DEFORMATION STUDIES OF THE FOLDED MYLONITES OF THE MOINE THRUST, ERIBOLL DISTRICT, NORTHWEST SCOTLAND

by

HENRIQUE DAYAN

THESIS SUBMITTED IN FULFILMENT OF THE

REQUIREMENTS FOR THE DEGREE OF

DOCTOR OF PHILOSOPHY

THE DEPARTMENT OF EARTH SCIENCES

THE UNIVERSITY OF LEEDS

SEPTEMBER 1981

VOLUME CONTAINS CLEAR OVERLAYS

OVERLAYS HAVE BEEN SCANNED SEPERATELY AND THEN AGAIN OVER THE RELEVANT PAGE

TO THE MEMORY OF MY FATHER

ABSTRACT

An area in the northern part of the Moine Thrust Zone of Loch Eriboll and in the NE side of Loch Hope, NW Scotland, has been mapped in the scale of approximately 1:10,560.

Detailed measurements have been made of structures such as foliations and lineations and these have been studied and analysed geometrically in terms of their relative age and the consistence over the whole area. The mapping has also traced the intricate pattern of thrust faults which trend roughly NNE/SSW. These thrust zones delimit different nappes and the deformation aspects of these faults indicate that the rheology of the rocks suffered changes during the thrust belt evolution. The easternmost major thrust zone is considered to have been developed first and clearly shows the characteristics of a ductile deformation zone. This zone is interpreted here as the Moine Thrust Zone, sensu stricto. A conspicuous mylonitic zone lies beneath and trends parallel to the Moine Thrust Zone and is limited in the west by a thrust which carried the mylonites onto clearly non mylonitic rock. The width of the mylonitic zone varies from Loch Hope in the north to the SE end of Loch Eriboll. This width variation is interpreted as due to thickening of the mylonitic zone by effects of folding and also due to the different deformation bands which anastomose and die out. Closely spaced cross sections, transverse to the extension of the belt of deformation are illustrated and discussed.

Strain analyses were carried out in two different domains of the mapped area. In the southern half of the area, where the frequency of folds is high, the distribution of fold hinges in sheath or curvilinear folds were used as strain indicators. Models , numerical methods and computer programmes for this strain evaluation have been thoroughly investigated. A detailed description of the methods used and tests performed with the constructed computer programmes is given. The

results are analysed in conjunction with the land geology and structure.

For the northerly half of the mapped area, strain estimations have been made using the grain shapes of the Paleozoic quartzites which are common in the two lowermost nappes. A new method for fitting the strain ellipsoid using three orthogonal ellipses was devised. A computer programme making use of this method was constructed and applied to the existent data. An alternative solution is also presented for the case where the fitted surface is not an ellipsoid. The strain results with the above methods are compared with those obtained using other published programmes and methods of strain estimation.

Microtextural variations in the Paleozoic quartzites of the northern domain have been studied. A detailed textural description and correlation is made between the textures and the available information on the deformation intensities shown by the quartz grains. An increase in the measured strain intensity is generally accompanied by an increase in the amount of recrystallized new quartz grains. These facts are consistent with the geology and structures of the nappes where sampling was done.

Paleostress estimates using recrystallized grain sizes have been performed at 31 localities in the Eriboll and Hope areas. The methodology of particle-size estimation is described in detail. The necessity for a standardization in the methods of particle-size measurement is emphasized with examples. The estimations of the differential stresses are greater in zones of greater relative deformation intensity. Although there are limitations and some adverse criticisms on the reliability of these paleostress estimates, the conclusion reached by this study is that they form a pattern that fits well with the geology and structure of the investigated area.

Rheologic considerations on quartz deformation constitutes the last part of the thesis. Deformation maps were constructed for this study using ranges of probable differential stress and the measured size of the newly recrystallized quartz grains. It is concluded that strain is predominantly accommodated by internal mechanisms operated by dislocation processes. It is also inferred that the operative strain-rate for the deformation conditions of this area, is between $10^{-13}.s^{-1}$ and $10^{-12}.s^{-1}$.

ACKNOWLEDGEMENTS

I wish to thank Mike Coward for his supervision, helpful discussions and ingenious ideas throughout the period of this study. I am most grateful to Rob Knipe for his assistance and valuable discussions regarding many aspects of this research. I should also like to thank Darcy Odloak and El-Amy Hefetz for helpful advice and patient introduction to 'computer trickery'. Charlie Allotey is also thanked for helpful discussions. All the technical staff of the Department of Earth Sciences, Leeds University are also thanked for providing ever-ready and competent assistance during the course of this study. Miss Caroline Hall is also thanked for patiently typing this thesis.

I would like to thank The British Council and the Conselho de Desenvolvimento Tecnológico e Científico-CNPq, Brazil, for their financial support during this research.

Finally, I am most grateful to my wife Rebeca for her continuous encouragement, support, great understanding and many sacrifices during some difficult periods of this work. Our parents and families are also heartfeltly thanked for their valuable support. I am sure they understand that I dedicated this thesis to the memory of my father.

CONTENTS

SYMBOLS AND ABBREVIATIONS USED IN THIS THESIS

AT	Arnaboll Thrust
BQ	Basal Quartzite
CC	Coble Creep
CPU	Central Processor Unit
DC	Dislocation Creep
DD	Dislocation Density
DF	Diffusional Creep
DL	Durness Limestone
DS	Dunnet and Siddan's Method
FB	Fucoid Beds
GBS	Grain Boundary Sliding
GR	Grid Reference
LG	Lewisian Gneiss
LM	Lewisian Mylonite
MG	Moinian Gneiss
MM	Moinian Mylonite
Mod I	Sanderson's (1973) model
Mod II	Variation of Sanderson's (1973) model used in this study
MP	Moine Psammite
MT	Moine Thrust Plane
MTZ	Moine Thrust Zone
NHC	Nabarro Herring Creep
OR	Oystershell Rock
PR	Pipe Rock
R	Finite Strain Ratio
R_f	Axial ratio of a particle in the deformed state
RGS	Recrystallized Grain Size
R_i	Axial ratio of a particle in the undeformed state

SA	Sample Average
SG	Serpulite Grit
SI	Shimamoto and Ikeda (1976) Method
SS	Subgrain Size
ss	sensu stricto
UAT	Upper Arnaboll Thrust
2D, 3D	Two and three dimensional

CHAPTER 1

GENERAL INTRODUCTION

1.1 Introduction to the Area of Study

The region of the Moine Thrust Zone in the Northwest Highlands of Scotland has been a classic area for the study of structural geology. This zone of Caledonian deformation extends some 190 km from Whitten Head in the extreme north near Loch Eriboll to Sleat in Skye (Fig. 1.1).

The area of this project constitutes a narrow strip of land which extends from the southeastern edge of Loch Eriboll to the northeastern side of Loch Hope, as shown in the map of Fig. 1.1. This area is located approximately 100 km northwest of Inverness and 20 km southeast of Durness. Access to the area can be gained via the A838 road which connects Durness and Tongue.

The southeastern border of Loch Eriboll can be described as a hilly and step-wise plateau with higher elevations in the south which are gradually lowered northwards. The relief is clearly controlled by the structural attitude of foliation, regionally dipping eastward.

Eastward-flowing consequent streams, frequently captured in small lochs on the plateau, flow towards Loch Hope. Obsequent and more active streams, flowing to the west, cut through the escarpment facing Loch Eriboll.

Peat covers parts of the area and glacial unconsolidated deposits lie along the lower ground near the coast of Loch Eriboll. The area contains a reasonable amount of outcrop, and Figs. 2.2 can give an idea of outcrop frequency and distribution throughout the domain of the mapped ground.

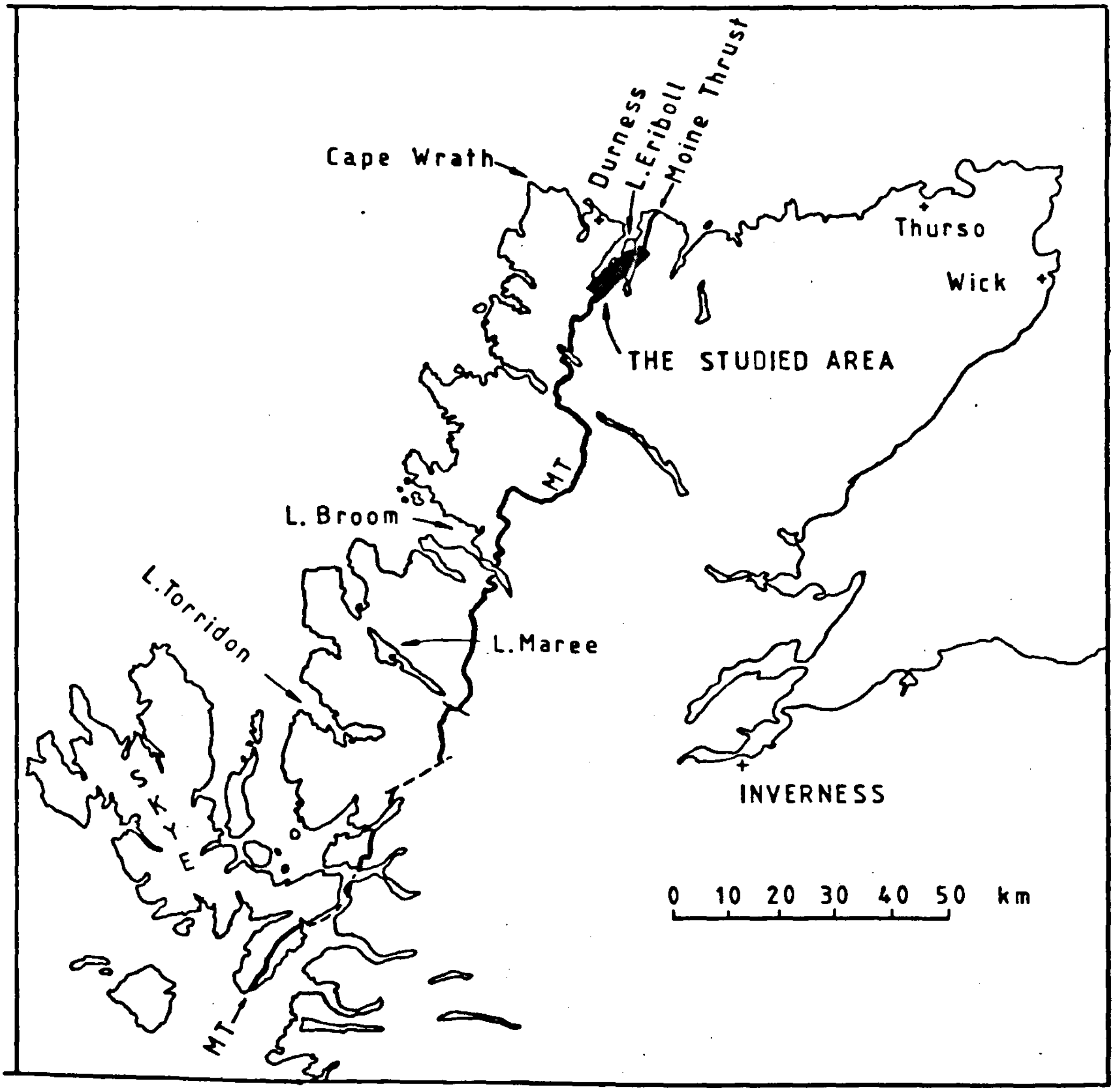

Figure 1.1. The northern part of Scotland. The thick black line displays the trace of the Moine Thrust. In shaded black is shown the studied area.

1.2 Review on the Early Research

Research in the area of the Moine Thrust Zone was marked from the beginning by controversial arguments and sometimes passionate discussions. This zone is often referred as the 'Belt of Complication', but from the available historic accounts it seems also appropriate to call this zone as the 'Belt of Dissention', as still there are controversial views on problems such as Thrust mechanics and emplacement which were first raised by the early geologists who worked in that area.

The early accounts on geologic research can be traced back to the beginning of the last century when Macculoch in 1819 (in McIntyre 1954) first pointed out that at Eriboll there were superposed gneisses on top of quartzites and limestones. The first interpretation of this was given by Cunningham (1839, in McIntyre 1954). He concluded that the gneisses and mica-slates (Moines) were younger than quartzites while the oldest of all were the underlying limestones, known at that time to contain fossils.

Nicol (1856) was attracted to this problem by the influence of Murchison and in this first paper he gave a poetic description of a first reconaissance of the area. He confirmed the existence of metamorphic rocks overlying fossiliferous limestone, near Ullapool, but he was in doubt whether the gneiss has formed in situ or had been pushed over the calcareous rock.

The prevalent idea at the time, as put forward by Murchison, was that the overlying gneisses and schists were younger than the limestone and formed a conformable succession. It is reported that Nicol disagreed publically with Murchison (see details in McIntyre 1954). After four years of research when Nicol visited the area four times and covered much of the ground around a line extending from

Eriboll to Skye, he published a paper, (Nicol 1860), which must be considered of utmost importance as it contains some lucid descriptions, good even by today's standards. In this paper (o.p. cited, p.86) Nicol formally disagrees with Murchison on the theory of conformable younger gneisses and schists and states that ".... where this conformable succession is said to occur is clearly a line of faulting ...." Nicol's (1860, p.91) comments were based on the criteria that the lithologic succession did not match in many different sections and that some beds were also missing in many sections. This in his opinion condemned Murchinson's "upward conformable succession".

Some of Nicol's terms and stratigraphic divisions are still used today. For instance denominations such as Pipe Rock, Fucoid-beds, Durness-Limestone, lower-quartzites (see Phemister 1960) were present in this 1860 paper.

It is reported, however, that the ideas by Murchison and his followers gained more acceptance at this period, so the polemic was temporarily closed only to be re-opened in 1878 by Hicks (in Lapworth 1885-a). In 1882 Lapworth initiated some studies in the Durness-Eriboll district. He opted for what he considered to be the only solution which could explain the geological phenomena at Eriboll, and this included, faulting, deformation, local stratigraphic inversion and partial metamorphism. While Nicol's descriptions are valuable, Lapworth's (1883, pl. v, Figs. 1, 5) cross sections are outstanding and detailed works of art.

Lapworth (1883) realised that there were no reasons for accepting Murchinson's ideas of superposed schists and gneisses younger than the underlying sedimentary and fossilferous rocks. Lapworth was also convinced of the existance of unconformity between the older Lewisian Gneiss and the younger paleozoic Quartzites but reported that the latter occurred tectonically emplaced on the former, as seen in the region above the Church Crag (see Geologic Map of figs. 2.1).

In his next paper (Lapworth 1984) it is clear that he was influenced by the ideas of Heim (1878) and interpreted the superposition of schists in Eriboll as due to gigantic overfolds (op. Cit., p.438). He interpreted the schists overlying the Paleozoic rocks as being composed of a mixture of Precambrian Lewisian Gneiss and Paleozoic rocks, so it is not clear whether he was referring to what are now considered as Lewisian mylonites or the younger Proterozoic Moinian rocks. It was also Lapworth's opinion that there were no rocks younger than the Durness Limestone. Lapworth was obviously impressed by the deformation effects shown by some of these rocks, as he referred to them as "..... crushed and mechanically metamorphosed ...." and repeatedly used the expression " ..... crushing effects ... " as referred to deformation. In this 1884 paper he clearly hinted the movement direction in the zone and stated (op. cited, p.441) that the rocks " .... travelled to west from east ...". It is quite clear that this was a prelude of his celebrated definition of mylonitic rock which appeared in a subsequent paper (Lapworth 1885-a).

Meanwhile B.N.Peach and J.Horne who were sent to the Eriboll area by Geikie, possibly to disprove the ideas of Nicol, arrived at the same conclusions as Lapworth thus favouring Nicol and rejecting completely Murchison's ideas. They also convinced Geikie who personally inspected the ground in Eriboll and immediately published an article in NATURE (1884). This paper introduces and preceeds a first analysis of the area by Peach and Horne (1884).

In Geikie's paper he criticised the interpretation of Murchison and introduced the name "Thrust-Plane", the expression "system of reversed faults" and also noticed the presence of "a fine paralled lineation, running in a west-north-west and east-south-east direction" (see op. cit., p.30).

Peach and Horne's (1884) paper on NW Scotland contains a stratigraphic description of the Paleozoic sequence (see fig. 1.2 for details) and also a detailed cross-section of the Durness-Eriboll region. The imbricate zone of Ben Heilam is represented in this section, the imbricates defined as reversed faults, and these two authors clearly differentiate it from the "Thrust-Plane" that brought the Lewisian over the Paleozoic suite of rocks. One can also find some remarks on the flattening, bending and rotation effects in the previously orthogonal (to bedding) pipes or worm-tubes of the so called Pipe-Rock. There are also descriptions of the thrust relationships in the region of the Arnaboll Hill and Creag-na-Faollinn, very much alike the modern interpretation.

The area of Durness-Eriboll was specifically treated by Peach and Horne in a subsequent paper (1885) where they describe the contrast between the west and east sides of Loch Eriboll. They also mentioned the formation of a secondary foliation in rocks subjected to the effects of mechanical deformation and this description also contains a remark about a " ... parallel lineation like slickensides trending in the same direction, over a vast area, while the minerals were oriented along these lines ... ", which refers to an important direction of stretching as will be discussed in the next two chapters.

The above work, in fact, preceded Lapworth's (1885-a) paper which contains the definition of mylonites as "finely laminated schists" (mylonites, gr. mylon, a mill) composed of shattered fragments of the original crystals set in a cement of secondary quartz, the lamination being defined by minute inosculating lines (fluxion lines) of kaolin or chloritic material and secondary crystals of mica". It

Series	Group / Zone	Description
C. Calcareous Series ...	VII. Durine Group ...	Fine-grained, light gray limestones, with an occasional dark fossiliferous band.
	VI. Croisaphuill Group	*c.* Fine-grained, cleaved, lilac-coloured limestones, full of flattened worm-casts; fossils distorted by cleavage. *b.* Alternations of black, dark gray, and white limestone, with an occasional fossiliferous band, like zone (*a*) of this group. *a.* Massive, dark gray limestone, chiefly composed of worm-casts which project above the matrix on weathered surfaces. Near the base are several lines of small chert nodules. This is one of the most highly fossiliferous zones in the Durness Basin.
	V. Balnakeil Group ...	Alternations of dark and light gray limestone, highly fossiliferous, with occasional impure, argillaceous, unfossiliferous bands. Most of the beds are distinctly cleaved, and contain few worm-casts.
	IV. Sangomore Group...	Fine granular dolomites, alternating near the top with cream-coloured or pink limestone. Near the base are two or more bands of white chert, one of which is about 5 feet thick.
	III. Sailmhor Group ...	Massive, crystalline-granular, dolomitic limestones, occasionally fossiliferous, charged with dark worm-castings set in a gray matrix; large spheroidal masses of chert near the base. This limestone is locally known as "the Leopard Stone."
	II. Eilean Dubh Group	Fine-grained, white, flaggy, argillaceous limestones and calcareous shales. As yet no fossils have been found in this division.
	I. Ghrudaidh Group ...	Dark leaden-coloured limestones, occasionally mottled, alternating near the top with white limestone. About 30 feet from the base there is a thin band of limestone charged with *Serpulites Maccullochii*, and a similar band occurs at the base.
B. Middle Series (partly calcareous and partly arenaceous)...	Upper Zone	At the base lies a massive band of quartzite and grit, passing upwards into carious dolomitic grit, crowded in patches with *Serpulites Maccullochii*, more especially in the decomposed portions (Serpulite-Grit).
	Middle Zone	Alternations of brown, flaggy, calcareous, false-bedded grits and quartzites with cleaved shales.
	Lower Zone	Calcareous mudstones and dolomitic bands, weathering with a rusty brown colour, traversed by numerous worm-casts, usually flattened, and resembling fucoidal impressions. These beds are often highly cleaved. This and the overlying zone form the "Fucoid-beds" of previous authors.
A. Arenaceous Series...	Upper Zone	Fine-grained quartzites, perforated by vertical worm-casts and burrows becoming more numerous towards the top of the zone ("pipe-rock" of previous authors). These beds pass downwards into massive white quartzites.
	Lower Zone	False-bedded flaggy grits and quartzites, composed of grains of quartz and feldspar. At the base there is a thin brecciated conglomerate, varying from a few inches to a few feet in thickness, containing pebbles of the underlying rocks, chiefly of quartz and orthoclase, the largest measuring about 1 inch across.

Figure 1.2. Stratigraphic section of the Lower Paleozoic rocks of Loch Eriboll (after Peach and Horne 1884).

must be remembered, however, that the expression " ... fluxion lines ..." and " .. mill .. " both connected with deformation were previously used by Geike, (1884, pp.30-31).

It is evident that all the workers were much impressed by the superimposed mylonitic foliation and, for instance, Lapworth (1885-a) reported that new minerals had been formed as a consequence of deformation. However, he interpreted the rocks to the east (the actual Moine succession) as a mixture of Hebridean (Lewisian) and patches of Paleozoic and igneous rocks.

There followed a profusion of reports and papers exploring the newly found ideas with advances not only in mapping but also in terms of experiments, such as the celebrated thrust modelling performed by Cadell (1888). This research along the Thrust Zone (Eriboll-Skye) received much attention till the end of the last century. Many of the present thrust-rules are partially derived from this work. The geology was summarised by the now classic reports Peach et al. (1907) and Peach and Horne (1930).

During this century the Moine Thrust Zone has been largely neglected, though there have been several structural projects since the fifties and sixties. Some of this research has become much more specialized. For instance, structures in rocks of the Thrust Zone are now investigated from a submicroscopic (see references in Chapter 6) dimension. On a larger scale the thrust tectonics of this zone have been described in a paper by Elliott and Johnson (1980) which applied new concepts and ideas drawn from the Rocky Mountains. Much of this recent literature will be discussed in the next chapters.

The specific area at Loch Eriboll was partially mapped and described by Soper and Wilkinson (1975) although some aspects have been described by Barber and Soper (1973). The area of the north has been the object of PhD theses (Allison 1974, Nadir, 1980) and recent papers by Coward and Kim (1981), Fisher and Coward (in preparation). Some aspects of the thrust geometry of the Loch Eriboll area have been discussed by Coward (1980); these papers will be discussed in the next chapters.

1.3 Scope, Methods and Organisation of this Study

The aims of the present study were to investigate the geometry of the rock fabrics, to evaluate the deformation intensities and also to establish the probable deformation mechanisms that operated within the context of the deformed rocks of the Moine Thrust Zone of the Eriboll-Hope region.

The area specified in fig. 1-1 has been remapped mainly at the scale 1:10,560, sometimes at approximately 1:5,000 or locally at 1:1100 (see fig 2-4). The bulk of field work was carried out in two summer seasons, but mapping for this study was also performed during two intermediate (short) visits to the area.

Well over 7,000 measurements of planar and linear structures were recorded for the Eriboll and Hope areas, during the course of field mapping. Oriented samples were collected for purposes of laboratory work which comprised measurements of grains and analysis of microstructures.

A great deal of time was spent with computer work during the research period at Leeds. The study consisted in the elaboration of programmes, in FORTRAN IV, for the methods of strain determination. Chapters 3 and 4 are strictly connected with this part of the research.

Chapter 2 contains a description of the lithologies involved in the area. The geometry of the structures in the mylonites has been described and systematically analysed. Fold geometry is specified in terms of class and shape. The structure of the area is reviewed in terms of detailed cross-sections.

Chapter 3 gives a numerical evaluation of the strains in the rocks, using directional data of re-oriented fold hinges. New methods of parameter estimation using optimization techniques allowed the application of two basic models. The results of these and the derivation of other possible models are discussed in the context of the present structural setting.

Chapter 4 is given to strain estimation using microscopic markers. Grain shape analysis of data were measured from oriented thin sections. A new method of fitting the ellipsoid using data from 3 orthogonal ellipses is presented. A new solution for the case of fitting a non-ellipsoidal surface is also proposed. Two computer programmes (corresponding to the above situations) were specially elaborated and applied to the available data. The results and comparisons with previously existent methods and programmes are discussed.

Chapter 5 consists of a detailed description of microstructures in rocks subject to a progressive increase of deformation. It correlates the amount of grain deformation to the percentage of recrystallization present in the sample.

Chapter 6 presents a study of Paleopiezometry using the recrystallized grain size of quartz. The methods used in this study are described and the results obtained are compared with the published results from the Moine Thrust Zone.

Chapter 7 is concerned with the Rheology of the rocks. The flow mechanisms and equations are dealt with in the form of deformation maps. These were calculated for the range of the measured grain sizes. There follows a discussion of the more probable mechanisms of deformation affecting the studied rocks.

Finally Chapter 8, covers a final discussion and main conclusions for the present work.

Appendices 1-4 fully list the computer programmes that were made by the author during the course of the present research. Every programme is accompanied by instructions for use.

There is not an uniform nomenclature in this thesis due to the fact that the chapters cover various different fields which make use of the same legend. In order to avoid duplicity it would be necessary to modify some well known symbols. Therefore it was decided to discriminate the necessary nomenclature, in each chapter, in order to make it compatible with the specialized literature.

All diagrams and maps are referred to here as figures (figs.), in the case of photographs and photomicrographs, these will be referred to as plates. Throughout this work all the illustrations and mathematical expressions have a composite numbering in which the first numerical is indicative of the chapter. The innumerable localities referred to in the text, with their complex Gaelic and Norse names, are given in figs. 2-1.

CHAPTER 2

GEOLOGY AND STRUCTURE

2.1 General

The first part of this chapter deals with lithological descriptions and related stratigraphic aspects of the rocks found in the studied area.

The second part of the chapter is more extensive and comprises a detailed description of the structures met in the mapped area. This is followed by a statistic and harmonic analyses of folds and finally by thrust description using detailed cross-sections. The final part is given to the interpretation, comments, comparisons and discussions which are based on the field mapping and data measurement.

2.2 Lithology

The succession of lithologic types found in the mapped area, together with their main rock-character, inferred time and group relationships, are summarised in table 2-1.

2.2.1 The Lewisian Suite of Rocks

The Lewisian rocks comprise a varied suite of lithologies. They are highly metamorphic rocks that have undergone a very complex deformation history. The Lewisian of the NW of Scotland was originally described in detail by Peach et al. (1907) and then studied by Sutton and Watson (1951, 1953 and 1962). They established a chronologic subdivision of this complex group, using dykes as stratigraphic markers. In the more recent years, other studies also attempted to establish a general chronology for these rocks and presently there is clearly a divergency of opinions (eg. Bowes 1968, 1969; in Park 1970) both on the methods employed in this kind of study and also in the interpretations

Table 2.1

Displays the series of rock types found in Eriboll and Hope areas.

Lower paleozoic	DL	7	Durness Limestone
		6	
		5	
		4	
		3	
		2	
		1	
	SG		Serpulite Grit
	FB		Fucoid Beds
	PR		Pipe Rock
600 Ma	BQ		Basal Quartzite

------------------------------ Probably Unconformable ------------------------------

?1250-1050?	Pelitic to Psammitic		Moinian and Oystershell rocks. Gneisses, schists and psammites which include acid and basic masses. Psammitic series can grade to semi-pelites and also include a feldspathic-rich member. Amphibolite sheets in different rock domains.
	Psam-mitic	Amphi-bol.	
	Gneis-sic.		

------------------------------ Probable Unconformity ------------------------------

1290-1600	Lewisian	Lewisian mylonite	Orthogneiss derived from a granite-gabbro-peridotite suite. Dykes, basic (minor) and acid composition, comprise part of the bulk of the rock.

given to the structure and sequence of events.

The Lewisian cropping out in the foreland region neighbouring Durness is of two main types: (i) a dominantly dark banded rock where the percentage of aplitic and veined material is minor and (ii) a domain visibly dominated by a rock-type characterised by intense injection of aplitic to pegmatitic material with a predominant pink colour. Most of the gneisses are considered to have been re-deformed and intruded by the aplitic/pegmatitic material during a Laxfordian episode at about 1800 my ago (cf Sutton and Watson 1962).

In the studied area, all the Lewisian rocks have suffered some effects of Caledonian deformation, dated along the Moine Thrust Zone (MTZ) as approximately 430 m. a. (see van Bremmen et al. 1979), and they exhibit characteristics of homogeneization due to:

(i) A very strong mechanical deformation which has brought to near parallelism all platy minerals and given the rock a thinly laminated foliation. It has also erased previous structures and brought dyke-contacts and their internal fabrics into concordance with the host rock.

(ii) Metamorphic changes which have caused the crystallization and recrystallization of grains, giving rise to the formation of a greenschist-chloritized series of minerals, in which the association of epidote-chlorite is responsible for the homogenous greenish appearance observed in the rocks.

In one locality it was possible to observe the original rock types relatively undeformed (see plate 2-1). This is on the westernmost face of the Creag-na-Faollinn, where the gneiss includes hornblende bearing rocks which vary from a type which is formed exclusively of hornblende aggregates to banded hornblende-plagioclase-gneiss. Also present in this locality are metabasic lenses which attest that

Plate 2.1. 'Undeformed' Lewisian rock of the western-most face of Creag-na-Faollinn.

Plate 2.2. Milky quartz-veins (arrow) in the Moinian psammitic rock.

the Lewisian suite was previously affected by basic intrusives. Elsewhere in Creag-na-Faollinn it is possible to identify biotite-gneisses.

There are two other localities where it was possible to locate metabasic-lenses; the first occurs in the area of the relatively less deformed Lewisian that constitutes the upper westernmost side of Arnaboll Hill, and the second occurs within the mylonitic zone overlying the Cambrian rocks in the top of the same hill. In the area of Lewisian mylonites of the NE side of Loch Hope serpentinized rocks form an extensive outcrop. That is the only occurance of ultra-basic rocks in the mapped area.

The rest of the area shows rocks of two types: (i) Leuco-gneiss massively impregnated by veins of varied thickness in which a dominant pink colour is a direct result of the microcline content. With the exception of Creag na Faollinn and the western top of the Arnaboll Hill, these veins are in perfect concordance with the host rock. (ii) Homogeneous green and greyish (both varying from light to dark) rocks which constitute the corresponding highly deformed versions of the rock-types (rich in mafics) described for Creag-na-Faollinn.

The feldspar-amphibole-epidote assemblage of the Lewisian rocks seem to grade to albite-epidote-chlorite due to effects of mylonitization (Soper and Wilkinson, 1975). The feldspars show polysinthetic twining and perthitic lamellae. Among the micaceous minerals, muscovite appears with chlorite and biotite. Apparently epidote is to be located within the micaceous bands. Calcite is also present in many sections and it is considered to be due to feldspar breakdown. Other minor components include sphene, zircon and opaques.

On the geologic maps of figs. 2-1, the Lewisian rocks appear to be confined to a narrow longitudianl NE-SW strip, bounded by the easternmost thrust traces. Two lithologic types appear in the legend and these correspond respectively to the mylonitic and non-mylonitic types.

2.2.2 The "Oystershell" and the Moine Series

2.2.2 a The "Oystershell" Rocks

These rocks seem to be part of the Moinian Series. There is some controversy over the genesis and the stratigraphic position of these rocks.

The "Oystershell" rocks are characterized by greenschist series of metamorphic grade. They have a green colour and exhibit quartz-bearing domains with milky colour which form small plates concordantly disposed in the foliation planes. These resemble oyster shells and hence the analogy and name by Peach and Horne (1907).

In the area north of Alt-na-Eisgil, between cross sections BB' and CC' (see geologic map of fig. 2-1) the succession of "Oystershell" rocks can be divided into two clearly distinct rock types: (i) a structurally lower member characterized by alternating bands of pelitic and quarzitic layers, the latter being formed by fine grained quartz which differentiates this lithology from the coarser Moinian psammite that underlies it. The thickness of the fine psammitic layers in the Oystershell rock vary from one to a few centimetres while the pelitic bands are thicker, and resemble the Oystershell rock, sensu stricto. (ii) The structurally overlying member grades to an almost entirely pelitic rock which exhibits some psammitic members resembling 'oysters' with milky colour and oblate shape. The green colour of this schist is probably due to chlorite content but there is also epidote present in this mineralogic suite which includes cholorite-muscovite and quartz.

There are some calcareous domains in these Oystershell rocks and calcite is frequently seen in thin section. Feldspar (albite?) is also present, especially close to the domain of the underlying feldspathic Moinian psammite.

Soper and Wilkinson (1975) have chemically analysed the Oystershell rocks and place their origin in the field of argillites (see op. cit., p.343, table I). They consider that this rock was derived from an 'off-shelf' pelitic facies of the Durness Limestone.

The thickness of these rocks is modified by the effects of multiple folding and the lithology cannot be traced both north and south of the studied area. This decrease in rock thickness (to zero) seems to be gradual in both directions. At the NE border of Loch Hope the 'Oystershell' seems to be confined to a single outcrop while south of Creag-na-Faollinn this schist is thin to non-existent in the SE of Alt-na-Craoibhe-Caoruinn.

In the geologic map of figs. 2-1, the 'Oystershell' rocks are represented by a single ornamented type. This lithology is always located to the right of the easternmost thrust trace (ie the Moine Thrust,sensu stricto).

2.2.2.b The Moine Series

This group of rocks structurally overlie the 'Oystershell' rocks in Eriboll and Hope areas. It is also shown in this area that there is a gradation to three rock types.

The lower member of the Moinian suite of rocks is an almost essentially psammitic, having a light colour, fine grained, but also presenting a small percentage of feldspars and micaceous minerals. It exhibits a granoblastic type of texture, in thin section.

The psammitic varieties of the Moines are characterised by the presence of milky quartz veins having varied thickness, oblate to signoidal shape and anastomosing at the ends. Some veins show rootless folds and are always concordant with the dominant mylonitic foliation (see plate 2-2). These veins are thought to be a product of quartz segregation processes.

In some parts of the mapped area, the Moine psammites show a gradual increase in the content of white micas and this seems to be approximately inversely proportional to the volume of the quartz segregations. With this increase in pelitic content there is a colour change from nearly white (psammite) to light green (intermediate or semi-pelitic member) and finally the extreme member which is dominantly pelitic. The pelites exhibit some scattered and large pink feldspars (up to 3 cm) concordantly disposed in the foliation planes. Some Moinian psammites exhibit feldspars closely associated with quartz veins (see plate 2-3). Accessory minerals include epidote and sphene.

Soper and Wilkinson (1975) placed this pelitic member, as pertinent to the Lewisian domain. Indeed the resemblance is striking in many cases, especially because the strongly deformed Moine schists can acquire the greenish colour of Lewisian Mylonites. Near to the top of Creagan Road, at Poll Mor, the contact between the psammitic and pelitic members is very sharp (thus lacking the intermediate member) so the described gradation is not visible and this is a situation that may lead one to consider a Lewisian origin for these pelites.

Furthermore to the north of the Creagan Road, towards the Arnaboll Hill the pelitic lithology changes by becoming more feldspathic and this gives the rock a distinct pink and very homogeneous appearance resembling that of strongly deformed and richly feldspathic Lewisian

Plate 2.3. Feldspars associated with quartz-veins in Moinian Psammitic rocks. Note pronounced lineation almost parallel to the pencil.

Plate 2.4. Cross-bedding in the quartzitic rocks of the Cambro-Ordovician sequence beneath the b-thrust near the Creagan Road.

mylonites.

Between cross sections EE' and FF' (see geologic maps of figs 2-1-a and b) there appear in the pelites, some lenses of amphibolitic material. These lenses are more common within the corresponding pelites located at the NE side of Loch Hope. The gradation from pelite to psammites is also present in this area where amphibolites occur not only within the pelite but as well within the psammitic member. It must be remembered that the rocks to the south of Melness show amphibolitic lenses also within the Moines. This gradation from psammite to pelite has lead me to place both groups in the Moines.

On the map of figs. 2-1-a and b, the Moinian lithology constitutes the easternmost sequence of rocks. Note also the presence of the psammitic member at several localities along the mylonitic zone between the two easternmost a and b - thrust traces.

2.2.3 The Lower Paleozoic Rocks

The lower Paleozoic rocks, which rest uncomformably on the Lewisian series, occur in the lower nappes of the thrust zone (see figs. 2-1). They are grouped in three series, according to the original division by Peach and Horne (1884) (compare table 1-1 with fig. 13 in Phemister 1960) as follows:

c - The Calcareous Series (top), which can have 7 subdivisions (see Phemister 1960).

b - The Passage or Middle Series, which is partly calcareous and partly arenaceous.

c - The Arenaceous Series.

2.2.3-a The Arenaceous Series

These rocks constitute the bottom part of the Paleozoic column and are probably of lower Cambrian age (see Phemister 1960, p.48).

2.2.3-a.1 The Basal Quartzite

These rest uncomformably on the Lewisian rocks (see fig. 2-1-b, the domain above Kempie Bay, between cross sections GG' and FF). They consist of coarse impure sandstones, with quartz grains up to a millimetre in size and even coarser pink feldspars (up to 5 mm). In places, this rock has the appearance of a microconglomerate but stratigraphically upwards a change is made to a better sorted suite clearly exhibiting cross stratification and bedding marked by thin darker bands which are richer in feldspars.

The upper horizon consists of a much more homogeneous, fine grained and massive rock. This type has a light white colour in which the only surfaces of discontinuity are some irregular partings. These could well be a result of pressure solution seams (concentrations of insoluble material). There are no indications of primary structures and this domain resembles very much the matrix of the immediately overlying 'Pipe-Rock'.

2.2.3-a.2 The 'Pipe-Rock'

This lithology has its name (from Nicol 1856) derived from the vertical tubes which are mostly interpreted as infillings of worm burrows - Skolithos and Monócraterion (Hallam and Swett, 1966). Apart from having cylinders normal to bedding, this sandstone contrasts with that previously described by presenting a better sorting, finer grain size and an absence of coarser feldspar grains. In thin section, it is possible to verify the presence of micaceous minerals, probably sericite.

The pipe-rock variations comprise 5 subzones according to their forms and frequencies - see Peach et al 1907, pp.372-373. However Hallam and Swett (1966, p.102) argue that these subzones do not constitute laterally continuous domains or even appear in constant chronological order. The present study distinguishes generally (not in sequence) three main groups with the characteristics as follows:

(i) In one group, 'pipes' and 'matrix', both have the same whitish colour. Bedding (very frequently cross bedding) is denoted by very thin darker bands. The perturbations seen in these layers, the downward drag into the pipes, allow one to recognise the right way up of those beds. In sections oblique to bedding, the traces of these burrows resemble cones while in the bedding planes the pipe sections (either circular or elliptical) can exhibit a wide area which decreases downwards - that is, the pipes have a funnel shape. This lithology is commonly referred to as the 'trumpet pipes' horizon (Peach et al. 1907, subzone III). Hallam and Swett (1966) believe that Monocraterion was the fossil responsible for the formation of these 'trumpets'.

(ii) In this group pipes and 'matrix' are nearly white in colour but with the difference that in this case the pipes shown in section have a lighter colour. Here bedding is not so conspicuous as in the previous case. This horizon could perhaps be correlated to the 'ordinary pipes' of Peach et al. (1907). In the view of Hallam and Swett (1966) these traces are attributable to the action of the fossil Skolithos.

(iii) Finally, there is a group of rocks where white pipes contrast with a purple 'matrix'. It is very easy to identify the white tubes -

perhaps longer than in case (ii) - but very difficult to locate bedding. In the present mapping area, this group was rare.

2.2.3-b The Intermediate or Middle Series

This is the thinnest sequence among the 3 series (see Phemister 1960, p.49) and it can be subdivided as:

2.2.3-b.1 The Fucoid Beds

These are the lowermost rocks and consist mainly of calcareous shales with some mudstones and layers richer in quartz. The rock characteristically exhibits a brown rusty colour that varies its shade from a darker to a lighter-brown perhaps according to the decrease in shale content. The term fucoid (a type of seaweed) is based on an early misinterpretation of flattened worm-casts found in the bedding planes.

Barber and Soper (1973) give a detailed description of these rocks for Kempie Bay. In the present study area, the most extensive outcrops of this lithology occur between the bottom of Creagan Road and Church Creag. Many of Barber and Soper's (1973) variations were observed within this area.

2.2.3-b.2 The Serpulite Grit

This upper member consists of a more gritty rock with a light brown colour. It is named after its fossil content (Serpulite Macculochi).

In the domain of the present mapping this rock type is restricted to a very few outcrops along the folds between the Creagan Road and Kempie Bay. It is possible that these rocks also crop out below the lower thrust at the front of the Creag na Faollinn area.

2.2.3-c The Calcareous Series

This is stratigraphically the highest group of rocks and in the foreland exhibits the greatest vertical thickness (see Phemister 1960. fig. 13).

This lithology is referred to here generically as the Durness Limestone. In the domain of this study area the calcareous rocks are confined to two localities: (i) a westernmost strip shown in the geologic maps (figs. 2-1-a and b) cropping out between the base of Creagan Road and Kempie Bay, (ii) and as an allochtonous mass of rocks, emplaced in the middle of the mylonitic rocks above the Church Creag.

2.3 Structure

2.3.1 Survey on Previous Work in the Study Area

In recent years, a considerable amount of work has been carried out in areas in or near the area of the present study. Some research on the eastern edge of Loch Eriboll was done previously by Wilkinson (1956). He recognised, in that area, 4 nappes which are named after their underlying thrusts. Soper (1971) and Soper and Brown (1971) applied Johnson's (1957, 1960) concept of a four-fold deformation sequence for the Moine Thrust of Eriboll. This was confirmed in the paper of Barber and Soper (1973) which also contains detailed maps (see op. cit. figs. 3, 4) and illustrates some of the difficulties encountered in that area. These two authors also modified the previous subdivision of thrusts and nappes.

Soper and Wilkinson (1975) mapped in great detail the ground between the south of the Arnaboll Hill and the south of Alt-na Craoibhe Caoruinn. They also adopted Barber and Soper's (1973) tectonic subdivision which can be summarised as follows (from east to west):

Moine Nappe	
------------- Eriboll Thrust	confined to Alt Eriboll area
Moine Thrust Zone	
------------- Moine Thrust	
South Eriboll Nappe	restrict to the southern part of the area
------------- Faollinn Thrust	
Arnaboll Nappe	occurring in the north of the area
------------- Arnaboll Thrust	
Heilam Nappe	north (off limits) of the area
------------- Sole Thrust	
Foreland	

The above division reveals that it is not possible to correlate thrusts - traces along the whole of the mapped area. Thrusts can branch, merge or even die out.

This study agrees with much of the mapping by Soper and Wilkinson (1975, compare their fig. 8 with the present figs. 2.1-a and b).

Some differences related to lithological aspects have already been mentioned (section 2.2.2-b) and others, relative to structures, will be discussed in detail in section 2.3.5.3.

Coward (1980) investigated domains along the thrust zone at Faollinn and the Arnaboll Hill. A model for the evolution of the Arnaboll area is also presented in his paper (op. cit. fig. 5).

Coward and Kim (1981) proposed models for strain evaluation using Cambro-Ordovician rocks of Eriboll. Recently the geology and structure to the north of the Creagan Road has been dealt with by McClay and Coward (1981) and Rathbone _et al_ (in press).

A number of theses have made use of the rocks of Eriboll area. For example, McLeish (1969) determined strains in the pipe-rock of Kempie Bay, while Allison (1974) investigated the strain and microstructures in the rocks of Ben Heilam. More recently Nadir (1980) studied the structure and the deformation of the Paleozoic rocks of the Lower Nappes, north of the An-t-Sron. More references on studies in Eriboll rocks, especially those dealing with microscopic textures, will be given in Chapters 5 and 6.

2.3.2 General

The distribution of the rock-types shown in the geologic maps of figs. 2-1 has been introduced in section 2.2. The present section aims to describe the relevant structures, encountered during lithological and structural mapping, and these are represented on the structural maps of figs. 2-2.

The structures to be described in this chapter were measured in the field and the conventions and systematics adopted during the mapping routine followed those proposed by Turner and Weiss (1963) in which the geometry of the various structures is grouped in terms of Planar and Linear elements.

For the purpose of structural analysis, the mapped area (figs. 2-1 and 2-2) has been subdivided into almost homogeneous domains, based mainly on the distribution of the attitudes of the most prominent Planar Fabrics. The data for each sub-area have been plotted on equal area (lower hemisphere) projections and these are shown in figs. 2-3 to 2-6.

One of the aims of the present analysis is to use the meso-scale structures (cf. Turner and Weiss, 1963, pp.15-16) in order to infer the geometry of the structures on the macro-scale.

It was noticed, in the field, that the meso-structures presented some characteristically persistent patterns of style and preferred orientation, resulting from several deformation phases, and this allowed them to be grouped, taking into account the following field criteria (see Weiss and McIntyre 1957; Johnson 1960-a):

(i) By observing the relationships (ie consistent) between structures that overprint and distrub previous structures and recording their position, general characteristics and pattern of preferred orientation.

(ii) by extending the criteria of similarity in their style and pattern of preferred orientation to those domains where over-printing is not clearly seen. It must be pointed out that a similarity in orientation does not necessarily define a particular generation.

The first of the above criteria is by far the most reliable. Based on this, three main groups of structures were recognised in the upper nappes of the Thrust Zone. However , one cannot expect to find a simple structural superimposition in every outcrop and for this reason, the second of the above criteria was widely used during mapping routines.

It is also the aim of the present section to analyse the various local preferred orientations of the meso-structures and to relate them to the pattern of the whole zone and ultimately to interpret the geometry in terms of the dymanic picture of the thrusting.

2.3.2-a The Sequence of Events and the Adopted Convention

As this mapping is almost restricted to zones of thrust faults and strong mylonitization, in which most of the rocks involved have their previous structures erased, it is convenient to place this mylonitization event as a reference guide. Therefore, the structural elements will be defined according to the following subdivision:

(i) Planar structures (S_i- Planes) - Foliation is the term adopted here (cf. Turner and Weiss, 1963. pp.97-101) in order to define the generation of planar fabrics, independent of their origin.

- (S_0), defines any identifiable primary structure such as bedding found especially in the Paleozoic rocks.
- (S_1), refers here to the foliation formed as a result of mylonitization whereas S_2, S_3 and S_4 are respectively axial planes developed during the subsequent folding phases.
- (S_A), can generically (or collectively) define any recognisable planar fabric, previous to S_1, found in the proterozoic rocks.

(ii) Linear Structures (L_i) - These are prominent linear features, found throughout the mapped area, which are due to structures generated sequentially, independent of the rock-type. These are divided in different sets:

- (L_1), refers to a characteristically (early) penetrative linear structure, thought to be syngenetic with S_1, which is given by longitudinal alignment of elongated minerals.
- $L_2 \equiv B_{S_1}^{S_2} \equiv F_2$, $L_3 \equiv B_{S_1}^{S_3} \equiv F_3$ and $L_4 \equiv B_{S_1}^{S_4} \equiv F_4$, refer respectively to the fold axes of the subsequent deformation phases.

It must be pointed out that the above convention is surely an oversimplification of the real facts. However, for the practical purposes of study and description (within the mapped domain) it proves convenient in that it avoids conflict between the numbering and definition of structures (Paleozoic and Proterozoic) formed previous to the mylonitic foliation.

2.3.3 Description of the Geometry and Analysis of the Structures

2.3.3-a The Main Domains of Planar Structures

The mapped area is composed of three distinct domains accordingly to their structural characteristics. In the north-west (i) the Lower Paleozoic rocks form a domain bounded by a thrust (b-type of thrust as discussed later) which separate them from (ii) the zone of strong mylonitized rocks and finally (iii) the Moinian sequence that overlie this second domain due to the effects of the a- or the easternmost thrust (see figs. 2-1). Thrust naming will be discussed later.

The rocks of domains (i) and (iii) have been described previously but those of the mylonitic domain need a brief description.

The largest and thickest part of the mylonite belt is made up almost entirely of Lewisian rocks and these lie immediately beneath a thick sequence of Moinian rocks. This generalized mylonitic zone comprises blocks of predominantly moderately deformed Lewisian rocks which are separated by zones much more intensely deformed rocks. These heavily mylonitized rocks form an elongated zone with a NNE-SSW trend and regionally they dip towards the ESE.

In the field it is easy to observe a transition from a strong deformed gneiss showing a persistent straight banding to an intermediate stage where lamination is even more intense and finally the extreme case where the rock is finely laminated, generally dark in colour and shows a fine grained texture of closely spaced mylonitic folia. This lamination (less than 1 mm thick) is characteristic of narrow tabular zones of intense deformation. It is formed by the parallel disposition of platy materials. This presumably originated by the re-shaping and size modification of leucocratic minerals, such as quartz. The net result is a fine grained and uniformly graded micro-structure exhibiting prominent parallel banding.

The characteristics of this foliation vary not only with intensity of deformation which seems to grade away from the mylonitic zones, but also accordingly the rock type. It is clear, that in conditions of intense deformation the appearance of a fine lamination is independent of the rock composition but in the less deformed stages the rocks with some percentage of micaceous materials tend to produce a more clearly defined cleavage than for instance a sample primarily composed of quartz and devoid of micaceous and platy minerals. We shall illustrate, in Chapter 5, the effects of this re-shaping, size grading and re-orientation of platy minerals in a zone of progressive deformation.

Another aspect of the foliation in the mylonites is that it forms a quite persistent and regular pattern which overprints and erases most of the previous structures, and generally produces a homogeneization of the whole rock. For instance, quartz-feldspathic dykes and veins in the Lewisian Gneiss, presumably of Laxfordian age, appear totally concordant with the host rock and even develop an internal planar fabric. In the more mafic parts there is a tendency for colour-homogenization (greenish) which is given by the development of equally spaced mica layers associated with epidote and chlorite.

The thickness of the mylonites varies considerably within the area. In the Paleozoic rocks, beneath the heavily mylonitic zones composed of Lewisian gneiss, there is clearly a rapid decrease in the intensity of the deformation. There is no transposition of fabrics, so primary structures can still be identifiable at only a short distance from the b-thrust, as can be seen in plate 2-4. Mylonitization is restricted to a few centimetres of the thrust and cataclasis may be present (see plates 2-5 and 2-6). Overlying these Paleozoic rocks there follows a thick zone of mylonites which are bounded by the upper or the easternmost thrust (the a-thrust). This upper fault is characterised by a wider zone of mylonites and also by the fact that it does not form a sharp contact. The apparent continuity of structures across the thrust often makes it more difficult to identify this fault.

The phase of mylonitic formation is envisaged here as representing the peak of the local deformation and this fabric is not totally obliterated by the subsequent fabrics, namely S_2, S_3 and S_4. The S_1-fabric is so dominant that it is believed it influences the orientation of the superposed fabrics.

2.3.3-a.1 The Geometry of S-Planes

The regional attitude of the foliation planes is given by a set of 34 stereoplots (fig. 2-3) which record nearly 3400 S-planes. The division into sub-areas is mainly based on the variability of the attitudes of the S_1-planes.

The stereoplots in fig. 2-3 show that the geometry of S_1 is apparently simple, and with a few exceptions the π-diagrams clearly exhibit a remarkably homogeneous fabric generally depicting a strong preferred orientation, given by a single maxima and their associated contours. In general the fabrics range from axial-orthorhombic to monoclinic. There are exceptions such as the apparently triclinic symmetry of sub-area no. 2, but this area has been mapped in a greater

Plates 2.5 and 2.6. Illustrate aspects of cataclasis in the Paleozoic quartzites in the vicinity of a thrust-plane at Creag-na-Faollinn.

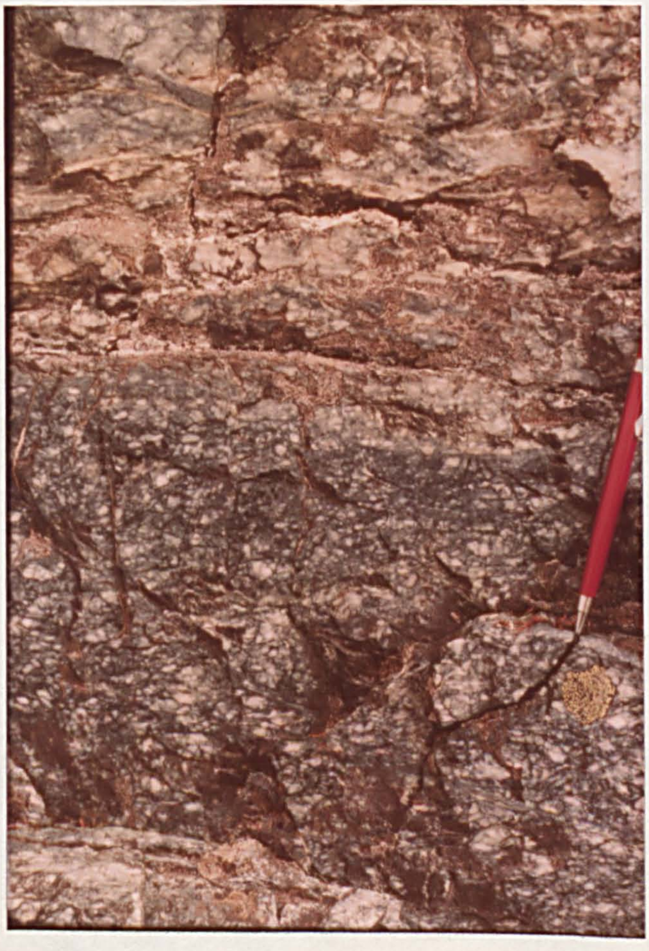

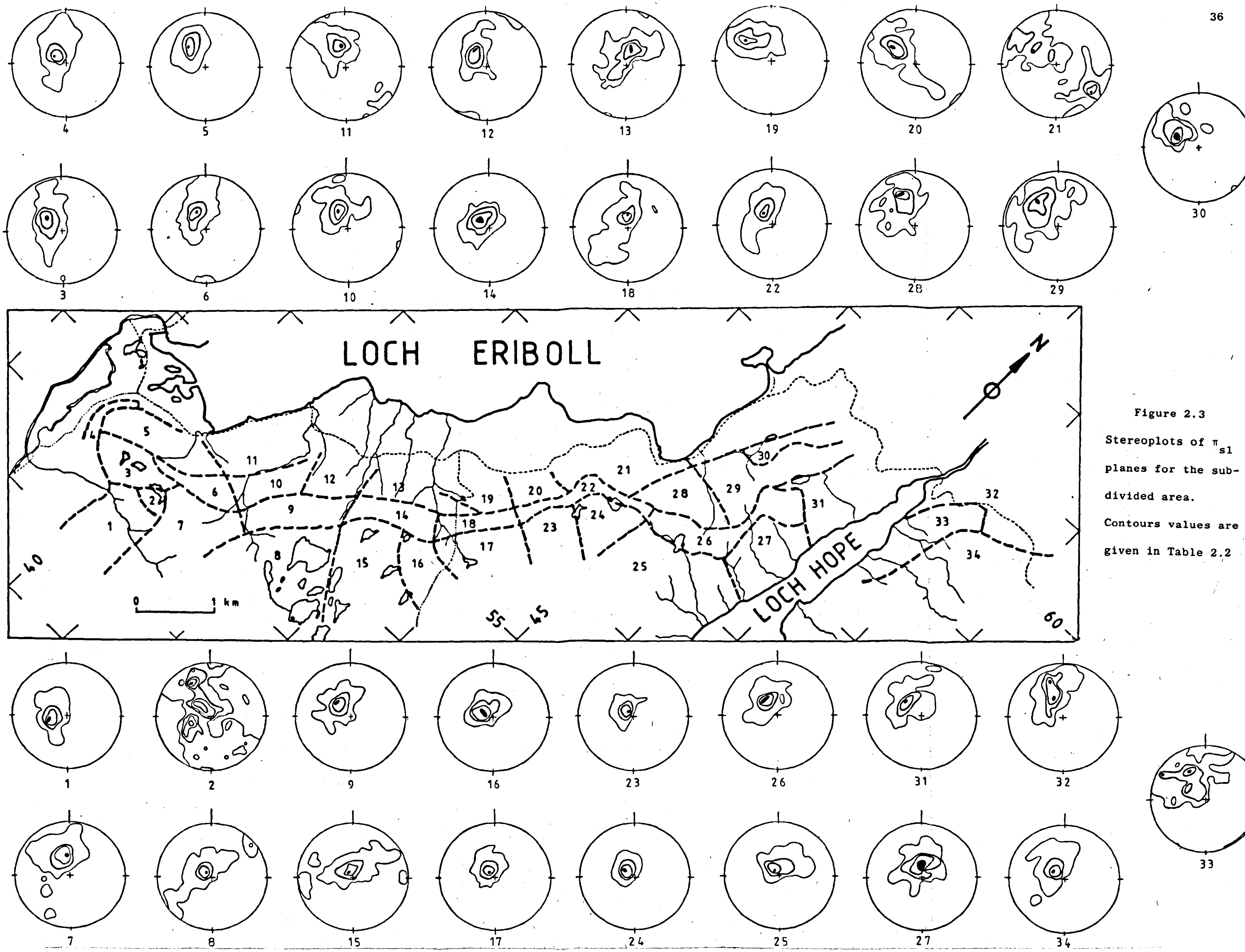

Figure 2.3 Stereoplots of π_{s1} planes for the subdivided area. Contours values are given in Table 2.2

detail and one can readily see from fig. 2-4 that the geometry of the S-planes is in fact composed of two fabrics with higher symmetry. It seems clear that the π-diagram in area 2 is made of two cross girdles that interfere, and this follows from the geometry of the folds which form Lunate shapes (ie Curvilinear-Hinges, see Turner and Weiss 1963, p.107) as illustrated in figure 2-4.

There are some localities which show less homogeneity in their π-fabrics (S_A-structures) and these include the contiguous zones 28 and 29 which constitute the domain of the so called 'undeformed' Lewisian block. Sub-areas 32 and 33 are from zones where deformation was inhomogeneous and perhaps a pattern of higher symmetry could be found by further subdivision in those sub-areas.

In general the homogeneity of π-fabric may be connected with a long history of strong and persistent deformation. Therefore if a certain fabric in an area does not exhibit a well defined high symmetry or constancy in direction except where it is refolded, such a domain may be interpreted as having suffered less deformation.

Zones showing fabrics of highest symmetry are those of sub-areas nos. 17, 23, 24, 25 and 27. In general there is a strong axial (sometimes tending to orthorhombic) maximum plunging steeply towards the NW which means that the planes dip gently towards the SW. The area represented by these diagrams corresponds exactly to the domain of the Moinian rocks. These rocks also show in the field that they are highly deformed and exhibit a strong effect of mylonitization.

A gradual change occurs towards the south, where in sub-areas 16, 15 and 8 there is a pattern of southward plunging folds. This is clearly reflected by the π-girdles (see in fig. 2-3, the diagrams for sub-areas 15 and 8). This change in fabric orientation, in sub-areas 16, 15 and 8, coincides with the greatest change in the apparent

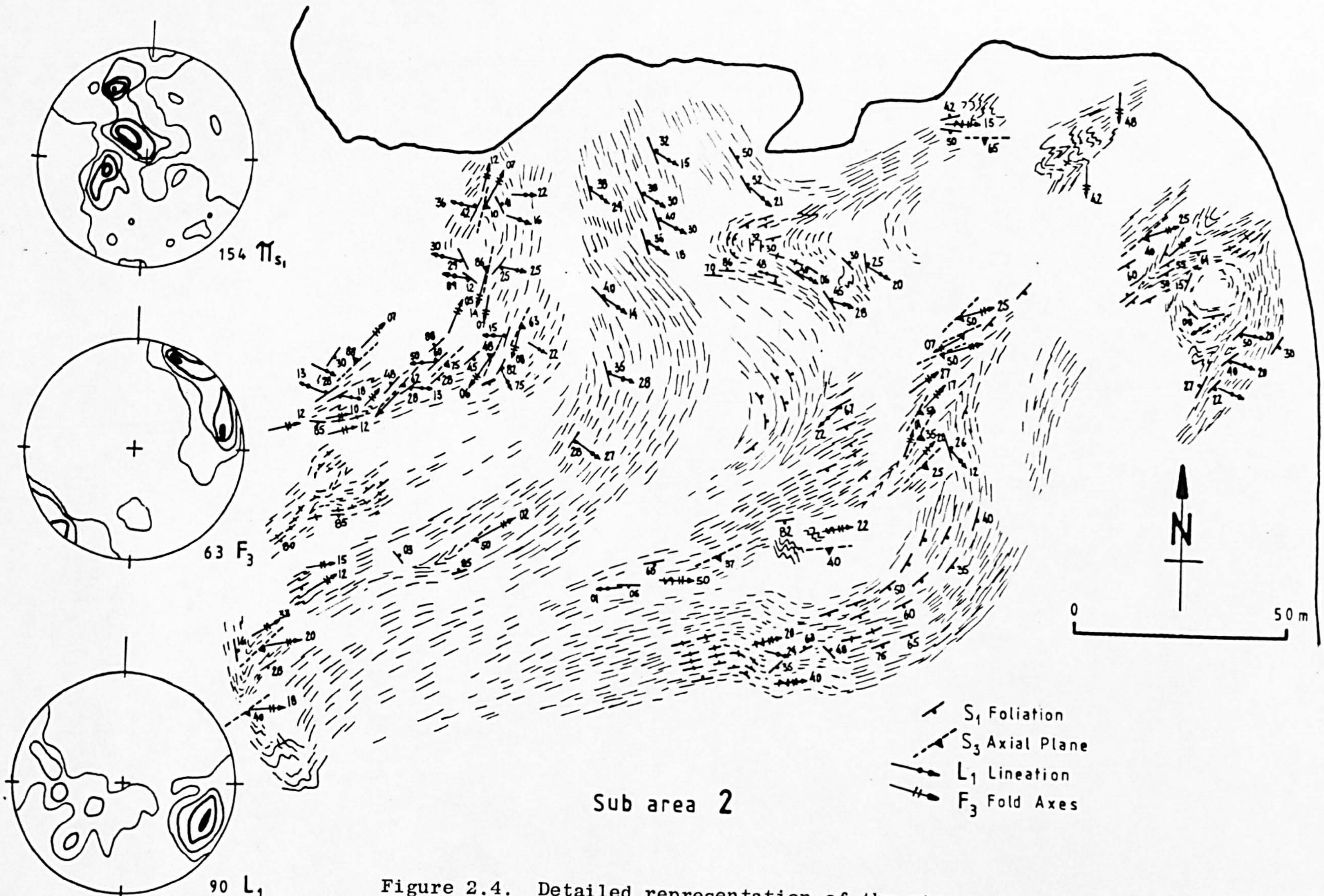

Figure 2.4. Detailed representation of the structures in sub-area 2.

width (hence thickness) of the underlying mylonitic zone, which was fairly constant in width, beneath sub-areas 17, 23, 24, 25 and 27.

Sub-areas 19, 20 and 21 are part of a large domain in which the stereoplots show a π-pole girdle striking WNW-ESE in which the β-axis coincides with the mesoscopic F_3-fold axes mapped in the field. Those 3 sub-areas are part of the An-t-Sron syncline which is illustrated in the cross-section EE' of fig. 2-20-e.

South of this area the stereoplots comprise domains of dominantly Lewisian mylonites which are characterized by the presence of folds in the meso and macro-scales. In sub-areas 13 and 14, no major fold-structure was recognised but in sub-areas 12, 9, 10 and 11 there is a substantial increase in the population of F_3-folds and this is reflected by the formation of π-girdles in which their β-axes roughly coincide with F_3-maxima (see figs. 2-3 and 2-7). However, areas 6 and 3 lie across a large overturned, S-shaped fold which plunges towards the East. This field observation is reflected in the stereoplot which show a girdle whose β-axis plunges to the East and is coincident with the maxima of the measured F_3-structures (fig. 2-7). The influence of this folding is also reflected in adjacent sub-areas 5 and 7 which show incomplete π-girdles but exhibit consistent F_3-maxima (fig. 2-7).

Sub-area 4 lies in a zone of Paleozoic rocks situated between two lower thrusts and field observations show this to constitute a huge overturned fold structure. The π-diagram from sub-area 4 gives an axis concordant with the axis direction of the fold in sub-areas 3 and 6. However the statistical maximum for its F_3-hinges does not coincide with the π-pole of the girdle formed by the S-poles in this diagram.

The structural maps of figs. 2-2 contain most of the planar structures described in this section. Other planar fabrics such as the axial planes of the different fold phases measured in the field, are not represented by stereoplots but these were plotted on the structural maps of figs. 2-2.

2.3.3-b The Main Domains of Linear Structures

Among all linear fabrics, L_1 is perhaps the most impressive because of its remarkably constant trend towards the ESE and occurrence practically in every rock type. There may be more than one generation or type of linear structures with this consistently parallel attitude towards the ESE direction (or WNW in case of folding). These may include; (i) striae given by the parallel disposition of minerals in the more quartzitic members. In the essentially pelitic rock types, such as the Oystershell rocks, such lineations are well developed in the so called 'oysters' and consist of very fine parallel lines given by different white shading in the 'milky-quartz' domains. (ii) Striae given by minute corrugations in the silky surface of psammites richer in micaceous minerals. (iii) The re-orientation and alignment of hornblende and augen or feldspar. (iv) The existence of flattened quartz rods (elongated parallel to the striations see plate 2-7) in a more pelitic matrix. This is characteristic of certain domains of the Moinian rocks.

Subsequent to the L_1 forming event there followed two phases of ductile deformation which superimpose and distort the previous structures. These two phases are termed F_2 and F_3. F_2 was observed to show an acute angle to L_1 while F_3 exhibited a more varied pattern of orientations relative to the early lineation.

The last folding phase (F_4) developed structures characterised

Plate 2.7. Flattened quartz-rods parallel to the L_1-lineation. Psammitic rocks of the Moinain sequence in Loch Hope area.

Plate 2.8. L_1-lineation folded obliquely to an F_3-fold axis. Moinian psammites in the Loch Eriboll area.

by sharp and straight hinges. These formed at an acute angle to the ESE lineation direction (L_1). This phase is clearly distinct from the previously described phases for the reasons to be explained later.

2.3.3-b.1 The Geometry of the L_1-Lineation

The stereoplots of nearly 1400 such linear structures, having a markedly persistent trend towards the ESE, are displayed in fig. 2-5. This shows the same sub-area division as for the S-planes and it can be seen that these diagrams tend to exhibit symmetries which in general also vary from axial to nearly monoclinic. The orientation of the maxima and their more closely associated contours are, without exceptions, to the ESE generally with gentle angles of plunge.

In some stereoplots the lineations tend to describe a girdle in direct analogy to the effects of lineations being subjected to folding (see plate 2-8). There are some diagrams which give girdles apparently close to great circles (see in fig. 2-5 the stereoplots for sub-areas 33, 17, 8, 7, 2, 6, 10 and 3). The poles to the great circles plunge up to 30^o, both to the NNE and SSE directions.

It must be pointed out that individually these folded lineations might not be contained in a plane, but collectively their diagrams can give an indication that they might be pertinent to a 'best fit' plane. These great circle girdles pass through the regional L_1 maximum to the ESE.

2.3.3-b.2 The Early Folds (F_2)

The collective display of nearly 400 F_2-fold axes are shown in the stereoplots of fig. 2-6. These folds have their hinges trending well within the SE quadrant and their angles of plunge are generally gentle. In general they form isoclinal structures with

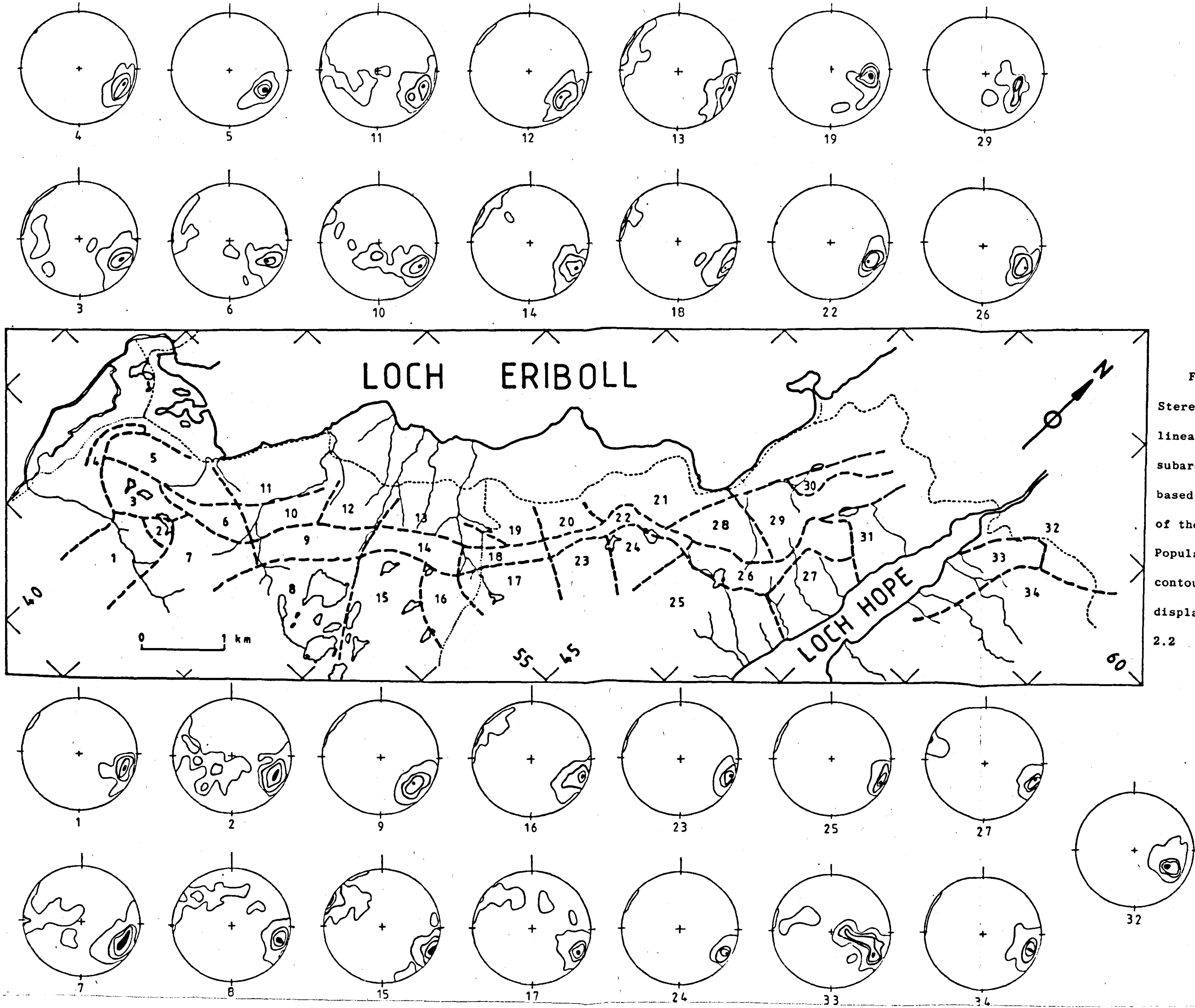

Figure 2.5

Stereoplots of L_1 lineations for a subarea division based on the pattern of the π_s-diagrams. Population size and contour values are displayed in Table 2.2

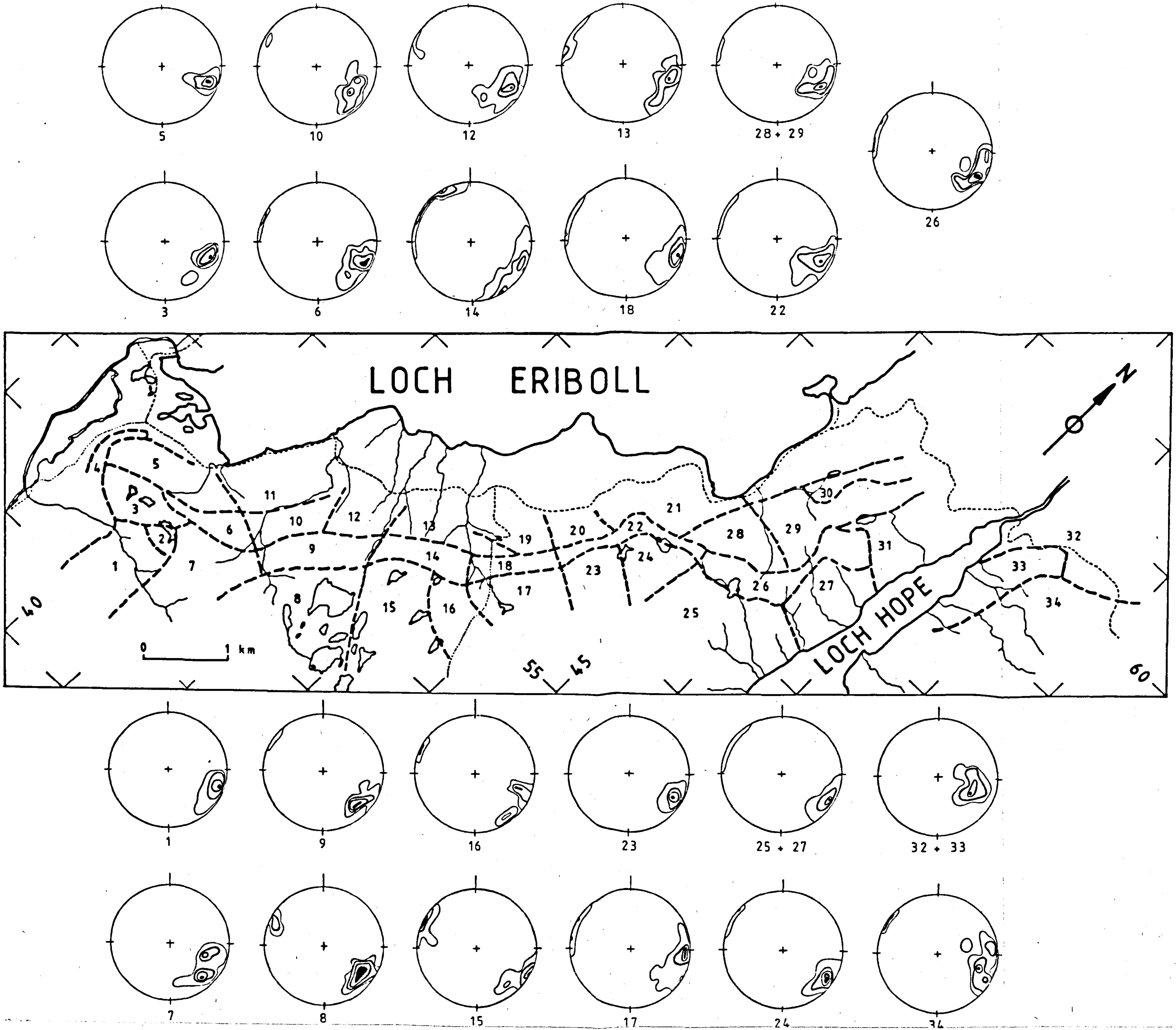

Figure 2.6

Stereoplots of the F_2 fold axes. Subarea division, as in Figure 2.3 Population size and contour values are listed in Table 2.2

axial planes subparallel to the dominant foliation. They occur not only in the domains of the mylonitic Lewisian rocks but also well within the Moine psammites.

It must be pointed out that not only the distribution of the F_2-folds is rather irregular but also their population is more restricted, when compared with the subsequent fold phase. The local scarcity of these structures in some of the heavily mylonitized zones is not just due to their possible destruction by effects of intense deformation as they are also absent in some less deformed zones. It is also important to notice that the F_2-folds occur throughout the whole area and are not confined to a particular nappe.

Another important point is that the F_2-folds both in the Lewisian mylonites and the overlying Moines share the same relationship with the early lineation L_1 and the subsequent folding F_3. It is not clear whether the F_2-folds are a result of a single phase.

2.3.3-b.3 The Second Folds (F_3)

The subsequent ductile phase of deformation produced folds (F_3) that clearly overprint and distort the F_2-structures. The pattern of preferred orientation of F_3-hinges is variable with gentle plunges to the NE and SW but also to the SSE. The axial planes of the F_3-folds are more oblique to the foliation planes. From their asymmetry, the structures show a clear vergence towards the WNW. The F_3-folds bend the mylonitic folation and in general they tend to form at high angles to the mineral lineation (L_1), but there are domains where that angle is considerably reduced.

The F_3-structures occur literally in all the nappes and lithologies met in the mapped area. Contrarily to the precedent F_2-folding phase the F_3-population is numerous and homogeneous in distribution and frequency (see structural maps of figs. 2-2). In general the F_3-folds are well developed where the foliation is well defined, either in the domain of the mylonitic rocks or in the Paleozoic rocks.

Most of the F_3-structures are ductilely folded surfaces but there are some examples where the layers can show some brittle deformation.

The wavelength of the F_3-folds range from a few centimetres to several tens of metres. As reported previously, sub-areas 3 and 6 comprise one such huge folded structure (see plate 2.9) and away from the Lewisian mylonites (sub-area 8) it is possible to follow the limb of an overturned F_3-fold for more than 100 metres. These larger F_3-structures are characteristically S-shaped (sub-areas 3 and 6) when plunging towards the NE direction or Z-shaped (sub-area 8), if plunging to the SE.

The style of the F_3-folds also differs from that of F_2, in that they are less tight, generally overturned, asymmetric and with straight limbs and sharp hinges. The F_3-axial cleavage is generally poor developed so it is easy to distinguish it from the mylonite banding. However the Oystershell rock exhibits a crenulation cleavage which dates from the F_3-phase.

Figure 2-7 displays 25 stereoplots which give the orientations of nearly 1200 F_3 axes for the whole mapped area.

2.3.3-b.4 The Third Set of Folds (F_4)

The last group of structures (F_4) which overprint the earlier two sets, comprise folds with a completely different style. The folds show sharp and straight hinges and straight planar limbs.

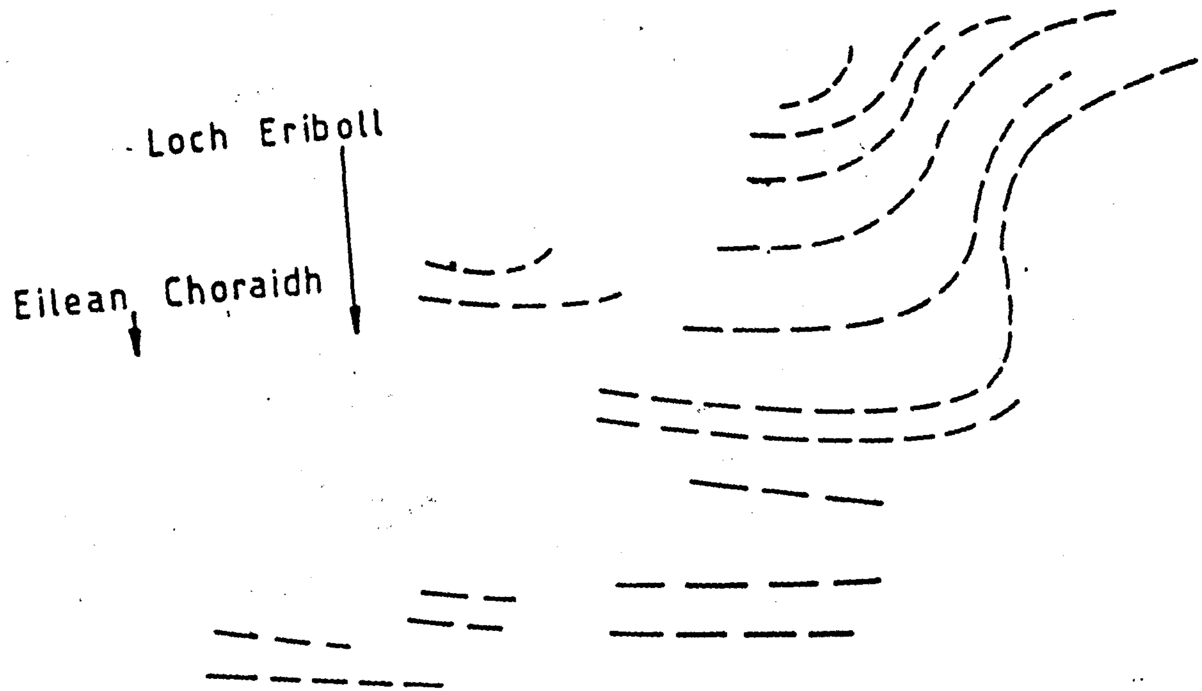
Loch Eriboll
Eilean Choraidh

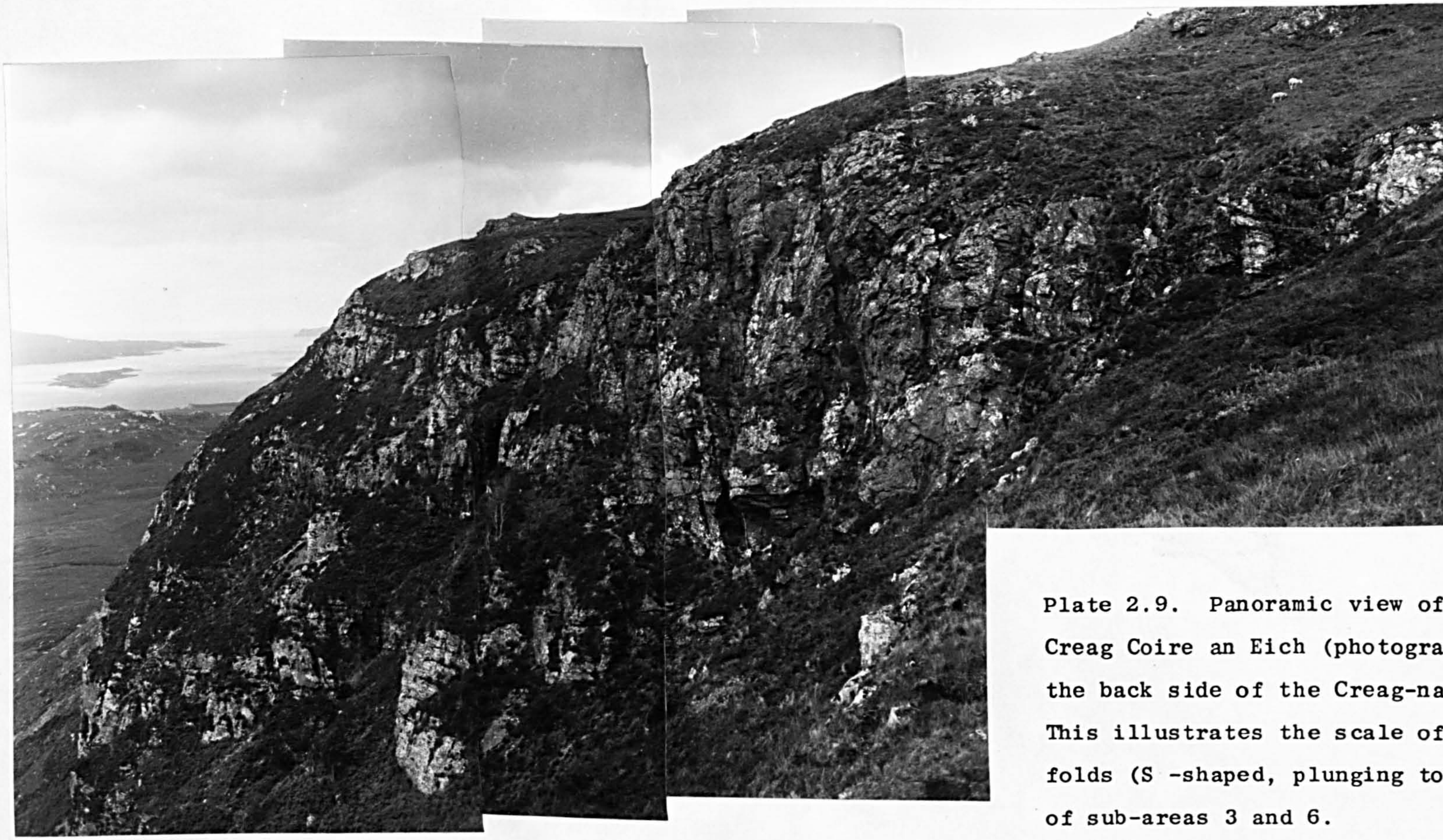

Plate 2.9. Panoramic view of the Creag Coire an Eich (photographed from the back side of the Creag-na-Faollinn). This illustrates the scale of the F_3-folds (S -shaped, plunging towards NNE) of sub-areas 3 and 6.

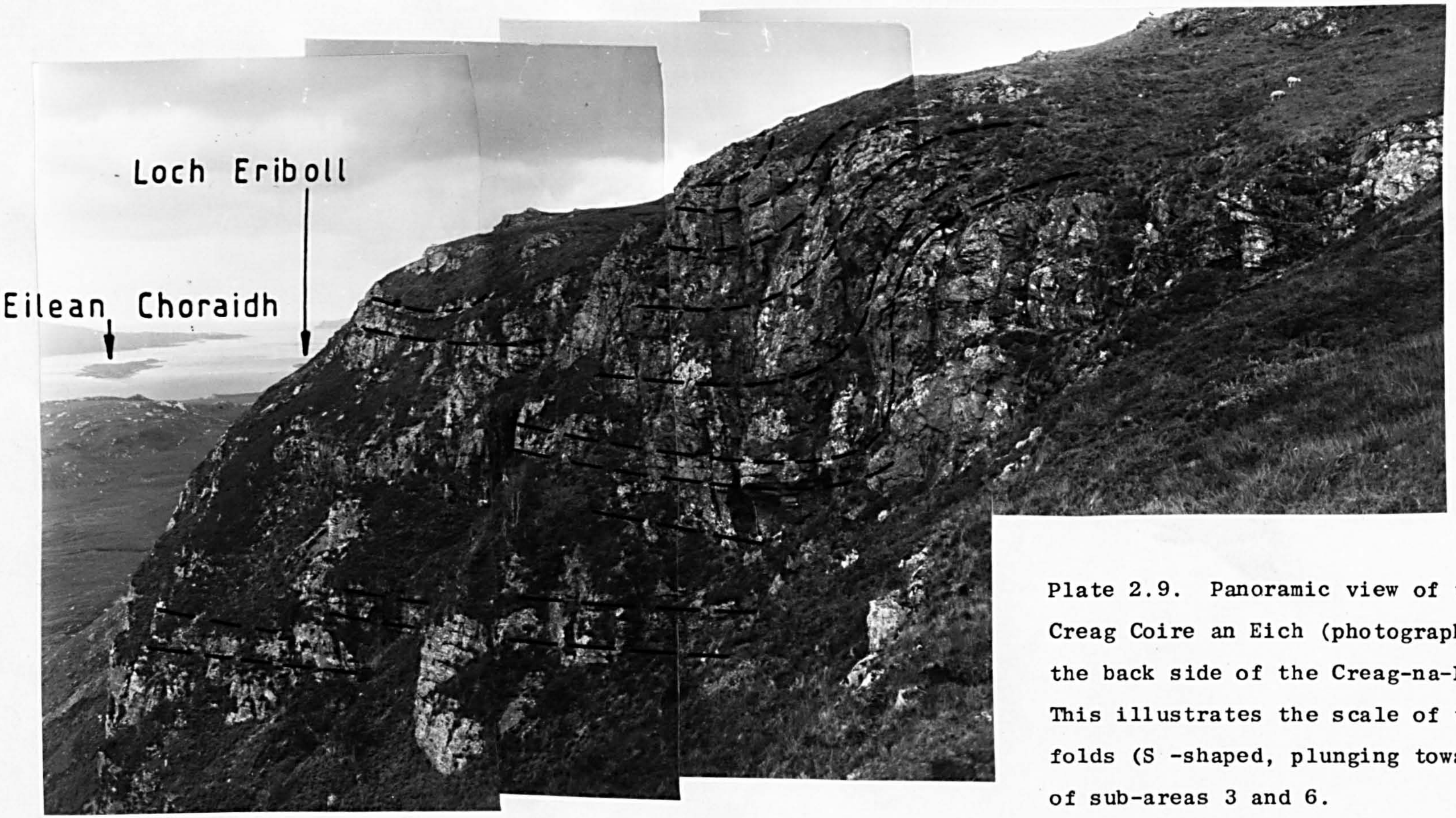

Plate 2.9. Panoramic view of the Creag Coire an Eich (photographed from the back side of the Creag-na-Faollinn). This illustrates the scale of the F_3-folds (S -shaped, plunging towards NNE) of sub-areas 3 and 6.

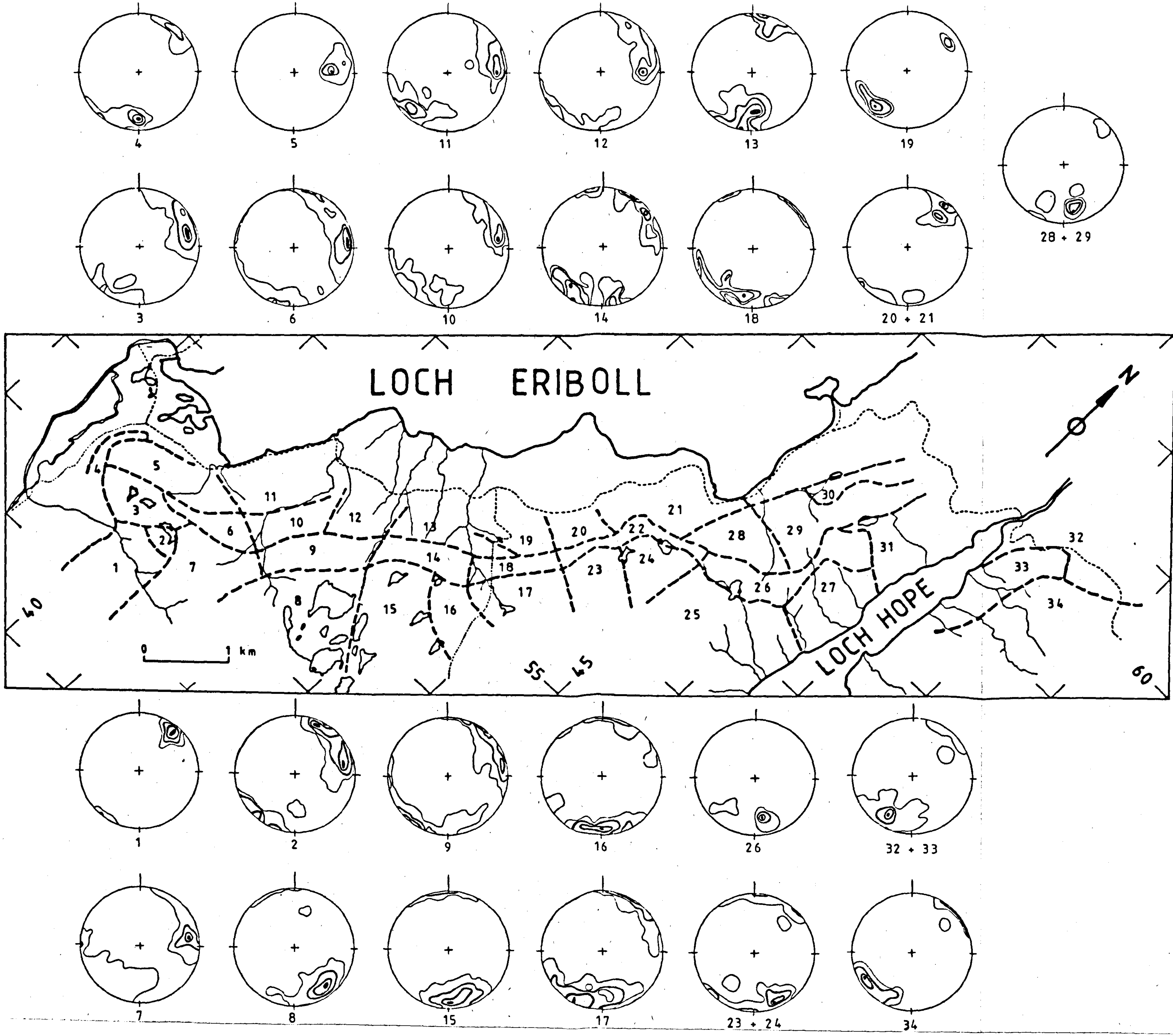

Figure 2.7
Stereoplots of F_3 fold axes orientations. Sub-area division based on the S-fabrics of Figure 2.3 Population size and contours are displayed in Table 2.2

Table 2.2

Note: The figures for contours refer to percentages per one percent of the stereonet area.

Sub area	Pop	πs_1-contours	Pop	L_1-contours	Pop	F_2-contours	Pop	F_3-contours
1	60	1-9-17-25	21	1-12.3-23.6-35	10	1-12.6-24.3-36	10	1-15.6-30.3-45
2	154	.4-1.8-3.2-4.6-6	90	1-3.5-6.5-8.5			63	1-4-7-10
3	219	1-6.3-11.6-17	81	1-7.3-13.6-20	10	1-3.6-26.3-39	67	1-6-11-16
4	150	.5-8.5-16.5-24.5	22	1-10.6-20.3-30			26	1-9-17-25
5	165	.5-10.3-20.1-30	28	1-16-31-46	10	1-16-31-46	20	1-21-41-61
6	221	1-6.3-11.7	64	1-10.3-19.6-29	20	1-8.7-16.3-24	99	1-5-9-13
7	137	1-5.3-9.6-14	76	1-4.3-7.6-11	23	1-23-19-25	93	1-4.6-8.3-12
8	61	1-10-19-28	60	1-11-21-31	9	1-8-15-22	84	1-10-19-28
9	118	1-9-17-25	89	1-7-14-21	9	1-14-27-40	91	1-4-8-12
10	107	1-8-15-22	55	1-7-14-21	19	1-10-19-29	103	1-5-9-13
11	156	1-7-13-19	45	1-6-11-16			68	1-5-9-13
12	92	1-9-18-27	61	1-9-18-27	33	1-10-19-28	57	1-7-13-19
13	105	1-5-9-13	51	1-7-13-19	26	1-8-15-22	29	1-5-9-13
14	100	1-7-13-19	65	1-9-17-25	31	1-8-15-22	31	1-4-8-12
15	137	1-6-11-16	107	1-8-15-22	19	1-14-27-40	131	1-6-12-18
16	46	1-7-14-21	44	1-10-19-28	5	1-20-40	26	1-8-15-22
17	106	1-13-25-37	111	.5-12-24-36	22	1-12-24-36	96	1-4-7-10
18	93	1-10-19-28	45	1-13-25-37	35	1-10-19-28	10	1-10-19

Table 2.2 (continued)

Sub area	Pop	πs_1-contours	Pop	L_1-contours	Pop	F_2-contours	Pop	F_3-contours
19	74	1-4-14-21	15	1-11-20-29			7	1-10-19-28
20	80	.5-5.5-10.5-15.5					12	1-11.6-22.3-33
21	102	.5-3,5-6.5-9.5						
22	60	1-10.6-20.3-30	25	1-13-6-23-6-39	27	1-8-15-22		
23	45	1-16-31-46	32	1-15-29-43	10	1-16-31-46	22	1-8-15-22
24	50	1-15-29-43	30	1-22-43-64	20	1-12-23-34		
25	71	1-9-17-25	28	1-17-33-49	17	1-16-31-46		
26	70	1-10-21-32	25	1-10-21-32	10	1-9.3-18.3-28	7	1-14.6-28.3-42
27	61	1-6-11-16	40	1-12-23-34				
28	50	1-5.5-10.5-15			11	1-9.6-18.3-27	10	1-10.3-19.6-29
29	141	.5-4.3-8.1-12	10	1-13.6-16.3-29				
30	25	1-17-13-19						
31	42	1-8.3-15.6-23						
32	80	.5-5.3-10.1-15	30	1-11.3-21.6-32	18	1-9.6-18.3-27	35	1-9-17-25
33	83	1-4.7-8.4-12.2	35	1-6-11-16				
34	95	.5-10.3-20.1-30	57	1-12.1-23.3-34.5	19	1-9.3-17.6-26	18	1-9.6-18.3-27

They invariably show very steep axial planes and exhibit a constant hinge direction which is nearly parallel to the L_1 direction.

The distribution of F_4-folds is more irregular than for any other of the previously described types. The F_4-structures are confined to rocks which develop very finely spaced foliation planes, forming types which range from kink bands to chevron folds.

There are no collective diagrams for this kind of structure, but they are illustrated in the structural maps of figs. 2-2.

2.3.3-c Comments

It is thought that the lack of identifiable mesostructures earlier than S_1 or L_1, in the mylonitic domains, is due to the fact that any such structures have been re-oriented during the Caledonian period of deformation. There is some evidence for the existence of primary structures not only in the Paleozoic rocks beneath the lower thrust of Creagan Road (plate 2-4), but also in the Moinian sequence (sub-area 15), however these features proved to be rare within the limits of the mapped area. The scarcity of these primary structures in the Moinian rocks could well attest the intensity of deformation. Barber and Soper (1973) report primary structures in the Moinian sequence but these were found (outside the present area of mapping) in a domain located further away from the mylonitic zones.

As reported earlier, sub-areas 28 and 29 constitutes domains of relatively less intensely Caledonized fabrics. Although there is a tendency for triclinicity of fabric in these areas, the foliation has attitudes similar to that in the neighbouring zones of strongly deformed fabrics.

Major and minor folds belonging to the first two generations (F_2 and F_3) tend to develop axial planes at low angles to the horizontal.

The tightness, reclined to recumbent character of these early F_2-folds are characteristic features not only in the mylonite zone but also away from them (sub-area 15 can provide good examples). The resultant attitude of the folds may be interpreted as being due to the rotation of the planar structures under the effects of progressive deformation. This can be confirmed by making a comparison between the attitudes of the F_2-folds and the subsequent fold phases (F_3). The latter shows axial planes not so concordantly disposed relative the dominant foliation. It is interpreted here that the F_3-axial planes suffered less re-orientation (rotation). These facts are supported by an analysis of fold axis orientation (see Chapter 3).

Figures 2-8-a to c show plots of the maxima taken from each of the stereoplots in figures, 2-5, 2-6 and 2-7. It is important to observe the scattering of the lineations, according to their age:

(i) For L_1 (see fig. 2-8-a) there is a clustering around the $113^o/15^o$ direction. The range of trend of their maxima is a mere 30^o.

(ii) Figure 2-8-b contains the maxima for F_2-lineations and it can be seen that there is a confinement of these to the SE quadrant. In fact the range of their trends is precisely between directions 090^o and 150^o (ie approximately 60^o).

(iii) Figure 2-8-c gives a maxima of F_3-lineations and these can be grouped in three sets: the first plunging towards NE-SW, the second to S-SE and the third to the ENE direction.

The above trends confirm field evidences that L_1-lineations have a conspicuous and constant direction. It also suggests that the older the lineation the more clustered it appears around the ESE direction.

The scatter of F_3-axes was interpreted by Soper and

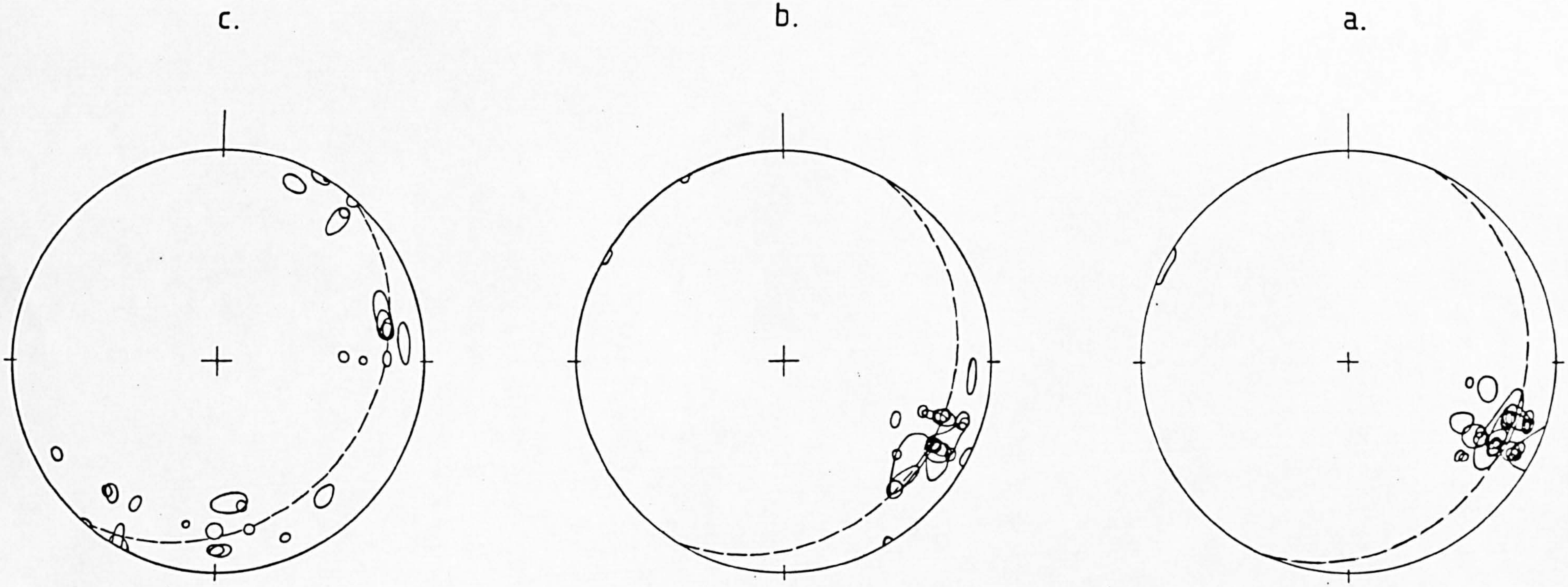

Figure 2.8. Synoptic diagrams, grouping only the strongly dominant maxima of the stereoplots for:

(a) L_1-fabrics,

(b) F_2-fold hinge directions and

(c) F_3-fold hinges. See text for explanation.

Wilkinson (1975, p.350) as being an original feature, due to the intersection of S_1 and S_3, the latter being at variable attitudes. However, the present study does not disregard the possibility of the F_3-phase being in fact a polyphase deformation event because: (i) as reported earlier the F_3-structures exhibit both the ductile and brittle characteristics. The deformation history of the Thrust Zone, in Eriboll, indicates that it evolved from an early ductile to a late brittle stage (this will be discussed later). (ii) the scatter of F_3-axes could well indicate a very long period of progressive deformation that would include spasmodic 'sub-phases'.

Also from fig. 2-8 it can be seen that the grouped maxima are contained on a plane which for L_1 dips 15^o to 115^o, while for F_2-axes the best fit plane dips at 20^o towards 120^o and the grouped maxima of F_3-hinges describe a girdle which dips at 25^o towards 130^o. Thus the picture of progressive rotation of fold axes towards the clustering direction of L_1 is corroborated by the fact that there is a progressive rotation of the best fit planes towards the attitude of the L_1 best fit plane. The girdle containing the lineations becomes shallower with age and increase in deformation intensity.

It is argued, in the next chapter that the above data agree with an interpretation of fold hinges having rotated under persistent strain to become arcuate or lunate-shaped, (forming curvilinear fold hinges), so that with intense deformation they direct their hinges towards the ESE direction.

2.3.4 Fold Geometry

2.3.4.1 General

The present section investigates the geometry of some of the mapped folds not in terms of their orientations or spatial location, as in the previous section, but instead using the elements seen in a profile section and applying the techniques of fold analysis developed by Hudleston (1973-a).

There are two important and distinct aspects of fold geometry: (i) that given by the trace line of a single surface and (ii) that given by the characteristics of a layer (or a sequence of layers) which comprise the domain bounded by two curvature lines, an 'inner' and an 'outer' form surfaces. The latter aspect contains elements that allow a fold classification using the inclination of the dip isogon lines (Ramsay 1967, pp.363-372), while the former can give quantitative information about fold shape.

The analysed folds (figs. 2-9 to 2-15) were drawn from photographs taken from F_2 and F_3-structures sampled both from the heavily and less mylonitized rocks in the area.

2.3.4.2 Fold Class

Dip isogons are defined as the lines joining points of equal slope on two adjacent trace surfaces (Elliott 1965). Ramsay (1967) classified folds according to the pattern formed by these lines; in Class 1 these are convergent downwards (in antiforms); in Class 2 the isogons are parallel, and in Class 3 they diverge downwards. The variation (or deviation) of these lines can give some information on how the layers interact or accommodate strains during folding or reflect fabric anisotropy, and yet to show variability in competency.

Parameters that can be used in conjunction with isogons are: (i) the ($t'\alpha$) orthogonal thickness (Ramsay 1967, p.359) or

Hudleston's (1973-a) parameter ($\phi\alpha$) which is defined as the angle between the dip (α) isogon and the normal to the tangent to the folded layer.

In the present study of folds, use was made of the graph relating $\phi\alpha$ vs α instead of $t'\alpha$ vs α because the former has the advantage (i) that it does not change its shape with the change in the dip reference line as in the case of the plot $t'\alpha$ vs α, and (ii) also it does not require the measurement of the length of a line, as the latter does. (iii) It presents the distinct advantage that the curves behave similarly to the first derivative $dt'_{\alpha}/d\alpha$, which make these curves very sensitive to geometric changes (see Hudleston 1973-a, pp.12-13). This is particularly convenient for the present folds.

Figures 2-9 to 2-14 illustrate the variations of the parameters for the F_3-folds not only in different lithological types but also within different zones of deformation. Figures 2-9-a and 2-10-a show F_3-folds from two different localities belonging to the Moine Psammites which overlie the Oystershell rocks. Being an essentially mechanically homogeneous rock, very little isogon deviations are to be expected as there should be no competence contrast (Gray 1979). However the observed isogons converge (Class 1) and diverge (Class 3) mainly due to difference in layer thickness which can cause competence differences possibly coupled with differences in layer properties due to grain size and of mica content. Whatever the reasons are, the above figures 2-9 and 2-10 also reveal that the folds thicken in the hinge areas and thin on the limbs. The $\phi\alpha$ vs α plots, also demonstrate that the curves are sometimes not smooth and these irregularities may be the result of (i) measurement bias or errors, (ii) to the nature of those parameters reputably very sensitive to slight changes in curvature. From these graphs $\phi\alpha$ vs α, the majority of isogon patterns plot

Figure 2.9. (a) Pattern of dip isogons for F_3-folds in Moinian Psammites.

(b) Diagram of $\phi\alpha$ vs α showing the different field classes.

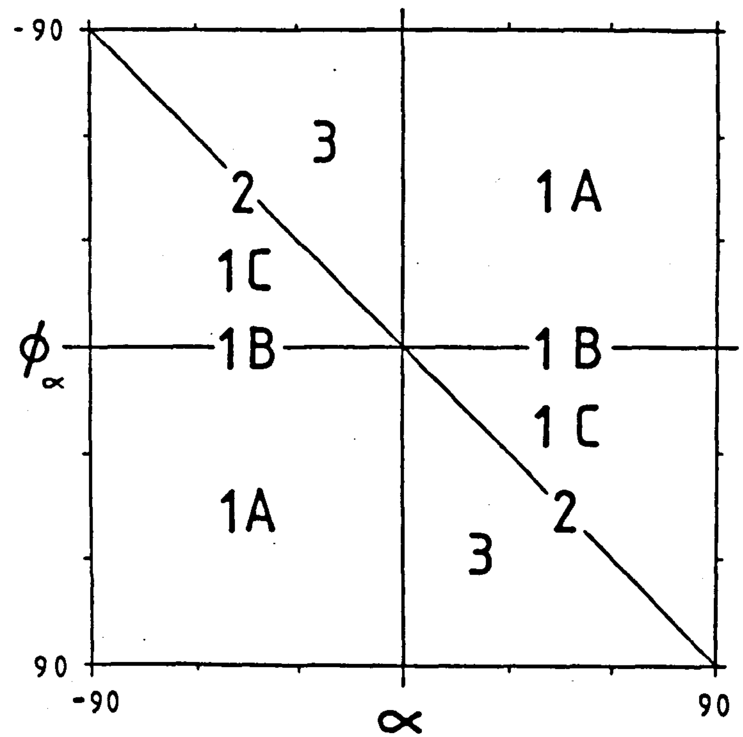

Figure 2.10. (a) Pattern of dip isogons for F_3-folds in the domain of Moinain Psammites.

(b) The obtained ϕ/α curves. See text for explanation.

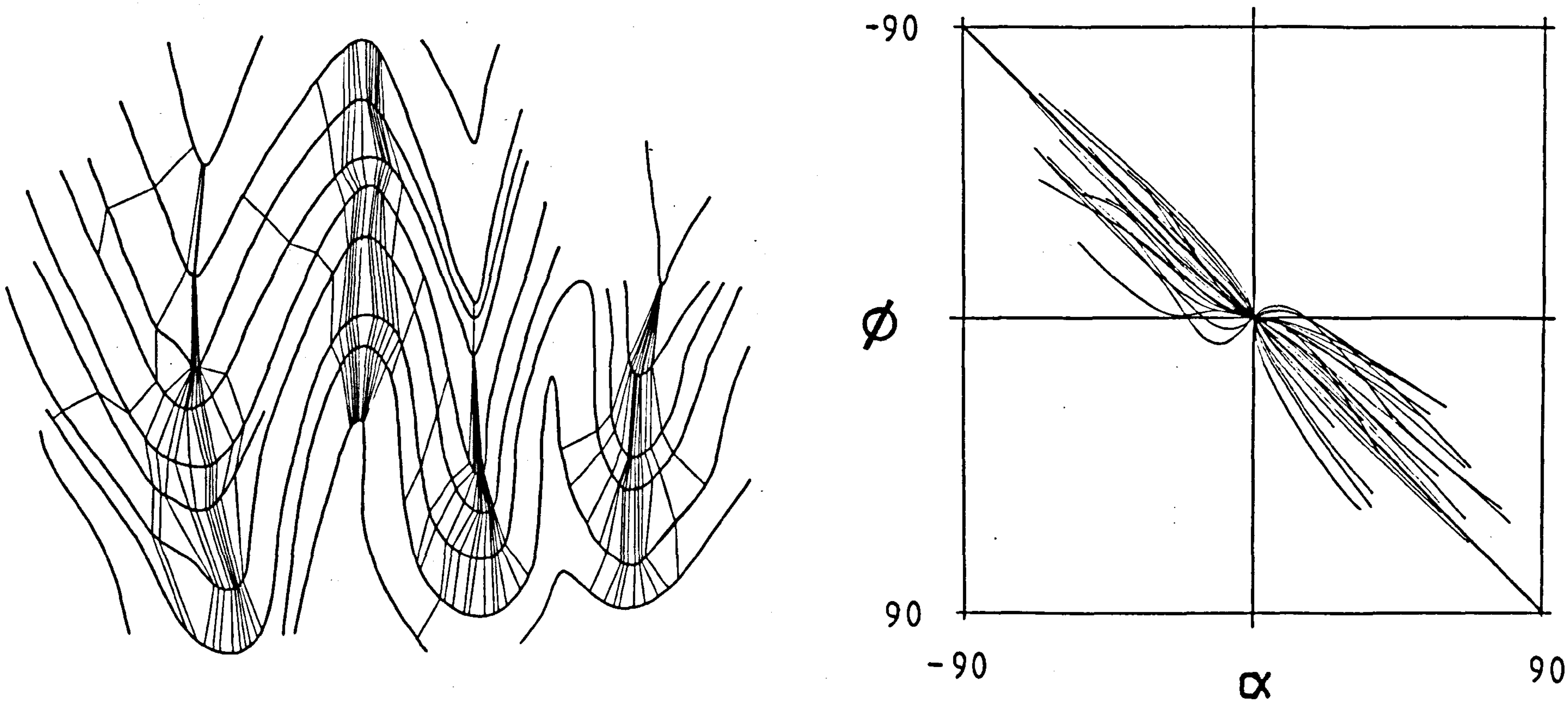

within the 1C field while some less competent layers with less rounded crests plot directly in the class 3 field, in general very near to the boundary line of class 2.

Figures 2-11 and 2-12 illustrate some of the isogon patterns for the F_3-folds in the domain of the Lewisian mylonites. For instance in 2-11-b the ϕ/α curves plot dominantly in the 1C field. Fold layers are characterised by more or less homogeneous layers that exhibit straight limbs and reasonably constant thickness. In the hinge regions the pattern varies from showing almost parallel isogon (inner layers) to those of Class 1C. Figure 2-12-a shows layers in a less tight fold and the corresponding $\phi\alpha$ vs α plot (fig. 2-12-b) exhibits a more irregular pattern which is due to irregularities in the curvature of the fold. Again, the dominant Class is 1C. The same pattern applies for figure 2.13 and its corresponding $\phi\alpha$ vs α plot (figure 2-13-b) which shows some Class 3 layers in the core of the fold.

Figure 2-14 comprises a sequence with different lithologic characters. The inner layers neither acquire the characteristics of thickened crests nor the almost cuspate forms of some previous examples. This is due to the presence of two layers which have a more quartz-feldspathic composition and this makes them contrastingly more competent than the surrounding pelitic members. The anisotropy is reflected by the isogon patterns and the position of the ϕ/α curves (figure 2-14-b) is ruled by differences in layer thickness and composition. There is a complete spectrum between fold Classes 1C, 2 and 3.

Figure 2-15 illustrates an F_2-fold from the psammitic layers of the Moinian sequence. The folds exhibit a distinctive tightness with proportionally longer limbs and thicker crests. The corresponding ϕ/α curves show the predominant 1C and 3 Classes with the

Figure 2.11. (a) Isogon patterns of F_3-folds affecting rocks of the Lewisian mylonites.

(b) The corresponding ϕ/α curves. See text for comments and explanations.

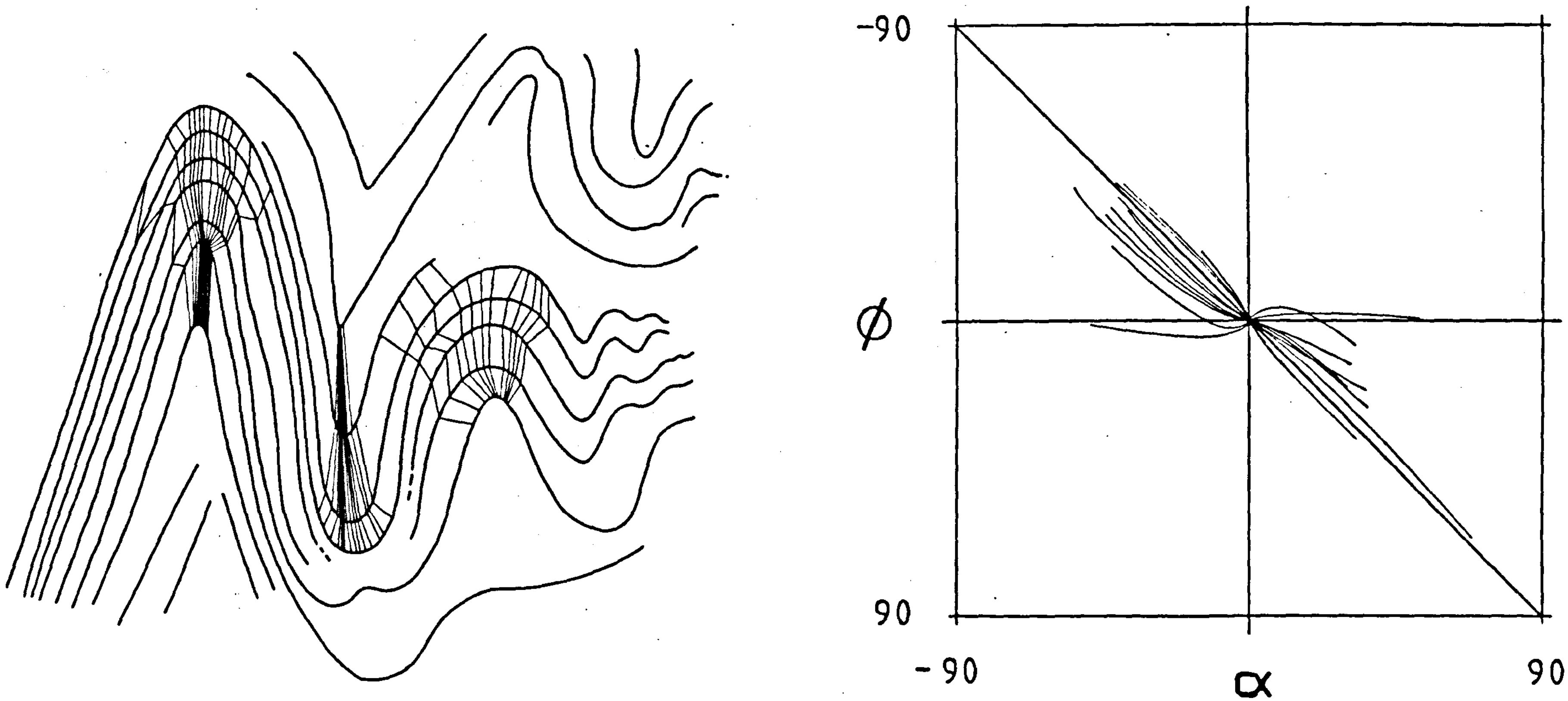

Figure 2.12. (a) Isogon patterns for F_3-folds in the Lewisian rocks.

(b) Refers to some of the corresponding ϕ/α curves. See text for details.

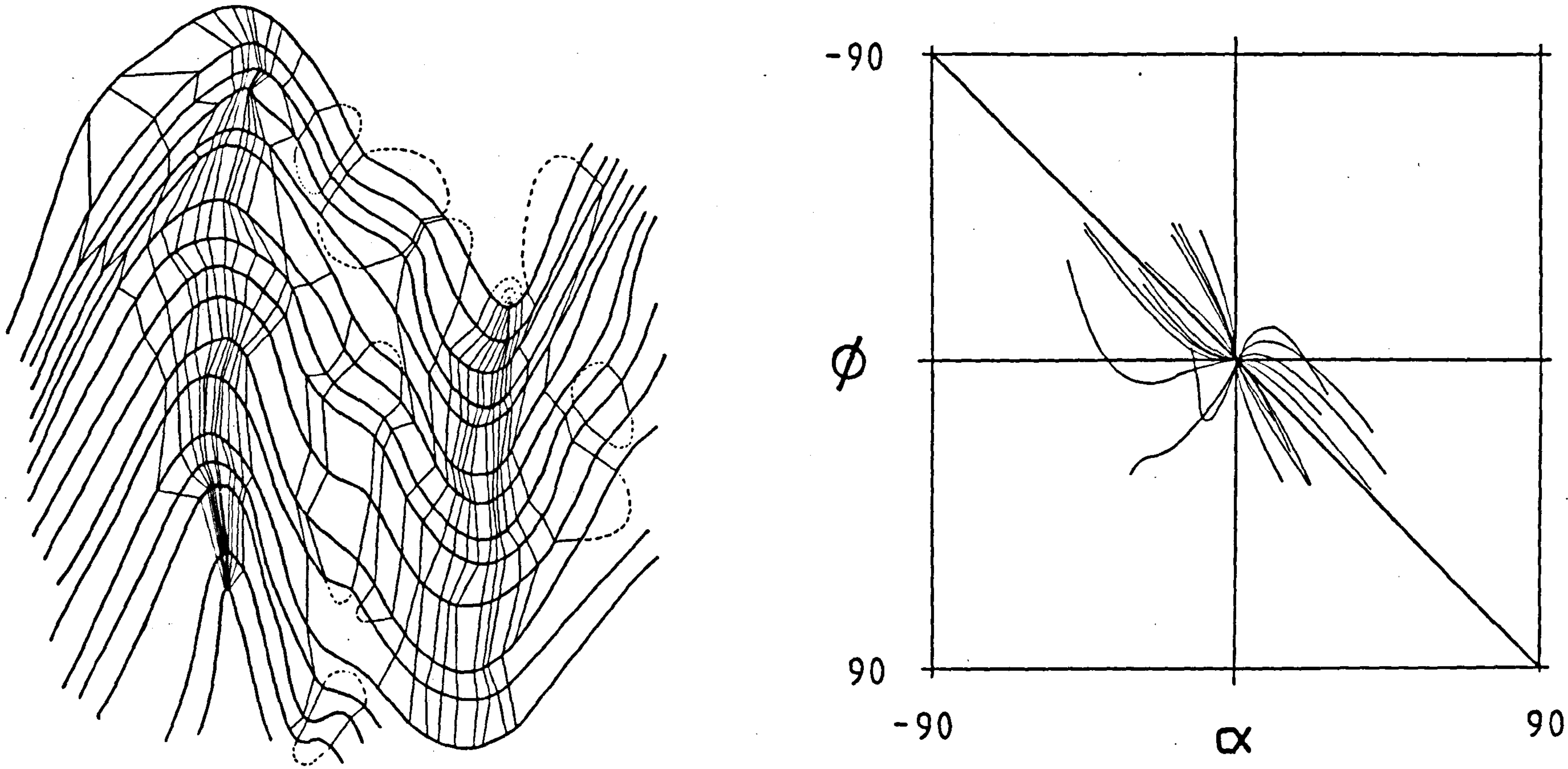

Figure 2.13. (a) Isogons of F_3-folds in the Lewisian mylonites.

(b) The corresponding ϕ/α curves. See explanation in text.

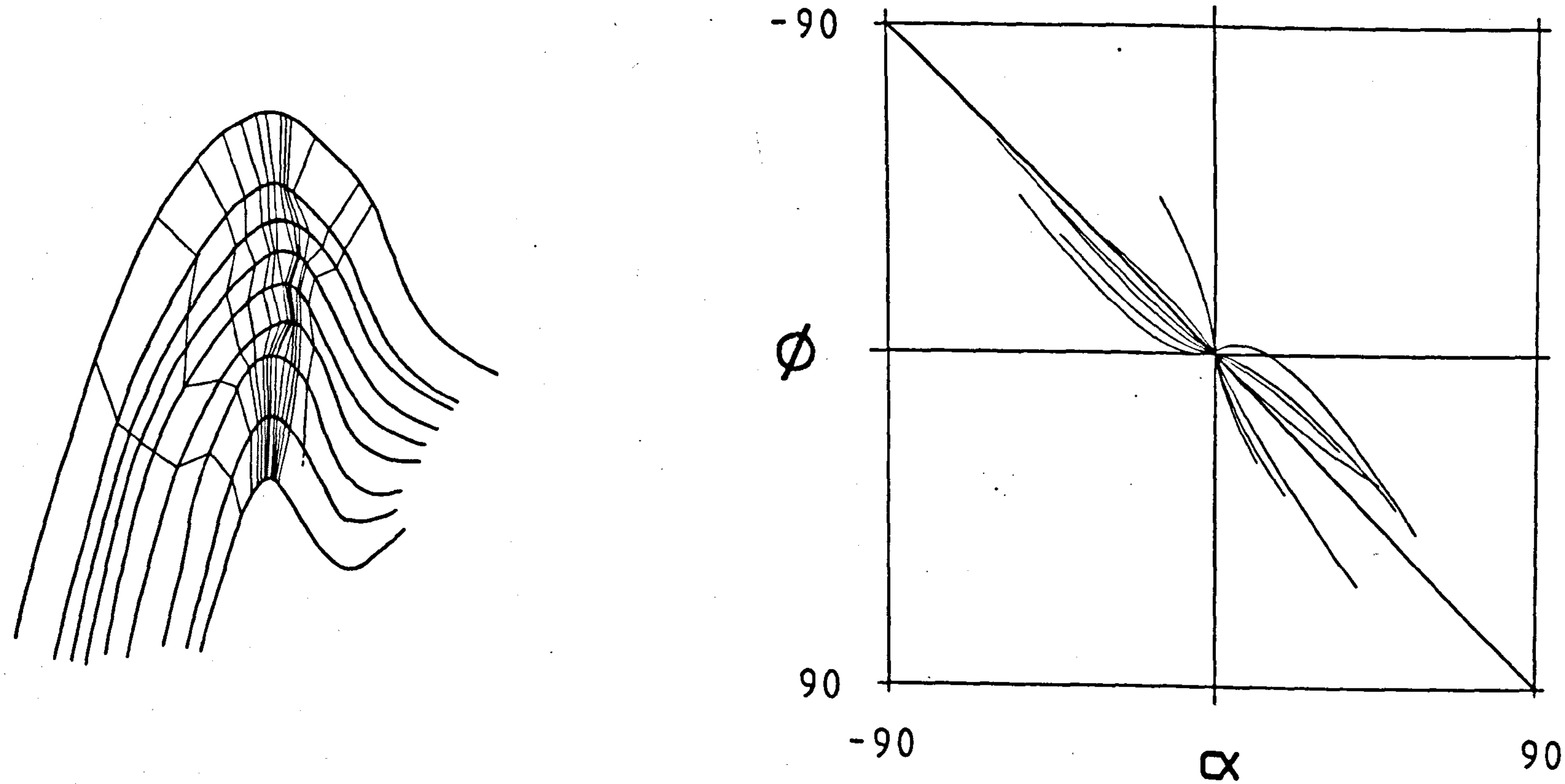

Figure 2.14. (a) Pattern of isogons for F_3-folds in mylonitic rocks of the Lewisian gneisses, Eriboll.

(b) The corresponding ϕ/α curves. See details in text.

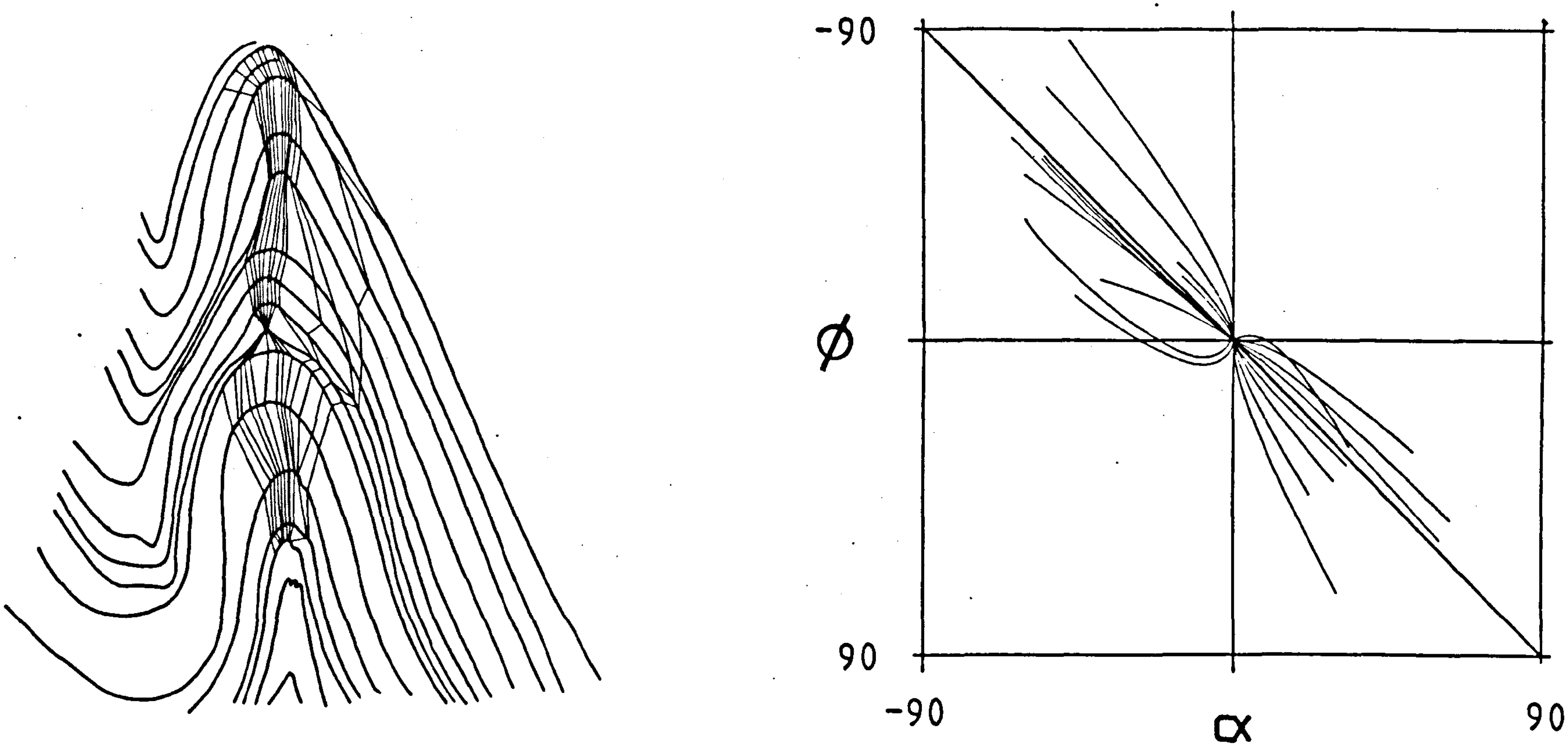

Figure 2.15. (a) Isogon pattern for F_2-fold in the psammitic layers of the Moinain sequence, Eriboll.

(b) The corresponding ϕ/α curves. See text for explanation.

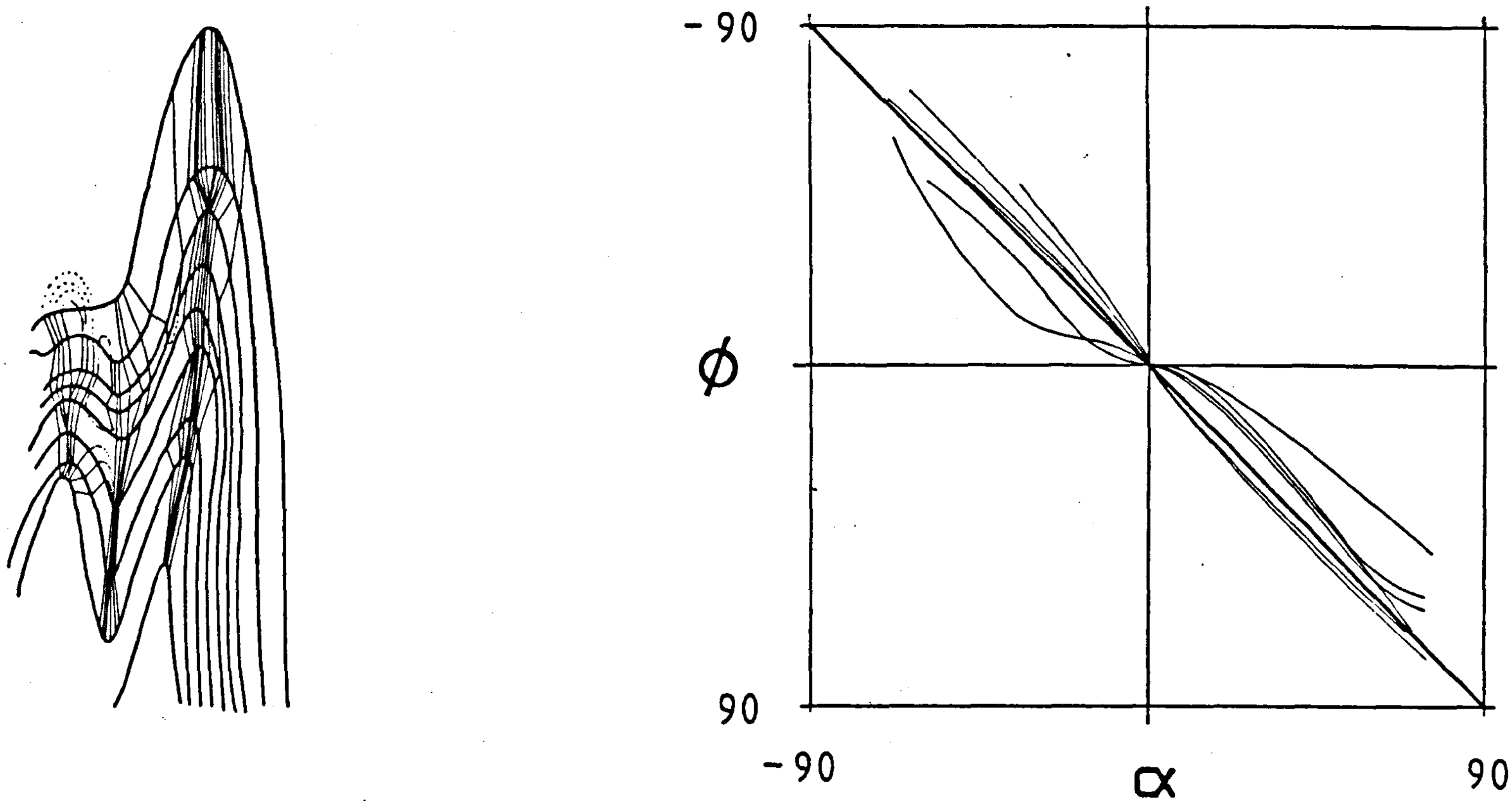

difference that in this example the curves are smoother and longer. This is due not only to the relative homogeneity in the layers but also to a higher degree of fold tightness.

2.3.4.3 Fold Shape

As stated earlier, fold shape can be quantitatively specified using the trace of the surface form in profile. The rates of change in inclination of these lines can be studied using the type of Fourier analysis proposed by Hudleston (1973-a). The method consists in dividing the folded surface in quarter wavelength segments and then fitting the Fourier function:

$$f(x) = 0.5a_o + \sum_{n=1}^{\infty} a_n \cos nx + \sum_{n=1}^{\infty} b_n \sin nx \qquad [2\text{-}1]$$

The above expression can be further simplified when all a constants, all cosine terms and even numbered sine terms are equal to zero (see Stabler 1968, p.345; Hudleston 1973-a, pp.18-19), so the shape of the curve can be obtained only in terms of the odd coefficients b_1, b_3, b_5 etc. Stabler (1968, p.346) points out that further simplification eliminates the high harmonics (greater or equal to 5) because in terms of a numerical contribution these become neglibible. Therefore, the shape of the form line can be fully defined in terms of b_1 and b_3.

Both Stabler (1968, p.345) and Hudleston (1973-a, p.19) preferred a quarter-wavelength unit ("W/4 unit"),as the former points out, this can avoid problems of asymmetry. The W/4 unit is obtained by establishing the Y-reference axis normal to the tangent line to the hinge and X as the normal to the Y-line passing through the inflexion point (see Hudleston 1973-a, pp.19-20). The coefficients b_1 and b_3 were obtained here using Hudleston's (1969) original programme which makes use of the IBM-subroutine FORIT for the summation of the Fourier series.

Figure 2-16 plots b_3 vs b_1 values of the analysed 78 units. These points tend to be constrained mainly along a relatively narrow strip bounded by $0.1 > b_3 > -0.1$ and b_1 up to 9.5. This undoubtedly defines a plot within the field of the sinusoidal type of waves.

Hudleston (1973-c) pointed out that b_1 values closely reflect the ratio amplitude/wavelength of fold tightness. Results for the first harmonic reveal that for F_2 and F_3-data the mean value is approximately 2.97, while for the b_3 coefficients, the mean is -0.011. A negative result in this second harmonic implies folds with sharp hinges and relatively straight limbs.

For F_2-folds, an average value for the b_1-coefficient is in the order of 5.1. This is nearly twice the corresponding average for the F_3-folds (where $b_1 \simeq 2.58$).

Figure 2-17 plots the b_3/b_1 ratio vs b_1 values. The parameter of the ordinates is very sensitive to changes in the fold shape. The mean b_3/b_1 ratio for the whole population is around -0.0028 while for F_2 folds this is approximately equal to -0.0002, which means that the F_2-folds tend to present more rounded hinges than the average.

The variances of the calculated b_3/b_1 ratios for both F_2 and the average fold are very close (4×10^{-4} and 6×10^{-4} respectively) which confirms that there is little to no change in type of fold shape. This can be seen in the b_3/b_1 vs b_1 plot, where the points are practically confined to a narrow strip bounded by ordinate values $\pm$ 0.5

Figure 2-18 used Hudleston's (1973-a) pictorial diagram for summarising and characterising the fold types found in the area. The

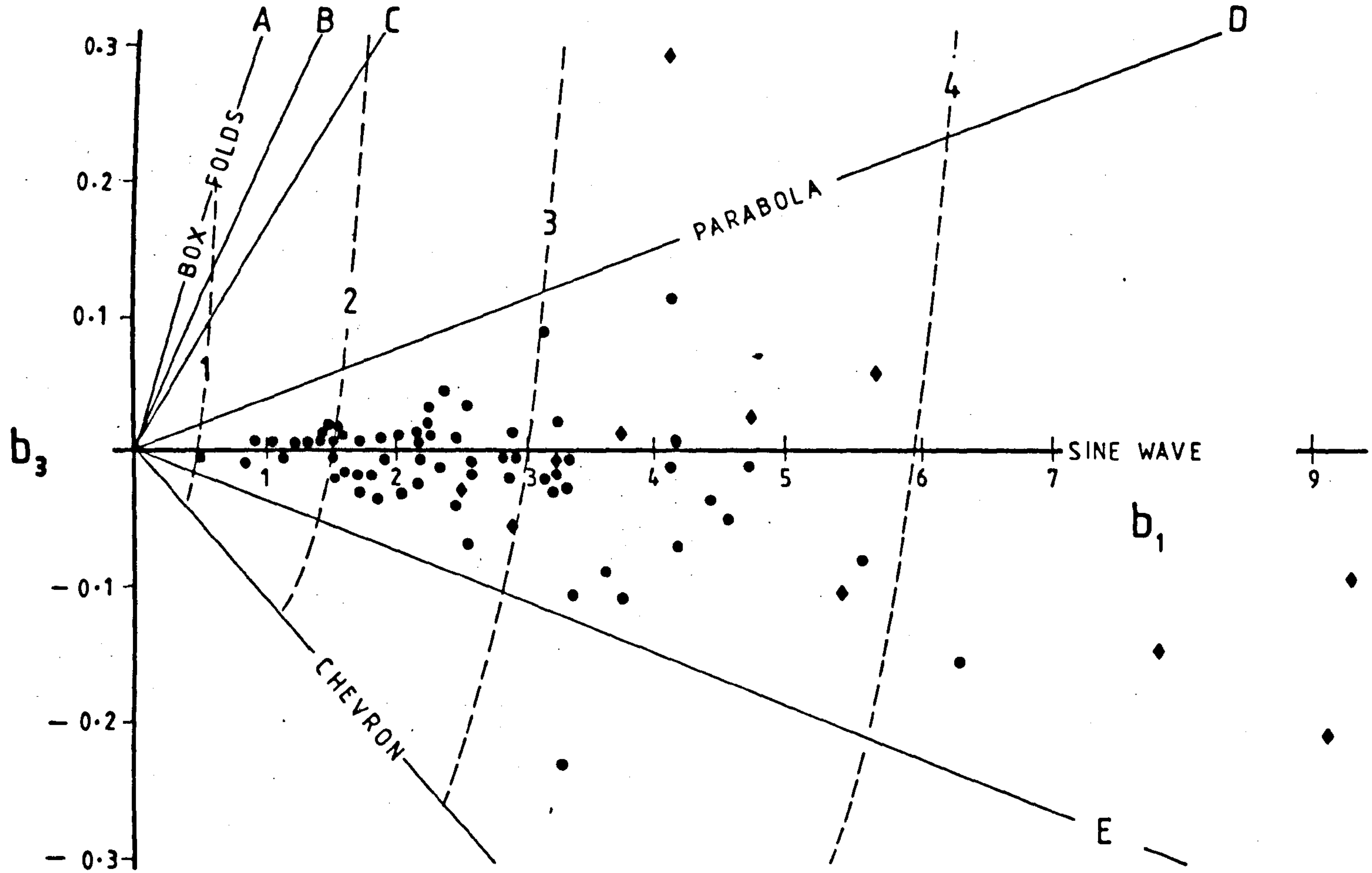

Figure 2.16. Plot of b_3 vs b_1 values of 78 units. Fold shapes tend to be confined to the sine wave type which presents different amplitudes. Circles refer to F_3-folds while 'diamonds' represent F_2-fold forms.

Figure 2.17. Diagram plotting (b_3/b_1) ratio vs b_1 values. Full circles correspond to F_3-folds while diamonds refer to F_2-folds. See text for explanation.

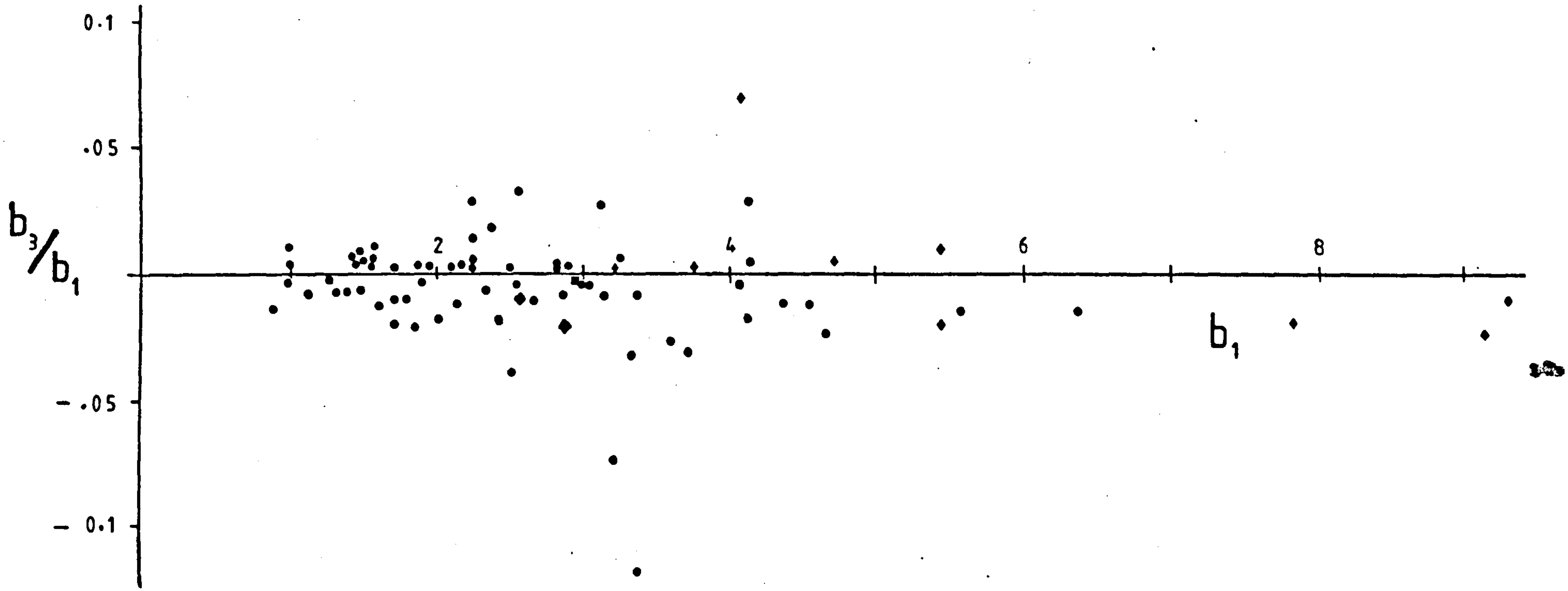

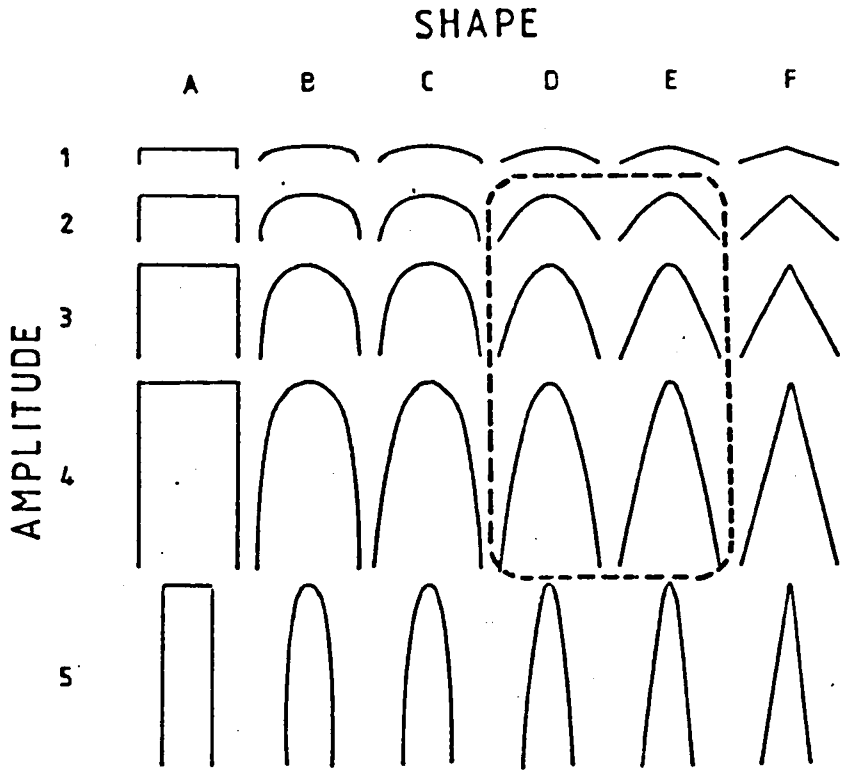

Figure 2.18. Hudleston's (1973-a) visual diagram of fold shapes. The area depicted by the dotted line represents the domain of the analysed folds in the mapped area.

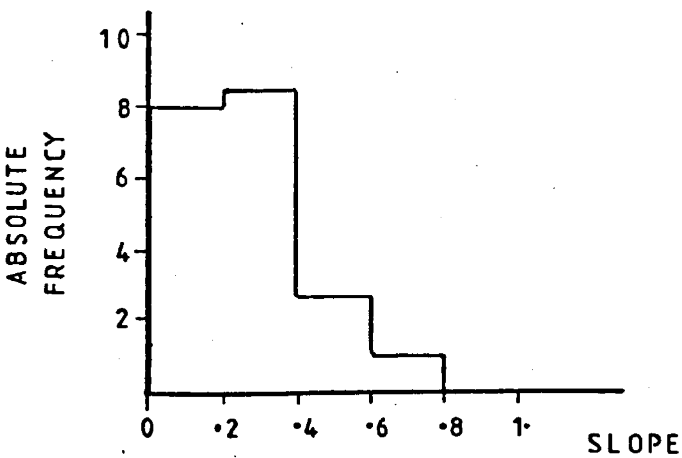

Figure 2.19. Frequency-histogram grouping 50 of the obtained slopes of the best fit lines with data values of tan (ϕ-α) vs tan α. See details in text.

figures given in the last two paragraphs also indicate that the amplitude of F_2-folds is considerably higher than that of the F_3-folds. There seems to be a change in fold shape with increasing amplitude to forms exhibiting more rounded crests (cf. Chapple 1968, Hudleston 1973-b). A change is represented here by a slight increase in the b_3/b_1 ratio followed by a large increase in b_1. This also supports Hudleston's (1973-a, p.119) comments that folds produced by buckling have a sinusoidal form but with an increase in the amount of flattening (parallel to the axial-plane) there is an increase in the amplitude but the shape remains unchanged.

2.3.4.4 Strain Superimposition and Comments

The results of fold classification show that similar (ie Class 2) folds are rare. This suggests that folding did not operate by simple shear parallel to the axial surfaces and it is reasonable to assume that at least a significant component of buckling was present during the fold formation. Another indication that buckling played an important role in the fold formation is that the folded lineations are not contained in a plane. Thus the idea of folds formed by heterogeneous simple shear alone cannot be applied in this area.

As the harmonic analysis suggests that the fold shape initially formed a low amplitude sine wave which then changed to a high amplitude sine wave with progressive deformation, it was decided to apply Hudleston's (1973-a, pp.35-39) technique that evaluates the amount of flattening by comparing isogon curves with theoretical models that have their isogons modified by effects of superimposed homogeneous strain. There are however some limitations to these models and also some conditions to be met (see Hudleston 1973-a, p.35, for full details).

Strictly speaking, flattening can only be invoked if at least one of the principal axes of stain is parallel to the fold axis (see Mukhopadyay 1965, Hudleston 1973-b). While this condition is not strictly true here, it must be pointed out that most of the illustrated F_3-folds have their hinges contained in a plane trending NNE-SSE, which should correspond (roughly) to the interpreted position of the principal plane of the strain ellipsoid formed by the least and intermediate principal axes. The F_2-fold of figure 2-15-a, however, is directed with its hinge line nearly parallel with the 'statistical' position of the X-principal axis of the ellipsoid while the axial plane of this fold is flat lying in the foliation planes. Therefore the F_2 fold profiles probably lie close to the XZ plane while the F_2 profiles are very close to parallelism with the YZ plane.

Two graphs are available for calculating the amount of superimposed flattening:

(i) The first uses the original ϕ/α curves and compares those which occur within the field of Class 1C, with a family of curves that are generated by the function:

$$\phi = \tan^{-1}\left[\frac{\tan\alpha(1-R'^2)}{R'^2.\tan^2\alpha+1}\right] \qquad [2\text{-}2]$$

where $R'_1 = \sqrt{\lambda_2/\lambda_1}$ is the reciprocal of the amount of flattening (see Hudleston 1973-a fig. 19).

(ii) The second graph is given by Hudleston (1973-a, fig. 21). This represents a fold by mean of a single parameter, the slope of the straight line on a graph relating tan $(\phi-\alpha)$ vs tan α. This slope is obtained from data by a simple best fit method.

The first method was not used because the ϕ/α curves obtained here do not strictly follow the contours set by [2-2]. Therefore the second technique was applied using the linear regression expressions [4-62] and [4-63] to 50 of the ϕ/α curves. In each fitting, a minimum of five pairs of tan $(\phi-\alpha)$ and tan α- values were used, and the amount of flattening $R = \sqrt{\lambda_1/\lambda_2}$ was assessed using:

$$R = [\tan (\Delta)]^{-\frac{1}{2}} \qquad [2\text{-}3]$$

where Δ corresponds to the slope of the best fitted line.

The results for F_3-folds are grouped in the frequency histogram of fig. 2-19. The calculated amount of flattening range from 1.11 to 6.83 while the mean of the values is roughly equal to 2.6. For the F_2 fold, the range is between 2.4 and 4.2 and the mean is 2.8 which apparently does not differ too much from the F_3-mean, except for the fact that this latter relates to profilès that lie near the YZ-principal plane of strain while the former is closer to the XZ section.

2.3.5 Structure in Macro-Scale

2.3.5.1 Cross-Sections Description

Having already described the statistic distribution of the various elements of the Caledonian fabric, it is now possible to present some inferences and comments about the general geometry of the structure (or macro-scale) of the studied area by means of a few selected cross sections.

Figures 2-20 (a to i) display 9 such sections. These were drawn from the Geology and Structural Maps (figs. 2-1, 2-2), transverse to the length of the deformation belt.

Section AA' (fig. 2-20-a) is the most southerly of the presented traverses. It comprises the thickest part of the mylonitic Lewisian domain which is bounded eastwards by a fault line (the a-thrust) that brought the Moinian succession on top of the Lewisian mylonites. In the middle of the Lewisian domain there are shown traces of the S-shaped and overturned (view downplunge, towards the NNE) F_3-folds.

The folded Lewisian may be bounded by a fault as the mesoscopic folds stop abruptly at this boundary (see locality c, in fig. 2-20-a). To the west, the topography is controlled by the orientation of the foliation planes (dip-slope) which are extremely parallel and show a restricted number of folds. There are a few folds on the summit of Creag na Faollinn which constitutes the domain of sub-area 5. The west face of Creag na Faollinn exhibits an intricate pattern of thrust planes that isolates a folded block which includes a succession of relatively undeformed Lewisian, Basal Quartzites and Pipe-Rock. This is the domain of sub-area 4.

Beneath the lower thrust there appear Fucoid Beds and Pipe-Rock and these are interpreted as making part of the imbricate zone. However, 200 m NE of this zone there is a good example of an associated parallel thrust beneath the lowermost thrust shown in this AA' section. (see plates 2-10 and 2-11, where Basal Quartzite rests on top of Pipe-Rock).

It is believed that the front face of Creag na Faollinn characterizes a domain of rocks with rheologic properties quite different from those located eastwards. This difference stems from the fact that in the west the thrust surfaces are clearly identifyable [Johnson's (1960) type of 'clean-cut-thrusts' see plate 2-12] and also show the existence of rock shattering and other brittle structures such as the cataclasis in the vicinity of thrusts (plates 2-6 and 2-5) and the

Figures 2.20

L I T H O L O G Y

STRUCTURE

Lewisian

LD MYL.

BD

Upper Proterozoic

MG MP OR

AS

Lower Paleozoic

BQ PR FS DL

TT

LC

FT

LD = Less Deformed
MYL = Mylonitic
BD = Basic Dyke

MG = Moinian Gneiss
MP = Moine Psammite
OR = Oystershell Rock
AS = Amphibolitic Sheet

BQ = Basal Quartzite
PR = Pipe Rock
FS = Fucoid & Serpulite beds
DL = Durness Limestone

TT = Thrust Trace (arrow points in the sense of movement).
LC = Lithologic Contact
FT = Foliation Trace.

Figures a to i refer to cross sections drawn from the map of figures 2.1-a and b. See text for detailed explanation and supplementary legend (thrust naming). The horizontal scale, in all sections, is identical to that on the geological map(ie ≃ 1:10,560).

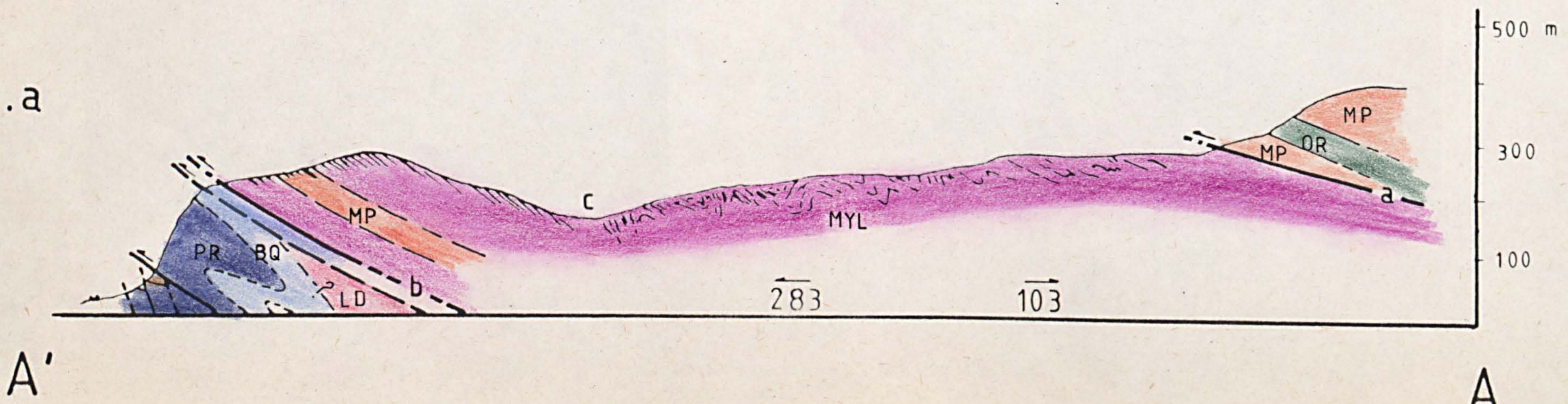

2·10

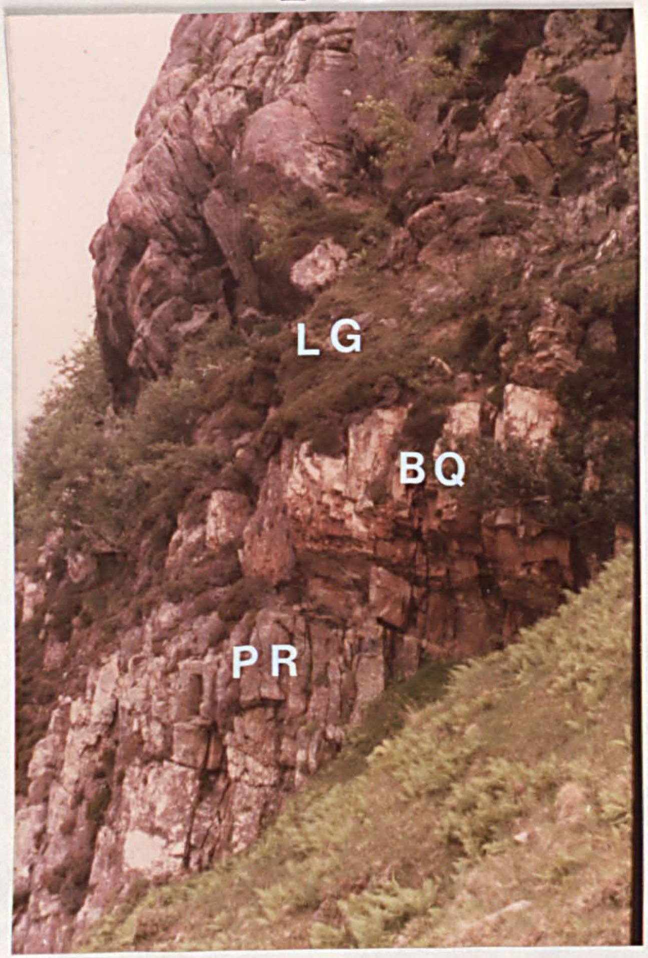

2·11

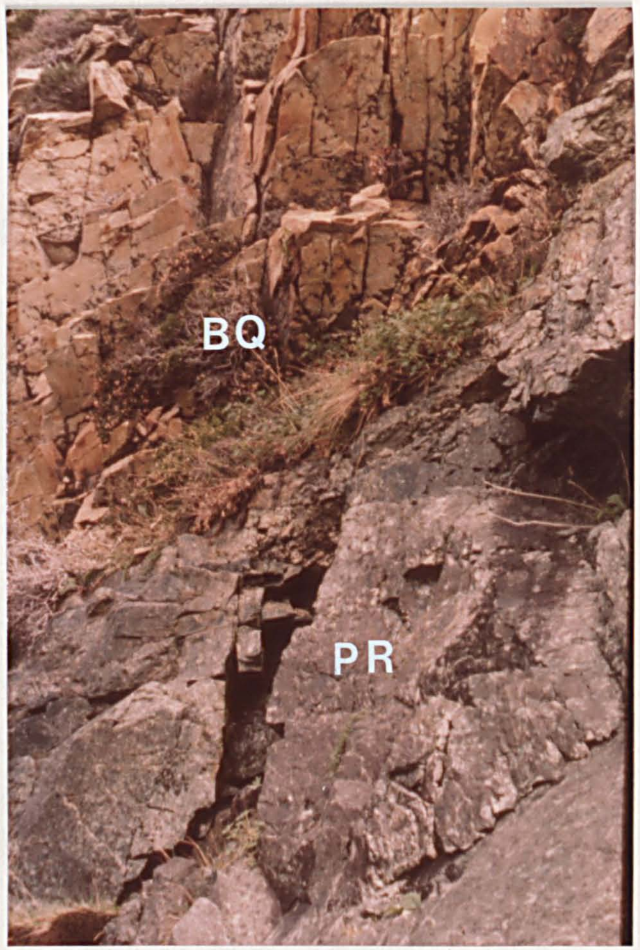

Plate 2.10. Illustrates stacking of thrusts on the Western face of Creag-na-Faollinn. From top to bottom: Lewisian Gneiss (LG), Basal Quartzite (BQ), Pipe-Rock (PR).

Plate 2.11. Detail of Plate 2.10. It shows the Basal Quartzite (BQ) thrusted over the Pipe-Rock (PR).

Plate 2.12. Basic rock of the Lewisian Domain thrusted over Paleozoic quartzites ('clean-cut-thrust'). Creag-na-Faollinn area, SE end of Loch Eriboll.

formation of imbricate faults.

Section AA' cuts across the thickest part of the mylonitic zone and this thins both to the south and north as it will be shown by the next section.

Cross section BB' (fig. 2-20-b) runs approximately SE-NW. In the east it comprises Moinian rocks of sub-areas 8 and 9. This is the section showing the more extensive and perhaps the thickest domain of the Oystershell rocks which show the variations in the pelitic and psammitic content as described in section 2-2. This variation was only noticed in this particular region.

As in section AA', there seems to be an association between the topographic slope change with the proximity of the a-thrust zone, which here shows no discordance in structures between hanging wall and footwall. In fact the very existence of a thrust in this zone has been a disputable subject since the days of Peach and Horne. Under conditions of intense deformation the rocks look very much alike, so the thrust is difficult to locate accurately. The existence of the fault is evident by the fact that some meters away (in both directions) the rocks prove to be definitely distinct, Moine and Lewisian.

The Lewisian and the fine laminated Moine psammites, located between the thrusts, show intense F_3-folding with overturned structural patterns. This is the section where it is possible to see the thickest pack of mylonitic Moinian psammites (below the a-thrust) interbedded within the Lewisian mylonites. This Moinian domain is the extension of another strip depicted in section AA' and it will be shown that the same pattern of interfingering of these rocks persists in the next two cross sections.

The Moinian psammite is truncated beneath by a fault that brings it into direct contact with the Paleozoic quartzitic rocks (see c.

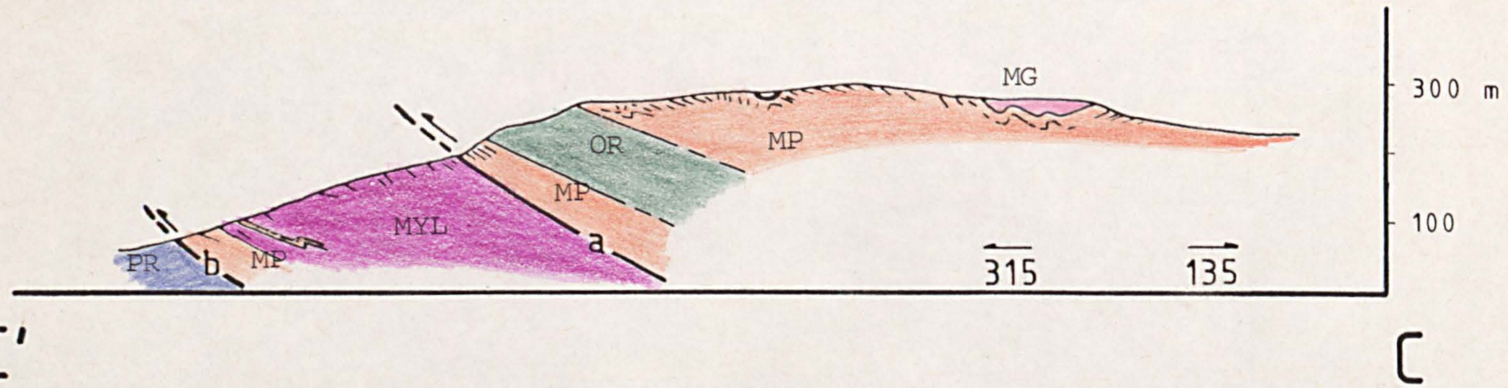
MG
OR
MP
MP
MYL
a
PR
b
MP
315
135
300 m
100
C'
C

b.

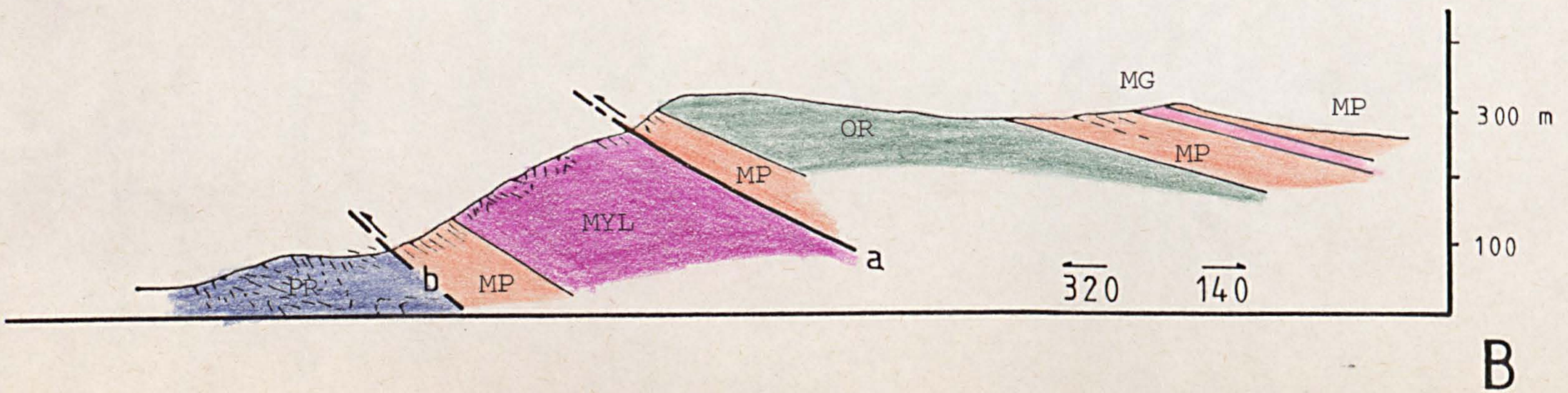
MG
MP
OR
MP
MP
MYL
a
PR
b
MP
320
140
300 m
100
B'
B

Geologic Map of figs. 2-1) which are represented in this point by the 'Pipe-Rock'. These are inverted by folding.

Section CC' (figure 2-20-c) trends 315°/135°. The Moinian rocks above the a-thrust are mainly the psammites of sub-area 15 which show the effects of an F_3-fold verging towards the WNW. The thickness of the Oystershell rock has diminished considerably from the previous section and on the western slope,the lower Moinian quartzite is in contact with the Lewisian mylonites through a fault (the a-thrust).

The Lewisian beneath the a-thrust is interfingered with Moinian psammites and to the west this occurs again and it is inferred that they are in thrust contact (b-thrust) with the Paleozoic rocks.

Section DD' (fig. 2-20-d) is almost parallel to the previous one. The Moinian sequence at this point shows additional displacements due to vertical faults.

This section runs through the region which was called the 'zone of complication' by Soper and Wilkinson (1975). The upper thrust zone (a-thrust) still has a mylonitic character but the contact with the Lewisian mylonites is much more complicated than to the south. It is difficult to map; in some places this contact is concealed by peat and therefore has to be inferred. It is quite probable that there are several associated thrusts like those associated with the allochthonous limestone cropping out just north of this section (see geologic map).

The Lewisian mylonites do not crop out continuously and some zones are entirely covered with peat. The interbedded Moinian rocks crop out in two separated horizons the westernmost being the one which comes directly into contact (through the b-thrust) with the large overturned structure consisting of Paleozoic rocks.

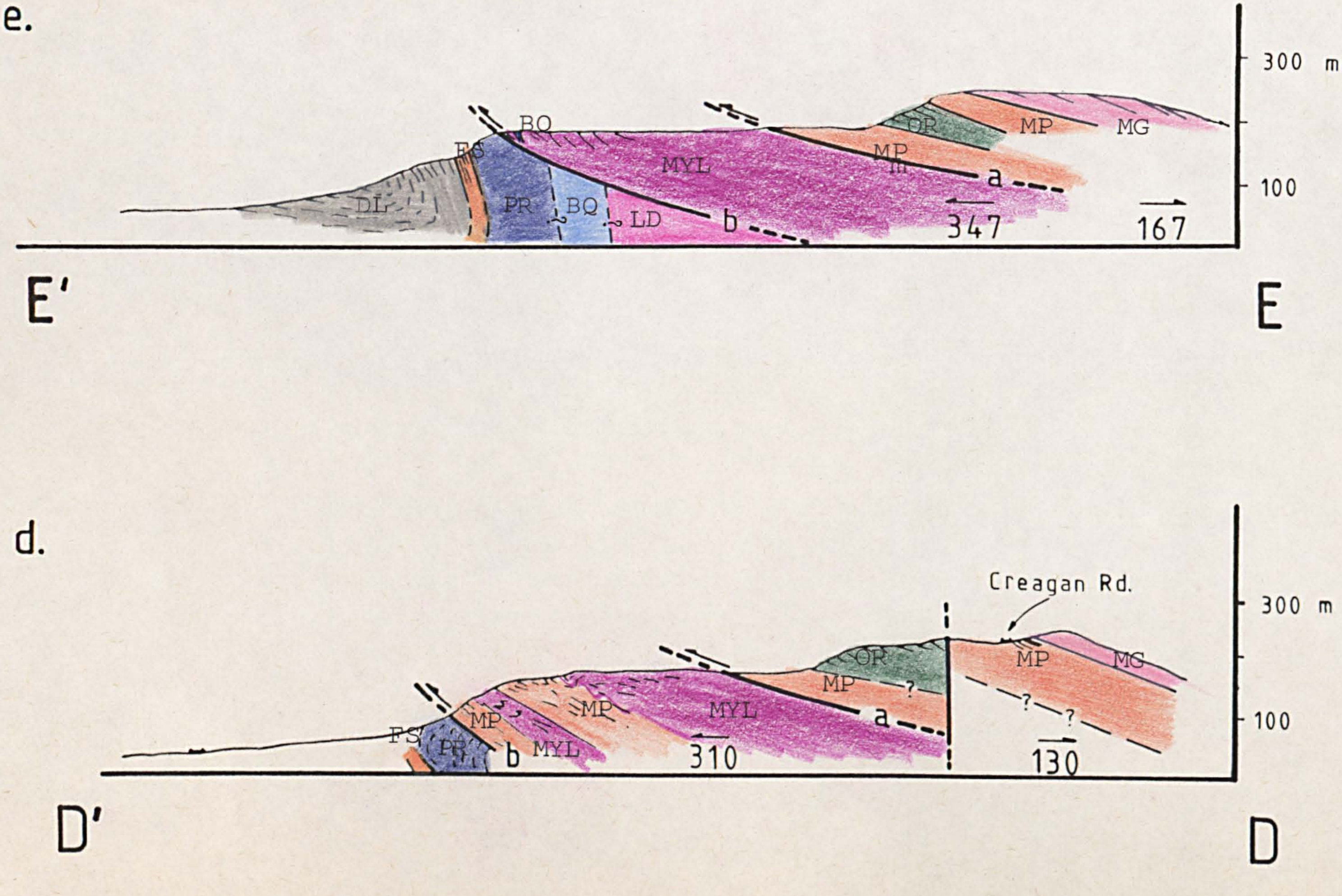
e.
300 m
100
BQ
FS
OR
MP
MG
MYL
MP
a
DL
PR
BQ
LD
b
347
167
E'
E
d.
Creagan Rd.
300 m
100
OR
MP
MG
MP
MP
MYL
FS
PR
MP
b
MYL
a
310
130
D'
D

The Precambrian rocks here show evidence of intense mylonitization but the underlying Paleozoic rocks clearly exhibit primary structures, such as cross bedding, at only a small distance (less than 10 m vertically) from the b-thrust (plate 2-4). This suggests that the Moinian and Lewisian domains have experienced a more prolonged deformation history than the adjacent Paleozoic rocks.

The section EE' (see fig. 2-20-e) trends SSE/NNW and shows the gneissic rock overlying the upper Moinian psammites. The Lewisian mylonites are devoid of Moinian psammites but show interbedded Paleozoic quartzites very near the edge of the b-thrust contact with the (underlying) truncated Paleozoic sequence. The overturned fold illustrates the structure of the An-t-Sron syncline.

Cross section FF' (fig. 2-20-f) exhibits a considerable reduction in the thickness of the Moinian sequence. The Lewisian mylonites do not include any of the Moinian psammites in this section, and the mylonite zone seems to be affected by presumably vertical-horizontal displacements possibly not related to Calėdonian movements. The mylonites are in direct contact with the Basal Quartzite which belongs to a block that also shows Lewisian gneiss,much less affected by deformation, and its contact with the Cambrian rocks is the original unconformity.

The subsequent section (GG', see fig. 2-20-g) has an orientation parallel to the ESE/WNW trend and shows in the eastern side that the Moinian sequence is warped synformically and this group together with the Lewisian mylonite zone might have been affected by the vertical faults.

It must be noticed that the thickness of the Lewisian mylonites, bounded by the a and b-thrusts, decreases significantly from g.

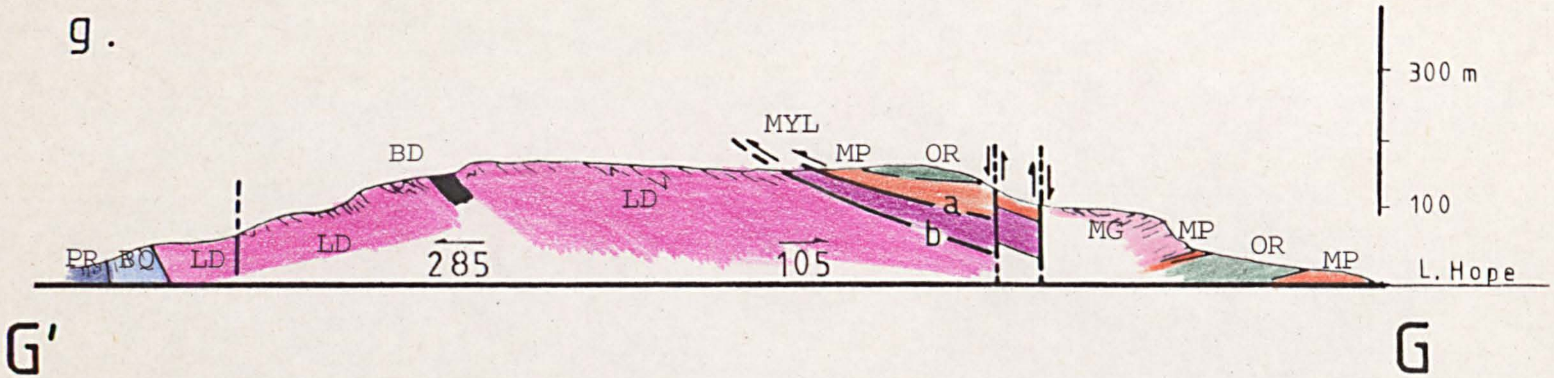
300 m
100
MYL
BD
MP
OR
LD
a
b
PR
BQ
LD
LD
285
105
MG
MP
OR
MP
L. Hope
G'
G

f.

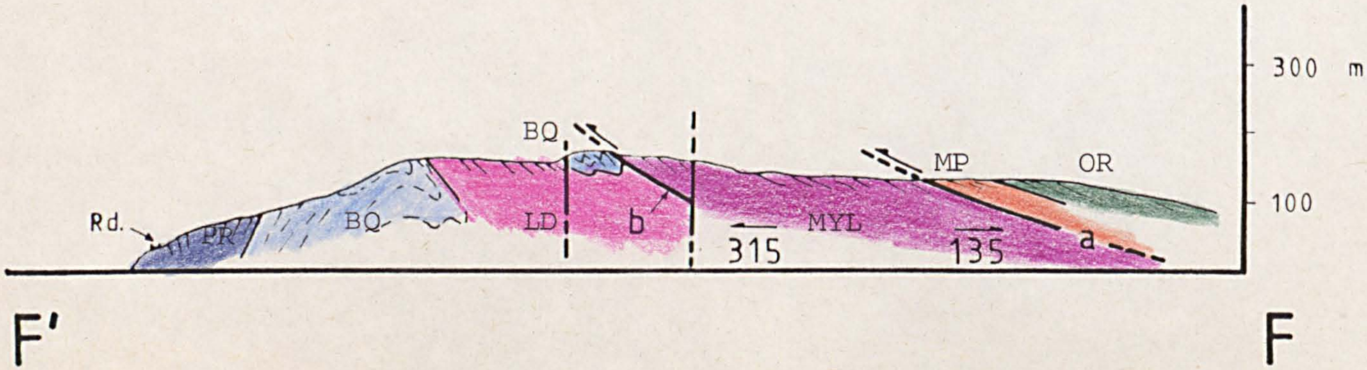
300 m
100
BQ
MP
OR
Rd.
PR
BQ
LD
b
MYL
315
135
a
F'
F

the south, while the block of the 'less deformed' Lewisian occupies the greatest area in this section. The contact with the Paleozoic rocks is presumably the continuation of the unconformity mentioned in section FF.

Cross section HH' (fig. 2-20-h) trends 296°/116° and crosses the top of the Arnaboll Hill. The Moinian sequence has been completely eroded away from the easternmost part of the section; therefore only the underlying Lewisian mylonite can be seen overlying the previously lowermost b-thrust. Beneath, there is another thrust, carrying Lewisian rocks, known as the Upper Arnaboll Thrust (Coward 1980). The name b-thrust, used throughout the present description, was taken from Coward's (1980, fig. 5) work, which explains the structural evolution of this very region. However it is necessary to emphasise that apart from the b-thrust trace illustrated in section HH', its use elsewhere is entirely the responsibility of the author. Rathbone et al. (in press) consider the Upper Arnaboll Thrust and the b-thrust to merge on the Arnaboll Hill, and call the southern continuation of both, the Upper Arnaboll Thrust. However the present study considers that the Upper Arnaboll Thrust branches-off laterally, to the NE, and this explains the geometry seen on the geologic map of fig. 2-1.

The present section also presents another speculative view and that is the backlimb thrusting beneath the trace of the Upper Arnaboll Thrust and the faulting of the trace of the Arnaboll Thrust. These interpretations are based on structures shown in the northernmost edge of the mapped area.

The cross section II' (fig, 2-20-i) is located on the NE side of Loch Hope and runs oblique to the previous section. It shows in the east, Moinian psammites on top of the Moinian Gneiss. The structure is characterised by an overturned S-shaped (plunge towards

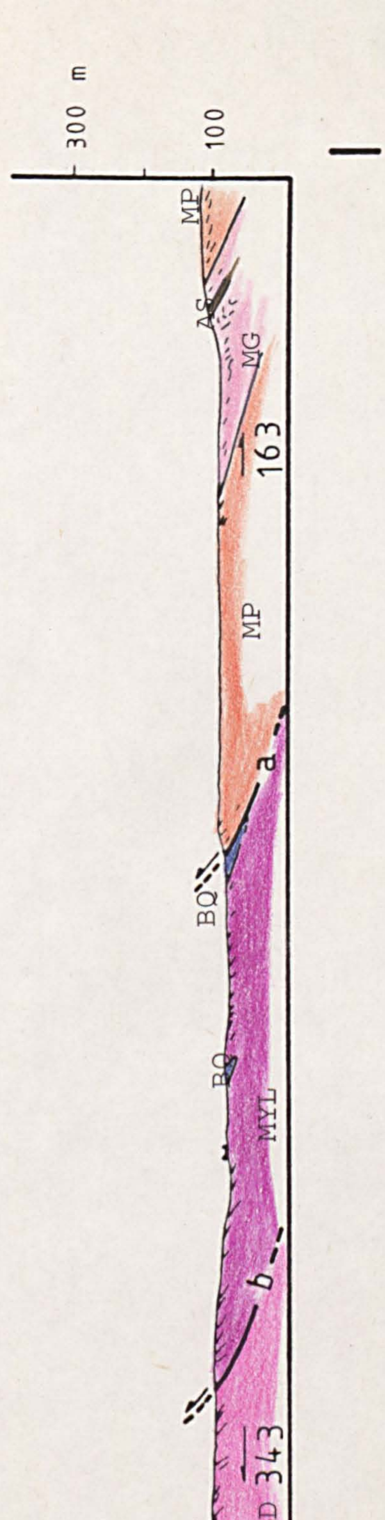
i.
300 m
100
I
MP
AS
MG
163
MP
a
BQ
BQ
MYL
b
343
LD
BQ
I'

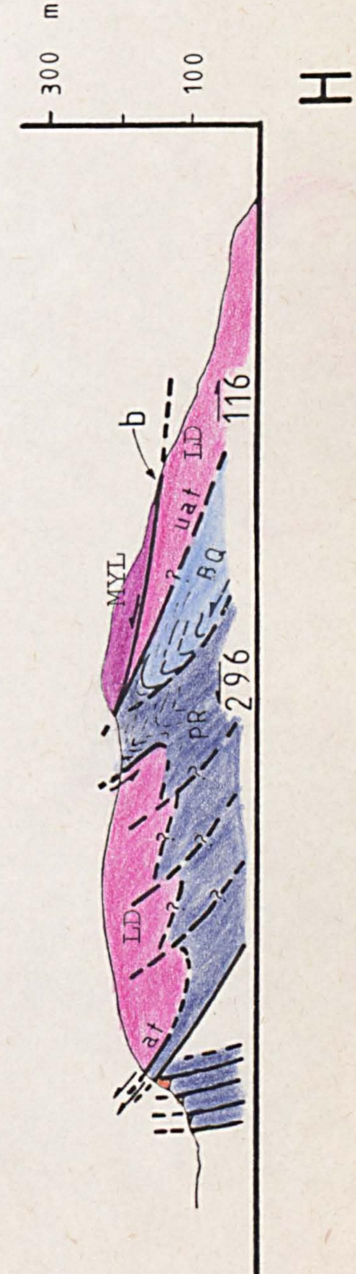
h.
300 m
100
H
b
116
LD
uaf
MYL
BQ
296
PR
LD
af
H'

NNE) F_3-fold. Amphibolites are represented in this section as occurring within the Moinian Gneisses. The 'Oystershell' rocks occur only at one locality north of section II' and the reason for them not being represented along this section is due to probable concealment by peat cover.

The Moinian sequence is in thrust contact with the Cambrian quartzites, similarly to the a-thrust in the Eriboll sections. The mylonitic Lewisian in this region shows numerous lenses of Cambrian Basal-Quartzite, and presents a pattern of mylonitic banding comparatively more heterogeneous than the corresponding domain at Eriboll. This heterogeneity will be discussed in studies of Grain Shape and Paleopiezometry in chapters 4 and 7. The western edge of these mylonites shows highly deformed rocks exhibiting characteristics of closely spaced foliated planes. This zone is in direct contact with the domain of the less deformed Lewisian gneiss. This is a situation very similar to that occurring in sub-areas 28 and 29 or as in the area between section FF' and GG'. The contact is interpreted as being similar to the b-thrust (type) as in Eriboll. This is supported by the fact that the 'less deformed' Lewisian gneiss also resembles that in sub-areas 28 and 29 and is similarly heavily impregnated by feldspathic pegmatites. The less deformed Lewisian rocks are underlain by Paleozoic quartzite rocks. This situation is similar to that for the Upper Arnaboll Thrust in the Eriboll area.

2.3.5.2 Thrust Emplacement Mechanisms

As in all the matters connected with thrust faults, the mechanics of thrust-emplacement is also a controversial subject. The available models vary according to the original approach which could be essentially analytical (Elliott 1976-a, b; Chapple 1978), experimental

(Ramberg 1980) or even empiric-analogic (R. Price and Mountjoy 1970; Dahlstrom 1970).

The exact forces governing the development of thrusts and nappes are not known. However, gravity forces are presently considered to play a leading role in the motion of thrust sheets,as applied lateral stresses would probably deform the sheet rather than solely transport it (Hubert and Rubey 1959). Among the gravity-types of mechanisms that could be related to the development of thrust movements (see discussion Elliott and Johnson vs N. Price et al. 1978), Gravity Spreading seems to be favoured by some that advocate the sequential development of thrusts in the direction of transport (R. Price and Mountjoy 1970; Dahlstrom 1970; Elliott 1976-a,b; Ramberg 1980), while Gravity Gliding (N. Price 1977, Blay et al, 1977) may cause faults to propogate opposite to the movement direction.

Elliott (1976-a) applied concepts of motion in glaciers (Nye 1952) when he derived his model for the motion of thrust sheets. He pointed out that the surface slope controls the gravitational forces, and formulated that

$$\tau = \rho g H \alpha \qquad [2\text{-}4]$$

where τ is the basal shear stress, ρ is the rock density, g the gravitational constant, H the nappe thickness and α is the surface slope.

Chapple's (1978) model conflicts in many aspects with that by Elliott (1976-a), principally by the fact that he envisages the topographic slope as a negligible factor and places more importance in the horizontal compressive stress. His model also takes into account the internal deformation of the slab which moves also because of the existence of a weak basal layer.

Ramberg (1980) approached the problem using experimental models. In his view of gravity spreading, the forward movement is due to the vertical shortening of the nappe and this not only implies a lowering of the centre of gravity (ie gravity potential) but also the lengthening of the horizontal plane.

Ramberg (1980, figs. 3 - 5) considered two models: (i) one where there is a free slip along the base of the sheet. Pure shear may occur both on the top and bottom of the model, while in the middle zone there is a combination of pure and simple shear. (ii) The second model has a complete coherence at the base. The top of the model is analogous to the previous one but towards the base simple shear becomes important due to the welded nature of the rock.

In Ramberg's opinion, the operational mechanism of a nappe is a combination of pure and simple shear, represented by a vertical shortening and shear along the shear direction in a quasi-horizontal plane.

This problem of strain in a thrust sheet will be returned to in later chapters.

2.3.5.3 Discussion

So far in this study, the thrusts have not been named. This is due to the fact that naming and correlation of thrusts can be a matter of personal interpretation and this has been a problem in the NW Highlands since the days of Peach and Horne.

One reason for disagreement stems from the fact that it is not always possible to follow a particular thrust line throughout an area; the trace may be lost by simple concealment or die out or yet anastomose with another fault.

Soper and Wilkinson (1975) conceived the existence of an upper Thrust in the Eriboll area and they termed it the Eriboll thrust. This bounded the Lewisian and Moinian mylonites and it was restricted to the area, roughly, between present cross sections CC' and FF'. This thrust trace corresponds exactly with the present a-thrust. However, what is not understood is why these authors did not extend this thrust line to the south and north of this area as it is quite clear in the field that the mylonitic zone persistently bounds the Moinian sequence and this is one of the most consistent boundaries in the whole area. It seems reasonable to extend the thrust trace as seen in the present maps (figs. 2-1 and 2-2).

The problem connected with the location of the Moine Thrust (s.s.) in fact dates from the days of Peach and Horne. Their original maps (IGS-Edinburgh) reveal that there were two conflicting positions for the MTP:

In the first interpretation, the Moine Thrust (s.s.) matches the position of present study's b-thrust. In this case they use the denomination ?MTP?, and along the thrust trace there are always interrogation marks.

In the second interpretation the Moine Thrust (s.s.) lies more eastwards, beneath the Moinian sequence, near or along the present position of the a-thrust. Along this fault line the word Moine (in Moine Thrust Plane) is clearly crossed out and replaced by the initials B.N.P.

Soper and Wilkinson (1975) pointed out that Peach and Horne were in disagreement on the above issue. Soper and Wilkinson also conceived the Moine Thrust as (i) underlying the thick mylonites, and (ii) forming a clean-cut, brittle type of thrust surface which developed during the last deformation (D_4). Thus Soper and Wilkinson clearly put the Moine Thrust with this study's b-thrust.

In the model suggested by Coward (1980, fig. 5) the sequence of faults develops from an initial movement along the MTP and then follows displacements in the direction of transport (Dahlstrom 1970) branching off from the lower thrust zone. Adopting Coward's model for the general development of the area, the MTP in this study would correspond exactly to the upper or the a-thrust and this is in agreement with B.N. Peach's opinion for this fault's position and is contrary to Soper and Wilkinson's view. McClay and Coward (1981) and Rathbone et al (in press) also placed the MTP in the position of the present a-thrust.

The age of the mylonites has been a problem in the past. Peach et al. (1907) attribute all the structures observed in the area of the thrust zone to the effects of thrusting movements. This seems to follow the original view of Lapworth (1885). Clough (in Peach et al..1907, p.46) postulates that folding of rock in the domains above and below the thrust preceded the formation of the latter. Bailey (1955, p.162) pointed out that folding, dislocation metamorphism in the thrust belt and the general metamorphism of the Moines dated from the Moine Thrust formation. Christie (1955) stated that the main transport of rock in the thrust zone of Assynt relates to an early phase of movement, developing mylonites and plastic folds. Christie (1963) was in the opinion that the thrusting events culminated in the formation of a mylonitic foliation and the ESE plunging folds.

Johnson's (1957) early view favoured the idea of mylonites preceding folding and recrystallisation and these were followed by brecciation indicating a time gap between the mylonite formation and the main thrust phase. Johnson (1960) modified his first opinion by stating that the events were discontinuous and there exists ... " no obvious relations betwen mylonites and the Moine Thrust fault, of which there is no evidence prior to the latest movement phase ...". In his opinion the mylonites of Loch Alsh contain two sets of folds unrelated to the thrust movements.

Barber (1965) studied the Thrust zone of Loch Alsh and Loch Carron and he emphasised that the thrusts and mylonites formed were completely different events. His sequence of evolution includes: mylonite formation, isoclinal folding (ESE-axes), recrystallisation constituting the dominant foliation and lineation, asymmetric folds (NS-axes), monoclinal folding and then thrusting.

Soper and Wilkinson (1975) considered a sequence of thrusting from W to E and attribute the Moine Thrust formation to a D_4 age because it is post D_2 and produces brecciation. It must be remembered, however, that they refer to a thrust that corresponds to this study's b-thrust which bounds rocks with contrasting intensities of deformation. If a "D_4-age" is assigned to this surface since (i) it does not represent this study's Moine Thrust (s.s.), and (ii) adopting Dahlstrom's (1970) view for the sequence of thrusting, it might be considered that the Moine Thrust (ie the a-thrust) developed earlier than the more 'brittle D_4 age' thrust of Soper and Wilkinson.

Elliott and Johnson (1978) were in the opinion that the thrusts formed progressively younger westwards while Soper and Barber (1979) doubted that the Moine Thrust was the earliest to be emplaced. Their objection was based on the argument that contrary to the evolution for the Canadian Rockies (Dahlstrom 1970) and Appalachians (Barton 1978), the tectonic style of the Moine thrust region was different because it involved both the Basement and Cover. Soper and Barber's (1979) sequence of events is:

(i) D_1-folding, with NNE trend and vergence towards the foreland and in the lower nappes.

(ii) D_2-emplacement of major nappes (Arnaboll). Formation of Duplex, Imbricates and Sole zone.

(iii) D_3-open folds co-axial with D_1.

(iv) Emplacement of the Moine Nappe.

(v) Box folding.

It must be realised, however, that the American literature (eg Hatcher 1981) gives us clear indication that the Appalachians contain large basement thrust slices so the argument of Soper and Barber (1979) is difficult to accept.

McClay and Coward (1981) considered that the tectonic style in the Eriboll area is geometrically and structurally similar to that of the Appalachians and Canadian Rocky Mountains. They pointed out that the thrust style and strain patterns are controlled by the position of the Sole Thrust and although adopting the sequence of fault stacking taking place in the direction of tectonic transport, they admit the possibility of reactivation of some thrusts causing reversals in that stacking order.

The data from the Eriboll-Hope areas, from this study, can be generally subdivided into 4 main zones corresponding to the major nappes (or Sheets, Elliott and Johnson 1980) which are delimited by 3 major thrusts. It will be shown that the stacking order fits well with mechanical and rheologic changes in the rocks, as seen in the textural studies of Chapters 5 and 7.

The westernmost zone comprises the domain of the imbricated Cambrian rocks. These generally occur west of the present area. This is however, an important zone which shows characteristic mechanics of brittle deformation. The present study has shown that the imbricates developed beneath the Arnaboll Thrust (section HH'). In the south of the area, in Alt-na-Craoibhe-Caoruinn, there is also the development of imbricated faults in the lowermost outcrops of Paleozoic rocks.

The second zone is a longitudinal domáin bounded by rocks with overall characteristics of comparatively more ductile deformation with mylonitization practically restricted to the neighbourhood of the thrusts. There are associated overturned folds such as at Creag na Faollinn (section AA') or at An-t-Sron syncline (Sections DD' and EE'). Generally the rocks beneath the thrust bounding this second domain are of Paleozoic origin but there are exceptions as in the case of the unmylonitized Lewisian in areas 28, 29, north of Hope and in the western face of Creag-na-Faollinn. Signs of cataclasis and brecciation (plates 2.5 and 2.6) are associated with the faults in this zone. These discontinuity surfaces also exhibit Johnson's (1960) characteristics of 'clean-cut-surfaces' (see plate 2-12). This is clearly a transitional domain because in some areas the lowermost thrusts acted as 'roofs' for the development of the underlying imbricates in the Paleozoic rocks, while in others the uppermost thrust bounds ductile folds.

The third zone is bounded to the west by the b-thrust. It must be stressed that the b-thrust is not used here in the strict sense, but instead it is used to characterise a thrust type which forms the lower boundary of a heavily mylonitized upper sheet. Most of the mylonites are mainly of Lewisian origin but there are domains where the rocks involved are Moinian and others where they are Paleozoic. In general the Moine mylonites are more abundant in the southern half of the area while the Paleozoic mylonites occur predominantly (but not exclusively) north of Creagan Road. This is a domain with clearly ductile deformation.

The fourth sheet is delimited underneath by the Moine Thrust (sensu stricto) or the a-thrust, which separates the last zone from the upper Moinian sequence. There appears to be a clear deformation gradient eastwards away from this junction, as the effects of mylonitization, although persisting in the Moine sequence, tend to decrease in that direction. The Moine Thrust differs from the lower thrusts in that it does not have the brittle characteristics of a clean-cut surface.

No imbricated structures have been recognised in the upper zones. They may exist but due to the relative homogeneity of the mylonites they may be inconspicuous. Alternatively, the absence of zones of contrasting weakness in the Precambrian sequence prevents imbricate fault formation. It is known that incompetent layers can act as gathering zones (Douglas 1950).

From the characteristics described in the present section it seems that the above 4 zones show a transition from brittle to ductile shear zones, in the sense defined by Ramsay (1980). The brittle clean-cut-thrusts differ from the a-thrust type because the latter comprises a domain of fault(s) where the displacement is continuous, without showing the sharp rupture surface and this explains why there is a perfect continuity in the attitude of the foliation planes across the a-fault zone. As it will be shown in the next chapter, the a-thrust zone presents the most intense strain magnitudes.

It is now the intention of this study to summarise the evolution of the deformation zone by correlating the mechanical and rheological characteristics of the zone. Firstly, there is no reason to believe that the mylonites are not related to the Moine Thrust (sensu stricto). Apparently, the intermediate thrusts were affected by the second phase (F_3) of folding, therefore preceded it (section HH').

Following a thin skinned model, with the sequential development in the direction of transport (Dahlstrom, 1970), the main movement plane could have first developed in an environment of plastic deformation (ie deeper level). There followed a climb up (cf. Rich 1934) to a transitional environment no more dominated by mylonite forming effects and finally reached the upper levels characterised by the brittle behaviour of the rocks. This would clearly conform with Ramsay's (1980, fig. 22) view of the relationships between brittle and ductile zones in an environment of crustal contraction. Evidence that the mylonitic rocks were affected by a superimposed phase of brittle deformation (cf. Sibson 1977) will be given by the description and analysis of microtextures of Chapter 5. This sequence of development would also explain why, in terms of intensity of deformation, the rocks above and below the b-thrust are clearly discrepant and this is due to the fact that the former was first developed or formed completely dissociated from the latter.

Another aspect of the Moine Thrust Zone is the formation of bulges, the biggest occuring in the Assynt area. In the mapped area there appears to be one such lunate shaped structure, which seems to have been formed where the traces of the main thrusts (a and b) do not run parallel. The mylonite zone exhibits a reasonably homogeneous thickness from the Arnaboll Hill southwards to the vicinity of Creagan Road, south of which the distance between the traces widens. This width is abruptly increased in the area of cross section BB', being widest near section AA'. To the south the thrust traces are closer again.

There is a strong connection between the increase in the frequency of folding and this widening of the mylonite zone. Large folds could be responsible for the thickening of the zone and would give rise to the observed bulge in analogy to Barton's (1978) explanation for the existence of the Assynt bulge. Field evidence suggests, for instance, that the frequency of F_3-folds (meso-scale) is high in sub-areas 12, 10, 11 but these clearly form large fold structures in sub areas 6, 3 but grade again to small scale folds in the adjacent sub-areas 7, 3 and 1. One could treat the bounding thrusts a and b respectively as the 'roof' and 'floor' structures, the 'horse' being the folding domain just described.

Johnson (1957, p.262) also pointed out the relationship of the intensity of folding relative to the thickening and thinning of nappes. This variation in thickness must have some effects in the adjacent nappes. As reported earlier, the F_3-fold hinges in the Moinian sequence above the Moine Thrust suffer a progressive deflection in their hinge direction, which changes from 180^o in sub-areas 17, 16 to approximately 145^o in sub-area 8. These changes seem to coincide with the widening of the underlying mylonitic zone.

There must be some reason for the increase in fold frequency. Could this mean that their existence is related to some differential rate of displacement along the strike of the thrust? Talbot (1979) points out that a moving sheet only forms folds when it accelerates or decelerates. Could it mean that sub-area 8 and 15 gradually decelerated relative to sub-areas 17, 23 and 24?

CHAPTER 3

FOLD HINGES AS STRAIN MARKERS

3.1 General

An aspect of thrust tectonics which has received considerable attention during the recent years is the problem of fold orientation within thrust zones (Bryant and Reed 1969, Sanderson 1973, Roberts and Sanderson 1974, Hobbs et al. 1976, Carreras et al. 1977, Williams 1978, Bell 1978, Coward and Kim 1980). The present chapter deals with some quantitative aspects of fold orientations. It investigates the tendency for folds and lineations to attain a constant orientation nearly parallel to the thrust movement direction. This pattern described in Chapter 2 is here interpreted as due to fold hinges being reorientated during progressive deformation. It deals with numerical methods and problems related with quantification of strains using fold hinges as markers. It also analyses and discusses the strain results and possible mechanisms in the context of geology and structural setting of the south of Eriboll area.

3.1-a Review of the Literature

There are two-central themes to be dealt with in this chapter. The first deals with the angular relationship between fold hinges and the direction of movement in the thrust zone. The second theme deals with the strain mechanisms - pure shear, simple shear or the combination(s) of these in the thrust zone.

Peach et al. (1907) referred to the ESE plunging lineation of the Moine Thrust Belt as the stretching direction-lineation. They considered it to show the thrust movement direction. This view was critdcised by some authors such as Phillips (1937, 1940, 1955), McIntyre (1954) and Christie (1955) who claimed that such lineations constituted a b-linear fabric (rather than an a-lineation) because of their parallelism to fold hinge directions. The views of Peach et al (1907) however, had the support of Anderson (1948) and Kvale (1948, 1953).

It seems that this controversy was an unfruitful discussion generated by the use (or misuse, see Weiss 1955, Whitten 1966, p.106) of Sander's (1930) concept of kinematic axes. It is considered that in progressive simple shear the a-axis is defined as being parallel to the movement or slip direction, while the b-axis is orthogonal to a but pertinent to this shear plane, the ab-plane. If these concepts are applied to folds, on the condition that their fabrics have a monoclinic symmetry, the b-axis is considered to be normal to the monoclinic plane of symmetry, thus parallel to the fold axis, whereas the a-axis is located in this symmetry plane parallel to the direction of movement (see Whitten 1966, pp.105-111; Hobbs et al. 1976 p.194).

Kvale (1953) clearly stated that Sander's (1930) theory of movement and fold formation need not to be applied in the Norwegian Caledonides. He criticised McIntyre's (see Kvale 1953, p.51) views and stressed that in E and W Norway there is a lineation in the thrusts which is parallel to fold axes and also to the direction of movement. Bryant and Reed (1969) reported similar relationships for the Blue Ridge, S Appalachians and they supported Lindstrom's (1961) ideas of fold rotation towards the direction of thrusting. There followed a number of examples showing the same behaviour of folds and lineations in different thrust belts. Escher and Watterson (1974) gave examples from Greenland, Nicholas and Boudier (1975), Minnigh (1979) presented examples from the Alps. Carreras et al. (1977) showed examples from NE Spain while Oleson (1971), Rhodes and Gayer (1977) and Williams (1978) gave examples from Scandinavia. Bell (1978) showed examples of fold hinges parallel to the transport direction for the Woodroffe Thrust Zone, Australia and Quinquis et al. (1978) described them for Brittany.

There were some studies which considered the geometry of folds which have their hinge distorted. Hansen (1971, figs. 20, p.43) illustrated the curvature of such hinges in the Trollheimen rocks, Norway. Carreras et al (1977) introduced the name of 'sheath-folds'. Other studies dealt with parameter quantification: Sanderson (1973) developed an analytical model for strain quantification with the conditions that the folds (either normal or oblique to the stretching direction) were deformed by a co-axial strain. In a subsequent paper, Roberts and Sanderson (1974) applied the model to folds from the SW Highlands of Scotland. Williams (1978) produced a contour map of the angular distribution of fold hinges, relative to the direction of movement of thrusts from East Lakesfjord, Finnmark. Cobbold and Quinquis (1980) produced sheath folds experimentally and also studied some of their theoretical aspects.

Ramsay (1981, fig. 15) has illustrated diagramatically the formation of curvilinear folds during simple shear. Minnigh (1981, fig. 11) also showed a scheme for the development of such folds. The present study also found examples of these folds with curved hinges within the mapped area (see plates 3-1 to 3-6) and the interpretation of these curvilinear folds forms the basis of this chapter. The present study's analogy for the formation of these arcuate-hinge folds is illustrated in plate 3-7.

There are two fundamental mechanisms which may produce the rotation of such fold axes in thrust belts. The first involves pure shear where the fold axes are passively rotated towards the direction of maximum elongation (Johnson 1967, Sanderson 1973, Roberts and Sanderson 1974). Other studies clearly advocate the development

Plates 3.1 and 3.2. These illustrate incipient curvilinear folds (F_3) in the Moinian Psammites cropping out north of Creagan Road. Notice the curved hinges which are flat lying in (or near) the foliation planes.

Plate 3.3. Curved hinge in the Moinian psammitic rocks of Loch Eriboll area.

Plate 3.4. Curved hinge in the Oystershell Rocks above the Moine Thrust Zone of Church Creag, Loch Eriboll. The yellow pencils (see arrows) were placed parallel to the curved hinge in 3 different locations.

Plate 3.5. Illustrates curved hinges with obliquely folded lineations (L_1).

Plate 3.7. Laminar flow showing the formation of curved and 'refolded' folds. Stream of the Alt-na-Craoibhe-Caoroinn.

Plates 3.6-a and b. Two different views from the same outcrop constituted of folded Lewisian mylonites, east of Alt-na-Eisgill, Loch Eriboll. Notice the pencils parallel to the curved hinges of F_3-folds.

of such folds in a shear zone (cf. Ramsay and Graham 1970) by means of a simple shear mechanism. Escher and Watterson (1974) used the term 'comtemporary folds' for these folds generated in this regime. Hobbs et al. (1976, fig. 6-15) showed diagrammatically the reorientation of fold hinges, while Ramsay (1980, fig. 16) illustrated the formation of curvilinear hinge folds using a simple shear mechanism.

The deformation with thrust and shear zones which causes the re-orientation of fold hinges should be largely that of simple shear, although some authors (Nicholas and Boudier 1975; Escher et al. 1975; Hobbs et al. 1976; Williams 1978; Bell 1978; Minnigh 1979; Ramberg 1981) assume combinations of irrotational (pure shear) and simple shear.

The models by Ramberg (1981) suggested that there is pure shear associated with simple shear leading to extension of the belt. Hossack (1968, 1978) has described extensional strains given by deformed conglomerates extended almost parallel to the shear plane in Norway.

The analysis developed in this chapter considers essentially co-axial deformation. This is obviously an oversimplified assumption but to admit a rotational deformation such as simple shear can also lead to innaccuracies as will be discussed in the end of this chapter.

3.1-b The Organization and Contents of this Chapter

The sections that follow in this chapter are mainly devoted to the quantification of deformation using curvilinear fold hinges as strain markers. The subdivided sections are organised as follows:

- Section 3.2 briefly describes a model proposed by Sanderson (1973). It explains how data are collected, treated and the results obtained using this techinque.

- Section 3.3 contains the derivation of a model proposed in this study.
- Section 3.4 describes in detail the techniques of optimization that were used or tried in the estimation of the parameters of the models described in sections 3.2 and 3.3. It also describes the structure of this study's computer programmes which were devised in conjunction with the investigated methods of optimization. Tests of these programmes are also discussed.
- Section 3.5 is devoted to data treatment. An analytical solution is here introduced, which selects data by weighting procedure.
- Section 3.6 deals with the results obtained using data from the study area.
- Section 3.7 presents a discussion of the hinge orientations in the context of the geology and structure of the area.
- Section 3.8 comments on the possibilities of using other models involving other mechanisms.

3.2 The Model Devised by D. Sanderson

The idea of estimating the strain using the distribution of fold hinges as markers was put forward by Sanderson (1973) and subsequently applied for a wide area in the SW of Scotland by Roberts and Sanderson (1974). It is suggested that folds are modified by tightening, flattening and passive rotation of limbs and hinges which formed at high angles to the movement direction of the thrust sheets. The assumption was that a population of fold axes, initially distributed around a mean as a Gaussian (or Normal) distribution,would give rise to a modified distribution as a result of superimposed strain (cf. Roberts and Sanderson 1974).

Sanderson (1973, pp.55-56) based his model on Dewey's (1969) assumption of parallelism between the finite strain ellipsoid axes, X, Y, Z (where X>Y>X) and the fold geometric axes α, β and γ where $\alpha\beta$ determines the axial plane and β is the fold axis. The analysis was restricted to two dimensions to changes within the XY-plane of the strain ellipsoid. Sanderson (1973) initially considered the case where the initial mean of fold axes was parallel to the Y-axis of the finite strain ellipsoid so the fold axes population was strained orthogonally to this mean direction. He then considered a more generalised model where the stretching (pure-strain) is oblique to the 'mean α-axis' (cf. Sanderson 1973, p.56).

During deformation, fold axes should have their lengths altered and axes rotated towards the X-direction of the strain ellipsoid. This change in length may be important because it will determine the probability of an axis being sampled. However, no actual measurements of fold axes lengths are normally made during the field routine, and from the practical point of view this factor presents some problems, as will be shown later.

Sanderson (1973, p.62, eg.10) derived an expression for his model involving stretching oblique to the mean of the original distribution of fold axes:

$$Y_\theta = \frac{N}{\sigma\sqrt{2\pi}} \exp\left\{-\tfrac{1}{2}\left[\frac{90-\theta}{\sigma}\right]^2\right\} \frac{[(X/Y)^2 \cdot \cos^2(\theta-\phi)+\sin^2(\theta-\phi)]^{3/2}}{X/Y}$$

[3-1]

where N is the population size, σ is the standard deviation from the mean fold axis ϕ, which is the angular distance from the Y-axis of the strain ellipsoid. θ_i is the angle between the i-fold axis and the X-strain axis.

Using the Sanderson technique, structural data are collected in the field according to criteria of homogeneity (cf.Turner and Weiss 1963) and fold generation. The reference frame (ie the XY-plane of the strain ellipsoid) is obtained for cases where poles of well defined (ie single) maximum of planar fabric define the mean axial plane (XY) while the X-direction is given by the maximum of the stretching direction lineations. A series of planes regularly spaced and orthogonal to the XY-plane is used to divide (and group) the population of fold axes into different class intervals, forming thus a frequency histogram.

The assessment of the unknown parameters ϕ, θ and the X/Y ratio is made, according to Sanderson's technique, by computing a series of distribution diagrams and then choosing the one with the closest correspondence with the frequency histogram (cf Roberts and Sanderson 1974).

3.3-a The Model Used in this Study

Experience gained during the early strain calculations using Sanderson's (1973) technique showed it to be very lengthy and CPU-time consuming. There were two solutions for this problem: (i) to try a more efficient method for parameter calculation, and/or (ii) to derive a more simplified model. Both solutions were tried here. The former is discussed in section 3.4, the latter is the object of the present section.

A model similar to that of Sanderson (1973) was devised. The basic idea developed from observations of what happened to data grouped in frequency histograms, subjected to a pure shear transformation (see figs. 3-1-a and b). It was seen that there was a change in the shape of the transformed histogram (fig. 3-1-b) but no alteration

Figure 3.1-a. See text for explanation.

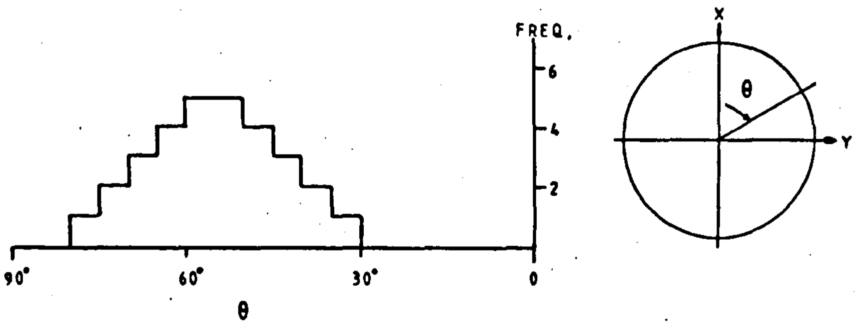

Figure 3.1-b. See text for explanation.

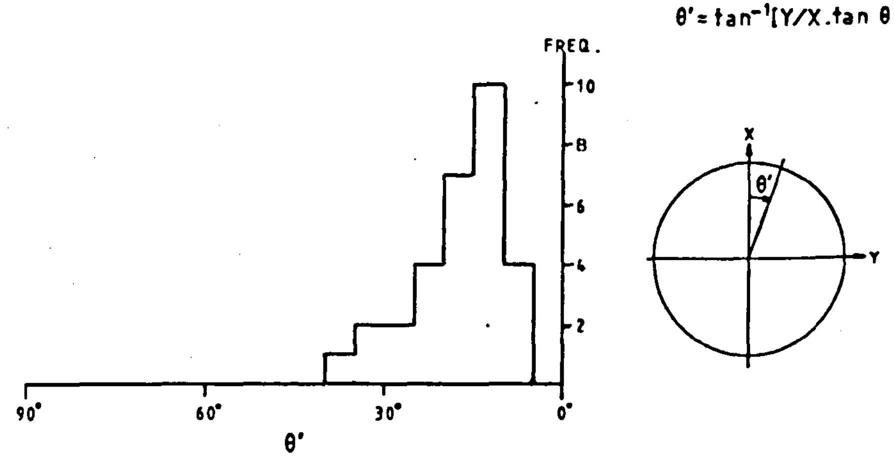

Figure 3.2-a. See text for explanation.

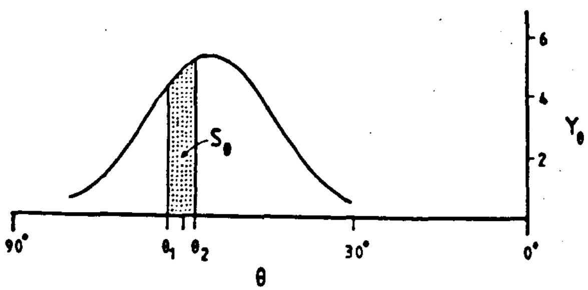

Figure 3.2-b. See text for explanation

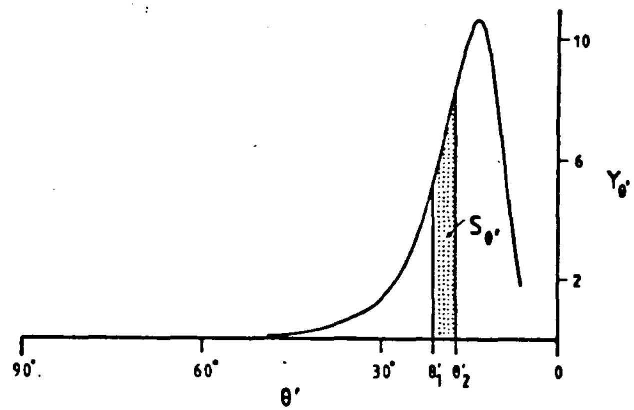

in the original area.

If instead of a histogram we deal directly with the best fitted curve $Y = f(\theta)$ (see fig. 3-2-a and b) it is reasonable to expect the same sort of shape change. Let a sector S_θ, under such a curve, be determined by its abscissae values θ_1 and θ_2. There will be a corresponding sector $S_{\theta'}$ in the transformed curve, and by simply asking for the area in the new sector S_θ to be the same as $S_{\theta'}$ we come across with a trivial problem of finding areas under a curve.

$$S_\theta = Y_\theta \cdot (\theta_1 - \theta_2) \quad \text{and} \quad S_{\theta'} = Y_{\theta'} (\theta_1' - \theta_2')$$

and

$$S_\theta = Y_\theta \ (\theta_1 - \theta_2) = Y_{\theta'} \ (\theta_1' - \theta_2') = S_{\theta'} \qquad [3\text{-}2]$$

By making $\Delta_\theta = \theta_1 - \theta_2$ and $\Delta_{\theta'} = \theta_1' - \theta_2'$ and substituting these in [3-2] we get $Y_\theta \ . \ \Delta\theta = Y_{\theta'} \ . \ \Delta_{\theta'}$

Hence

$$Y_{\theta'} = Y_\theta \ \frac{1}{\Delta_{\theta'}/\Delta_\theta} \qquad [3\text{-}3]$$

By taking the limit when $\Delta_\theta \to 0$

$$\lim_{\Delta_\theta \to 0} \frac{\Delta\theta'}{\Delta_\theta} = \frac{d[\theta']}{d\theta} \qquad [3\text{-}4]$$

which substitutes in [3-3] giving

$$Y_{\theta'} = Y_\theta \ \frac{1}{d[\theta']/d\theta} \qquad [3\text{-}5]$$

Equation [3-5] gives the height of the ordinate in the transformed curve, in the condition of no area change.

By taking the derivative $d[\theta']/d\theta$ where θ' is given by the well known strain transformation (Ramsay 1967)

$$\theta' = \tan^{-1}[\tan\theta/R] \qquad [3\text{-}6]$$

where R corresponds to the X/Y ratio of the finite strain ellipsoid, then

$$Y_{\theta'} = Y_{\theta} \cdot \frac{1 + \cos^2\theta(R-1)}{R} \qquad [3\text{-}7]$$

The final step is the choice of the initial curve $Y = f(\theta)$ which gave the ordinate Y_θ in the fig. 3-2-a. As the specific model assumes a population of fold axes initially formed with a symmetric distribution. This may be expressed by the Gaussian function:

$$Y_{\theta'} = \frac{N.\ell}{\sigma\sqrt{2\pi}} \exp\left[-\tfrac{1}{2}\left[\frac{\theta-\mu}{\sigma}\right]^2\right] \qquad [3\text{-}8]$$

where N = population size

ℓ = histogram class interval

σ = standard deviation about the original mean

μ = the original mean direction (measured from the X-axis).

The rest of the elements are as defined previously.

Remembering that $\theta = \tan^{-1}[\tan\theta'.R]$

and substituting [3-9], [3-8] in [3-7], we can get

$$Y_{\theta}' = \frac{N.\ell}{\sigma\sqrt{2\pi}} \exp\left[-\tfrac{1}{2}\left[\frac{\tan^{-1}(R.\ \tan\theta')-\mu}{\sigma}\right]^2\right] . \frac{1 + \cos^2\left[\tan^{-1}(R.\ \tan\theta')\right](R^2-1)}{R} \qquad [3\text{-}10]$$

Equation [3-10] produces some different results from that of [3-1] and for this reason both models were here used in parallel, with the same input data. Sanderson's (1973) model will thereafter be simply termed Mod. I,while the variation just derived will be referred to as Mod. II.

3.3-b Method of Parameter Estimation

It is appropriate to describe some of the difficulties faced during the course of this investigation. Firstly it is necessary to define the problems associated with the calculations using the described models. It is clear that we are dealing with a histogram to which an appropriate curve should give a fair representation of it (it applies for both Mod I and II). A statistical population is a representation concept that an individual can take in terms of probabilities, while a histogram is a concrete realisation of the variation in the sample in question. The shape of the histogram is dependent on the particular set of finite observations, but to some extent it should reflect the main characteristics of the universe sampled. Secondly, the choice of the shape of the curve that fits (or represents) a particular histogram is perhaps not unique but it should fulfil all the necessary conditions of the model. Thus there are two aspects which we need to consider in this section:

(i) A model which is expressed by a mathematical relation, and

(ii) A technique which makes possible the parameter estimation.

These two aspects are completely independent since there could be more than one particular method for parameter estimation. A problem envisaged here is one of curve-fitting to frequency histograms, with the added difficulty that such a histogram is generally skewed.

The models, Mod I and Mod II, are expressed by simple equations containing three unknowns. The curve-fitting may be done by a method that iteratively estimates the values of the unknowns. An iterative solution is the one which tends towards the Optimum (ie a Minimum or a Maximum, it depends on the sign) by successive approximations. In general, it requires an initial guess, or a starting point x_o, and then proceeds by generating a sequence of points $x_{i,j}$; $i = 1,2, \ldots m$, $j = 1,2, \ldots n$, according to information gained previously.

Figure 3-3 illustrates an hypothetical iterative path towards the Optimum where progress is made in the direction of movement d_J according to the iterative rule:

$$x_{i,j+1} = x_{i,j} + d_{i,j} \qquad [3\text{-}11]$$

3.4 Optimization Procedures

In this section we describe the techniques that were used with both Mod I and Mod II. Section 3.4.3 applies only to Mod II.

3.4.1 The Objective Function

As described before, Roberts and Sanderson (1974) handled the parameter estimation by the computation of a series of distribution diagrams from which they chose the one with the closest correspondence to the frequency histogram. There is apparently no indication on how the choice was made and for this reason, it is interpreted here that such a choice was performed by visual means rather than by a mathematical mode.

Initially in this study, data were treated by this visual method but it was considered that manual process of plotting diagrams for visual comparison was too ambiguous, not safe and above all, very laborious. It was felt that there should be a mathematical algorithm for this choice of parameters, as human judgement alone is often unable to optimize systems with only three variables (see Adby et al, 1974). (Optimize means finding the best solution or the closest correspondence).

The first step in the search for an optimization method in the present case, is to create the mathematical condition of 'choice' and this means that we need to find the correspondence between a curve and the histogram , that is to say, we find the best possible approximation

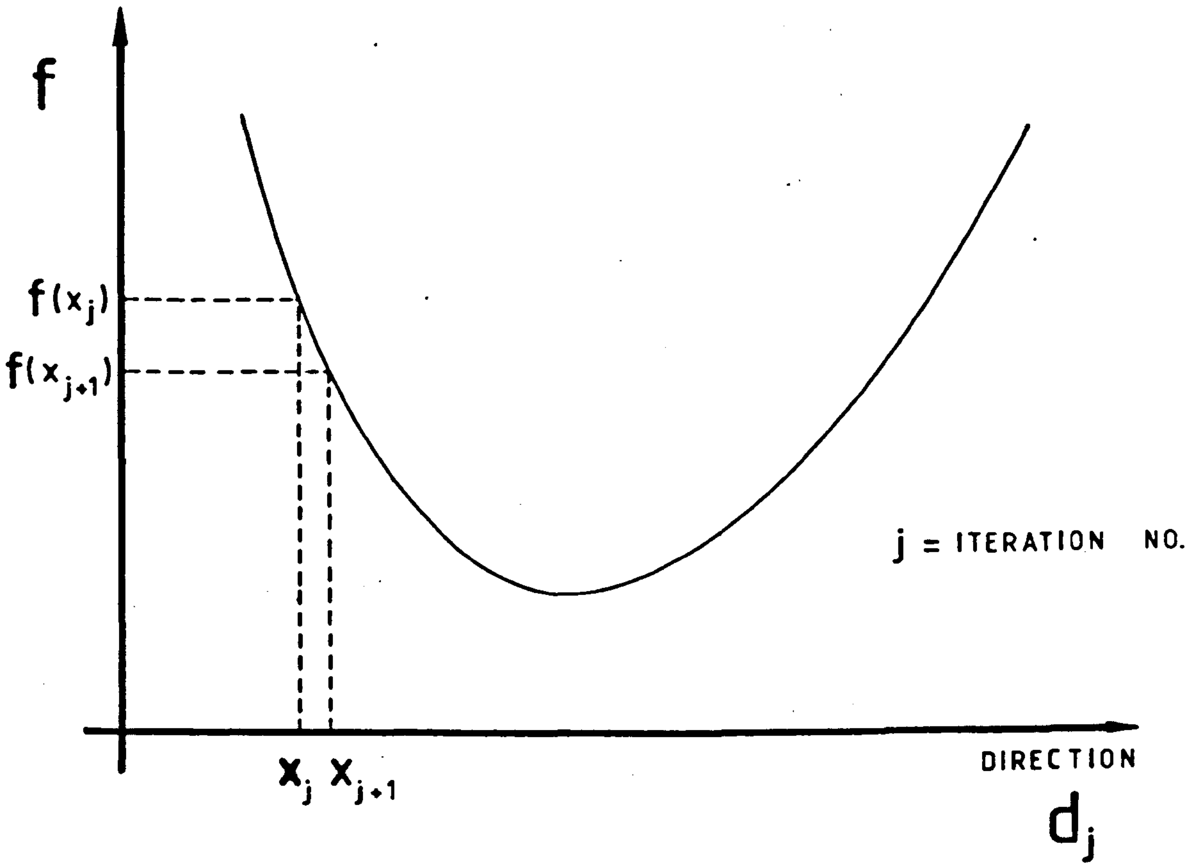

Figure 3.3

Hypothetical iterative path towards the optimum where progress is made in the direction of movement d_j.

or the one which produces the smallest error. This error could simply mean a condition such as:

$$\text{Error} = |f(x_0) - g(x_o)| \qquad [3\text{-}12]$$

which is true for the case of deviation between f and g at the point x_o. However the problem here concerns an approximation over an entire interval - say a, b - and not a single point. Intuitively the simplest method is to choose the approximation g(x) with the least overall error satisfying the condition:

$$\text{Error} = \int_a^b |f(x) - g(x)|dx \qquad [3\text{-}13]$$

While [3-13] is the straightforward theoretical condition, for practical purposes (ie numerical procedures) the following algorithm is widely used:

$$\text{Error} = \sum_{i=1}^{n}[f(x_i) - g(x_i)]^2 \qquad [3\text{-}14]$$

Thus the application of the above condition [3-14] to the present problem means that the closest approximation is the one which produces the least error between an i-fitted curve and a given histogram. Relation [3-14] can also be called the OBJECTIVE FUNCTION and is expressed here as:

$$Z_{min} = \sum_{k=1}^{n}[Y(\theta')k - Ht(\theta')k]^2 \qquad [3\text{-}15]$$

where $Y(\theta')_k = f(x_i|\theta'_i)_k$ or more simply Y_k and Ht_k are respectively the ordinates of the fitted curve and the heights of the histogram columns for k-class intervals.

Methods of finding the minimum (or maximum) of a function of n-variables have been devised (see Dixon, 1972) that involve:

(i) only the function and variable values themselves

(ii) only the first partial derivatives

(iii) the first and second partial derivatives.

There are many factors to be considered in each problem and these can make one of the above methods more convenient than the others. This study initially applied the first of the above 3 methods, for both Mod I and Mod II. This method constitutes the Direct Search Method and will be described in section 3.4.2. For reasons to be explained later it was decided also to make use of the second and third methods (1st and 2nd derivatives) with Mod II and these constitute the Gradient Method which is described in section 3.4.3.

These methods of Optimization are only beginning to find applications in Structural Geology. It is hoped that the following discussion of the different methods will be of use not only in work on strain analysis but also in other branches of geology.

3.4.2 The Direct Search Method

3.4.2-a Introduction

The 'simplest' technique of finding the Optimum value of a function f(x) of n-variables, x, all bounded between an upper and lower interval would be to divide the entire range of each x_i into a set of r_i grid points and then evaluate f(x) at each of the $\Pi_{i=1}^{n} r_i$ combinations of variables x lying on the grid.

This was the initial idea in this study. However it was not carried out, as the appropriate grid requires a large number of combinations and this makes the particular method prohibitive. Consider for instance the situation where it is required to search for the maximum of the present objective function [3-15] using different values for the Mod II parameters μ, σ and R, in a grid defined by successive increments of 0.1, in the following range (also referred to as upper and lower bounds):

(i) The mean-μ in the range between 45° and 135° in increments of 0.1°, comprising exactly 900 different values.

(ii) For the standard deviation,σ in the limited range between 1° and 31°, in increments of 0.1°, comprising 300 different values.

(iii) The parameter, R in the range between 1 and 21 at 0.1 increments comprising 200 values.

Thus, constraining the search to the above limits will require a number of combinations; 900 x 300 x 200,that is,equal to 54×10^{6}. Such a solution is clearly out of the question. However it is possible to overcome this difficulty by changing the search mode and this is the aim of the next section.

3.4.2-b The Multivariate Constained Method

Direct Search Methods are usually the initial step in an Optimization investigation and preferable especially for cases where the exact behaviour of the function is not known (see Beveridge, 1970). For cases where it is suspected that the function is non-unimodal, there is a chance for the solution to converge to a local optimum rather than the global one. This situation is illustrated geometrically in fig. 3-4.

Text books on Optimization techniques describe several Direct-Search-Methods, but the one to be described here has no particular name simply because it was intuitively developed, directly from

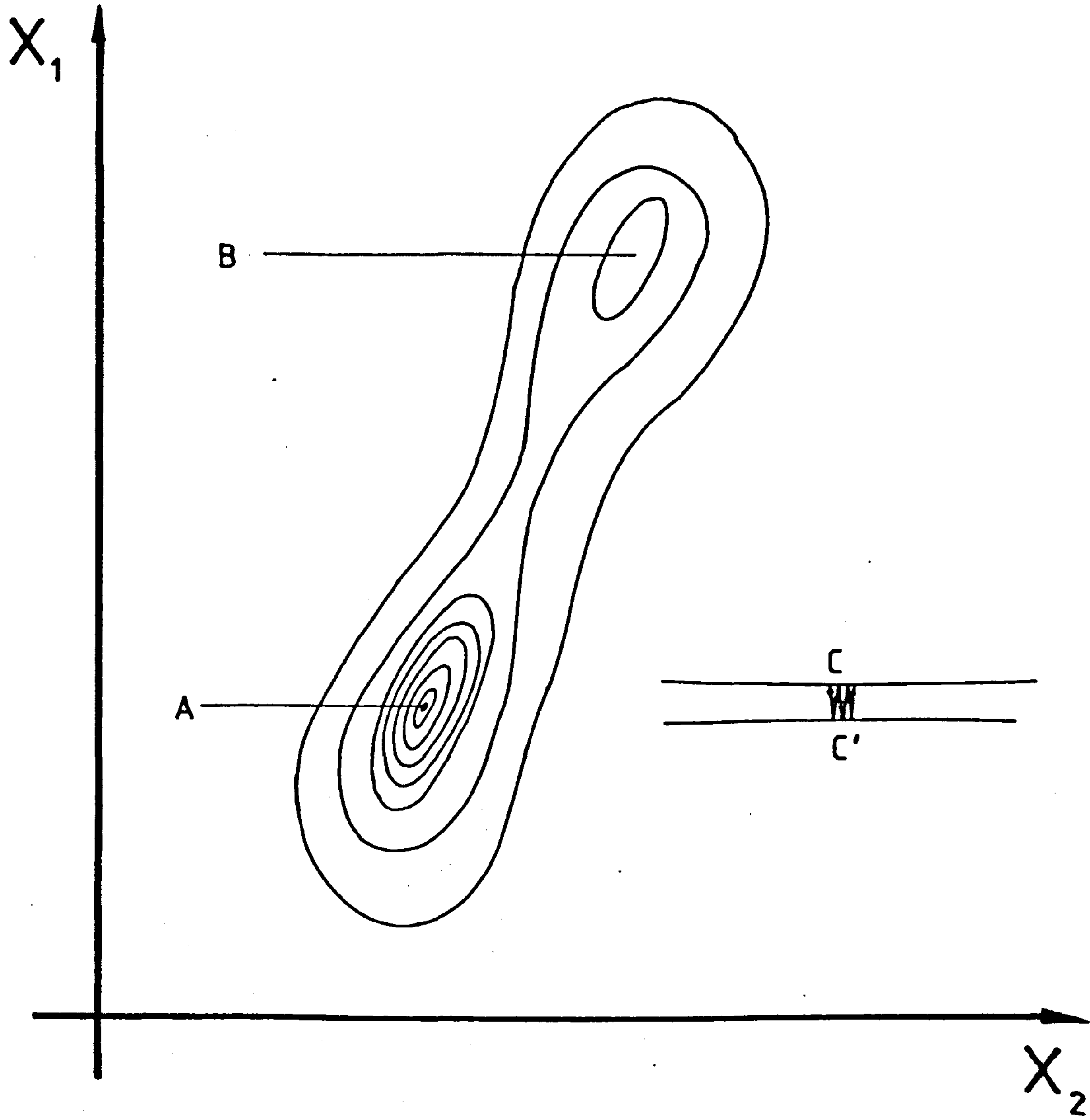

Figure 3.4. Hypothetical representation of a function. A, B, C and C' are points which satisfy the equation

$$\frac{\partial f}{\partial x_i} = 0$$

A is the Global Optimum, B is the Local Optimum, C and C' represent points along a narrow valley (Saddle Point). The arrows (in CC') show the gradient direction of movement, orthogonal to the contours. Notice that progress along this region is minimal.

the situation just described in 3.4.2-a.

Consider the initial situation, as set in 3.4.2-a, where there are 3 parameters in the range limited by their upper and lower boundaries. Now, suppose that we start the search for the least error using initially a much coarser grid of increments (say 10, instead of 0.1) and then reduce the size of this increment substantially as we move towards the Optimum. This would eliminate most of the unnecessary operations of the situation described in 3.4.2-a.

This method is in essence an interval elimination routine, where the region, in which the Optimum lies, is sequentially reduced by the search procedure. The next section examines this method in more detail.

3.4.2-c Description and Routine

The problem consists of minimizing the Objective Function set up by [3-15].

$$Z_{min} = \sum_{k=1}^{n}[Y_{(\theta')k} - Ht_{(\theta')k}]^2 \quad , \; k = \text{class interval number},$$

here taken as 1 to 18, and $Y_{(\theta')k} = f(x_{ij}\ ,\ \theta'_{kj})$; subject to the inequality constraints $a_{1j} < x_{1j} < b_{1j}$, for $i = 1,2,3$, or $x_{1j} = \mu_j$, $x_{2j} = \sigma_j$ and $x_{3j} = R_j$ and θ'_{kj} = mid point of the k class interval. a_{1j} and b_{1j} are respectively the lower and upper bounds of the (j) cycle of combinations.

The search for the minimum [3-15] is carried out by the elimination of intervals and if this routine is the only method of Minimization, the interval, in which the Optimum value of the function occurs, is subsequently reduced to some final figure, the magnitude of which depends on the desired accuracy. Thus the desired accuracy will determine the number of function evaluations and consequently the consumed processor time.

For reasons that will be apparent later, this routine initiates the search covering a broad range of intervals which need not be the same in number or in magnitude, for each variable. The algorithm proceeds as follows:

(i) Determine the initial search interval for each variable x_i, with boundaries a_i and b_i.

(ii) Set the initial sum of squared differences to a very large number, much larger (eg 10^{20}) than any possible value that the Objective Function [3-15] can take.

(iii) Evaluate the Objective function at x_{ij} compare the sum of squared differences (with the previous Optimum). Store the best value (here the minimum) as the temporary Optimum and save the corresponding parameters x_{ij}, as $x_{i,best}$.

The routine proceeds through the whole specified interval and then comes to a decision:

- If the programme is used alone, at the end of the first of the j cycles of iterations, new boundaries $a_{i,j+1}$ and $b_{i,j+1}$ are assigned in a new range covering a large proportion of the previous interval (see fig. 3.5). In general these are arranged half symmetrically around each $x_{i,best}$. As the number of intervals remain as defined initially, their length will be sequentially reduced in each cycle. The routine ends at the specified number of cycles.

- Alternatively, we can make use of another method to finalize the

Figure 3.5. It illustrates schematically the search for the mean (μ). At every cycle-i ($i = 1,2 \ldots n$) a length I_i is searched in intervals Δ_i. Both the length I_i and the interval Δ_i are sequentially reduced in each iteration. Notice the magnitudes of I_{13} and Δ_{13}. M_i are the optima of each iteration.

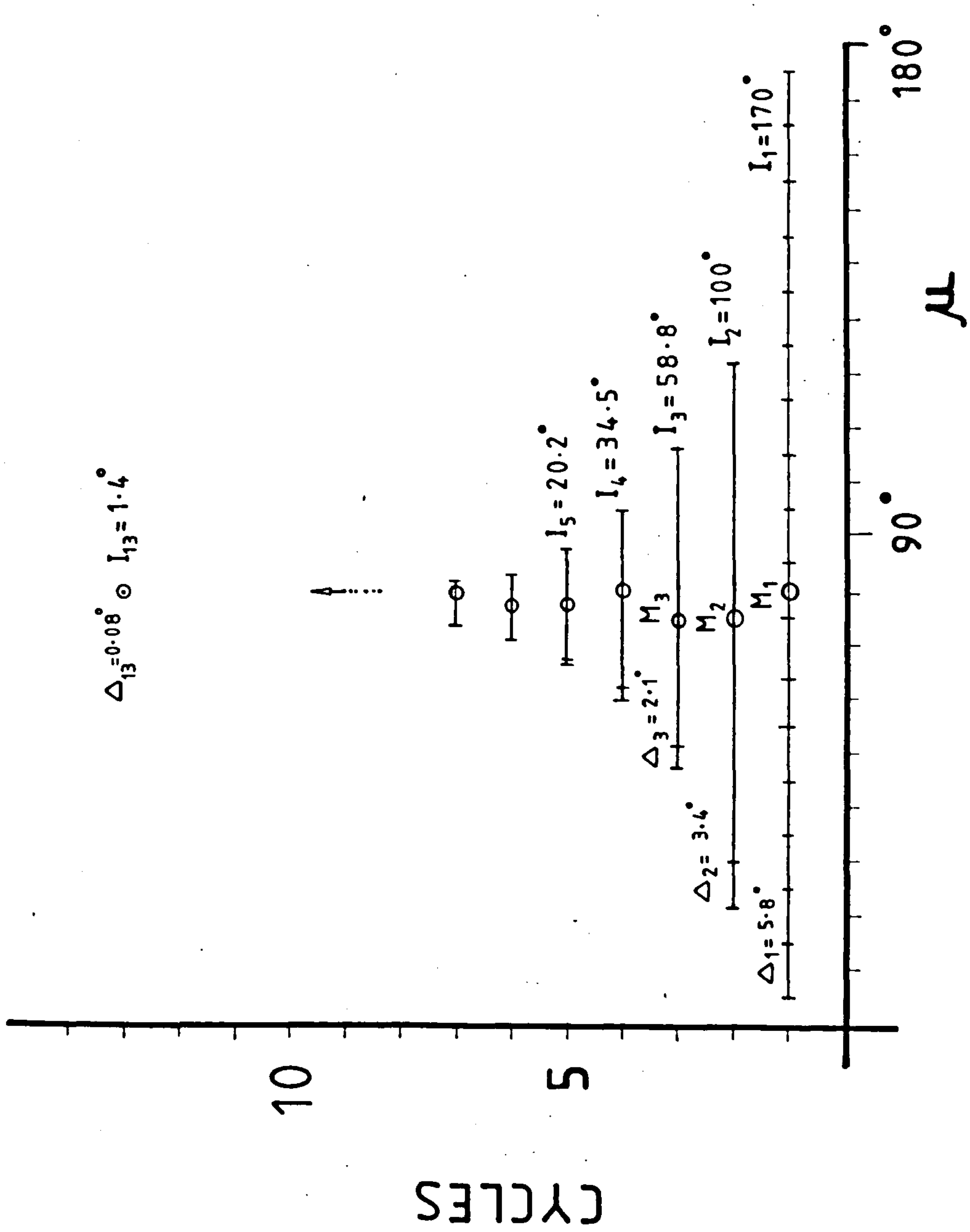

minimization. This method and the reasons for its choice are explained in the next section.

3.4.3 Unconstrained Gradient Methods

3.4.3-a General

The Gradient Methods are based on the Taylor expansion series with terms involving first and second derivatives (higher orders are neglected). Optimization methods which neglect the second derivatives are termed first order methods while those using first and second derivatives are termed here second order methods (see Adby and Dempster, 1974).

According to the objective function, the required derivatives can be obtained either analytically or numerically. In the present study,use was made of the second order method in which the first derivatives were taken analytically while the second ones were derived numerically.

There are, however, situations where analytical derivatives are not possible to obtain (or not worth obtaining) so numerical estimates must be used instead. The efficiency in these cases can be seriously compromised because of the errors introduced in the computations (see Box, Davies and Swann 1969).

The Gradient Direction at any point is the direction whose components are proportional to the first partial derivatives of the objective function at the point in question (see Wismer and Chattergy, 1978, p.139).

This method is distinguished from the Direct Search technique in three fundamental ways: (i) it selects the direction of search, (ii) it optimizes the step length of movement in the chosen direction of search, and (iii) there are no boundary constraints, so the search is free to take any appropriate value. This method also profits by information gained from earlier iterations. For full details on the method and its innumerable variations see: Box et al. (1969), Beveridge and Schechter (1970), Dixon (1972), Adby and Dempster (1974), Wismer and Chattergy (1978).

The algorithm is perhaps best illustrated using fig. 3-3 in which we could introduce a variation, or update the concept expressed in [3-11] by writing instead

$$x_{i,j+1} = x_{i,j} + h_j d_{i,j} \qquad [3\text{-}16]$$

where h_j is the length of movement in the d_i direction.

Figures 3-6 and 3-7 illustrate the geometry of the gradient path towards the optimum region in two hypothetical cases. It can be observed that the process is initiated at points $x_{i,o}$ and subsequent movement is orthogonal to the contours.

3.4.3-b Description and Routine

The method consists of determining the partial derivatives of the objective function [3-15] in order to establish the gradient direction as follows:

$$\frac{\partial Z}{\partial x_i} = \sum_{k=1}^{n} [Y_{(\theta')k} - Ht_{(\theta')k}]^2 = 2\sum_{k=1}^{n} [(Y_{(\theta')k} - Ht_{(\theta')k} \cdot \frac{\partial Y_{(\theta')k}}{\partial x_i}] \qquad [3\text{-}17]$$

k = 1,2, ... n, are numbered of class intervals and i = 1,2,3 as defined already.

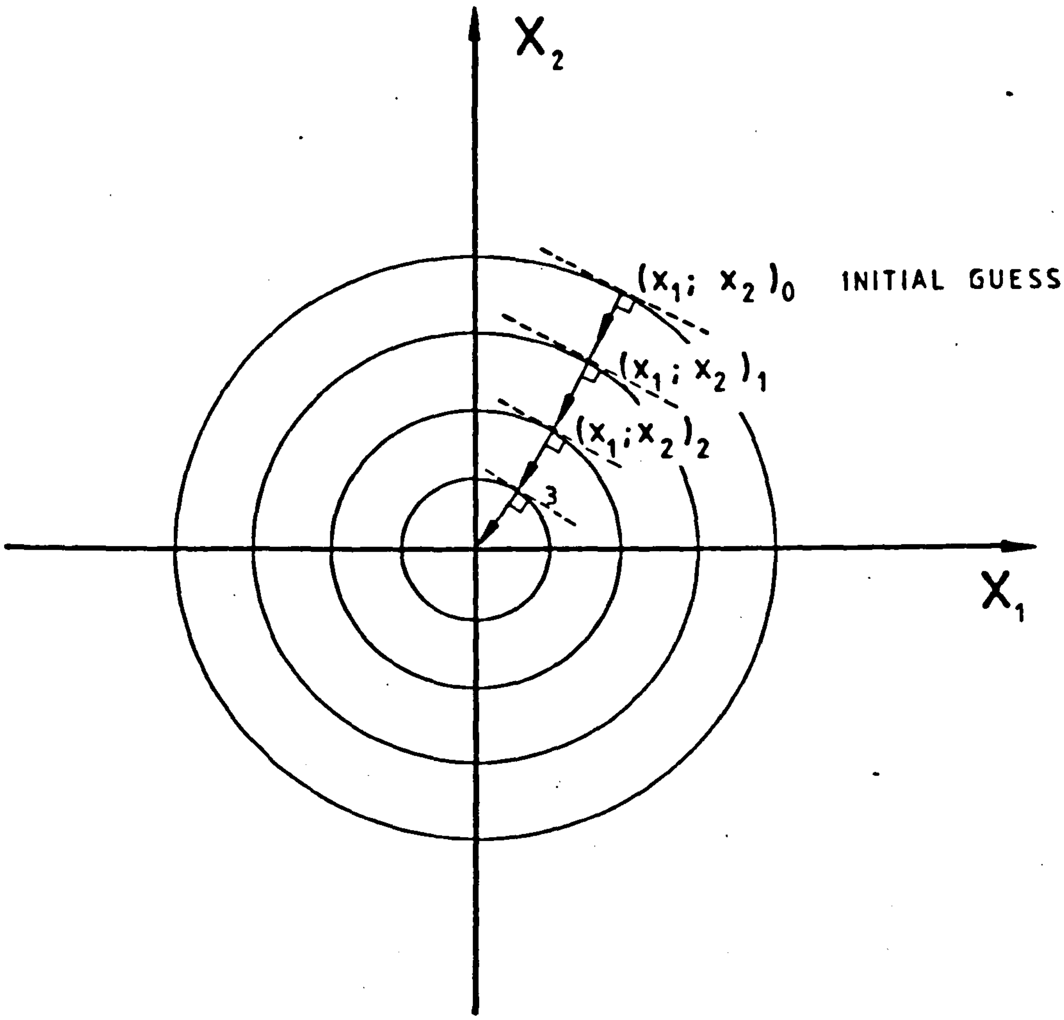

Figure 3.6. Graph illustrating the gradient path, towards the optimum, starting from an initial guess $(x_1)_o$. The contours approximate to a quadratic function. Notice that the hypothetical steps (1-4) are in a direction orthogonal to each contour.

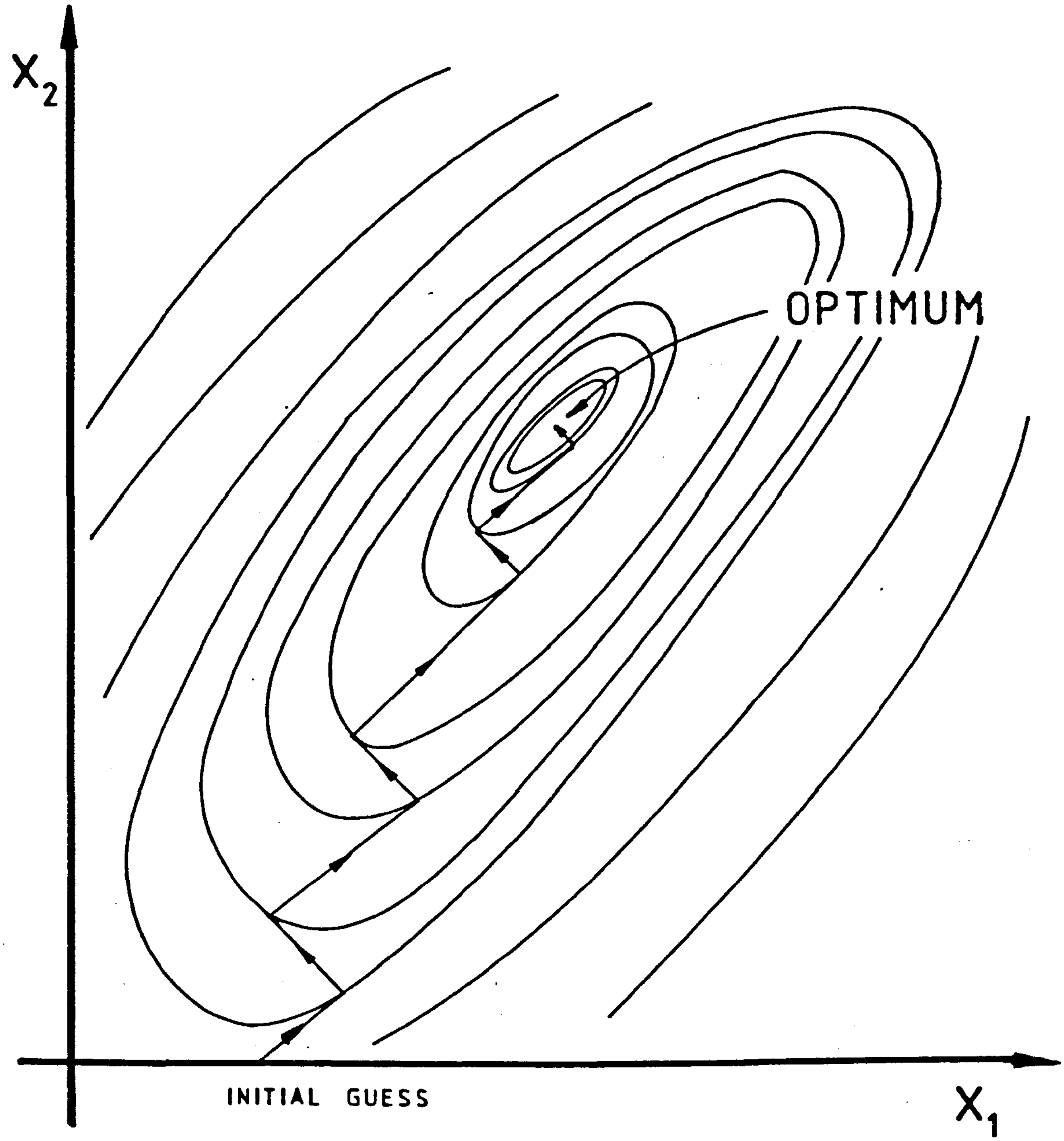

Figure 3.7. This illustrates an hypothetical situation for the gradient path where the contours are elliptical. Notice that the steps are orthogonal to each contour.

The normalized Gradient Vector at the current point, or iteration L, is defined as:

$$g_{i,L} = \frac{\frac{\partial Z}{\partial xi}}{\left[\sum_{i=1}^{n} \left(\frac{\partial Z}{\partial x_i}\right)^2\right]^{\frac{1}{2}}} \qquad [3\text{-}18]$$

If conditions are such that only the first derivatives are required, then all elements necessary to the routine are met here and the method is called Steepest Descent (see Box et al. 1969) or First Order Method (cf Adby and Dempster, 1974), or condition number two, in section 3.4.1. The algorithm proceeds as follows:

i) Set the Optimum value to a very large number, for the reasons already explained in (ii) of section 2.4.2-c.

ii) Input the so called initial 'guesses' $x_{i,o}$, for each variable and set the value of the function as the new optimum.

iii) Calculate the components of the Gradient vector $g_{i,L}$ using [3-17] and [3-18].

iv) Generate new points $x_{i,L+1}$ according to the iterative rule

$$x_{i,L+1} = x_{i,L} - h_L \cdot g_{i,L} \qquad [3\text{-}19]$$

which is an updated version of the general expression [3-16], where h_L is the appropriate step length for the L iteration, and is found by a direct search procedure using the following algorithm.

$$h_L = h_{L-i} + \frac{\Delta h}{p} \qquad [3\text{-}20]$$

where p = constant (it can be any number, here it was equal to 10.0).

v) The objective function is then compared with the previous (stored) value, subject to a convergence limit

$$\left| Z_L - Z_{L-1} \right| \leqslant \text{Limit} \qquad [3\text{-}21]$$

where Limit is the desired accuracy of search, and fixed _a priori_ in the Programme. The actual value of Limit is determined empirically according to the formulated problem. In the present case Limit is dependent on the type of frequency histogram. For cases of relative frequency, Limit amounts to a lower figure than for cases of absolute frequency.

If the condition [3-21] is satisfied, the procedure stops. Otherwise store new parameters as the Optimum values and the process returns to step number three. However, if conditions are such that progress can be made using the Second Order Method (the programme tests it), the algorithm of [3-19] changes (once more) by the inclusion of the second partial derivatives:-

$$H_{iJ} = \frac{\partial^2 Z}{\partial x_i \partial x_J} \qquad \text{for } i,j = 1,2,3, \qquad [3\text{-}22]$$

and remembering that $\dfrac{\partial^2 Z}{\partial x_i \partial x_j} = \dfrac{\partial^2 Z}{\partial x_j \partial x_i}$ [3-23]

The matrix formed by elements

$$[H_{ij}] = \begin{bmatrix} \partial^2 Z/\partial x_1^2 & \partial^2 Z/\partial x_1 \partial x_2 & \partial^2 Z/\partial x_1 \partial x_3 \\ \partial^2 Z/\partial x_2 \partial x_1 & \partial^2 Z/\partial x_2^2 & \partial^2 Z/\partial x_2 \partial x_3 \\ \partial^2 Z/\partial x_3 \partial x_4 & \partial^2 Z/\partial x_3 \partial x_2 & \partial^2 Z/\partial x_3^2 \end{bmatrix} \qquad [3\text{-}24]$$

is referred to as the Hessian Matrix and the method which makes use of it, is frequently referred to as Newton's Method (Box et al 1969) or as the Second Order Method (Adby and Dempster, 1974).

The basic algorithm proceeds as follows:

i), ii) and iii) - Same as for the Steepest Descent Method

iv) Define the Hessian Matrix $[H_{ij}]_L$ of [3-24] bearing in mind [3-23] for programme economy. Find the inverse $[H]_L^{-1}$ of the Hessian Matrix.

v) Generate new points $x_{i,L+1}$, according to the iterative rule:

$$x_{i,L+1} = x_{i,L} - h_L \, [H]_L^{-1} \, g_{i,L} \qquad [3\text{-}25]$$

where h_L is as defined before in [3-20].

vi) Same as (v) for the Steepest Descent Method.

The flow chart of fig. 4-5 (Chapter 4) illustrates the Newton-Raphson Routine, which in essence is the basis of Newton's Method just described here.

3.4.3-c Preliminary Comments

It seems advisable at this stage to comment on the methods described above:

a. Second Order or Newton's Method: This method has some drawbacks and cannot always be used. The advantages will be listed later in the discussion, whereas in the present section we are directly concerned with the disadvantages, these are:

(i) The matrix of the second derivatives must be evaluated at each iteration, either by analytical differentiation or by numerical techniques. If processor time is not in consideration, then this is a minimum disadvantage. In the case of second derivatives found by a numerical method, the round off errors or the approximation errors normally affect the efficiency of the technique, especially if f(x) is small.

ii) There is a subsequent matrix inversion operation. Again if processor time is not the main concern, then this is a minor disadvantage.

iii) Caution must be taken because if $[H_{ij}]$ is singular, the inversion is impossible. Return to Steep Discent if it happens.

iv) Progress towards the Minimum is only ensured if $[H_{ij}]$ is Positive Definite.

The method is particularly useful (or ideal) for cases when the Objective Function is Quadratic, so the Minimum can be reached in a single iteration (see Wismer and Chattergy, 1978, p.51). However even with functions not truly quadratic, but near the Optimum region, the method can still particularly be useful, as in the neighbourhood of the Optimum most objective functions behave near quadratically. Otherwise if conditions are adverse,the direction $- h_L[H]_L^{-1} \cdot g_{iL}$ is unhelpfull and the Steepest Descent Method is then preferable.

Thus, what are the advantages or reasons for persisting in using this method? The answer to this is simply that if conditions can be arranged for this method to be operative, it will prove far superior not only in convergence rate (ie time involved) but will also give an accuracy unmatched by the Direct Search Method.

b. Steepest Descent or First Order Method - This work has made an extensive use of this routine. Although progress towards the Optimum proved to be continuous, the pace was too slow to an extent that the method was considered inefficient if used alone. For this reason the change was made towards Newton's Method.

There are some variants of the Steepest Descent technique which can produce good results. One variant consists of scaling the variables x_i (see Box et al, 1969, p.36) so the net effect is to transform the contours shown in fig. 3-4 to become more circular (ie quadratic) and this produces a faster convergence. With suitable scaling, ellipses can be transformed into circles and ellipsoids into spheres. Because the direction of steepest descent is orthogonal to the contours of constant function value, it follows that for circular contours the direction of steepest descent must pass through the centre of the system of circles (see fig. 3-6) that is, through the Optimum of the objective function.

The present study attempted firstly a scaling for the mean (μ) and then for both μ and σ. This was done because it was noticed that the magnitude and sign of the first derivatives changed constantly in every iteration, and this was accompanied by a very slow progress towards the optimum. This situation was interpreted as analogous to that shown in fig. 3-4 at CC'. This scaling technique worked successfully in some cases but failed in many others. The scaling of variable was thus abandoned. This unsuccessful attempt, however, does not invalidate the technique, it only means that suitable scaling was not found.

3.4.3-d The Partial Derivatives

As indicated in section 3.4.3-b the Gradient Method requires evaluation of partial derivatives of the Objective Function and their analytical expressions are listed in this section. Let initially transcribe[3-17].

$$\frac{\partial Z}{\partial x_i} = 2\sum_{k=1}^{n}\left[\left(Y_{(\theta')k} - Ht_{(\theta')k}\right)\frac{\partial Y_{(\theta')k}}{\partial x_i}\right] \quad \text{where}$$

$x_1 = \mu$, $x_2 = \sigma$ and $x_3 = R$, so:

$$\frac{\partial Y_{(\theta')k}}{\partial \mu} = \frac{N.\ell}{\sqrt{2\pi}}\,\frac{1}{\sigma}\cdot\frac{1+(R^2+1)\cos^2[\tan^{-1}(R.\tan\theta')]}{R}.\left[\frac{\tan^{-1}(R\tan\theta')-\mu}{\sigma^2}\right]\cdot$$

$$\exp\left[-\tfrac{1}{2}\left[\frac{\tan^{-1}(R\tan\theta')-\mu}{\sigma}\right]^2\right] \qquad [3\text{-}26]$$

$$\frac{\partial Y_{(\theta')k}}{\partial \sigma} = \frac{N.\ell}{\sqrt{2\pi}}.\,\frac{1+(R^2-1)\cos^2[\tan^{-1}(R.\tan\theta')]}{R}.\left[\frac{[\tan^{-1}(R.\tan\theta')-\mu]^2-\sigma^2}{\sigma^4}\right]\cdot$$

$$\exp\left[-\tfrac{1}{2}\left[\frac{\tan^{-1}(R.\tan\theta')-\mu}{\sigma}\right]^2\right] \qquad [3\text{-}27]$$

and

$$\frac{\partial Y_{(\theta')k}}{\partial R} = \frac{N.\ell}{\sqrt{2\pi}}.\,\frac{1}{\sigma}\left[\left\{\frac{1}{R}\left[2\cos^2[\tan^{-1}(R.\tan\theta')] - \frac{(R^2-1)\sin 2[\tan^{-1}(R.\tan\theta')].\tan\theta'}{1+(R.\tan\theta')^2}\right]\right.\right.$$

$$\left.-\left[\frac{1+(R^2-1)\cos^2[\tan^{-1}(R.\tan\theta')]}{R^2}\right]\right\} -$$

$$\left.\left[\frac{[\tan^{-1}(R.\tan\theta')-\mu].[1+(R^2-1)\cos^2[\tan^{-1}(R.\tan\theta')](\tan\theta')]}{\sigma^2[1+(R.\tan\theta')^2]R}\right]\right]\cdot$$

$$\exp\left[-\tfrac{1}{2}\left[\frac{\tan^{-1}(R.\tan\theta')-\mu}{\sigma}\right]^2\right] \qquad [3\text{-}28]$$

During the step number (iii) of section 3.4.3-b - in both First or Second Order Methods - equations [3-26], [3-27] and [3-28] are evaluated and substituted in [3-17] which in turn allows for the calculation of the normalized gradient vector g_{iL} given by [3-18].

If the position is favourable for the Newton Method to work, then the elements of the Hessian matrix could be set up as follows:

$$\frac{\partial^2 Z}{\partial x_i \partial x_j} = \frac{\partial^2 Z}{\partial x_j \partial x_i} \simeq 2\sum_{k=1}^{n} (Y_{(\theta')k} - Ht_{(\theta')k}) \frac{\partial^2 Y_{(\theta')k}}{\partial x_i \partial x_j} \qquad i,j = 1,2,3$$

and in terms of the higher order are neglected.

However due to the excessive length of the expressions [3-26],[3-17] and [3-28] it was decided not to try to obtain the analytical expressions of the second derivatives and instead to estimate them numerically, by a finite difference method, using the first partial derivative routines in the process, as follows:

$$\frac{\partial^2 f}{\partial x_i \partial x_j} = \frac{f'(x_j+h_j)_i - f'(x)i}{h_j} \qquad [3\text{-}29]$$

where $i,j = 1,2,3$ $\qquad f'(x)i = \frac{\partial f}{\partial x_i}$

$h_j = x_j \cdot \Delta$, and $\Delta \simeq$ small increment (eg here taken as 10^{-3}).

3.4.4 Tests

Some tests were performed in order to evaluate and compare the capabilities of the models in estimating the three parameters. One way of testing a model is to produce stochastic variables (see footnote) characterised by a statistical behaviour which parallels or simulates the actual variable. In these simulations it is necessary to combine

---

Deterministic variable is the one which contains no element of chance (eg a sine function). A Stochastic variable is that whose behaviour can be described statistically (eg Theoretical Distribution: Poisson Distribution of grain sizes etc ...).

deterministic and random components (cf Harbaugh and Boham-Carter 1970).

The technique which makes use of random numbers to simulate a sample population with determined characteristics is called a Monte Carlo simulation (see Harbaugh and Boham-Carter, 1970, p.74). Usually the routine consists of generating pseudo-random numbers forming an initially uniform distribution (or a rectangular frequency distribution) and then using these in order to obtain a random sample from a known distribution (see full details in Harbaugh and Boham-Carter, 1970, p.74).

In the present test there was a need for numbers to be drawn from a population of fold axes having a normal distribution, characterised by its mean and standard deviation.

There are many ways of generating these numbers on a computer. Some of the usual methods are known as the Congruential Methods (Harbaugh, et al. 1970). These require such small amounts of computer memory that they can be performed by modern pocket calculators. The methods vary according to the computer installation and most computer libraries include subroutines for the purpose.

In the present test, use was made of the NAG subroutine G05DD5 which can draw a random sample from a normal distribution having specified its mean and standard deviation. This population of fold axes, was subjected to the angular rotation, due to a specified strain and finally grouped into frequency histograms. These histograms constituted the input data for the early versions of programme SAND (Mod I) and MODEL2 (Mod II proposed here). Both programmes are fully listed in the Appendices.

Figure 3-8 illustrates one such simulation and the results obtained with programmes SAND and MODEL2. It can be seen that Mod I slightly underestimated the true X/Y-value, while Mod II produced an overestimation. Both models gave underestimates for the standard

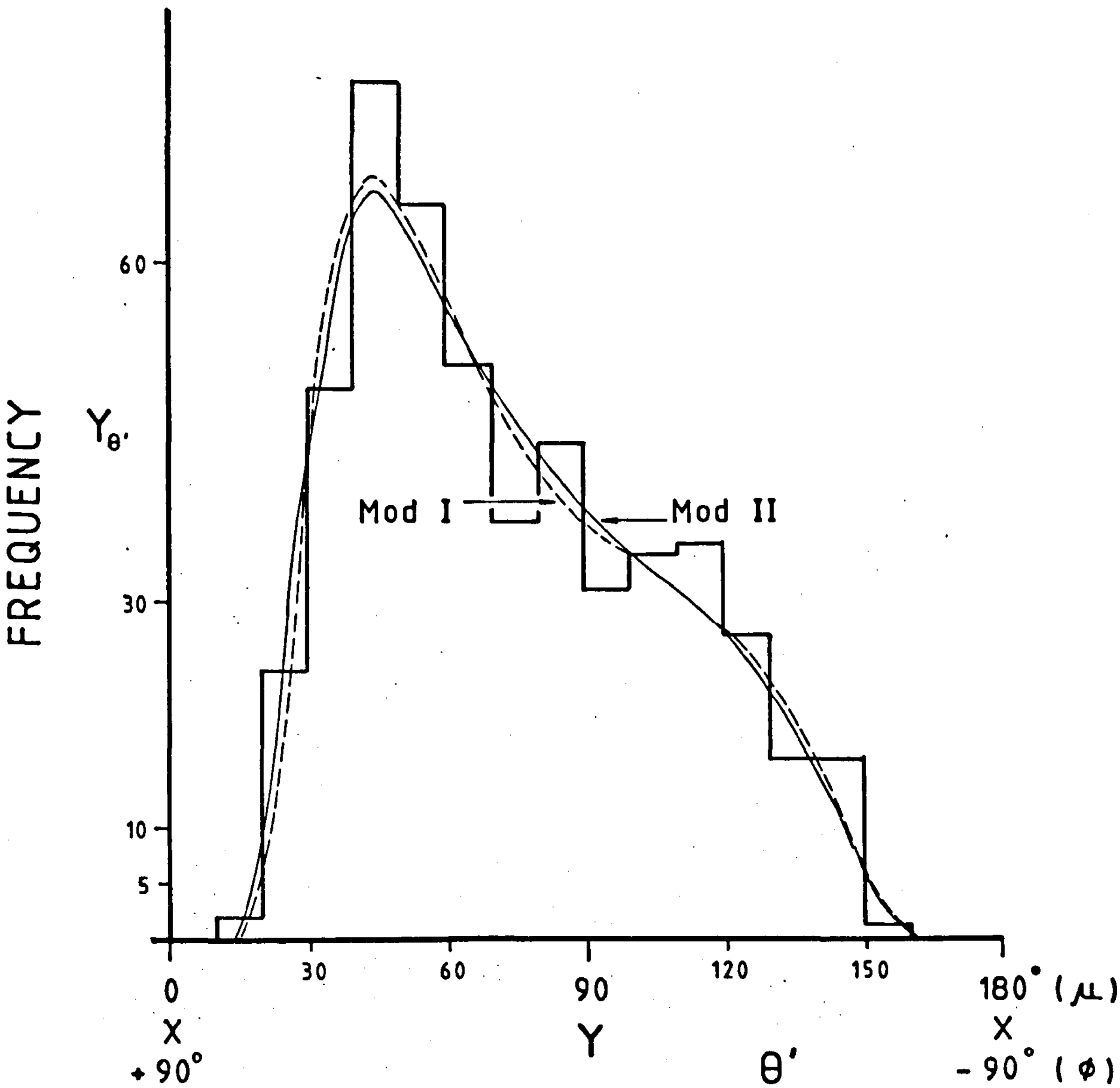

Figure 3.8. Illustrate a Monte Carlo simulation. Population of 500 axes drawn from an originally normally distributed population (μ = 85, σ = 10°).that subsequently was subjected to a pure shear transformation (R=5). The graph also shows the results for the fitted curves for both models:

- True values: μ = 85° (or ϕ = +5°), σ = 10°, R = 5
- Mod I results: ϕ = 3.96°, σ = 9.01°, R = 4.444
- Mod II results: μ = 85.84°, σ = 8.12°, R = 5.510

deviations, Mod II gave a closer estimation of the mean.

Although these results are similar and not unreasonable, the methods used and the programme versions were far from efficient. For instance, the parameter estimation of Mod II required 180 secs of CPU-time while for Mod I to perform the same operation it required three times (CPU) this. However different and independent aspects were being treated at the time: (i) the two models, (ii) the method of estimation, and finally (iii) the two computer programmes which were constantly changed, due to experience gained with both models and methods.

Both programmes (SAND and MODEL2), have the same structure and the differences (both in estimates and CPU-time) stem from the fact that Mod I includes in its equation a sampling-factor (see Sanderson, 1973, pp.57-58) which alters the area of the curve to be fitted. Consequently at every curve fitting, normalization is required and this implies a numerical integration and other additional operations that are non-existent in the simpler formulation of Mod II. This normalization operation, done by summing frequencies, can give innaccurate results, especially with high strains (Sanderson, 1977, pers comm.). For these reasons it was decided to make use of Mod II thereafter.

Another type of test was sought and this gave a measure of the programme capability to converge to the right solution. This type of test - a convergence or curve fitting test - was carried out by generating a series of theoretical curves, simply by inputing different values of σ, μ and R in expression [3-11] and then submitting the ordinates to the available programme and verifying if the estimated $\bar{\mu}$, $\bar{\sigma}$ and $\bar{R}$ values departed from the true ones. Table [3-1] lists five of these trials using a Direct Search Method for Mod II.

Table 3.1

Params. True Values	TRIAL No.	BOUNDARIES OF SEARCH — INPUT						No. of CYCLES	RESULTS — ESTIMATES				TOTAL CPU TIME (SECS)
		μ Lower	$\Delta\mu$	σ Lower	$\Delta\sigma$	R Lower	ΔR		$\bar{\mu}$	$\bar{\sigma}$	$\bar{R}$	Minimized Error or Final Value of The Least Sum of Squared Diffs.	
$\mu = 75$	A	5-175	10	1-76	15	1-16	3	17	74.783	10.054	4.947	0.02234045	129
$\sigma = 10$	B	5-175	10	1-51	10	1-16	3	17	74.837	10.096	4.942	0.01355647	129
$R = 5$	C	5-175	10	5-55	10	2.5-17.5	3	17	75.666	9.666	5.225	0.07364522	129
$\mu = 85$	A	5-175	10	1-51	10	1-16	3	17	85.527	9.046	5.555	0.63703251	129
$\sigma = 10$	B	5-175	10	5-55	10	2.5-17.5	3	17	84.286	11.330	4.404	0.651433952	120
$R = 5$													
$\mu = 95.5$	A	5-175	10	5-55	10	1-16	3	17	95.967	24.505	2.112	0.0201466212	120
$\sigma = 23$	B	5-175	10	5-55	10	2.5-17.5	3	15	95.06	21.36	2.400	0.01213815	110
$R = 2.23$													
$\mu = 106$	A	5-175	10	5-55	10	2.5-17.5	3	17	108.078	18.590	2.006	0.0719753291	120
$\sigma = 17$	B	5-175	10	1-76	15	1-16	3	17	106.419	17.111	2.226	0.0097095333	120
$R = 2.27$	C	5-175	10	5-55	10	1-16	3	15	105.83	16.84	2.29	0.0005308924	110
$\mu = 115$	A	5-175	10	1-76	5	1-16	3	17	130.711	39.361	1.125	0.476201200	120
$\sigma = 33$	B	5-175	10	1-56	15	2.5-17.5	3	17	111.629	29.361	1.754	0.0664935393	120
$R = 1.56$	C	5-175	10	5-55	10	2.5-17.5	3	17	114.720	32.200	1.580	0.007995710	120

Table 3.1 (continued)

This table displays some results for parameter estimation using only the Direct Search method in a programme for Mod II. Parameters μ, σ and R are as defined previously in [3-10], while $\bar{\mu}$, $\bar{\sigma}$ and $\bar{R}$ are the obtained estimates. $\Delta\mu$, $\Delta\sigma$ and R are the initial increments of search. In the input column are specified the initial boundaries of search (lower and upper) for each parameter. In each case, the first column gives the true parameters, while the second column specified the number of trials. All experimental runs had 17 cycles of iterations. The columns of results specify the different estimates in each trial and the final or the minimized error. The last column reports the necessary CPU time (in seconds) for the LEEDS' ICL 1906-A computer.

Compare results of this table with that of Table 3.2. The simulated data for parameter estimation (ie the histogram) is common to both these tests. Notice the results obtained for Table 3.2, which consumed generally between 1/6 and 1/10 of the present table's average CPU time.

A first consequence of this type of test was the confirmation that results could be greatly improved if the appropriate number and intervals of search for each parameter were used. Many of the earlier tests were carried out using 10 intervals of search for σ, μ and R, giving a total of 1000 combinations in every cycle of interations. Better results were obtained when numbers of intervals for the mean increased from 10 to 15, and decreased from 10 to 5 for both σ and μ. This not only improved the final results but also gave a total of 375 combinations per cycle, a little more than a third of the previous amount.

These tests also reveal that in this direct search technique it is important that the increments (relative to each parameter) are sequentially and proportionately reduced in every cycle of iterations. In other words, the range and the number of intervals for each parameter and the number of cycles of iterations must balance in such a way that at the end, the magnitude of these increments for each parameter must be roughly the same. In other words, in the last cycle, all the parameters μ, σ and R are searched in increments of say approximately 0.1.

One specially valuable piece of information obtained from these tests is the fact that a lot of care must be taken with the search for the mean. Compared to σ and R, there should be a greater number of intervals of search, allocated to finding μ, because this parameter governs the success in finding the right convergence direction. The Mod II function relies on the mean and neglecting this could give spurious results.

The results of the type of the Monte Carlo simulation shown in fig. 3-8 showed improvements with the change in the intervals of search for the mean:-

- Mod I, ϕ changed from 20 to 30 intervals, and the estimated R is 4.8, while Mod II changed from 10 to 33 intervals and the estimated

R is 5.3. Therefore both results came closer to the desired value 5.0.

Another important observation is the fact that the models' function are very sensitive. Minor differences in the values of the minimised errors can lead to many different estimates of μ, σ and R. This fact is shown in table 3.1.

Experience gained with the use of the Direct Search Method showed that it loses its efficiency as the iterations progress. In other words, the method is quite efficient in the early iterations as it eliminates intervals and locates the most likely region where the optimum lies. Thereafter, the progress towards the optimum becomes less efficient and requires too many iterations. This showed the necessity of finding another solution, and the investigated method was the Gradient Method described in section 3.4.3. Section 3.4.3-c describes the disadvantages of the Gradient Method, while table 3-2 illustrates the advantages in terms of accuracy and time necessary to reach the optimum, using data listed in table 3-1. In both tables 3-1 and 3-2 it is important to compare not only the values of the estimates but also the final values of the minimised error, (ie the final value yielded by the objective function). Compare the columns of the minimised errors in both tables 3-1 and 3-2. The analysed data is the same for both tables.

Table 3-2 also gives an idea about the direction towards which there is a convergence. It can be seen that in each trial there were different initial guesses, as shown in the input columns, but the results, both the estimated parameters and obviously the minimised errors, are nearly the same. It is clear that the method shown in table 3-2 leads more accurately to an Optimum solution than the Direct Search Method of table 3-1. It must be reported that the input 'guesses' in table 3-2 were taken from results of the early three iterations using

Table 3.2

Direct Search Method Cycle No.	INPUT			RESULTS			
	INITIAL GUESSES			ESTIMATES			Minimal error or Final Value of The Sum of Squared Diffs.
	μ	σ	R	μ	σ	R	
1st	75	16	4	74.988	9.985	5.002	0.42875×10^{-2}
1st	75	11	4	74.911	10.026	4.975	0.37143×10^{-2}
1st	85	15	2.5	74.916	10.023	4.976	0.37490×10^{-2}
2nd	78.705	6.700	6.940	74.921	10.021	4.978	0.37048×10^{-2}
3rd	78.84	7.498	7.494	74.921	10.021	4.978	0.37051×10^{-2}
	TRUE VALUES			75	10	5	
1st	85	16	4	84.995	10.006	4.995	0.19431×10^{-2}
1st	85	15	2.5	84.996	10.004	4.997	0.15309×10^{-2}
2nd	82.825	18.10	2.98	84.996	10.054	4.970	0.45560×10^{-2}
3rd	83.965	12.799	3.613	85.002	9.993	5.002	0.89724×10^{-3}
	TRUE VALUES			85	10	5	
1st	105.00	41.00	1.00	95.499	22.997	2.230	0.25266×10^{-6}
1st	95	15	4.00	95.499	22.997	2.230	0.25282×10^{-6}
2nd	91.058	10.00	4.960	95.499	22.997	2.230	0.25271×10^{-6}
3rd	95.66	17.695	2.900	95.499	22.997	2.230	0.25266×10^{-6}
	TRUE VALUES			95.5	23	2.23	

Table 3.2 continued

Direct Search Method Cycle No.	INPUT			RESULTS			
	INITIAL GUESSES			ESTIMATES			Minimal error of Final Value of the Sum of Squared Diffs.
	μ	σ	R	μ	σ	R	
1st	125.00	31.00	1.00	106.00	16.999	2.27	0.43680×10^{-8}
2nd	105	15	2.5	106.00	16.999	2.27	0.43657×10^{-8}
3rd	106.41	16.197	2.306	106.00	16.999	2.27	0.43657×10^{-8}
TRUE VALUES				106	17	2.27	
1st	135	46	1.00	114.818	32.283	1.583	0.79539×10^{-2}
1st	105	25	2.5	114.819	32.284	1.582	0.79539×10^{-2}
2nd	132	37	1	114.818	32.283	1.582	0.79539×10^{-2}
3rd	106.41	26.197	2.306	114.818	32.284	1.583	0.79539×10^{-2}
TRUE VALUES				115	33	1.56	

This table displays the results of the Gradient Method, which used Mod II formulation. The input data (ie initial guesses) were originated from the 1st, 2nd and 3rd results or cycles of the Direct Search routine. Notice:

(i) The similarity in values of the estimates (ie consistency) in each case.
(ii) Similarity between the estimates and the true values.
(iii) The accuracy of search in the errors column.
(iv) No matter what the input, the convergence is to the same point.

the Direct Search Method.

This study also found that the Gradient Method proved to be unhelpfull when the initial guesses were far away from the Optimum region. It cannot be defined here what is the appropriate range for the Gradient routine to function properly, because it varied accordingly the tested case. The Steepest Descent method always operates (in all tested circumstances) but the rate of its convergence towards the optimum can be infinitely slow. This is a clear indication that these methods (either 1st or 2nd order method) show that their weaknesses lie in those circumstances where the initial steps are far away from the optimum. This contrasts very much with the Direct Search Method which proved to be more efficient exactly in this region—ie it locates and approximates very quickly to the optimum region.

An all purpose, error-free and globally-convergent method is not yet available, due to the fact that the objective functions may vary considerably according to the formulation of each problem. Functions can have more than one optimum. There could be a saddle-point (see CC' in fig. 3-4) or narrow valley, where progress is very slow. In these situations it is important to search in another direction and see if there is an improvement in the value of the Objective Function. An alternative method is to generate various initial guesses using a random number generation routine, but a successful convergence cannot be guaranteed.

Based on experiences gained in the innumerable simulated estimations it was decided not to try yet another method, or any variation on the methods already available. This was due to two reasons:

(i) The problem of having to deal with local minima would persist, no matter which method was chosen.

(ii) The methods already tested have complementary characteristics on efficiency, as explained above.

Thus the chosen strategy was to use the Direct Search Method to initiate the Optimization process and eliminate intervals where the optimum is less likely to occur. The Gradient routine was then activated and on average it locates the Optimum in less (generally) than 10 iterations, with great accuracy and at a fraction of the time that would be spent by the Direct Search alone (usually at 1/6 to 1/10 of that time).

Programme ISTRAES (see appendix, for listing and instructions of use) was devised incorporating the version of the Direct Search Method (Mod II) under a subroutine named MODEL2. The Gradient Method-Programme was modified to subroutine GRADIT. Thus ISTRAES initiates the cycles of iterations by activating subroutine MODEL2 , in a range as broad as possible, restricting this range at every cycle. The output results are submitted to the subroutine GRADIT which finalises the whole operation. Table 3-2 shows different runs in which the initial guesses for GRADIT were taken from MODEL2 's cycles numbers 1, 2 and 3. It can be seen that there was convergence towards the correct solution in every single test. Theoretically, using the results of the second and third cycles of MODEL2 increased the safety of search and also the processor time. It does mean that good results could be achieved only using the first cycle results. The running times for the LEEDS' 1906-A ICL computer, amounted on average to 32 seconds, and this includes inputing data, 3 cycles with MODEL2 , finalization with GRADIT and then printing (line printer) the fitted curve on the analysed histogram.

3.5 Data Treatment

Many of the earlier results were obtained by treating data in the way described by Roberts and Sanderson (1974). That is manually as explained in section 3-2 (see diagram in figs. 3-11 and 3-12). This is a reasonable procedure if the number of estimations is relatively small, otherwise there is a need for a quicker process, and this is the aim of the present section.

The method here is based on the technique introduced by Loudon (1964, see also Whitten 1966, pp.582-585) and subsequently simplified by Ramsay (1967,pp.18-19).

Loudon (1964) applied the least squares fitting method in order to find the fold axis of conical and cylindroidal folds. While his method required matrix inversion for solving three simultaneous equations, Ramsay (1967) approached the problem by introducing a constraint which reduced the unknowns to two simple expressions. The method used here introduces another constraint thus restricting the problem to a simple expression.

Geometrically what is required is a plane that best fits the normal to the S-planes, with the condition that such a plane contains the resultant vector of the stretching direction, that is the statistical X-direction, of the finite strain epplisoid. The normal of such plane constitutes the Y-axis and as explained in section 3-2, the XY-plane is used in order to group data into frequency histograms.

The conditions that a line, given by its direction cosines l, m, n, should lie in a plane are

$$al + bm + cn = 0 \qquad [3\text{-}30]$$

and

$$ad_{j1} + bd_{j2} + cd_{j3} = 0 \qquad [3\text{-}31]$$

(see Bell, 1937, p.43)

An S-pole (d_{ji}) lying on this plane should be perpendicular to the plane's normal. This condition of orthogonality can be expressed by the fact that the product of their cosines equals to zero. (Ramsay, op. cit., p.18). By making $A = a/c$ [3-32]

and $B = b/c$ [3-33]

and substituting these in the former expressions, we get

$$Al + Bm + n = 0 \qquad [3\text{-}34]$$

and

$$Ad_{j1} + Bd_{j2} + d_{j3} = 0$$

Taking the value of B in [3-34] and substituting in [3-35], yields

$$B = -\frac{Al - n}{m} \qquad [3\text{-}36]$$

and

$$Ad_{j1} + d_{j2}\left[\frac{-Al - n}{m}\right] + d_{j3} = 0 \qquad [3\text{-}37]$$

Now, the minimization of errors using the Least Squares Method is carried out (see Dixon, 1972, p.42) by creating an Objective Function $Z = f(A)$

$$Z_{min} = \sum_{j=1}^{n} e_J^2 = \sum_{j=1}^{n}[d_{j3} + Ad_{j1} + d_{j2}\left[\frac{-Al - n}{m}\right]]^2 \qquad [3\text{-}38]$$

This gives the condition of optimum at

$$\frac{\partial Z}{\partial A} = 2\sum_{j=1}^{n} e_j \cdot \frac{\partial ej}{\partial A} = 0 \qquad [3\text{-}39]$$

where

$$\frac{\partial ej}{\partial A} = \frac{dj_1m - dj_2l}{m} \qquad [3\text{-}40]$$

so

$$\frac{\partial Z}{\partial A} = 2\sum_{j=1}^{n}\left[\left[\frac{md_{j3} + mAd_{j1} - Ald_{j2} - nd_{j2}}{m}\right]\cdot\left[\frac{md_{j1} - ld_{j2}}{m}\right]\right] = 0 \qquad [3\text{-}41]$$

which simplifies, after expanding and collecting the terms, to

$$A\sum_{j=1}^{n}[(ld_{j2} - md_{j1})^2] + \sum_{j=1}^{n}[(ld_{j2} - md_{j1})(nd_{j2} - md_{j3})] = 0$$

and therefore

$$A = -\frac{\sum_{j=1}^{n}[(ld_{j2} - md_{j1})(nd_{j2} - md_{j3})]}{\sum_{j=1}^{n}(ld_{j2} - md_{j1})^2} \qquad [3\text{-}42]$$

Back substitution of [3-42] in [3-36] yields the value of B. The fitting plane is given by the direction cosines of its normal (the Y-axis) which are assessed by means of Ramsay's (1967) expression no. 1-13.

$$C = (1 + A^2 + B^2)^{-\frac{1}{2}} \qquad [3\text{-}45]$$

which substitutes in [3-32] and [3-33] giving a = Ac and b = Bc.

Having established the ellipsoid axes, X and Y, the task is now to find the θ'_i angles that each vector projection makes with the X-direction in the XY-plane. Figure 3-9 illustrates the situation. In a cartesian system (U,V,W), a unity vector $\overline{OP}_i$ makes angles α and β with two orthogonal axes OX and OY. The projections of this vector on each of the axes is given by the lengths of $\overline{ox}'$ and $\overline{oy}'$ respectively. The angle θ' in the XY plane is assessed as follows:

$$\overline{OP}'^2 = \overline{Ox}'^2 + \overline{Oy}'^2$$

Figure 3.9. See text for explanation.

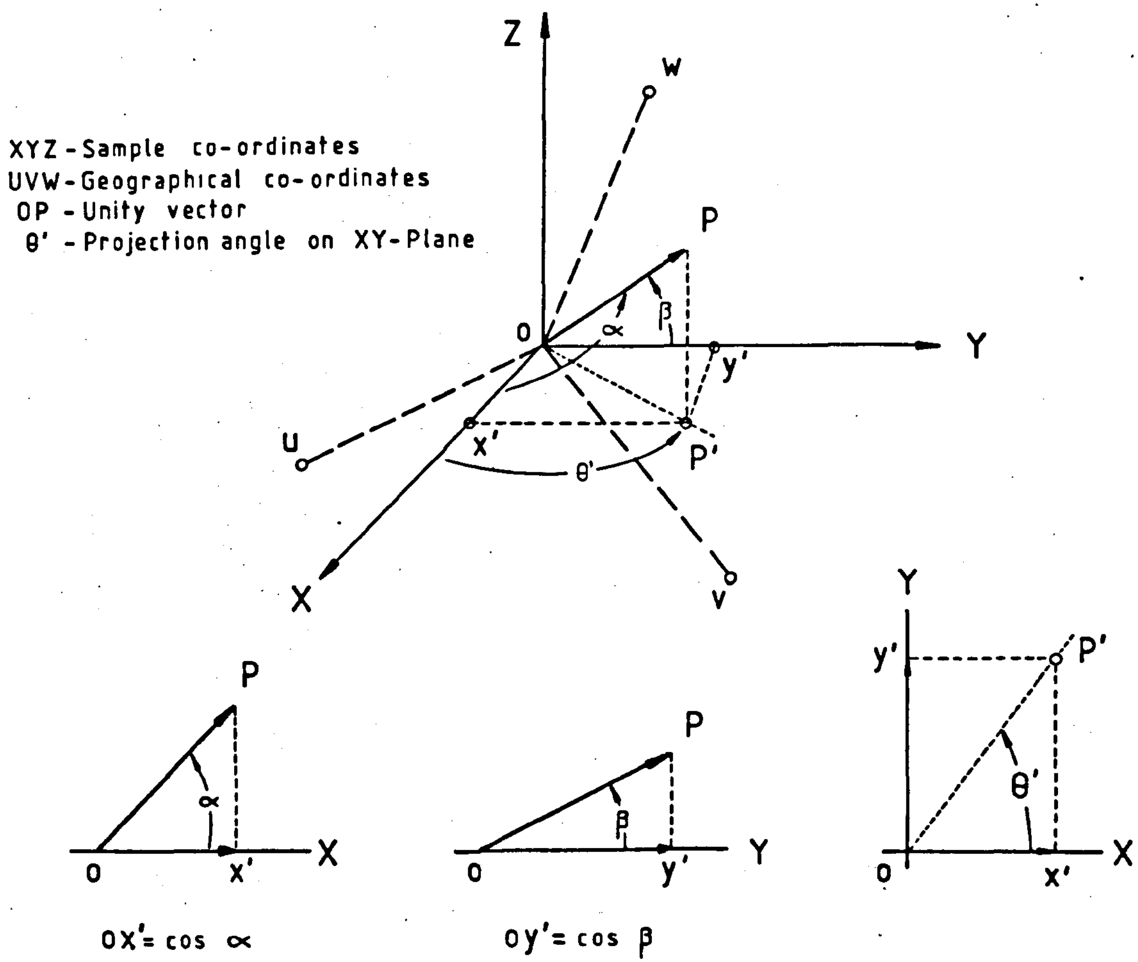

$$\overline{OP}'^2 = (\cos^2\alpha + \cos^2\beta)^{\frac{1}{2}} \quad , \text{ but } \overline{Ox}' = \overline{OP}' \cos\theta'$$

therefore

$$\theta' = \cos^{-1}\left[\frac{\cos\theta}{(\cos^2\alpha + \cos^2\beta)^{\frac{1}{2}}}\right] \qquad [3\text{-}46]$$

The angles α and β can be easily calculated by remembering that two straight lines make an angle λ according to the relationship (see Kindle, 1972).

$$\cos\lambda = \frac{x_1P_1 + x_2P_2 + x_3P_3}{\rho_1\rho_2} \quad , \quad \text{where} \qquad [3\text{-}47]$$

P_i are the co-ordinates of each vector, and ρ_i are the lengths of each vector (here taken as unity).

The operation is easily carried out by matrices

$$\begin{bmatrix} \cos\alpha \\ \cos\beta \end{bmatrix} = \begin{bmatrix} x_1 & x_2 & x_3 \\ y_1 & y_2 & y_3 \end{bmatrix} \cdot \begin{bmatrix} P_1 \\ P_2 \\ P_3 \end{bmatrix} \quad \text{or} \quad [\cos\lambda_j] = [E_{jk}]^t\,[P_{ki}]$$

[3-48]

for $i = 1,2, \ldots n$; $j = 1,2$, and $k = 1,2,3$. $[E_{jk}]^t$ are the co-ordinates for the X and Y axes in a transposed disposition.

Subroutine HISTGM (listed in Programme ISTRAES) was devised to group data into frequency histograms. Data are dealt with in terms of azimuth and plunge, in the following steps:

(i) Input data come from subroutine READAT and comprises the poles of the S-planes and the resultant vector of the stretching direction lineation, the X-axis. These are used in the described Least Squares routine, in order to find the XY-plane.

(ii) Each fold axis is projected onto the XY-plane using [3-46] and the angle θ'_i is recorded.

(iii) The frequency histogram is formed by grouping the obtained angular projections according to the class intervals.

3.5.1 Data Weighing

Some comments are necessary at this stage, because the algorithm described in the previous section produces perfect results only in ideal conditions. Where conditions depart from the ideal, some unwanted results may come out. It is believed, however, that there is nothing wrong with the method, and the results are a direct consequence of the type of input data. The method, as explained in the last section, takes into account all the entered data without any sorting (or 'cleaning') criteria.

Data treatment by the manual construction of the frequency histogram allows one to take field criteria into consideration and thus individually evaluate each entered datum. However, even after the most careful handling of data the resultant histogram may contain some subjectivity. The routine explained in the last section does not take into consideration any criteria of data selection and every measurement no matter how discrepant, has the same weight. It is believed that it is possible to partially overcome, or at least to lessen the problems of sampling, by using a modified routine of the least squares technique which weights each S-pole according to its proximity to the resultant pole-distribution vector. The axes which depart too much from the centre of gravity of the poles distribution will be given less weight.

The degree of clustering of each distribution of S-poles can be assessed and used in the weighting process. Here, use was made of Fisher's (1953) k-parameter as a measure of the degree of clustering.

Thus the situation in [3-38] is changed to

$$Z_{min} = \sum_{j=1}^{n} w_j e_j^2 = \sum_{j=1}^{n} w_j \left[d_{j3} + Ad_{j1} + d_{j2} - \left(\frac{-Al - n}{m} \right) \right]^2 \qquad [3\text{-}49]$$

and also in [3-42] which becomes

$$A = - \frac{\sum_{j=1}^{n} wj[(ld_{j2} - md_{j1})(nd_{j2} - md_{j3})]}{\sum_{j=1}^{n} wj[(ld_{j2} - md_{j1})^2]} \qquad [3\text{-}50]$$

for j = 1,2, ... n; where w_j are weighting factors which could be chosen arbitrarily from the following standard approaches (remembering that j = 1,2, ... n are data numbers):-

(i) the sum of squares of the errors is minimised if $w_j = 1$

(ii) the sum of squares of the percentage errors is minimised if $w_j = (1/e_j)^2$

(iii) the probability of a set of errors occurring can be minimised if σ_j is the expected error in the measurement σe_j (ie if this is possible to determine) so $w_j = (1/\sigma_j)^2$.

The tests carried out in this study lead us to choose (more or less intuitively) the results relative to σ_j, the closest angular distance between each S-pole and the distribution-resultant in one of the following relationships:-

(i) $w_j = \cos|\alpha_j|$, (ii) $w_j = \cos|\alpha_j|/[1-\cos|\alpha_j|]$

(iii) $w_j = k \cos|\alpha_j|$, or (iv) $w_j = 1/[k.\tan|\alpha_j|]$,

where k is the well known Fisher (1953) concentration parameter, only used on the constraint that $k \geqslant 1$.

The more satisfactory results were obtained with the fourth expression above. Figures 3-10-a and b are stereoplots of two solutions using the above described methods. It can be observed that for 3-10-a,

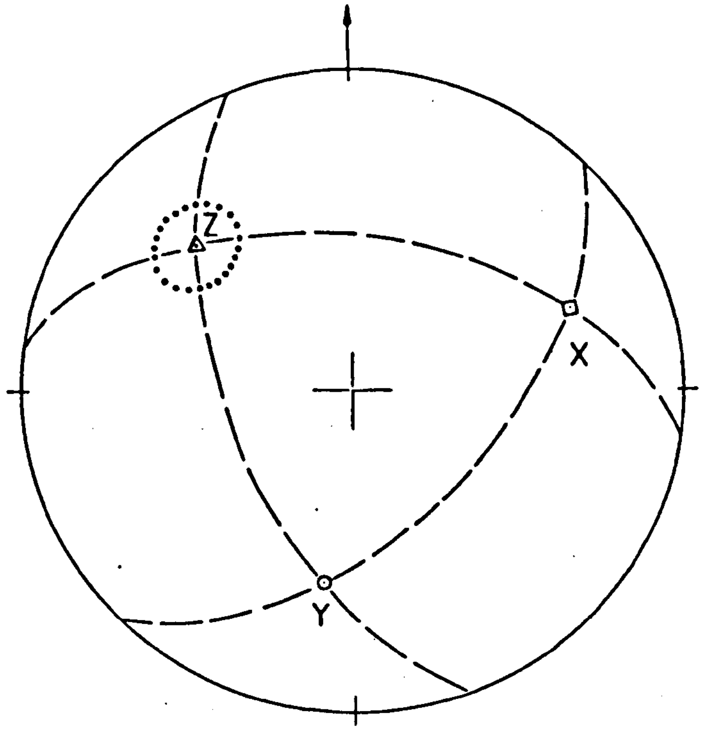

Figure 3.10-a

Hypothetical ('ideal') case of poles of S-planes clustered at a resultant direction which constitutes the pole of the best fit plane containing the X-axis.

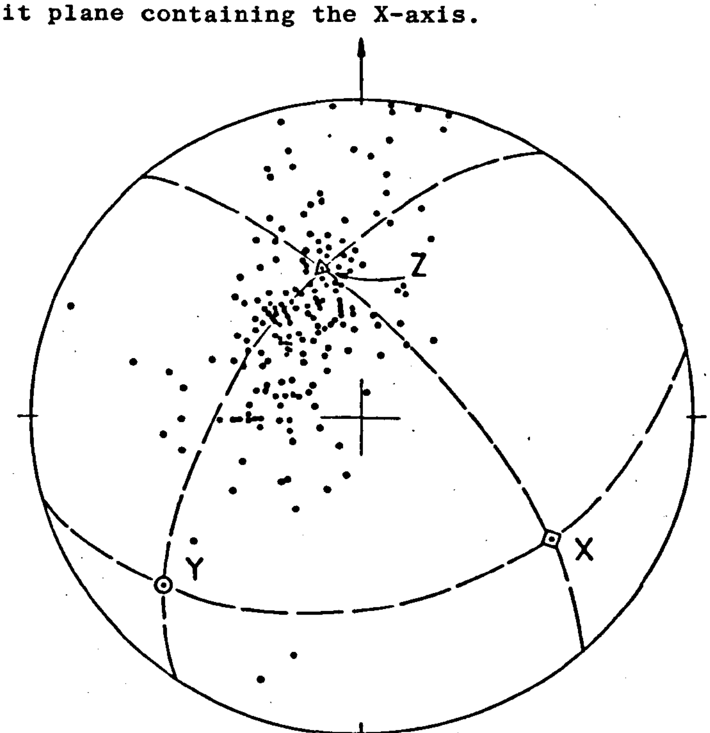

Figure 3.10-b

Data from sub-area 6, 221 πs-planes, illustrates the chosen best fit plane (XY).

the ideal case, the fit is perfect. Figure 3-10-b is made from data of sub-area 6 (see fig. 2-3) and it is displayed here for comparative judgement.

3.6 Parameter Estimation

3.6.1 General

Figures 3-11 and 3-12 contain the resultant parameter estimations using both Mod I (Sanderson's) and Mod II (present study) using a Direct Search Method, for two fold generations, F_2 and F_3 in the studied area. The sub-area numbering, as indicated in every diagram corresponds exactly to that described previously for Chapter 2. It must be stressed that such sub area division fits better for the F_3-folds, than for the F_2-generation. The estimations are restricted to the southern part of the mapped area (fig. 2-1) simply because data are more abundant in this domain. The estimated parameters, for both models and fold generations, are displayed in the sequence of figs. 3-13 - 3-17.

Figure 3-13 compares the means estimated by Mod I and Mod II, using data for F_2 and F_3 fold axes. The best fit regression line, given by relation [4-62] (see next chapter), for F_2-folds has a slope of 42.1° while that for F_3 is 45.4°. The linear correlation coefficients $r\mu$ (see Chapter 4, relation 4-63) present values very close to unity. It is quite clear that the estimates were almost identical, no matter which model was used. The existent differences are certainly due to the low accuracy of search-programmes that only used the Direct Search Method. Figure 3-13 also shows that 85% of the estimated means are located within the range of 85°-115° from the finite X-direction,

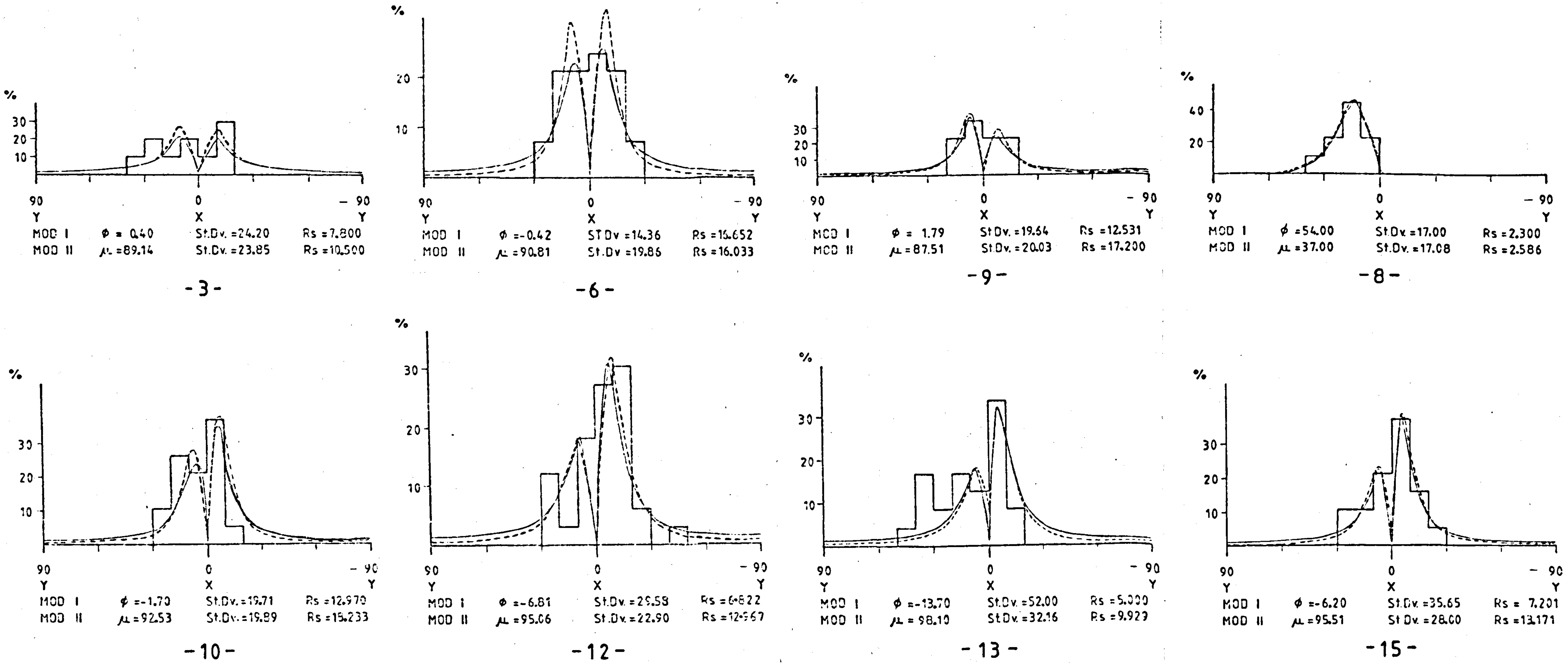

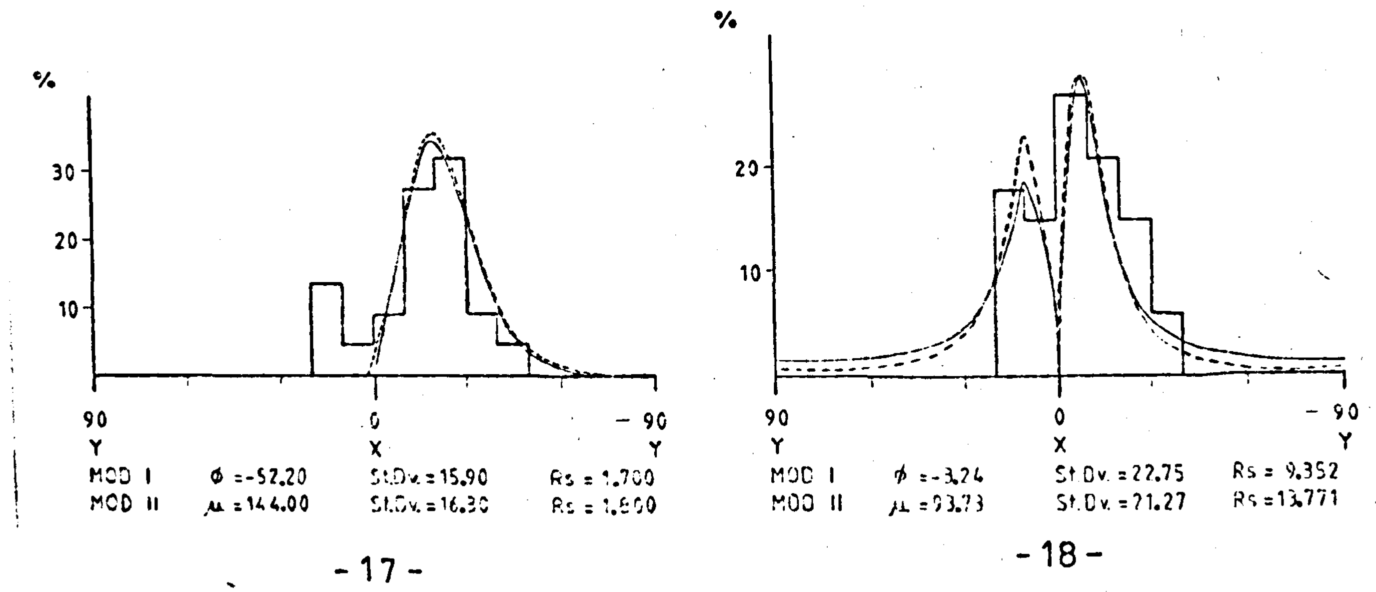

Figures 3.11. Refers to F_2 folds. Best fit curves to frequency histograms. Dashed lines correspond to curves for Mod I (Sanderson's) and full lines refer to Mod II. Numerals beneath each diagram refer to sub-area location (described in Chapter 2). Results for both models were obtained from programme using a Direct Search method (see text for details).

Figures 3 -12

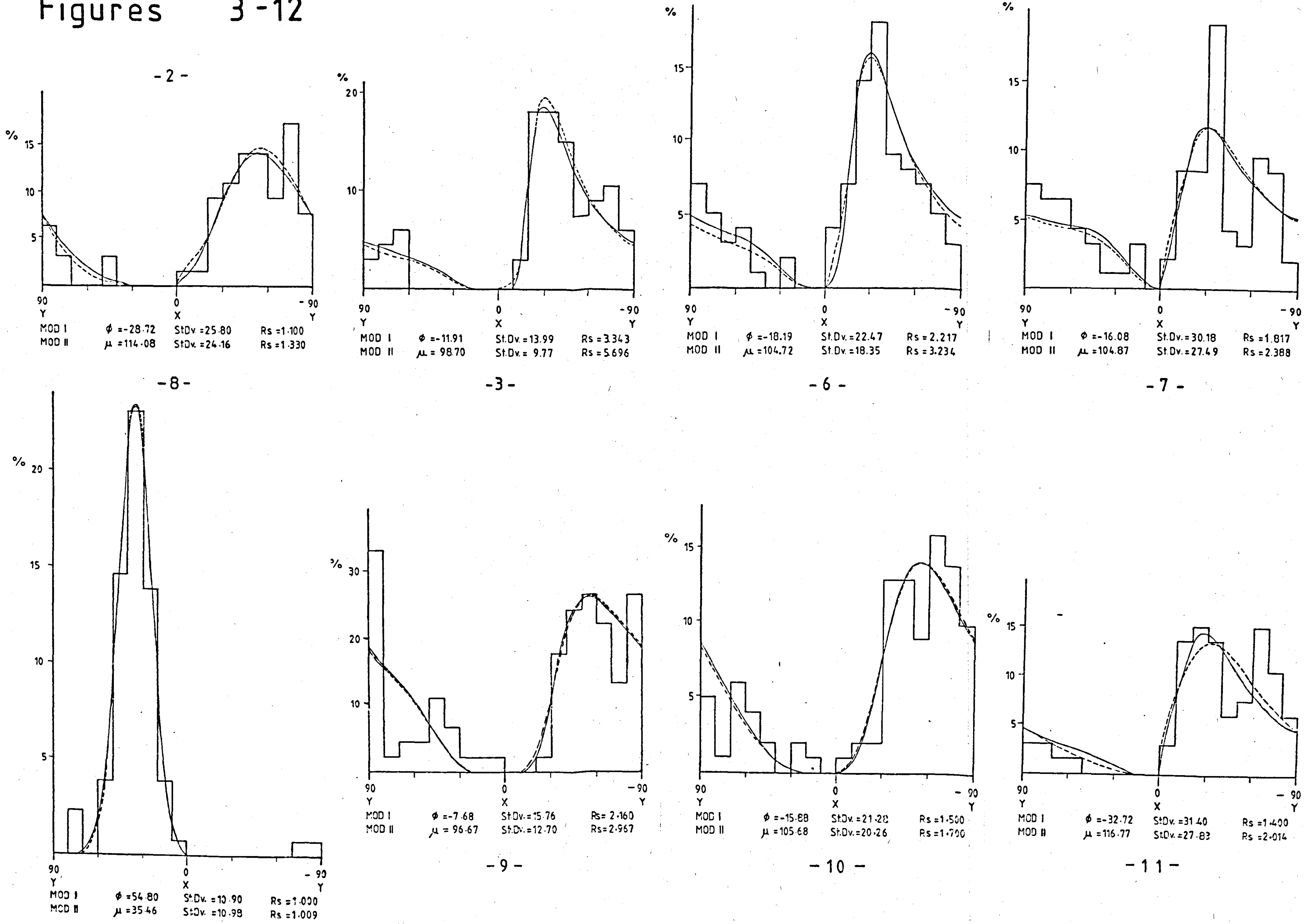
-2-
MOD I ϕ =-28.72 StDv. =25.80 Rs =1.100
MOD II μ =114.08 StDv. =24.16 Rs =1.330
-3-
MOD I ϕ =-11.91 St.Dv. =13.99 Rs =3.343
MOD II μ = 98.70 St.Dv. = 9.77 Rs =5.696
-6-
MOD I ϕ =-18.19 St.Dv. =22.47 Rs =2.217
MOD II μ =104.72 St.Dv. =18.35 Rs =3.234
-7-
MOD I ϕ =-16.08 St.Dv. =30.18 Rs =1.817
MOD II μ =104.87 St.Dv. =27.49 Rs =2.388
-8-
MOD I ϕ =54.80 StDv. =10.90 Rs =1.000
MOD II μ =35.46 StDv. =10.98 Rs =1.009
-9-
MOD I ϕ =-7.68 StDv. =15.76 Rs= 2.160
MOD II μ = 96.67 StDv. =12.70 Rs=2.967
-10-
MOD I ϕ =-15.88 StDv. =21.20 Rs =1.500
MOD II μ =105.68 StDv. =20.26 Rs =1.700
-11-
MOD I ϕ =-32.72 StDv. =31.40 Rs =1.400
MOD II μ =116.77 StDv. =27.83 Rs =2.014

Figures 3-12 (cont'd)

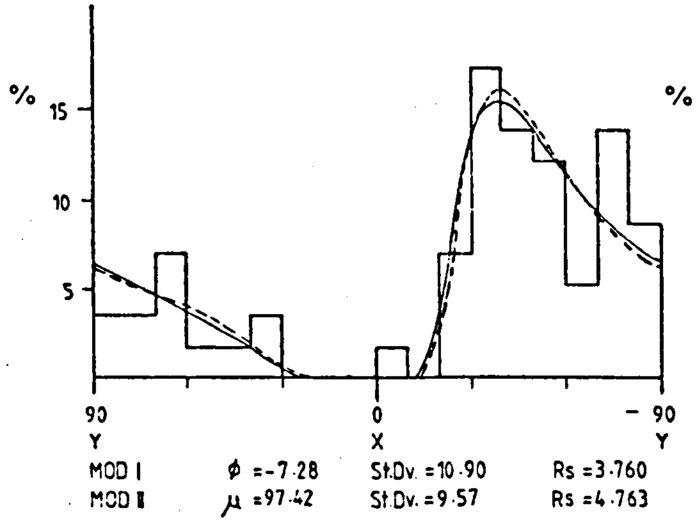

- 12 -

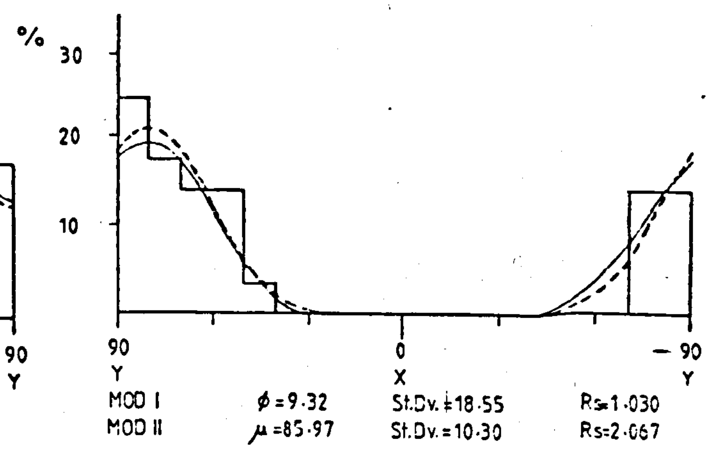

- 13 -

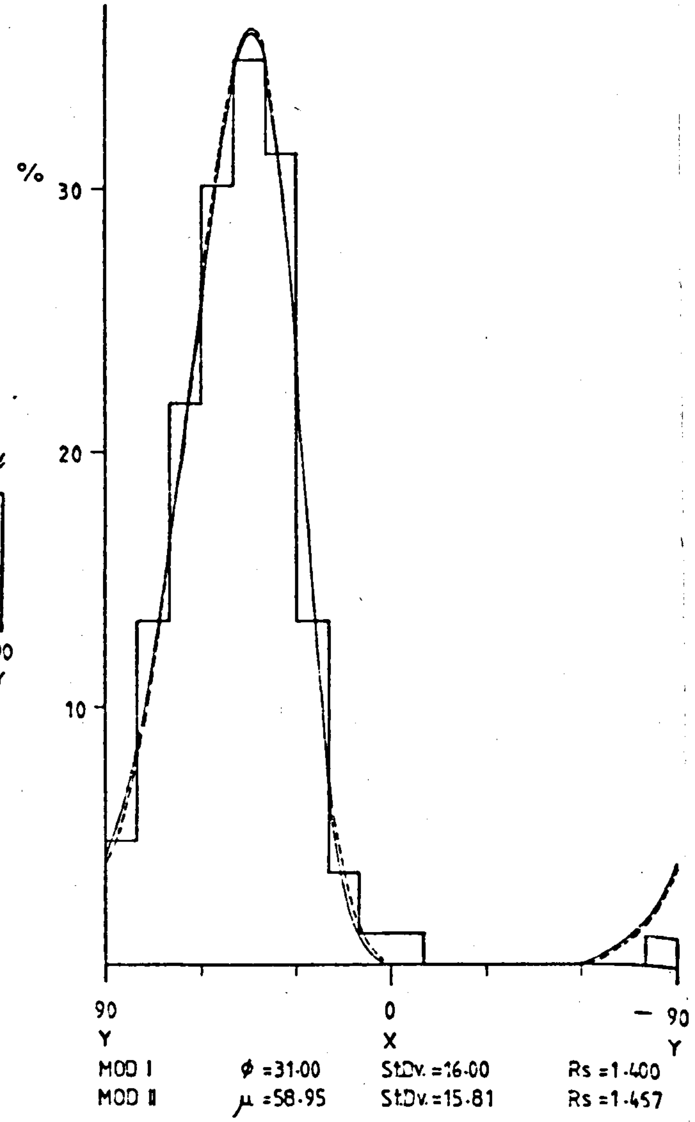

- 15 -

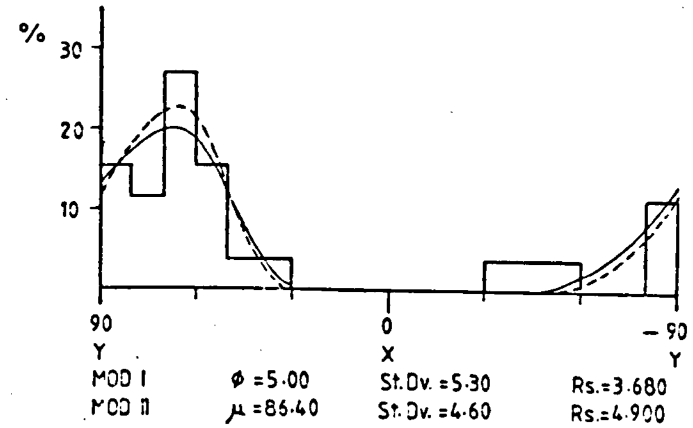

- 16 -

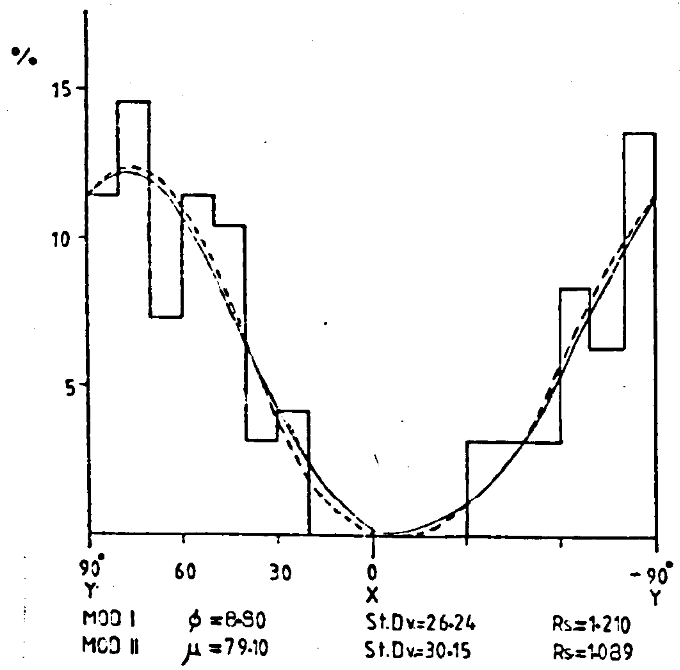

- 17 -

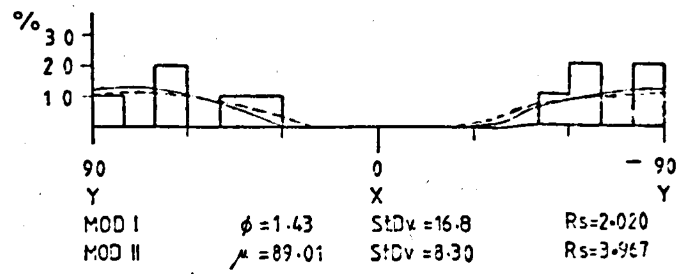

- 18 -

Figure 3.12. There refer to F_3-folds, showing the best fit curves to frequency histograms. Dashed lines correspond to curves for Mod I (Sanderson's) and full lines refer to Mod II. Numerals beneath each diagram refer to sub-area location (described in Chapter 2). Results for both models were obtained from programmes using a Direct Search method (see text for details).

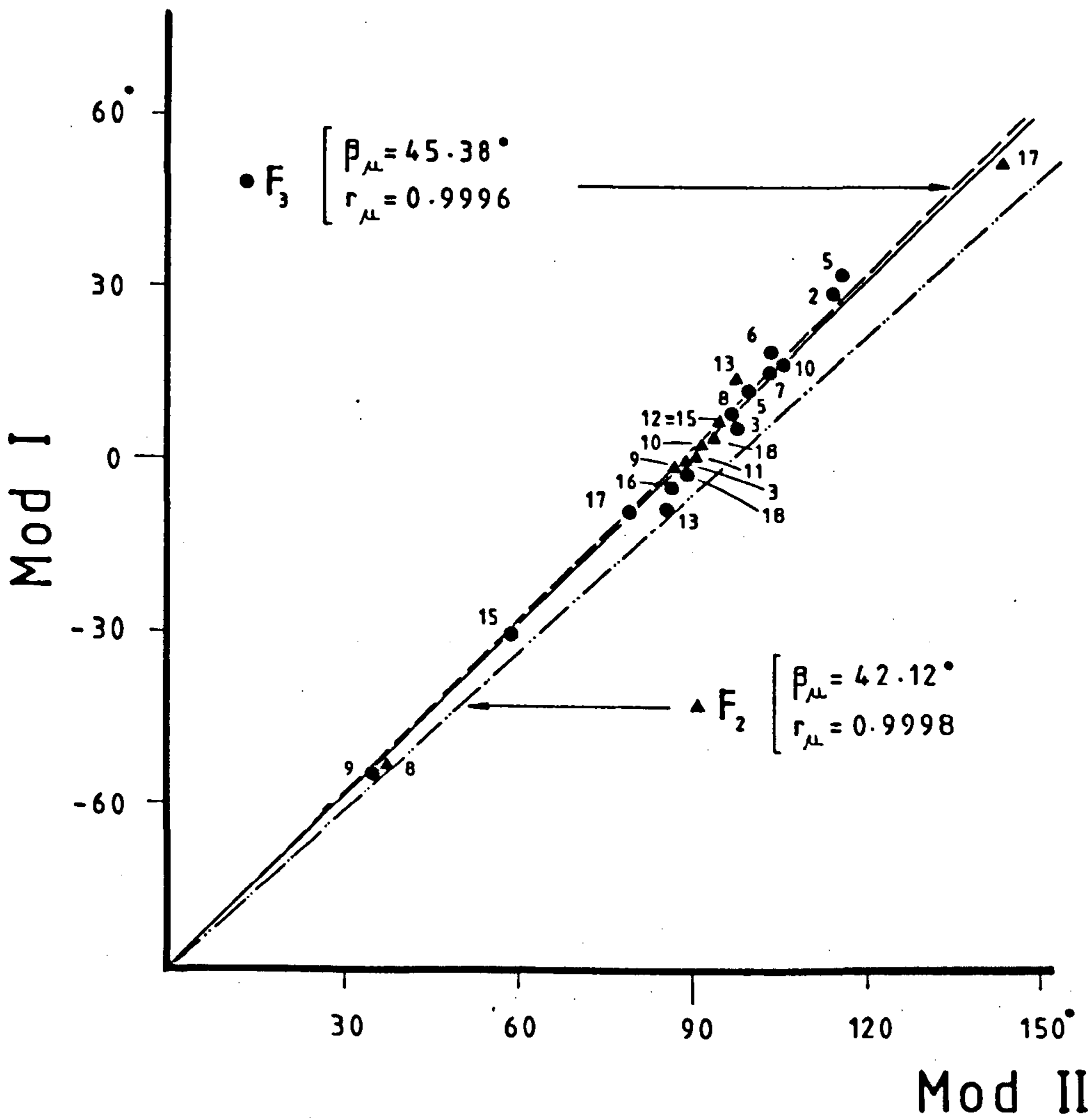

Figure 3.13

Correlates the estimated means obtained from the two models used. Dashed lines correspond to the best fit regression lines as indicated. This full line has a 45^{o}-slope. See text for full details.

that is, with high obliquity to the thrust movement direction. The position of the original mean directions are plotted in figs. 3-23 and 3-24, and a further discussion is given later.

Figure 3-14 compares estimates of original standard deviation σ. This diagram clearly shows that the regression lines for both populations, F_2 and F_3-folds, departed slightly from the ideal 45^o-slope line. Compared to fig. 3-13 the scattering of this plot is larger and a measure of this scatter is given by the calculated linear correlation coefficients, $r\sigma$ (see fig. 3-14). The estimates for σ are in the range up to 30^o, and this range should constitute a constraint for the following reasons:

(i) Both models, Mod I and Mod II, make use of the Gaussian function of [3-8]. This relation is appropriate for linear measures (cf Mardia 1972, p.18) whereas the present cases (ie both models) require a circular function such as the von Mises function (see Mardia 1972, p.42 for details). However for values of σ less than 30^o, both functions, Gaussian and von Mises, tend to approximate one another (Agterberg 1973).

(ii) Also, measurements made by the author on photographs of experimentally produced folds (Dubey, 1976) show that the standard deviation of fold axes is in the range of 6^o to 12^o. Folds being formed with standard deviation values greater than 12^o are perhaps due to inhomogeneities that were not present in Dubey's (1976) experiments.

The results given in fig. 3-14 plot within the 10^o-30^o range. It is suggested that all results in which $\sigma > 30^o$ are geologically meaningless.

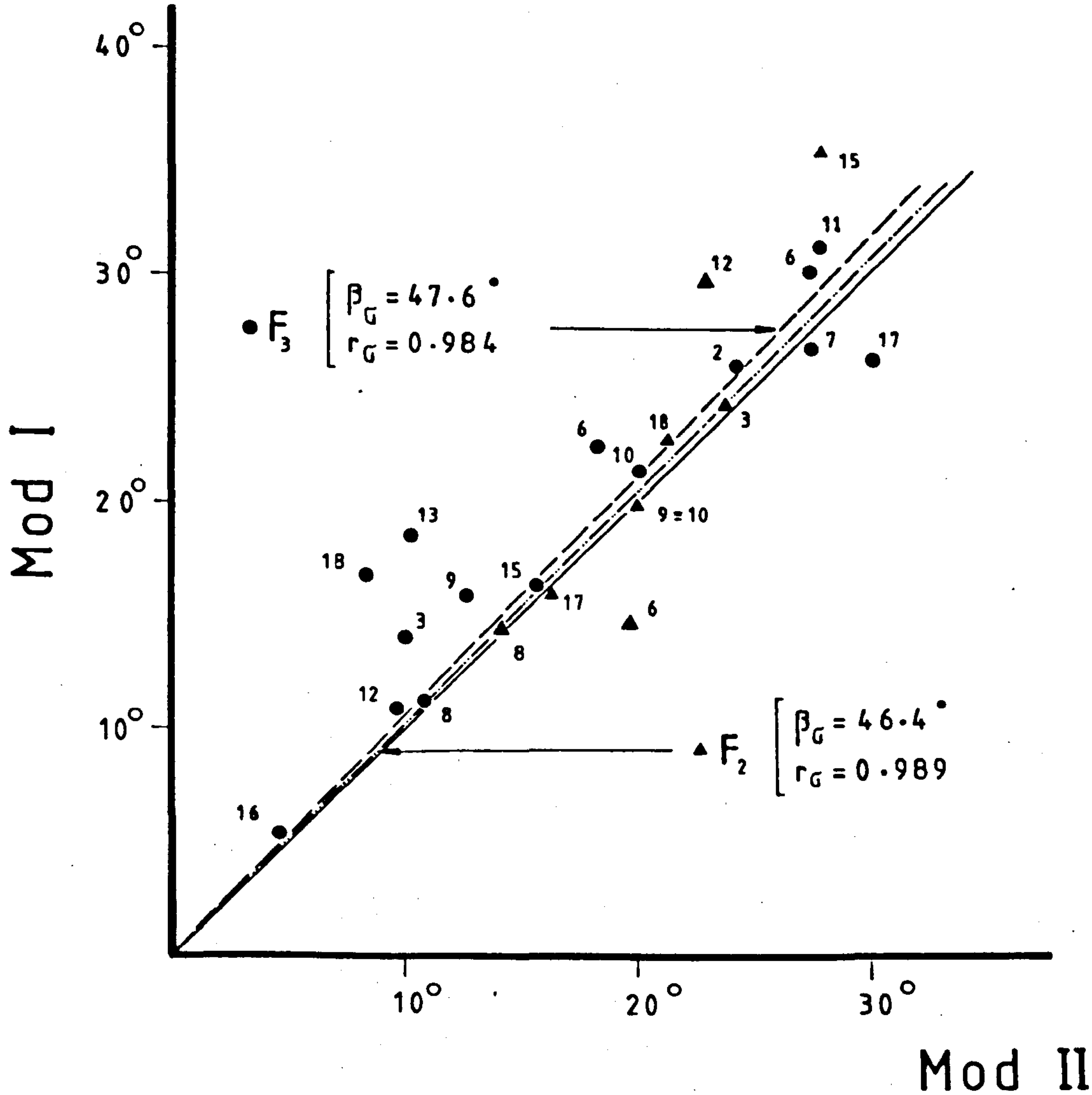

Figure 3.14

This correlates the values of the estimates for the Standard Deviations using the two models. Notice the range up to 30^{o}. Dashed lines are the best fit regression lines as specified. The full line has a 45^{o}-slope. See text for full details.

The estimates of the strain ratio, R, both for Mod I and Mod II and F_2 and F_3-folds, are compared in fig. 3-15. It can be seen that such diagrams exhibit a plot with strong departure from the 45^o-slope line. The slope for both regression lines have very close values around a 35^o slope. Thus, Mod II overestimates the ratios obtained by Mod I. The scattering for F_2-folds on this graph is comparatively greater than for F_3 estimates, as this is measured by the correlation coefficients in fig. 3-15. Also from this diagram is the indication that F_2-folds show a much higher strain ratio than do F_3-folds. The latter range from 1.0 to 5.5 while the former reach ratios as high as 18.0.

It is apparent from figs. 3-13 - 3-15 that the differences in models tend to:

(i) Produce no discrepancies in the location of the means (μ or ϕ) of the original fold distributions.

(ii) Give higher estimates of standard deviation for Mod I than for Mod II.

(iii) Assign higher estimated values for strain in Mod II than in Mod I.

It is also clear that both models tend to produce practically the same ordinate values for the fitted curves. This is obvious and is due to the fact that both programmes (SAND for Mod I and MODEL2 for Mod II) make use of the same objective function [3-15]. Thus the differences in the results of σ and R are due to the differences in the original formulation of each model.

Figures 3-16 and 3-17 constitute a visualisation of the magnitude and orientation of strain estimates for the southern part of the mapped area.

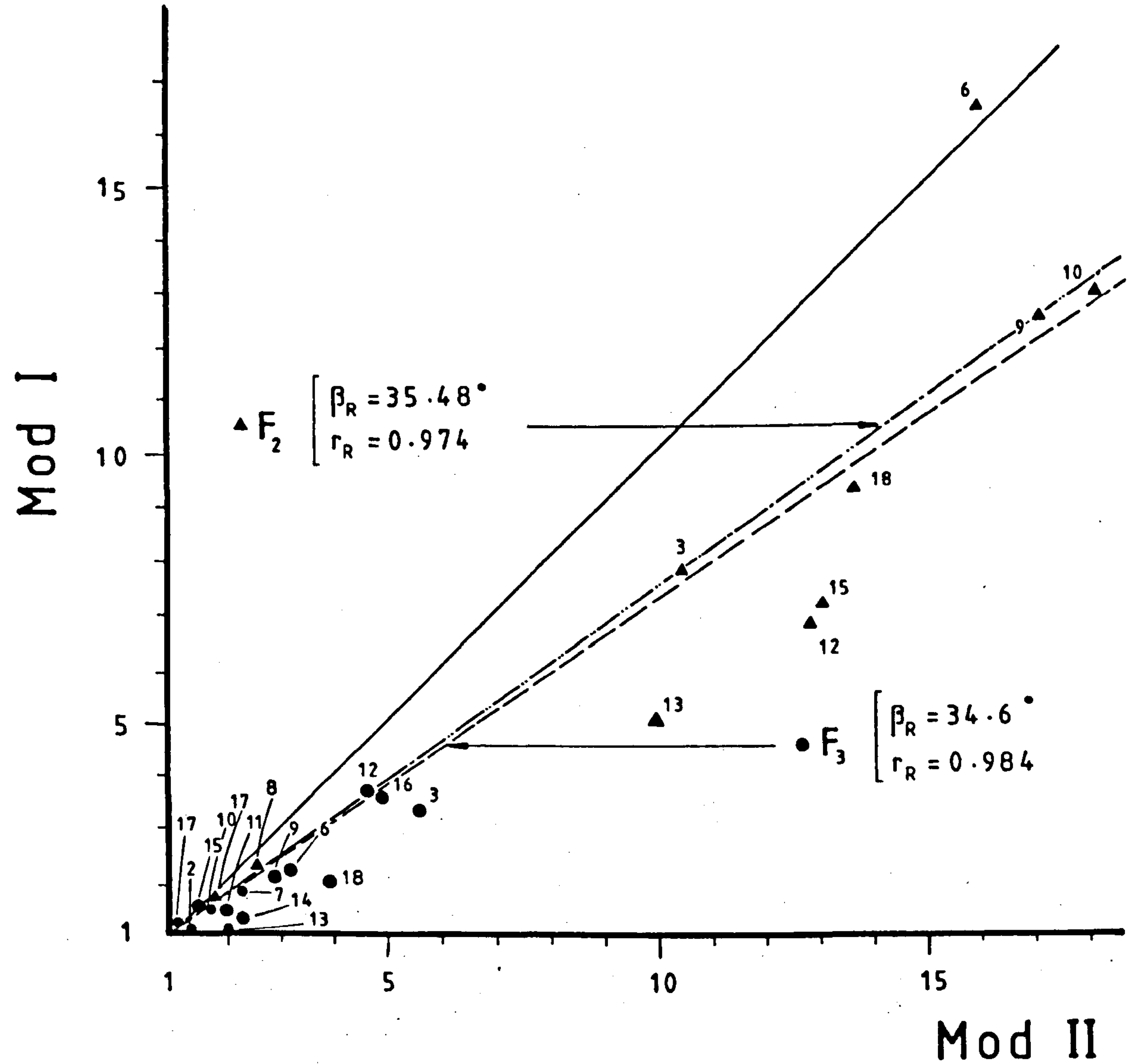

Figure 3.15

This correlates the strain ratio estimates using the two models. Dashed lines refer to best fit regression lines as indicated. This full line has a 45^{o}-slope. See text for full explanation.

Figure 3.16. The different ellipses illustrate the magnitudes and orientations of the X/Y ratios determined using F_3-fold axes orientations with Mod I, in a Direct Search Method. See diagrams of figures 3.12 and text for full explanation.

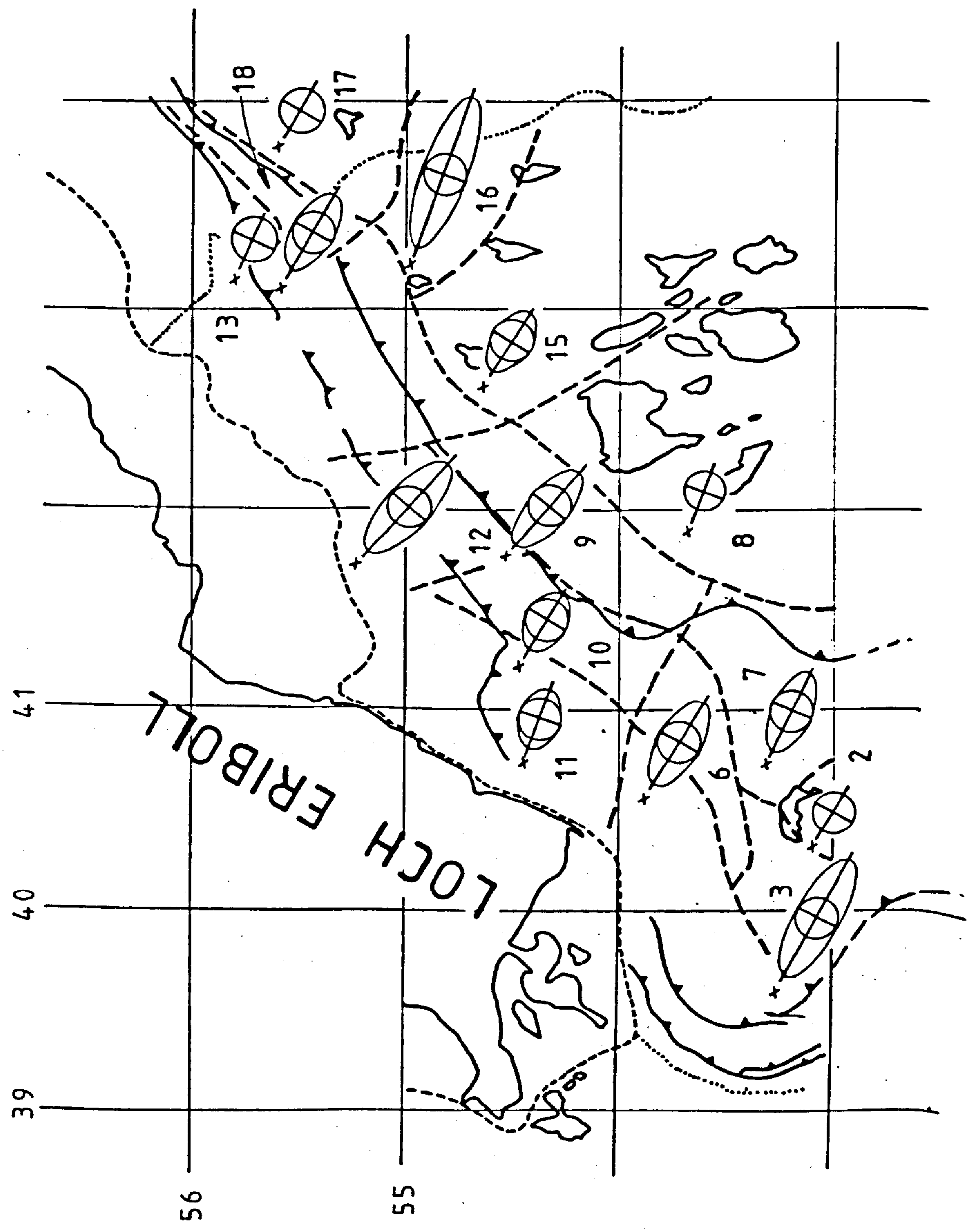

Figure 3.17. The different ellipses illustrate the magnitudes and orientations of the X/Y ratios determined using F_3-folds axes orientations with Mod II, in a Direct Search Method. See diagrams of figures 3.12 and text for full explanation.

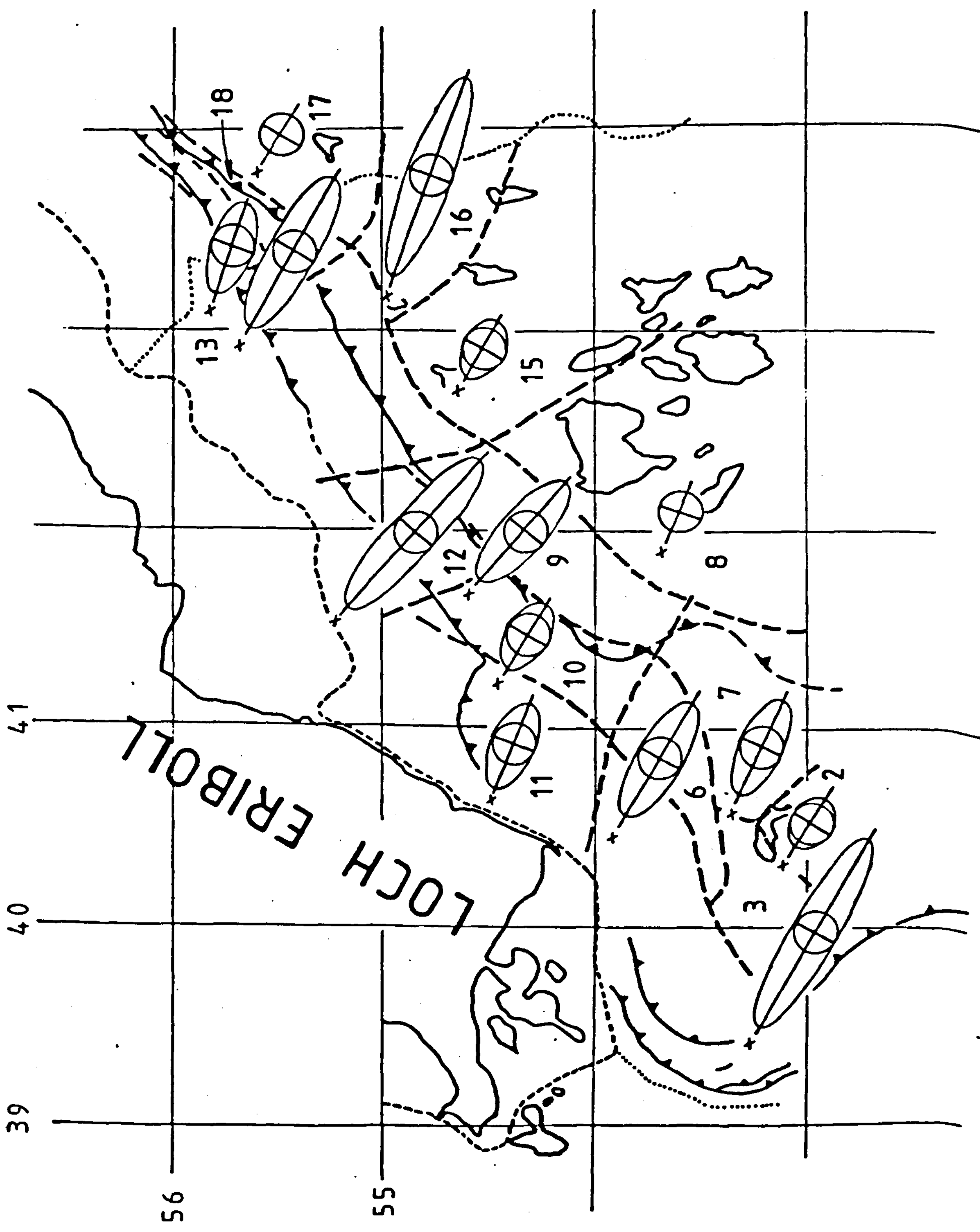

3.6.2 Multiple Cells Sub-division

The results based on a sub area division as given in figures 3-16 and 3-17 can be considered subjective, no matter what criteria were used to obtain the best sub-area division. A different approach is introduced here which tries to reduce this subjectivity.

The analysed area is subdivided into overlapping 'cells' and data input from each 'cell' are submitted for parameter estimation using programme ISTRAES (ie Direct Search and Gradient Methods). Each cell covers an area in which part of its data have been used in the neighbouring cell. This kind of overlap is taken both laterally and longitudinally to a particular frame or reference orientation.

The idea behind this procedure is that, if subjectivity is introduced by a particular choice of sub-area, this should be eliminated by this gradual coverage, provided sampling is ideally perfect.

3.6.3 Procedure

Mapping was originally carried out by measuring field structures and numbering stations. The density of such measurements amounted to roughly 500 per km^2. However the distribution of the collected data is far from homogeneous as it is dependent upon factors such as accessibility, availability of outcrops etc .... For example the present analysis is constrained to the southern half of the mapped area as data are more readily available there. A great effort was made to establish a sampling net as homogeneous as possible (see structural map, figs. 2-2 for an idea on density of measurements and outcrop availability) and this proved to be a time consuming task.

The geographical coordinates of each station were calculated and each datum was filed (computer input) according to its co-ordinates.

The whole set of measurements formed initially a huge matrix of approximately 4,000 x 4, in which the columns included: azimuth direction, angle of plunge, vertical and horizontal (map) co-ordinates.

The actual calculations were carried out by the programme (ISTRAES) not in azimuth and plunge but in terms of direction cosines. However the subroutine READAT can cope with both situations provided that the input mode is specified in the main programme by CONTRL (3) (see appendix for details). If data are to be used intensively, as in the present case, it is more efficient to transform the whole set to direction cosines.

Sorting data from the above matrix was carried out by an auxiliary routine that selected those in which the co-ordinates were within the limits of the frame of each individual cell. However, another modification proved to be necessary soon after the early estimations were carried out. It can be seen from the maps of figs. 2-2 that structural control is important in the mapped area. The thrusts, foliations and other structures trend approximately NE-SW. Field observations showed that changes in the structural pattern is done preferentially along zones more or less parallel to this direction. For this reason the whole set of data had its co-ordinates rotated by 45^{o}, so that scanning could be performed parallel to these structural zones and thrust traces. Both the size of each cell and the amount of data it contained varied in these determinations as data are not homogeneously distributed throughout the area.

Over 200 estimations were carried out using programme ISTRAES, which stands for Irrotational STrain RAtio EStimation. This outputs not only the numerical results but also a graphic plot (line printer-type) of the fitted curve and histogram.

The results are shown on the map in fig. 3-18 while fig 3-19

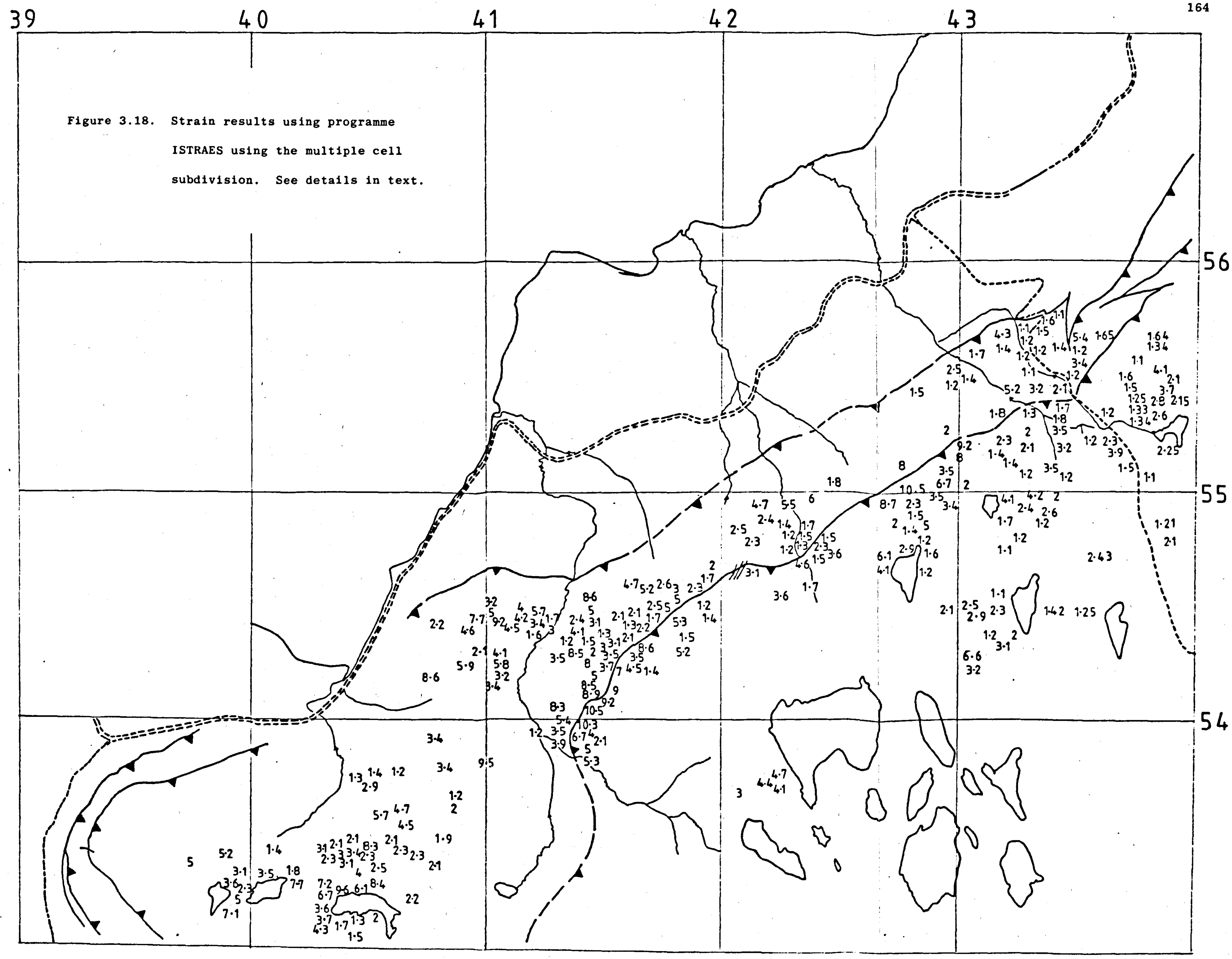

Figure 3.18. Strain results using programme ISTRAES using the multiple cell subdivision. See details in text.

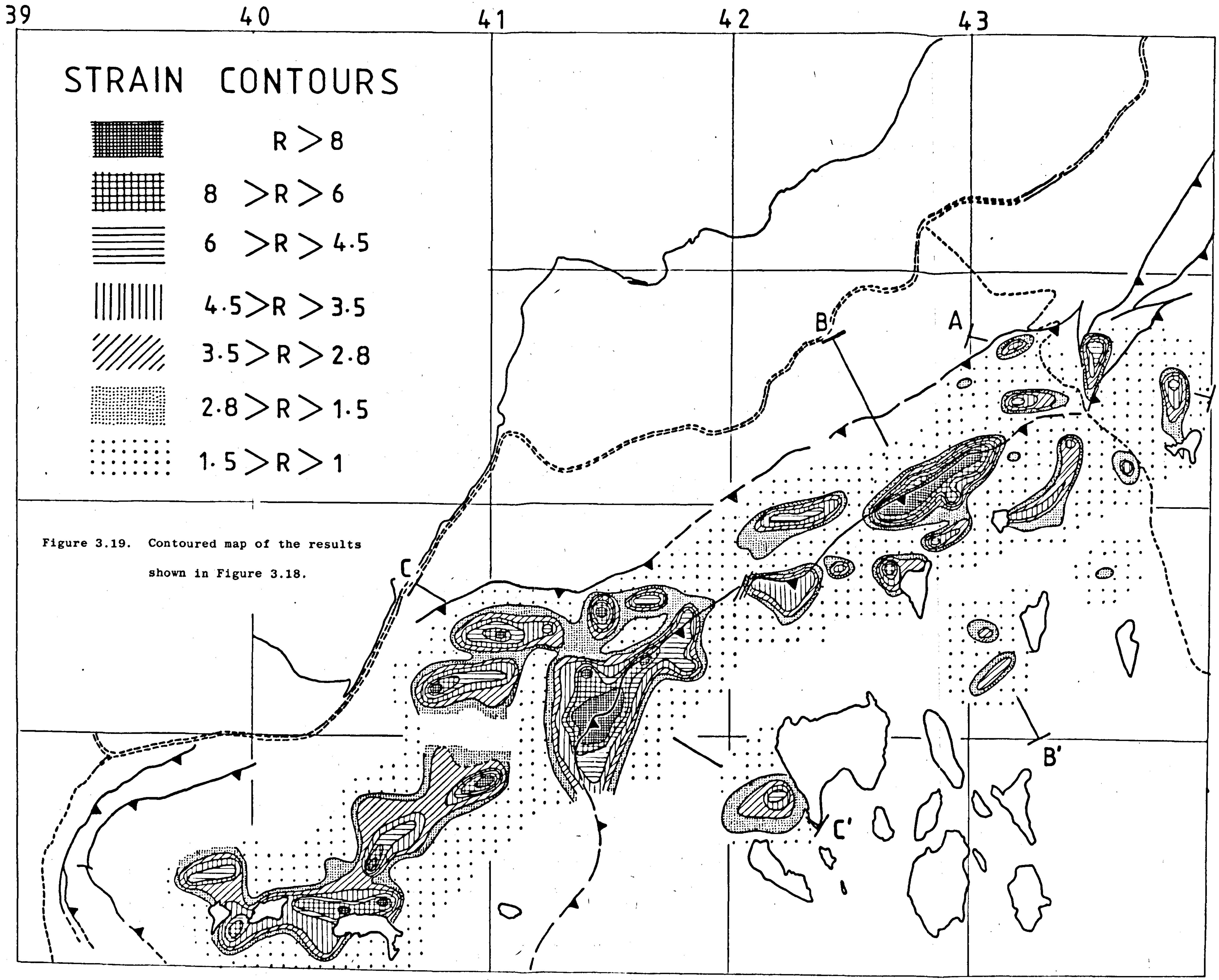

Figure 3.19. Contoured map of the results shown in Figure 3.18.

displays hand constructed contours of these values. From the above maps it is possible to draw some preliminary geological conclusions.

(i) The R-estimates have higher values near the Upper Thrust (the MTP) and decrease with increasing distance from the thrust trace .

(ii) Within thrusts there are domains where deformation values are different and this confirms field observations that there are zones with different intensities of deformation.

(iii) Variations in the Means of the original distribution confirm the sub area division displayed in figures 3-11 and 3-12.

(iv) From figure 3-20 it is clear that the distribution of the original Means is as follows:

- 70% within the range $90^{o} \pm 10^{o}$
- 20% within $100\text{-}110^{o}$ and $70\text{-}80^{o}$
- approximately 10% in the limits of $60\text{-}70^{o}$ and $110^{o}\text{-}120^{o}$
- The modal class is not at 90^{o} but in general it is shifted to approximately 5^{o} from this.

(v) From fig. 3-21 which deals with the variations in estimates of the original Standard Deviation, we can draw the following conclusions:

- 45% are localised within the range of $\sigma \leqslant 10^{o}$
- 33% are between 10^{o} and 20^{o}
- 22% are in the range $20\text{-}30^{o}$

(vi) There was not a single example where the estimated Mean was greater than 135 or less than 45^{o}.

(vii) Far less than 5% of the results gave estimated Standard Deviations greater than 30^{o} and none less or equal to 1. The values of σ greater than 30^{o} are geologically meaningless and also inappropriate with the used function (Agterberg 1963, Sanderson 1973)

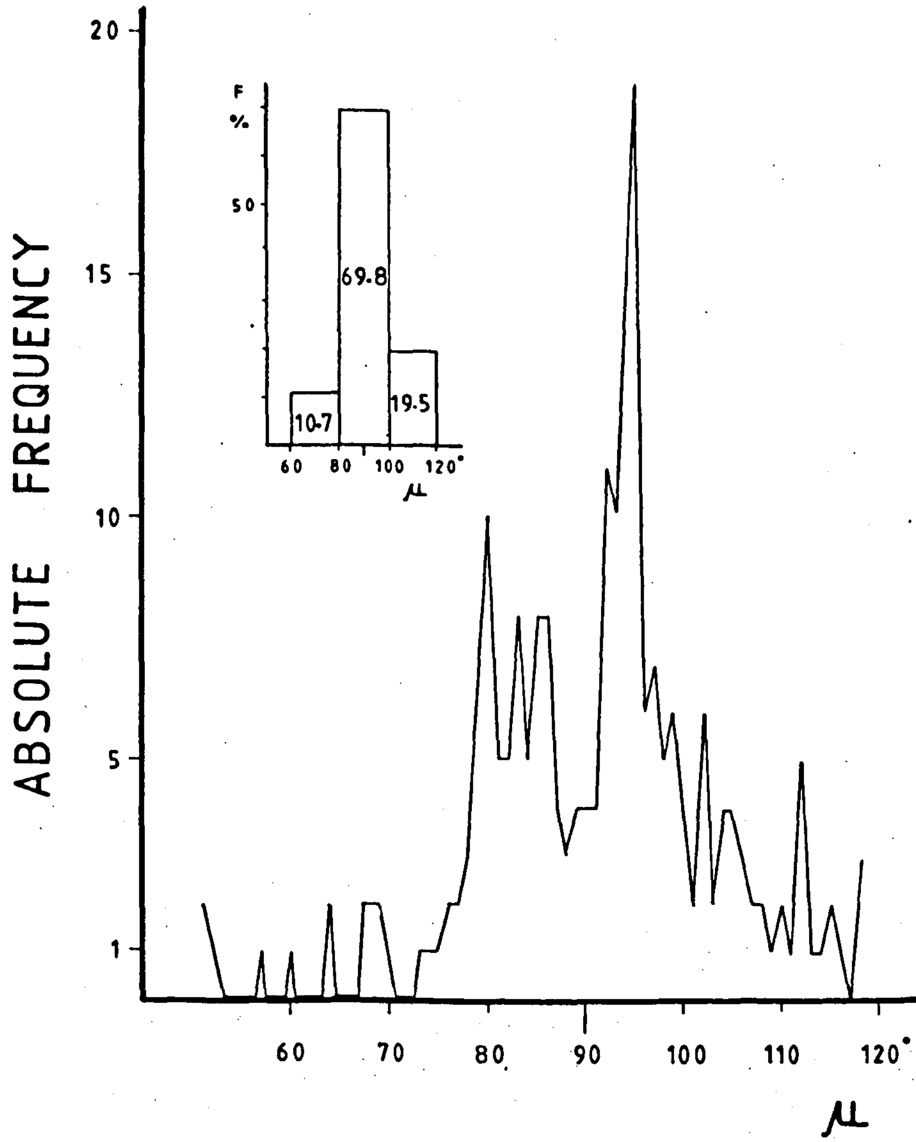

Figure 3.20. Diagram of the frequency of the estimated original means, prior to the deformation. Inset, grouped histogram, featuring relative percentages. See details in text.

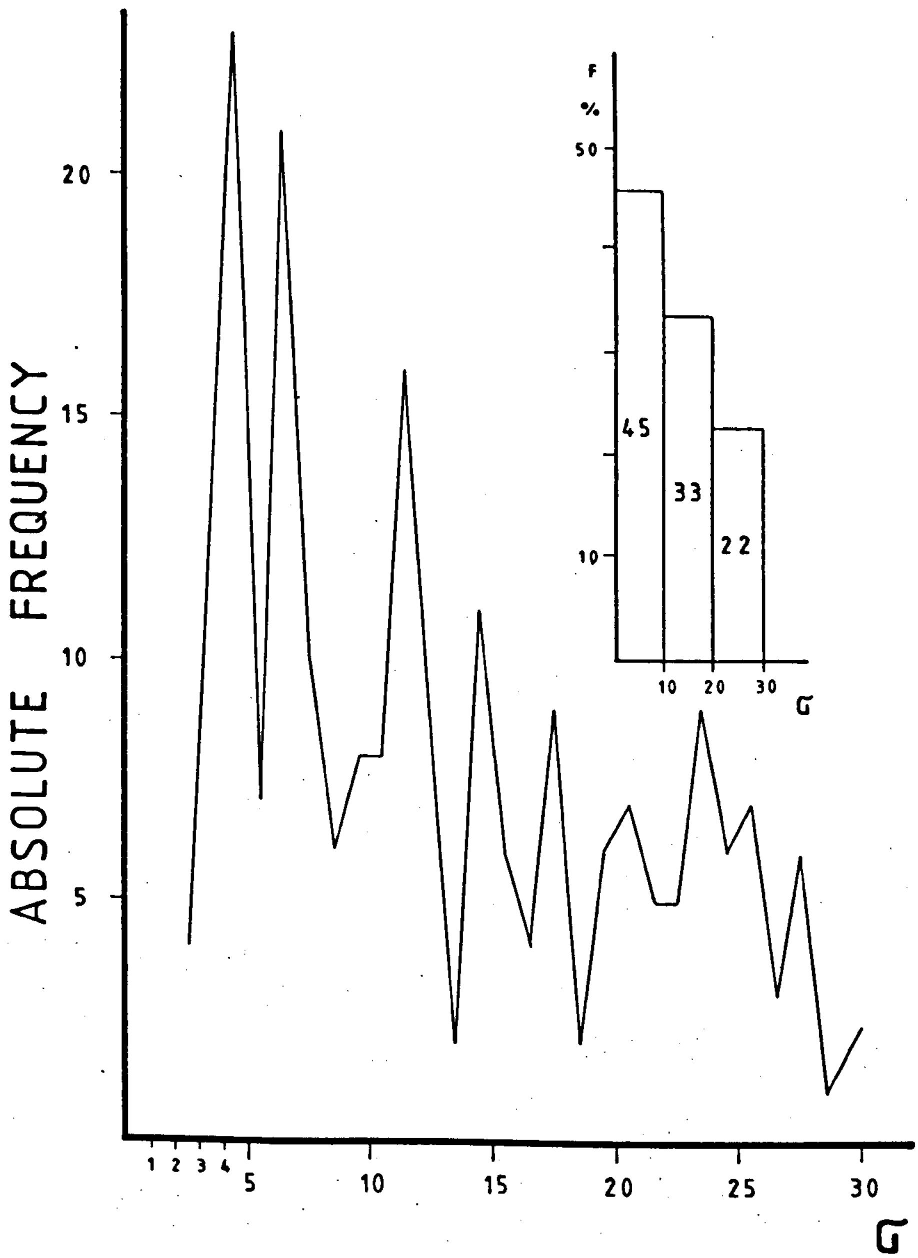

Figure 3.21. Diagram of the frequency of the original standard deviations. Inset, grouped histogram, featuring relative percentages. Full details in text.

Thus in conclusion:

1 - Over 200 estimations were obtained from Eriboll area and the results are within the geological limits of acceptance.

2 - If we accept the initial proposition of the model, folds formed in the Eriboll area are initially formed with hinges at very high angles to the direction of movement.

3 - The estimates for the Standard Deviation around the mean do not follow strictly the theoretical limits taken from the measurements made on experimental models of folds made by Dubey (1976).

4 - Results of the 'Multiple Cell Subdivision' corroborates the values found earlier by the Direct Search Method. These are displayed in figs. 3-11, 3-12, 3-16 and 3-17.

5 - The Multiple Cell Subdivision reveals the existence of high values of strain near the upper Thrust trace (the MTP) and also in the zones within the mylonitic belt.

3.7 Discussion

Figure 3-22 displays three strain profiles across the deformation belt. The indications are that the Upper Thrust Zone (the MT) constitutes a ductile shear zone with a progressive increase of deformation towards the thrust trace. In profiles AA' and CC' strain also increases westwards but near the b-thrust the strain intensities drop. However it must be remembered that there are considerably less data available in vicinity of this b-thrust than near the upper MTP, so these results must be taken cautiously.

Figure 3.22.

Strain profiles taken from the map of figure 3.19. Horizontal scale is approximately 1:10,560. Arrows indicate the positions of the Moine Thrust (MT) and the b-thrust along the considered sections.

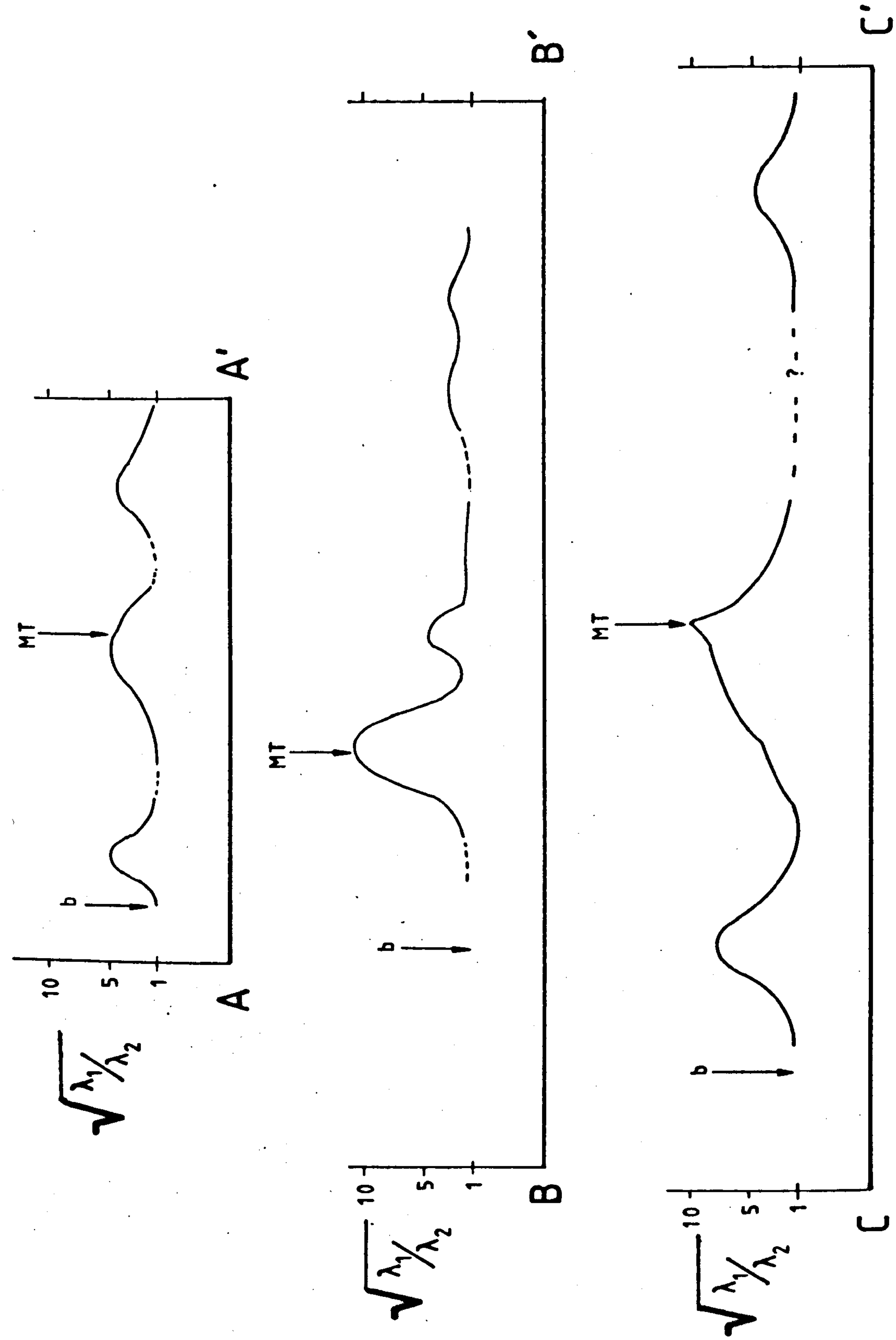

The histograms of figs 3-11 and 3-12 enhance some aspects of the information already contained in the structural maps of figs. 2-2 and the stereoplots of figs. 2-5 and 2-6. That is, they show the preferential distribution of fold axes maxima in the sub areas covered by the strain determinations dealt with in this Chapter (ie the area of figs. 3-16 and 3-17).

Figures 3-23 and 3-24 plot the directions of the dominant maxima in each sub-area, taken from the histograms of figs. 3-11 and 3-12. The length of the arrows is proportional to their relative frequency, as read directly from the ordinate of each histogram.

Figure 3-23 concerns the F_2-folds and there are clearly two different asymmetrical patterns. Throughout most of this area the dominant maxima lies to the left of the X-direction (view down-plunge of X). However the opposite asymmetry is seen for sub areas 8 and 9. The original means (μ) of the fold axes, previous to the superimposed strain, are also plotted in each diagram. With the exception of data in sub-areas 17 and 8, all the μ-directions plot to the NE or SW, normal to the movement direction in the thrust belt. The two exceptions trend respectively 083^{o} (sub area 17) and 150^{o} (sub area 8) which clearly conflict with the neighbouring results. It is more likely that these two results for parameter estimation should not be taken into account as they reveal contrastingly low strain estimates, if compared with the other diagrams.

Figure 3-24 show the plots of the enhanced maxima taken from the F_3 histograms of figs. 3-12. For this fold phase the analysis is more complex as the histograms may exhibit more than one sub-maxima. Grouping of diagrams according to similarity in maxima directions reveals 3 main domains: In domain (1) the dominant maxima is directed towards the east (sub areas 3, 6, 7 and 12). In domain (2) the dominant maxima is towards south (sub areas 8, 9, 13, 14, 15, 16 and 18). In

Figure 3.23. See explanation in text.

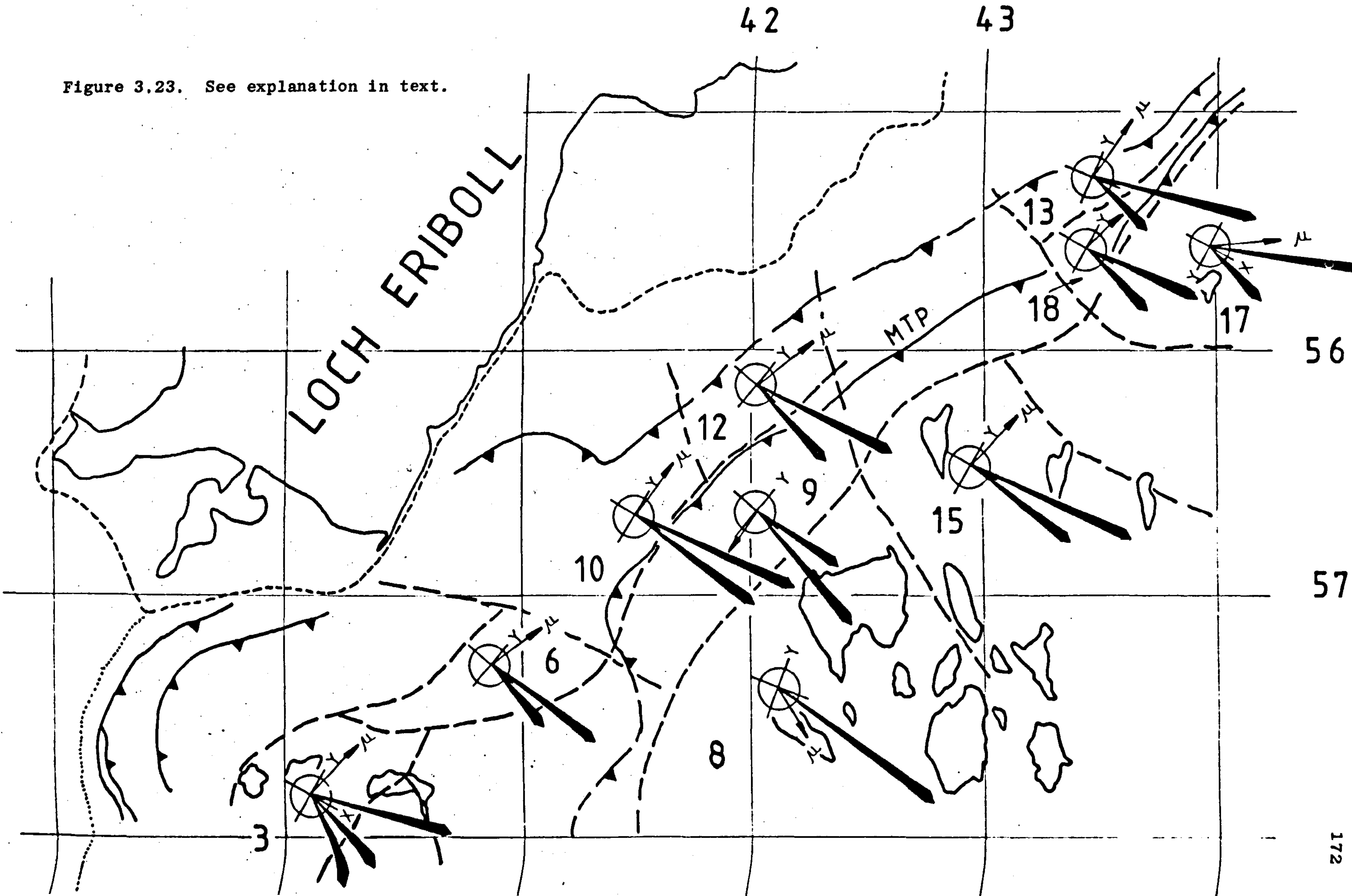

Figure 3.24. See explanation in text.

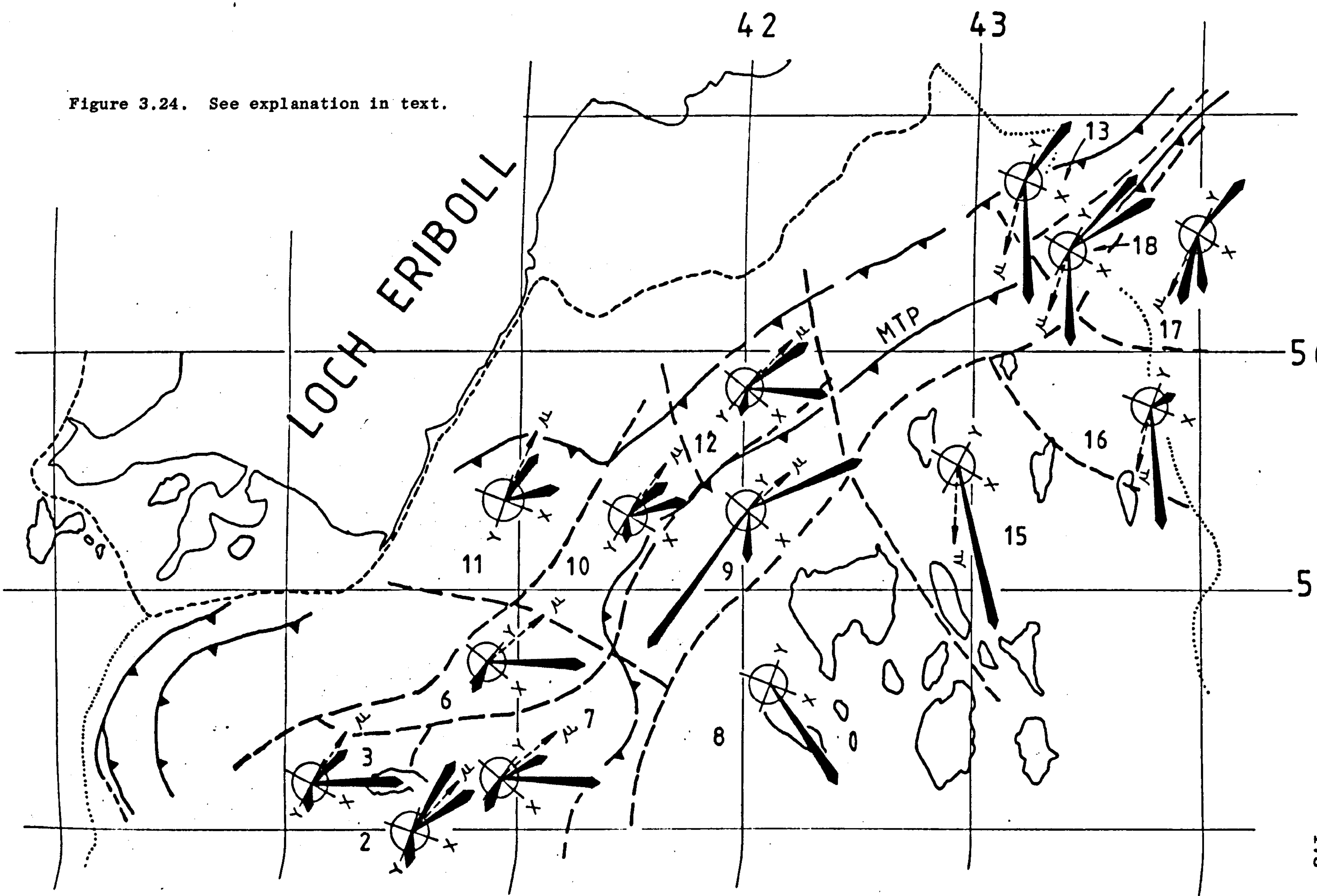

domain (3) the dominant maxima is directed to the NE quadrant (sub areas 10 and 11). However most of these diagrams include one or more sub maxima that might be parallel to the dominant maxima of another domain. For example the diagrams of sub-areas 2, 3, 6, 7, 9, 12, 13, 18 and 17 contain elements oriented to the NE quadrant (of the third domain). Diagrams classified in the first and third types, contain sub-maxima directed to the SSW. As it will be shown later, there could be factors influencing in the sampling collections and this can cause the predominance of one trend.

There could be several possible interpretations for the distribution of fold axis orientations shown in fig. 3-24.

1 - The discrepancies between the directions of the maxima in sub-areas 3, 6 (domain 1) and 8, 15, 16 (domain 2) may lead us to the conclusion that these two directions had completely independent development with non-coeval structures as the trends of their dominant maxima are at high angles. This would be corroborated by the fact that the western domain 1 (3, 6, 7) contains mainly Lewisian rocks while that to the east (sub areas 8, 15,16 in domain 2) is made up of Moinian rocks. If this is true,it would invalidate most of the strain determinations along the a-thrust trace (ie the MTP) as shown by figs. 3-18 and 3-19. The results that would be valid are those which were plotted away from this fault zone.

- However it is believed that the F_3-structures of the Lewisian and Moinian sub-areas are coeval because of the following reasons:

(i) These discrepancies in orientations are not observed northwards where there is a reasonable similarity between the diagrams plotted for sub areas 13, 18 and 17.

(ii) Field observations clearly do not corroborate the non-coeval hypothesis for F_3-structures as these can be traced across the a-thrust zone

(iii) The F_3-folds in both nappes (ie above and below the MT zone) have the same relationships to the F_2-folds, L_2-lineations and S_1-foliation.

(iv) North of the area of fig. 3-24 where the thickness of the mylonitic domain is reasonably constant there are no such discrepancies in the orientations of fold maxima, as observed for the southern sub areas 3, 6, 1 and 8, 15, 16. It seems that there is a relationship between the widening of the mylonitic zone and the development of oblique fold orientations.

(v) The diagram for sub area 9 refers almost entirely to structures of the Moinian Nappe. This diagram seems to exhibit the directional elements of the both contrasting sub areas (ie 3, 6, 7 and 8, 15, 16).

2 - Another possible explanation for the existence of such discrepancies in orientations between domains 1 and 2, is the possibility that the two nappes had initially (previous to folding) different regional attitudes: the foliation in the lower nappe dipping perhaps to the NE quadrant while in the Moinian Nappe the dip was to the SE. In the event of folding, with movement towards the WNW direction, this would produce mostly NE plunging folds in the Lower Nappe while the hinges in the Upper Sheet should plunge towards the south. At the junction of the two sheets the fabrics would develop elements of the two zones and that is why it is difficult to differentiate the structures and lithologies along the a-thrust zone.

The hypothesis of different initial tilts to the foliation and consequently different plunge directions towards the NE and SE quadrants seems reasonable. These plunge directions are also confirmed by plotting the azimuth of the original means (μ) as deduced from diagrams of figs 3-11 and 3-12 (see dashed arrows in figs. 3-23 and 3-24). For F_2-folds most of the means are oriented towards the NE. For the F_3-phase the azimuth of the original means (μ) are towards SSW (200^o) for sub areas 13, 18, 17 and 16. In the domain of sub area 15 it was oriented towards 180^o and for sub-area 8 the indications are that it was towards 150^o. In the rest of the sub-areas the original means plot in the NE quadrant ranging between directions 025^o and 050^o (see fig. 3-23), and these accord very well with the folds being formed at high angle to the WNW direction of movement of the thrust belt.

3 - Another possible reason is due to differential movement of the thrusts. The discrepancies in preferred orientations become enhanced in the zone where the nappe above the b-thrust thickens and this thickening might be connected with the deflection of the directions of the structures of the upper Moinian Nappe. Perhaps this thickening is related to the differential flow in the rocks of the Moinian Nappe and the observed effects are the gradual deflections in the directions of fold hinges from SSW plunge (sub area 17 and northwards) to SSW (sub area 15 and 16) and finally to the SW (150^o) as in sub area 8. The effects of this thickening in the rocks (sub areas 3, 6, 7) below the a-thrust, would be analogous to the creation of a vertical (ductile) shear zone with sinistral displacement, in the Moinian Nappe. This would gradually deflect the hinge directions as explained before. Measurements of the orientation of the finite X-axis in this area (fig. 3-24) reveals that in sub-area 8 it plunges towards the 109^o direction while in the neighbouring sub-areas 9 and 12 it is directed towards 129^o. The

azimuth of the X-axis in sub-areas 15, 10, 6 and 2 is towards 118°. This reveals that the ellipsoid X-axis for sub-area 8 is deflected (anticlockwise) relative to the surrounding sub-areas by 10-20°.

A sinistral relative displacement for sub-area 8 may also explain the pattern of F_2-folds in figs. 3-23. However this fold generation seems not to have developed the same pattern of different maxima orientations as observed for the F_3-phase. This apparent more uniform maxima orientation for F_2-hinges, as observed in fig. 3-22, supports the idea of the coeval nature of the fold structures across the two nappes, at least in the limits of this study area.

3.8 Comments on Other Possible Models

The model described in this chapter may appear unsatisfactory to some geologists especially to those who advocate a simple shear mechanism as the only strain mechanism in a thrust or shear zone. Let us first consider the difficulties in devising a simple shear model and then discuss the possibilities of more complex situations which make use of composite mechanisms.

The first difficulty that one faces in simple shear is the problem of finding a reference frame and co-ordinate system. In the co-axial model of Sanderson (1973), this was tackled by finding the position of the XY-principal plane of the finite strain ellipsoid, defined statistically by the best fit plane which contained the resultant direction of L_1 (cf sections 3.2 and 3.5). However if one accepts the parallelism between the above structures and the principal XY-plane for the simple shear case (eg Escher et al. 1975, p.163, fig. 4) then there is an additional difficulty in that the position of this XY-plane changes at each strain increment (see Ramsay 1981, fig. 15). It would be helpful if we knew the accurate attitude of shear plane. It may be possible to find this where the boundaries of the zones are shown on vertical cliffs (see Escher et al 1975) but in the great majority of the thrust zones the only available information is the field location of the thrust trace and not its overall attitude. Sometimes the thrust dip is obtained from structural contour lines but in many areas thrusts are not constant in dip and warp around bulges (cf Elliott and Johnson 1980). However many shear and thrust zones contain strains which are not just due to simple shear. In some areas there is evidence for variations along the longitudinal direction of the deformation zone (ie along the supposed Y-axis). This is incompatible with a simple shear model. The grain shape analysis (Chapter 4) suggests that there may be variations along the longitudinal direction of the thrust zone at Eriboll.

A further complication is the relationship between two fold phases (F_2 and F_3) and the shear zone. Would these be considered 'contemporary folds' (cf Escher and Waterson 1974, p.224)? If the strain pattern in shear belts followed the model by Ramsay and Graham (1970) no folds should form (Carreras et al 1977). Perhaps this simple shear condition could be invoked here in order to explain the early phase of mylonite formation (S_1) which could be marked by flowage and may not necessarily include folding.

Ramsay (1981, p.92 figs. 13) has shown that for buckling of planar structures to occur it is necessary that the angle between the shear direction and the surface to be folded be obtuse. This is considered unlikely in this thrust zone. The folds studied here are mainly in 1C Class (see Chapter 2) and this suggests a component of layer parallel shortening present in the zone.

It might be argued therefore, that if a model involving only a simple shear mechanism was readily available, the nature of its results and its applicability would be perhaps as much debatable as the co-axial model presented here. The two fundamental mechanisms, pure and simple shear, are perhaps too simplistic to account for the observed structures in such zones of complex deformation history.

Perhaps it is possible to obtain a better approximation of the real deformation if we include a combination of strain mechanisms. One way to explain the orientation of fold axes with axes plunging towards the stretching direction would be by admiting the existence of two simple shears in which the shear planes are at high angles to each other. The hypothesis of the existence of such mechanisms in shear belts has been advanced previously by Escher et al (1975), Grocott (1977). Another possibility would be to allow the operation of pure and simple shears in varied proportions (cf Ramberg 1981, see also chapter 2). This combination would allow one to explain fold initiation of buckling by a layer parallel shortening component and a further tightening and reorientation by the rotational strain. Bell (1978) considered that this mechanism operated in Woodroffe Thrust Zone, Australia. Still another way to combine mechanisms is by reversing the order of these two last strains, though this fails to produce folds. Perhaps if we allow another mechanism to actuate in conjunction with this combination (eg horizontal shortening ± subhorizontal simple shear ± flattening component) we might obtain a better analogy to observed geology and structures in thrust zones.

It is worth pointing out that curvilinear folds used in the way explained in this chapter give strain results that must be considered poor estimates if compared with other markers such as deformed particles. These limitations are inherent to the nature of the original formulations of the models (Mod I and II). These two models can only take into account the modification in hinge orientations during deformation, and were compelled to neglect the changes in length which occured during this event. We should envisage this type of strain analysis as giving a comparison of deformation intensity rather than absolute strain values. In this respect it is believed that both the basic mechanisms, simple or pure shear, will yield relatively the same qualitative results.

CHAPTER 4

GRAIN SHAPE ANALYSIS

4.1 Purposes

This work is based on fabric analysis made from the shape of quartz grains in Cambro-Ordovician rocks. The early intention was to quantify the variation in deformation intensity in the quartzitic rocks from an area which shows a complex deformation history. Rock samples of quartzites were collected from the Thrust Zone so it was possible to investigate if there was any systematic variation in the pattern of deformation throughout the area. This could perhaps confirm field evidence that the deformation intensities appeared to vary along the mylonitic zones.

The Paleozoic Quartzites are suitable for this kind of study and they crop out as strips within the domain of mylonitic rocks (ie above the b-thrust, figs. 2-1) of the northern part of the mapped area. This simplified map of fig. 4-1 shows the limits of this area. The distribution of the quartzitic rocks in the mylonitic zone is irregular. For this reason, sampling could not obey an ideal or systematic grid-pattern as it depended solely on the availability of the quartzites within the mylonites. Some samples were collected from below the b-thrust, to compare the results from these with the ones found for the quartzites from the above mylonites.

In general the quartzites above the b-thrust form isolated, elongated and anastomosed lenses with thickness ranging from centimetres up to metres. Above the Church Creag (Kempie Bay) there extends a discontinuous fringe of basal quartzites, for nearly 1 km, very near the b-thrust surface. In the area to the NE of Loch Hope there are numerous bands of quartzite within the Lewisian mylonites. In the region of the Arnaboll Hill the samples come from below the b-thrust and most of them are from Pipe-Rock.

Altogether 50 samples were selected from domains shown in fig. 4-1. These will be referred to after their geographical location

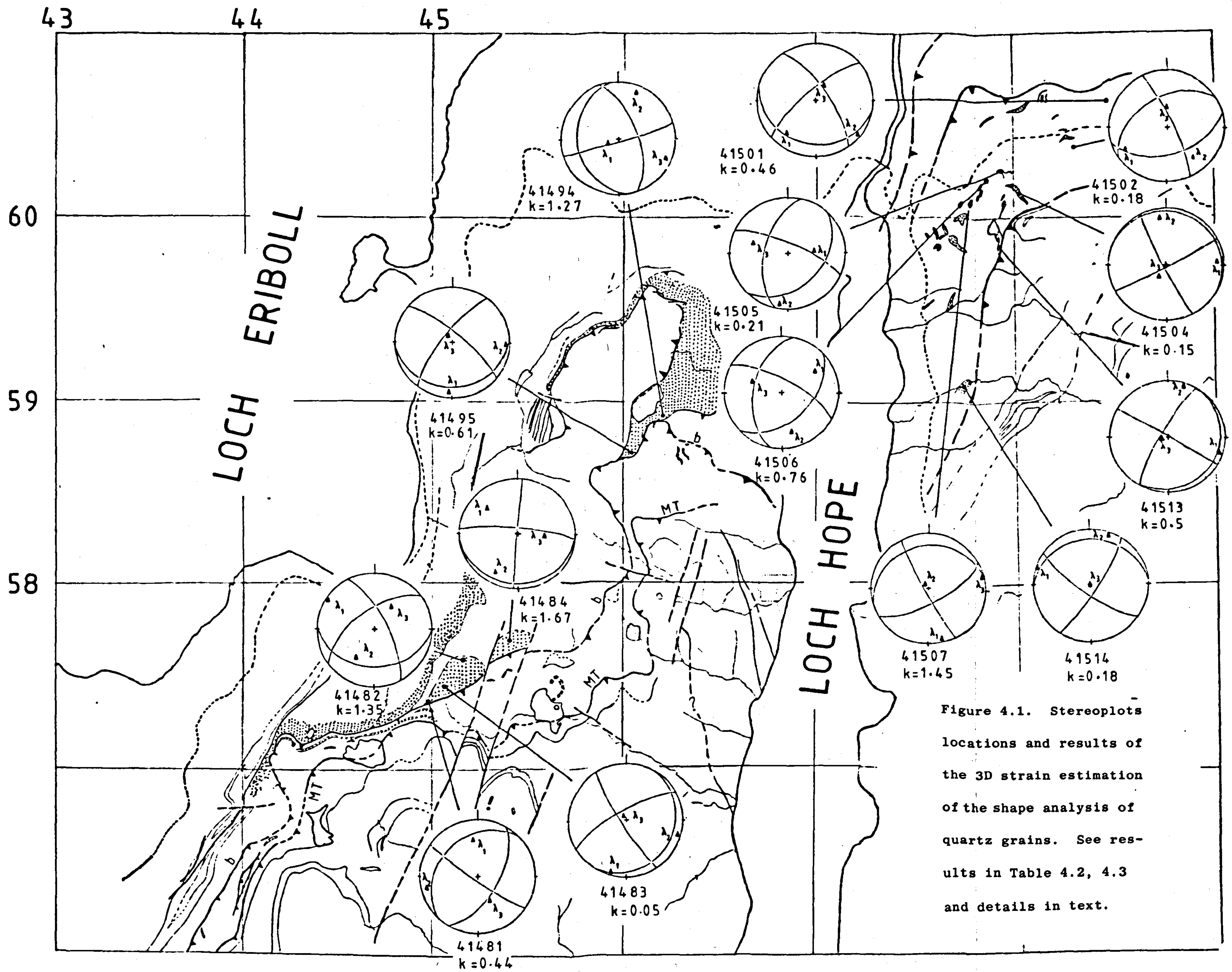

Figure 4.1. Stereoplots locations and results of the 3D strain estimation of the shape analysis of quartz grains. See results in Table 4.2, 4.3 and details in text.

as the Kempie, Arnaboll and Hope sub-areas. However, only 14 samples provided reasonable clasts for measurement. The microtextures in the other samples exhibited a very high proportion of recrystallization which made them unsuitable for shape evaluation. These recrystallized grains proved to be very useful for Paleopiezometric determinations, discussed in Chapter 6.

The distribution of the 14 remaining samples, in the context of the 3 sub-areas, is also far from ideal; for example in Kempie sub-area the determinations do not come from quartzites within the main mylonitic zone (ie above the b-thrust) but from the edge-zone of basal quartzites. The sub-area of the Arnaboll Hill provided only two suitable specimens while the rest of the samples were from the mylonitic domain of the Hope sub-area.

It is the aim of this chapter firstly to describe in detail an analytical method of determining the ellipsoid using data collected from 3 orthogonal planes, and also to introduce an alternative solution for the case where the fitted conic is not an ellipsoid. Secondly the results from Eriboll-Hope quartzites using this method are compared with those obtained from previously existent routines. There follows a discussion on the 'strain' determinations relative to the geology and structure of the area.

4.2 Two and Three Dimensional Strain Determination

4.2.1 Comments on Some of the Available Methods

Strain measurements with initially non circular objects seem to be the most commonly encountered situation and there is an extensive record of such examples for geographically different tectonic environments (Flinn 1956, Staufer 1967, Hossack 1968, Dunnet 1969, Gay 1969, Mukhopdyay 1973, Hutton 1979). Usually the strain is evaluated from two dimensional surfaces and eventually these are combined in order to give a three dimensional ellipsoidal surface. The evaluation of the shape of the ellipsoid is a problem that might be handled geometrically in different ways, but in general the three most common situations are:

(i) Data may be collected on the principal planes of the strain ellipsoid. This presents a great advantage in terms of simplicity and speed of computation for it needs data in only two of the principal planes to perform the determination (Ramsay 1967, Dunnett 1969), the third plane being used as a check for the internal inconsistencies originated during routines of data collection, sectioning and measuring.

(ii) Commonly, measurements may be taken from any three perpendicular planes and the resultant ellipses are combined in order to best fit an ellipsoid (Ramsay 1967, pp.142-147).

(iii) In some cases data must be gathered from any three planes which are neither orthogonal nor parallel. Situations such as these could arise in cases where the samples cannot give three orthogonal surfaces or in the case of particle measurement being performed directly in the field, where the conditions of 3 orthogonal surfaces are seldomly found.

Depending on the method used and the availability of strain markers, there are always conditions or assumptions to be met. Assumptions frequently involve the correlation between the position of the finite strain axes and rock structures such as lineations, cleavage or foliation. Sometimes where the available deformed markers cannot be considered as having had a predeformational spherical shape, there are assumptions on their initial orientation fabric.

In the present study data were not collected on the principal planes. Due to the poor content of pelitic material in the quartzites, many rocks did not exhibit a well developed cleavage and had instead a massive appearance. In many cases it was very difficult to identify the stretching lineation. It was also this study's intention to make use of a method which was free, as possible, from the assumptions mentioned above.

Usually the two dimensional evaluations are made in terms of shape (ie ratio of particle dimensions) rather than in terms of absolute dimensions (size). The commonly used two dimensional strain methods are listed as follows:

1. Means of Final Particle Ratios (Rf) - Cloos (1947) used the arithmetic mean ($\bar{R}$) of particle ratios as an estimate of the 2D-strain. Dunnett (1969) considered the geometric mean (G) of the ratios (Rf) as a better estimate, while more recently Lisle (1977) introduced the use of the Harmonic mean (H). Lisle (1977) also confirmed the relationship.

$$\bar{R} \geqslant G \geqslant H \qquad : \qquad [4-1]$$

which is in fact Cauchy's Theorem (see Bartch 1974, p.39). The above inequalities should increase with the increase in the dispersion of particle ratios $(Rf)_i$, $i = 1,2, \ldots n$.

All the above means do in fact overestimate the strain ellipse ratio, R (see Lisle 1977).

2. Non Spherical Markers - Ramsay (1967, pp.207-211) dealt with strain determination from a group of elliptical and passively deformed markers. He correlated the final ratio (Rf) and orientation (ϕ) to the initial orientation (θ) and ratio (R_i) and strain (R). Subsequently Dunnet (1969) devised a method based on mathematically

derived curves. The condition of this model is that there is a pre-deformation random distribution of the particles longest axes orientation (θ). Dunnet's method used the visual best fit of Rf/ϕ data to the curves and this procedure carries a great deal of subjectivity.

The Rf/ϕ-method was subsequently modified (Dunnet and Siddans 1971) to deal with primary structures (planar or imbricated) and adapted as FORTRAN IV computer programme named STRANE, listed in Siddans (1971). This method, also referred to here as the DS method, assumes a knowledge of the strain principal axes, and the strain estimation is carried out by an unstraining routine using co-axial deformation.

3. Elliott (1970) suggested a method where finite strain is determined by means of a shape factor grid which allows for the estimation of the orientation and magnitude of the strain ellipse. The method does not require any assumption of initial spherical forms of particles nor an initial random distribution of their elongated axes.

4. Matthews et al (1974) derived a numerical technique which requires the data to be collected on the principal planes of the strain ellipsoid. This method relates the axial ratios and orientations of particles to the finite strain transformations. The method only requires an initial symmetric distribution (either random or non-random) of the markers relative to bedding.

   The method has been adapted, by the same authors, for a computer programme under the name X.ROT. This method does not require an unstraining operation, and is also capable of dealing with error estimation as a function of sample size.

5. Ramsay's (1967, p.195) centre-to-centre method is useful for rocks

that have suffered effects of pressure solution. The method assumes distances between particles' centres to be independent of direction and considers that, by strain, these centres will be relatively displaced.

6. Fry (1979) has recently proposed a centre-to-centre technique which assumes an initially strictly isotropic distribution. The method requires a minimum sample of 300 objects and is limited to strain ratios up to 6:1. A computer programme POINTS is fully documented in Milton (1980).

7. Mukhopadhyay(1980) has also presented a simple refinement of Ramsay's centre-to-centre technique for the case of adjacent particles with constant distance between grain centres.

8. Shimamoto and Ikeda (1976) derived a very simple technique which makes only the assumption that the elliptical particles may initially have had varied shapes and sizes but their overall distribution of axes was uniform.

They derived a set of equations which are extremely simple for a numerical method. Data are handled in terms of Rf and ϕ measurements (cf. Dunnet and Siddans 1971). The method is also valid for two and three dimensional strain analyses. This method will be thereafter referred as the SI-method.

9. The Rf/θ-method by Lisle (1977) involves a test of goodness of fit and the input data do not depend on any fixed reference direction. The principle of the method consists of unstraining the distribution of deformed ellipses by applying a co-axial progressive strain, orthogonal to the ellipse preferred orientation (ie the vector mean) and then testing the distribution with the Chi-Squared test (χ^2)

The lowest value in the χ^2-test is chosen as the inverse of the imposed strain, R. The value of $\dot{\chi}^2$ at the best-fit is in itself the goodness of fit of data to the model. A FORTRAN IV computer programme names THETA, based on Lisle's (1977) method is fully documented in Peach and Lisle (1979).

Among the listed methods, the Rf/ϕ method of Dunnet (1969) seems to have had a wide acceptance and usage over the years. Seymour and Boulter (1979) have performed comparative tests using programmes STRANE (Dunnet and Siddans 1971) and X.ROT (Matthews et al 1974), and they showed the importance of following each model's restrictions in order to avoid errors. De Paor (1980) extended the range of Seymour and Boulter's (1979) limitations to include problems of ductility contrast. He also doubted some of the alleged capabilities of the Rf/ϕ model (see Siddans 1981, DePaor 1981). Hanna and Fry (1979) and Siddans (1980) have performed comparative strain evaluations using some of the above listed techniques and their best results pointed towards Dunnet's method.

It is the opinion of the present study that the tests by Hanna and Fry (1979) and Siddans (1980) are restricted because of their limited range of tested values. Their quoted differences and/or magnitudes may be not valid in another range. However the results of these tests give an indication of the magnitude of the differences in the final values of strain ratio. For oolitic limestone, a comparison between the DS and the SI methods shows an average overestimation for the former of less than 1% (see table I in Hanna et al 1979, p.156).

Siddans' (1980) test involves a simulation using randomly oriented ellipsoids prior to deformation. It compares results from methods of Dunnet and Siddans (1971) against:

(i) The SI method, where contrary to the test of Hanna and Fry (1979) the overestimation is for the SI method and the magnitude is 1.5%

(ii) The method of Matthews et al (1974) which also overestimates the results of the DS method by approximately 1.23%

Whether or not these differences can be generalized for all ranges of strain values is not the concern here. What can be readily concluded is that the magnitude of the quoted differences is less than the errors introduced during procedures of sampling, sectioning, measuring, etc...

Siddans (1980), contrary to Seymour and Boulter (1978), also concluded that the SI, DS and Rf/θ-methods are equally valid when data are not sampled from the principal planes of the strain ellipsoid.

In view of what is described above, the best choice for a two dimensional strain method should be towards the one which produces the best results at the expense of the least effort. There can be no doubt that the SI method fulfils the requisites. Indeed this technique is so simple that its programme is restricted to only a few lines (compared with the hundreds of lines requires both by STRANE and THETA programmes) and can be easily performed by a pocket programmable calculator.

Comparisons, made by the author, between the SI and Rf/θ methods clearly reveal a tendency for the Rf/θ method to present overestimated values (see tables 4-2, 4-3; also fig. 4-7-a). If we recall that the Rf/θ method uses the harmonic mean, and that Lisle (1977-b) showed it to overestimate the strain ratio, R (at least in the range $1 < R < 10$), it is therefore concluded that the SI-method holds the best characteristics of simplicity and also precision. For these reasons the SI-method was fully incorporated in the present routine and programme of strain evaluation.

4.2.2 Some Problems Involved with Shape Measurements

As was shown in the previous sections of this chapter, there are many methods of estimating the strain based on particle shape. However what has been largely neglected in many previous papers is that it is equally possible to perform grain measurements in many different ways, and this influences the final results.

In the present study the shape measurements were carried out by means of a Shadowmaster (with cross polars) which projects the image of a transparent section onto a frosty surface. The details of each grain boundary were carefully transferred onto a transparent perspex sheet which could be used for direct measurement or copied on tracing paper. Some of the possible errors involved in this routine are listed below:

(i) Errors in the measuring device - every instrument carries errors inherent to its characteristics and scale.

(ii) Errors due to distortions of the projected image. These increase with the distance from the centre of the field.

(iii) Errors due to copying. These could be avoided if photomicrographs were used instead of the shadowmaster projection.

(iv) Errors due to sectioning effects. It would not be guaranteed that perfectly orthogonal sections were cut from each sample. The present sections were cut at approximately 90 ± 5^{o} to each other.

(v) Errors due to resolution of the equipment. Errors due to diffusiveness of the particle boundaries are inherent to the shadowmaster routine, due to the projection on a translucid surfaee. Pickering (1976, p.11) gives a relationship for error due to microscope resolution and this can be useful perhaps when measuring from photomicrographs.

(vi) Errors due to irregularities in particle shape. As expected the shapes of quartz clasts departed from an ideal ellipse especially in the less deformed specimens.

Measurements of the longest and shortest axes of particles can pose some difficulties as it is sometimes difficult to locate these positions. The more circular the particle the more difficult to determine the axes locations. On the other hand if the grain boundaries are too irregular, due to recrystallization or pressure solution effects, then the availability of a clear preferred elongation of the grain might not help, because the location of the orthogonal axes poses some problems. Consider for instance, the situations illustrated by figure 4-2. These were based on examples found in this study. In the case (i), the position of the (a) and (b) axes reasonably satisfy the requirements of an elliptical section, where the axes are respectively parallel and orthogonal to the elongation direction and the intersection is midway along their lengths. In case (ii), the above conditions are hardly met; the (a) axis is easily located but the position of the shortest b-axis must be chosen, for instance, between chords b_1, b_2 and b_3. The situation in particle (iii) is one in which neither of the chosen (a) and (b) axes satisfy the ideal conditions of an intersection midway along each axis.

In view of these numerous difficulties it was decided to measure the shape by inscribing the grain in a rectangle (case IV) and then taking axes (a) and (b) as the projections of length and width. This arrangement in practical terms is very convenient because it can be performed using a cheap and commercially available measuring device which consists of two dislocating orthogonal rulers (quadrograph nr.7010), and it also combines the advantage of speed and guarantees orthogonal axes during measurement because the readings from (a) and (b) axes are made in one position. The measurement of ϕ, the angle

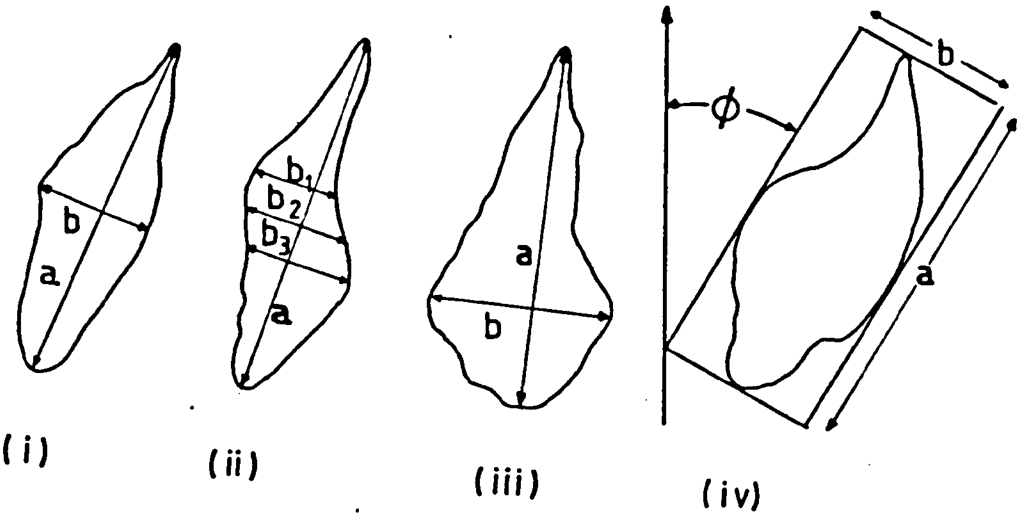

Figure 4.2. Illustrates particle ratios and some problems in locating their axes. See text for explanation.

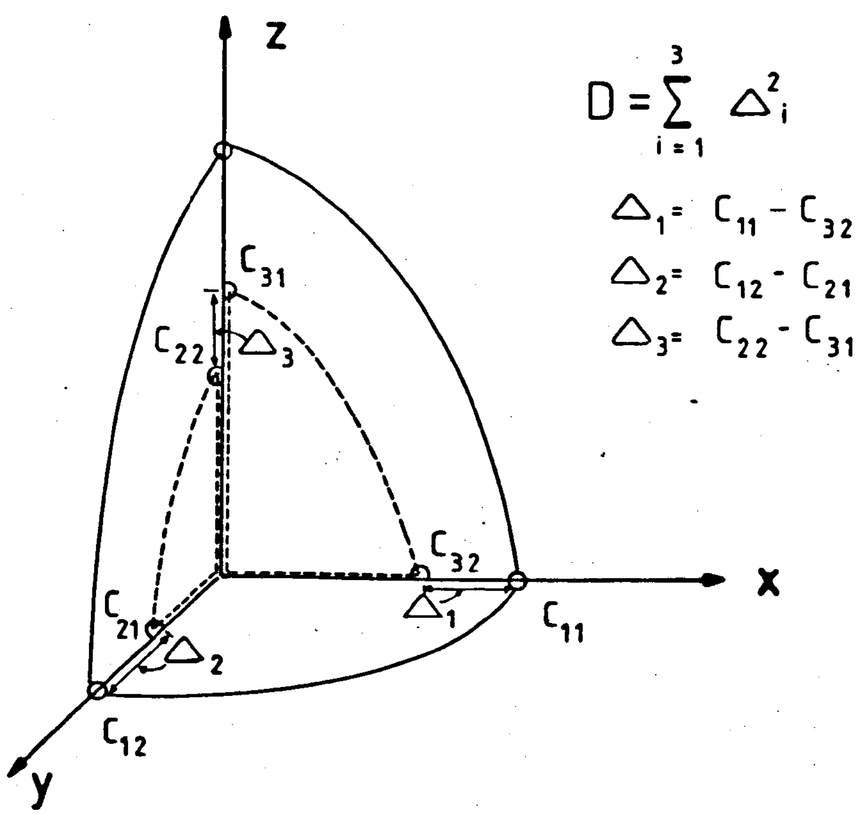

Figure 4.3. Scaling of 3 orthogonal ellipses. The previous positions of the ellipses in zx and yz planes are given by dashed lines. The ellipse in the xy plane remains unchanged because scaling is made on the other two planes (full lines) by minimizing the Δ_i differences between adjacent chords. See text for details.

between the a-axis and the co-ordinate axis, is taken separately.

The chosen way of particle measurement is clearly open to criticism, but then so are many other possible ways. Underwood (1970, p.195) has shown that the quantitative description of shape or form of particles is the most difficult and indeterminate of the stereologic aspects. He (see Underwood 1970, p.228) also lists 10 such shape indices, which may vary according to the scope of the subject in question. It is believed that these errors should decrease with the increase in the number of measurements (see Chapter 6), provided that the sample was deformed homogeneously. There have been some attempts to estimate the minimum number of particles necessary for shape analysis, but the quoted figures seem to vary. For pebbles Flinn (1956) measured up to 33 particles, while Hossack (1968) has shown that 30 is a sufficient number for accurate results. Gay (1969) took samples with populations varying from 4 up to 63, while Dunnet (1969) considered populations between 60 and 100.

In cases where the particles were oolites: Cloos (1947) used population size of 35; for Dunnet (1969) 40 is a number large enough. Tan (1976) found 30 sufficient, while Elliott(1970) considered that the measurements should be carried out until they became reproducible.

For deformed quartz grains Mukhopadhyay(1973) found reproducible results with sample sizes of 70 grains. In a study of elliptical markers Matthews et al (1974, eq32) derived the expression

$$n_m = 4\nu(\gamma_i)/(E_{Rs})^2 \qquad [4\text{-}2]$$

where n_m = minimum sample size, E_{Rs} = fractional error of strain determination, γ_i is the angular deflection in the undeformed state and $\nu(\gamma_i)$, the variance of γ_i. They give an example where 39 markers are required on the condition that the fabric was derived from initially elliptical and circular markers exhibiting random orientation. Matthews et al (1974) also pointed out that error decreases with the increase in the number of markers and they show that 53 particles produce an error in the magnitude of around 10% while 212 should give errors of 5%.

Probably, Elliott (1970) is correct in saying that there is not a unique sample size and reproducibility is the limit (ie the convergence) of measurements. Presumably the number of measurements is influenced by the availability of strain markers during data collection. For example, sampling from pebbles in the field poses far more problems and restrictions than measurements on oriented thin sections.

In the present study, the average size is around 110 grains per section and the effective range is 70-212 grains (quite similar to that of Mukhopadhyay, 1973). The routine is very laborious and time consuming. It is estimated that the average time per sample determination is around 20 hours and this includes image transfer measurements of axes dimensions and finally data input for computer calculation. The computation itself required only 4 seconds (ICL-1906-A) of CPU-time.

4.2.3 Determination of the Ellipsoid from Orthogonal Sections

4.2.3.1 General

Ramsay (1967) has shown that it is possible to combine data from 2D-strain analyses and obtain the 3D ellipsoid in two different situations:

(i) When the 2D data are collected on 3 mutually perpendicular planes and,

(ii) For cases where 2D data are collected in any three non parallel planes. The latter makes use of a projection of the results on to 3 mutually perpendicular planes - using a stereonet and Mohr circle - and then the process reverts to the first case. The procedure for determining the length of each axis of the resultant ellipsoid relies on the solution of a cubic equation and further manipulation can give the attitude of each axis.

Roberts and Siddans (1971) approached the problem of combining 2D data in 3 perpendicular planes using eigenvalues and eigenvectors in order to derive the magnitudes and orientations of the ellipsoid axes. The programme in FORTRAN IV is named PASE5 and is listed in Siddan's (1971). The method makes one of the tensor relationship derived by W. Owens (in Siddans 1971) in which the scaling ratios are used to combine results in 6 different ways. The final result is obtained by an average of the 6 results (see details in Siddans 1971).

Shimamoto and Ikeda (1976) also dealt with the problem of fitting the ellipsoid from 2D-data and their method resembled that of Roberts and Siddans' (see Siddans 1980, p.11).

Oertel (1978) and Miller and Oertel (1979) approached the problem of adjusting the 3 perpendicular strain ellipses using techniques of weighted least squares for scaling.

Casey and Powell (TSG-meeting, Nottingham Univ. 1979) presented a solution for 2D data collected in any 3 non-parallel planes. Also recently Milton (1980-a) presented a solution for measurements in any 3 non-parallel planes, and the programme, TRISEC, is fully listed in Milton (1980-b).

4.2.3.2 The Proposed Method of Fitting the Ellipsoid from Three Perpendicular Planes

The method to be introduced here, consists in adjusting the proportional magnitude of the three intersecting ellipses by an algebraic operation and then obtaining the fitting of the ellipsoid by means of a Least Squares Method. Clearly, the existence of 3 elliptical sections over-specifies the problem and it is appropriate to solve it by means of a best fit procedure (see Rogers and Adams, 1976 , p.80).

Another reason for opting for the followed routine stems from the fact that a perfect adjustment of intersecting ellipses is not always expected and then a procedure which minimizes the remaining discrepancies would appear to be very appropriate.

Let the equation of a Quadratic surface be written as

$$a_{11}x^2+a_{22}y^2+a_{33}z^2+2a_{12}xy+2a_{13}xz+2a_{23}yz-1 = 0 \qquad [4\text{-}3]$$

or in matricial form $\tilde{x}^t \tilde{A} \tilde{x} - 1 = 0$ [4-4]

where $\tilde{x}^t = [x \ y \ z]$ [4-5]

and

$$\tilde{A} = \begin{bmatrix} a_{11} & a_{12} & a_{13} \\ a_{21} & a_{22} & a_{23} \\ a_{31} & a_{32} & a_{33} \end{bmatrix} \qquad [4\text{-}6]$$

for $a_{21} = a_{12}$, $a_{13} = a_{31}$ and $a_{32} = a_{23}$

It is possible to rotate the xyz-co-ordinate axes so that the equation of the conic in the new system x'y'z' has no cross product term. This is carried out by finding a matrix

$$\tilde{p} = \begin{bmatrix} p_{11} & p_{12} & p_{13} \\ p_{21} & p_{22} & p_{23} \\ p_{31} & p_{32} & p_{33} \end{bmatrix} \qquad [4\text{-}7]$$

which orthodiagonalizes $\tilde{A}$ and ensures the transformation (rotation)

$$\tilde{x} = \tilde{P}\tilde{x}' \quad \text{or} \quad \begin{bmatrix} x \\ y \\ z \end{bmatrix} = [\tilde{P}] \cdot \begin{bmatrix} x' \\ y' \\ z' \end{bmatrix} \qquad [4\text{-}8]$$

Substitution of [4-8] in [4-4] yields

$$[\tilde{\tilde{P}}\tilde{x}']^t \; \tilde{A} \; [\tilde{\tilde{P}}\tilde{x}'] - 1 = 0 \quad \text{or} \quad \tilde{x}'^t \; [\tilde{P}^t \tilde{\tilde{A}}\tilde{\tilde{P}}]\tilde{x}' - 1 = 0 \qquad [4\text{-}9]$$

Since P orthogonally diagonalizes A

$$\tilde{P}^t \tilde{\tilde{A}}\tilde{\tilde{P}} = \begin{bmatrix} \bar{\lambda}_1 & 0 & 0 \\ 0 & \bar{\lambda}_2 & 0 \\ 0 & 0 & \bar{\lambda}_3 \end{bmatrix} = \tilde{B} \qquad [4\text{-}10]$$

where $\bar{\lambda}_1$, $\bar{\lambda}_2$ and $\bar{\lambda}_3$ are eigenvalues of $\tilde{A}$, the rotation being accomplished by [4-7]. Thus [4-9] can be written as

$$[x'y'z'] \cdot \begin{bmatrix} \bar{\lambda}_1 & 0 & 0 \\ 0 & \bar{\lambda}_2 & 0 \\ 0 & 0 & \bar{\lambda}_3 \end{bmatrix} \cdot \begin{bmatrix} x' \\ y' \\ z' \end{bmatrix} - 1 = 0 \qquad [4\text{-}11]$$

or

$$\bar{\lambda}_1 x'^2 + \bar{\lambda}_2 y_1{}^2 + \bar{\lambda}_3 z'^2 - 1 = 0 \qquad [4\text{-}12]$$

which means that the conic is in the standard position.

Data input for each perpendicular plane is in axial ratios. This means that the absolute magnitudes of the axes are not known. In order to make 3 perpendicular ellipses part of the same ellipsoid it is necessary to make them mutually compatible and this means scaling them.

In the present routine, scaling is attained by minimizing the differences between adjacent chords of the intersecting ellipses (see figure 4-3) using the Newton-Raphson Technique.

It is required to minimise the sum of differences Δ_i between chords C_{ij} ($i = 1,2,3$; $j = 1,2$), which are parallel to the co-ordinate axes (see figure 4-3). An objective function is set as

$$D_m = \sum_{i=1}^{3} \Delta_i^2 = \Delta_1^2 + \Delta_2^2 + \Delta_3^2 \qquad [4\text{-}13]$$

Figure 4-4 is a representation of the ellipse in terms of its polar equation

$$r_i^2 = \frac{b^2}{1 - \varepsilon_x^2 \cos^2\theta} \qquad [4\text{-}14]$$

where ε_x is the excentricity ($\varepsilon_x < 1$) and is given by

$$\varepsilon_x = \sqrt{a^2 - b^2} / a \qquad [4\text{-}15]$$

in which (a) and (b) are respectively the major and minor semi-axes of the ellipse, r and θ are chord lengths and angles with the major axis (a) of the ellipse.

It is possible to alter the absolute magnitude of a chord, without changing the ellipse-ratio by simple modifying the length of its shortest axis (see eqn. [4-14]). Therefore, by substituting C_{ij} by $F_i C_{1j}$, where F_i is a multiplier, in each of the co-ordinate planes on figure 4-3, we obtain an appropriate scaling of ellipses. It is also necessary to alter the objective function [4-13] firstly to:

$$D_{min} = \sum_{i=1}^{3} \Delta_i^2 = [F_1C_{11}-F_3C_{32}]^2 + [F_2C_{21}-F_2C_{32}]^2 + [F_3C_{31}-F_2C_{32}]^2 \qquad [4\text{-}16]$$

However, as scaling is made proportionately among the 3 intersecting ellipses, which means that their absolute magnitudes are not important (or even known), this allows us to set F_1, arbitrarily, as equal to 1 and the above expression becomes:

$$D_{min} = \sum_{i=1}^{3} \Delta_i^2 = [C_{11}-F_3C_{32}]^2 + [F_2C_{21}-C_{32}]^2 + [F_3C_{31}-F_2C_{32}]^2 \qquad [4\text{-}17]$$

This is the case for the Newton-Raphson technique, which makes use of the algorithm represented by the flow-chart (single

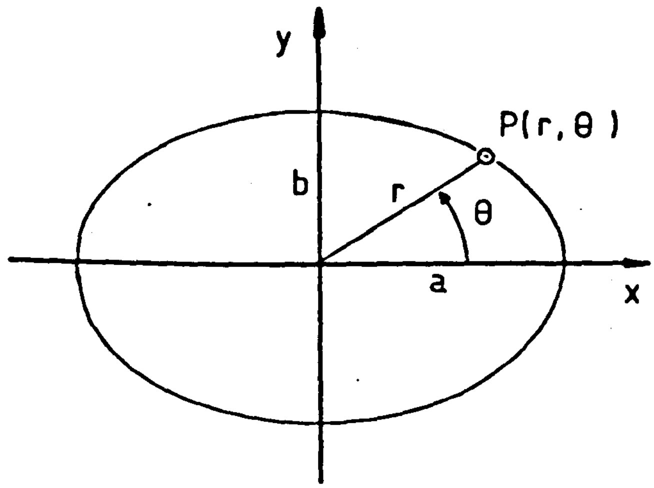

$$\varepsilon_x = \frac{\sqrt{a^2 - b^2}}{a}$$

$$r^2 = \frac{b^2}{1 - \varepsilon_x^2 \cos^2\theta}, \quad \varepsilon_x < 1$$

Figure 4.4 Representation of an ellipse in terms of its polar equation. ε_x is the eccentricity.

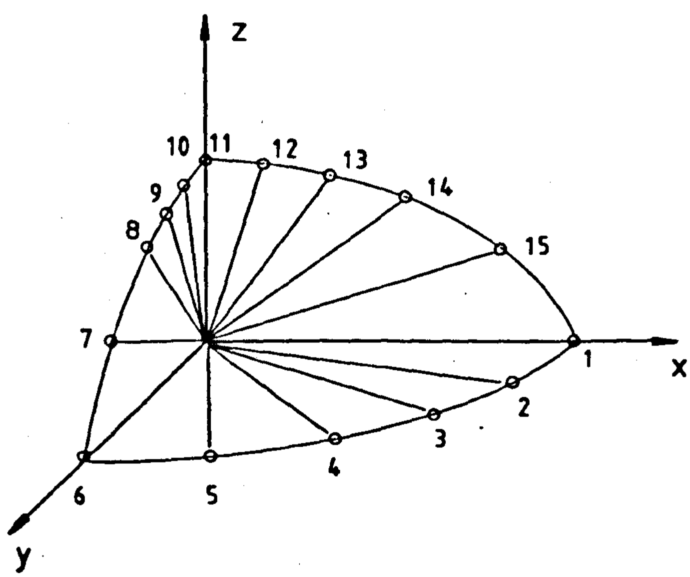

Figure 4.6. Sequence of chords obtained in each co-ordinate plane using polar equation of Figure 4.4.

variable for ease of explanation) in figure 4-5:

$$x_{i+1} = x_1 - \frac{f'(x)_i}{f''(x)_i} \qquad 4\text{-}18$$

where $i = 1,2, \ldots n$ is the iteration number, x_i, $f'(x)_i$ and $f''(x)_i$ the values of the variable, the first and second derivatives respectively, in the i-iteration.

In the present case (two variables, F_2 and F_3), the required analytical expressions are:

$$\frac{\partial Dm}{\partial F_2} = 2F_2(C^2_{21} + C^2_{22}) - 2F_3C_{31}C_{22} - 2\,C_{12}C_{21} = 0 \qquad [4\text{-}19\text{-}a]$$

$$\frac{\partial Dm}{\partial F_3} = 2F_3(C^2_{31} + C^2_{32}) - 2F_2C_{31}C_{22} - 2C_{11}C_{32} = 0 \qquad [4\text{-}19\text{-}b]$$

$$\frac{\partial^2 Dm}{\partial F^2_2} = 2(C^2_{21} + C^2_{22}) \qquad [4\text{-}19\text{-}c]$$

$$\frac{\partial^2 Dm}{\partial F^2_3} = 2(C^2_{31} + C^2_{32} \qquad [4\text{-}19\text{-}d]$$

$$\frac{\partial^2 Dm}{\partial F_2 \partial F_3} = \frac{\partial 2_{Dm}}{\partial F_3 \partial F_2} = -2C_{22}C_{31} \qquad [4\text{-}19\text{-}e]$$

The elements of equations [4-19] form a symmetric matrix, termed the Hessian Matrix $[H_{ij}]$, so the algorithm of [4-18] becomes:

$$F_{i+1} = F_i - [H_{ij}]^{-1} \frac{\partial Dm}{\partial F_i} \qquad [4\text{-}20]$$

for $j = 1,2$ and $i = 2,3$.

This is an iterative process which requires an initial guess. For this particular case,this could be any value as the convergence is assured due to the quadratic character of the present objective function (see Wismer and Chattergy, 1978 p.51 for details).

THE NEWTON-RAPHSON ROUTINE

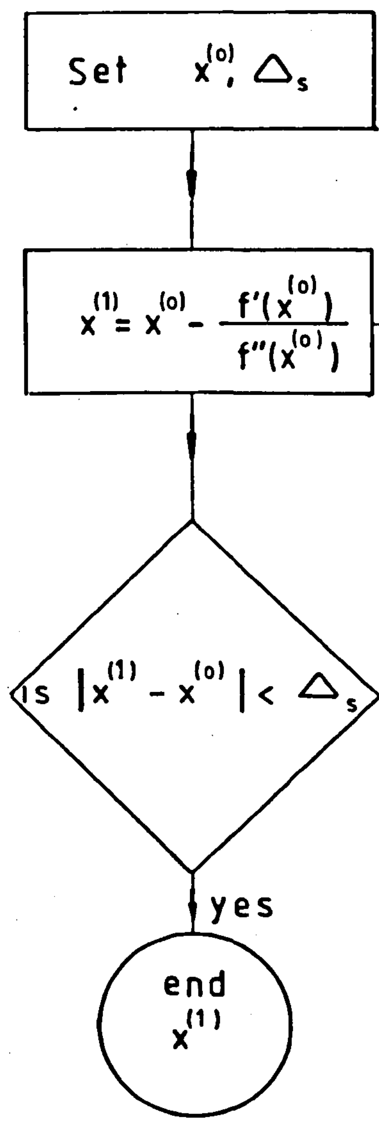

Figure 4.5. The scheme of iteration of the Newton-Raphson routine. (one variable).

At first sight this method might appear lengthy and complex but there are real advantages in terms of programming which make this technique convenient. The matrix (2 x 2) inversion and the whole iterative process has to be performed only once, as the convergence is immediately achieved due to the quadratic character of the objective function.

The scaling operation tends to minimise the differences between the adjacent chords of the intersecting ellipses, but does not eliminate them completely, because these discrepancies are thought to be due to cumulative errors generated during sampling procedures, as explained before, and perhaps also due to possible deformation inhomogeneities that might exist. Therefore before obtaining the best fitting ellipsoid it seems useful to derive a measure of the compatibility of the 3 ellipses. This is useful in judging the reliability of a strain estimation result.

So using the elements of fig. 4-3, we expect that

$$C_{11}C_{21}C_{31} - k(C_{12}C_{22}C_{32}) = 0 \qquad [4\text{-}21]$$

where k is a necessary factor in order to satisfy the above equality. The value of k approaches unity as the differences between ellipses decrease. A measure of the percentage of incompatibility between intersecting ellipses is given by the expression

$$\text{Perc. Incompatibility} = \left| \frac{C_{12}C_{22}C_{32} - C_{11}C_{21}C_{31}}{C_{11}C_{21}C_{31}} \right| \times 100 \qquad [4\text{-}22]$$

After the scaling operation we need to obtain the attitude of the ellipsoid through the Least Squares Fitting. The conditions for determining the coefficients $[V_j]^t = [a_{11}a_{23}a_{33}a_{12}a_{13}a_{23}]$ [4-23] are the existence of a number of a number of data sets (n) equal or or greater than the number of parameters (j) to be determined. In the present case the data sets are obtained by means of the polar equation of [4-14], according the scheme illustrated in figure 4-6. The required objective function is set as follows:

$$Er_i = a_{11}x_i^2+a_{22}y_i^2+a_{33}z_i^2+2a_{12}x_iy_i+2a_{13}x_iz_i+2a_{23}y_iz_i-1 = 0 \qquad [4\text{-}24]$$

for $i = 1,2, \ldots n$,ie admitting that there is an error Er_i between the theoretical and the obtained values. It is required that we minimise the squares of these deviations so we first define (s) as the objective function:

$$s_{min} = \sum_{i=1}^{n} Er_i^2 = \sum_{i=1}^{n}(a_{11}x^2+a_{22}y^2+a_{33}z^2+2a_{12}xy+2a_{13}xz+2a_{23}yz-1)_i^2 \quad . [4\text{-}25]$$

The conditions for (s), a function of (j) variables, to attain an extremum,are $\partial s/\partial V_j = 0$, in which case this equation can be generalised as;

$$\frac{\partial s}{\partial v_j} = 2 \sum_{i=1}^{n} Er_i \cdot \frac{\partial Er_i}{\partial V_j} = 0 \qquad [4\text{-}26]$$

where V_j is the transpose of [4-23]. After expanding [4-26] and collecting the terms, this gives the following system of equations:

$$
\begin{bmatrix}
\sum x_i^4 & \sum x_i^2 y_i^2 & \sum x_i^2 z_i^2 & \sum x_i^3 y_i & \sum x_i^3 z_i & \sum x_i^2 y_i z_i \\
\sum x_i^2 y_i^2 & \sum x_i^4 & \sum y_i^2 z_i^2 & \sum x_i y_i^3 & \sum x_i y_i^2 z_i & \sum y_i^3 z_i \\
\sum x_i^2 z_i^2 & \sum y_i^2 z_i^2 & \sum z_i^4 & \sum x_i y_i z_i^2 & \sum x_i z_i^3 & \sum y_i z_i^3 \\
\sum x_i^3 y_i & \sum x_i y_i^3 & \sum x_i y_i z_i^2 & \sum x_i^2 y_i^2 & \sum x_i^2 y_i z_i & \sum x_i y_i^2 z_i \\
\sum x_i^3 z_i & \sum x_i y_i^2 z_i & \sum x_i z_i^3 & \sum x_i^2 y_i z_i & \sum x_i^2 z_i^2 & \sum x_i y_i z_i^2 \\
\sum x_i^2 y_i z_i & \sum y_i^3 z_i & \sum y_i z_i^3 & \sum x_i y_i^2 z_i & \sum x_i y_i z_i^2 & \sum y_i^2 z_i^2
\end{bmatrix}
\begin{bmatrix}
a_{11} \\ a_{22} \\ a_{33} \\ a_{12} \\ a_{13} \\ a_{23}
\end{bmatrix}
=
\begin{bmatrix}
\sum x_i^2 \\ \sum y_i^2 \\ \sum z_i^2 \\ \sum x_i y_i \\ \sum x_i z_i \\ \sum y_i z_i
\end{bmatrix}
\qquad [4\text{-}27]
$$

or in matrical representation $[U][V] = [W]$ [4-28]

The solution of the above system leads to $[V] = [U]^{-1}[W]$, which contains the coefficients of equation [4-4]. These can be arranged to give the real and symmetric 3 x 3 matrix of $\tilde{A}$ (see [4-6]).

The characteristic equation of $\tilde{A}$ is

$$|A - \bar{\lambda}I| = \begin{vmatrix} a_{11}-\bar{\lambda}_1 & a_{12} & a_{13} \\ a_{21} & a_{22}-\bar{\lambda}_2 & a_{23} \\ a_{31} & a_{32} & a_{33}-\bar{\lambda}_3 \end{vmatrix} = 0 \qquad [4\text{-}29]$$

where I is the 3 x 3 identity matrix, and the roots $\bar{\lambda}_1$, $\bar{\lambda}_2$ and $\bar{\lambda}_3$ are the eigenvalues of $\tilde{A}$. The solution of the 3 equations

$$|A - \bar{\lambda}_1 I|\cdot|\,p_{i1}| = 0,\ |A - \bar{\lambda}_2 I|\cdot|\,p_{i2}| = 0 \text{ and } |A - \bar{\lambda}_3 I|\cdot|\,p_{i3}| = 0 \qquad [4\text{-}30]$$

for i = 1,2,3 allows the calculation of the matrix of eigenvalues defined by $\tilde{B}$ in [4-10].

The magnitudes of the semi-axes X,Y,Z (for X>Y>Z) of the ellipsoid are obtained from

$$X = (\bar{\lambda}_1)^{-\frac{1}{2}}, \qquad Y = (\bar{\lambda}_2)^{-\frac{1}{2}} \text{ and } Z = (\bar{\lambda}_3)^{-\frac{1}{2}} \qquad [4\text{-}31]$$

where $\bar{\lambda}_3 \geq \bar{\lambda}_2 \geq \bar{\lambda}_1$. The attitude of each axis is given by its corresponding vector column in the matrix of eigenvectors $\tilde{P}$ (see [4-8]). The eigenvalue-eigenvectors programming routine was devised by the author using the Jacobi Method following the scheme and equations proposed by Greenstadt (1960; see also Gourlay and Watson, 1973; Hornbeck, 1975 pp.236-241). This programme was subsequently incorporated in programme FITELI as subroutine EICOBI.

The routine calculation is restricted to the following steps (for data input and output and also for full details see listing of the FORTRAN IV programme FITELI in appendix).

A. First Mode: Programme performs 2D strain estimation in 3 orthogonal planes, then obtains the ellipsoid-fitting by the Least Squares Method:

1) Input data from each plane for the calculation of the 2D strain ellipse using the equations of Shimamoto and Ikeda (1976).

2) Use the Newton-Raphson routine for scaling the mutually perpendicular strain ellipses.

3) Calculate the amount of incompatibility (lack of fit) between the intersecting ellipses using [4-22].

4) Compute the chords in each ellipse using the sequence of figure 4-6.

5) Form the matrix of the sum of cross products [U] and the vector of the sum of products [W] according to [4-27].

6) Invert and find the solutions of [4-27], which is the vector column of [4-23], and form the symmetric matrix of $\tilde{A}$ [4-6].

7) Call subroutine EICOBI to obtain the eigenvalues and eigenvectors of matrix $\tilde{A}$ by the Jacobi Method.

8) Compute ellipsoid axes using [4-31].

9) Normalise axes X, Y, Z to the equivalence of sphere of unit ratio by

$$t = (XYZ)^{1/3} \text{ so: } X' = X/t, \; Y' = Y/t \text{ and } Z' = Z/t \qquad [4-32]$$

10) Calculate the Amount of Distortion, (Flattening and Stretching) in each axis by: Distortion = (Axis - 1) x 100 [4-33]

11) Calculate the following parameters:

(i) Flinn's (1962) parameter $K_{(f)} = a-1/b-1$ [4-34]

where $a = X/Y$; $b = Y/Z$,

(ii) Ramsay's (1967) parameter $K_{(r)} = \ln a/\ln b$, [4-35]

(iii) Lode's (see Hossack,1968) parameter

$$\nu = \frac{2E_2 - E_1 - E_3}{E_1 - E_3} \qquad [4-36]$$

where E_1, E_2 and E_3 are the natural logarithms of X', Y' and Z' respectively. For constant volume ($E_1 + E_2 + E_3 = 0$) the above expression reduces to $\nu = 3(E_1 + E_3)/(E_3 - E_1)$.

(iv) Nadai's (1963) natural Octahedric Strain

$$\gamma_o = 2/3 \left[(E_1-E_2)^2 + (E_1-E_3)^2 + (E_3-E_1)^2 \right]^{\frac{1}{2}} \qquad [4\text{-}37]$$

Again, which reduces to

$$\gamma_o = (8/3)^{\frac{1}{2}} \left[E_1^{\;2} + E_1E_3 + E_3^{\;2} \right]^{\frac{1}{2}} \text{ at constant volume.}$$

(v) And also Nadai's (1963) effective strain

$$\varepsilon_s = (3/4)^{\frac{1}{2}} . \gamma_o \qquad [4\text{-}38]$$

which constitutes a very useful representation of the three dimensional strain in that it is independent of the shape of the ellipsoid.

12) Finally obtain the attitude of the ellipsoid using the correspondent vectors of matrix $\tilde{P}$ in [4-7]. Output the results in terms of Azimuth and Plunge of each axis.

B. Second Mode: Programme only performs ellipsoids fitting (any number) by the Least Square Method:

1) Input data such as ellipses' Rf/ϕ in the following order of measurements: Rf_{xy}, Rf_{yz}, Rf_{zx}, ϕ_{xy}, ϕ_{yz}, ϕ_{zy}. It is very important to observe the SENSE of angular measurements given by the ORDER of the subscripts. Otherwise there will be spurious results.

Steps 2 to 12 as explained in the First Mode.

4.3 Possibility of Fitting a Non-Ellipsoidal Surface

4.3.1 Introduction

Sometimes the fitted surface of [4-25] results in other than an ellipsoid. This can occur because the general form of a conicoid (eg eqn. [4-3]) also represents other distinct surfaces such as the Hyperboloid of one and two sheets (see Kindle 1950, p.131). The result in such a case is the appearance of at least one negative eigenvalue (ie the matrix $\tilde{A}$ is not Positive-Definite, see Cohn 1961 p.63) and for the present purposes this is considered 'geologically meaningless' (cf Mittlefehldt and Oertel 1980).

Milton (1980-a, b) has recently reported to have found such negative eigenvalues especially when using 2D-strain estimation by the Shimamoto and Ikeda (1976) method. In one locality the frequency of these negative roots occurred in the proportion of 7:9 (see Milton 1980-b, p.98) and this made him to opt for Lisle's Rf/θ method, because it produced negative results, using the same data, only in the proportion of 2:9.

Mittlefehldt and Oertel (1979) however reported to have overcome this difficulty by performing adjustments and rotations in all three planes, thus removing the negative principal length.

In this section will be introduced a new technique for overcoming the problem of negative eigenvalues. An experimental version of this method was incorporated to the previous routines of programme FITELI described in the last section. The main programme of this experimental version (the subroutines were excluded because they are exactly the same as in FITELI) was named FTELAM and is listed in the Appendix.

4.3.2 The Constraint Method

Clearly, what is required is a method which constraints the choice of the quadratic surface to that of an ellipsoid. A possible solution is to use the method of the Langrange Multipliers in order to impose certain conditions during the fitting operation.

We shall complement the explanation of section 4.2.3.2 by defining the Invariants of the surface of second order (cf Brohnstein and Semandaiev 1971, p.268). Let us expand the general equation of the second degree given by [4-3]:

$$a_{11}x^2+a_{22}y^2+a_{33}z^2+2a_{12}xy+2a_{13}xz+2a_{23}yz+2a_{14}x+2a_{24}y+2a_{34}z+a_{44} = 0 \quad .$$

The Invariants of the surface of the second order are:

$$\tilde{D} = \begin{bmatrix} a_{11} & a_{12} & 1_{13} & a_{14} \\ a_{21} & a_{22} & a_{23} & a_{24} \\ a_{31} & a_{32} & a_{33} & a_{34} \\ a_{41} & a_{42} & a_{43} & a_{44} \end{bmatrix} \quad ; \qquad \tilde{A} = \begin{bmatrix} a_{11} & a_{12} & a_{13} \\ a_{21} & a_{22} & a_{23} \\ a_{31} & a_{32} & a_{33} \end{bmatrix} .$$

$$T = \begin{bmatrix} a_{11} & a_{12} \\ a_{12} & a_{22} \end{bmatrix} + \begin{bmatrix} a_{22} & a_{23} \\ a_{23} & a_{33} \end{bmatrix} + \begin{bmatrix} a_{33} & a_{31} \\ a_{31} & a_{11} \end{bmatrix} \quad ; \text{ and} \quad s_t = a_{11} + a_{22} + a_{33}$$

The conditions for a conicoid to represent an ellipse are:

$$\tilde{A}.s_t > 0, \qquad T > 0 \qquad \text{and} \qquad \tilde{D} < 0 \qquad . \qquad [4\text{-}39]$$

In the above determinants the relation $a_{ij} = a_{ji}$ holds (Bartsh 1974, p.277), and for the present conditions we have

$$a_{14} = a_{41} = a_{24} = a_{42} = a_{34} = a_{43} = 0 \qquad [4\text{-}40]$$

and $a_{44} = -1$.

Therefore it is possible to simplify the above invariants (except the Trace of $\tilde{A}$, s_t) to the form of:

$$\tilde{D} = (+1)^{4+4} \begin{bmatrix} a_{11} & a_{12} & a_{13} \\ a_{12} & a_{22} & a_{23} \\ a_{13} & a_{23} & a_{33} \end{bmatrix} \qquad \tilde{A} = a_{11}a_{22}a_{33}+2a_{12}a_{13}a_{23}-a_{13}^2a_{22}-a_{23}^2a_{11} -a_{12}^2a_{33}$$

$$[4\text{-}41]$$

and $$T = a_{22}a_{33}+a_{11}a_{33}+a_{11}a_{22}-a_{12}^2-a_{13}^2-a_{23}^2 \qquad . \qquad [4\text{-}42]$$

The general procedure when dealing with a problem which includes an inequality constraint of the form

$$h_j(a_{ij}) \geqslant 0 \qquad i, j = 1,2, \ldots\ldots n \qquad [4\text{-}43]$$

is firstly to convert the inequalities to equality constraints and then to solve by the Lagrange Multipliers Method (see Wismer and Chattergy 1978).

Thus we define a Slack Variable b_j for each inequality $h_j(a_{ij})$, then if

$$b_j^2 = h_j(a_{ij}) \geqslant 0 \qquad [4\text{-}44]$$

we satisfy the inequality by satisfying the above equality in b. The inequality constraints of [4-39] are defined respectively as:

$$\left[(a_{11}+a_{22}+a_{33})\cdot(a_{11}a_{22}a_{33}+2a_{12}a_{13}a_{23}-a_{13}^2a_{22}-a_{33}^2a_{11}-a_{12}^2a_{33})\right] \geqslant 0 \qquad [4\text{-}45]$$

$$(a_{22}a_{33}+a_{11}a_{33}+a_{11}a_{22}-a_{12}^2-a_{13}^2-a_{23}^2) \geqslant 0 \qquad [4\text{-}46]$$

and

$$(a_{11}a_{22}a_{33}+2a_{12}a_{13}a_{23}-a_{13}^2a_{22}-a_{23}^2a_{11}-a_{12}^2a_{33}) \leqslant 0 \qquad [4\text{-}47]$$

However, as $\tilde{A}.s_t > 0$ and $\tilde{D} < 0$, but $D \equiv \tilde{A}$, hence $s_t < 0$, therefore $\tilde{D} = \tilde{A} < 0$ and $(a_{11}+a_{22}+a_{33}) < 0$ or $-(a_{11}+a_{22}+a_{33}) > 0$. [4-48]

Now using the above slack variables b_j, $j = 1,2,3$ we get

$$b_1^2 = -(a_{11}+a_{22}+a_{33}) \geqslant 0, \quad \text{therefore} \quad b_1^2+a_{11}+a_{22}+a_{33} = 0 \qquad [4\text{-}49]$$

$$b_2^2 = (a_{22}a_{33}+a_{33}a_{11}+a_{11}a_{22}-a_{23}^2-a_{31}^2-a_{12}^2) \geqslant 0 \qquad \text{or}$$

$$a_{22}a_{33}+a_{33}a_{11}+a_{11}a_{22}-a_{23}^2-a_{31}^2-a_{12}^2-b_2^2 = 0 \qquad [4\text{-}50]$$

and finally $b_3^2 = -(a_{11}a_{22}a_{33}+2a_{12}a_{13}a_{23}-a_{13}^2a_{22}-a_{23}^2a_{11}-a_{12}^2a_{33}) \geqslant 0$

which gives

$$b_3^2+a_{11}a_{22}a_{33}+2a_{12}a_{13}a_{23}-a_{13}^2a_{22}-a_{23}^2a_{11}-a_{12}^2a_{33} = 0 \qquad [4\text{-}51]$$

We then define and apply the Lagrangian (see Wismer and Chattergy, 1978,pp.55, 66).

$$L(a_{ij},l_j,b_j) = f(a_{ij}) + \sum_{j=1}^{m} l_j[h_j(a_{ij}) - b_j^2] \qquad [4\text{-}52]$$

where l_j are Lagrange Multipliers. The necessary conditions are

$$\frac{\partial L}{\partial a_{ij}} = 0 , \qquad \frac{\partial L}{\partial l_j} = 0 \quad \text{and} \quad \frac{\partial L}{\partial b_j} = 0 \qquad [4\text{-}53]$$

again, for i,j = 1,2,3.

In the present case the Lagrangian conditions are specifically:

$$L(a_{ij},\tilde{A},s_t,T,\tilde{D}) = L(a_{ij},l_j,b_j) = \sum_{k=1}^{n} E_k^2+l_1(b_1^2+s_t)+l_2(-b_2^2+T)+l_3(b_3^2+\tilde{D}) \qquad [4\text{-}54]$$

substituting [4-25], [4-49], [4-50], [4-51] in [4-54] yields

$$L = \sum_{k=1}^{n}(a_{11}x^2+a_{22}y^2+a_{33}z^2+2a_{12}xy+2a_{13}xz+2a_{23}yz-1)_k^2+l_1(b_1^2+a_{11}+a_{22}+a_{33}) +$$

$$l_2(a_{22}a_{33}+a_{33}a_{11}+a_{11}a_{22}-a_{23}^2-a_{31}^2-a_{12}^2-b_2^2)+l_3(b_3^2+a_{11}a_{22}a_{33}+2a_{12}a_{13}^2a_{23} -$$

$$a_{23}^2a_{11}-a_{12}^2a_{33}) \quad . \qquad [4\text{-}55]$$

Applying the necessary conditions of (5-50) we must first form and then solve the following system of equations:

$$\frac{\partial L}{\partial a_{11}} = 2\sum_{k=1}^{n}(a_{11}x^4+a_{22}x^2y^2+a_{33}x^2z^2+2a_{12}x^3y+2a_{13}x^3z+2a_{23}x^2yz-x^2)_k+l_1+l_2(a_{22}+a_{33})+l_3(a_{22}a_{33}-a_{23}^2) = 0$$

$$\frac{\partial L}{\partial a_{22}} = 2\sum_{k=1}^{n}(a_{11}x^2y^2+a_{22}y^4+a_{33}y^2z^2+2a_{12}xz^3+2a_{13}xy^2z+2a_{23}y^3z-y^2)_k+l_1+l_2(a_{33}+a_{11})+l_3(a_{11}a_{33}-a_{13}^2) = 0$$

$$\frac{\partial L}{\partial a_{33}} = 2\sum_{k=1}^{n}(a_{11}x^2z^2+a_{22}y^2z^2+a_{33}z^4+2a_{12}xyz^2+2a_{13}xz^3+2a_{23}yz^3-z^2)_k+l_1+l_2(a_{22}+a_{11})+l_3(a_{11}a_{22}-a_{12}^2) = 0$$

$$\frac{\partial L}{\partial a_{12}} = 4\sum_{k=1}^{n}(a_{11}x^3y+a_{22}xy^3+a_{33}xyz^2+2a_{12}x^2y^2+2a_{13}x^3yz^3+2a_{23}xy^2z-xy)_k-2l_2a_{12}+2l_3(a_{13}a_{23}-a_{12}a_{33}) = 0$$

$$\frac{\partial L}{\partial a_{13}} = 4\sum_{k=1}^{n}(a_{11}x^3z+a_{22}xy^2z+a_{33}xz^3+2a_{12}x^2y+2a_{13}x^2z^2+2a_{23}xyz^2-xz)_k-2l_2a_{13}+2l_3(a_{12}a_{23}-a_{13}a_{22}) = 0$$

$$\frac{\partial L}{\partial a_{23}} = 4\sum_{k=1}^{n}(a_{11}x^2yz+a_{22}y^3z+a_{33}yz^3+2a_{12}xy^2z+2a_{13}xyz^2+2a_{23}y^2z^2-yz)_k-2l_2a_{23}+2l_3(a_{12}a_{13}-a_{23}a_{11}) = 0$$

$$\frac{\partial L}{\partial l_1} = b_1^2+a_{11}+a_{22}+a_{33} = 0$$

$$\frac{\partial L}{\partial l_2} = a_{22}a_{33}+a_{33}a_{11}+a_{11}a_{22}-a_{23}^2-a_{13}^2-a_{12}^2-b_2^2 = 0$$

$$\frac{\partial L}{\partial l_3} = b_3^2+a_{11}a_{22}a_{33}+2a_{12}a_{13}a_{23}-a_{13}^2a_{22}-a_{23}^2a_{11}-a_{12}^2a_{33} = 0$$

$$\frac{\partial L}{\partial b_1} = 2l_1b_1 = 0$$

$$\frac{\partial L}{\partial b_2} = -2l_2b_2 = 0$$

$$\frac{\partial L}{\partial b_3} = 2l_3b_3 = 0$$

equations [4-56-a to e]

From the last 3 equations we can have, either

$$\bar{l}_j = 0 \qquad \text{and/or} \qquad \bar{b}_j = 0 \qquad [4\text{-}57]$$

(where $\bar{l}_j$ and $\bar{b}_j$ are estimates of l_j and b_j). For the above, if $\bar{l}_j = 0$ and $\bar{b}_j \neq 0$, then the constraint of [4-43] is ignored and [4-44] becomes

$$\bar{b}_j^{\,2} = h_j(\bar{a}_{ij}) > 0 \qquad [4\text{-}58]$$

(where $\bar{a}_{ij}$ are estimates of a_{ij}) and this satisfies the conditions of [4-39].

Confronted with the systems of equations of [4-27] and [4-56-a to l] one readily concludes that the price paid for including the conditions [4-39] is higher dimensionality and also a non-linear character of the set of equations of [4-56]. The Augmented Function [4-55] leads to a significant computational problem, because what is required is the solution of 12 simultaneous equations in 12 unknowns, resulting from the necessary conditions of [4-53] . The Gauss-Seidel iterative method is a widely used technique for solving nonlinear sets of simultaneous equations (cf Hornbeck 1975, p.106). However, we make use (once more) of the already defined Newton-Raphson technique (cf [4-18], see fig 4-5), although this method could give some problems or convergence, depending on the character of the function. It is expected, however, that the initial guesses will be close enough to the optimum region so convergence can be achieved.

Once more the algorithm of [4-18] yields

$$a_{ij}^{(m+1)} = a_{ij}^{(m)} - [H]^{-1} . \frac{\partial L}{\partial a_{ij}} \qquad [4\text{-}59]$$

$$l_j^{(m+1)} = l_j^{(m)} - [H]^{-1} . \frac{\partial L}{\partial l_j} \qquad [4\text{-}60]$$

and $$b_j^{(m+1)} = b_j^{(m)} - [H]^{-1} \cdot \frac{\partial L}{\partial b_j} \qquad [4\text{-}61]$$

where the Hessian Matrix [H] of $L(a_{ij}, l_j, b_j)$ is displayed in table 4-1.

In terms of computation, the routine described in 4.2.3.2 is modified in step number 8, where there is a check for possible negative eigenvalues. In case there is a negative argument in [4-31], the programme branches to:

8. (i) - Save the values of elements $a_{ij}(i,j = 1,2,3)$ of matrix $\tilde{A}$ and these will constitute the initial guesses $a_{ij}^{(0)}$ or [4-59].

(ii) - Set initial guesses of $b_j^0 = 1$, and variable SUMIN to 10^{10}.

(iii) - Recall elements of matrix [U] and column vector [W] and incorporate them both in the Hessian [H] and vector column of first derivatives of [4-56-a - l].

(iv) - Update elements of matrix [U] and vector [W] by performing an iteration of the algorithm or [4-59]. Also update values of Slack Variables by using [4-61].

(v) - Compare the sum of the squares $SUMIN^{(m+1)} = \sum_{k=1}^{6} (\partial L/\partial a_{ij})_k^2$ [4-62]

with the previous result (m). Check for any negligible improvement (less than 10^{-3}) or divergence. In either case this will interrupt the iterative process. In case of slow improvement, enter the updated matrix $\tilde{A}$ in step number 8. However in case of divergence, try to confirm it with some additional iterations. Abandon the solution if divergence persists.

In case there is a considerable improvement towards minimization (ie convergence) revert to step 8(iii) until improvement

Table 4.1

The Hessian Matrix of [4-61]

$$H=\begin{bmatrix}
2\sum x^4 & 2\sum x^2y^2+l_2+l_3a_{33} & 2\sum x^2z^2+l_2+l_3a_{22} & 4\sum x^3y & 4\sum x^3z & 4\sum x^2yz-2l_3a_{23} & 1 & a_{22}+a_{33} & a_{22}a_{33}-a_{23}^2 & 0 & 0 & 0 \\
2\sum x^2y^2+l_2+l_3a_{33} & 2\sum y^4 & 2\sum y^2z^2+l_2+l_3a_{11} & 4\sum xy^3 & 4\sum xy^2z-2l_3a_{13} & 4\sum y^3z & 1 & a_{11}+a_{33} & a_{11}a_{33}-a_{13}^2 & 0 & 0 & 0 \\
2\sum x^2y^2+l_2+l_3a_{22} & 2\sum y^2z^2+l_2+l_3a_{11} & 2\sum z^4 & 4\sum xyz^2-2l_3a_{12} & 4\sum xz^3 & 4\sum yz^3 & 1 & a_{11}+a_{22} & a_{11}a_{22}-a_{12}^2 & 0 & 0 & 0 \\
4\sum x^3y & 4\sum xz^3 & 4\sum xyz^2-2l_3a_{12} & 8\sum x^2y^2-2l_2-2l_3a_{33} & 8\sum x^2yz+2l_3a_{13} & 8\sum xy^2z+2l_3a_{13} & 0 & -2a_{12} & 2(a_{13}a_{23}-a_{11}a_{33}) & 0 & 0 & 0 \\
4\sum x^3z & 4\sum xy^2z-2l_3a_{13} & 4\sum xz^3 & 8\sum xyz+2l_3a_{23} & 8\sum x^2z^2-2l_2-2l_3a_{22} & 8\sum xyz^2+l_3a_{12} & 0 & -2a_{13} & 2(a_{12}a_{23}-a_{13}a_{22}) & 0 & 0 & 0 \\
4\sum x^2yz-2l_3a_{23} & 4\sum y^3z & 4\sum yz^3 & 8\sum xyz^2+2l_3a_{13} & 8\sum xyz^2+2l_3a_{12} & 8\sum y^2z^2-2l_2-2l_3a_{11} & 0 & -2a_{23} & 2(a_{12}a_{13}-a_{11}a_{23} & 0 & 0 & 0 \\
1 & 1 & 1 & 0 & 0 & 0 & 0 & 0 & 0 & 2b_1 & 0 & 0 \\
a_{22}+a_{33} & a_{11}+a_{33} & a_{11}+a_{22} & -2a_{12} & -2a_{13} & -2a_{23} & 0 & 0 & 0 & 0 & -2b_2 & 0 \\
a_{22}a_{33}-a_{23}^2 & a_{11}a_{33}-a_{13}^2 & a_{11}a_{22}-a_{12}^2 & 2(a_{13}a_{23}-a_{12}a_{33}) & 2(a_{12}a_{23}-a_{13}a_{22}) & 2(a_{12}a_{13}-a_{11}a_{23}) & 0 & 0 & 0 & 0 & 0 & 2b_3 \\
0 & 0 & 0 & 0 & 0 & 0 & -2b_1 & 0 & 0 & 2l_1 & 0 & 0 \\
0 & 0 & 0 & 0 & 0 & 0 & 0 & -2b_2 & 0 & 0 & 2l_2 & 0 \\
0 & 0 & 0 & 0 & 0 & 0 & 0 & 0 & 2b_3 & 0 & 0 & 2l_3
\end{bmatrix}$$

in SUMIN becomes negligible.

The above steps were fully incorporated to programme FITELI, thus constituting the experimental version of a programme named FTELAM, which worked very well with the available examples. The process aims towards rapid convergence. However, there was little opportunity to gain experience with this modified programme because of lack of suitable input data (ie data that provided negative eigenvalues).

4.4 Results and Interpretations

4.4.1 Correlation Between Methods and Programmes

Both Oertel (1978) and Milton (1980) placed great importance on the ellipses-scaling down operation. Milton (1980) not only introduced a scaling factor F_i but also adjustment factors, in order to get compatibility between ellipses.

In the method used here, scaling is restricted to the minimization process described above and the other 'adjustments' are implicit in the fitting operation, the Least Squares Fitting, which minimizes errors but does not impose any further deformation of the 2D strain ellipses.

Two-dimensional data for fitting ellipsoids in 6 different Standard Positions (ie ellipsoids' axes coincident with the co-ordinate axes) were given to both FITELI and PASE5 programmes for comparison purposes and the output results of the ratios and orientations of all axes were perfectly coincident.

Tables 4-2 and 4-3 contain the results obtained by both FITELI and PASE5, when using data input from sampled quartzites. As mentioned before, this study also made use of the Lisle's Rf/θ method,

SPECIMEN IDENTIF.		ELLIPSOID PRINCIPAL AXES (NON VOLUME CHANGE)		PERCENTAGE OF DISTORTION						CHARACTERIZATION PARAMETERS						INCOMPATIBILITY IN THE 2D-STRAIN ELLIPSES	
ORDER	DEPT. NO. / FIELD NUMBER	PROGRAMME		PROGRAMME													
		FITELI	PASE5	FITELI			PASE5			FLINN'S k		NADAI'S ε_s		LODE'S ν		PERCENTAGE	
		$\surd\lambda_1 : \surd\lambda_2 : \surd\lambda_3$	$\surd\lambda_1 : \surd\lambda_2 : \surd\lambda_3$	STRETCHING X	Y	SHORTENING Z	STRETCHING X	Y	SHORTENING Z	FITELI	PASE5	FITELI	PASE5	FITELI	PASE5	FITELI	PASE5
1	41481 860	2.34:1.18:0.36	2.32:1.21:0.36	134	17.9	-63.8	132.0	21.0	-64.0	0.437	0.381	1.336	1.337	0.265	0.301	6.66%	6.87%
2	41482 868-A	1.60:0.96:0.65	1.56:0.98:0.65	60	-3.6	-35.2	56.0	-2.0	-35.0	1.353	1.193	0.641	0.619	-0.121	-0.062	7.38	7.64
3	41483 868-B	1.53:1.40:0.47	1.58:1.33:0.47	53.2	40.0	-53.4	58.0	33.0	-53.0	0.047	0.102	0.936	0.927	0.848	0.562	19.19	21.02
4	41484 925	1.82:0.93:0.59	1.48:1.01:0.67	82.2	-7.0	-41.0	48.0	1.0	-33.0	1.664	0.914	0.802	0.560	-0.193	0.036	24.73	27.67
5	41494 1084	1.96:0.96:0.53	1.74:1.07:0.53	96.5	-3.8	-47.1	74.0	7.0	-47.0	1.274	0.624	0.929	0.845	-0.089	0.182	27.30	30.85
6	41495 1046	2.05:1.09:0.45	2.03:1.10:0.45	108.8	9.0	-55.2	103.0	10.0	-55.0	0.613	0.584	1.080	1.071	0.170	0.187	15.29	16.45
7	41501 1185	1.80:1.13:0.49	1.83:1.10:0.50	80.1	12.9	-50.8	83.0	10.0	-50.0	0.459	0.561	0.930	0.924	0.281	0.215	18.13	19.74
8	41502 1189	1.48:1.22:0.56	1.54:1.18:0.55	47.7	21.8	-44.4	54.0	18.0	-45.0	0.179	0.273	0.732	0.755	0.604	0.483	15.80	17.04
9	41504 1206	1.58:1.28:0.49	1.59:1.28:0.49	58.3	28.1	-50.7	59.0	28.0	-51.0	0.147	0.148	0.878	0.885	0.637	0.632	12.19	12.93
10	41505 1207	1.40:1.17:0.61	1.40:1.18:0.61	40.2	17.5	-39.3	40.0	18.0	-39.0	0.206	0.199	0.624	0.620	0.579	0.588	2.67	2.71
11	41506 1220	2.61:1.05:0.36	2.22:1.10:0.41	160.9	5.2	-63.6	122.0	10.0	-59.0	0.782	0.592	1.394	1.200	0.153	0.169	7.72	8.00
12	41507 1223	2.44:0.93:0.44	2.60:1.00:0.39	143.5	-7.2	-55.8	160.0	0	-61.0	1.479	1.018	1.210	1.341	-0.131	-0.007	43.29	51.34
13	41513 1250	1.87:1.12:0.48	2.25:1.08:0.41	87.2	11.8	-52.2	125.0	8.0	-59.0	0.504	0.652	0.975	1.207	0.245	0.138	29.64	33.77
14	41514 1293	2.06:1.36:0.36	2.05:1.36:0.36	105.6	35.8	-64.2	105.0	36.0	-64.0	0.184	0.182	1.295	1.285	0.525	0.528	0.58	0.58

Table 4.2 - Results by Programmes FITELI and PASE5 with input data by Shimamoto and Ikeda (1976) method.

SPECIMEN IDENTIF.		ELLIPSOID PRINCIPAL AXES (NON VOLUME CHANGE)		PERCENTAGE OF DISTRIBUTION						CHARACTERIZATION PARAMETERS						INCOMPATIBILITY IN THE 2D-STRAIN ELLIPSES	
ORDER	DEPT. NO. / FIELD NUMBER	PROGRAMME		PROGRAMME													
		FITELI	PASE5	FITELI			PASE5			FLINN'S k		NADAI'S ε_s		LODE'S ν		(PERCENTAGE)	
		$\sqrt{\lambda_1}:\sqrt{\lambda_2}:\sqrt{\lambda_3}$	$\sqrt{\lambda_1}:\sqrt{\lambda_2}:\sqrt{\lambda_3}$	STRETCHING X	Y	SHORTENING Z	STRETCHING X	Y	SHORTENING Z	FITELI	PASE5	FITELI	PASE5	FITELI	PASE5	FITELI	PASE5
1	41481 860	2.55:1,16:0.34	2.55:1.16:0.34	155.1	15.5	66.1	155	16	-66.2	0.503	0.491	1.436	1.436	0.214	0.218	1.38%	1.41%
2	41482 868-A	1.67:0.96:0.63	1.62:0.99:0.63	66.7	-4.2	-37.4	60.1	-1.00	-36.9	1.392	1.096	0.695	0.668	-0.130	-0.042	15.40	15.58
3	41483 868-B	1.57:1.39:0.46	1.61:1.34:0.46	57.3	38.7	-54.2	60.8	34	-53.5	0.066	0.107	0.959	0.957	0.795	0.706	18.31	19.95
4	41484 925	1.76:0.96:0.60	1.47:1.02:0.66	76.6	-3.5	-40.3	46.9	2.0	-33.6	1.291	0.798	0.757	0.567	-0.099	0.087	23.74	26.46
5	41494 1084	2.06:0.97:0.50	1.79:1.09:0.51	105.9	-3.0	-49.9	79.2	9.0	-48.8	1.198	0.567	1.000	0.894	-0.065	0.209	24.61	27.52
6	41495 1046	2.30:1.04:0.42	2.30:1.05:0.42	129.5	4.3	-58.2	129.5	5.0	-58.4	0.802	0.787	1.206	1.204	0.074	0.077	16.10	17.34
7	41501 1185	1.85:1.17:0.46	1.89:1.13:0.47	85.1	16.6	-53.7	85.4	13.0	-53.1	0.386	0.486	0.997	0.995	0.334	0.260	18.90	20.55
8	41502 1189	1.53:1.20:0.55	1.57:1.17:0.54	52.5	19.8	-45.3	56.8	17.0	-45.5	0.229	0.296	0.758	0.780	0.529	0.448	8.34	8.73
9	41504 1206	1.55:1.30:0.49	1.55:1.31:0.49	55.3	30.2	-50.5	54.8	31.0	-50.6	0.118	0.111	0.871	0.880	0.692	0.708	2.44	2.49
10	41505 1207	1.46:1.20:0.57	1.45:1.20:0.57	46.4	20.3	-43.2	45.4	20.1	-43.0	0.194	0.187	0.706	0.696	0.585	0.594	4.4	4.40
11	41506 1220	2.18:1.14:0.40	2.55:1.05:0.37	118.2	14.7	-60.1	155.26	5.0	-62.7	0.481	0.792	1.212	1.366	0.243	0.081	11.97	12.67
12	41507 1223	2.48:0.93:0.43	2.76:0.96:0.38	148.1	-6.7	-56.8	175.6	-4.0	-62.2	1.433	1.219	1.239	1.403	-0.120	-0.065	36.9	42.92
13	41513 1250	1.93:1.10:0.47	2.49:1.05:0.38	92.7	10.6	-53.1	148.6	5.0	-61.7	0.549	0.789	1.006	1.331	0.213	0.081	32.6	37.46
14	41514 1293	1.06:1.37:0.35	2.11:1.35:0.35	105.5	37.5	-64.6	111.2	35.0	-65.1	0.172	0.195	1.303	1.323	0.524	0.502	9.43	9.88

Table 4.3 - Results by programmes FITELI and PASE5 with input data by program THETA (Peach and Lisle 1979).

through programme THETA by Peach and Lisle(1979). For 2D strain estimation the results of THETA generally overestimate the values found by the SI-method (see figure 4-7-a).

In order to analyse the variations in results with the above methods and programmes it was decided to correlate linearly the values obtained with both models (see Wonnacott and Wonnacott 1977, p.407-412):

$$\hat{\beta} = \frac{\sum x_i y_i}{\sum x_i^2} \qquad [4\text{-}62]$$

and

$$r = \frac{\sum x_i y_i}{[\sum x_i^2 \sum y_i^2]^{\frac{1}{2}}} \quad , \quad i = 1,2, \ldots\ldots n \qquad [4\text{-}63]$$

Where x and y are respectively the correlated methods. The angle of $\hat{\beta}$ is the slope of the straight line of best-fit through the origin (regression of y on x) while r is the linear correlation coefficient. The more the absolute value of r approaches to unity the closest the correlation between x and y. For the present case $\hat{\beta}$ values also reach their optimum condition towards 1.

As programme FITELI has one option which allows it to perform only ellipsoid fitting using the second mode of 4.2.3.2, it was decided to check whether or not the discrepancies between the SI and Rf/θ-methods would affect the resultant ellipsoids.

Figures 4-7-b and 4-7-c correlate Flinn's - k and Nadais' ε_s parameters. For the ε_s-values, PASE5 presents a slightly better regression line. However the k-parameter presents nearly the same value for r but contrasting positions for the regression lines.

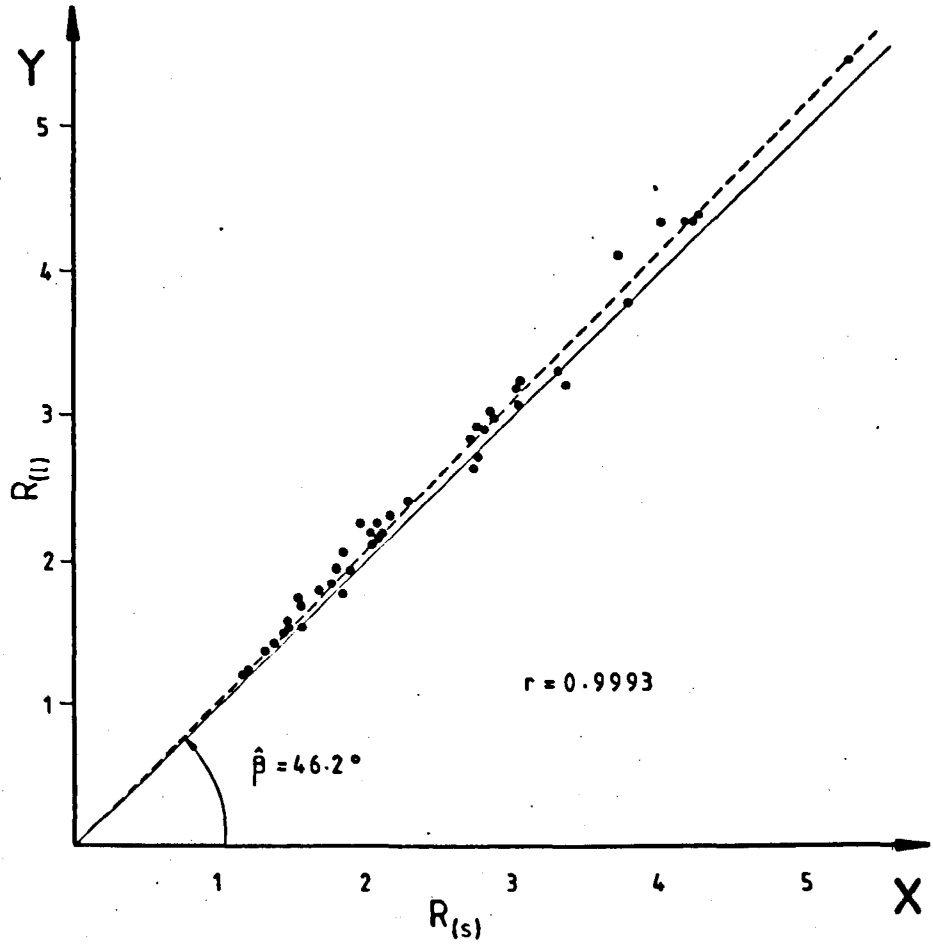

Figure 4.7-a. This correlates 2D-strain estimates obtained by two different methods. In the abscissae are strain ratios (R_s) obtained using the Shimamoto and Ikeda (1976) method while the ordinates contain strain ratio values (R_l) obtained by the Rf/θ method of Lisle (1977).
The position of the regression line clearly shows that the latter method overestimates the results of the former (R_s).

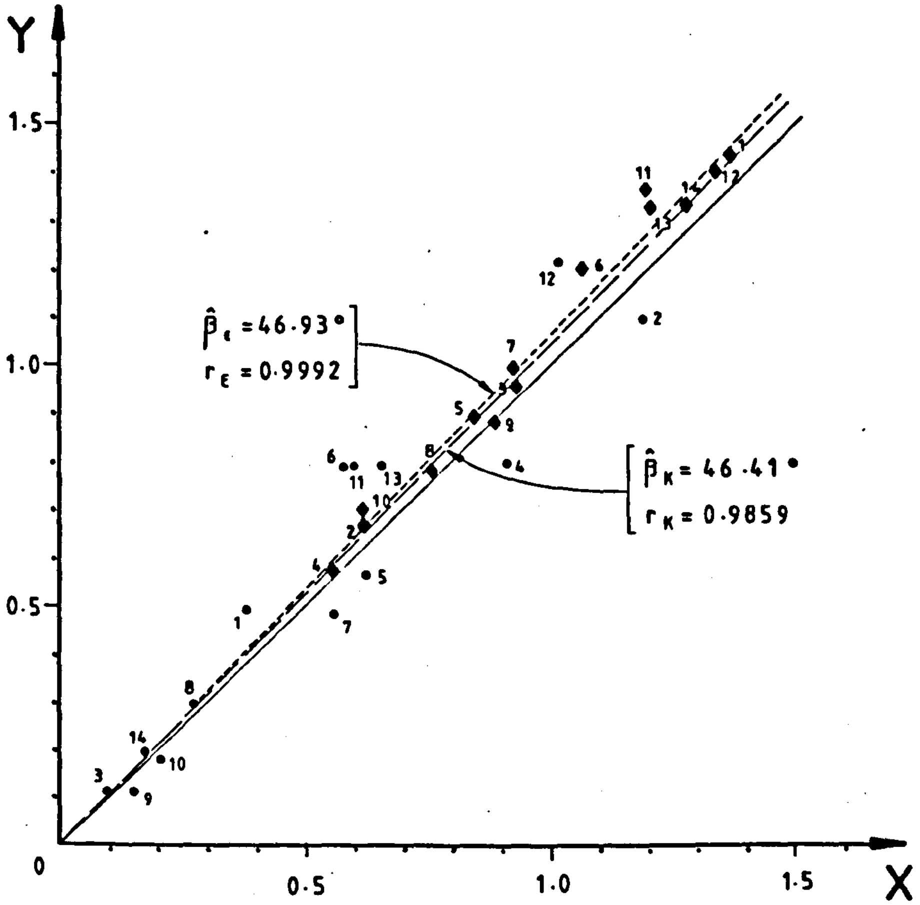

Figure 4.7-b. Diagram of linear correlation (using Programme PASE5) of values of Flinn's (1962) k (●) and Nadai's ε_s (♦) parameters. The X-axis refers to 2D results from the Shimamoto and Ikeda (1976) method, while for the Y-axis the 2D results were obtained from Lisle's (1977) Rf/θ method.

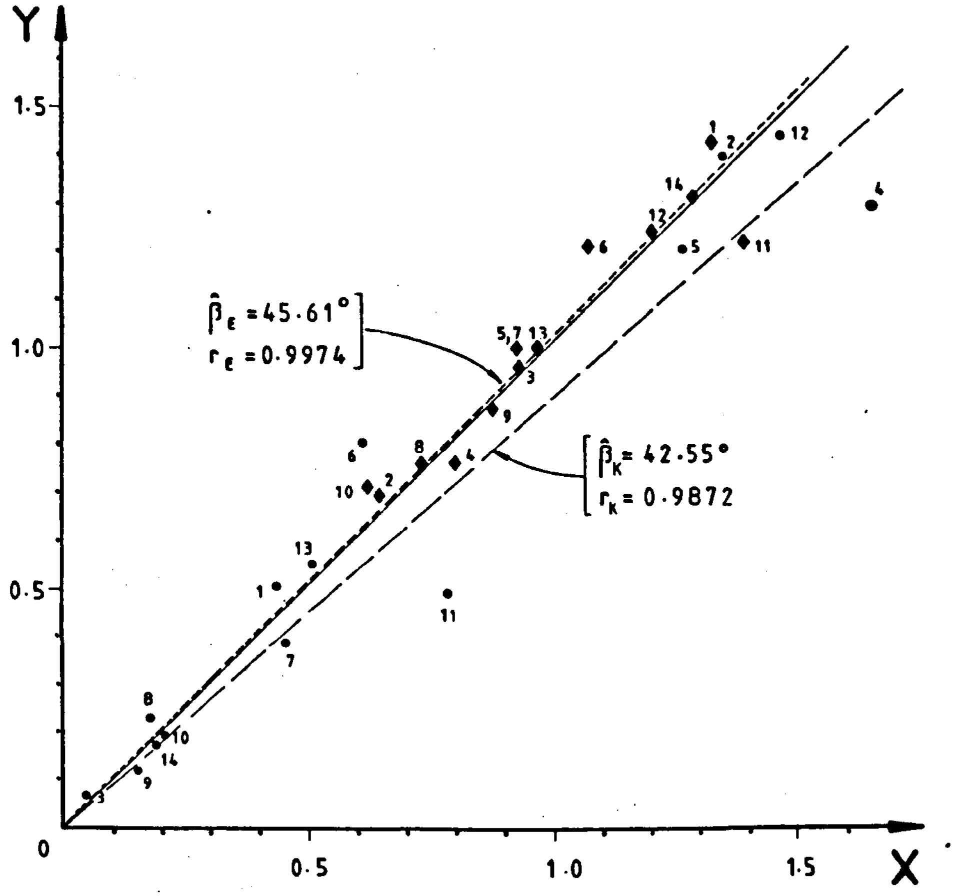

Figure 4.7-c. Diagram of linear correlation (using Programme FITELI) of values of Flinn's (1962) k (●) and Nadai's ε_s (♦) parameters. The X-axis refers to 2D results from the Shimamoto and Ikeda (1976) method while for the Y-axis the 2D results were obtained from Lisle's (1977) Rf/θ method.

Figure 4-7-d plots k and ε_s-values obtained (input data using the SI-method) with PASE5 and FITELI programmes. Here again, the ε_s results give very good regression line and have a good correlation coefficient while the k-parameter showed a scattered plot and its regression line produces a slope which is shifted by approximately 10° off the ideal 45° position.

4.4.2 The Shape of the Ellipsoids

The results obtained (fig. 4-8) reveal that the dominant pattern in the area is for ellipsoids which occupy the flattening field of Flinn's (1956) diagram. Some fabrics plot within the constrictional field, 2D strains given by the SI-method (see table 4-2). Three of the prolate ellipsoids show high levels of incompatibility of their conjugate ellipses and for this reason these must be considered as of low reliability.

Other strain estimates have been carried out in the northern part of the Moine Thrust. McLeish (1971) has used data from the Pipe-Rock around Kempie Bay and he found X/Y ratios in the range between 2:1 to approximately 10.3:1, the mean being around 5:1. His model, however, makes the assumption that pipes lie in the $\lambda_1\lambda_3$-plane of the strain ellipsoid which deforms by plane strain. This is the condition to be expected in shear zones.

Nadir (1980) estimated the 3D strain within grains for rocks of the lower Eriboll Nappes, using rutile needles. These gave mainly oblate strains. He also performed 2D strain determinations using elliptical sections of 'pipes' on bedding surfaces, and by measuring the shape of quartz grains. The former reveal low values of R in this area - 1.5:1 to 3:1 - while the latter show greater ratios ($\simeq$4.3:1).

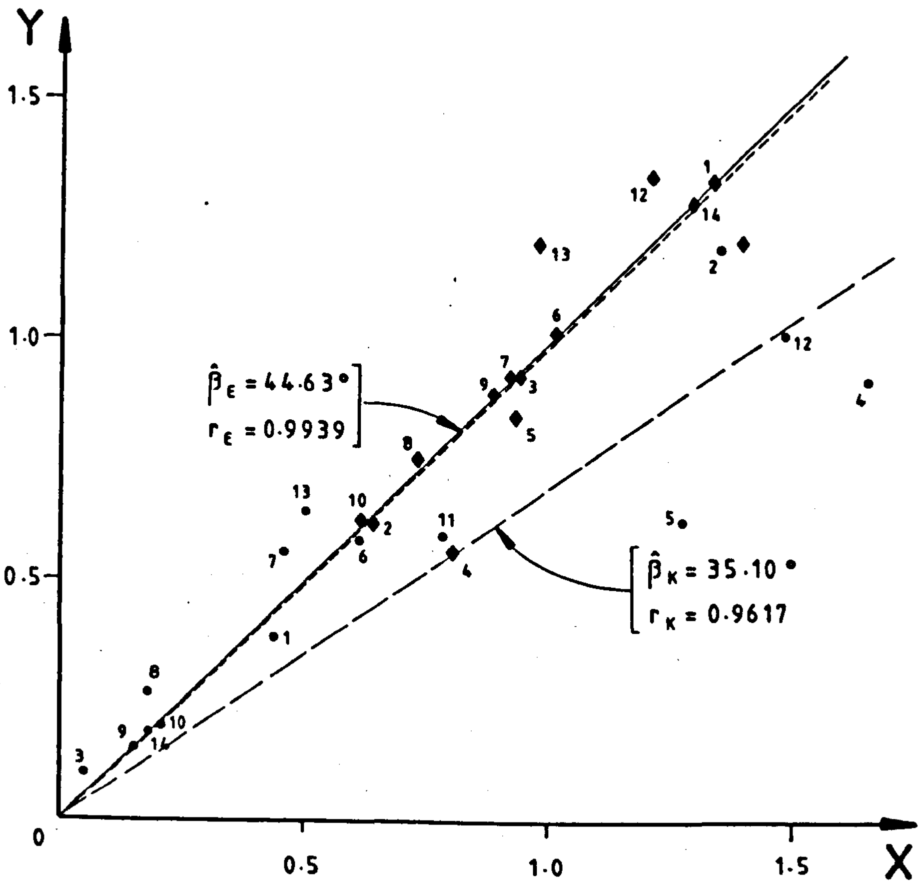

Figure 4.7-d. Correlates Flinn's k (●) and Nadai's ε_s (♦) values, obtained with FITELI and PASE5 programmes: the X-axis refers to values from programme FITELI while the Y-axis refers to values from PASE5. Full line has a 45° slope while dashed lines refer to regression lines (see text for full details) as indicated. Note that the discrepancies are greater for k-values than for ε_s.

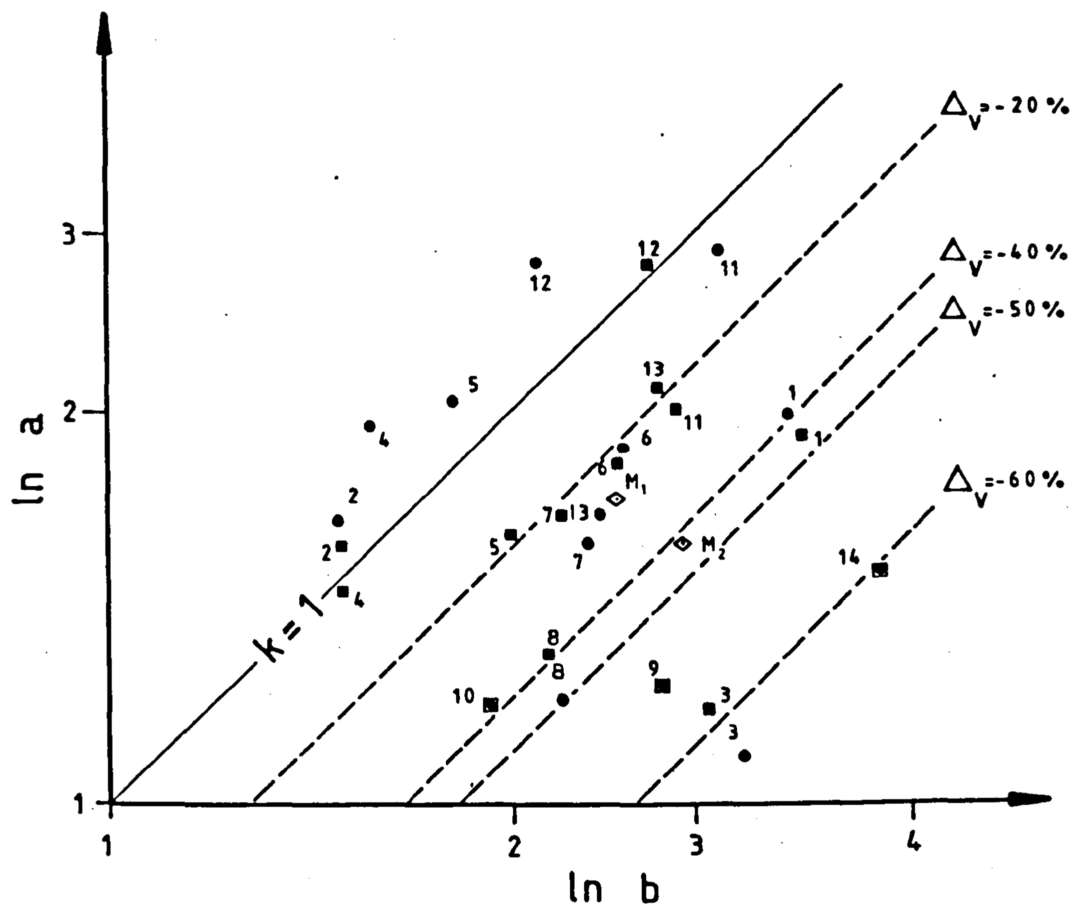

Figure 4.8. Logarithmic plot of Flinn's (1962) diagram showing results of strain measurements in the Eriboll area using programme FITELI (●) and PASE5 (■). Numbers refer to data from Table 4.2. M_1 and M_2 are the means of the plotted k-values. Dashed lines refer to volume change (see text for details).

Mendun (1976) performed strain evaluation using pebbles of the Strathan Conglomerate of Melness, west of Tonge. He obtained very low k-values, all oblate and ranging between 0.012 to 0.0013. He estimates X/Z ratios to be in the proportion of 51:1.

In the present study the X/Z ratios range between 2.5:1 to 6.5:1 for the Eriboll area while those specimens from Loch Hope were in the range of 2.3:1 to 7.2:1.

These shape values may be compared with others determined elsewhere within thrust zones. Chapman et al (1979) reported the predominance of oblate shape fabrics for pebbles deformed in Ifjord region, N Norway. They noticed the existence of isolated domains which show the constrictional type of ellipsoids. Hossack's (1968; 1978, fig. 5) results also show a predominance of oblate pebble fabrics for the Bygdin area, S Norway.

Among the 4 prolate values found by the present study, 3 are known to be in the vicinity of major fold hinges (see fig. 4-1 localities for diagrams nos. 41482, 41484 and 41494). Could this be correlated in some way with Ramsay's (1967, p.220) explanation that a prolate fabric might develop a hinge region provided that there was an earlier compactional fabric present in the rock? However the non-plane strain oblate fabrics also need to be explained.

One way to explain the oblate fabrics obtained in the rocks is to invoke volume change. Ramsay and Wood (1973) discussed the effects and implications of volume reduction during conditions of plane strain deformation. They illustrated the case in which the tectonic strain is of k = 1, but with volume change the finite strain plots in the oblate domain of Flinn's (1956) plot. Slate might well lose 10-20% volume during lithification from mudstones and even greater volume losses from unconsolidated sediment. However it is unlikely that quartzites would suffer such large volume loss due to compaction processes. The fabrics from Eriboll would plot in field suggesting volume losses up to 65% , according to the model of Ramsay and Wood (1973, p.274). Probably the deformed sandstones experienced some volume loss during the whole period of their history, but the amount required (up to 65%) is far too great.

The mean of all ellipsoids, including the prolate ones, plots within the flattening field as M_1 (see fig. 4-8) while the mean of the oblate ellipsoids plot as M_2. The former would give Flinn's k-parameter a value of 0.514 while the latter gives k = 0.340. If these means are considered as representative of the studied population they would plot along lines of 20% and 40% of volume loss respectively.

Another possibility is that this apparent flattening may be interpreted as a result of reduction of the volume of individual grains due to effects of polygonization and recrystallisation processes at their grain boundaries (see Chapter 5 and 6 for details). This may occur when there is no bulk volume change during deformation. Let us consider some situations which are based on microstructural observations (Chapter 5):

(i) Consider the partition of clasts along preferential directions in the grain (see Chapter 5, plate 5.33). The increase in the amount of recrystallization along the parting surfaces leads to the isolation of the remaining parts of the original clast and these can be easily mistaken as completely unrelated clasts (see plate 4.1). The outer parts of the grains form a rim of recrystallized new grains commonly referred to as mantle (cf Gifkins 1975; White 1976-a) around the remaining clast, termed the core (see fig. 5-10).

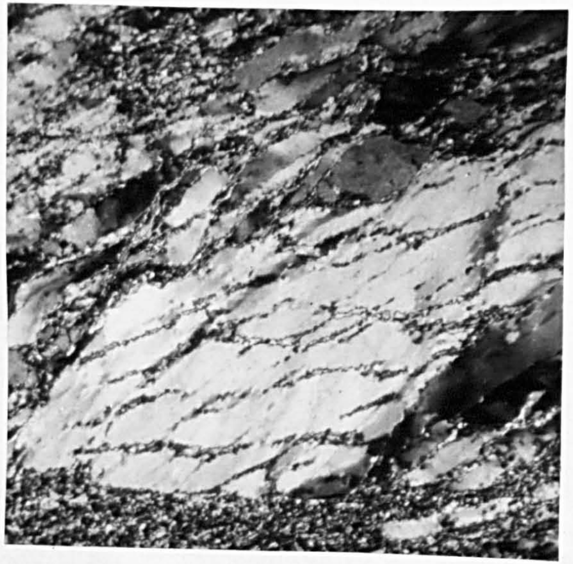

Photomicrograph (cross polars) magnified 38 times.

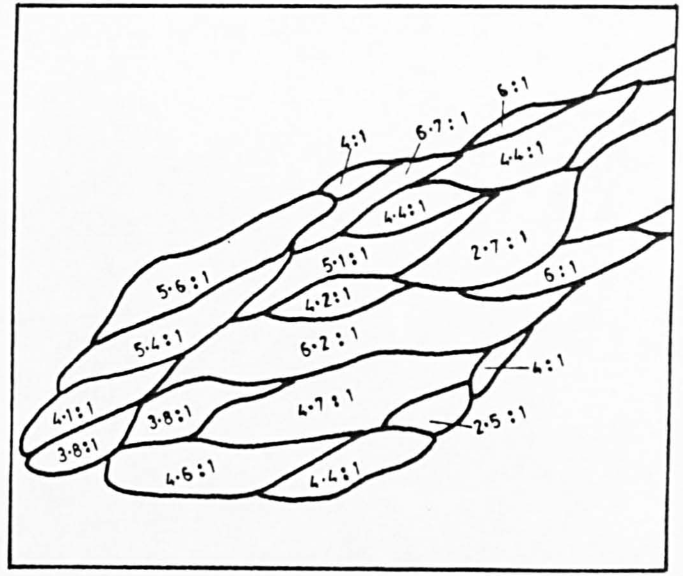

Plate 4.1. Illustrates the partition of a quartz grain with new grains having recrystallized along the parting surfaces. The progressive increase in the thickness of these recrystallized mantles leads to complete separation of the remaining cores and they could easily be mistaken for separate clasts. Notice in the diagram, made from the photomicrograph, the outlined new cores present a clear, preferred orientation and shape ratio ranging from 2.5:1 to 6.7:1. The mean ratio of these cores is 4.6:1.

(ii) Consider for instance the situation illustrated by fig 4-9. The development of preferential recrystallization in a particular direction in a clast can lead to a deceptive strain estimation.

(iii) Another example of the effects of the recrystallization on the grain shape is given by figs. 4-10 and 4-11 which examines mantles around particles of different shape ratios. These show no preferential recrystallization. It can be seen that for the perfectly circular grain the ratios are always equal to unity, no matter what the amount of the recrystallization of the surrounding rim. With an elliptical grain section, the shape ratio of the core increases as the amount of recrystallization (measured as the area of the mantle) increases. Figure 4-11 plots the shape ratios given by cores with different initial ratios. It is clear from this diagram that the initial excentricity of the grain will determine the relative increase in the shape ratio of the remaining core. A corollary of this is, if the initial particles are well rounded in such a way that their initial dimensions do not exceed ratios of nearly 1.5:1, the amount of recrystallization does not add too many errors to the shape measurements of the cores.

(iv) A more reàlistic situation, combines (ii) and (iii) above, where there are unequal increases in the thickness of the mantles, according to preferential directions of recrystallization coupled with intracrystalline deformation of the core.

The above discussion deals only with 2D ratios. In 3D there may be preferential recrystallization parallel to particular strain axes and this could influence the 3D shape ratio.

It is also possible that the tectonic strains may not have been of $k = 1$ and may have involved extension in the Y-directions

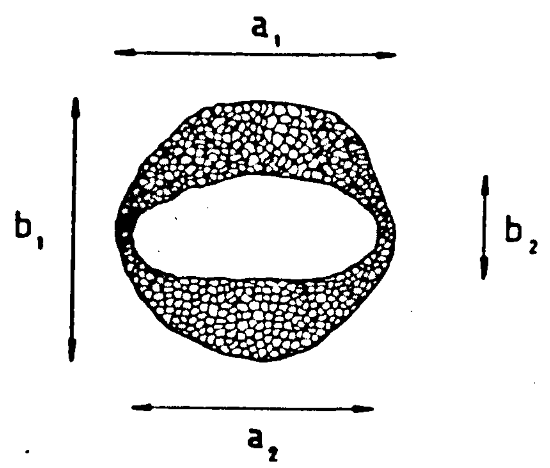

Figure 4.9. Illustrates the preferential development of newly recrystallized grains. The previous axes ratio, a_1/b_1, is modified to a greater (a_2/b_2) value and this could give a false impression that the shape of the particle was a product of intracrystalline deformation.

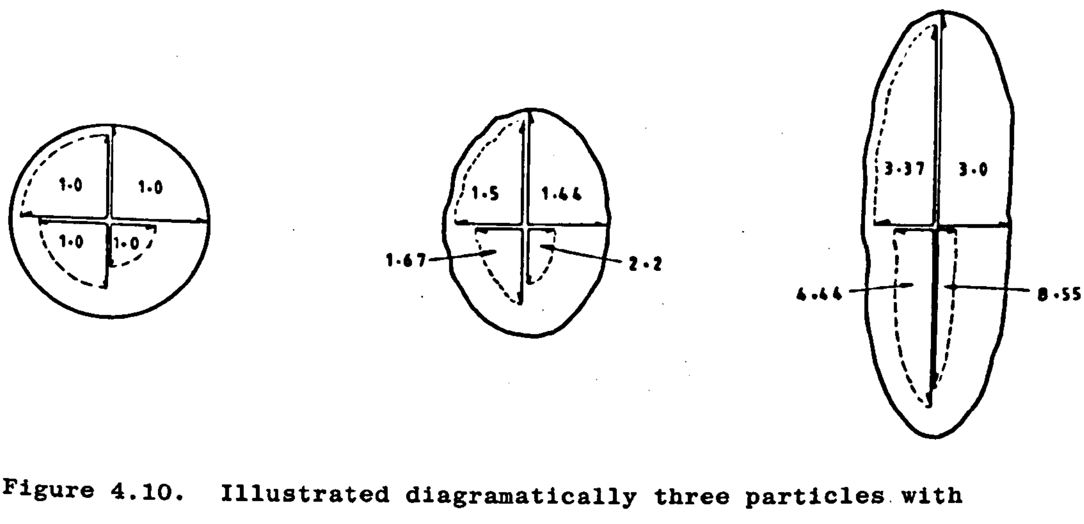

Figure 4.10. Illustrated diagramatically three particles with different external shapes. These particles suffer homogeneous regression of their external boundaries thus reducing their areas respectively to: 80%, 50% and 20% of the initial area. This is represented only in the quadrants of each diagram, in which the dashed lines refer to the regressed external boundary and the figures indicate the modified axes ratio.

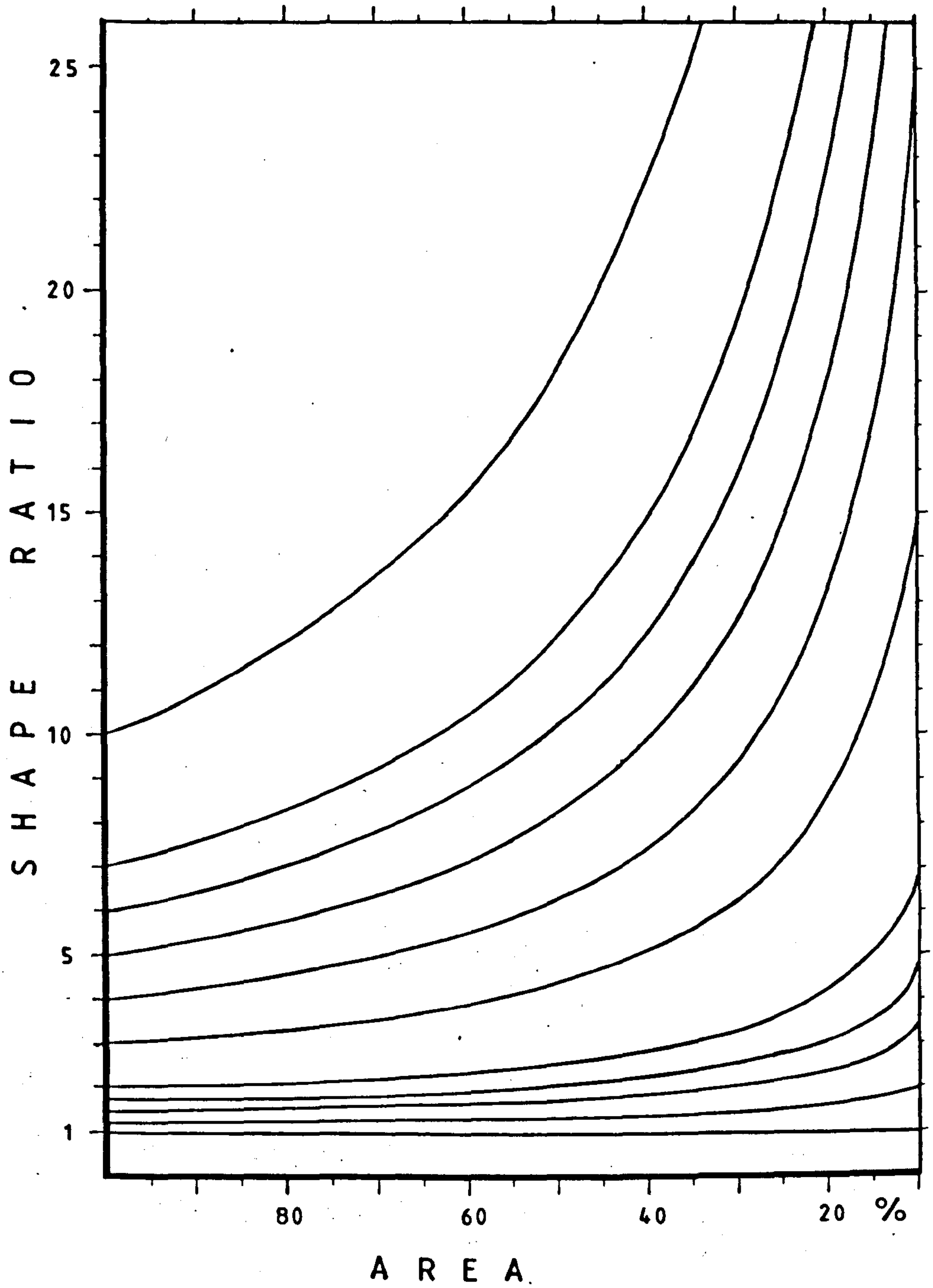

Figure 4.11. This correlates the change of the particle ratio with homogeneous area reduction, according to the initial shape of the particle.

or the strain ellipsoids. Hossack (1978, p.232) calculated the elongation along the Y-direction for the Bygdin area which ranges from 11 to 15%. Chapman et al (1979) also reported an average extension of 17% along the Y-direction for the Ifjord area, Norway. The means found in this study, M_1 and M_2, correspond respectively to ellipsoid ratios 1.93:1.12:0.46 and 1.89:1.19:0.44 (no volume change) in which the extension along the Y-axis corresponds respectively to 12% and 19% while shortening along the Z-directions are of magnitued of -53.5% and -55.5%. From the individual ellipsoids (see tables 4-2 and 4-3) the extensions along the Y-direction are up to 40% while shortening along Z-axes ranges from 35% to 64%. We shall see however that we cannot judge extension along a deformation belt based solely on figures from the ellipsoid axes, because there could be a lack of parallelism in the orientation of these axes, throughout the belt.

Another way of interpreting ellipsoid fabrics is by superposition of strains. Sanderson (1976) has investigated cases where the total strain results from plane strain superposed on compactional strains. An oblate final fabric could result where a coaxial superposed strain has its least principal axis normal to bedding while the extensional direction is nearly parallel to bedding. The superposition of non-coaxial irrotational strain (see Sanderson 1976, p.46) such as simple shear parallel to an oblate (compactional) type of fabric would also produce a fabric that plots in the flattening field.

The domain of the present mapping does not include undeformed quartzitic rocks. However the quartzites from the foreland away from the thrust belt yield a very weak or no fabric at all (G. Potts,Pers. Comm. 1981). The absence of such an initial fabric, excludes the fabric interpretation based on the mechanisms suggested by Sanderson (1976).

Grocott (1979) interprets shape fabrics from quartz-grains, sampled from the Ikertoq Belt in W Greenland, as due to the superposition of two simple shear strains and the majority of his results plot in the oblate field. Coward and Kim (1981) presented a range of possible ellipsoids that can result from the combination of irrotational and rotational strains, which might be expected in a thrust zone. None of these strains involved length changes of the belt normal to the transport direction. They showed (op. cit. pp.268-288) that the field where the final ellipsoid plots depends whether or not there is a shortening (oblate) or an extension (prolate) along the displacement direction.

As many of the rocks in the mapping area are folded and it is argued (Chapters 2 and 3) that there is layer parallel shortening or compressional flow (cf Nye 1952) forming these folds, then it is not surprising that many of the strain ellipsoids are in the oblate field.

It must be concluded that the interpretation of deformation based solely on shape fabrics of quartz grains proves to be no simple matter.

4.4.3 Orientation of the Ellipsoid Axes

It is important to take into account the orientations of the semi-axes of the obtained ellipsoids and relate them to the regional structure of the belt. Figure 4-1 shows the stereoplots of the ellipsoid axes at each locality and it can be seen that there are some variations in the attitudes of these axes.

It is possible to group and describe orientations as follows:

(i) In the Kempie sub-area, the orientations of the 2 closest samples underneath the lower thrust (nos. 41481 and 41483) bear some resemblence in that both are oblate and the differences between their $\lambda_1\lambda_2$ planes appears to exhibit only a relative tilt, which if it is eliminated,would practically restore analogous axes in both ellipsoids to nearly parallelism. The other two samples (41482, 41484) however are prolate. They are further from the thrust surface and underwent less deformation. These two samples have their λ_1 and λ_2 axes trending parallel and concordantly with the expected Caledonian trend (ie λ_1 plunging towards ESE and λ_2 oriented to NNE/SSW).

(ii) The two samples from Arnaboll Hill probably have been influenced by the antiformal hinge in this area (see structural map of figs. 2-2). One of the samples is prolate (41494), while the oblate one presents a subvertical λ_1-direction and λ_2 plunging gently to the NNE.

(iii) The samples in the Hope sub-area, show a spread of their λ_1-axes which describe a precession arc of nearly 180^o.

Samples 41501 and 41502 show similar orientations of their principal axes, the $\lambda_1\lambda_2$-plane being subhorizontal and λ_1 directed towards the SE.

The orientations of the λ_1-principal axes in samples 41504 41505 and 41506 show some similarity,while sub-parallelism of λ_3 axes occurs in specimens 41505 and 41506.

Specimen 41507 shows a curious orientation of the λ_3-principal axis,being subhorizontal towards the ENE, while λ_1 plunges gently towards the SSE. This specimen presents a prolate shape (both by FITELI and PASE5) and the highest lack of fit (nearly 40%) for the intersecting ellipses. This result should be considered as unreliable, as the amount of recrystallization is also considerably higher than in the rest of the samples.

Samples 41513 and 41514 are those with clearly similar principal axes, parallel to the expected positions of a Caledonoid fabric. Specimen 41513 is the nearest to the calculated mean $\bar{M}_1$ in the diagram of figure 4-8.

A general plot of the axes (see fig. 4-12) reveals that there is a tendency for the λ_1 and λ_2 principal axes to be at subhorizontal while λ_3 is generally steeply plunging. The positions of the λ_1 and λ_2-principal axes seem to resemble many of the orientations of the F_2 and F_3 hinge directions, described in Chapters 2 and 3.

This study also compared the attitude of ellipsoid axes for programmes FITELI and PASE5, in 34 different determinations. The results correlate very well. It was observed that the differences in the attitudes of the axes given by these two programmes increased proportionately to the amount of incompatibility (see section 4.2.3.2, also the last column of tables 4-2 and 4-3) that is, the lack of fit between the 3 orthogonal ellipses. Therefore, in conditions of poor lack of fit, the input data is unreliable for both methods. However, both tests converged to exactly the same answers in a series of 6 tests in which the simulated input data had levels of incompatibility equal to zero.

4.4.4. The Estimated Strain Intensities

The strain intensities vary throughout the area. At Kempie

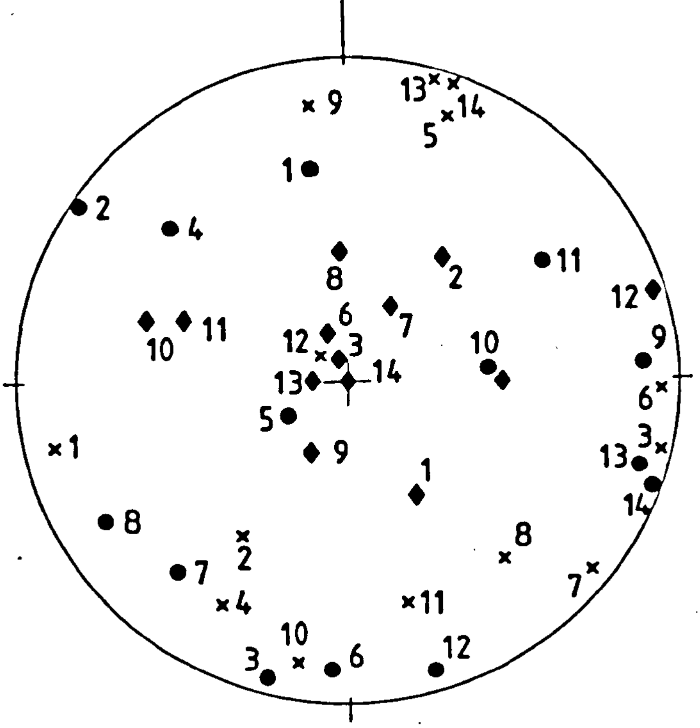

Figure 4.12. Stereoplot of the principal axes of the obtained ellipsoids. ●-λ_1, X-λ_2 and ◆-λ_3 directions. See text for full explanation.

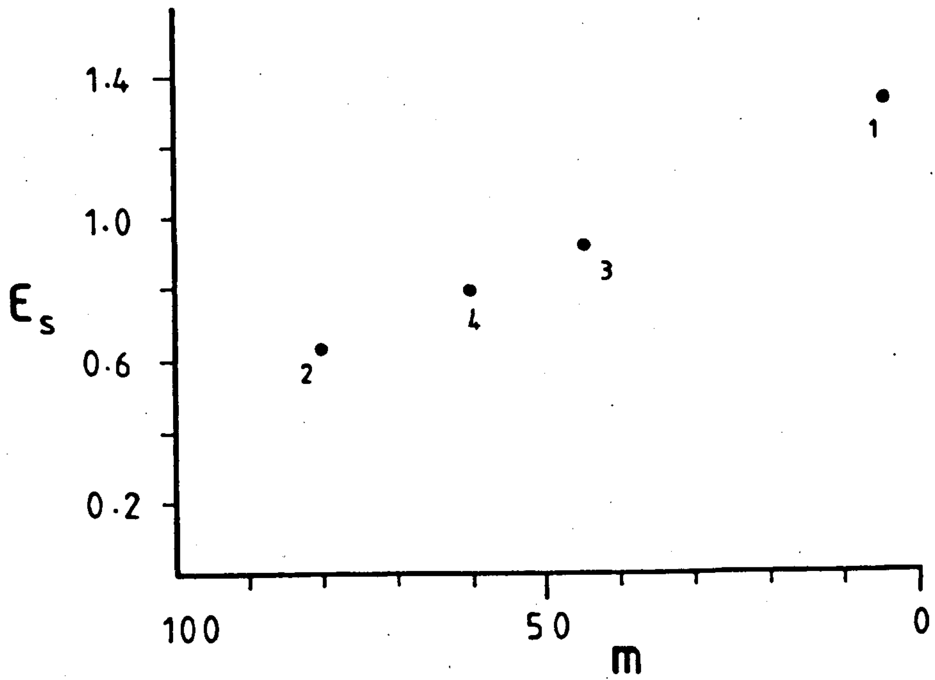

Figure 4.13. Relates the amount of strain with sample proximity (metres) to the b-thrust at Kempie. Sample order numbers and ε_s values are given in Table 4.2.

there seems to be a gradual increase in the amount of deformation with the proximity of the thrust belt (ie a strain gradient, see fig. 4-13). Due to large amounts of recrystallization, it was not possible to estimate the shape factor within the Kempie mylonitic belt. Compared with other strain studies (see Kohlstedt et al 1979) the ratios given here are low. The maximum measured particle ratio is 26:1 while the ε_s estimates range from 0.64 to 1.39 (see tables 4-2 and 4-3). It is believed however, that the values for Nadai's-ε_s parameter in the mylonite zone of Kempie would reach figures considerably greater than 1.4, as there were some samples from this zone showing individual particles with ratios in the proportion of 62:1.

Perhaps only pebbles can provide good strain estimations in these conditions of more severe deformation. In fact, deformation estimates using pebbles very often reach ε_s-value around 3.0. Hossack (1978, fig. 5) has shown that εs in the Bygdin area varies between 1.0 and 2.6, while Chapman et al (1979) reports ε_s-estimations in the range of 0.8 and 3.9 for Ifjord area, Norway. The calculation of ε_s-values for the strain results reported by Hutton (1979, table I) in Horn Head, N Ireland, also range between 1.56 and 2.87.

On the other hand, the ε_s values for strained quartz grains in slates from the Ardennes (Mukhopadyay, 1973) range from 0.42 up to 1.0. Perhaps the strain values obtained from the Eriboll and Hope areas should be considered as minimum values. Quartz generally allows a limited amount of intracrystalline deformation before recrystallization processes interfere. As will be illustrated in chapter 5, recrystallization takes place early during deformation events almost concomitantly with clast distortion. Recrystallization then progresses rapidly towards grain destruction.

One aspect neglected in the preceeding sections relates to the role of grain boundary sliding during deformation. In Chapter 7 it will be shown that grain boundary sliding affects the creep rate in rocks (Gifkins, 1976, Etheridge and Wilkie 1979). Some of the deformation could have taken place by sliding or rolling effects instead of strictly intracrystalline deformation of grains, and this could account for any discrepancies between the bulk strain and the strain given by shape of individual grains. Borradaile (1981) has defined three different flow regimes, relating the role of grain boundary sliding to intracrystalline processes. He showed that during deformation there could be a change from one of these three schemes to another.

It is possible that the deformation exhibited by the less deformed specimens began by dominantly intracrystalline processes but as deformation progressed by size reduction of the clasts, newly recrystallized grains were formed along the boundaries so there could be some grain sliding contribution to the bulk rock deformation. Perhaps in the stage of ultramylonite formation (see Chapter 5, plate 5.20) where grains are finely reduced (sizes range 70-30μm), grain boundary sliding process may be quite important.

Finally I give some concluding remarks concerning the possibility of strain variations with deformation phases present in the area:

(i) The fabric results were obtained from samples measured not in the principal planes of the ellipsoid thus removing an additional assumption and therefore a possible bias.

(ii) Much of the observed fabric seems to be connected with the early phase of ductile deformation which gave rise to the Caledonian foliation. This is interpreted as being the peak of deformation intensity. Subsequent ductile phases may also have been responsible for additional strains, as shown for instance, by bent fold hinges. However these did not transpose completely the earlier foliation.

(iii) The positions of the least principal axes λ_3 tend be approximately parallel to the Z-finite ellipsoid axes determined in the fold hinge analysis of Chapter 3.

(iv) The discrepancies in the positions of the intermediate and longest axes of the obtained ellipsoids could be due to strains produced during the later ductile phases and it is possible that some differential rotations developed.

(v) Any argument that the oblate shape of the 3D ellipsoid might be due to extension along the Y-direction, normal to the transport direction of the belt, might not be valid because some λ_2 directions are not even nearly parallel to this Y-direction.

CHAPTER 5

MICROTEXTURAL ANALYSIS

5.1 Introduction

The aim of this chapter is to describe and comment on the microstructures and the deformation mechanisms of the quartzitic rocks of the Eriboll and Hope areas as shown in fig. 4-1. This follows on from the study of grain shape (Chapter 4) when it was observed that the thin sections of the measured grains exhibited a great variety of microstructures. It is believed that the rock textures can be used to indicate not only different strain magnitudes (Chapter 4) but also different conditions of temperatures, strain rate and deformation mechanisms.

In the present study, deformation mechanisms will be divided into three main groups: (i) Cataclastic, (ii) Intracrystalline, and (iii) Diffusional Processes (see McClay 1977, p.58, Kerrich and Allison 1978, p.109).

Cataclastic flow involves rupture of particles, frictional sliding and rotation of these grains (Sibson 1977). It may correspond to an overall dominant process during a tectonic regime or can constitute a mechanism only operative in one of the phases (eg quartz may deform by a ductile process while feldspar porphyroclasts behave in a brittle manner, see plate 5.35). Intracrystalline processes are those in which most of the strain is achieved by deformation within grains, eg by the gliding and climb of dislocations (Nicolas and Poirier, 1976). An intracrystalline process that particularly concerns the present study is that of Dislocation Creep which allows extensive plastic flow by glide motion of dislocations, the velocity of these dislocations being controlled by their rate of climb (see Ashby, 1972, p.887).

The last group of deformation mechanisms are by Diffusional Processes which occur where strain is accomplished by the transfer of matter within the grains or along their boundaries (Ashby 1972). Diffusive fluxes can be caused by the deviatoric stresses (Stocker and Ashby, 1973) so ions are removed from domains under high compressive stress to such places where low or tensile stress conditions occur. There is the implicit constraint that grain boundary sliding is also involved in the diffusion creep, thus preventing voids from forming and consequently preventing volume increases (Stocker and Ashby, 1973, McClay 1977, p.59 fig. Ic). If the diffusion path is intragranular, ie lattice diffusion, the deformation is termed Nabarro-Herring creep (Nabarro, 1948, Herring 1950). This kind of material transfer is important in metals at high temperatures and low stresses and occurs by the movement of point defects. However, if the diffusion path is along grain boundaries, the process is termed Coble Creep (Coble 1963).

Other deformation mechanisms may contribute to the overall rock flow, under certain conditions, and these include: Twinning, Defect-Less Flow (Ashby 1972), Grain Boundary Sliding (Gifkins 1975,, Etheridge and Wilkie 1979), Superplastic Flow (Boullier and Gueguen 1975). Details of the constitutive equations of some of these mechanisms and also the problems of their usage will be dealt with in Chapter 7.

There are several studies where microfabrics and strains have been interrelated in zones of progressive deformation (White 1973-a, b, 1976-a; Wilson 1973; Bell and Etheridge 1973, 1976; Marjoribanks 1976; Bouchez 1977; Kerrich and Allison 1978). For the Eriboll area, Allison (1974, 1979) investigated the microfabric of the quartzitic rocks of Ben Heilam while more recently Nadir (1980) studied microstructures in the Cambro-Ordovician sequence of the Lower Nappes (below the b-thrust) north of the Kempie Area. Other contributions from the Eriboll area are specifically discussed in Chapter 6.

Recent studies (White 1973-a, b; Bell and Etheridge 1973;

Majoribanks 1974; Nicolas and Poirier 1976; Hobbs et al, 1976) have indicated that there are a number of microstructural changes which accompany deformation by dislocation processes in which undulatory extinction is usually the first optical indication,as this represents small lattice distortions (White 1973-a) and appears before any visual grain-elongation takes place. Deformation lamellae and deformation bands constitute domains of equal extinction (ie same sense of tilt), developing either parallel or perpendicular to the active slip plane (Wilson 1975, White 1976-a). The presence of deformation lamellae and bands are indicative that further deformation within the grains has taken place, while the formation of subgrains and newly recrystallized grains marks the extreme limits of this microstructural evolution (see White 1976-a).

Most of the specimens analysed in this study, were collected from the Cambrian quartzites located within the Lewisian rocks as shown in figs. 6-4-a, b and c. The samples analysed for the grain shape analysis (Chapter 4) clearly indicate that there are no undeformed rocks among the collected specimens. This is certainly due to the fact that rock-sampling was performed from the vicinity of thrust surfaces and from within the mylonitic zones. However, towards the west (on the foreland), away from the faulting zones,the rocks exhibit characteristics of less deformation.

The descriptions of microscrutures in this chapter's thin sections are restricted to the optical microscopy of the Paleozoic quartzites. It will be shown that there is a sequence of microfabrics exhibiting the characteristics of progressive deformation. The systematic observations of this study led to a division of the analysed specimens into two main categories based on the phyllosilicate content. Further subdivisions, within each group are possible, based on the intensity of deformation. There follows, in this chapter, a discussion of the textural types in the context of the geology and structure of the area. The last part of the chapter is given to numerical correlations between the amount of recrystallization and the deformation experienced by some samples.

5.2 Textural Types

5.2.1 General

In order to give a systematic account of the existing textures, the selected specimens were divided into two groups according to the amount of phyllosilicates present in the section. Group A comprises those samples with very low phyllosilicate content (1-2%). Group B includes those specimens where the phyllosilicate contents reach proportions from 2 to 10%

It will be shown that Group A includes textures in which the grains show evidence of ductile deformation processes (Group A1) while some specimens show signs of a cataclastic flow (Group A2). A further subdivision, within Subgroup A1 can be made and as will be explained in section 5.2.2., this is based on combined criteria of an increase in the amount of clast elongation and grain recrystallization. Four classes of microtextures are presented here: (i) comparatively low to moderately deformed specimens, (ii) moderately to highly deformed fabrics, (iii) highly to extremely highly strained fabrics, and (iv) completely recrystallized fabrics, due to high mylonitization.

5.2.2 Group A1

The textures to be described in this section apply to samples with up to 2% phyllosilicate content. It will be shown that the microstructures characterize a progressive increase in the amount of deformation towards the mylonitic zone (bounded by UAT, b and MT planes). This is evidenced by sections exhibiting progressive elongation of clasts, accompanied by an increase in the amount of grain recrystallization. The totally recrystallized section is the predominant textural type within the highly deformed domains of the above defined mylonitic zone.

5.2.2.1 Comparatively Low to Moderate Deformation Fabrics

The least deformed specimens of the present collection are those in which the detrital grains have length/width ratios of less than 2.5:1 and were sampled at vertical distance of approximately 60-80 m from below the b-thrust (see localities of samples 41482 and 41484 in fig. 4-1). Such specimens (plates 5.1 and 5.2) have a preferred orientation of clast long axes and contain a number of microstructures indicative of slight intracrystalline deformation. These are: (i) undulose extinctions, (ii) incipient deformation bands and (iii) zones of sub grains and newly crystallized grains along clast boundaries and deformation band walls.

Clasts, characteristic of the present deformation stage, shown an increase in the misorientation associated with undulatory extinction, giving rise to the formation of deformation bands, which in many cases lie at high angles to the boundaries of the slightly elongated grains. Detrital grains can have clast-to-clast contact but there is a tendency for some recrystallization to be present along the clasts' boundaries and for these newly recrystallized grains to form a thin film. In some cases this recrystallization concentrates along isolated domains or in those areas with greater misorientations such as deformation band boundaries (see plates 5.1, 5.2 and 5.3). In many cases the clasts show effects of deformation by exhibiting 'trails'

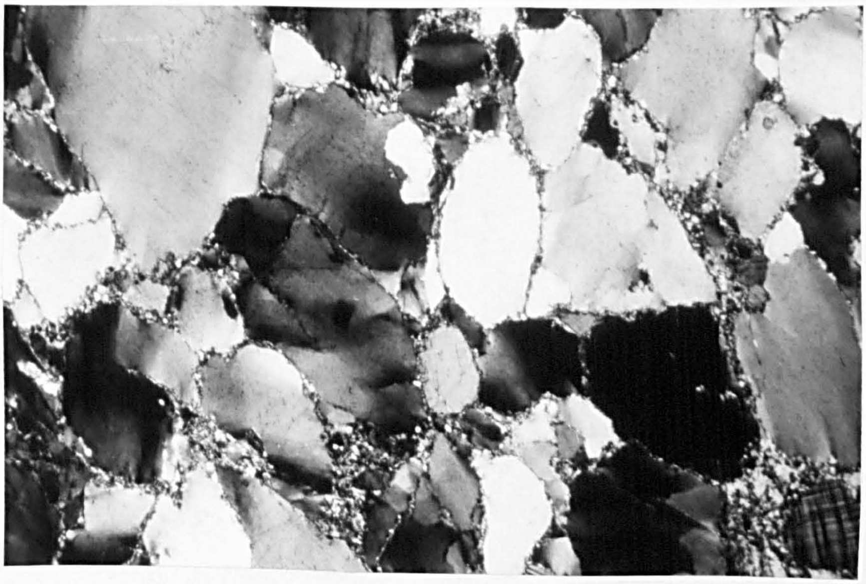

Plate 5.1. Texture of the least deformed of the sampled specimens. Sample collected at 85 m (vertical distance) of the b-thrust at Kempie, Loch Eriboll. Notice that grains show signs of deformation by exhibiting undulatory extinction, incipient deformation bands (diffuse) and some elongation. Photomicrograph (cross polars) magnified 38 times. Grid reference NC 45145752.

Plate 5.2. Section with characteristics of low deformation. Development of deformation bands and recrystallized grains along the boundaries. Photomicrograph (cross polars) magnified 38 times. GR. NC 45345760.

of subgrains which very often do not cut entirely across the grain.

The microstructures at this stage indicate that recovery processes have taken place, even though the shape change of the clasts is relatively low. The development of serrated grain boundaries (see plate 5.3) , with the size of the serration being equivalent to the sizes of the newly recrystallized grains, indicates that the clasts' boundary regression may be associated with the recrystallization processes along grain boundaries. The formation of this migration interlock (see plate 5.12) of grains with increasing misorientation along these boundaries, leading ultimately to the detachment and formation of a new individual grain, can be driven by a change in the dislocation density on each side of the grain boundary. This stage is known as dynamic recovery in order to differentiate it from static recrystallization (White 1976-a), where recrystallization takes place after deformation. As pointed out by White (1976-a), the increase in misorientation with the transition from undulose extinction to subgrain formation is governed by strain rather than temperature. He also mentioned that this transition is an indication that grains are ductile features.

At these comparatively low strain intensities the clast grains are continuous and exhibit domains with slight optical misorientation, characteristic of subgrain formation. As the process of deformation continues, the misorientation increases and the result is a complete isolation of that domain, forming a new grain. Another characteristic feature of this process is the narrow width of this mantle of new grains surrounding the clast. Very often such mantles are only one grain wide and this is important because as deformation increases that mantle of new grains gradually widens (compare plates 5.1 and 5.2 with 5.8) and leads to the complete isolation of each clast.

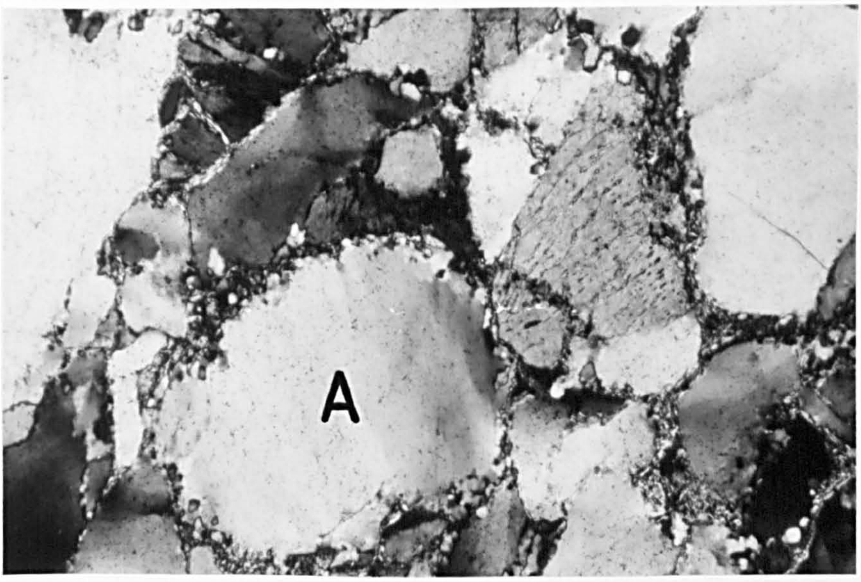

Plate 5.3. Illustrating microstructures in a regime of low deformation intensity. Large clast (A) shows serrated grain boundaries, and develop a core and mantle structure. Photomicrograph (cross polars) magnified 90 times. Grid reference NC 45145720.

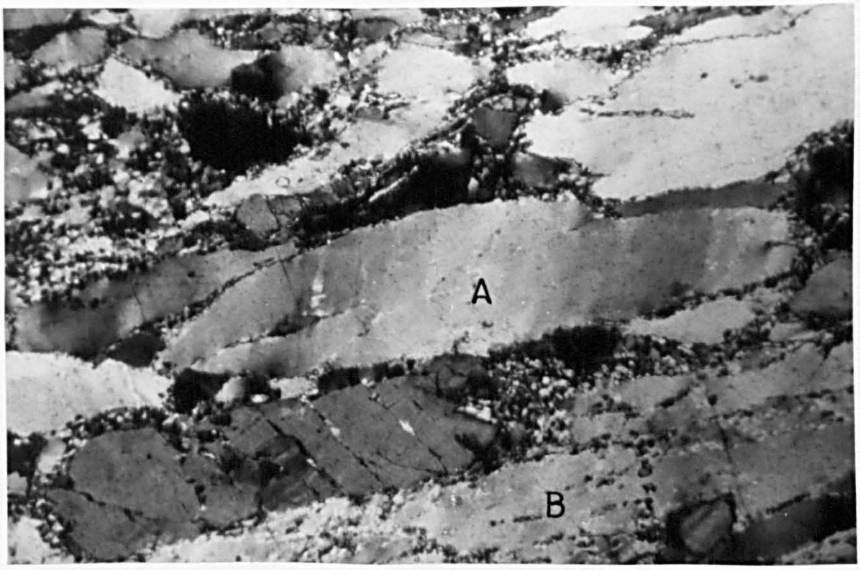

Plate 5.4. This section has developed bands of extinction at high angles to the elongation direction of the grain (A). Notice the increased amount of subgrains and new grains within the bottom quartz grain (B). Photomicrograph (cross polars) magnified 38 times.

Grid reference NC 45035738.

Also present in the specimens of this subgroup, are narrow zones with parallel boundaries cutting across the microfabric of the sections. The grains within these zones have extremely constant sizes and are much finer than the detrital clasts. These zones, will be referred thereafter as bands of recrystallization ,increase their width in the more deformed textural-types.

5.2.2.2 Moderately to Highly Deformed Fabrics

Two microstructural features are characteristic of this group of specimens: (i) the clastic grains are progressively more elongated than the previously described type (see plates 5.4 , 5.5 , 5.6 and 5.7). Ratios of clasts length/width in the proportion of 10:1 are not uncommon (see plate 5.14) and in the present study there are records of 26:1. It is clear that the textures, at this stage,also show a well defined preferred orientation of these particle long axes (see plate 5.6). (ii) The percentage of the newly formed grains (size in the range 30-70 μm) is also higher than in the previously described type. Proportions of 20-30% in volume, of recrystallized new grains,are usually common at this stage.

The localities where the present section's specimens were collected also shows characteristics of higher deformation, if compared with last described type. For example, the sample illustrated by plate 5.5 was collected at 20 m from below the b-thrust, at Kempie, while the samples of plates 5.6 , 5.7 and 5.10 come from within the mylonitic zone of the NE side of Loch Hope.

Other characteristics readily observed in these textures are the omnipresence of undulatory extinction within relic grains and the increased proportion of deformation bands (compare plates 5.8 , 5.9 and 5.10). Subgrains change their shape from nearly

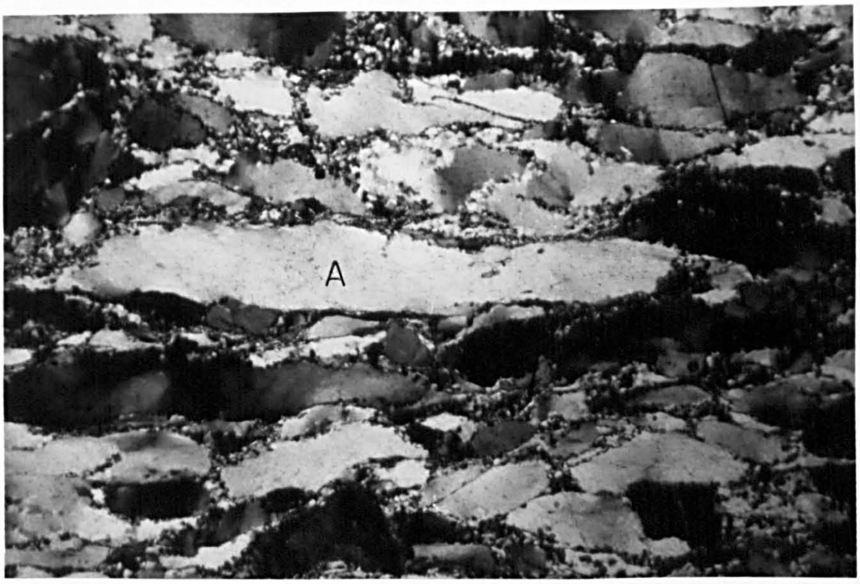

Plate 5.5. Basal Quartzite of Eriboll area, collected at 20 m (vertical distance) from the b-thrust. It shows a grain (A) stretched in the proportion of 7:1. The calculated amount of deformation for this sample is $\varepsilon_s = 0.95$. Photomicrograph (cross polars) magnified to 38 times. Grid reference NC 45005740.

Plate 5.6. Texture of highly deformed clastic grains forming 'ribbon' type structures. Photomicrograph (cross polars) magnified 38 times. Grid reference NC 47675910.

Plate 5.7. Quartzitic rock showing elongated clasts in 'ribbon' type of structure. The central clast (A) has a ratio ≃ 10:1. The percentage of recrystallized grains is approximately 30% in volume of the sample. Specimen collected within the mylonitic zone of the NE border of Loch Hope. Photomicrograph (cross polars) magnified 12 times. Grid reference NC 47825976.

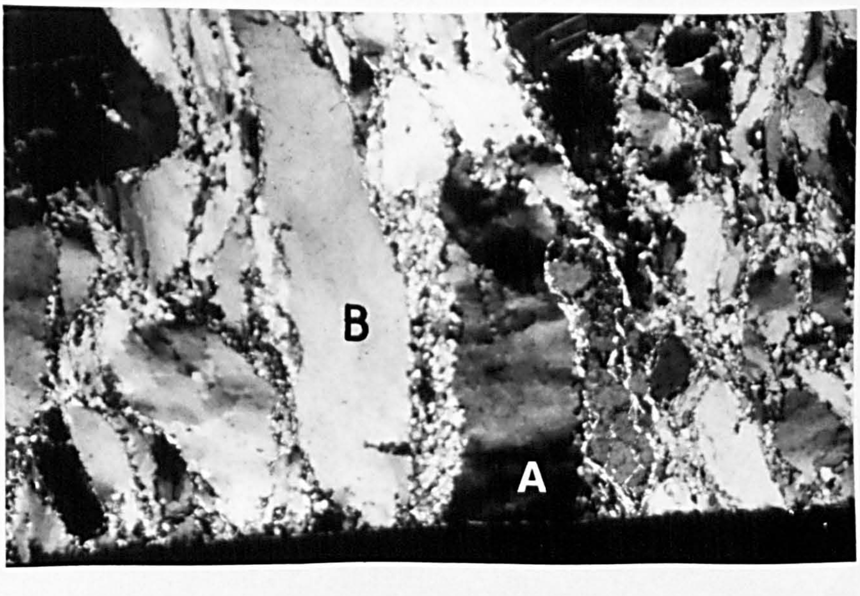

Plate 5.8. Illustrates the deformation bands orthogonal to the boundaries of clasts (A). Notice the amount of recrystallization between clasts A and B (mantle formation). Photomicrograph (cross polars) magnified 38 times. Grid reference NC 47825976.

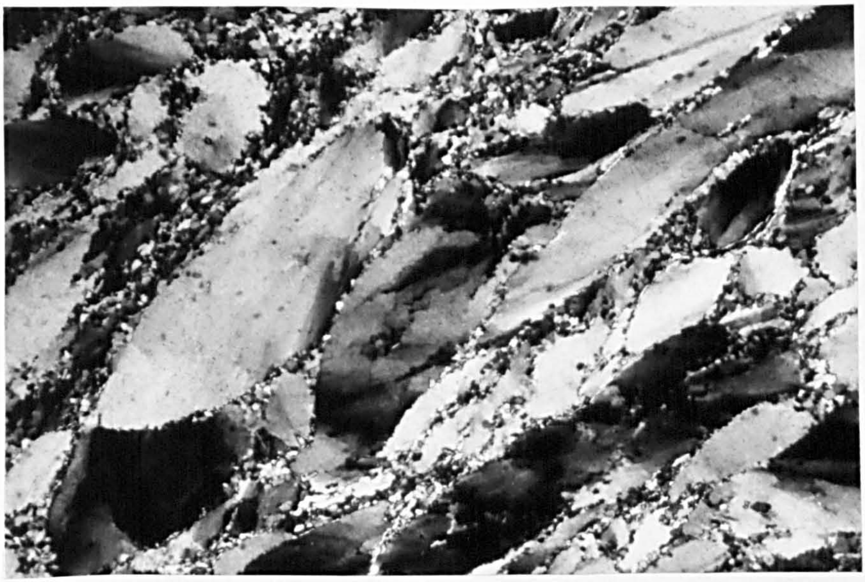

Plate 5.9. Illustrates deformation bands and new grain development within old grains. Notice effects of partitioning of grains by increased recrystallization. Photomicrograph (cross polars) magnified 38 times. Grid reference NC 47825976.

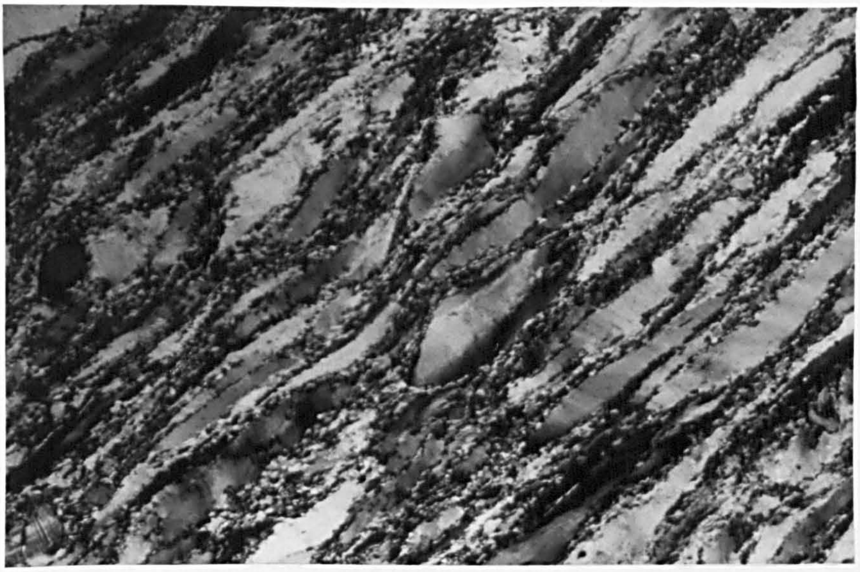

Plate 5.10. Quartz 'ribbon' structures with deformation bands at a high angle to the elongation direction. Notice the percentage of recrystallized grains. Photomicrograph (cross polars) magnified 38 times. Grid reference NC 47675908.

rectangular to a more equidimensional polygons as strain increases. However due to the poor resolution of the optical microscope it is difficult to conduct subgrain and size determinations as this equipment might not reveal that aggregates of smaller subgrains may be present in the observed microstructures (Tullis 1979).

In this textural stage, 'trails' of subgrains and new grains cutting across the relic clast, are more frequent than in the microstructures of section 5.2.2.1. In some cases this process leads to the complete partition of the grain (plates 4.1, 5.31). However there are cases where polygonization spreads over the entire clast, so that its physical continuity can only be inferred by rotating the microscope stage (see plates 5.11-a and 5.11-b) and/or with the help of a tint plate. In this stage the 'grain' is in fact an aggregate of a mosaic of finer and differently orientated new grains.

The increase in deformation is also accommodated by an increase in misorientation of subgrains which tend to form along the grain boundaries. Continuity of this process leads to the formation into new grains by development of high angle boundaries (plate 5.12). This sequence repeats itself by exposing a new grain boundary to the same effects, provided the operative stresses continue to build up dislocations and recovery is not capable of absorbing them (White 1976-a). It will be noted that such a mechanism gives rise to the formation of rims of recrystallized grains (size in the range 30 μm-70 μm) that progresisively isolate the remaining clasts as their boundaries suffer regression towards the inner parts. This type of structure is currently termed mantle and core structure (Gifkins 1975, White 1976-a, see plates 5.3 and 5.8), and has been referred to previously in Chapter 4. The boundaries of the clasts are rarely straight, but are invariably serrated (subgrained, see plate 5.13), following new grain boundaries.

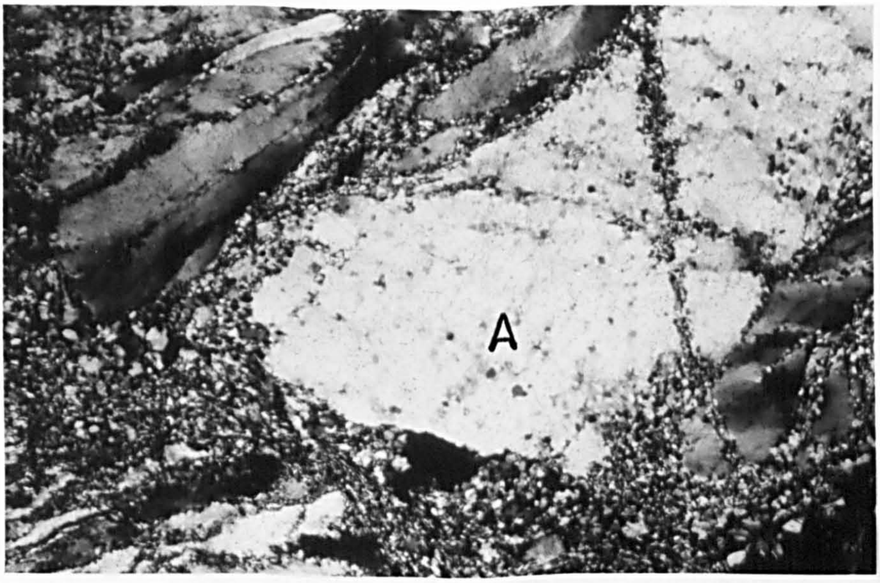

Plates 5.11-a and 5.11-b. Illustrates the effects of polygonization, which is verified by (microscope) stage rotation. The same grain (A) is in both plates, and it can be seen that it constitutes an aggregate on smaller oriented domains. Both micrographs (cross polars) are magnified 38 times. Grid reference NC 45385716.

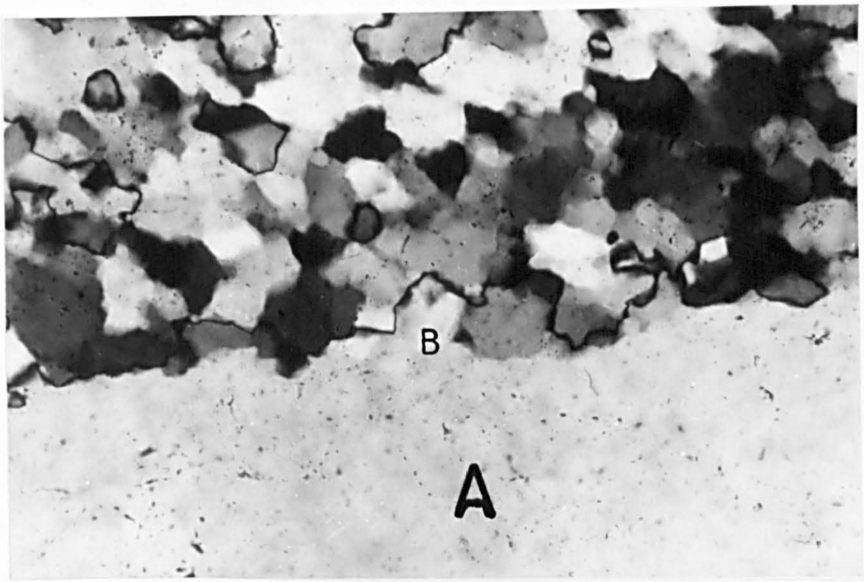

Plate 5.12. Illustrates grain boundary regression by the effects of recrystallization. Notice the 'detachment' of grains, (eg. B) in the boundary of grain (A), Photomicrograph (cross polars) magnified 363 times. Grid reference NC 47825976.

Plate 5.13. Illustrates the serrated grain boundaries. Notice the polygonal shape of the newly formed grains. Photomicrograph (cross polars) magnified 90 times. Grid reference NC 47825976.

The narrow zones, constituted entirely of recrystallized grains (bands of recrystallization, referred to in the previously described textural type), are more frequent and also wider in this stage. However, the diameter of the newly formed grains, in both textural types, may show little change and this will be discussed in more detail in the next chapter. The edges of such zones can still exhibit parallel sided boundaries approximating to straight lines (see plate 5.15).

5.2.2.3 High to Extremely High Strained Fabrics

Deformation features characteristic of this group are (i) a strict parallelism of the extremely elongated clasts which have not been destroyed by (ii) extensive recrystallization (see plates 5.16, 5.17).

The specimens in the present category were invariably collected from within the mylonitic zone of the nappe which is bounded underneath by the b-thust . The number of thin sections still exhibiting clasts is limited, but when these do appear, the ratios length/width of these grains can reach proportions up to 62:1. The amount of recrystallized grains in this stage, is far more than 60% in volume. It is worth mentioning that these specimens were totally unsuitable for the grain shape analysis of Chapter 4, due to this high percentage of newly recrystallized grains and also because of the difficulties in determining clast boundaries.

The textures of the samples in the present section fill the gap in the evolution from a texture described for the previous type (see 5.2.2.2) and the contrasting different textural-type to be described in section 5.2.2.4. Microscopic observations clearly indicate that this process of progressive deformation by clast elongation and area

Plate 5.14. Illustrates the general aspect of the stretched clasts. Photomicrograph (cross polars) magnified 12 times. Grid reference NC 47825976.

Band of Recrystallization

Plate 5.15
Illustrates the boundary between clastic domain and the zone or band of recrystallization. Photomicrograph (cross polars) magnified 90 times. Grid reference NC 47756015.

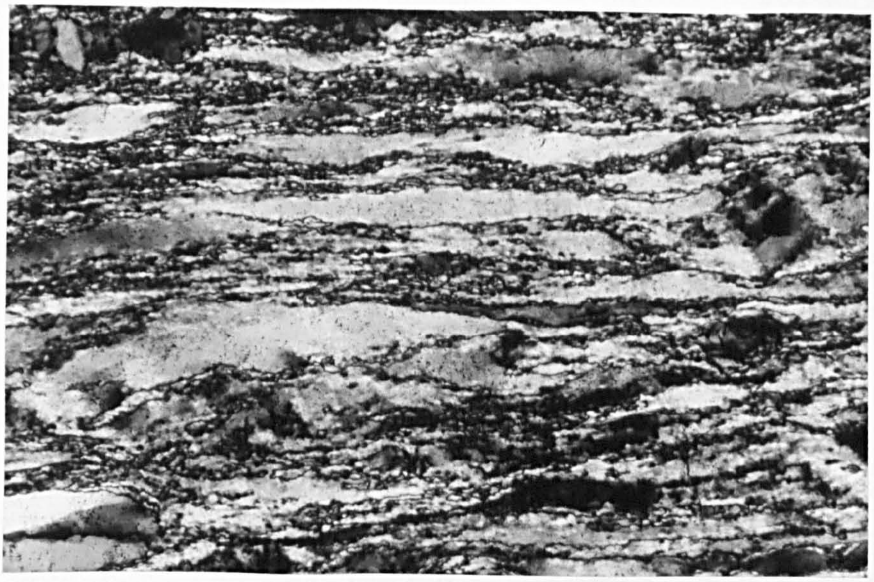

Plate 5.16. Specimen with a highly deformed fabric showing very elongated quartz grains. Photomicrograph (cross polars) magnified 90 times. Grid reference NC 45585717.

Plate 5.17.
Texture characteristic of a heavily mylonitized specimen. Notice the extreme elongation of quartz grains and the rounding effects of the grains of feldspar. Photomicrograph (cross polars) magnified 38 times. Grid reference NC 45705720.

reduction (ie volume reduction) by recrystallization can have another concomitant contribution to the already described bands of recrystallization. In the present fabrics, these latter microstructural features are clearly widespread and predominate over the amount of remaining clasts.

5.2.2.4 Completely Recrystallized Fabric

The characteristic microtextures of the present class is that of almost complete recrystallization (>95%). Possible grain relics (see plate 5.20) account for a minute proportion of the total slide area and are a few times the average recrystallized grain size. The reason for the existence of some relics can be perhaps explained by their orientations. Those most unfavourably oriented to slip or those perfectly oriented to it are likely to be more resistant to recrystallization (Carreras et al, 1977, Bouchez 1977).

The majority of the specimens of the present group are pertinent to the mylonitic nappe, bounded underneath by the b-thrust. The slides of the present type always show an extremely fine grained texture. A strong alignment of the phyllosilicates is occasionally seen and this defines a very close spaced foliation in which some feldspar grains with rounded boundaries are also distinguishable. A rock with such characteristics may be termed ultramylonite (Sibson 1977) and therefore comprises the end product of the present picture of progressive deformation (see plates 5.18 , 5.19 and 5.21).

The ultramylonitic texture may appear at first sight to exhibit a pattern of extremely fine grains with a constant size. However, a close inspection in some of the sections revealed that the

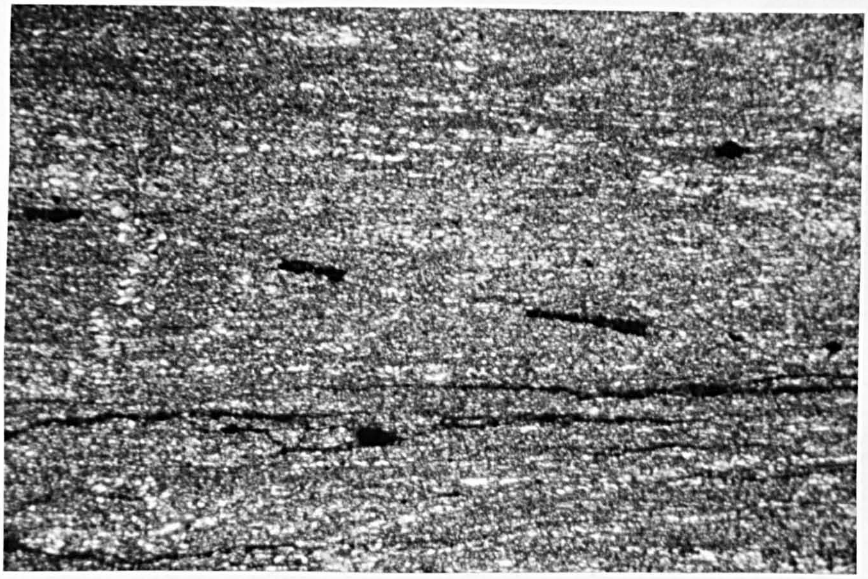

Plate 5.18. Ultramylonitic foliation. Specimen from within the Eriboll mylonite. Photomicrograph (cross polars) magnified 38 times. Grid reference NC 48196048.

Plate 5.19

Ultramylonitic folation exhibiting a weak transposition (see sketch) by alignment of grain boundaries oblique to the dominant (vertical) foliation. See sketch below. Photomicrograph (cross polars) magnified 38 times. Grid reference NC 47575975.

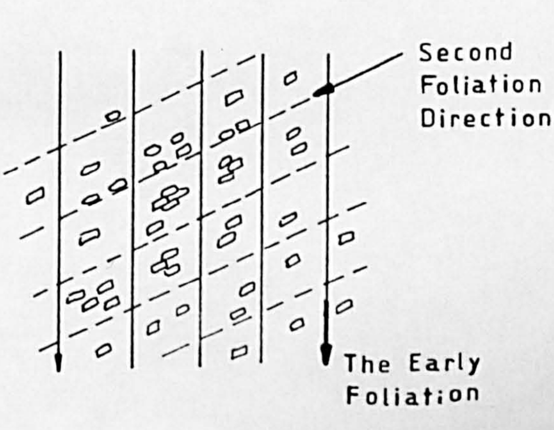

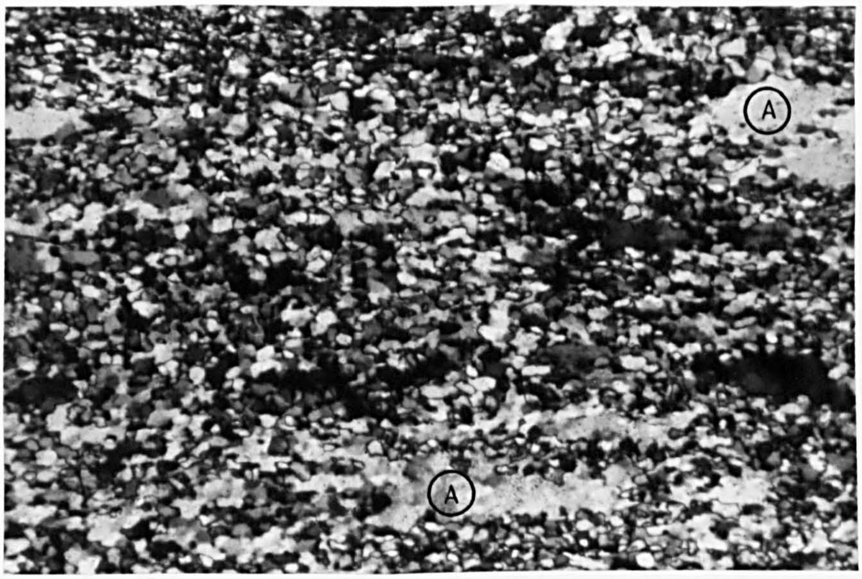

Plate 5.20. Recrystallized domain showing some small relic grains (A). Photomicrograph (cross polars) magnified 90 times. Grid reference NC 46045870.

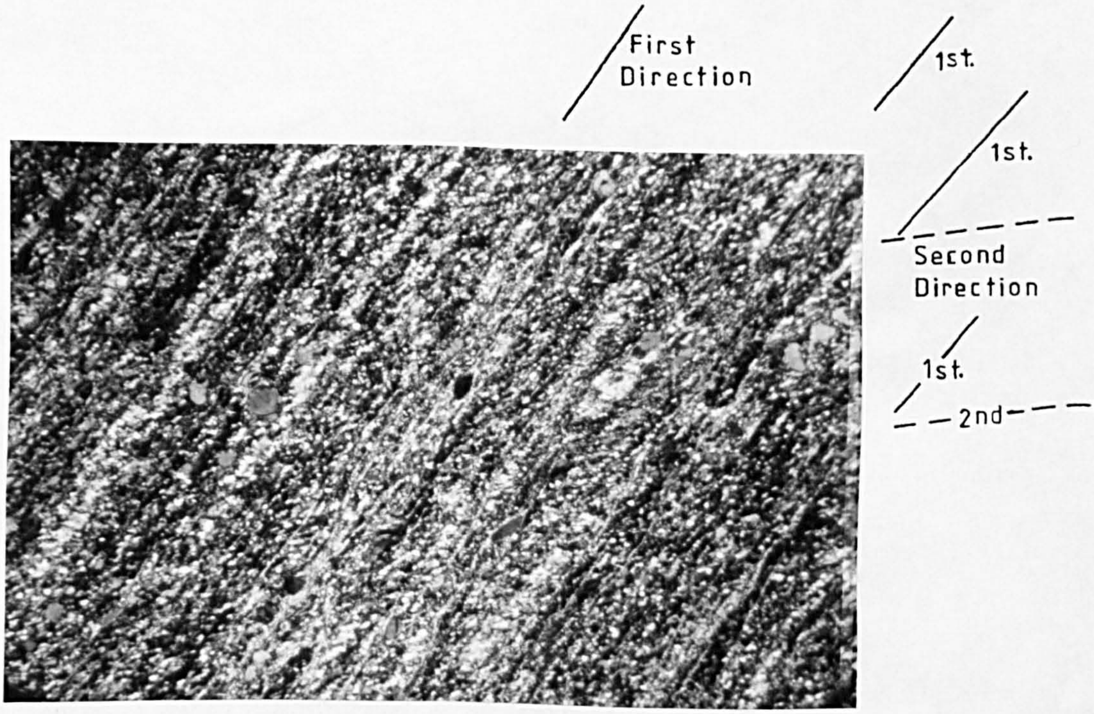

Plate 5.21. Ultramylonitic foliation showing alignment of phyllosilicates which are intersected by grain growth (tabular shape) of quartz, at an oblique angle of approximately 30°. Notice rounded feldspar grains. Photomicrograph (cross polars) magnified 38 times. Grid reference NC 47766047.

grains are equidimensional and there are fine disseminated phyllosilicates (see plate 5.26), . while other sections show signs of coarsening with aggregates having changed size and developed a tabular shape , parallel to the axial planes of microfolds which are superimposed on the mylonitic foliation (see plate 5.32).

Another equally important aspect,observed in some of these ultramylonites,is the development of an incipient late foliation , clearly cutting through the trace of the still dominantly ultramylonitic fabric, as shown by plates 5.21 and 5.19 . From the observations made in the sections it appears that:

(i) The incipient transposition of fabric takes place at low angles (around 30°) to the early foliation.

(ii) The effects of this new fabric alignment develops both by mineral re-orientation (phyllosilicates) and shape change, with quartz grains becoming clearly rectangular and this is accompanied by some coarsening.

(iii) This new fabric development occurs in different locations of the studied zones of mylonitization.

(iv) The continuation of this process would lead to the complete destruction of the previous mylonitic foliation. Thus some of the textures observed in the present study may not have evolved directly from primary structures and instead might be the result of the last transposition.

Another important question concerns the reason(s) for the rectangular shape in the newly formed grains. Exner (1972, p.36) gives a useful explanation why grains present a habit-shape, in that the reason for a group or a domain of grains to grow with a determined habit must be linked with features of minimum suface energy of a particular shape. This means that the grains will be spherical , or equidimensional, only if the specific surface is isotropic. In the case of antisotropy, those crystal planes having the lowest energy, the habit planes, are preferentially developed, forming a crystal of higher symmetry.

5.2.3 Group A2

5.2.3.1 Cataclastic Textures

Only three specimens were found to belong to this textural group and all were collected in the area located in the NE border of Loch Hope. Morphologically they are characterized by a clear cataclastic or microbrecciated texture, superimposed on a ductile type, such as those described in Group A1.

In the studied specimens it is clear that the quartz grains are broken into angular particles with a range of sizes, thus contrasting with the previously described textures in which the common characteristics are coarser clasts with finer and more uniform recrystallized new grain size. Quartz grains in the present group show microstructures with characteristics analogous to the brittle behaviour exhibited by feldspar grains in some of the section belonging to Group A1. Particles comprise a variety of different sizes and their grain boundaries do not show the characteristics of intense serration already described for the previous Group A1.

Although polygonization and bulging of the newly formed grains are ubiquitous, the deformation appears to involve different processes, as the presence of an early ductile fabric is clearly overprinted by a brittle deformation episode. White (1976-a) points out that cataclastic processes may take place in conjunction with the ductile mechanism and both are capable of producing steady flow

(Bell and Etheridge 1973).

Due to the restricted occurence of this textural type in the studied area, the significance of the brittle deformation must be interpreted with caution. For example, a cataclastic texture was not observed in the rocks of the Eriboll areas, Kempie and Arnaboll, which are very near to the Hope domain. The brittle fabric could perhaps be correlated with the late faulting events that took place in the area, but that argument is speculative due to the restricted number of samples.

Sibson (1977) uses a conceptual model where a brittle texture superimposed on a previously ductile microfabric (Quasi-Plastic zone cf Sibson, 1977, p.191) could indicate that the rocks were subject to a further deformational regime (Elastico-Frictional, cf. Sibson, op. cited) in which the rheologic characteristics of the rocks have changed.

There is also an alternative explanation where the presence of fluids in the 'pores' have the effect of reducing the mechanical resistence of the rock by lowering the frictional resistence to slip (cf Verhoogen et al 1970, p.464). This leads to the rock fragmentation and rotation (cataclastic-flow) under conditions where it would be normally ductile. However this condition is considered unlikely in the present case because the existence of an early ductile fabric would imply in a previous 'dry' condition for the rocks, thus the fluids would have to be inserted (by veins?) in the structure after the ductile deformation stage in order to induce it to a cataclastic flow.

5.2.4 Group B

Samples belonging to this group are less numerous compared with those in the previous Group A, but they proved to contain completely different microstructures. The rocks analysed in the present chapter constitute quartzites containing up to 10% of phyllosilicates. However, the composition of these rocks is far from homogeneous, or at least there seems to be some modification in the textural pattern that can be correlated with the increased proportion of phyllosilicate present in the sample. Rocks from the previous Group A have some phyllosilicates present but in a very small percentage (around 2% is the estimated average) while the amount for Group B is between 4 and 8%. This seems to be enough to cause modifications in the microstructures, at least in the less advanced stages of recrystallization.

Relatively less deformed rocks, which still exhibit some clastic grains,have a texture where grains have not deformed by progressive elongation accompanied by a process of polygonization, but instead there appears to have been a continuous reduction of grain size without extensive stretching of the remaining clast (plate 5.22) and also the formation of anastomosing or lenticular quartz domains showing intense polygonization (see plate 5.23).

In the whole area of sampling (fig. 4-1), the phyllosilicates are present:

(i) Along grain boundaries of larger clasts, causing some interference as illustrated by plate 5.24.

(ii) Forming localized concentrations (ie aggregates) in some less deformed types (see plate 5.25).

(iii) In parallel alignment, associated with the mylonitic and ultramylonitic fabric, especially in such specimens where the transformation to new grains was almost complete (see plates 5.26 , 5.27).

(iv) Forming a phase with minute diameter,uniformly disseminated along the boundaries of the newly formed quartz grains.

Plate 5.22. Illustrates quartz clasts reduced in size by effects of recrystallization but no signs of extreme elongation within the 'cores'. Photomicrograph (cross polars) magnified 90 times. Grid reference NC 46255884.

Plate 5.23. Shows the presence of phyllosilicates forming anastomosed lenticular domains of quartz recrystallized grains. Photomicrograph (cross polars) magnified 38 times. Grid reference NC 47706010.

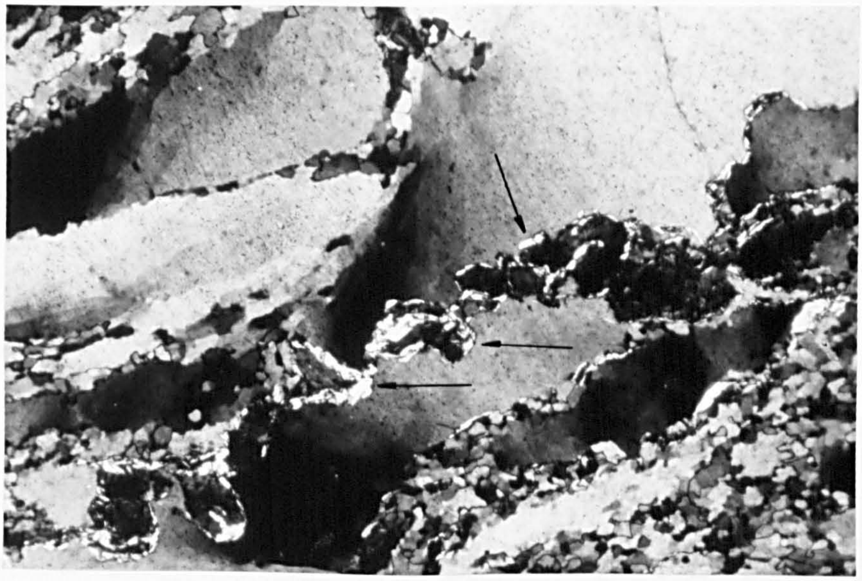

Plate 5.24. Phyllosilicates along quartz grain boundaries (arrows) giving stylolitic appearance. Photomicrograph (cross polars) magnified 90 times. Grid reference NC 47825976.

Plate 5.25
Illustrates aggregates (arrows)of plyllosilicates. Photomicrograph (cross polars) magnified 38 times. Grid reference NC 48386058.

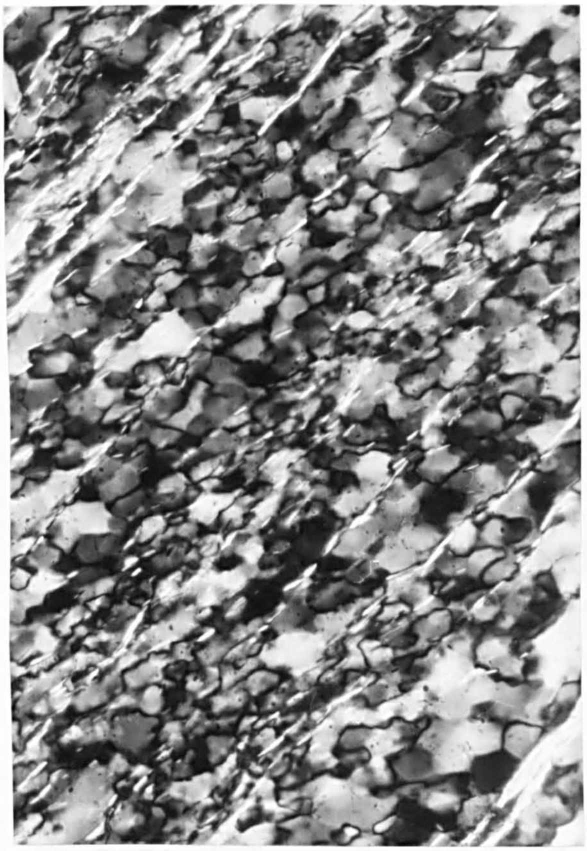

Plate 5.26
Shows the parallel alignment of micas within recrystallized quartz grains. Photomicrograph (cross polars) magnified 363 times. Grid reference NC 45515718.

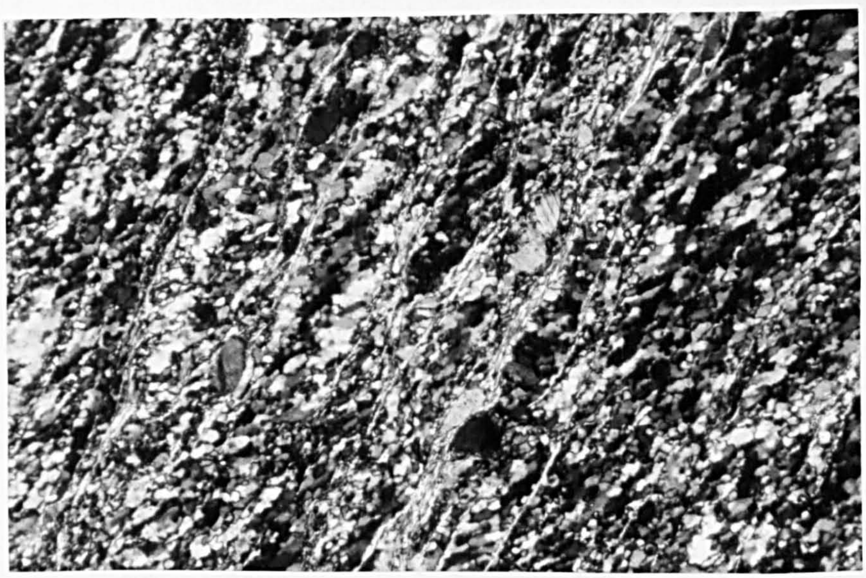

Plate 5.27. Mylonitic foliation given by parallelism of phyllosilicates suffer interference of quartz recrystallization obliquely to the dominant foliation direction. Photomicrograph (cross polars) magnified 90 times. Grid reference NC 47760047.

Wilson (1973) noticed that micas can interfere by inhibiting clast deformation. He pointed out that grains retained their detrital shape and there was little evidence of new grain development. Bell and Etheridge (1976) studied an area of granulites (0.2% HOH) and amphibolites (1% HOH) and concluded that for the same degree of recrystallization the rocks with granulitic composition contained sub-grains and new grains smaller in diameter than those of the amphibolite side. Etheridge and Wilkie (1979) suggested the importance of phyllosilicates in the recrystallized grain size (hydrolitic control) as the key factor controlling the diameter of the newly formed grains. In a given mylonite zone the presence of a 'hydrous phase' can produce coarser sizes, independently of the position with respect to the thrust (Woodroffe and Davenport Thrusts, Australia, see Etheridge and Wilkie 1979, p.458).

The systematic measurement of recrystallized grain size, described in Chapter 6, reveals that for rocks where deformation was less severe, the specimens with phyllosilicates presented new grains only slightly bigger than those with comparatively the same deformation, but devoid of phyllosilicates. However in the case of the heavier mylonitized specimens, there was apparently no noticeable differences in the recrystallized grain sizes in those sections richer and poorer in phyllosilicates. It was noticed that some comparatively mica-rich specimens exhibited sub-grains and recrystallized grains with polygonal shape (see plate 5.30).

It may be argued that the amount of phyllosilicates present in the rocks of the study area may not be directly comparable to that in the rocks studied by Bell and Etheridge (1976). The observations by Etheridge and Wilkie (1979) can be confirmed in some of the studied specimens but cannot be applied as a general rule for the whole of the Eriboll-Hope area. The preceeding descriptions in this chapter also do not conform with Wilson's (1973) observations.

The present interpretation for the study area is that the effects of hydrolitic weakening may be present but the pattern was not clearly differentiated.

5.3 Discussion

The descriptions of section 5.2 reflects this study's interpretation that Group A1 represents a structural evolution developed during the progressive deformation, while Group B shows comparable rocks in the same regime influenced by an additional phase. Group A2, the cataclastic rocks, may indicate a complete change in the value of the state variables as the rock response to the imposed regime was different.

With the exception of the deformation lamellae the present study made use and illustrated the occurence and modes of most of the microstructural indicators discussed section 5.1. Considerable attention has been given to these deformation lamellae (Christie <u>et al</u> 1954, McLaren <u>et al</u> 1970, Tullis <u>et al</u> 1973, White 1973-a, b and c). Nicolas and Poirier (1976) define them simply as domains within the crystal with different refractive index, but there is some controversy about the nature and origin(s) of these microstructures (White 1976-a, p.72; Bouchez 1977).

The present study reports that these lamellae are not abundant. These observations cannot be generalized for the whole of the Eriboll area as Allison (1974, p.74) has reported their occurence in the imbricate zone of Ben Heilam. More recently Nadir (1980) has photographed well defined deformation lamellae but referred to them as rare. Therefore it is suggested that the occurance of these microstructures may be more restricted to the nappes beneath (lower nappes) the ones mapped by this study. The presence or absence of these microstructures could characterize a certain deformation level or regime. If it is true that deformation lamellae decrease in frequency with strain (Bouchez, 1977),the upper nappes of Eriboll experienced a greater amount of deformation than the lower imbricated zones.

In the present section it is necessary to comment on some aspects characteristic of the stúdied rocks irrespective of their morphologic classification. The first aspect is related to the contrast of the boundaries between clasts and the newly formed particles. To the limit of the resolution of the optical microscope, the new grains appear to have sharp boundaries (see plate 5.28), and exhibit a misorientation relative to the host grains. It is possible to correlate the recrystallized grains to their hosts, in the following modes:-

(i) As small, individuals along boundaries of the hosts as shown in plates 5.9 and 5.29.

(ii) As 'isolated' grains within the domain of the host (see plate 5.30.

(iii) As an aggregate of small new grains occuring in a localized domain of the host grain or in that portion of the host particle exhibiting concentrated misorientation (White 1976-a).

(iv) Forming 'trails' of new grains, transecting the host (plate 5.31). The progress of this process can lead to the complete sectioning, or partitioning of the old grain (cf Chapter 4, plate 4.1),thus forming several smaller 'host' grains.

The mode firstly described may occur in all stages of the deformation process, in which there are still remanent clasts. The second mode may also appear in more than one particular stage of the deformation process. It is useful to comment on the possible causes of

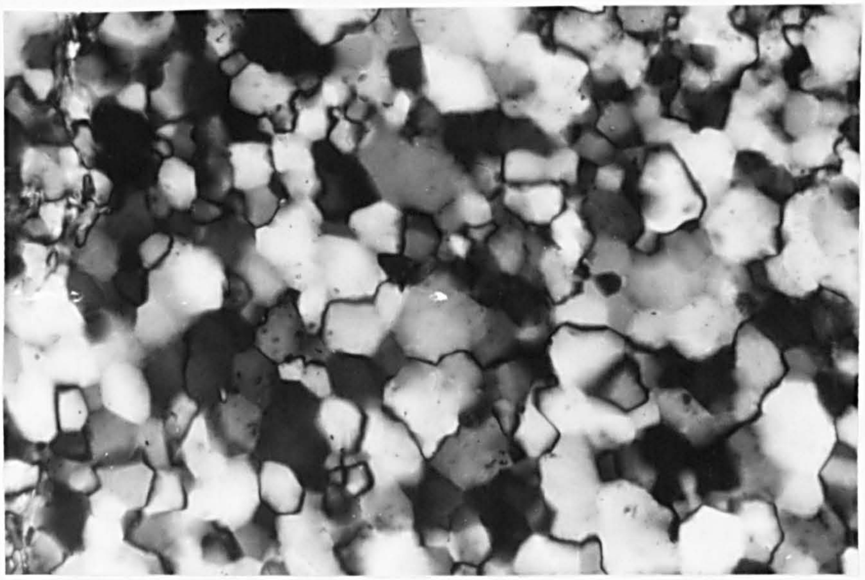

Plate 5.28. Polygonal recrytallized grains. Modal class of grain size is around 33 μm. Photomicrograph (cross polars) magnified 363 times. Grid reference NC 46255884.

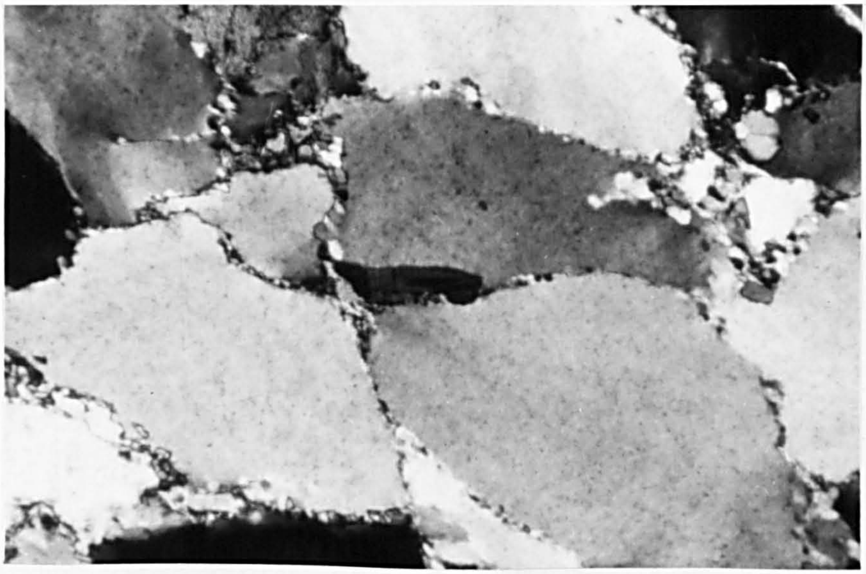

Plate 5.29. Clasts exhibiting only a limited amount of recrystallized grains along the boundaries. Photomicrograph (cross polars) magnified 90 times. NC 45145752.

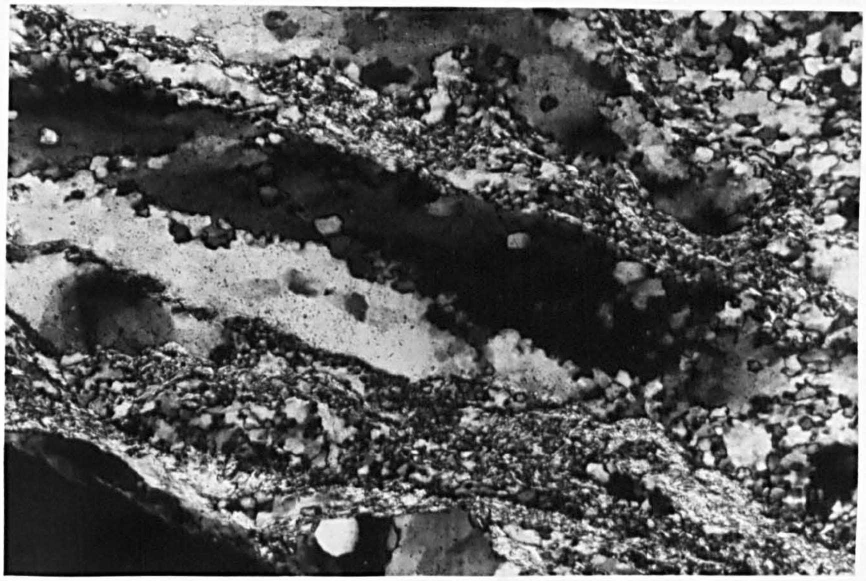

Plate 5.30. Illustrates the formation of isolated new grains within the clasts. Notice the presence of phyllosilicates along the boundaries. Photomicrograph (cross polars) magnified 90 times. Grid reference NC 47706010.

Plate 5.31. Shows the partitioning of clasts with recrystallization along the parting surfaces. See text for explanation. Photomicrograph (cross polars) magnified 38 times. Grid reference NC 47825976.

the different modes of occurence of recrystallized grains. Consider, for instance, the case of a grain under effects of increasing deformation being distorted by heterogeneous strain so that the crystal becomes subdivided into sectors of different lattice orientations. Much of White's (1977) fig. 3 was used here as an analogue of such a hypothetical grain (see fig. 5.1). As recrystallization is an effective way of lowering the stored strain energy (Nicolas and Poirier 1976) this could take place selectively. It could be that there are domains more favourably oriented for recrystallization processes than other parts of the clast. The net result could be the situation described for mode number 3. The fourth mode was already explained in Chapter 4.

Another important aspect of recrystallization deals with its mechanisms rather than mode of occurence. Dynamic recrystallization is a recovery process which should occur in the grain when it is not possible to deal with the increase in strain energy (White 1973-a, 1976-a). The result is that new grains form along deformation bands by establishing high angle boundaries (cf White 1977, p.152). Kohlstedt et al (1979, figs. 2 and 3) illustrate the mechanism of 'bulging' (see plate 5.13) as strain induced grain boundary migration. The progressive subgrain rotation (see White 1973-b, Nicolas and Poirier 1976) is a way of absorbing the free dislocations thus causing reduction in the dislocation density. In the case of subgrain rotation the misorientation of subgrains increases (with strain) and when it exceeds 10-15^{o} (see Tullis 1979) this implies that high angle boundaries have been established;thus a new grain is formed. White (1976-a, quoting Hull 1965, p.182) gives an interesting explanation for sub-grain rotation during a dynamic recovery process which is based in the increase of the angle of misorientation (θ):

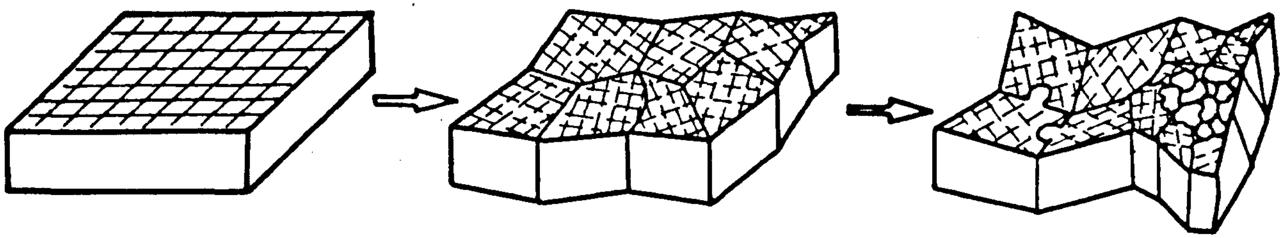

Figure 5.1. Schematic evolution of a grain in which there are distortions at different locations (by effects of progressive deformation) so the crystal becomes subdivided into sectors of lattice orientations. Recrystallization could take place selectively, thus firstly along those sectors more favourable oriented. For that reason, it is possible to observe new grains occurring in localized sectors within a host grain. Diagram based on White's (1977) Figure 3.

$$2 \sin \frac{\theta}{2} = \frac{b}{h} \qquad [5\text{-}1]$$

where b = Burger's vectors and h = spacing between dislocations. Thus the misorientation increases as the dislocation density in the wall, increases. Mercier et al (1977) and more recently Poirier et al. (1979) presented a critical discussion on modes of nucleation.

In the present study the recrystallized grains show (ie at the resolution of the optical microscope) sharp boundaries but their morphological aspect can be grouped into:

(i) Grains with apparent equidimensional sections (plates 5.28 , 5.26).

(ii) Elongated grains (plates 5.32 and, 5.33-b). Under conditions of annealing (static recrystallization) new grains should be strain free and with polygonal boundaries, while dynamic processes may produce elongated particles containing sub-grains and undulatory extinction. Nicolas and Poirier (1976) pointed out that it is difficult to distinguish between recrystallization due to a syntectonic process and that which originated by a post deformation (annealing) condition.

It is also important to comment on the characteristics of those zones exhibiting grains with uniform diameters (ie bands of recrystallization). Such zones are common in most of the studied sections where clasts are still the dominant phase. In the low to moderately deformed specimens they appear as discrete parallel sided bands of recrystallized new grains, bound by relatively straight edges. Their frequency and width increase with the degree of deformation to an extent that they include practically the whole of the area of the

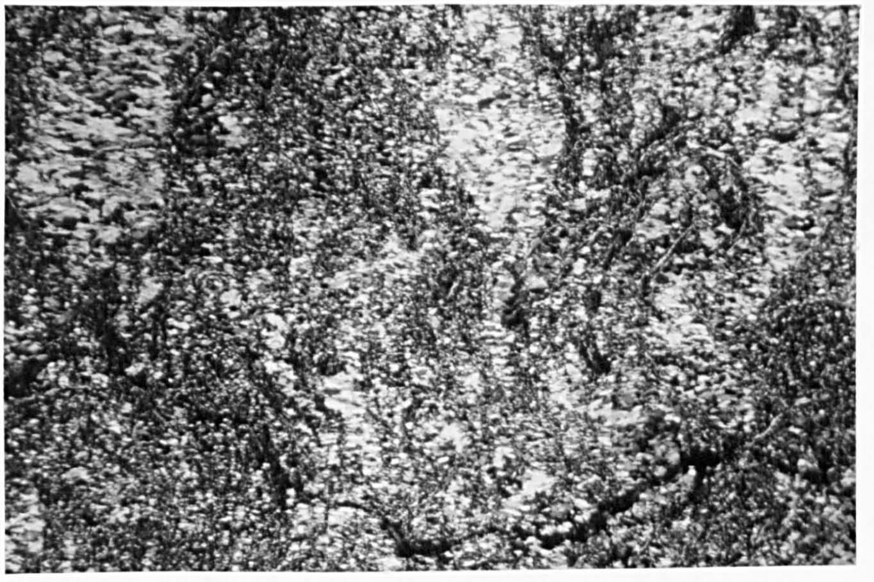

Plate 5.32. Phyllosilicates being microfolded. Quartz grains adjust their shape by coarsening and elongation parallel to the axial plane direction. Photomicrograph (cross polars) magnified 90 times. Grid reference NC 47625979.

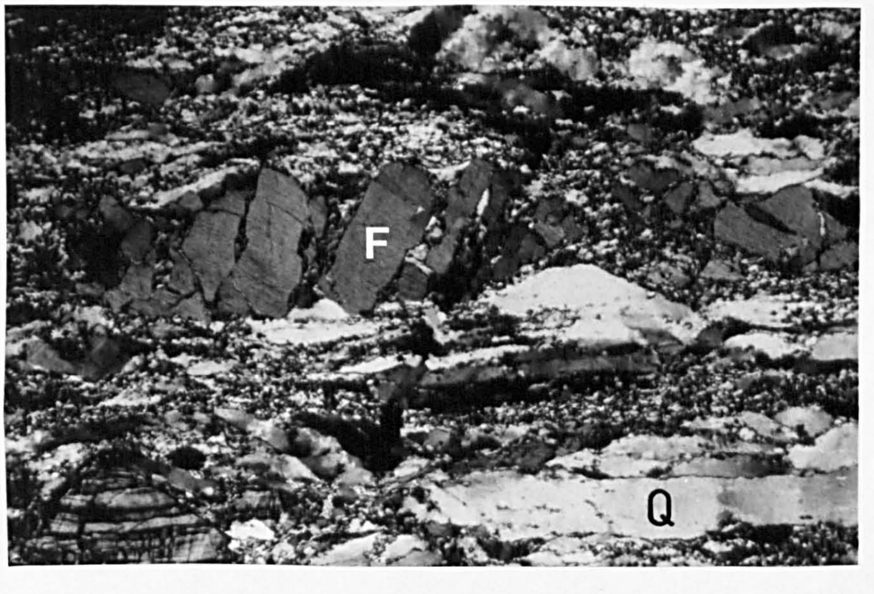

Plate 5.35. Feldspar (F) grains flows by fragmentation and rotation of the angulose particles. In contrast notice the ductile deformed quartz grain (Q). Photomicrograph (cross polars) magnified 38 times. Grid reference NC 45855731.

thin section. The recrystallized grains exhibit those two morphologic types - polygonal and elongated grains - which might indicate possibly different regimes.

These bands of recrystallization are here correlated to shear zones or zones of strain localization (see Poirier et al (1979) as they seem to indicate that once the deformation regime is installed in this domain, it is preferable to continue to deform this already deformed zone (weakness?) rather than to initiate the process of deformation elsewhere (Poirier et al. 1979). Plate 5.34 illustrates one such zone of strain localization (although not essentially a recrystallized zone). It can be inferred that zones such as these can also occur both on meso and macroscopic scales (cf Turner and Weiss 1963), which might mean that such deformation processes are quite independent of the scale and density of the rocks, but solely dependent on the mechanical conditions of the deforming domain.

Despite the great amount of recent research, the genesis of these zones is not fully understood. Analogy with laboratory experiments suggests that such zones cause a stress reduction (White et al. 1980). This fact can be illustrated with the diagrams of figs. 7-3 by following a contour of strain-rate as grain size is progressively reduced. However the gradient of reduction can be very small, under the dominant conditions of dislocation creep. The gradient may change more rapidly if the mechanism of deformation changes to diffusional creep (see discussion in Chapter 7, and maps of figs. 7-3).

Shear zones are often planar domains that allow strain to be accommodated by ductile processes, which limit their width so as to balance stress build up and the capacity of accommodating that energy. It is interesting to notice that various thin sections exhibited bands of recrystallization in which there were

Plate 5.34. Non-homogeneous deformation shown by a narrow zone of differential stretching developed in a domain of localized strain. There is the development of a new penetrative fabric (top left-bottom right) obliquely to the trace boundaries of the clasts. Photomicrograph (cross polars) magnified 38 times. Grid reference NC 45385716.

clearly differentiated two zones of quite distinct grain sizes (see plates 5.33-a and b). The pattern is always the same; the edge of the recrystallization zone forms a narrow rim of smaller grains while the centre shows a larger grain diameter (cf zones B and C in plates 5.33).

A possible explanation for the formation of this bimodal grain size is that as the boundary of this band of recrystallization migrates, by clast-recrystallization, it could be necessary to re-distribute the grain boundary surface area, by a grain growth, hence the very uniform size for the whole of this inner zone (see plate 5.33-a). This could mean that there is an energy gradient (stress build up?) not only between the margin of the band of recrystallization and the outer clasts (regions A and B in plates 5.33) but also between this edge and the inner part of the band of recrystallization (regions B and C in plates 5.33). There should be some energy concentration along the margin (A-B in plates 5.33) in order to produce the widening of this zone.

It is also important to comment on the behaviour of the heavily twinned feldspar grains, which comprise the secondary phase (up to 10%) in many of the studied sections.

Firstly it is quite clear that no matter what the strain intensity is, the feldspars deform characteristically by brittle rupture and rotation, rather than by ductile elongation typical of the quartz grains. Plates 5.35 , 5.36 , and 5.17 , show this mineral in different textural types. For example in the low-moderate level of deformation of plate 5.35 , the feldspar grains are broken apart, and the rotated fragments retain the angular shape, in contrast to the quartz grains which show signs of stretching. In the

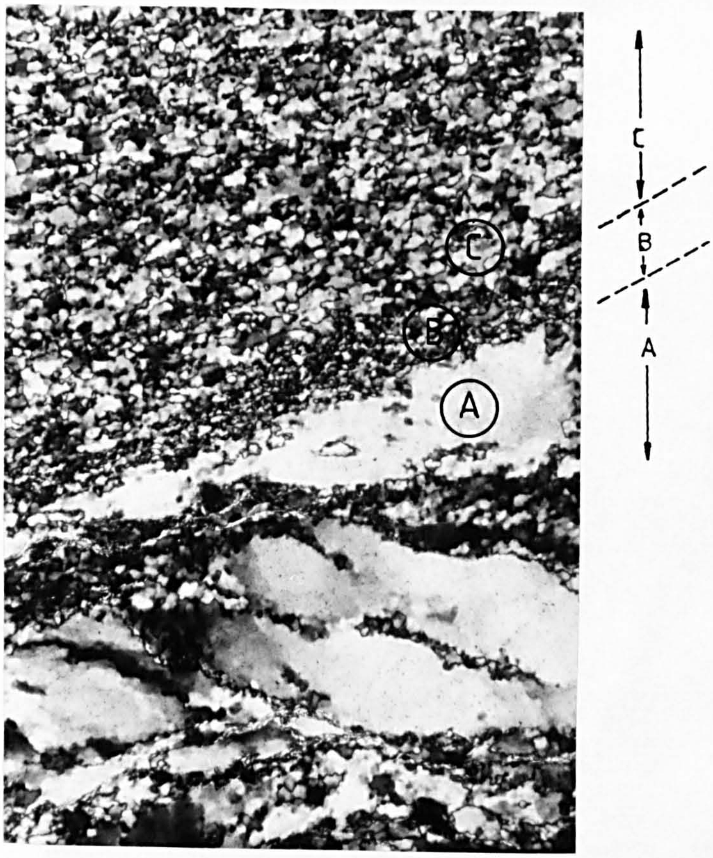

Plate 5.33-a
Illustrates the variation in the grain sizes, across a band of recrystallization (ie zones B and C). Photomicrograph (cross polars) magnified 38 times.
Grid reference
NC 45855731.

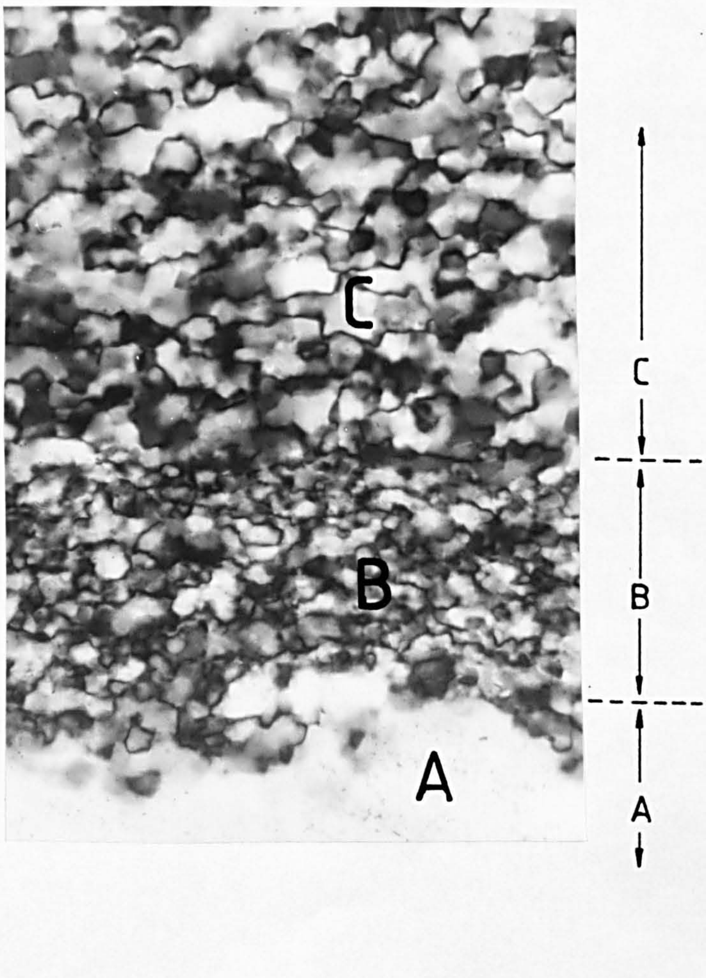

Plate 5.33-b
Detail of the above plate 5.33-a. It illustrates the grain diameters of the 3 zones, according to the relationship
$A \gg C > B$.
Photomicrograph (cross polars) magnified 363 times.
Grid reference
NC 45855731.

Plate 5.36. Ultramylinitic foliation showing signs of incipient transposition. Feldspar grains retain their angular or polygonal shape. Photomicrograph (cross polars) magnified 38 times. Grid reference NC 48060054.

heavily mylonitized samples some feldspar fragments still have angular shapes (plate 5.36), while in others this mineral exhibits rounded shapes, which may indicate that grinding effects by rolling action may have taken place (see plates 5.19 and 5.21).

Etheridge and Wilkie (1979) have reported that the recrystallized grain sizes for feldspar grains in shear zones is 1/3 to 1/5 times that of the neighbouring quartz grains. No attempt was made in this study in establishing systematically any such comparisons because of the obvious problems of optical resolution of the minute size of those particles.

The present study also confirms Kohlstedt et al's (1979) observations that feldspar grains interact differently with quartz than do quartz with quartz grains. Quartz-feldspar contacts invariably do not show the characteristic serrated boundaries but instead a sharp line defines the two mineralogic domains.

It was noticed that feldspars appear more abundant in the less deformed specimens while, contrarily, phyllosilicates seem more predominant in the domain of the increasingly recrystallized rocks. There are however some points to be considered:

(i) There was not a systematic evaluation that could confirm these observations in a more quantitative way.

(ii) The proportions of both feldspar and phyllosilicates is in a sense restricted (less than 10% either) and this not only poses some problems of accurate measurements but also shows the necessity of a rigorous percentage evaluation of these minerals.

(iii) If feldspar recrystallized in sizes, 1/3 to 1/5 of neighbouring quartz grains (Etheridge and Wilkie, 1979), it would be very difficult to estimate the percentage of feldspars in a recrystallized sample, by optical means, because the range of recrystallized size for quartz grains (Chapter 7) is between 10 and 30 μm.

The textures described in groups A1 and A2 might indicate that the mylonitic zones of Eriboll and Hope areas were formed during a QP-type regime (cf Sibson 1977) with some evidence that an EF-regime (Sibson 1977) might have operated later, at least in the Loch Hope domain.

Microstructures in the studied quartzites of Eriboll and Hope areas cannot give any clue on the relative ages between the mylonitic zones of these areas. However the microstructural pattern for Eriboll seems to be more homogeneous than that for the Loch Hope domain. The microscopic study confirms field evidence that the strain gradient is relatively simple for the Eriboll area. The microtextural pattern changes gradually with the proximity of a single mylonitic zone, whereas the Hope area shows a more varied pattern of different strain intensities and textures which confirms the field evidence that in such domains there developed more than one such mylonite zone.

5.4 Correlation Between the Dynamic Recrystallization Phase, and Relative Amount of Progressive Deformation

5.4.1 Preliminary Considerations and Methods

So far this study has shown that the pattern of progressive deformation is also reflected in the microstructures, either (i) by analysis of the shape factor measurements of clastic grains, or (ii) by the description of textural modifications that are associated with different amounts of clast elongation and proportions of newly recrystallized grains. This section aims to correlate quantitatively these two indicators of progressive deformation. The calculation of the three dimensional shape of particles has been explained in detail in Chapter 4. The present section deals with the estimation of the relative percentage of the recrystallized phase present in the samples analysed for shape factor.

The assessment of the volume phase in a sample is not new in geology and the basic mathematical framework seems to have been set up more than a century ago by Delesse (1848). Subsequent research was carried out by Rosiwal (1898, in Underwood 1970, Pickering 1976), Shand (1916) and many others since then. There are other approaches which originated in other branches of science that also deal with three dimensional solids (eg serial sectioning in medical and biological sciences), estimations.

In the present case it is necessary to evaluate the volume of a phase using information from a thin section. Therefore there is the implicit condition of a correlation between two-dimensional data and spatial distributions. The basic principle states that the volume fraction of a phase is equal to the area fraction. This is the Delesse's principle (see Underwood 1970, p.25 for full description). Rosiwal (1898) extended the principle to include the equivalence between volume and linear fractions. Today it is commonly accepted to obtain the proportion of a volume phase by a convenient technique of point counting (Underwood 1970, p.15) which extends the above principle to include an equivalent fraction of randomly distributed points.

Comparatively, point counting is to be preferred because it requires the least amount of effort and provides good precision. Pickering (1976, p.14) illustrates the efficiency of the method by comparing the following relative errors: Areal analysis = 12.5% relative error

Linear analysis = 12.5% relative error

Point counting:

- systematic = 10.5% relative error

- random = 16.6% relative error

Systematic point counting seems to have a good acceptance both in petrography (Chayes, 1956) and metallurgy. The usual procedure is to superimpose a counting grid over the image (projection or photo) of the elements to be measured and to estimate the proportion of a phase by simply counting the number of points laid on the elements of the phase evaluation. The estimated is given by working out the sum of those points out of the total number in the grid (see figs. 5-2-a). The grid spacing should be greater than the maximum intercept length of the phase being measured. Ideally this should mean that no element of the phase should be big enough to include two such counting points and it is also implicit in the above principle and figure, that the position and orientation of the counting net, relative to the sampled population is invariant, simply because the spatial distribution of the elements of the phase is a random one.

The pattern of the last paragraph changes completely if the elements of the sample have a partially oriented structure. In analogy to the explanation given for fig. 6-2c, the length of the traverse in a lineal analysis (section 6.4.2) or the spacing of points in point analysis, will depend on the direction in which the test is being taken, relative to the orientation of the structure. This means that the results will vary when for instance an analysis in a section parallel to the sample's preferred orientation is compared to an analysis performed obliquely or perpendicularly to the oriented structure. The situation becomes even more complex if the structure exhibits (apart from preferred orientation) segregated or lamelae domains because the position of the counting grid also will determine the probability of phase elements being sampled (the diagram in fig. 5-3 clearly illustrates

Figures 5.2

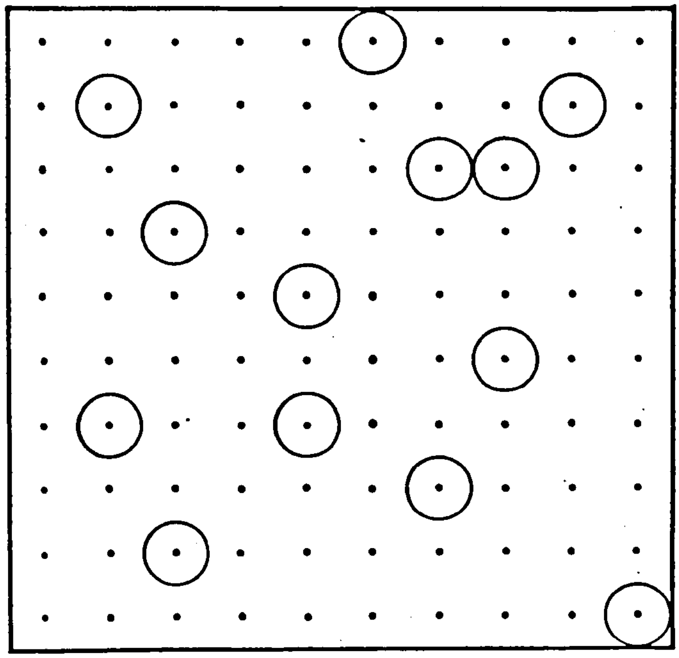

$$\frac{\sum \text{elements}}{100 \text{ points}} = \% \text{ phase}$$

•a

Point counting grid for a phase with the characteristics of random distribution of its elements.

•b

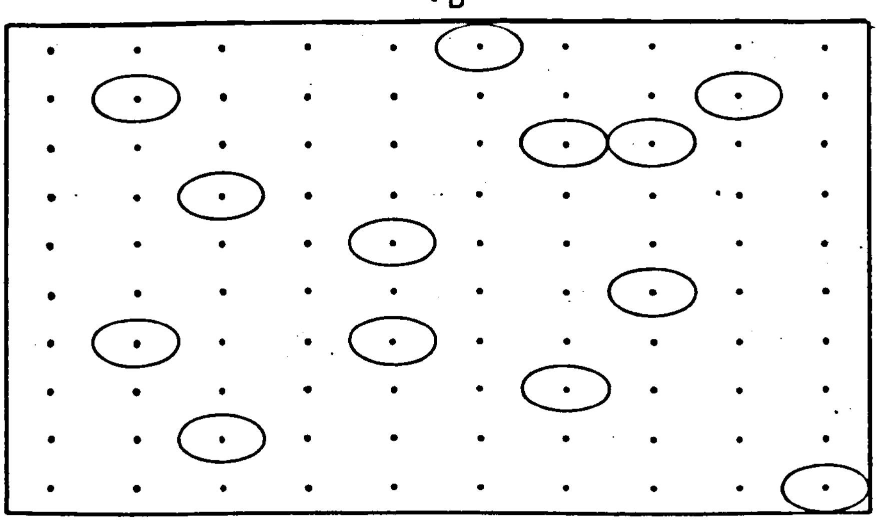

Point counting grid adapted to conditions of phase anisotropy (ie orientation and shape) present in that section.

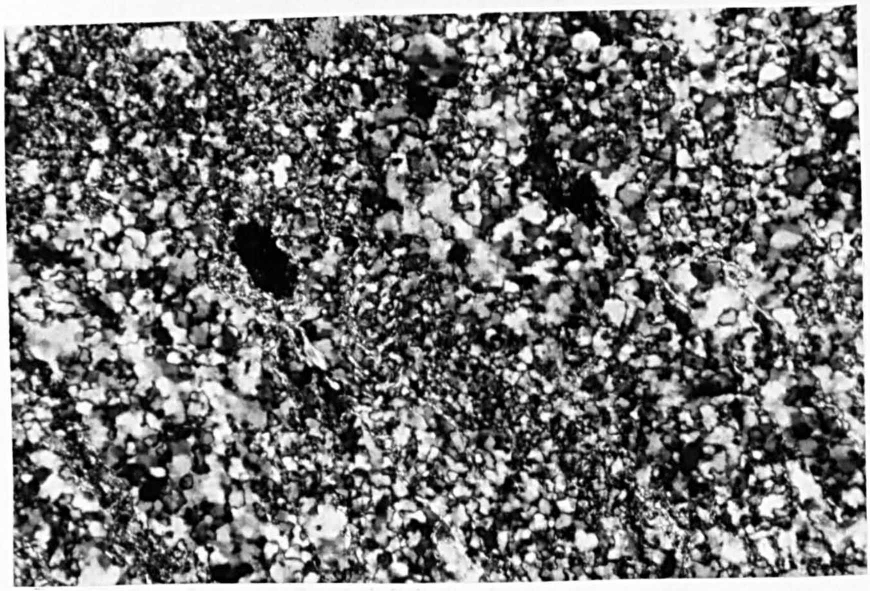

Plate 5.37. It shows the apparent 'equilibrium' of two distinct sizes of quartz grains. Grid reference NC 45605740. Photomicrograph (cross polars) magnified 90 times.

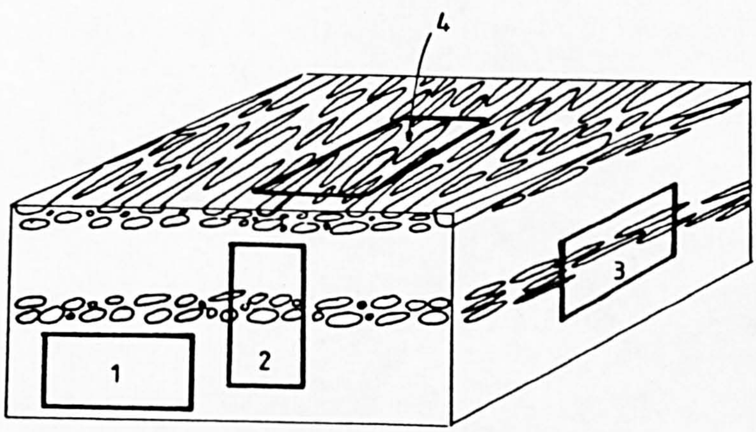

Figure 5.3. Block diagram illustrating rock with banded domains. The estimated phase measurements will depend very much on the position of the counting sections. It is clear that neither section 1 nor section 4 produces representative estimates of the phase proportions. Sections 2 and 3 should give a more reasonable result note that shape of particle relative to the orientation of the counting section (grid) should very much influence the final results.

this point).

Microstructural anisotropy given by elements with preferential parallelism of certain dimensions and forming stratified domains is a common feature in geology. Therefore these conditions invalidate completely the use of the grid shown by fig. 5-2-a (see explanation in fig. 5-3). Unfortunately there is not a simple and definitive method that would overcome these problems brought about by the presence of preferred orientation and/or segregation bands. It is not surprising to note that most of the texts, dealing with techniques of phase estimation, avoid the present problems, precisely because each case must be analysed separately.

There are many errors involved in this kind of phase estimation (ie 2D measurements to infer a 3D phase) and these in general arise from different sources such as: sampling, sectioning, equipment resolution and many others, depending on the particular case. It is however very difficult to try to evaluate how these quantities, if properly assessed, will interact (ie summing up, or can some of them anhilate each other) and affect the final result.

No mathematical expression for error evaluation will be produced here, simply because the technique used in the present study does not follow any of the usual methods and instead it comes from an intuitive variation of the ideas put forward by Chayes (1956), Hutchinson (1974) and Pickering (1976, p.14). To compensate this lack of an expression for error estimation, two different sections (here orthogonally oriented) were analysed for each sample and the differences in results used in order to check the internal consistency level.

The problem of choosing section planes has been discussed by Chayes (1956) and Hutchinson (1974). The latter also deals with the 'anisotrophy problem' without providing any specific mathematical formulation. Hutchinson (1974, p.49) advises the selection of thin sections made perpendicular to banding and/or the preferred oriented structure and also the avoidance of sections which are close to the foliation plane. Chayes (1956) dealt with this problem of anisotropy and considered that banding could be an advantage rather than a handicap. He pointed out that the best section for measurement could be a plane normal to banding, in order to obtain maximum information (ie measurements) in that area. Chayes (1956) is of the opinion that in case of anisotropy the technique of measurement should include a rectangular-measuring grid, rather than a square one.

Thus the simple technique used here included preliminarly, an inspection of the three orthogonal sections of each rock specimen, to eliminate the one close to bedding or foliation. A counting grid was then made compatible with the anisotropy present in each section. The results of the grain shape analysis (Chapter 4) were used here in order to construct for each section, its measuring grid. The followed method consists simply:

(i) The point spacing followed the anisotropy or the shape ratio (the Rf, cf Siddans, 1971) present in each section. For the present case use was made of the results of the SI-method (cf Chapter 4). This gives a rectangular grid, with 100 points, as shown by fig. 5-2-b.

(ii) The orientation of the longest dimension of each rectangular counting grid was parallel to the preferred grain direction (ie the ϕ-angle, cf Siddans 1971) determined for each section (Chapter 4), as illustrated in fig. 5-2-a.

(iii) Counting was performed in at least 10 different and parallel positions throughout the section. Therefore the total number of points per section came at least to 1000.

Figures 5-2-a and b illustrate the general idea behind this simple method. Notice that ideally,the grid should be made in such a proportion that no two (or more) counting points should pertain to the same grain.

5.4.2 Results

The estimated volumes of the recrystallized grains present in the rocks used for grain shape analysis of Chapter 4, are plotted as abscissa values in fig. 5-4. The results of the calculated Nadai's ε_s parameter (table 4.2) were plotted as ordinate values of fig. 5-4, in order to correlate the volume of recrystallized new grains with the intensity of the 3D strain present in each sample. These results require the following comments:

(i) With the exception of three specimens all the measurements were made in two perpendicular thin sections. The results from those samples that could provide two orthogonal thin sections, rarely showed differences greater than 10%. This indicates the validity of the 'made-to-measure' rectangular counting grid.

(ii) The calculated percentages of recrystallized grains are interpreted here as underestimated values, because as it is explained in section 6.4.2, the diameter of the particle will determine the probability of a grain being sampled. Therefore the smaller fraction in those cases are always underestimated.

(iii) The counting operation was performed on an apparatus which projects the thin section image onto a translucent screen (Leeds Baty-Shadowmaster Junior 500 Projector). The net result is a poor resolution image which causes some details of the boundaries between grains to be missed. This introduces a false continuity

Figure 5.4. See Text for full explanation.

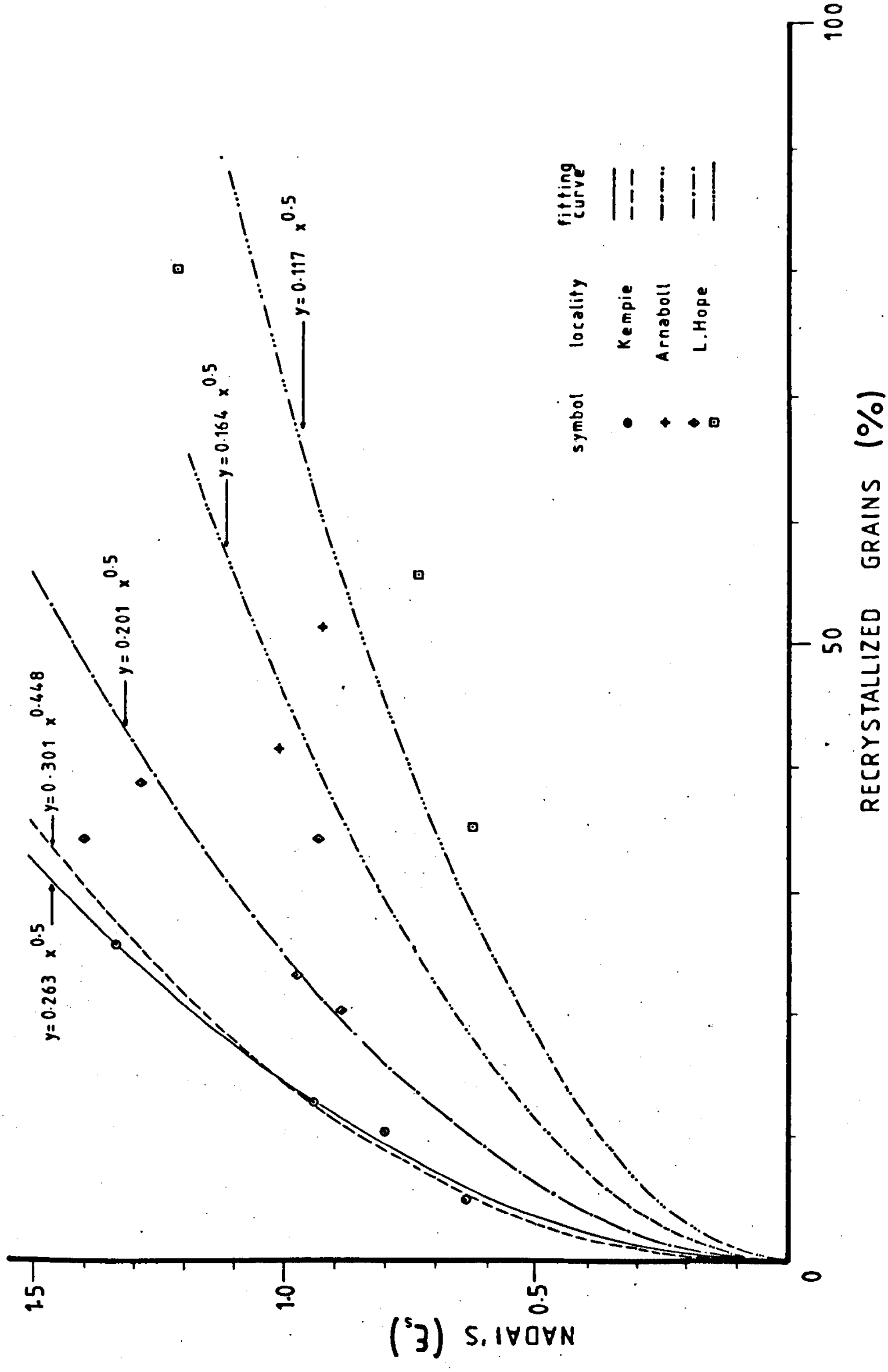

of non-existent domains and is also another contribution to the underestimation of the finer phase.

For the above reasons the obtained results are to be considered as the minimum estimates of the percentage of recrystallized new grains present in each sample. The correlated values in fig. 5-4 were plotted with different symbols, according to geographic domains. The samples from Kempiė constitute a more reliable and homogeneous domain. These rocks were collected from an almost continuous outcrop, at distances of approximately 80, 60 45 and 5 m below the b-thrust surface (cf Chapter 2, or fig 4-1). The specimens from the Hope area exhibit a greater scatter in the graph, and these rocks were sampled from different outcrops scattered over a wide area.

It is interesting to note that the results for the Kempie area indicate that the correlation between (i) volume of recrystallized grains, and (ii) the relative strain intensity, gives a plot obeying to a certain extent , a power-law of the form $y = ax^{\frac{1}{2}}$. The value of a for Kempie is approximately equal to 0.263 while for the Hope area it is 0.201. For Kempie results, an attempt was made to fit (by least squares) a curve of the form $y = ax^{p}$, for (p) to assume any real value (see dashed line in fig. 5-4). The obtained results are: $a \simeq 0.301$ and $p \simeq 0.448$, which are not too different from the previously imposed parabolic fitting.

It could be very significant that a more homogeneous domain such as Kempiė should produce a plot that almost fits perfectly on a parabolic curve. The existence of different fitted curves for each area should be expected because this reflects that there are many factors and conditions affecting the mapped domains of Kempie and Hope areas. The interaction between internal and external agents (eg P, T, HOH, Phases etc) affecting these rocks might have influenced the production of recrystallized new grains (eg inhibiting or accelerating) and also interfering in the capabilities of the rocks in accommodating strain by grain elongation.

Weathers et al (1979-a) also observed a change in the proportion of the recrystallized grains with distance from Moine Thrust Plane. They reported that at 100 m from the Thrust plane, at Glencoul, 5% of the quartzite is recrystallized while at 0.01 m (of the thrust) that proportion increased up to 100%. Figure 5-5 correlates some data of percentages of recrystallized grains, for Eriboll and Glencoul areas, with the appropriate distance from the a thrust plane. The traced lines are an attempt to show that the increase in the recrystallization with the proximity of a fault has a relatively constant gradient up to nearly 10 m of the fault. This gradient seems to change abruptly in these last 5-10 m from the fault, becoming less inclined, but the percentage of recrystallization very rapidly reaches the level of 100%.

It has been reported previously (Chapter 4, also in section 5.2.2.2) that there are some stages of the evolution of the microstructure in which the grains develop rims or mantles of newly recrystallized grains as the core becomes progressively elongated. White (1976-a) points out that the mantle protects the core (buffer?), but the observed textures of this study indicate that the process of mantle formation continues, and there seems to be competition between what it is interpreted here as two different processes: (i) the first which 'consumes' the existing clast by sequentially reducing its volume through a dynamic recrystallization process and (ii) the second which accommodates strain by grain elongation, presumably by intracrystalline deformation of the individual grains. This will cause some grain boundary sliding in the mantle and the result is called the 'ribbon-like' structure.

This study has also shown that there are occasions where the internal deformation of the clasts does not fully develop and instead the dynamic recrystallization of grains is the dominant process (compare plates 5-8, 5-10, 5-14 and 5-22).

Excluding all the mentioned external influences on the recrystallization processes (eg second phase impurities, etc ...) we could correlate the stored strain energy with the available surface area of grain during deformation. During recrystallization, a new surface of the 'core' is generated during the regression and grain refinement process, according to the density dislocation levels (White 1976-a). The remaining surface area of the clast is continuously reduced due to volume loss of each clast. However if the strain energy does not decrease during that process, or in other words, if the necessary surface area required by the deformation process remains constant, the rate of core reduction will be continuously increased.

Perhaps the explanation given by the preceeding paragraph plays a part in the deformation process. It could justify the continuous and sharp increase in the percentage of the recrystallized grains that can be observed (especially in the limits of 0-10 m) in fig. 5-5.

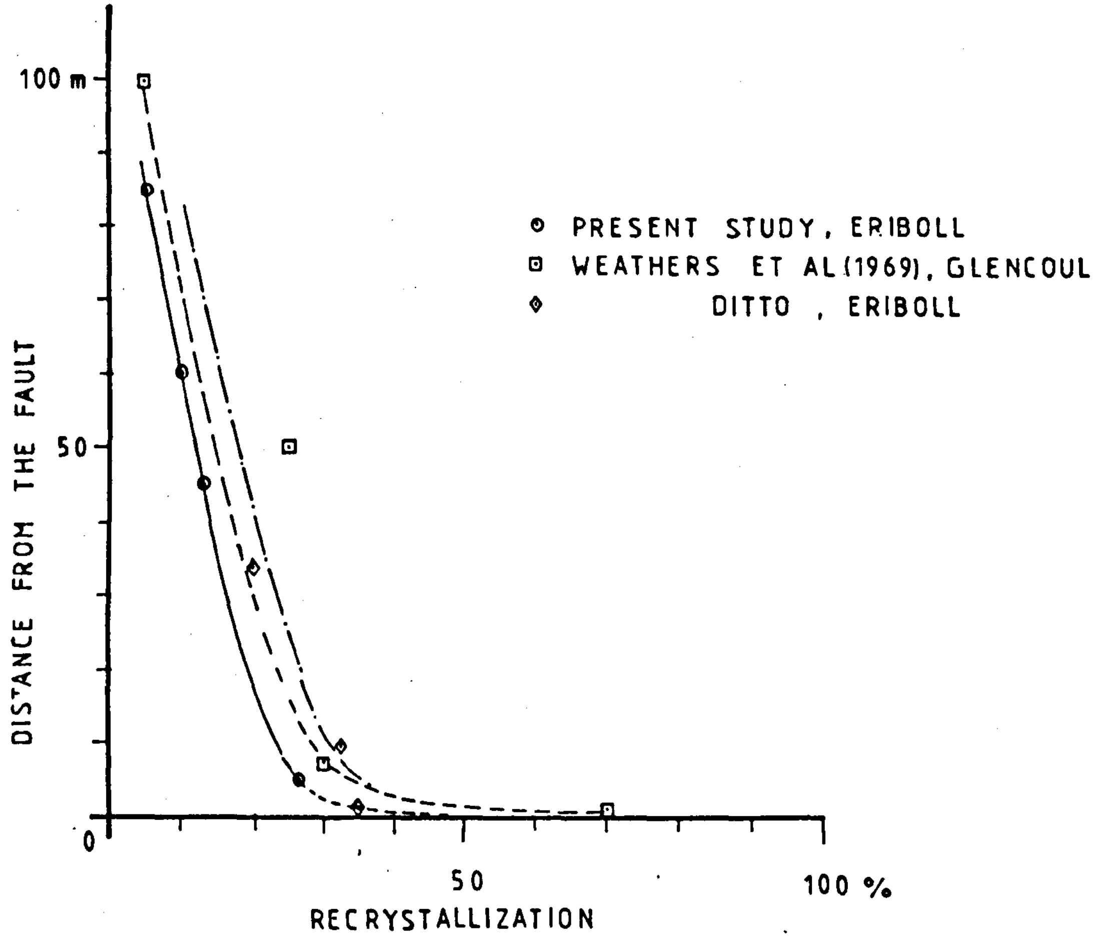

Figure 5.5. See text for full details.

CHAPTER 6

PALEOPIEZOMETRY

6.1 General

This chapter concerns the applications of Paleostress Estimates in the context of the geology and structural evolution of the northern part of the mapped area.

- Section 6.2 introduces the parameters and equations currently used in the determination of differential stresses.
- Section 6.3 describes briefly the current problems in applying the concepts and equations described in section 6-2. It also reviews briefly the recent literature of paleostress estimates.
- Section 6.4 is entirely concerned with geometrical problems and methodology of grain size estimation.
- Section 6.5 comprises the discussion of the results obtained in this study and the comparison with other studies in the mapped area. It also illustrates some of the problems introduced in section 6.3. Finally there is a brief discussion of the present results in the context of the geology and structure of the studied area.

6.2 Introduction

In the recent years there has been some attention to the study of microstructures in order to assess the magnitude of the differential stress operating during deformation. This chapter attempts to use quartz microstructural features in order to estimate paleostresses in the zone of mylonitization of the Moine Thrust Zone of the Eriboll and Hope areas. (fig. 4-1, see details of the 3 areas in figs. 6-4-a to c).

Both experimental and theoretical studies (eg Raleigh and Kirby 1970; Post 1973; Goetze, 1975; Kohlstedt _et al_ 1976; Mercier _et al_, 1977; Twiss 1977) show the validity of using steady state microstructure such as dislocation densities, subgrain size and recrystallized grain size to estimate the paleostress. The basic assumption is that these microstructures are generated during deformation and are thought to be solely dependent on the level of the differential stress.

Estimates of stress based on measurements of dislocation densities and subgrain sizes are calibrated by laboratory experiments (Mercier et al. 1977), but the measurements require the use of the Transmission Electron Microscope (TEM). This restricts the use of these two microstructures and makes the estimations more expensive when compared to the estimates made using the syntectonic recrystallized grain size, which are easily made using the ordinary petrographic microscope. In fact the measurements of the recrystallized grain size can even prescind from photomicrographs.

The relationships between the differential stress (σ_1-σ_3) and the three microstructural parameters listed above are considered separatedly in more detail below:

1) Dislocation density (DD) - Is correlated to the differential stress (Kohlstedt et al 1974; Takeuchi and Argon, 1976 in Weathers et al 1979-a, White 1979-a, b) by

$$\sigma_1-\sigma_3 = k\mu b\rho^{\frac{1}{2}} \qquad [6\text{-}1]$$

where k is constant, μ is the shear modulus compensated for temperature and pressure, b is the Burgers vector and ρ is the Dislocation Density.

2) Subgrain size (SS) - The adopted relationship is given by Raleigh and Kirby (1970, in Weathers et al 1979-a, White 1979-a, b).

$$\sigma_1 - \sigma_3 = l\mu b/Sg \qquad [6\text{-}2]$$

where l is a constant and Sg is dimensioned to the Burger's vector b. There appears to be some disagreement in the value of (l). Raleigh and Kirby (1970) derived the value of (l) based on optical observations while White (1976-a, b) using a TEM suggests a different value. The discussion of section 6.5.2-a will deal in more detail with the problems in dealing with subgrain size.

3) Recrystallized grain size (RGS) - This is related to stress by a simple relationship of the form (Mercier et al 1977; Twiss 1977):

$$(\sigma_1 - \sigma_3) = mD^{-p} \qquad [6\text{-}3]$$

where (m) and (p) are constants and (D) is the newly recrystallized grain size.

In the preceeding equations, the values of k, l and m can be determined experimentally for each mineral. In the case of quartz, the observations were calibrated at 900°C and a stress of approximately 100 MPa (see White 1979-b).

The present study is concerned with the estimation of the differential stress using the recrystallized grain size (RGS) of quartz grains measured from thin sections using the petrographic microscope.

Relation [6-3] has both experimental (Mercier et al, 1977; Kohlstedt et al, 1976 in Zeuch and Green, 1979) and theoretical (Twiss 1977) justifications. There is however, a range in the values of the parameters m and p for each mineral. This acoounts in part for the possible discrepancies in the stress estimation. Mercier et al. (1977) characterized their study for quartz in a condition termed 'wet' quartzite, ie 'wet' means a hydrolytically weakened state. Twiss (1977) arrived at the same expression by means of a regression analysis (see 1977; fig. I p.212):

$$\sigma/\Gamma = k(D/b)^{-p} \qquad [6\text{-}4]$$

$$\Gamma = \mu/1-\nu \qquad [6\text{-}5]$$

where ν is the Poisson ratio, k is a constant, μ is the shear modulus. Twiss (op. cited) used the best fit of two groups of relevant data and obtained the following values for the above parameters: $p = 0.68 \pm 0.02$, $\log_{10} k = 0.38 \pm 0.01$. Relation [6-4] can easily be applied provided the values of the elastic parameters and the Burger's vector of the analysed material are known. Data for quartz can be taken from Birch (in Clark 1966, table 7-16) as follows: $\mu = 4.2 \times 10^4$ MPa, $\nu = 0.15$, $b = 5 \times 10^{-7}$ mm, therefore $\Gamma \simeq 4.9 \times 10^4$ MPa, so relation [6-4] becomes:

$$\sigma_1-\sigma_3 \equiv \sigma \simeq 2.4 \times 4.94 \times 10^4 \, (D)^{-0.68} \quad \text{or simply}$$

$$\sigma \simeq 6.157 \, (D)^{-0.68} \qquad [6\text{-}6]$$

This relation will be referred to in the present chapter as the Twiss Model or simply as the Twiss equation for quartz-RGS. Mercier et al (1977 p.125) established the relation between the quartz-RGS (mm) and the differential stress (MPa) as:

$$D = 6.5 \, (\sigma)^{-1.4} \qquad [6\text{-}7]$$

which gives in the form of [6-3]; $\sigma = 3.808 \, (D)^{-0.71}$. [6-8]

This relation will thereafter be referred to as the Mercier model or simply as the Mercier equation for quartz-RGS for wet-quartzite.

The present study uses both relations [6-6] and [6-8] for the reasons to be explained in the next section. Figure 6-1 is a graph comparing the magnitudes (MPa) for recrystallized quarts grains (μm)

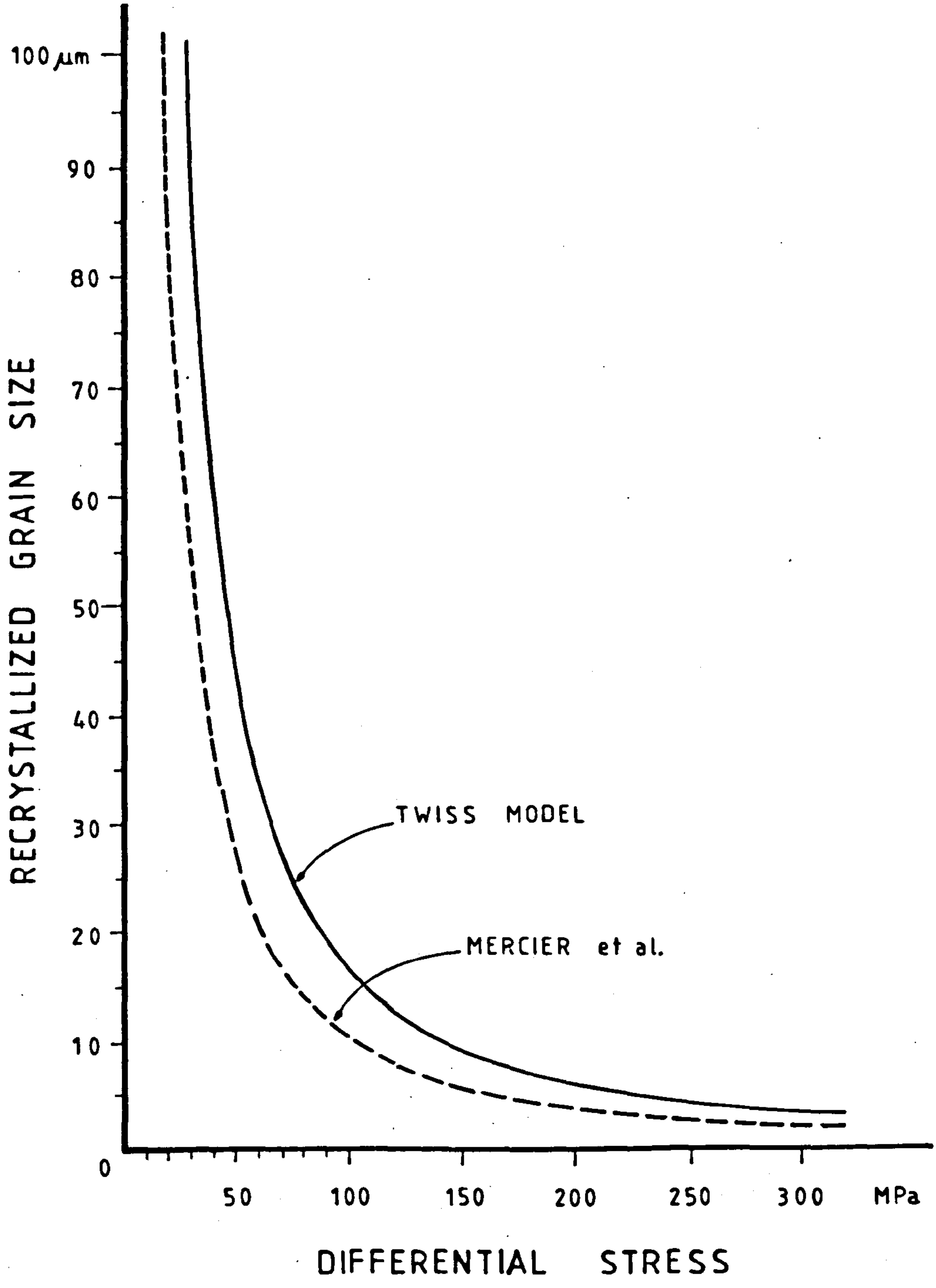

Figure 6.1. Graph relating particle grain size, in the range up to 100 µm, to differential stress in MPa, for models by Twiss (eqn 6-6) and Mercier et al (eqn 6-8). See text for explanation.

using Twiss and Mercier models.

6.3 Problems and Use of Microstructures for Paleopiezometry

The first part of this section described briefly some of the factors affecting the use of microstructures to estimate the paleo-stress. A more detailed and specific treatment of some of these factors is dealt with in the sections dealing with the results and discussion (see also White 1976-a).

The second part of this section is a review of previous work on Paleopiezometry.

6.3.1 Problems and Difficulties in the Paleostress Calculations

There are seven important problems associated with Paleo-stress Estimations; each is discussed briefly below:

1) The described equations [6-1] to [6-3] are only applicable in the constraint of a steady state deformation (cf Stocker and Ashby 1973) during disolcation creep mechanisms (cf White 1979-b, p.222).

2) White (1979-a, p.211) points out that there is no theoretical basis for equation [6-2], nor is there a perfect accordance in the values of the parameters k, l and m, used in equations [6-1], [6-2] and [6-3].

3) A model of the general form of [6-3] is only valid on the condition that the origin of the RGS is due to migration by 'bulging' type of migration boundaries (cf Kohlstedt _et al_ 1979). This arises

simply because this was the only type of mechanism of dynamic recrystallization observed in the experiment by Mercier et al (1977), as pointed out by Tullis (1979) (cf Poirier et al. 1979).

4) Equations [6-1] to [6-3] are clearly temperature independent and perhaps this is an oversimplified assumption. Recently Ross et al (1980) have reported experimental results from a study made for Olivines under both 'wet' and 'dry' conditions. They concluded that with 'wet' olivines the RGS are slightly temperature dependent, while for the 'dry' dunite the size is only stress dependent.

5) Another important aspect not taken into account by equations [6-1] to [6-3] is the influence of impurity phases or elements, which could influence the recrystallized grain and thus the stress estimate. Mercier et al (1977) invoked conditions of 'wet' quartzite for their model, as implying the presence of OH. Ross et al (1980) also referred to 'wet' conditions for deformation of olivines. Other studies considered that the presence of a second mineral phase, such as micas, interfered in the growth of quartz grains (Hobbs et al 1976). Knipe (1980) pointed out that impurity atoms are present in deformed quartzites. He also argued that the segregations present at sub-grain boundaries and dislocations may affect the size and shape of these two microstructures. It is known that in metals, the impurity content affects the subgrain size and the disolcation density (see Knipe 1980, T15). It is possible, therefore, that the shape and size of the RGS may have been influenced by these impurities and other phases present in quartz rocks.

6) Another factor to be taken into account is the behaviour of the three

microstructures, DD, SS and RGS with variations in the stress level. Recently Ross et al (1980) has noted that the subgrain size (SS) decreases with the stress increase, but if a subsequent reduction in the stress occurs, this causes no alteration in the previous subgrain size. It means that the SS records the maximum attained stress level. However we cannot expect a similar behaviour for both the dislocation density (DD) and the recrystallized grain size (RGS) (Tullis, 1979).

7) There are other equally important factors associated with measurements which are here classified as 'stereologic factors'. White (1979-b) points out that SS and RGS determined by the optical microscope are larger than those measured by Electron Microscopy. However, what has been neglected in most of the papers dealing with Paleopiezometry is the specification of the method used for size (SS or RGS) measurements (eg White 1979-a, b, c; Weathers et al 1979-a). With the exception of a few papers, such as Etheridge and Wilkie (1979), most of the papers restrict their discussion of the validity of the stress estimates to the arguments given in the 6 previous paragraphs in this section and they do not care to mention the necessity of having a standard method of size measurement. The implication of this last observation is obvious; if there is not a standard procedure of size evaluation, there is not a common basis for comparison and discussion of the results in the different works. This problem will be illustrated quantitatively in section 6.5.2-b of the present chapter.

The present study goes further and questions the validity of applying models both by Twiss (1977) and Mercier et al (1977) on stereologic grounds only. In other words, if we do not perform the size evaluation in the same way as each of these two studies did, it is even more irrealistic to try to apply these. It is unfortunate that these two papers (Twiss 1977 and Mercier et al 1977) neglected completely this important aspect,which restricts much of the application of their models.

On the other hand we can adopt a more pragmatic attitude and consider for instance that the size, (D) in [6-6] and [6-8],corresponds to a true spatial size of the RGS. In this case it is also the aim of the present chapter to describe and suggest the methodology used here for size of particle measurement (see section 6.4).

6.3.2 Brief Review on Previous Work on Paleopiezometry

The overall number of papers on Paleopiezometry is relatively limited. We shall briefly mention some of these, grouping the different papers firstly according to their nature: (i) Theoretical studies such as by Twiss (1977), Poirier and Guillopé (1979). (ii) Experimental studies as in the case of Mercier et al (1977), Zeuch and Green (1979), Ross et al (1980-a, b) and (iii) studies which are concerned only with the applicability to natural examples in some particular areas (White 1979-a, b, c, Weathers et al, 1979-a, Kohlstedt et al 1979, Etheridge and Wilkie 1979, Ross et al 1980-b).

Another way of grouping the previous work is according to the particular mineral used for the stress estimation. Two minerals account for the majority of the published results and these are olivine and quartz. Poirier and Guillopé (1979 p.73, fig. 5) dealt with halite. Tullis (1979, p.1144) lists references for other minerals. For olivine there are many experimental results (Mercier et al, 1977, Zeuch and Green 1979, Ross et al 1980-a, b) and also some attempts to use this mineral for natural stress estimates; Mercier et al (1977) used xenoliths of kimberlites, Ross et al(1980-b), applied the concepts to rocks of the Vourinos complex in Greece.

The present study is concerned only with the use of quartz, and that is why we reserve the final part of this section for a more detailed explanation of a few selected papers which used information from naturally deformed quartz rocks.

White (1976-b) estimated paleostress for Loch Eriboll, though the exact locations of specimens are not reported. Subsequently White (1979-a) made some stress determinations using what are here interpreted as Moinian Psammites, from the south of Creag-na-Faollinn. White (1979-b) published results for samples taken from two distinct localities in Eriboll: (i) at Alt Oldhrsgaradaidh, south of Creag na Faollinn, presumably from rocks of the Moinian Schists, and (ii) at Ben Heilam from Cambrian Pipe-Rocks, in the imbricate zone (see Peach and Horne 1907, Soper and Wilkinson 1975). White (1979-c) further described optical and TEM studies of Pipe Rock sampled from a mylonite of the Heilam Nappe at Ben Heilam, Eriboll.

Weathers et al (1979-a) studied rocks from three different localities in the Moine Thrust Zone: (i) at the stack of Glencoul, in Assynt District, (ii) at Knockan Creag, and also (iii) at Eriboll with no clear specification for the exact locality but the indications on their map (see Weather's et al 1979-a, fig. 2) suggest some place in the vicinity of Kempie Bay. Kohlstedt et al (1979) published comparative analyses of the Moine Thrust rocks and the Iquertoq shear zone, Western Greenland.

Another important study using quartz, is given by the paper Etheridge and Wilkie (1979) in which they re-analysed much of the microstructural relations for various different zones of thrusts in Australia. The present study profited from the information contained in the Etheridge and Wilkie (1979) paper as we shall be referring to it in the next section.

We shall be dealing with the above papers that used quartz-rocks of the Moine Thrust Zone, when we compare the paleostress estimates found in the present study (ie section 6.5).

6.4 Stereology

6.4.1 Preliminary Considerations

Before describing the methods of size of particle measurement it is appropriate to comment and also to justify the reasons for choosing here some particular stereologic methods. This study aims to emphasize the importance that the method of size measurement plays in the final result of the paleostress estimate.

The models by Twiss (1977) and MerCier et al (1977) require the determination of the recrystallized grain size (RGS) and this can be performed in several ways, depending on many factors such as: size of the particles, time to be spent and available equipment for measurements etc .... It is necessary to take into account those factors before choosing a method. However the final selection aims at a method which can produce the most reasonable results with the least effort (ie an Optimized method, ss). That last condition implies that the chosen method should not only be compatible with the available equipment but also that the amount of time to be spent in each determination should be taken into account. As we shall see, time can ultimately determine the accuracy of the size-estimation.

The study of grain or particle distribution is a long, and sometimes controversial subject which has many applications in many branches of science. For that reason similar problems seemed to have been handled and solved independently many times.

The present study requires that the measurement of data transmitted from a two dimensional image is used to estimate the spatial (statistic) behaviour of each population (phase) by means of their characterizing distributions. The most convenient approaches, for the present conditions, are those developed for quantitative metallographic studies which may be performed with an ordinary petrographic microscope, equipped with a micrometric ocular. It is important to characterize the above conditions because there are other suitable methods, for example, for reflected light or for observations made with the Transmission Electron Microscope (TEM) and these are not covered by the present study.

For cases where grain size measurements constitute a frequent routine,it is advisable to make use of a more sophisticated system which integrates recording and calculating devices in such a manner that it enables very accurate measurements to be made and also allows a vast quantity of data to be handled in a quick and effective way (see Exner 1972). Usually the commonly measurable parameters for most microstructures are: (i) the estimation of the proportion or the volume fraction of each of the component phases, (ii) the mean grain size, and (iii) the determination of particle size distribution.

The last two parameters are the particular concern of the present section while the first one was dealt with in more detail in section 5.4 of the previous Chapter 5.

In the geological literature there are some excellent texts dealing with the determination of particle size distributions (Krumbein 1935, Chayes 1956, Pettijohn 1957, Griffiths 1967). As a result of continuous research in the field of statistical-sedimentology, the current reference list is vast. However, for the present work it was decided to follow a 'stereologic' approach, which treats such problems from the purely geometric (solid) point of view. The excellent book by Underwood (1970) presents a comprehensive study in a very accessible text. The paper by Exner (1972) is an outstanding review of the particle and size distributions from a metallurgic point of view. More recently, Pickering (1976) published a monograph which has an essentially practical viewpoint and he describes most readily applicable stereological methods, leaving little room for lengthy considerations of a theoretical or purely conceptual nature. The methods used throughout the present chapter are primarily those to be found in these last three references.

6.4.2 The Grain Size Estimation

This constitutes a particular difficult problem because in nature the grains may not have ideally spherical forms but instead have polyhedrical shapes and very different sizes. This poses some difficulties, from the mathematical point of view, because the obtained measurements must be corrected for effects such as particle overlapping and surface truncation (cf Figs. 6-2-d, e).

Two main methods can be employed in these circumstances: (i) areal analysis, (ii) linear-intercept-length method. In general the latter is to be preferred not only because the areal analysis may demand sophisticated equipment for area estimation (apart from being a rather time consuming method) but also because the latter usually allows greater accuracy.

It must be pointed out that the spatial shape of the grains greatly influences a two dimensional analysis of size, and that for most of the natural cases it seems very difficult to derive a definite and precise analytical solution.

The linear-intercept or the intercept-length method is a very convenient technique when sizing is an occasional procedure. It consists in counting the number of grains intercepted by a traverse line of known absolute length, L (cf Fig. 6-2-a). Therefore the mean-linear-intercept (m.l.i) $\bar{l}$, can be obtained by:-

$$\bar{l} = \frac{L}{N_g} = \frac{L}{N_b} = \frac{L}{N} \qquad [6\text{-}9]$$

where N_g is the number of intercepted grains, N_b is the number of intercepted boundaries. The above relationship only holds for a microstructure where there is only one phase, as shown in fig. 6-2-a. For such cases where the traverse line intercepts more than one phase (see fig. 6-2-b for comparison) relation [6-9] does not apply and it is necessary to take into account the proper relation of (N) as depicted in figs. 6-2-a and b.

The complexity increases, however, because the condition explained in the last paragraph is true for cases of particles with the same size, randomly distributed through the sample and ideally spherical in shape. These conditions are seldomly met in nature. For such cases where there is a preferred orientation of particles, the number of intersections should vary according to the direction of measurement (see fig. 6-2-c). Underwood (1970, Chapter 3) gives a comprehensive treatment and derives simple expressions for dealing with such cases. However the measuring procedure becomes more complicated because it is first necessary to locate the preferred direction of particle-orientation and then to perform the counting routine along two orthogonal grids of parallel lines, the spacing of which is chosen according to particle-size criteria (see Underwood 1970, pp.48-71, for full details).

Figures 6.2

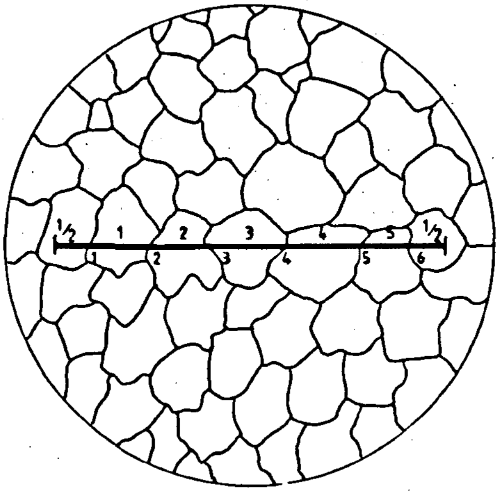

·a

N_g = No. of intercepted grains

N_b = No. of intercepted boundaries.

L = Absolute length of the traverse line.

$$N_b = N_g = N = 6$$

$$\text{m.l.i.} = \bar{l} = \frac{L}{N}$$

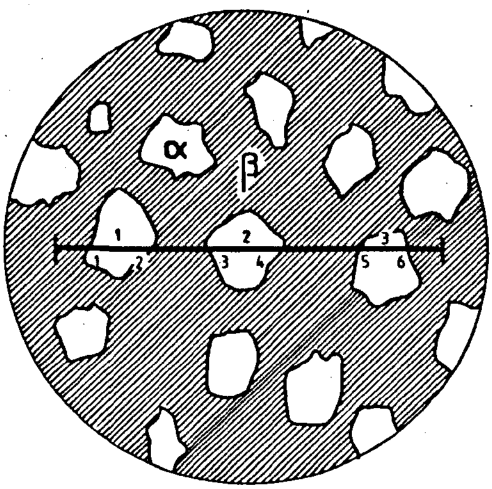

·b

$N_g = 3$

$N_b = 6$

$$\therefore\ 2N_g = N_b = N$$

$$\text{m.l.i.} = \bar{l} = \frac{L}{N}$$

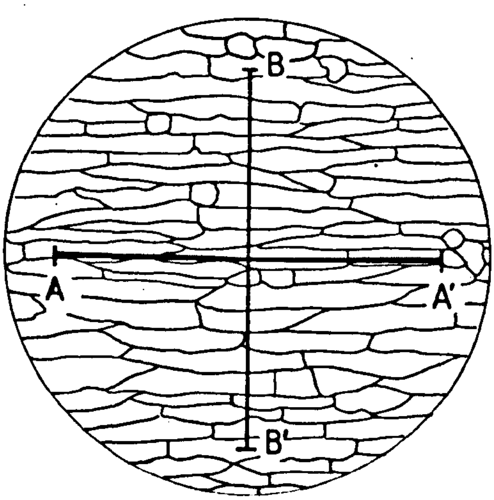

·c

$\overline{AA'} = L_{\overline{aa'}}$, $N_g = 3$

$$\therefore\ \bar{l}_{\overline{aa}} = \frac{L}{3}$$

$\overline{BB'} = L_{\overline{bb'}} = L$, $N_g = 20$

$$\therefore\ \bar{l}_{\overline{bb'}} = \frac{L}{20}$$

Illustrates the results variations according to the measurement direction.

To satisfy the conditions explained in the last paragraph, using an ordinary petrographic microscope equiped with a micrometric ocular, seems quite difficult. However the above measurements can be more easily performed on photomicrographs. Care is needed for correction of distortion and also for the determination of the absolute lengths of the grid. However, this method was not used here, and there are two main reasons for this:

(i) The great majority of the section measured initially exhibited textures which seemed to approach conditions of very weak to no preferred orientation of grain shape. In such circumstances the usual procedure is to admit (ie for practical purposes) that the conditions illustrated in figure 6-2-a are acceptable. However there were a few cases when these conditions were not met and the most convenient solution was to exclude these sections from the measurement scheme.

(ii) Mercier et al (1977) and also White (1979-a) mentioned that they measured in a direction perpendicular to the preferred orientation of grain long axes and this procedure was followed here only in very few occasions mainly to fulfil an indication of one of the used models (Mercier's) and also to compare the result with these of White's (1979).

Another problem to be subsequently solved was related to the conversion between two dimensional into three dimensional distributions of elements. This situation is particularly complex but the approach here was to simplify the problem by considering the following:

(i) The truncation or sectioning effects of particles can be clearly observed and analysed from the scheme in fig. 6-2-d, where the plane ABCD contains circles in which the diameters are probably smaller than the true particle diameters. Therefore a mean-linear-intercept (m.l.i.) directly taken from this sample does not correspond directly to a particle-size. It is most probably an underestimate of it and therefore should be corrected for spatial size equivalence.

(ii) Another equally important aspect is that the probability of cutting a particle as in fig. 6-2-d, increases with the particle diameter. This means that the smaller phases are always underestimated. This can be called a sampling effect, which tends to diminish with the uniformity of the size of the particle and also as grain size approaches the thin section thickness.

(iii) For the present case of projected images there are additional effects of overlapping (see fig. 6-2-e). This effect also diminishes if the thickness of the section approaches the size of the phase that contains it.

These are some of the innumerable 'difficulties' encountered in this study. They were here described in order to highlight a few of the more important problems that one faces before 'judging' and deciding on a particular method of size estimation. It must be stressed that the above described effects are thought to be additive and that the above treatment only applies if the particles have a simple shape. Underwood (1970) describes, but in many cases only mentions, methods using a more rigorous approach and these invariably end in very complicated problems of differential geometry. For the present study it was decided to follow a more simplistic approach mainly because of compatibility with the models by Twiss and Mercier.

Based on the distribution of probabilities, Exner (1972, p.32) was able to show that the diameter for perfect and equallized

Figures 6.2. (cont'd)

.d

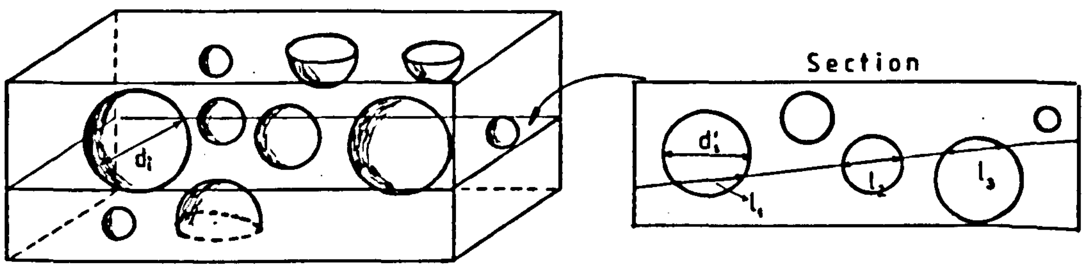

Illustrates truncation of particles by sectioning effects. Note that the intersected-diameters (d_i') are, in general, underestimated values of the particle-diameters (d_i). Note also the differences between (d'_i) and (l_i).

.e

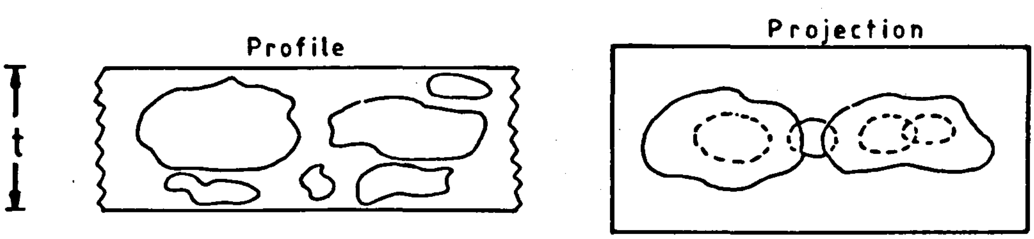

Illustrates effects of particle-overlapping relative to size and section thickness (t). It is clear that such effects are attenuated as particle-size approaches the thickness (t).

spheres which present a random distribution, can be estimated if the average mean (arithmetic) intercept diameter ($\bar{d}'$) is known (see fig. 6-2-d for definition of this diameter), by using:

$$D = \frac{4}{\pi}\,\bar{d}' \qquad [6\text{-}10]$$

the above conditions, however, are hardly met in this study. For cases of a spatial-size distribution (D) and the mean-intercept-length ($\bar{d}$ or m.l.i.), the relation is also found to be based on a probability function of sampling a linear-intercept (see some details in Exner 1972, p.33. Full details are in Exner 1967) as follows:

$$D = \frac{3}{2}\,\bar{d} \qquad [6\text{-}11]$$

where ($\bar{d}$) corresponds to a mean of numerous ($\bar{l}$) measurements in a section (see [6-14] to [6-17]). There are many other approaches which are listed in Underwood (1970, p.129). The method by Hilliard (1962), for example, is reputed to be the best but it is difficult to apply because, apart from requiring the measurement of the linear intercept, it is also necessary to have the distribution of the projected equivalent-circular area of the particles. Both Exner and Underwood mention Spektor's (1950) chord analysis as one of the best approaches for size estimation, but this will not be applied here because it may depart too much from the original method used by Twiss (1977), in constructing his empirical method.

In view of so many difficulties and constraints it was decided in this study to follow Pickering's (1976) practical approach, which defines the average particle size as:

$$D \simeq 1.75\,\bar{d} \qquad [6\text{-}12]$$

According to Pickering's treatment, the relative error of the m.l.i. can be assessed by

$$\frac{s(\bar{d})}{\bar{d}} \simeq \frac{0.7}{\sqrt{\sum N_i}} \qquad [6\text{-}13]$$

where, $\sum N_i$ is the population size, and $s(\bar{d})$ is the standard deviation of the m.l.i. ($\bar{d}$). Figure 6-3 plots the relative error as a function of the sample size.. This is a particularly useful graph especially when planning an experiment in terms of the cost of the results. It can be seen that the difference between the relative errors of 7% and 1% could imply a difference between approximately one hour and one week of continuous work (ie ≃ 4900 grains, roughly measured at 120 grains/h).

The final step in the grain size determination concerns the construction of the curve of size-distrubution. However the choice of the appropriate distribution function is also an intricate problem as it depends heavily on the shape of the elements being measured. Exner (1972, p.32) points out that the shape of the phase is so important that he constrains the possibility of determining the true spatial size distribution on the condition that the shape factor of the phase is known. Otherwise it is virtually impossible to establish the spatial size distribution by means of measurements on a plane thin section. In addition , the 'known' shape of the particles must be of simple geometry, otherwise it will make the mathematical treatment too complicated. There are some attempts to establish relationships between 2D measurements and the 3D particle shapes such as: ellipsoids, platy and rod-like cylinders, cubes and spheres. DeHoff (1962) developed a technique for ellipsoidal-spatial particles but this method is limited by the fact that it considers the whole population as particles with the same axial ratio and with the same shape type (ie Prolate or Oblates, there can be no mixture).

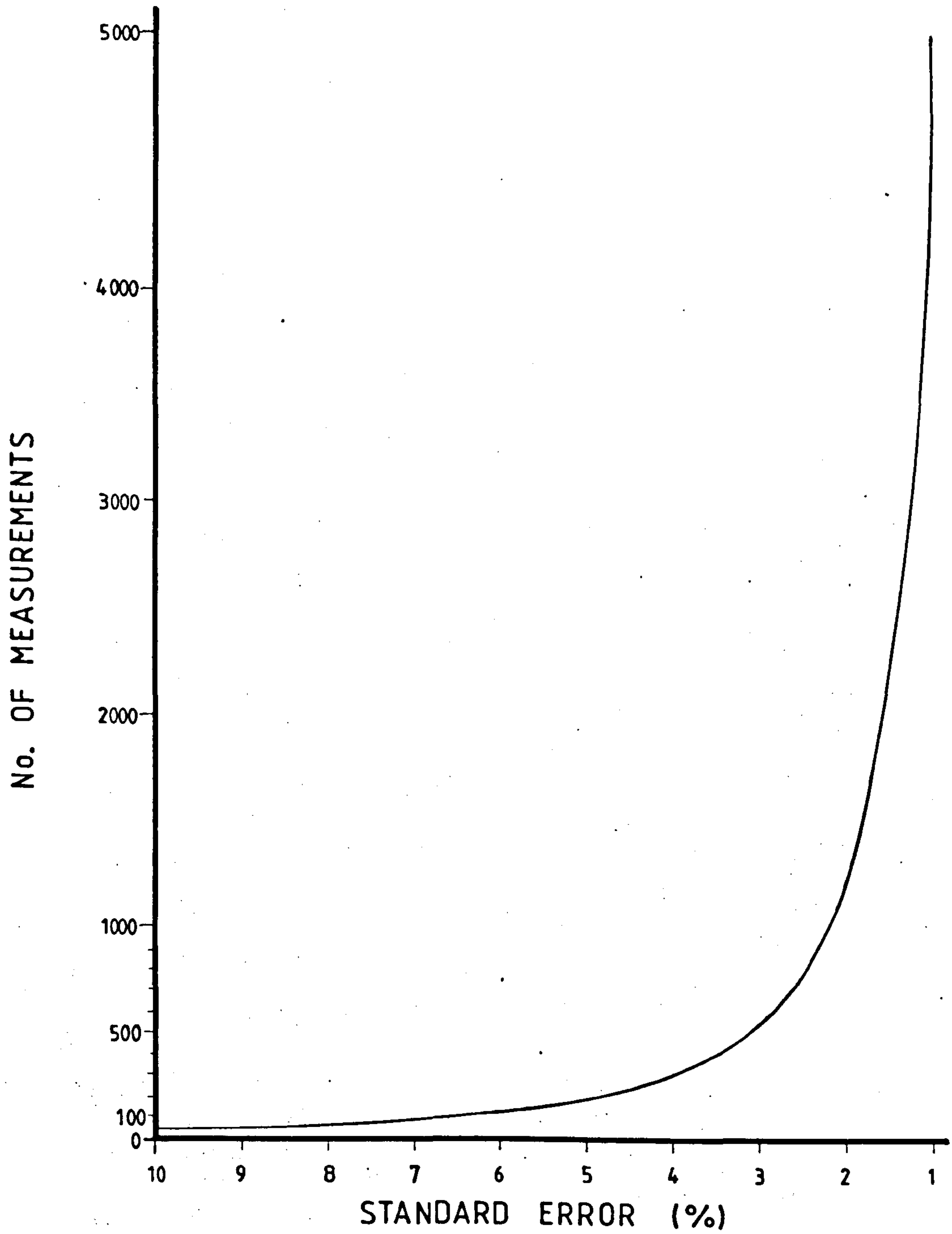

Figure 6.3. Curve estimating the error of the method (m.l.i.) in function of the amount of measurements performed.

If the described difficulties are supposedly overcome, the rigorous mathematical approach will require the constuction of the distribution curve for characterizing the sizes of the elements in question. However this is not the procedure chosen here, and in view of the existent difficulties it was decided to adopt a simple solution which employs simple parameters such as the average particle size (D), the standard deviation $[s(\bar{d})]$ of the m.l.i. the population size $\sum N_i$, etc.... Data can be grouped in finite class intervals, either with arithmetic (equidistant) or geometric (log equidistant) scale. In general, size distributions are skewed (Mitra 1978) and for this reason the geometric scaling is to be preferred. The best results using this geometric scaling are shown in figs. 6-4. It must be pointed out that some samples did not obey a log-normal law,so that their plots give asymmetrical patterns. There can be several reasons for this:

(i) The population size is insufficient, therefore the available population did not achieve the necessary reproducibility level.

(ii) Perhaps different class interval division could produce a symmetrical pattern.

(iii) The population may be heterogeneous and present grains that may have originated by mechanisms other than Bulging. For example the RGS may be due to subgrain rotation in polygonized domains [cf Mercier et al (1977);Poirier and Guiloppé (1979); Kohlstedt et al (1979); White (1979-a)] and this could produce a characteristic particle size distribution and hence there is a possibility of bimodal population, depending on the contribution of each mechanism.

(iv) Perhaps the particle shape interferes to such an extent as to make the chosen method totally incompatible, hence the discrepancies.

Figures 6.4. Distribution of grain-sizes in Logarithmic scale. Ordinates refer to absolute frequencies in all diagrams.

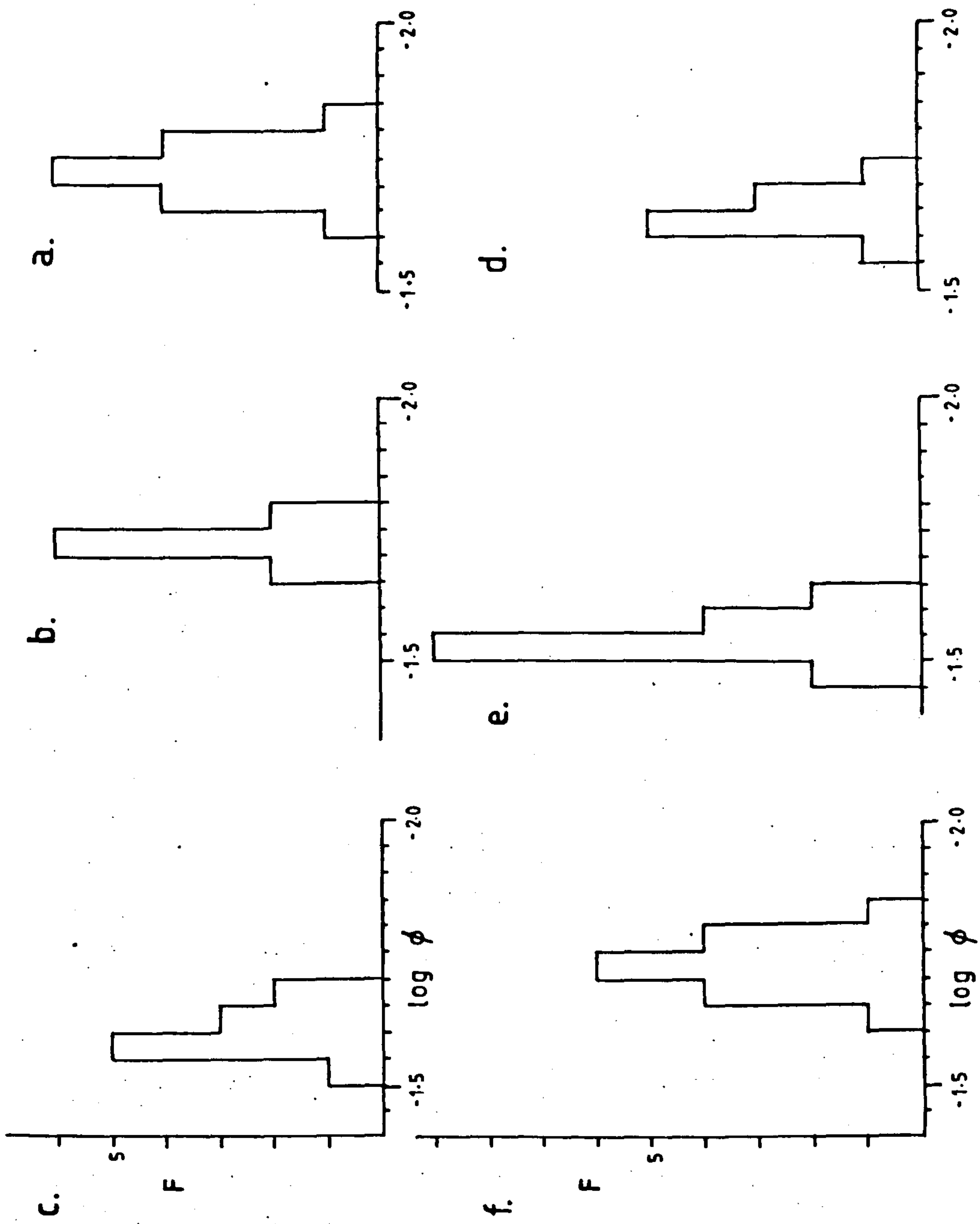

The systematics followed in the present study are listed below, and presented in tables 6-1-a to c.

1) The calculated mean (linear) intercept length (columns 7-11 in tables 6-1).

(i) Arithmetic

$$\bar{d}_a = \frac{\sum N_i \bar{l}_i}{\sum N_i} \qquad [6\text{-}14]$$

(ii) Geometric

$$\bar{d}_g = (\Pi \bar{l}_i)^{(\sum N_i)^{-1}} \qquad [6\text{-}15]$$

or taking logarithms

$$\log_{10} \bar{d}_g = \frac{\sum (N_i \log_{10} \bar{l}_i)}{\sum N_i} \qquad [6\text{-}16]$$

(iii) Harmonic

$$\bar{d}_h = \left[\frac{1}{\sum N_i} \sum \frac{N_i}{\bar{l}_i} \right]^{-1} \qquad [6\text{-}17]$$

The geometric mean represents the value with the greatest frequency if the distribution confirms with the log-normal law. The harmonic mean is mainly used for cases when it is necessary to correlate specific surface areas. The magnitudes of the above means relate to each other (following Cauchy's theorem) as $\bar{d}_a \geqslant \bar{d}_g \geqslant \bar{d}_h$, the inequalities increasing with the degree of dispersion of diameters.

2) The estimated errors (columns 10-11, tables 6-1).

(i) The standard deviation $s(\bar{d}_a)$ of the arithmetic mean may be expressed as the root mean square deviation (see Underwood 1970) as follows:

$$s(\bar{d}_a) = \left[\frac{1}{\sum N_i} \sum (N\bar{l}^2)_i - \left[\frac{1}{\sum N_i} \sum N_i \bar{l}_i \right]^2 \right]^{\frac{1}{2}} \qquad [6\text{-}18]$$

and

(ii) the relative error is given by:

$$s(\bar{d}_a)/\bar{d}_a \qquad [6\text{-}19]$$

3) The 'corrected' grain size estimates, are obtained using both [6-14] and [6-16] in [6-12] (columns 12-13 in tables 6-1).

4) The paleostress estimations (columns 14-17, tables 6-1). These are worked out, for the Arithmetic and Geometric Mean grain sizes ($\bar{D}_a$ and $\bar{D}_g$), using the models by Twiss [6-6] and Mercier et al [6-8] (see columns 16-17 in tables 6-1).

Tables 6-1-a, 6-1-b and 6-1-c represent respectively the domains of Eriboll (at Kempie and Arnaboll Hill) and Hope areas, as defined previously for Chapter 4. Altogether there were 57 sections representing 31 different localities in these three areas. Where a sample presented more than one thin section, the calculations were performed in both, in order to check for the consistency of the measurements. In general the discrepancies were below 10% and these samples have their results characterized by their means and are listed as rows of sample average (SA) in tables 6-1-a to c. The maps of figs. 6-5-a to c, contain the geographic locations (scale 1:10,560) of the estimates of tables 6-1.

6.5 Results and Discussion

6.5.1 From the Present Study

The following consistent relationships between the recrystallized grain sizes and the related microstructures have been obtained in the present study:-

Table 6-I-a

Thin Sect. No.	Dept. Refer. No.	Grid Reference	Section	Pop size $\sum ni$	M.L.I. standard error %	Mean Intercept Length: Arimeth. $\bar{d}a$ (μm)	Mean Intercept Length: Geometric $\bar{d}g$ (μm)	Mean Intercept Length: Harmonic $\bar{d}h$ (μm)	Error Estimation: St. Dev. $s(\bar{d}a)$ (μm)	Error Estimation: Rel. Error $s(\bar{d}a)/\bar{d}a$	Grain Size (Corrected): Arithmetic $\bar{D}a$ (μm)	Grain Size (Corrected): Geometric $\bar{D}g$ (μm)	Paleostress Determination (MPa): Based on Twiss (1977) for $\bar{D}a$	Paleostress Determination (MPa): Based on Twiss (1977) for $\bar{D}g$	Paleostress Determination (MPa): Based on Mercier (1977) for $\bar{D}a$	Paleostress Determination (MPa): Based on Mercier (1977) for $\bar{D}g$
1	41466	NC44155659	A	147	5.77	17.006	16.671	16.384	3.663	0.21541	29.761	29.174	67.181	68.098	46.87	47.54
2			C	136	6.00	18.382	18.290	18.012	1.878	0.10216	32.169	32.007	63.721	63.939	44.34	44.50
			SA			17.69	17.48	17.20			30.97	30.59	65.45	66.02		
3	41467	NC45265718	A	124	6.39	22.177	21.990	21.800	2.843	0.12821	38.810	38.483	56.086	56.409	38.77	39.01
4			C	132	6.09	20.833	20.833	20.171	3.855	0.18507	36.458	35.861	58.522	59.182	40.55	41.03
			SA			21.51	21.24	20.99			37.63	37.17	57,30	57.80		
5	41468	NC45135711	A	80	7.83	28.125	26.786	25.773	9.796	0.34830	49.218	46.875	47.719	49.328	32.72	33.88
6			B	73	8.19	30.821	29.921	29.014	7.324	0.23765	53.938	52.361	44.838	45.752	30.65	31.31
			SA			29.47	28.35	27.34			51.58	49.62	46.28	47.54		
7	41469	NC45365713	A	107	6.77	23.264	23.034	22.668	3.822	0.16360	40.877	40.310	54.132	54.658	37.36	37.74
8			B	112	6.60	22.321	22.094	21.875	3.223	0.14443	39.062	38.665	55.839	56.229	38.60	38.88
			SA			22.84	22.56	22.28			39.98	39.49	54.99	55.44		
9	41470	NC45745722	A	175	5.29	20.000	19.389	18.849	5.239	0.26196	35.000	33.931	60.169	61.450	41.74	42.68
10			B	105	6.83	21.428	21.146	20.849	3.377	0.15760	37.500	37.006	57.411	57.931	39.74	40.12
			SA			20.71	20.27	18.85			36.25	35.47	58.79	59.69		
11	41471	NC45655720	A	115	6.53	17.391	17.130	16.881	3.070	0.17657	30.434	29.979	66.168	66.850	46.13	46.63
12			B	133	6.07	16.917	16.786	16.649	2.045	0.12090	29.605	29.377	67.423	67.779	47.05	47.30
			SA			17.15	16.96	16.77			30.02	29.68	66.80	67.31		
13	41472	NC45575717	A	139	5.94	17.985	17.814	17.648	2.5014	0.13908	31.474	31.176	64.673	65.094	45.03	45.34
14			C	119	6.42	19.320	19.089	18.956	2.402	0.12500	33.653	33.406	61.795	62.106	42.93	43.16
			SA			18.31	18.45	18.30			32.56	32.29	63.08	63.60		
15	41473	NC45325713	A	111	6.64	18.018	17.978	17.937	1.164	0.6410	31.531	31.462	64.594	64.690	44.98	45.34
16			B	121	6.36	18.595	18.454	18.322	2.341	0.1259	32.541	32.296	63.224	63.550	42.93	43.16
			SA			18.31	18.22	18.13			32.04	31.88	63.91	64.12		
17	41474	NC45425718	A	111	6.64	22.522	22.290	22.076	3.357	0.14907	39.414	39.008	55.500	55.891	38.35	38.63
18			C	145	5.81	22.413	22.114	21.850	3.889	0.17355	39.224	38.699	55.683	56.195	38.48	38.85
			SA			22.47	22.20	21.96			39.32	38.85	55.59	56.04		
19	41475	NC45575720	B	145	5.81	15.517	15.130	14.789	3.682	0.23733	27.155	26.478	71.502	72.739	50.04	50.95
20			C	146	5.79	17.123	16.940	16.758	2.511	0.14665	29.965	29.645	66.870	67.360	46.64	47.00
			SA			16.32	16.04	15.77			28.56	28.06	69.19	70.05		
21	41481	NC45955734	A	110	6.67	22.727	22.444	22.177	3.681	0.16199	39.772	39.278	55.159	55.631	38.10	38.44
22			B	107	6.77	25.700	25.574	24.745	5.054	0.19666	44.976	44.125	50.735	51.398	34.90	35.38
			SA			24.21	23.88	23.46			42.37	41.70	52.95	53.52		

Table 6-I-a continued

Thin Sect. No.	Dept. Refer. No.	Grid Reference	Sec-tion	Pop size $\sum ni$	M.L.I. Standard %	Mean Intercept Length Arimeth. $\bar{d}a$ µm	Geometric $\bar{d}g$ µm	Harmonic $\bar{d}n$ µm	Error Estimation St. Dev. $s(\bar{d}a)$ (µm)	Rel. Error. $s(\bar{d}a)/\bar{d}a$	Grain Size (Corrected) Arithmetic $\bar{D}a$ (µm)	Geometric $\bar{D}g$ (µm)	Paleostress Determination (MPa) Based on Twiss (1977) for $\bar{D}a$	Based on Twiss (1977) for $\bar{D}g$	Based on Mercier (1977) for $\bar{D}a$	Based on Mercier (1977) for $\bar{D}g$
23	41482	NC46165758	A	107	6.77	21.028	20.834	20.656	2.964	0.14096	36.799	36.460	58.153	58.519	40.28	38.65
24			C	101	6.97	22.277	22.145	22.013	2.417	0.10850	38.985	38.754	55.195	56.141	40.54	38.61
						21.65	21.49	24.29			37.89	37.61	57.03	57.33		
25	41483	NC46035742	A	102	6.93	26.960	26.449	25.967	5.371	0.19925	47.181	46.286	49.110	49.754	33.73	34.19
26			B	129	6.16	25.193	24.229	23.454	7.740	0.30724	44.089	42.400	51.427	52.811	35.40	36.40
						26.08	25.34	24.71			45.64	44.34	50.27	51.28		
27	41484	NC46385767	B	117	6.47	23.504	23.203	22.905	3.753	0.15971	41.132	40.605	53.913	54.388	37.07	37.54
28			C	121	6.36	22.727	22.623	22.524	2.226	0.97960	39.772	39.590	55.159	55.332	38.10	38.23
						23.12	22.91	22.71			40.45	42.82	54.54	54.86		
29	41486	NC46675741	B	136	6.00	18.38	18.28	18.18	1.897	0.10324	32.17	31.99	63.72	63.95	44.34	44.51
30	41487	NC46675744	C	108	6.74	27.77	27.50	27.22	3.893	0.14015	48.17	48.13	48.12	48.45	33.01	33.25
31	41488	NC4662547	A	127	6.21	19.69	19.52	19.35	2.589	0.13155	34.45	34.15	60.82	61.18	42.22	42.48
				$\sum 3739$												
Average for Kempie area				120.61	6.37	21.53	21.22	21.09		0.16614	37.67	37.28	58.17	58.72	40.35	40.76

SA = sample average

MLI = mean intercept length (method)

Table 6-I-b

Thin Sect No	Dept. Refer. No	Grid Reference	Sec-tion	Pop size $\sum ni$	M.L.I. standard %	Mean Arithm. $\bar{d}a$ (µm)	Intercept Geom. $\bar{d}g$ (µm)	Length Harmonic $\bar{d}h$ (µm)	Error St. Dev. $s(\bar{d}a)$ (µm)	Estimation Rel. Error $s(\bar{d}a)/\bar{d}a$	Grain Size Arithm. $\bar{D}a$ (µm)	(Corrected) Geomet. $\bar{D}g$ (µm)	Paleostress Determination (MPa) Based on Twiss (1977) for $\bar{D}a$	for $\bar{D}g$	Based on Mercier (1977) for $\bar{D}a$	for $\bar{D}g$
32	41477	NC46175890	A	133	6.07	30.10	29.92	29.77	3.006	0.9997	52.63	52.36	45.59	45.75	31.19	31.31
33	41490	NC45975868	B	123	6.19	21.484	21.363	21.248	2.000	0.10846	37.597	37.386	57.310	57.529	39.66	39.82
34			C	116	6.50	21.551	21.435	21.323	2.275	0.10556	37.715	37.512	57.188	57.399	39.58	39.73
			SA			21.58	21.40	21.29			37.66	37.45	57.25	57.46		
35	41491	NC46035870	A	134	6.05	22.39	22.21	22.04	2.787	0.12450	39.18	38.87	55.73	56.02	38.51	38.73
36	41492	NC46025872	A	122	6.34	22.54	22.33	22.11	3.203	0.14210	39.45	39.08	55.47	55.83	38.33	38.59
37	41493	NC46035891	A	199	6.42	29.41	29.09	28.80	4.687	0.15936	51.47	50.90	46.29	46.44	31.69	31.95
38	41494	NC46285894	A	109	6.70	22.935	22.666	22.427	3.732	0.16273	40.137	39.666	54.818	55.260	37.85	38.18
39			C	129	6.16	23.255	23.026	22.791	3.224	0.13867	40.697	40.295	54.304	54.672	37.48	37.75
			SA			23.10	22.85	22.61			40.42	39.98	54.56	54.97		
40	41495	NC46055878	A	108	6.74	25.462	25.369	25.280	2.239	0.8797	44.560	44.396	51.057	51.184	35.13	35.22
41			B	107	6.77	25.700	25.274	24.837	4.594	0.17876	44.976	44.229	50.735	51.316	34.90	35.32
			SA			25.58	25.32	25.06			44.77	44.31	50.90	55.25		
42	41496		A	123	6.31	23.36	22.21	22.07	2.573	0.11511	39.13	38.87	55.78	56.02	38.55	38.73
			$\sum$	1328												

Average values for the upper part of the Arnaboll Hill	120.73	6.37	24.76	24.41	24.22		0.12940	43.09	42.73	52.70	52.99	36.62	36.85

Table 6-I-c

Thin Sect. no.	Dept. Refer no.	Grid Reference	Section	Pop size	M.L.I. Standard	Mean Intercept Length Arithm. $\bar{d}a$	Geometric $\bar{d}g$	Harmonic $\bar{d}h$	Error Estimation St. Dev. $s(\bar{d}a)$	Rel. Error	Grain Size (Corrected) Arithmetic $\bar{D}a$	Geometric $\bar{D}g$	Paleostress Determination Based on Twiss (1977) for $\bar{D}a$	for $\bar{D}g$	Based on Mercier (1977) for $\bar{D}a$	for $\bar{D}g$
				$\sum ni$	%	(μm)	(μm)	(μm)	(μm)	$s(\bar{d}a)/\bar{d}a$	(μm)	(μm)				
43	41497	NC47866052	A	123	6.31	20.32	20.20	20.08	2.235	0.1100	35.57	35.36	59.51	59.76	40.46	41.44
44	41498	NC48076061	A	126	6.24	19.84	19.53	19.25	3.636	0.18329	34.72	34.19	60.50	61.14	41.98	42.45
45	41499	NC48156068	A	120	6.39	20.83	20.80	20.78	1.101	0.52890	36.46	36.41	58.52	58.58	40.55	40.59
46	41501	NC48426066	A	106	6.80	33.018	32.276	31.622	7.421	0.22475	57.783	56.483	42.787	43.454	29.18	29.66
47			B	108	6.74	32.407	31.655	30.963	7.214	0.22263	56.712	55.397	43.334	44.032	29.57	30.07
			SA			32.71	31.97	31.29			57.25	55.94	43.06	43.74		
48	41502	NC48296040	A	119	6.42	25.210	24.628	24.128	5.820	0.23086	44.117	43.100	51.404	52.226	35.58	35.98
49			B	113	6.59	22.123	21.791	21.482	3.971	0.17949	38.716	38.134	56.178	56.760	38.84	39.26
			SA			23.67	23.21	22.81			41.42	40.62	53.79	54.49		
50	41505	NC47886028	A	104	6.86	28.85	28.09	27.43	6.921	0.23993	50.48	49.17	46.90	47.75	32.14	32.75
51	41506	NC47836017	A	113	6.59	22.123	21.495	20.972	5.757	0.26024	38.716	37.617	56.178	57.289	38.84	39.65
52			C	114	6.56	30.701	30.351	30.000	4.628	0.15075	53.728	53.115	44.957	45.309	30.74	30.99
			SA			26.41	25.92	25.49			46.22	45.37	50.57	51.30		
53	41507	NC47796010	B	99	7.04	37.88	37.24	36.67	7.368	0.9453	66.29	65.17	38.94	39.43	26.45	26.78
54	41509	NC47615991	A	125	6.26	20.00	19.93	19.87	1.738	0.8692	35.00	34.88	60.17	60.31	41.74	41.85
55	41512	NC47585952	B	90	7.38	30.55	30.07	29.61	5.582	0.18270	53.47	52.62	45.10	41.60	30.84	31.20
56	41513	NC47925984	C	122	6.34	34.84	34.34	33.89	6.107	0.17532	60.96	60.10	41.26	41.66	28.08	28.37
57	41514	NC47765910	C	123	6.31	36.58	35.69	34.90	8.566	0.23415	64.02	62.46	39.90	40.58	27.12	27.60
				$\sum 1705$												

Average values for Loch Hope	113.67	6.57	27.71	27.25	26.84		0.1819	48.49	47.69	49.85	50.36	34.13	34.57
Average values for all three areas ($\sum$6772 grains)	118.81	6.42	24.23	23.87	23.52		0.16319	42.35	41.84	54.29	54.76	37.99	38.37

(i) Within a sample and to a certain extent within a homogeneous domain (more than one shape) and RGS can be considered constant (compare the results of tables 6-1 which are plotted in the maps of figs. 6-5-a - c).

(ii) The sizes of the recrystallized new grains seem to be constant no matter what was the size of the original clasts in that sample.

(iii) The general pattern is that of a decrease in the size of the newly recrystallized grains within the mylonite-ultramylonite zones, although there can be exceptions to this 'rule'.

(iv) In the more advanced stages of recrystallization (ultramylonitic textures) the presence of phyllosilicates did not interfere (apparently) with size of the grain refinement process. This seems to contrast with those samples exhibiting a less advanced stage of recrystallization where, the new grains, in the specimens richer in phyllosilicates,are coarser than the RGS in samples poorer in phyllosilicates (see Chapter 5).

Etheridge and Wilkie (1979) have studied several thrust zones in Australia and correlated the measured RGS with the strain variation (measured in terms of grain stretching) in these zones. For each of the analysed nappes they found a remarkable constant modal class which does not change with the increasing strain. However, this pattern changed totally when the samples are totally recrystallized because the RGS becomes coarser (see op. cit.,fig.6). In the present study it has been demonstrated (Chapter 5) that strains can be easily correlated with the proximity to the mylonitic zones and it seems to be directly related to the production of the recrystallized grains. However, the general pattern for the studied area is as follows:

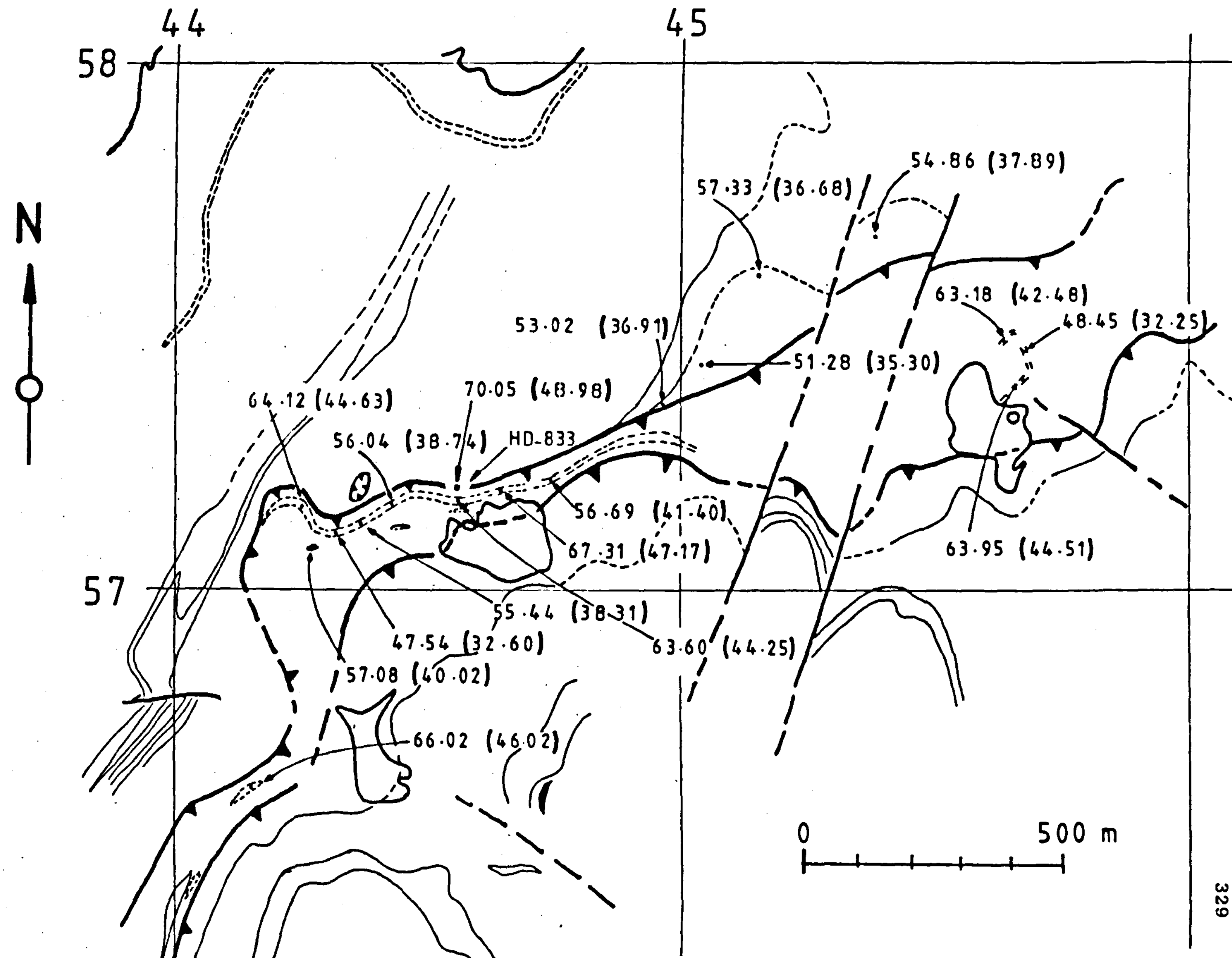

Figure 6.5-a. Region above Kempie Bay, Loch Eriboll. See explanations in figure 6.5-b.

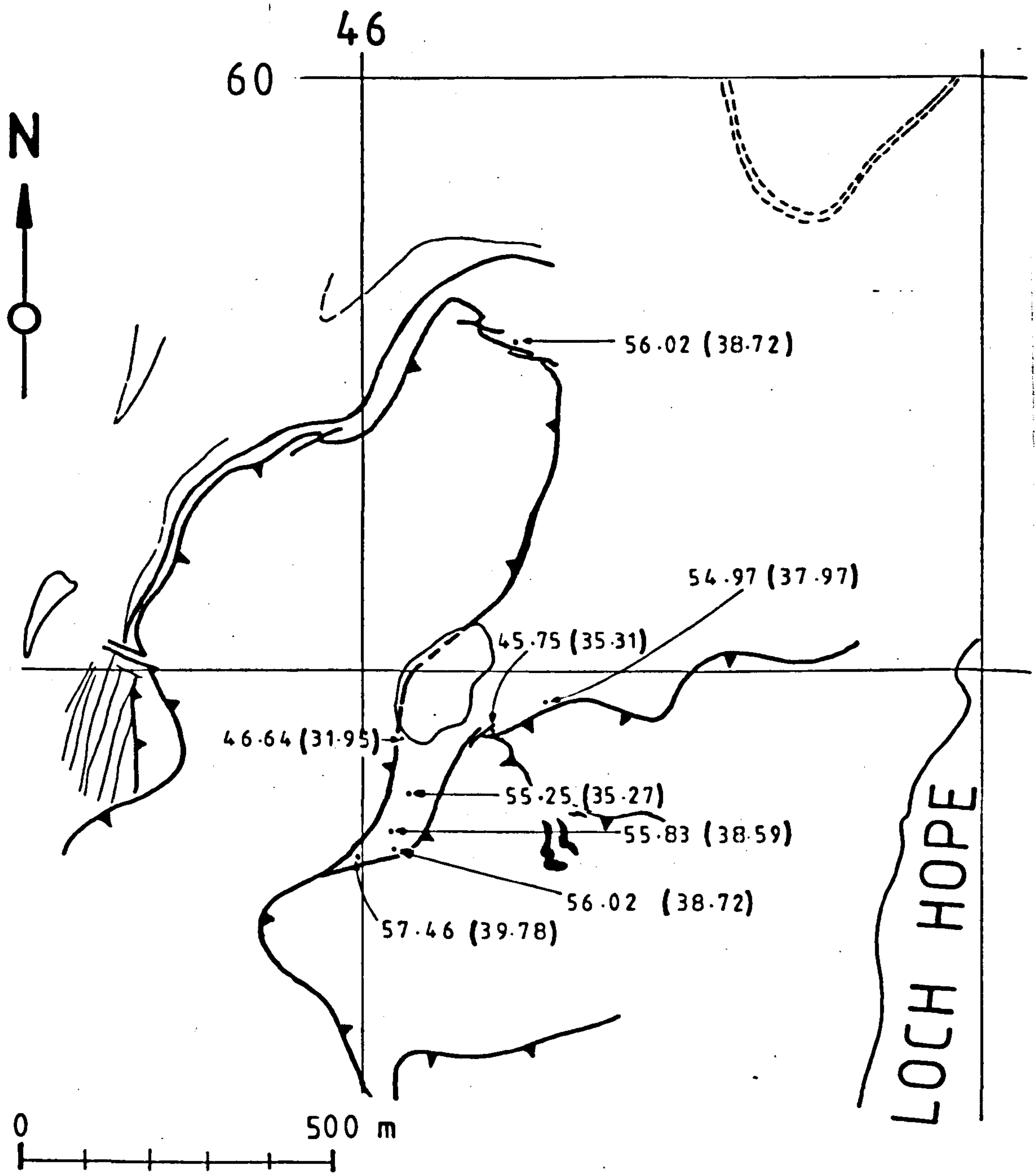

Figure 6.5-b. Area of the Arnaboll Hill, Loch Eriboll. Maps at a scale 1:10,560, showing the sampling localities for the collection of psammitic Paleozoic rocks used for paleostress estimates.
Values for each locality are in MPa, following the models by Twiss (1977) and Mercier <u>et al</u>. (1977). The results following Mercier <u>et al</u> are shown here in brackets.

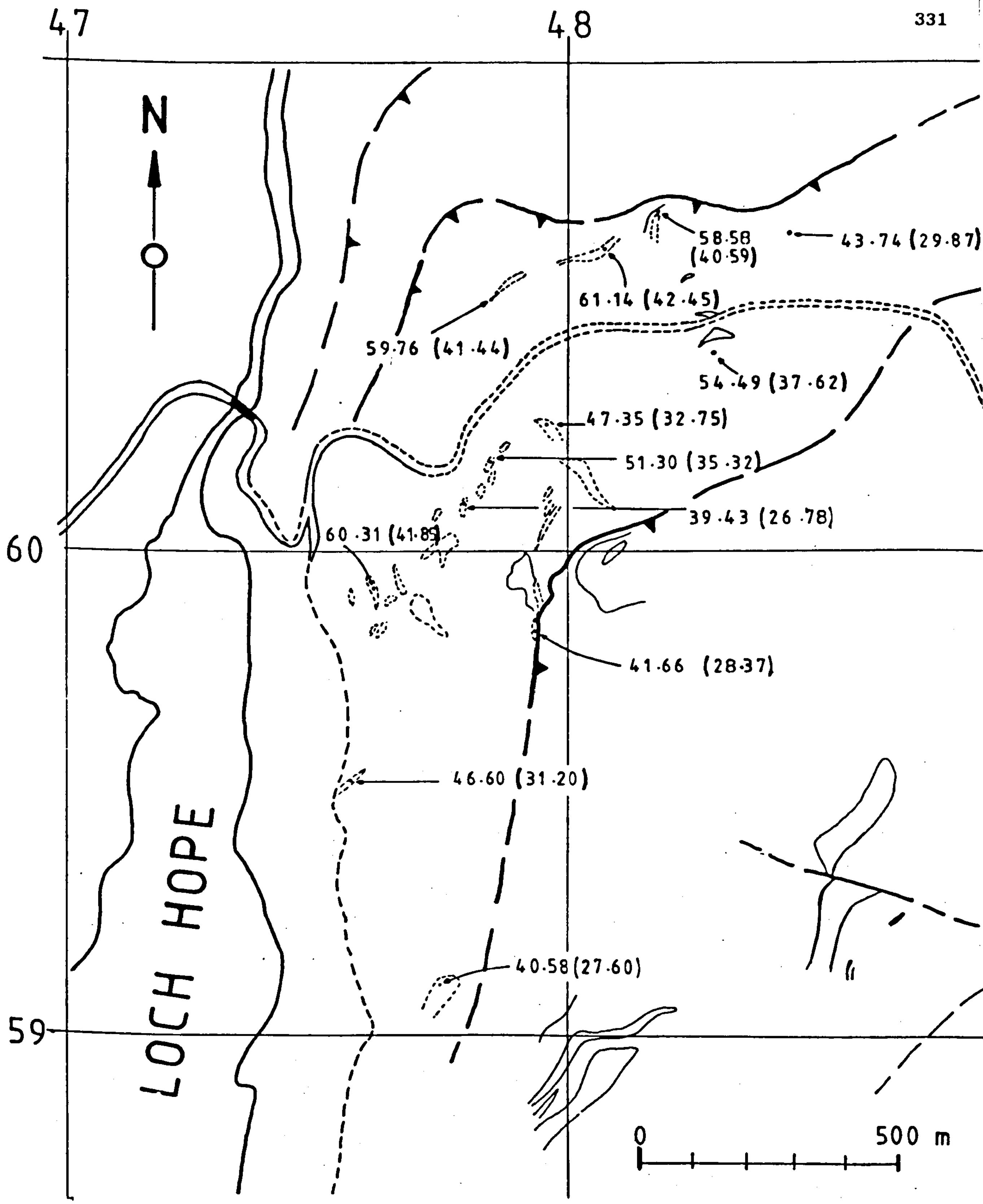

Figure 6.5-c. Area at the NE side of Loch Hope. See map for details and explanation in figure 6.5-b.

(i) In Loch Hope a greater variation in sizes of the recrystallized grains is present. This distribution is less homogeneous than that at Eriboll (see fig. 6-6).

(ii) For the samples with totally recrystallized grains there are no measurements of the intensity of deformation, such as Nadai's ε_s-parameter, because of the obvious lack of original clasts. However, there can be no doubt that these samples come from domains more deformed than the specimens used in grain shape analysis. Therefore, these totally recrystallized specimens would certainly plot in the graph of fig. 6-6 with abscissae values greater than 1.4. With one exception, the general trend for these totally recrystallized sections from the Kempie area, is for smaller RGS with increasing strain. This contrasts with Etheridge and Wilkie's (1979, fig.6) observations.

The magnitudes of the estimated differential stress have been tabulated in 6-1-a to c. However, in order to group and analyse these results according to specimen location, use was made of a Log-Log graph relating ratios σ/Γ and d/b (see fig. 6-7). It seems that each one of the three geographic sampling domains (Kempie, Arnaboll and Hope) occupy different locations in the graph. This may reflect the different conditions that operated in the three areas. The rocks sampled above Kempie Bay occupy mainly one end of the graph line, while specimens from the Arnaboll Hill fall within the Kempie range but clearly occupy the lower part of it. These differences may be related to the following factors:

(i) The specimens in Eriboll area come from two distinct nappe domains which are separated by the b-type or the UAT thrusts (cf Chapter 2). Arnaboll and Kempie specimens are separated by distances

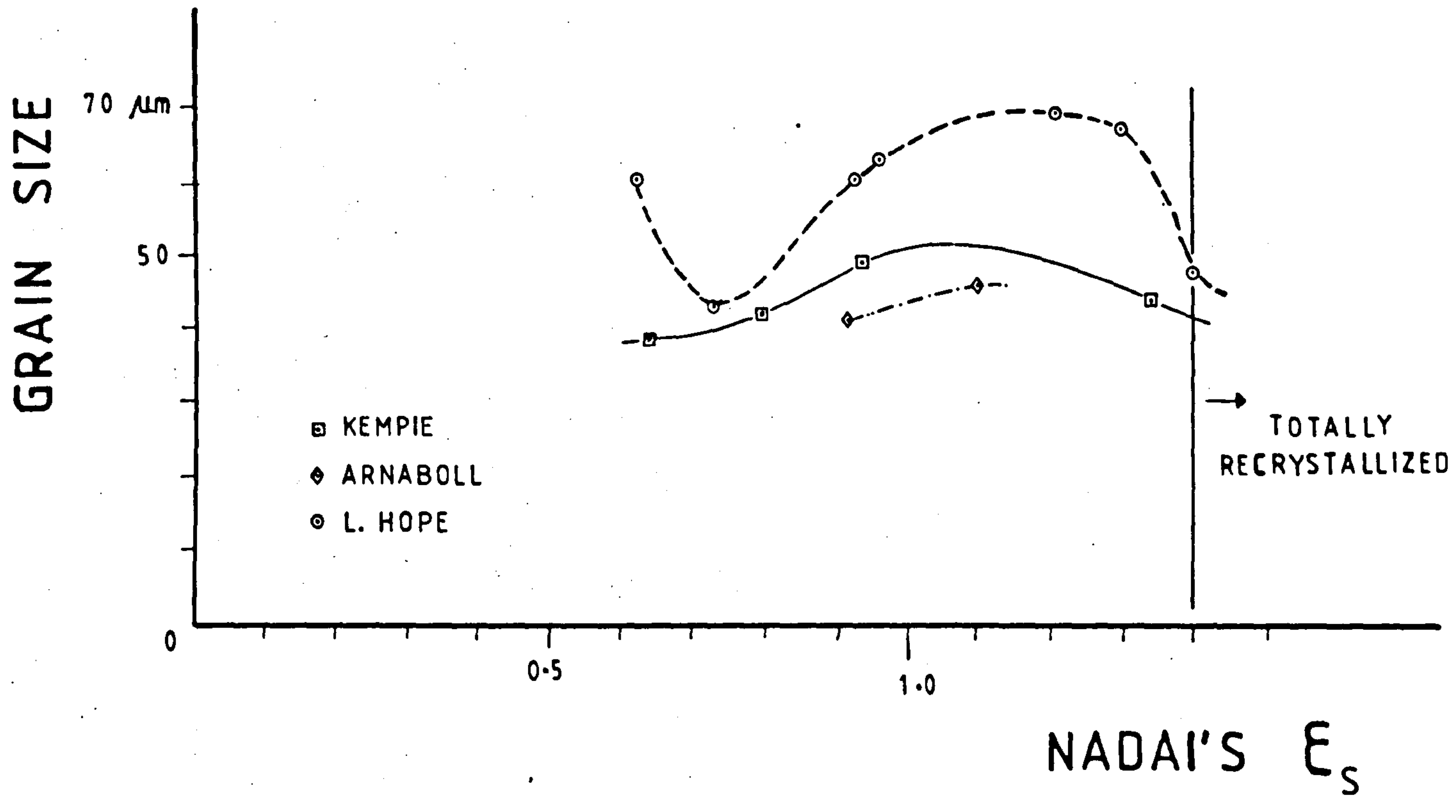

Figure 6.6. See text for explanation.

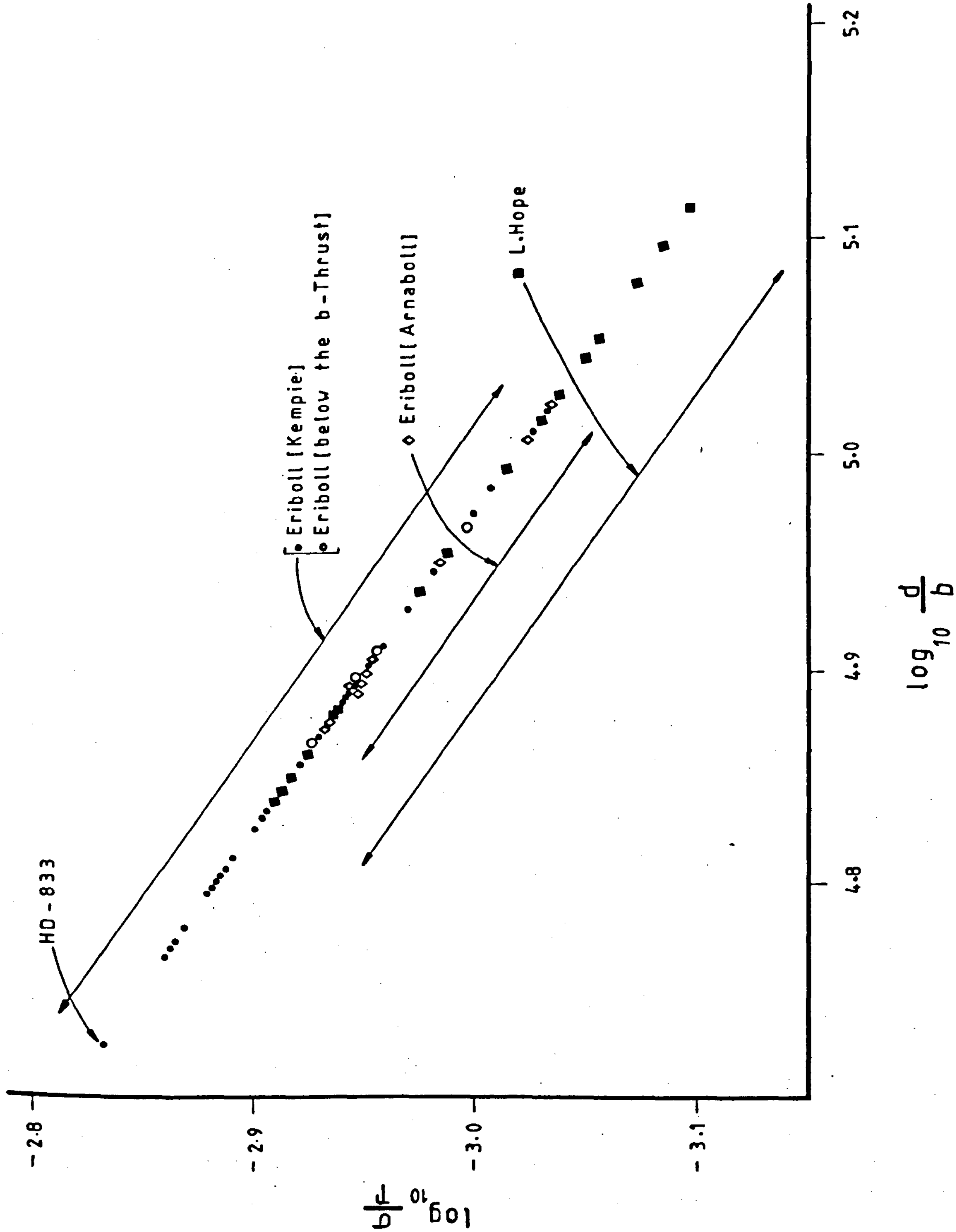

Figure 6.7. See text for explanation.

which vary from 1.5 to nearly 3.0 km, so stress could vary in this distance.

(ii) The specimens from Kempie which lie in the basal quartzites beneath the b-thrust, plot in the graph of fig. 6-7 in a range very similar to that for the Arnaboll Hill (see fig. 6-7, plots as open circles).

(iii) The rocks above and below the b-type (or the UAT) thrust may have different stress distributions. Kempie rocks above the b-thrust come from slabs of quartzites emplaced in a suite of mylonitic rocks which include the phyllonitic Lewisian rocks. Comparatively, the domain from the Arnaboll Hill constitutes a much thicker pile of Paleozoic Quartzites which are more competent and therefore stress propagation in these should be distinct.

The mean differential stress (eg Twiss Model) for all the 31 specimens at Kempie amounts to 58.5 MPa, while the four samples beneath the thrust (at Kempie) present a mean estimate of 53.97 MPa. The 11 estimates for the Arnaboll rocks place their mean at a level of approximately 52.8 MPa. Finally, samples from Loch Hope area occupy the other extreme of the graph line in fig. 6-7, and exhibit a wide range of values. This correlates with field evidence, that the Loch Hope deformation zones present characteristics of varied strain intensities, when compared with Eriboll Zones. The mean of the fifteen sections is approximately 50 MPa, which is precisely 5.3% and 15.6% below the Arnaboll and Kempie means, respectively.

The present geographic distribution of paleostress estimates together with the geologic and structural descriptions of Chapter 2, leads to the suggestion that there is a stress gradation towards the upper zone of the b-type of thrust. Etheridge and Wilkie (1979) generally found higher values of stress at upper thrust levels. They believed this to be inconsistent with their concept of stress increasing with depth, along a narrow zone, towards the proximity of the 'root' zone. They justify this discrepancy by the possible presence of a higher fluid pressure at depth or possibly due to hydrolytic weakning. This study presents an alternative interpretation which accords with the tectonic evolution explained in Chapter 2, and also conforms with Etheridge and Wilkie's (1979) concept of increasing stress towards 'a deeper root zone'; the rocks of the upper nappe were deformed at high stress in deeper levels and then carried out to higher levels (climb-up westwards) where the stress was reduced.

From the last paragraph, it is implicit that there is some correlation between the variability of stress and strain. The plot of stress intensities can present some inconsistensies for reasons to be discussed elsewhere in this chapter, but apart from this there seems to be an intrinsic relationship between the estimated relative stress and strain, in that the former generally appears to increase in those zones of more intense ductile deformation. It seems very significant in that context,that the Kempie mylonitic (above the b-thrust) zone could not provide a single suitable sample for grain shape evaluation while the lower stress zone of the Loch Hope mylonites provided 7 samples. Therefore, this study cannot agree with Weather's et al (1979) observations that for the Moine Thrust Zone , only strain (and not stress) increases towards the Thrust surface. Perhaps this is a mere coincidence, but the highest recorded stress estimate for the whole studied area of fig. 6-4, was sampled from the b-thrust (ss) plane - ie the slip surface of Pipe Rock in direct contact with the above Lewisian Gneiss, in locality HD-833 - and this exhibits the characteristics of higher deformation levels. The position of this estimate in fig. 6-7 is the uppermost plotted point, and this contrasts with the rest of plotted estimates (see the geographic location in fig. 6-4-a).

It is important to know that there are some factors influencing the stress estimates but it is difficult to establish the appropriate weight of these influences:

(i) Errors in the measurements. The average number of grains per section in this study is nearly 120. The estimated standard error (m.l.i.) in such cases varies from 5 to 10%, which is likely to cause a difference in the estimated differential stress of the order of magnitude of less than 10%. Thus within the analysed area, the stress variation can be considered within the limits of the standard error or close to it. Between areas the differences in the estimates can reach values of nearly 85%.

(ii) The second aspect is related to temperature. As mentioned before temperature is not taken into account in the used models. Mercier et al (1977) proposed a relation for the case of grain size dependence on temperature variation:

$$\sigma = m\ D^{-p}\ \exp\ (A/RT) \qquad [6\text{-}20]$$

where A is the stress sensitivity, R is the universal gas constant, T is the absolute temperature and the rest of the elements are as defined previously. White (1979-a, b) suggests that both D and S_g have temperature dependence. Perhaps, in the future the relation between stress and the RGS will include factors such as temperature.

(iii) Another important factor is the nature of the mechanism which produces the new recrystallized grains. White (1979-a) and Kohlstedt et al (1979) adopt the classification for polygonization taking place either by Bulging mechanisms or by subgrain rotation establishing high angle boundaries, hence a new grain (cf Chapter 5).

An unanswered question at the present is: does the type of the mechanism of RGS formation affect the size of the grain and consequently the stress estimation? Metallurgists have shown that the relation between differential stress and the RGS only applies for the mechanism of 'Bulging' by grain boundary migration (see Tullis 1979, pp.144). White (1979-a) goes even further by pointing out that both the Twiss and Mercier models are appropriate for 'Bulging' simply because in the event of RGS by rotation of subgrains this would imply in production of new grains of the same size as the subgrains. This means that the appropriate relation to be used in subgrain rotation is that of [6-2] rather than [6-3].

Etheridge and Wilkie (1979 p.461) pointed out that their Paleopiezometric study indicates that the RGS originated from rotation of subgrains. Poirier and Guillopé (1979, p.67) stressed the importance of recognizing the regime of grain recrystallization. Their observation for halite indicates that if the nature of the recrystallization is neglected there could be an error of an order of magnitude in the results. However one cannot be sure of the origin of the grains in the case of sections showing grains completely recrystallized. Plate 6-1 is the only sample where it was observed that two markedly different RGS(s) were present. The rest of the sections showed a much more constant size distribution. This size difference in plate 6-1 can be interpreted as: (i) due to the presence of phyllosilicates, (ii) as a result of superimposed deformation events in which it was not possible to reset completely the size range of the new grains, or (iii) due to different mechanisms of the production of the recrystallized grains.

Another aspect to be discussed relates to the presence of second phases (phyllosilicates and/or feldspars) and their influence on the RGS, and this appears to be a controversial issue. Bell and Etheridge (1976) reported an inhibition on quartz refinement due to the presence of micas. White (1979-a, b, c) pointed that there is grain reduction in the mica rich layers of quartzitic rocks in two localities at Loch Eriboll. In Chapter 5 of this study it was reported that the presence of phyllosilicates could be correlated with the observed coarser RGS provided the quartz-porphyroclasts accounted for at least 50% of the section. When recrystallization was complete,or very near that limit,there was no noticable difference between samples richer and poorer in phyllosilicates.

6.5.2 From Other Studies in the Mapped Area

6.5.2-a The Microstructural Parameters, Other than the RGS

The first topic to be discussed in this section relates to the interaction between the microstructural parameters defined earlier in this chapter and the possibilities of interference and over-printing effects. Care must be taken when applying paleopiezometric techniques because of the possible post-deformation recovery effects which may alter the deformation induced microstructures and this invalidates the use of relations [6-1] to [6-3]. In other words, it must be assured that the dynamic induced microstructures have not suffered any significant modifications after the stresses have been removed.

The analysed fabrics lead us to believe that the studied sections clearly exhibit quite different microtextures, characterizing the evolution of a zone of progressive deformation. There seems to be little evidence of annealing effects having taken place which means that the records of the deformation conditions might well be still 'frozen in'. The reason for this could be perhaps due to (i) the driving forces at low stresses (and temperatures) were insufficient to cause grain growth in the post deformation regime. That is, the grain growth kinetics become too slow to allow any significant grain size increase (cf Twiss 1977, p.235). (ii) The presence of a second mineral-phase may interfere causing an inhibition on grain growth (Hobbs et al 1976).

As explained in the first two sections of this chapter, the dislocation density (ρ) and the subgrain size (Sg) also bear definite relationships with the differential stress but these two microstructural parameters require the use of the TEM. Twiss (1977) points out that optically measured (ρ) are unreliable and this restricts the use of such parameters. The present study did not include measurements of (ρ) and (Sg) but these have been estimated for some of the rocks within the studied area, and therefore it is worthwhile to use the results as a complement of the present study.

As stated in section 6-2 the recorded dislocation density (ρ) in the rocks is liable to further changes due to recovery or any other stresses that might have operated on these rocks which may not be directly connected with the episode of interest. Weathers et al (1979-a, figs. 9, 10) report that for the analysed quartz-rocks of Glencoul and Knockan Creag areas, the dislocation density was independent of the distance from the Moine Thrust Fault. For Eriboll they reported that there were only a 'few' samples but their estimations indicated that the (ρ) remained the same on both sides of the fault (in the zone of the Moine Thrust?). Compared to Knockan Creag the dislocation density decreased by a factor of 4 but the estimate differential stress is in the order of 100 MPa (see Weathers et al 1979-a, Table I). which is approximately 41% higher than the highest RGS-estimate of the present study.

As pointed out by Kohlstedt et al (1979, p.404) the above discrepancy in the value of the estimates could result from the slow response to stress change by the recrystallized grains, compared with the dislocation density, or there could be some errors due to the reduced amount of data. The last argument is the one favoured by Kohlstedt et al (1979).

The relevant information in the present case, is the existence of large densities of dislocations, which make it less probable that the recrystallized grain size (RGS) is a structure due to an annealing phase but favours an origin due to syntectonic deformation of the measured new grains.

Subgrain size can be assessed using the optical microscope. However, Mercier et al (1977) pointed out that the optical measurements overestimate the subgrain size. White (1973) warns that a TEM gives smaller figures for (Sg) because it reveals that optical subgrains are constituted of a clustering of even smaller subgrains. The same seems to apply to the recrystallized grains and the reason for the non-detection of such 'grain in grain' structure (ie by optical means) is possibly due to the similarity in orientations of those domains (see White 1973).

White (1979-b) measured subgrain sizes in both Moinian and Paleozoic quartzitic rocks at Eriboll. The values decreased into the mylonitic zones (Ben Heilan and Alt Oldhrsgaraidh) and then remained constant. For the Pipe-Rock of Ben Heilam these sizes range from 13.7 μm to 3.7 μm while for the Moinian Mylonites the decrease was from 13.6 μm to 2.6 μm. The estimated differential stresses indicate 37 MPa outside the mylonite of Ben Heilam, increasing up to 130 MPa. For the Moine

Mylonite the increased reached 180 MPa. White (1979-c, table 2) used subgrains to estimate the differential stress across Pipe-Rock mylonite from a shear zone of the imbricates of the Heilam Nappe at Ben Heilam. He used equations derived by Ardell et al (1973) and Twiss (1977) in which the former overestimate the latter by a factor of approximately 2.65. However, both equations reveal that stress increases across 20-25 cm (maximum) of Pipe-Rock mylonite, by a factor of exactly 3.5.

Subgrains, which are structures of low angle boundaries, do not restore or change with stress relief (cf section 6.2). These are low energy structures and are more stable than the other two microstructural parameters, whose behaviour has been described before. These three distinct 'behaviours' are very convenient in that they work as different sensors, recording more information about the deformation history of a study zone. Subgrains record the maximum stress intensity, while recrystallized grains reveal more about the latest intense deformation event and the dislocation density can tell us about the post deformation conditions (see Ross et al 1980). The difference in the behaviour between the last two microstructural parameters is that the former require comparatively greater strain intensities to be totally reset (and for that reason they may show the existence of two distinct stress phases) while the latter are liable to be modified or partially readjusted by a change to new stresses and-or temperature regimes.

Comparing White's (1979-b, c) paleostress estimates using subgrains with the RGS estimates of the present study we can observe that: (i) White's lower estimates are in excellent agreement with this study's results for Arnaboll, Hope or even Kempie's samples below the b-thrust. (ii) However, White's highest stress values exceed by a factor of nearly 3 the highest paleostress estimate for the whole studied zone. White (1979-b) associates these high localized stresses recorded by (Sg) with the mylonite formation, while the results using (D) he suggests, tend to approximate to the regional background stresses.

6.5.2-b Comparison of Results Using RGS

The comparison with other estimations related to the present study area is aimed not only to complement the information contained in tables 6.1 but also to give some idea of the reliability of the estimates obtained by the present work. This section also intends to highlight some of the difficulties discussed in section 6.3-b.

The paleostress determinations, using RGS, for Eriboll area are listed as follows:

1) White (1979-a, Table II) measured RGS both optically and with the TEM. Results relate (from sampling, at grid ref.399516 ,which is outside the limits of the present mapping) with distance of the Moine Thrust as follows:

Lithology	Optical	TEM	Distance from the Fault
a - Mica-rich Quartz Mylonite	42.9 µm	-	far
b - Mica-rich Quartz Mylonite	12.8 µm	-	20 m
c - Mica-free Quartz Mylonite	14.0 µm	9.8µm	10
d - Mica-free Quartz Mylonite	18.6 µm	11.8	0.5

2) White (1979-b) reported a decrease in RGS towards the studied mylonitic zones, and then a stabilization of the measured grain size. Results refer to samples from the Pipe-Rock of Ben Heilam and to Moine Mylonites of Alt Odhsgaradaidh and have the following range:

(i) Pipe-Rock (PR): 24.6-14.6 μm; (ii) Moine Mylonites (MM) 42.9-18.6 μm. White also concluded that the estimates of the differential stress range from 50 to 100 MPa. The above measurements, if used directly in the 2 models, give the following stress estimates: Model by Twiss: (PR) 75.8-108.1 MPa; (MM) 52.0-91.7 MPa, or Model by Mercier: (PR) 52.7-76.4 MPa; (MM) 35.5-64.3 MPa.

From the above stress estimations it is difficult to guess which model was used to determine the mentioned range of 50-100 MPa. It is not known if the quoted sizes of White: (i) represent the mean of the measurements taken directly from the planar sections, or (ii) have been corrected for truncation and overlapping effects, in analogy to that explained in section 6.4. In case the first possibility is correct, there should be a correction factor. For instance if we use [6-12] for the reasons explained in section 6.4.2 we obtain:-

Model by Twiss: (PR) 51.8-73.9 MPa; (MM) 35.5-62.7 MPa or

Model by Mercier (PR) 35.4-53.3 MPa; (MM) 23.9-43.2 MPa.

These estimates are now very similar to the range of results displayed in tables 6-1. This also illustrates some of the difficulties in interpreting and comparing results which have not been described in detail.

3) White (1079-c, table 2) describes the measurements (both optical and TEM) across a narrow Mylonitic Zone of Pipe-Rock of the Ben Heilam Nappe.

TABLE 6.2-a				
Sample	Optical	TEM	Stress (MPa)	
	μm	μm	Twiss	Mercier
PR	24.6	-	68	39
PRM1	22.2	-	73	42
PRM2	18.2	-	84	49
PRM3	16.0	7.8	91	53
PRM4	14.6	6.0	97	57
PRM5	-	2.8	300	183

TABLE 6.2-b	
Stress (MPa)	
Twiss	Mercier
51.8	35.5
55.6	38.1
63.6	43.9
69.4	48.1
73.9	51.3
-	-

Table 6.2-a refers to White's (1979-c, Tables 1 and 2) observations. It can be seen that the Optically measured RGS overestimates the TEM estimates by more than 100%. The range or stress estimates in this table do not conform with those found in the present study.

Table 6.2-b represents this study's stress estimates using the optical sizes of table 6.2-a.; ie the optical sizes quoted in White (1979) are interpreted here as correspondent to ($\bar{d}$) and therefore require correction to (D) using [6-12]. The stress values in table 6.2-b accord extremely well with those in tables 6.1.

4) Finally we deal with the related work in the papers by Weathers et al (1979-a) and Kohlstedt et al (1979). It is unfortunate that these two papers do not give precise information about: (i) the exact location of sampling in Eriboll, (ii) the method of measurements, and (iii) the exact number of samples used.

Kohlstedt et al (1979, pp.402-403) reports that grains were measured optically for the Glencoul area and that the estimations (for Glencoul, Knockan Creag and Eriboll) involved 30 samples.

It is clear that they used Mercier's Model for the stress estimation. However there seems to be a contradiction in some of the quoted values (see Weathers et al 1979-a, p.7506, table I results in the last two columns) because if the RGS for Eriboll is 20 μm, we obtain approximately 63.23 MPa (for Mercier et al, 1977) or 88.03 MPa (using Twiss 1977), instead of their quoted value of 45 MPa (Mercier Model). An estimate of 45 MPa corresponds (see fig. 6-1, for Mercier's curve) to 31.507 μm using the appropriate relation [6-7].

Once more, their only indication of the sampling size(s), in both papers, points to some place above Kempie Bay, Eriboll. If their specimens come from the same rocks used in the present study, their size measurement does not coincide with that listed in table 6.1-a. However we cannot exclude two possibilities:

(i) again, if corrections for truncation and overlapping effects are applied for the quoted figure (ie $\bar{d} \simeq 20$ μm) we obtain $D \simeq 35$ μm which gives 41 MPa (Mercier) and 59.6 MPa (Twiss). These are well within the present study's results for Kempie area (see bottom line of table 6.1-a).

(ii) On the other hand if 20 μm does correspond to this study's ($\bar{d}$), we might conclude that they used a correction factor for spatial distribution of nearly 1.575, in order to give $D \approx 31.507$ μm, thus $\sigma = 45$ MPa. This correction factor is closer to relation [6-11] derived from Exner (1972).

The above comments and speculations on these five works on Paleostress estimates at Eriboll should justify some of the comments on the difficulties mentioned in section 6.3 and emphasize the need for standardization in the methods used. White (1979-b) warned about the problem of standardization and mentioned that he measured 100 grains in every sample, in a direction perpendicular to grain elongation. From this it was concluded that he used an intercept length estimation procedure, rather than for instance, an area equivalence method. That is the only clue to the method used for size measurement, contained in White's (1979-b) paper.

Another important question is how do the results presented in this section compare with those found by the present study? Weathers et al (1979-a) report variations in stress estimates in order of 100% between Glencoul and Eriboll areas, which are separated by 50 km. The stress estimates for the analysed 57 sections of tables 6.1 also show variations of nearly 85% in a much shorter distance. However, if the means of the estimates in each area do represent the real 'gradient' between locations, the difference then reduces to approximately 15% as can be shown by the synoptic results of tables 6.1.

In White's (1979-c) case, the reported results produced differences of 460% in a mere 20-25 cm. Perhaps this is only a localized result, but it is quite clear that both White's and this study's results, cannot share the views by Kohlstedt et al (1979) and Weather's et al (1979-a) in that for Eriboll the stress was independent of the distance of the (unspecified) fault.

6.6 Concluding Remarks

Poirier and Guillopé (1979) considered that the RGS is best piezometer, even better than dislocation density or subgrainsize, although this latter is the more reliable (White 1979-a, Ross et al 1980-a) in that it is not affected by stress relief. Ross et al (1980-a) emphasised the usefulness of the RGS in recording both the increase and decrease in stress levels occuring during the deformation history of an area. They point out the possibility of the existance of more than one modal class of RGS present in the section being due to the interference of more than one deformation event.

There are still some matters not fully understood and for this reason the technique of paleostress estimation should improve in the coming years. However the existence of some discrepancies and the lack of standardization neither discourages nor invalidates the actual use of those measurements. On the contrary, the estimates for the studied area show very coherent correlations with field observations. The variation in the recrystallized grain size, in the broad sense, reflects the stress-gradient that should be present during the development of the zones (Nappes) in the studied area. The mylonitic microstructures are here interpreted as being developed by recrystallization accompanied by decrease of the RGS towards the sheared domain and this seems to follow a pattern of increase in the amount of the finite strain.

The present study was unable to reach a definite conclusion on the role of the presence of phyllosilicates. It relies on an analysis based solely on textural descriptions and RGS measurements did not give the necessary arguments for firm conclusions. Therefore this matter deserves a closer scrutiny by other methods.

The results obtained with paleostresses estimators should not be crudely utilized but instead carefully analysed and correlated with field and textural observations. In this way paleostress estimators do help to develop an overall interpretative view.

CHAPTER 7

RHEOLOGIC CONSIDERATIONS

7.1 Introduction

The ultimate aim in a study of deformation of a zone is to determine or at least to correlate the stress and the strain history in a domain during a certain period and to explain the existence of some of the observed microstructures.

To deal with the various rates and mechanisms of deformation that would lead to steady flow (cf Stocker and Ashby 1973) in a deformation zone it is necessary firstly to know the conditions under which these mechanisms are dominant. The main difficulty is, however, to establish the correct flow-laws governing the relation between stress-strain at the time of deformation. One difficulty stems from the fact that flow laws are generally extrapolated from laboratory experiments in which only one phase is the object of the analysis. However, the natural geological examples involve polycrystalline aggregates in which the components (phases) may have different dimensions and were submitted to deformation conditions not exactly matched by laboratory simulations.

The theoretical knowledge about isolated mechanisms responsible for deformations come mainly from metallurgical studies and have been initally proposed by Nabarro (1948), Herring (1950), Weeterman (1955) and Coble (1963). However, the confirmation of their operation dates only from the early sixties (Squires et al 1963; in Elliott, 1973). For non-metallic crystalline aggregates the situation is more speculative due the the greater complexity of these substances and also the comparatively lower amount of research on these materials.

A few years ago, Ashby (1972) developed the concept of deformation maps based on the idea of the creep diagrams introduced by Weetèrman (1968, see Atkinson 1976-a). Ashby's (1972) maps are systems of stress - temperature co-ordinates displaying the dominant mechanism of flow. The field is divided into three independent mechanisms and a point in that plane indicates not only which is the dominant process but also the amount of strain-rate corresponding to the stress-temperature co-ordinate. That concept was subsequently applied to olivine, by Stocker and Ashby (1973) in a rheological study of the upper mantle. It was then extended to other minerals such as quartz (White 1976-a; Rutter 1976), galena (Atkinson 1976-a, 1977; McClay 1977), calcite (Rutter 1976).

From a study of deformation of pure aluminium, Mohamed and Langdon (1974) modified Ashby's (1972) original approach by introducing deformation maps based on a co-ordinate system of stress-grain size. They also simplified much of Ashby's original mathematical treatment. From the engineering point of view the approach by Mohamed and Langdon (1974) seems to be more realistic because it is quite probable that temperature is specified (or can be controlled), thus allowing stress and grain size as the variables.

More recently, a slightly different idea was put forward by Etheridge and Wilkie (1979) in that they used the Evans and Langdon (1976) treatment which, takes into account the effects of grain boundary sliding and this was not included in any of the previously mentioned maps. Evans and Langdon (1976) used Gifkin's (1975) constitutive equations in their work.

In the present study we shall deal with both types of maps: (i) Ashby's (1972) and (ii) Mohamed and Langdon's (1974), as it will be shown these two types prove to be useful in different situations, thus allowing complementary views in the same study.

7.2 Flow Mechanisms and Equations

As defined previously for section 5.1 the deformation mechanisms are divided into three groups (cataclastic, intracrystalline and diffusional). Particular attention will be given in the present section to the constitutive equations of the last two groups of mechanisms: (i) intracrystalline flow by dislocation creep (DC) mechanism, and (ii) diffusional transfer of matter which can be accomplished either via bulk [Nabarro-Herring (NH) mechanism] or boundary [Coble Creep (CC) mechanism] of the matter.

7.2-a The Constitutive Equations

Each of the defined deformation mechanisms are described by rate equations that are functions of stress, temperature and some structural parameters characteristic of each material. These constitutive equations are presented below:

1. Dislocation Creep (DC) - The equation used here is the one given by Ashby (1972) and it is widely adopted in the geological literature (see White (1976-a, Atkinson 1976-a, 1977).

$$\dot{e} = \dot{e}_{DC} = \frac{D_v G b}{kT} \left[\frac{\sigma}{G} \right]^n \qquad [7.1]$$

where $\dot{e}$ is the strain rate and the following parameters' values are here for quartz: G is the shear modulus ($\simeq 4.2 \times 10^{11}$ dyn.cm^{-2}); b is the Burger's vector ($\simeq 5$Å); k is Boltzmann's constant [$\simeq 1.38 \times 10^{-16}$ eng. mol^{-1}(^{o}k)$^{-1}$], T is the absolute temperature; σ is the stress either differential or deviatoric (bar). D_v is the bulk diffusion coefficient, defined by the relationship:

$$D_v = D_o \exp\left[-H_v/RT\right] \qquad [7-2]$$

where the following parameters' values are defined for quartz: D_o is the absolute diffusivity ($\simeq 5 \times 10^{-14}$ cm^2.s^{-1}, cf White 1976-a);

R is the Universal Gas Constant [$\approx 8.31434 \times 10^7$ eng. mol^{-1} $(^{o}k)^{-1}$]; H_v is the activation energy for volume diffusion ($\approx$84 KJ. mol^{-1}, cf White 1976-a, see also Rutter 1976) and finally the Dorn-parameters (n) and (A) which proved to be dependent (cf Stocker and Ashby 1973, pp.402-403) on the following empirical relationship:

$$n = 3.07 + 0.29 \log_{10} A \qquad [7\text{-}3]$$

The value of (n) varies from substance to substance. For quartz, a value of 4 has been used (cf Rutter 1976, White 1976-a, p.80) which makes Dorn's (A) parameter equal to 1610.263 (dimensionless).

2) Diffusional Creep (DF) - The representation for the two mechanisms Nabarro-Herring (NHC) and Coble Creep (CC) is based on combined equations (see Raj and Ashby 1971, Ashby 1972). Adopting White's (1976-a, 1977) notation, constants and values of parameters for quartz:

$$\dot{e} = \dot{e}_{df} = 21 \frac{D_v V\sigma}{kTd^2} \cdot \left[1 + \frac{\pi\delta}{d} \cdot \frac{D_b}{D_v} \right] \qquad [7\text{-}4]$$

where V is the atomic volume ($\approx$23.6 $cm^3.mol^{-1}$, see Robie et al 1966); d is the particle grain size; δ is the grain boundary width ($\approx 2 \times b \approx 10^{-7}$ cm). D_b is the boundary diffusion coefficient, defined by an analogous relationship to that of [7-2].

$$D_b = D_o \exp [-Hb/RT] \qquad [7\text{-}5]$$

where H_b is the activation energy for boundary diffusion. Usually the followed relationship is $H_b = 2/3\ H_v$ (cf Rutter 1976), but for the deformation maps constructed in this chapter, use was made of White's (1976-a) value, as: $H_b = \frac{1}{2}H_v$ = 42KJ mol^{-1}. The other parameters in [7-4] are as defined previously for [7-1].

The combined equation [7-4] yields two processes: Nabarro-Herring Creep (NHC) when $[\pi\delta D_b/dD_v] \gg 1$ and Coble Creep (CC) in the limit that $[\pi\delta D_b/dD_v] \ll 1$.

It has been shown that the above constitutive equations require a great deal of information about rheologic parameters and state variables such as P-T (cf Stocker and Ashby, 1973), many of which have been obtained by combinations of experimental work and experimental observation. In this study the values for the different parameters were listed together with their definition in order to avoid possible confusion. It must be pointed out, however, that there are currently some disagreements about relationships and values for some parameters, not to mention the fact that the original constitutive equations were derived for metals, which are significantly less complex than silicates. The following comments on the construction of maps are noteworthy:

(i) Equations in papers such as Stocker and Ashby (1973), Mohamed and Langdon (1974) and White (1976-a), differ in some aspects, and thus diversity can lead to some confusion, apart from preventing direct comparisons.

(ii) It is clear that diffusivity data for quartz is rather poor (White 1976-a, 1977) and this is due to the fact that the available values are solely based on experiments conducted by Tullis <u>et al</u> (1973). This could possibly mean that the subsequent extrapolations do not correspond to the real values just described and referred to in many studies. Published maps for quartz have only corrected Tullis <u>et al</u>'s (1973) data for temperature variation. Pressure effects (see Atkinson 1976-a) on diffusivity of quartz have been ignored. R. Knipe (pers. Comm. Sep' 80) has attempted a correction for pressure - which gives an increased diffusivity at lower temperatures. The result is a relative increase in the strain rate at lower temperatures.

(iii) Shear modulus (G) is most certainly affected both by (P) and (T). For studies using quartz, there is no expression for a P-T correction. It seems that the correction could consist of a simple linear interpolation. Stocker and Ashby (1973) took into account P-T variations in their study for olivine, using:

$$G(T,P) = G_o \left[1 + \frac{1}{G_o}\left[\frac{\partial G}{\partial T}\right](T-T_o) + \frac{1}{G_o}\left[\frac{\partial G}{\partial P}\right](P-P_o) \right] \qquad [7\text{-}6]$$

where G_o and G correspond to the shear modulus at (T_o) and (P-T) respectively, while $(1/G_o)(\partial G/\partial T)$ and $(1/G_o)(\partial G/\partial P)$ are the temperature and pressure dependent shear moduli respectively. Atkinson's (1976-a) work for galena derived a shear modulus expression taking into consideration only temperature corrections:

$$G_t = G_{293} \; [1 - (T-293)(1/293)(dG/dT)] \qquad [7\text{-}7]$$

where the subscript stands for $t=20^{o}C$ and the rest are as defined in [7-6] .

(iv) The molar volume has also temperature dependence and this is neglected here.

(v) The boundary width (δ) was taken here as equal to 2b ($\simeq 10^{-7}$ cm), a procedure used for metals (Rutter 1976, White 1976-a, 1977). However, McClay (1977) gives us an indication that for non metallic materials, δ could well be as high as 100 b.

7.3 Deformation Maps

The prime aim of this section is to deal with deformation mechanism(s) responsible for the achievement of large strains. This can be done by using simple plots such as the deformation maps (cf Ashby 1972) which are diagrams having their areas divided into three fields, each one characterizing the domain in which a deformation mechanism becomes dominant. However the fact that a deformation mechanism is dominant does not exclude the possibility of contributions by other mechanisms. This is particularly important especially in region of the boundaries which limit the three mentioned fields. The balance of contributions for different mechanisms increases with the proximity of the junction line.

The deformation maps show strain rate contours and these maps give information about the range and conditions where the contribution of each mechanism is important. There seems to be more than one way of obtaining the strain-rate contours: (i) using Ashby's (1972) original method in which for each specific field we completely ignore the contributions of other mechanisms (Atkinson 1976-a), or (ii) as in Mohamed and Langdon's (1974) simplified approach, which is suitable where computer facilities are not to be used. (iii) An idea put forward by Stocker and Ashby (1974, p.401-407) is to consider that the total strain takes into account compatible contributions such as:

$$\dot{e}_{total} = \dot{e}_{\substack{dislocation\\creep}} + \dot{e}_{\substack{diffusion\\creep}} \qquad [7\text{-}8]$$

This makes use of relations [7-1] and [7-4] which are substituted in [7-8] and then solved either for one of the variables σ or T. The boundaries between the fields of the deformation mechanisms can be determined by finding the loci of points where contributions of pairs of mechanisms are equal. Boundaries between dislocation and diffusional creep can be obtained by equalizing equations [7-1] and [7-4], while in order to delimit the junction between Nabarro-Herring and Coble

Creeps, this study equalized Hertzberg's (1976) equations:

$$\dot{e}_{NHC} = \frac{7\sigma D_v b^3}{kTd^3} \quad [7\text{-}9]$$

and

$$\dot{e}_{CC} = \frac{50\sigma D_b b^4}{kTd^3} \quad [7\text{-}10]$$

where subscripts NHC, CC stand for Nabarro-Herring Creep and Coble Creep respectively, and the elements of each equation are as defined previously in section 7.2.

Equations 7-9 and 7-10 emphasize the importance of the grain size in a grain boundary diffusion mechanism, while for dislocation creep this parameter is non existent. It can also be seen that the strain rate is inversely proportional to the square of the grain size if the field is for Nabarro-Herring Creep (higher temperature) while for Coble Creep this relation is inversely proportional to the cube of the grain size.

The deformation maps, for quartz, constructed in the present study are displayed in figs. 7-1-a to h. The co-ordinate axes in these diagrams are Stress (bar) in logarithmic scale and Temperature (^{o}C). Many papers also make use of log-normalized scales of σ/G (eg Ashby 1972, Stocker and Ashby 1973) or $\sigma/\sqrt{3}\ G$ (eg Atkinson 1976-a) versus homologous temperature ratio T/Tm, where Tm is the absolute temperature at the melting point of the substance. The purpose of these normalized ratios is mainly to allow comparisons between different materials (Atkinson 1976-a). In the present study only one mineral is analysed and for that reason no other scales are provided in the diagrams of figs. 7-1.

In order to fulfil the most probable range of meaningful geological conditions, the co-ordinate axes were calibrated as follows:

Figures 7.1. Deformation maps for quartz according to grain sizes. Strain rates contours are shown in diagrams from a to h. See text for explanation.

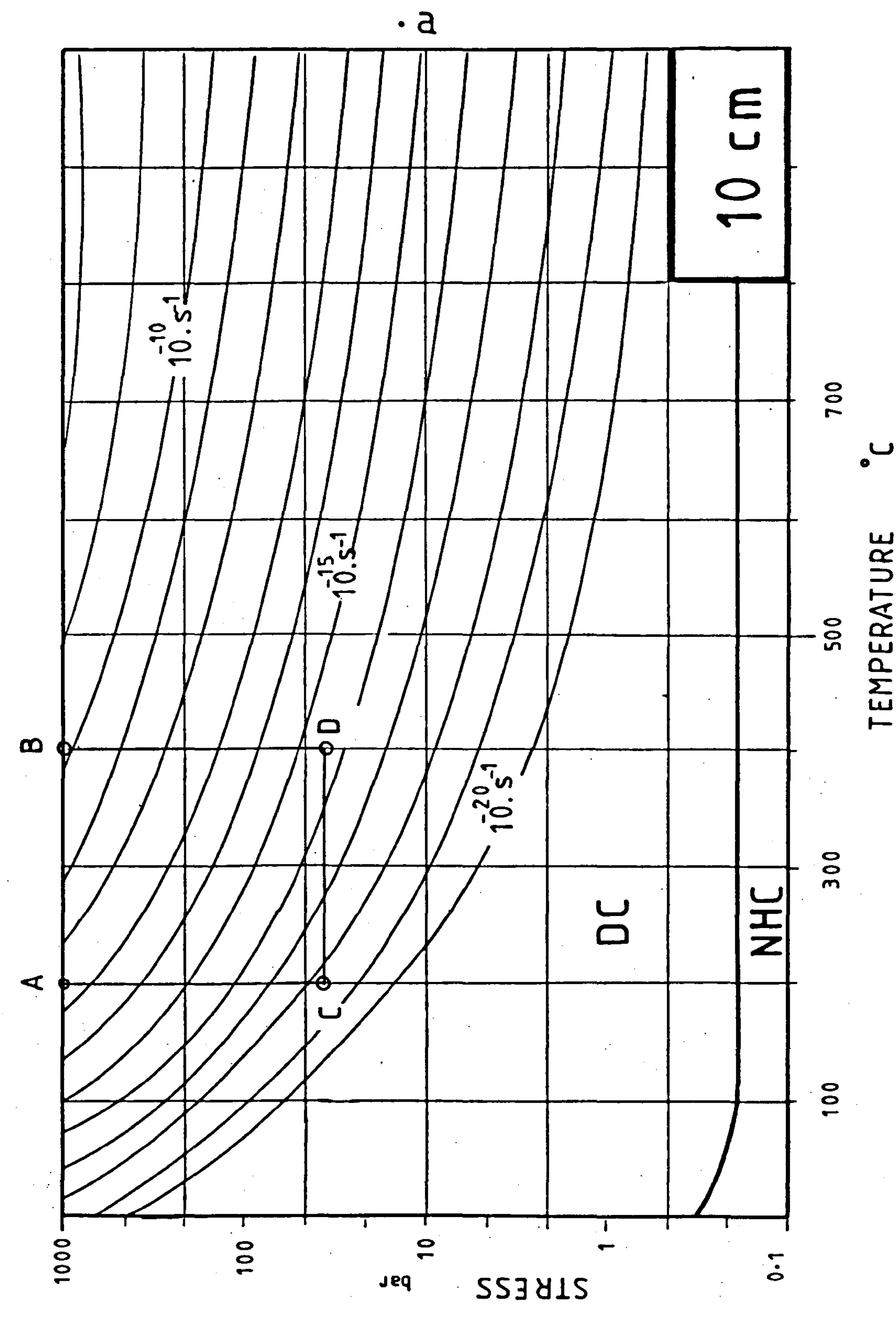

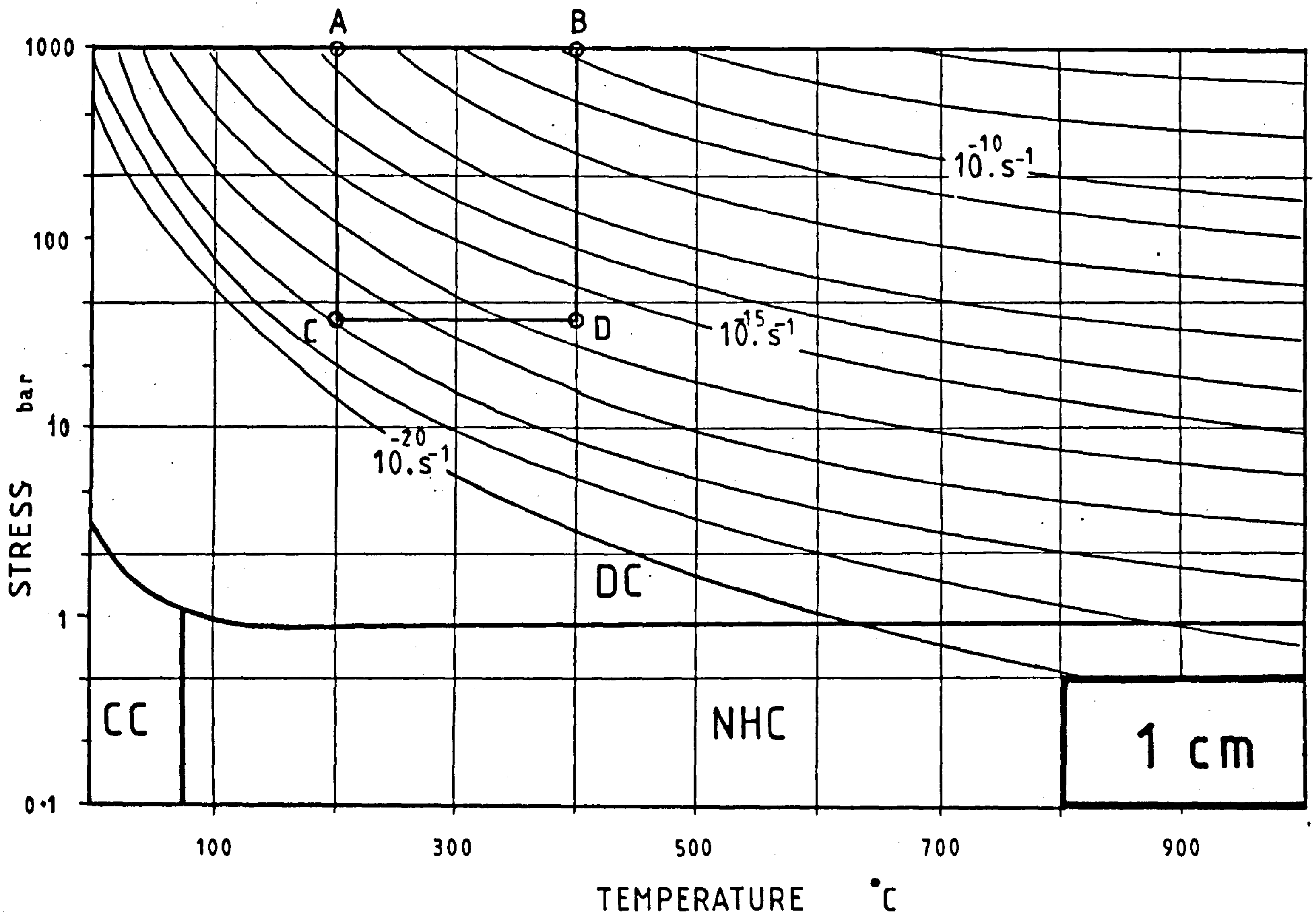
A
B
C
D
1000
100
10
1
0·1
STRESS bar
$10^{-10}.s^{-1}$
$10^{-15}.s^{-1}$
$10^{-20}.s^{-1}$
DC
CC
NHC
1 cm
100
300
500
700
900
TEMPERATURE °C

b.

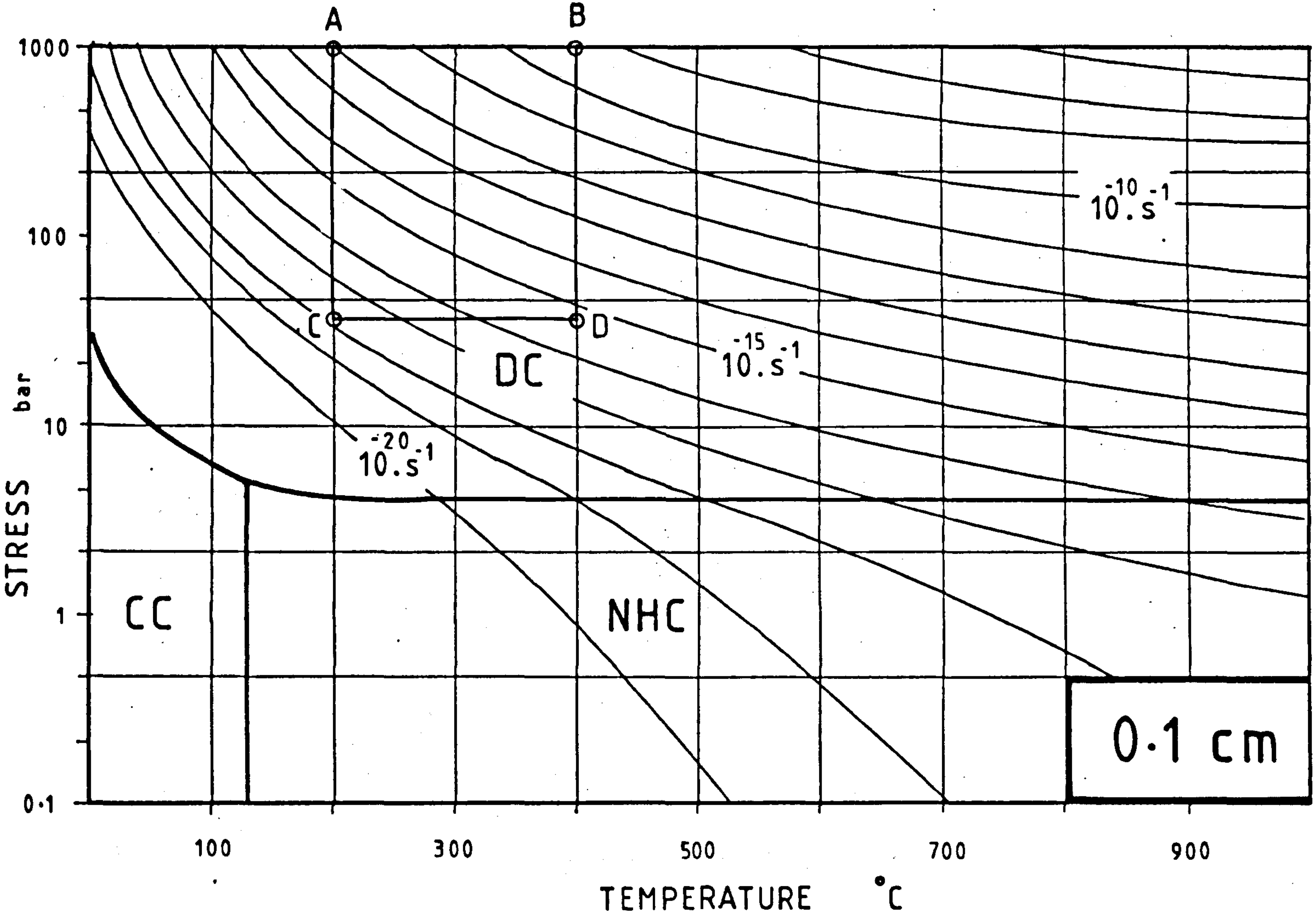
A
B
1000
100
10
1
0·1
STRESS bar
C
D
DC
CC
NHC
10.s-1 (exponents -10 and -1)
10.s-1 (exponents -15 and -1)
10.s-1 (exponents -20 and -1)
100
300
500
700
900
TEMPERATURE °C
0·1 cm

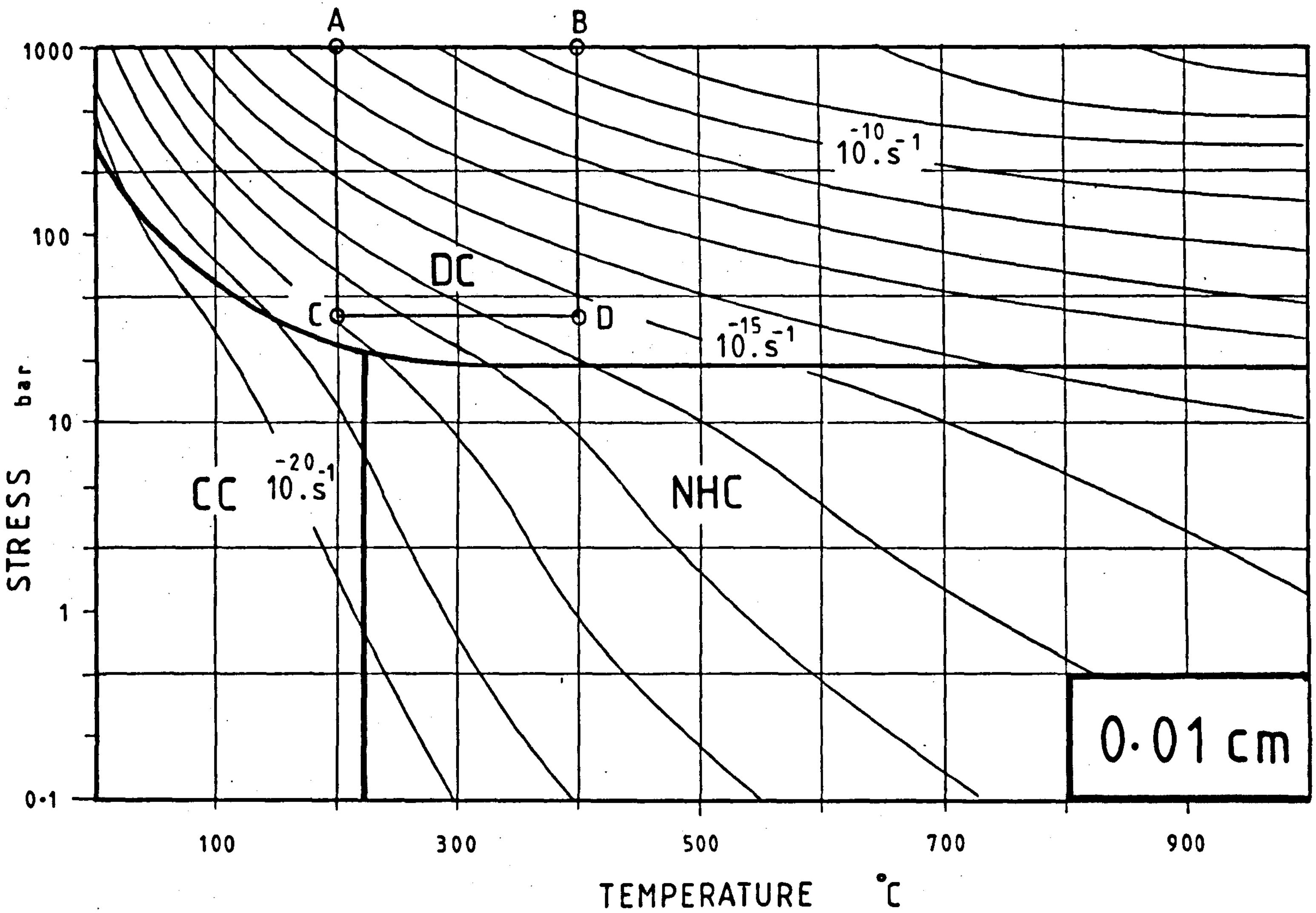

A
B
1000
100
10
1
0·1
STRESS bar
DC
C
D
$10^{-10}.s^{-1}$
$10^{-15}.s^{-1}$
$10^{-20}.s^{-1}$
CC
NHC
0·01 cm
100
300
500
700
900
TEMPERATURE °C

d.

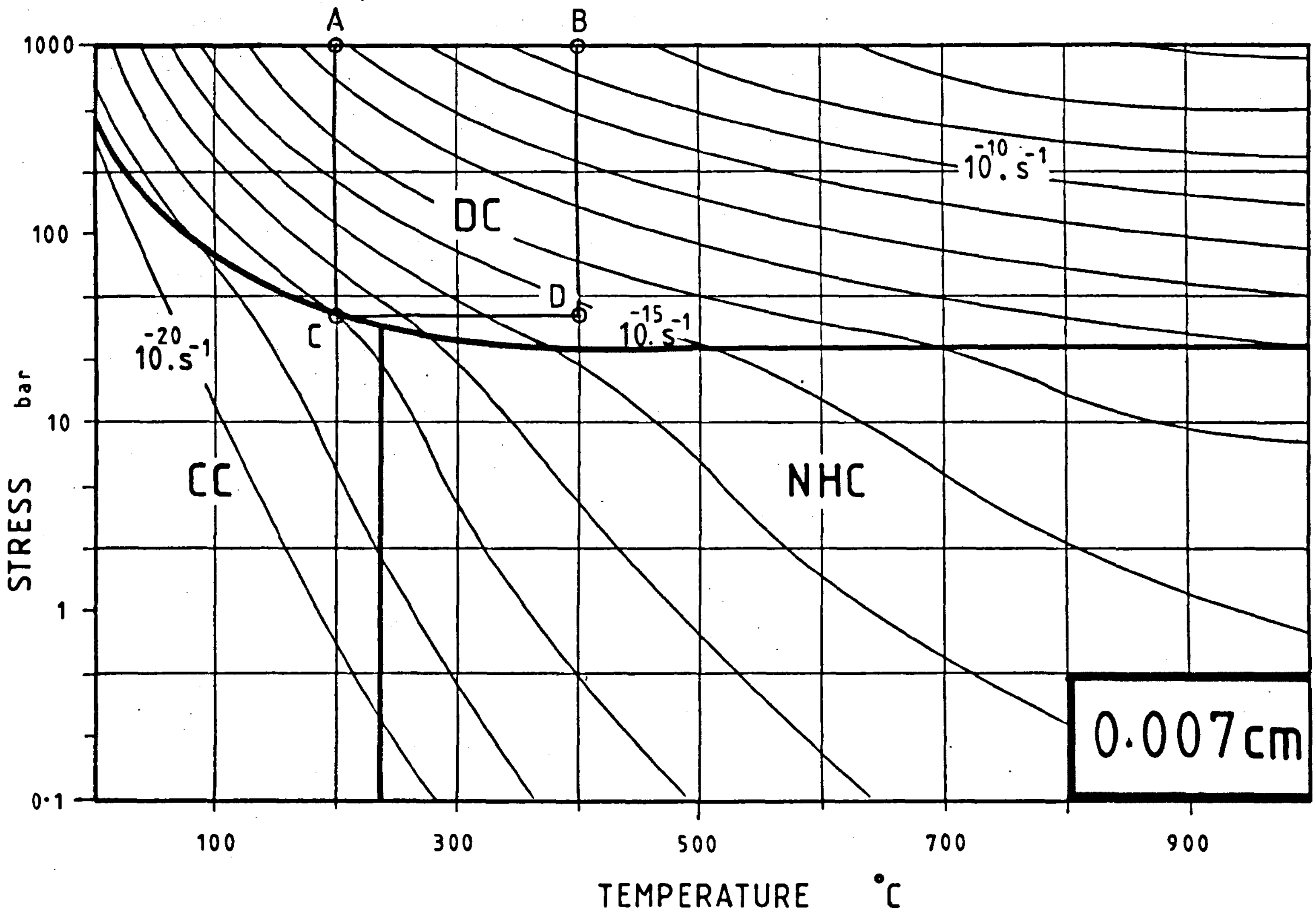

A
B
1000
100
10
1
0·1
STRESS bar
10^{-10}. s^{-1}
DC
D
C
10^{-15}. s^{-1}
10^{-20}. s^{-1}
CC
NHC
0·007cm
100
300
500
700
900
TEMPERATURE °C

e.

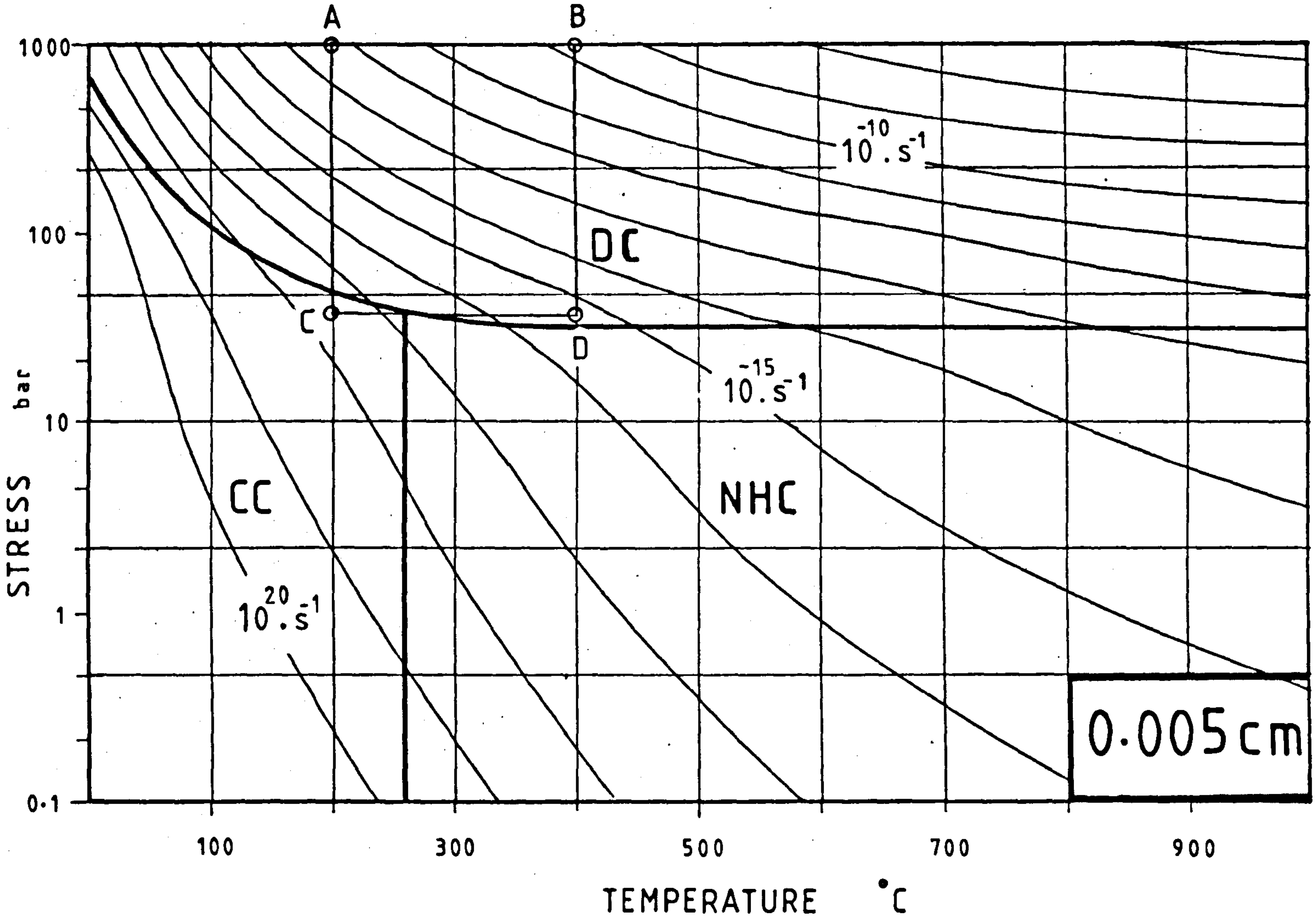
A
B
1000
100
10
1
0·1
STRESS bar
DC
C
D
10^{-10} . s^{-1}
10^{-15} . s^{-1}
10^{-20} . s^{-1}
CC
NHC
0·005cm
100
300
500
700
900
TEMPERATURE °C

g.

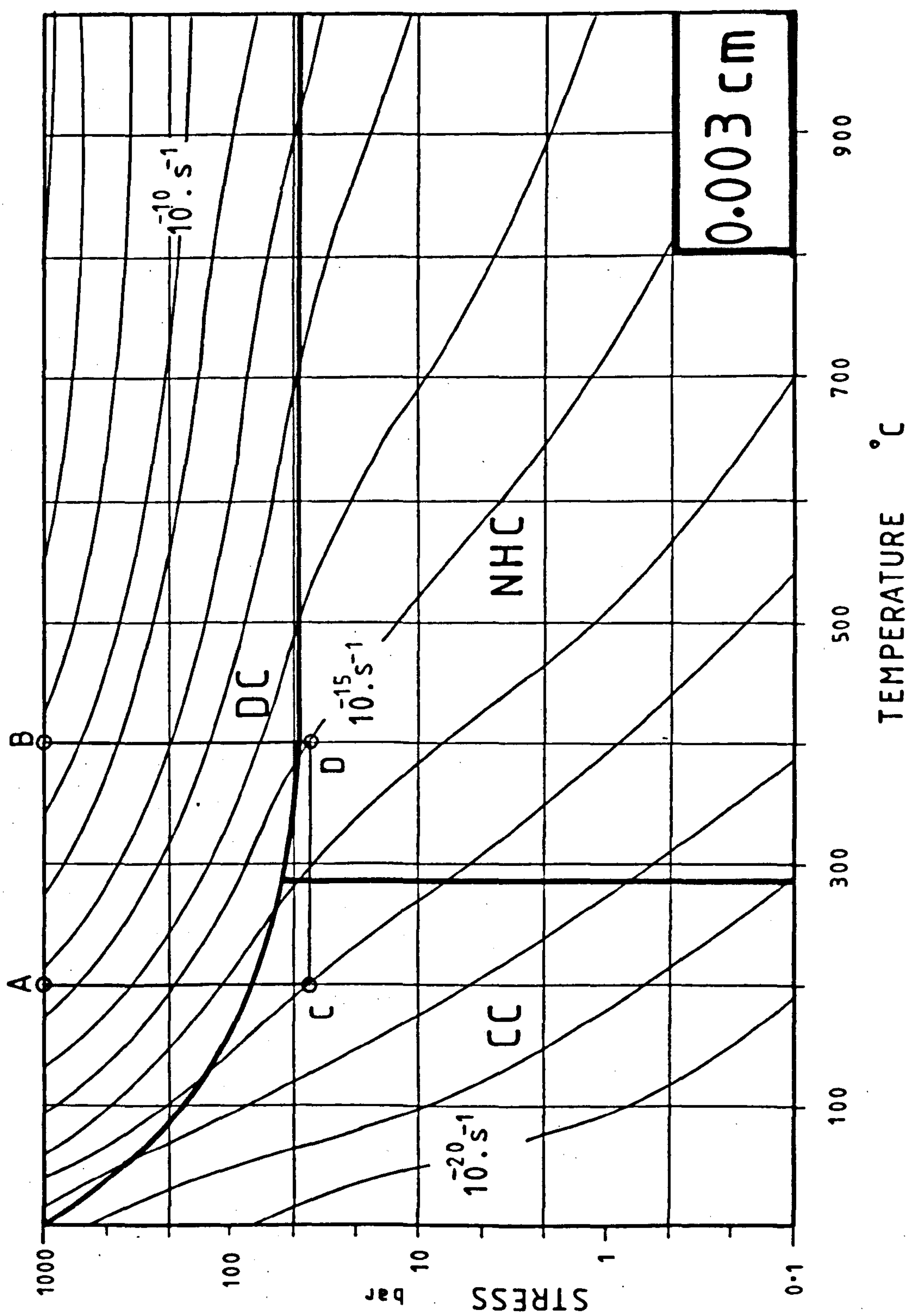

0.003 cm
DC
NHC
CC
A
B
C
D
$10^{-10}.s^{-1}$
$10^{-15}.s^{-1}$
$10^{-20}.s^{-1}$
STRESS bar
1000
100
10
1
0·1
TEMPERATURE °C
100
300
500
700
900

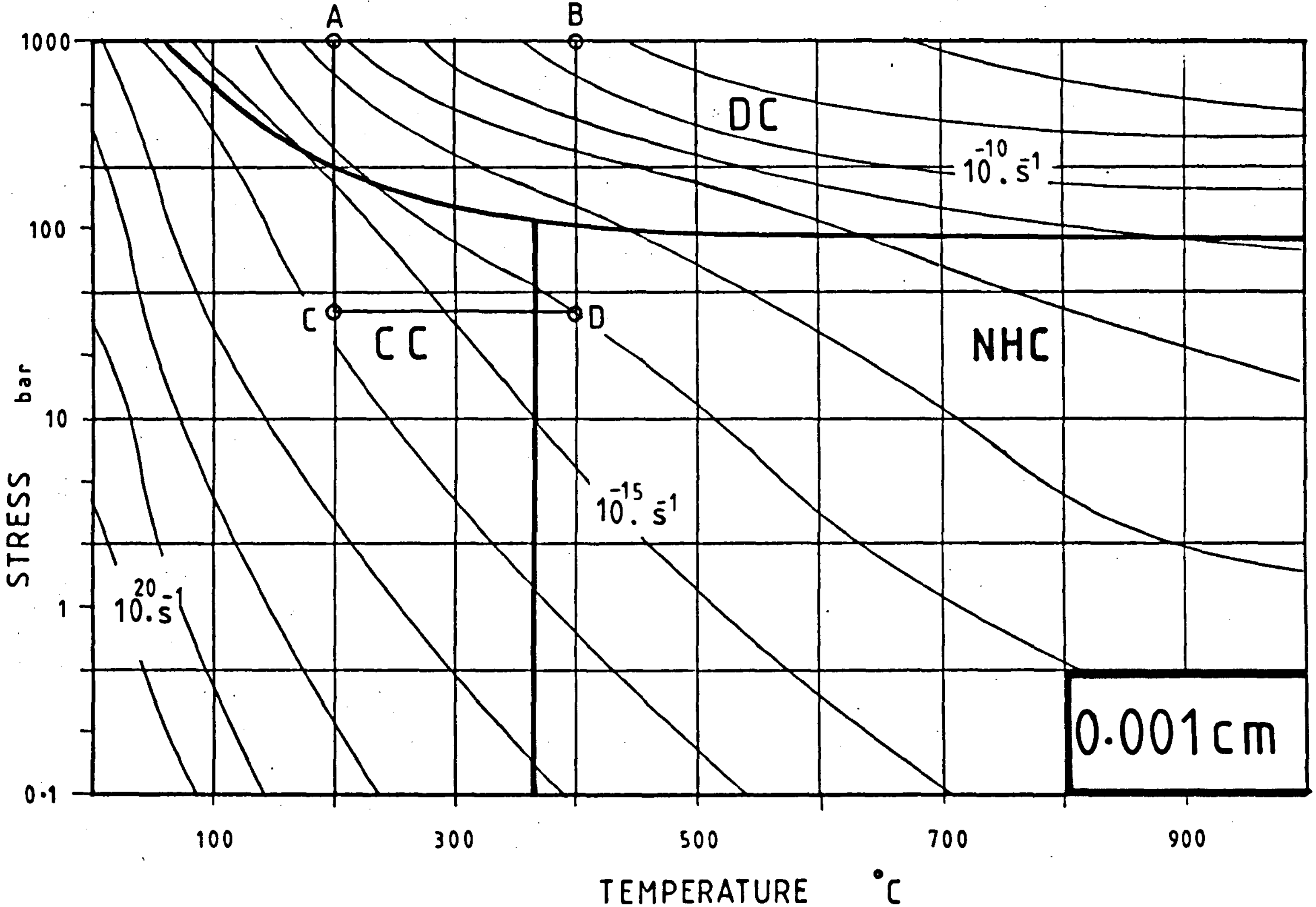
A
B
1000
100
10
1
0·1
DC
10^{-10}. s^{-1}
NHC
CC
C
D
10^{-15}. s^{-1}
10^{-20}.s^{-1}
0·001cm
STRESS bar
100
300
500
700
900
TEMPERATURE °C

h.

(i) The ordinates, with the differential stress (σ) are up to 10^3 bar or 100 MPa, following (White 1976-a, 1977), Rutter (1976) and also based on the range of paleostress estimates (using Twiss 1977 and Mercier et al 1977) which were listed and discussed in Chapter 6.

(ii) Temperatures are up to 1000°C, mainly because some experiments were carried out at values around 600°C-900°C (eg Tullis et al 1973).

(iii) Each map corresponds to particular grain size, (D), specified in the lower right corner). The range of the grain sizes is from 10 cm to 10 μm, because microstructural observations, given in the description of textures in Chapter 5 on grain size (D) evaluations, in Chapter 6 ,place the size distribution for quartz, well within the mentioned range.

(iv) Finally, the strain rate contours have a lower limit of $10^{-20}.s^{-1}$ which is in itself an exaggerated slow value (see Price 1975). Perhaps a more meaningful limit would be 10^{-16} (see also White 1975).

7.4 Discussion

In this section we discuss the application of the deformation maps for the conditions of the studied area. The microstructures and the mineralogy of these quartzitic rocks can be used in conjunction with the stress estimates and the deformation maps, for pure quartz, in order to gain further insight into the deformation conditions that operated in the area (eg.probable range of temperature and strain rate).

It is difficult to stipulate the precise temperature of a deformation belt such as the one of Eriboll-Hope areas. The present study believes that the Quartz-Muscovite-Chlorite mineral suite, which is present in the quartzitic rocks of the studied zone, is characteristic of low grade of (P-T) metamorphism (Cf Winkler, 1974). This mineral assemblage could indicate an upper range of temperatures in the region of lower greenschist facies, while the observed textures in these rocks indicate that the lower boundary of this range is certainly above the diagenesis field. Therefore, this study places the extremes of the probable range of temperatures for the conditions in the Eriboll-Hope areas in the region of 300 ± 100^{o}C (see explanations in Miyashiro 1973, p.439; also Winkler's 1974 figs. 7-1, 7-2).

Before we discuss the conditions of deformation in the area, a brief description of the deformation maps, their uses and limitations will be given. Each of the σ-T diagram of figs. 7-1 can give limited information because it is limited to a particular grain size, and as we saw previously, (Chapters 5 and 6), many of the studied thin sections exhibit more than one modal class. It is possible to combine all the maps of figs. 7-1 in the three dimensional block diagram of the type sketched in fig. 7-2 but this type of diagram is rather difficult to handle. Perhaps the range of temperatures in the studied deformation zone does not vary as much as the observed grain sizes and this could lead to consider the case where the plotting space is in terms of stress and grain size (ie at constant temperature as in figs. 7-3).

It is possible to observe in figs. 7-1 the effects of grain size reduction on changes in strain rates and deformation mechanisms. Suppose we establish, for Eriboll-Hope areas, the most probable range of values for the three co-ordinate parameters as follows:

$$5 < \sigma < 100 \text{ MPa}; \quad 200 < t < 400^{o}\text{C} \quad \text{and} \quad 10 < D < 0.001 \text{ cm}.$$

This corresponds to an area limited, in each diagram of fig. 7-1 by the polygon ABCD (see figs. 7-1). It can be seen that for the coarser

Figure 7.2. Block diagram combining the maps displayed by figures 7.1-a to 7.1-h.

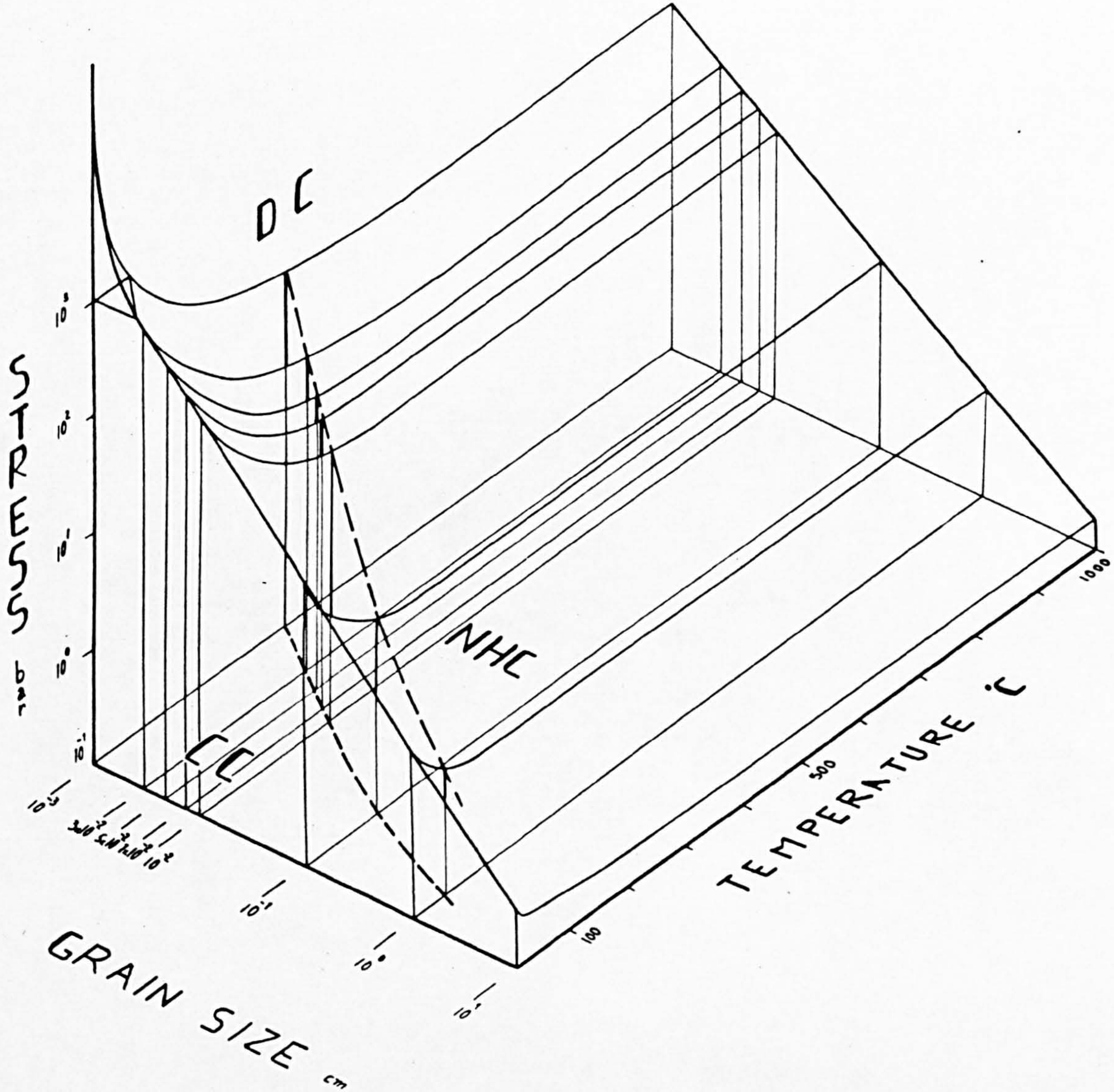

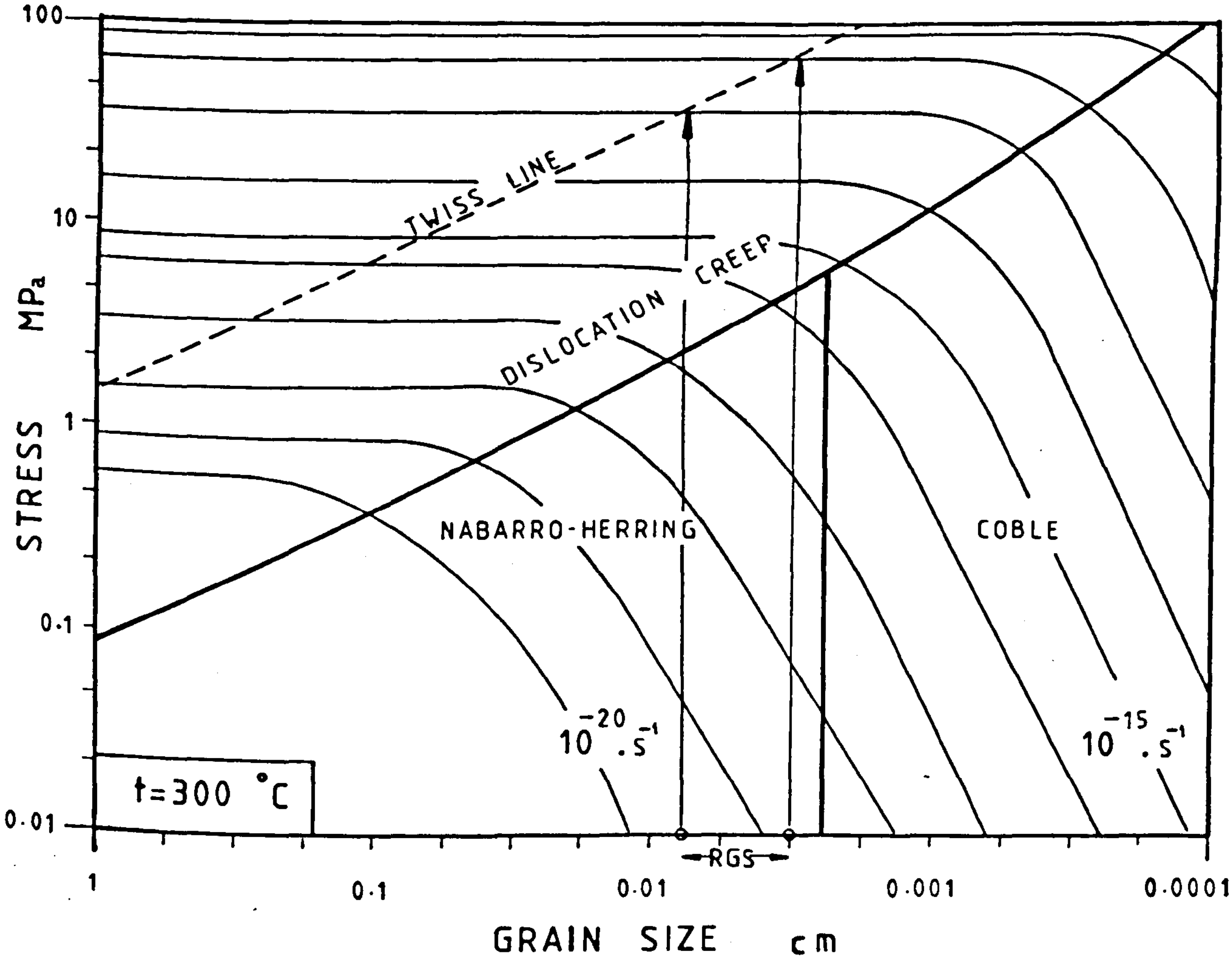

Figure 7.3-a. Deformation map for quartz relating differential stress (MPa) and grain size (cm). Strain rate contours and the dominant type of mechanisms are shown at t = 300^{o}C. The range of the measured Recrystallized Grain Size (RGS, 70-30 μm) is also indicated in this diagram.

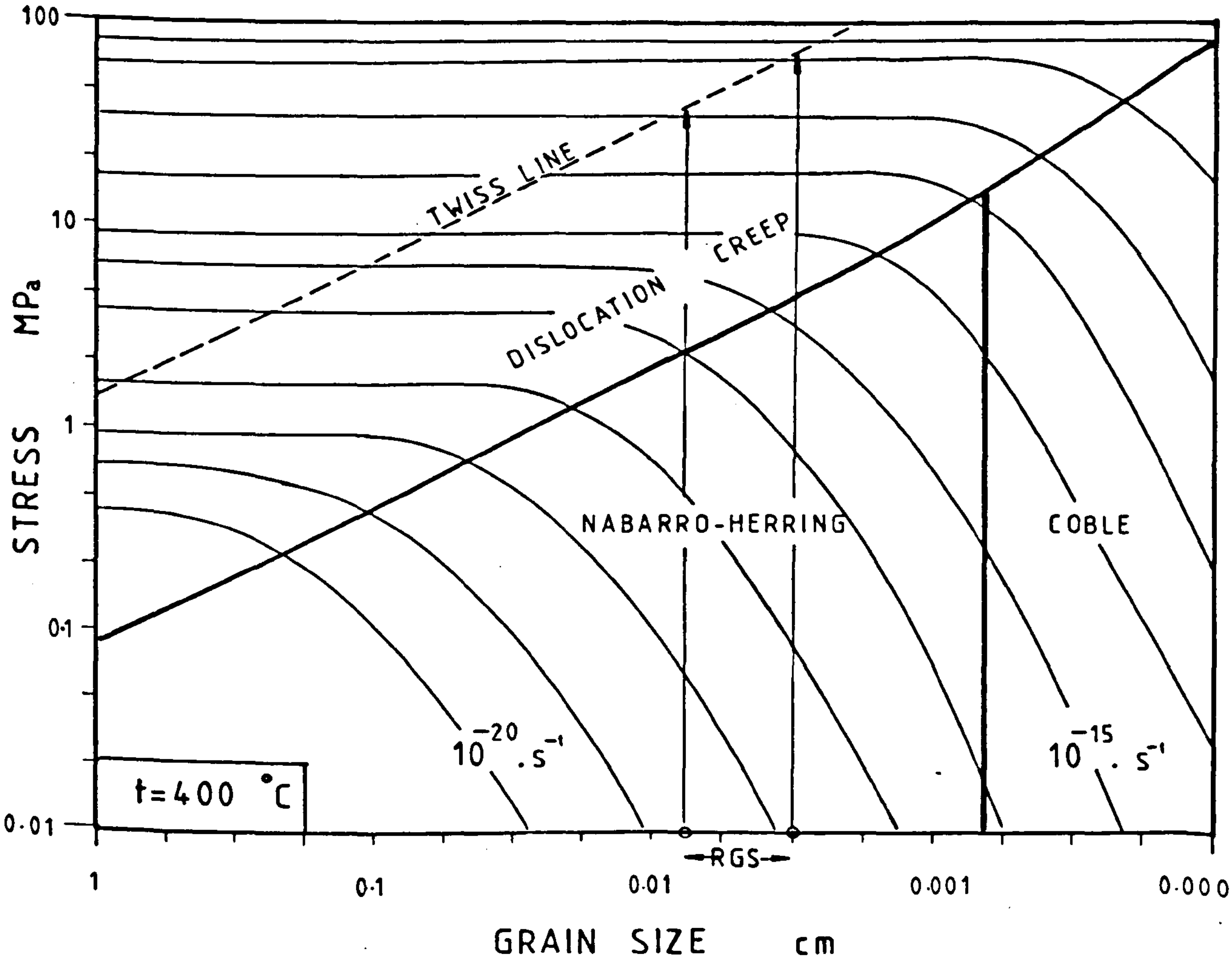

Figure 7.3-b. Deformation map for quartz relating differential stress (MPa) and grain size (cm). Strain rate contours and the dominant type of mechanisms are shown at t = 400°C. The range of the measured Recrystallized Grain Size (RGS, 70-30 µm) is also indicated in this diagram.

grain sizes (eg range 10 cm - 100 μm) the most effective deformation mechanism is by dislocation creep (DC), while the strain rate (range 10^{-19} - $10^{-9}.s^{-1}$) changes approximately by one order of magnitude (see figs. 7-1-a to d). The boundary between DC and the diffusion process (either CC or NHC) approaches the lower limits of the polygon ABCD in fig. 7-1-d (or D = 0.01 cm). Here the contribution of these diffusional processes might be relevant but only for stresses below the stipulated range (ie σ < 5 MPa). This means that for greater stresses the DC still makes an important contribution.

With the progress in grain refinement, by effects of deformation, the area of the static points ABCD (ie constant σ-T) encounters the junction line separating DC and DF processes and this is accompanied by an increase in the strain rate. Thus for the finer grain size fractions, the most effective process of deformation is by a diffusional mass transfer (for lower stresses, see the lower part of the areas limited by the polygon ABCD in figs. 7-1-e to h).

Figure 7-4 is a logarithmic graph correlating strain rate to differential stress, which allows the ready visualization of the range where each one of the deformation mechanisms, dislocation or diffusional is dominant. It can be seen from this graph that each grain size is represented by a line presenting a curved domain linking two straight lines. It is clear that along these straight lines, dislocation or diffusional mechanisms are dominant, whereas, where the lines become curved represents the domain where there is a significant contribution of these two deformation mechanisms (see fig. 7-4). The accurate position of the boundary line which separates the dislocation and diffusional fields in figs. 7-1-a to h, could be represented in fig. 7-4 by the intersection between the straight lines. Compared with figs. 7-1, fig- 7-4 shows a more realistic view of the change of the

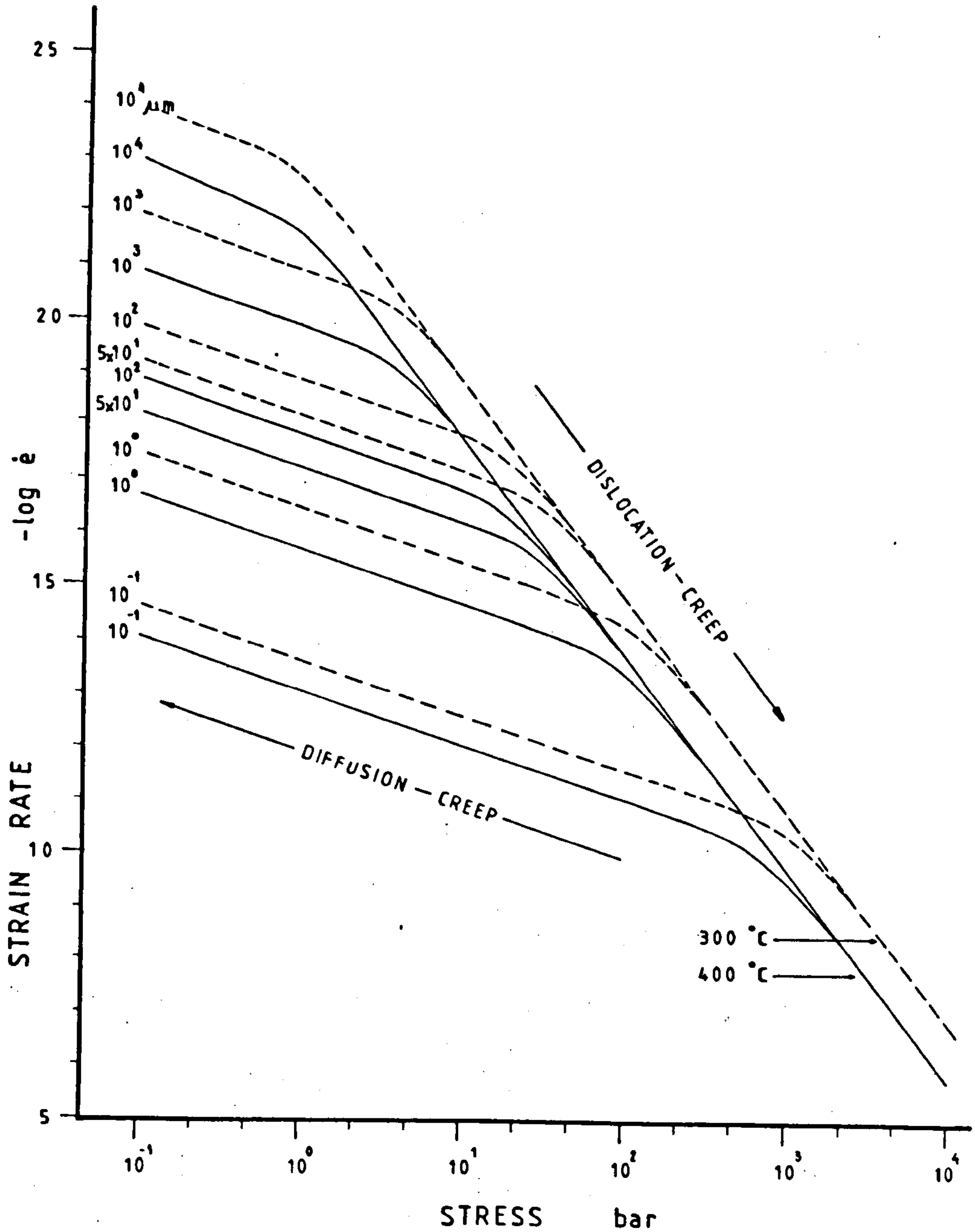

Figure 7.4. Log-Log graph relating strain rate to differential stress, for quartz, at the temperatures 300 and 400°C. It illustrates the clear transition (curved) between two main dominant mechanisms of deformation (straight lines) for each of the above particle sizes (μm)..

deformation mechanism . While in the figs. 7-1 there are sharp boundary lines separating the diffusional and the dislocation fields, in fig. 7-4 we can see instead,that the curved domains indicated that there is a gradual increase in the contribution of one mechanism followed by decrease of the other. This also represents more fairly the idea behind equation [7-8].

Other valuable information that can be drawn from fig. 7-4 is related to temperature variations. The net effect from a change of $100^{o}C$ is a shift between the set of curves (see fig. 7-4), which shows that there is an acceleration in the strain as the temperature increases. This can be observed by comparing figs. 7-3-a and b, however in fig. 7-4 these differences are enhanced. It can be also seen that for a given stress, there is a decrease in the rate of acceleration as the sizes of the particle decrease .

The effects of heating due to mechanic energy conversion are presently drawing some attention (Brun and Cobbold, 1980; Fleitout and Froidevaux, 1980) with inferences about the amount and the extent of heat dissipation (see White et al 1980). However, it is not yet possible to evaluate the role of shear heating accurately. It must be remembered that temperature variations can cause strong softening effects (cf White et al 1980), that might in turn allow variations in the strain rate.

There are still some important aspects not directly covered in the preceeding graphs and constitutive equations. One of these is the role of grain boundary sliding, GBS (cf Gifkins 1976, 1977; Etheridge and Wilkie 1979-b). As mentioned in section 5.1,grain boundary sliding is an implicit condition operating in conjunction with the diffusional mechanisms, otherwise this deformation would require an impossible volume change. However, GBS is not represented in the constitutive equations of section 7-3 and the deformation maps of figs. 7-1. Etheridge and Wilkie (1979-b) investigated the effects of GBS in conjunction with the deformation mechanisms, using relationships derived by Gifkins (1976, 1977). They constructed logarithmic graphs (log-log) relating stress to grain size (D) and plotted strain rate contours for temperatures in the range 400, 500 and 600^{o}C. The area in these log-log diagrams is divided in three different regimes, which are defined as follows:

(i) Regime IIa, is characterized by GBS accommodated by grain boundary diffusion. This field would include the whole diffusional field in a comparable temperature diagram given by fig. 7-3-b.

(ii) Regime IIb intends to include GBS accommodated by glide and climb of dislocations at the grain margins only,

(iii) Regime III comprises GBS accommodated by dislocation glide and climb throughout the grains.

Etheridge and Wilkie (1979-b) also claimed that the effects of GBS are to accelerate creep rates by one order of magnitude. Their diagram number 4 resembles this study's fig. 7-3-b, in that there are areas with comparable magnitudes of strain rates. The differences between these two diagrams are of course due to their different constitutive equations. It must be remembered that the deformation maps are not accurate, for at least two reasons: (i) due to contouring errors which involve interpolation of values (for obtaining the iso-strain rates of contours) in the logarithmic space.. (ii) Due to poor diffusional data, as discussed earlier. Perhaps we should consider the accuracy of those maps, within a factor of 10 (cf Etheridge and Wilkie 1979-c).

It is also necessary to speculate about the influence of grain size reduction on deformation processes (see White 1976-a). Again, figs. 7-3-a and b will prove very useful, as it can be seen that within the field of feasible strain rates - ie ultimately faster than $10^{-20}.s^{-1}$ (cf Price 1975), but most probably within the range 10^{-16} and $10^{-10}.s^{-1}$ - the reduction in grain size does not alter the strain rate provided that the boundary condition limiting the different mechanisms is not in the proximity. In other words, the grain size reduction by recrystallization, at constant T and σ, shows an extremely constant strain rate while the deformation operates well within the domain of the dislocation creep. However with continued grain size reduction,the mechanism of deformation may eventually approach the zone where diffusional creep becomes important and this can cause the strain-rate to accelerate dramatically: eg. reduction in grain size from 10 μm to 1 μm at 100 bar (see fig. 7-3-b) can change the rate from $\dot{e} \approx 10^{-14}.s^{-1}$ (dominantly dislocation creep regime) to almost $\dot{e} \approx 10^{-11}$ in conditions of dominant diffusional flow. As deformation progresses by grain refinement, and if the state variables σ and T are held constant, the strain rate will remain relatively constant as long as dislocation creep is the dominant mechanism of deformation (see figs. 7-3). It also implies that even with the most uniform distribution of σ and T, there will be strain rate differences due to grain size variations.

Another speculative view, based on the studied microstructures (Chapter 5) is that the rock can be reduced in grain size by dynamic recovery and recrystallization processes, and the end product is a rock with a uniform particle size, in equilibrium with T and the applied stress. By Twiss's (1977) theory, reduction in grain size, for a certain stress level, reaches an equilibrium as Twiss's line is approached.

This is because it solely relates size to stress. That line defines a strain rate for a particular level (cf Etheridge and Wilkie 1979-b) and figs. 7-3 shows it is in the dislocation creep field.

It is also possible to conclude that under conditions of constant strain rate, the development of localized deformation zones (ie grain reduction processes) causes an overall stress reduction (cf White et al 1980). Again, this stress reduction gradient increases sharply if the deformation mechanism changes to diffusion, otherwise it is negligible (see figs. 7-3). The conditions for strain softening (cf White et al 1980) must be invoked, ie softening must occur during some stage of the deformation period, otherwise there would be an indefinite migration of the boundaries of the deformation zones. (ie indefinite increase in thickness of such zones) and this is highly improbable.

Using the information of the preceding Chapters 5 and 6, it is possible to estimate some of the deformation variables which will allow an inference of the strain rate during deformation. The recrystallized grain sizes (cf Table 6.1) are in the range 26-66 μm, indicating that the magnitudes of the differential stress have values between: 26-51 MPa (Mercier model) or 39-73 MPa (Twiss model). Taken with the expected temperature conditions (300-400^{o}C), the grain size and stress estimates, when plotted on the deformation maps, indicate that dislocation creep is the dominant deformation mechanism. The differences between deformation at 300 and 400^{o}C (see figs. 7-3-a, b) do not affect this conclusion. Figures 7-3 show that at conditions of low stress and temperature the diffusion mechanisms are indeed too slow to account for any of the observed strains found in the studied area (notice the magnitude of these rates in figs. 7-3). Diffusional processes may play an important role in conditions where particle size is around 10 μm or less. The maps of figs. 7-3 clearly show that the strain-rates under conditions of formation of recrystallized quartz grains are roughly in the range: 10^{-13} to $10^{-12}.s^{-1}$ (300^{o}C) and 10^{-12} to $10^{-11}.s^{-1}$ (400^{o}C).

So far in this discussion we did not take into account the effects of other phase(s) being present, thus interfering with the rheology of quartz. Second phase effects were not taken into account in the described constitutive equations, consequently they do not appear in any of the displayed deformation maps. In this study we observed that phyllosilicates might have influenced the microstructures (cf Chapters 5 and 6) in some domains of the studied area, as their proportional increase can be correlated with textural changes associated with increasing deformation. The evidence presented in Chapter 5 includes the increase in the amount of the recrystallized grains and also certain increases in the size of these new grains, where phyllosilicate content is relatively higher. These characteristics might indicate induced recrystallization and softening effects. However as pointed out in Chapters 5 and 6, not only the frequency of these increases in the amount of recrystallization but also the variation in the sizes of the new grains did not reveal any clear pattern that would lead to the conclusion that effects of pressure solution played an important role during period(s) and process(es) of deformation in the mapped area. There are a few isolated microstructures which could be interpreted as being indicative of pressure solution effects (see plate 5-24), but these may have other explanations.

To summarise, the data and the interpretations in the present discussion lead us to the following conclusions:

1. The deformation of the analysed rocks operated dominantly by a dislocation creep mechanism.
2. Assuming that σ and T are held constant during a certain period, the existence of different grain sizes in a sample implies that these grains deformed at different rates.
3. The deformation conditions in the mylonites of Eriboll and Hope areas could have operated at temperatures around $300^{o}C$ and differential stresses in the approximate ranges: 40-75 MPa (using Twiss model), or a 25-50 MPa (Mercier).
4. The inference of the probable range of σ-T conditions, together with the measured recrystallized grain sizes (for quartz) place the operative strain rate for this deformation zone, in the ranges: 10^{-11} to $7 \times 10^{-13}.s^{-1}$, (following Twiss' model for stress calculation) and 1.2×10^{-13} to $2 \times 10^{-12}.s^{-1}$ (following Mercier's model for stress estimation).

CHAPTER 8

CONCLUSIONS AND INFERENCES

The data collected in this study are based on two main scales of observation: (i) mesoscopic measurements of structures in the field using normal mapping routines, and (ii) microscopic observations of microstructural parameters and fabrics. The analysis of the collected data allows us to infer the characteristics of this deformation zone in (iii) a macroscopic scale, keeping in mind the context of the regional geological setting. Some of the main points to come out in this study are summarised below.

1. The rocks of the eastern side of Loch Eriboll are here subdivided into four main zones, each with different rheologic and deformation intensities. These are as follows: (i) the westernmost imbricate zone of brittle deformation which is bounded eastwards by (ii) more ductilely deformed, but unmylonitized blocks of either Lewisian and/or Cambro-Ordovician rocks. This second domain is bounded eastwards by (iii) the b-thrust, which is the lower limit of a nappe composed mainly of Lewisian mylonites, exhibiting slabs of Moinian Psammites and Paleozoic rocks. This third zone is bounded eastwards by the Moine Thrust (ss), which brings a thick sequence of Moinian rocks on top of this third nappe.

2. There is a clear gradient of deformation towards the mylonitic nappe. This gradient is less abrupt on the eastern margin of the mylonites than on the western margin. Below the b-thrust there is a clear indication of a strain gradient as ε_s values increase progressively towards the mylonitic zone.

3. Another way of illustrating the differences in the deformation is given by the characteristics of the thrust faults. In the western

imbricate faults, the predominance is for brittle deformation. There are no indications that this zone suffered ductile deformation, due to thrusting effects. The imbricate zone is also characterized by abrupt lithological changes. In contrast, in the second nappe, there are clearly signs of progressive brecciation (up to 1 m thick) and/or mylonitization (up to 10 cm from the thrust surface). The b-thrust separates this second zone from the third which is entirely made up of heavily mylonitic rocks. The b-thrust discontinuity surface is easy to identify because of the contrasting intensities of deformation across the fault. The Moine Thrust however separates domains with similar intensities of deformation and thus is less conspicuous than this lower thrust.

4. The main component of the mylonitic nappe, below the Moine Thrust (ss), is the Lewisian Gneiss. Within this mylonitic Lewisian domain there are slivers or lenses of mylonitic Moinian and Cambrian quartzitic rocks; the former predominate south of Creagan Road while the latter are more abundant north of this road. This mylonitic zone is also composed of blocks of moderately deformed rocks, separated by zones of much more intensely deformed rocks. This strain-localization can be observed on different scales, from outcrops to microscopic scale.

5. The mylonitic foliation produced a homogeneization in the rocks. This is given by a closely spaced lamination which is present in the rocks independent of their mineral composition. However the presence of phyllosilicates tends to produce a more clearly defined planar fabric than a rock sample composed massively of quartz-grains. The stereoplots of this foliation confirm field observations that

later deformation episodes do not obliterate this early planar fabric. It is believed that the formation of the mylonitic fabric corresponds to the peak of the deformation intensity because it clearly obliterated and re-oriented any previously formed fabrics.

6. The development of structures (thrusts and faults) is interpreted to be from east to west, in the direction of the tectonic transport. The strains and textures of the rocks in the area indicate that this deformation zone developed in an environment of greater confinement (deeper level?) characterized by plastic deformation. The structures become more brittle westwards which implies that the structures climbed to shallower levels and thus show a transition from ductile to brittle shear zones (cf Ramsay 1981).

7. With the exception of the Moine Thrust (ss), it is not possible to trace continuously from NE to SW, any thrust fault as they branch-off, merge or even die out.

8. The homogeneity of a fabric in the studied zone is connected with strong and persistent deformation. The older the lineation, the closer it lies to the ESE direction ($\simeq 115^{o}$). The older the foliation, the closer, its parallelism with the mylonitic foliation containing the stretching direction. Thus the tendency is for the re-orientation of structures (due to increase in strain) towards a plane dipping approximately 15^{o} in the direction 115^{o}.

9. There were two ductile fold phases after the mylonitic foliation formation. The early phase has hinges which lie closer to the stretching direction, but folds of this phase are irregularly

distributed across the studied area. The second phase is more abundant, showing folds of varied amplitudes (cm to tens of metres) and more varied hinges directions. The multi-directional orientation of hinges, together with the existence of brittle and ductile folds of the same generation, may indicate a spasmodic of polyphasic nature of this folding event.

10. Fold shape analyses indicate that there was a strong component of buckling in the formation of these F_2 and F_3 folds. The dominant fold Class is in the 1C field, although some examples belong to Class 3. Very few folds belong to Class 2. The folds belong mainly to the sine-wave type and this supports their initiation by buckling (cf Hudleston, 1973-a, p.119).

11. There is a local thickening of the mylonite zone, south of the Creagan Road, and this appears to be associated with an increase in the frequence of folds in the area. This local thickenning might be due to differential displacements along the strike of the thrust.

12. The strain estimations, using the curved hinges of folds as strain markers, confirms that the MT zone presents characteristics of a ductile deformation zone in which there is a gradual decrease in strain intensity away from the trace of the fault.

13. The majority of the mean directions of fold axes previous to imposed strain, were distributed at high angle to the X-direction, nearly parallel to the longitudinal direction of the thrust belt. Most of these axes, were in range of up to 20°.

14. The use of a pure-shear mechanism to explain deformation in the thrust belt is debatable. However the simple shear mechanism advocated by many geologists may also generate as much criticism as that of pure-shear, in that neither of these mechanisms can wholly account for the structures observed in this deformation belt. A combination of pure and simple shears could better explain the structures met in this study area.

15. The models for strain estimation using curved fold hinges have rather limited or simplistic formulations. Therefore the strain results must be considered more as qualitative estimates.

16. It is the view of this study that the efficiency of some iterative methods for function-optimisation depend on the type of the objective-function formulated for the problem. For example the Direct Search method, developed during the course of this study, can be relatively simple to program, but apart from consuming excessive time of computer calculation, the results may lack the necessary accuracy. If an extensive use of the routine is required, the method is rather inefficient. The variations of the Newton-Method extensively applied in Chapters 3 and 4, however, can produce far more accurate results in a shorter time. However these methods have a drawback that convergence to the correct solution is not guaranteed in every case. The Gradient Method needs a more sophisticated set of equations than the Direct Search technique, apart from requiring a more elaborate programing.

In the present case the two investigated methods of optimisation, the Direct Search and the Gradient Methods, presented complementary characteristics of efficiency and in this situation it is valid to make use of both methods to solve for the unknowns.

This study also made use of the method of the Lagrange Multipliers as a mean of imposing a choice of a particular surface on a Least Squares fitting routine. Although the method is valid, this type of solution increased the complexity of the equations, originated from the augmented function and also resulted in the solution of a set of non-linear simultaneous equations.

17. The strain estimates using the shape of quartz grains provided only a limited range of values, because at high strains, dynamic recrystallization interfered, causing grain destruction. In some cases it is possible to observe extensive intracrystalline deformation of clastic grains accompanied by progressive recrystallization (ie ≈30% in volume). However no general rule should be made as there may be other influences such as different mineral phases which might interfere with the process of intracrystalline deformation.

18. Quartz grain shape analyses in this study must be considered as minimum strain estimates, because of the effects of grain destruction by recrystallization processes. The ε_s values found in this study range up to 1.4 and it is believed that the effective strain in more deformed zones reaches much greater values.

19. Most of the 3D strains, provided by the analyses of quartz grain shapes, plot in the oblate field of the Flinn-diagram. There are several explanations for this, one of which is to invoke volume reduction. It is believed that volume reduction could have taken place in the formation of these rocks but the amount (up to 65%) indicated by the nearly oblate shape (cf Ramsay-Wood, 1973) is far

too great. One of the reasons for obtaining oblate fabrics could be that there was differential displacement of layers along the transport direction (cf Coward and Kim, 1981). Such differential movement could also account for the origin of some folds which are found throughout the whole area, with axes parallel to the NNE/SSW direction.

20. The orientations of the axes of the various ellipsoids, given by the quartz shape analyses are not constant throughout the area. In general the least principal axes have a steeply plunging attitude, while the intermediate principal axes occupy various positions within the 180^o precession arc from NNE to SSE. This may be due to interfering strains produced during subsequent deformation phases and/or possible differential rotations due to differential movement along the deformation zone. The discrepancies, between some λ_2-directions and the Y-direction of the deformation belt, invalidates the hypothesis of extension normal to the transport direction of the belt.

21. Microtextural investigations attest the existence of progressive intracrystalline deformation of clasts, accompanied by grain recrystallization with proximity of the deformation zones. The existence of cataclastic textures affecting early ductile micro-structures may confirm that the rocks of this deformation belt were subject to deformation events during a regime where the rheologic characteristics have changed from ductile to brittle conditions.

22. The presence of phyllosilicates (from 2-10%) apparently (i) causes the increase in the amount of the recrystallized quartz grains and (ii) in those samples where there are clastic grains, the newly

formed quartz grains are coarser than in rocks devoid of phyllosilicates. (iii) In those samples totally recrystallized, the presence of phyllosilicates seems not to influence the size of the new grains. (iv) The amount of phyllosilicates is greater in samples which showed lower proportions of feldspars, so perhaps there was a chemical breakdown of feldspars to quartz and micas.

23. An argument based in field observations, that the mylonitic domain of Eriboll (at Kempie) exhibits characteristics of more homogeneity of deformation than the mylonitic zone at the NE side of Loch Hope, is corroborated by microscopic textural evaluations.

24. The paleostress estimations seem to characterise different stress domains which have also distinct geographic and structural positions in the analysed area. The stress estimates above the b-thrust at Kempie are higher than in the rest of the area. Strain intensities also seem to achieve higher magnitudes in the Kempie mylonites than for example, at Hope and Arnaboll areas. It is believed that there is a close correspondence between the estimated increases of stress and strain.

25. This study also emphasises that stereologic considerations on grain size measuring routines are not a matter to be neglected. On the contrary, the lack of standardization on measuring techniques for grain size evaluation, for paleopiezometric studies, not only prevents any correlation between different studies but also questions the validity of using an experimentally derived model such as that of Mercier et al (1977) if there are no clear indications on size evaluation technique(s) used by this work.

26. The evidence deduced from the deformation maps used in this study leads to the conclusion that the dominant mechanism of deformation for the study area is that of Dislocation Creep. The operative strain rate for temperatures around 300°C, is between $10^{-13}.s^{-1}$ and $10^{-12}.s^{-1}$. However the existence of different particle sizes in the same sample leads to the conclusion that in these grains, deformation may operate at different rates.

27. The deformation maps show that if the strain rate and the temperature are held constant, during a process of grain size reduction, this causes an overall stress reduction. The gradient of this reduction is negligible in the field of the Dislocation Creep, but should increase if the mechanism of deformation changes to diffusion. However for the conditions in the study area (ie temperatures around 300°C, recrystallised grain size greater than 30 μm) there can have been very little contribution of deformation by diffusional processes.

APPENDICES

```
C
C   P R O G R A M M E   S A N D
C
C*****************************************************************************
C
C
C  STRAIN RATIO ESTIMATION PROGRAMME
C  DIRECT SEARCH METHOD
C  BASED ON A MODEL BY D. SANDERSON(1973)
C  SEE TECTONOPHYSICS,16 : 55 - 70 .
C
C
C*****************************************************************************
C*****************************************************************************
C
C  VERSION : NOV 1978
C  DEVELOPED AT LEEDS' ICL 1906-A COMPUTER
C  BY  HENRIQUE DAYAN
C
C*****************************************************************************
C
C  THE FIRST CARD TO BE READ CONTAIN THE CONTROL PARAMETERS  :
C  COLUMN  INTEGER VARIABLE
C   1- 5          N          : POPULATION (AXES) SIZE
C   6- 10      NCTRL2        : THE REQUIRED CYCLES OF ITERATIONS
C
C  THE NEXT THREE CARDS CONTROL THE BOUNDARIES AND THE INTERVALS  OF
C  SEARCH FOR THE : THE M E A N  , THE S T A N D A R D  D E V I A T I O N
C  AND THE S T R A I N   R A T I O  RESPECTIVELY . IN EACH CARD INPUT
C  AS FOLLOWS :
C  COLUMNS
C   1 - 10     : THE LOWER BOUNDARY OF SEARCH
C  11 - 20     : THE UPPER BOUNDARY OF SEARCH
C  21 - 30     : THE INITIAL INTERVAL OF SEARCH
C
C  THE FIFTH AND SIXTH CARDS CONTAIN THE ORDINATES OF THE FREQUENCY
C  HISTOGRAM (FORMAT 9F8.0). ENTER THE 9 VALUES IN EACH CARD IN COLUMNS
C  1-18 , 9-16 , 17-24 , 25-32 , 33-40 , 41-48 , 49-56 , 57-64 , 65-72.
C  THE ORDER REFERS TO : 0 TO +90 DEGREES ON THE FIRST CARD AND
C  -90 TO 0 DEGREES IN THE SECOND.
C
C*****************************************************************************
C*****************************************************************************
C
C
C
      DIMENSION Y(37),HIS(18),YM(37),THETA(37),TTHETA(37),TETLIN(37)
      PI=ATAN(1.0)*4.0
C  READ INPUT PARAMETERS
      READ(5, 900) N,NCTRL2
C
C  READ BOUNDARIES OF SEARCH
C  FI0,FI1 =INF. AND SUP. LIMITS OF SEARCH  FOR THE MEAN
C  SIG0,SIG1 =DITTO FOR THE  ST. DEV. ESTIMATE
C  XY0,XY1= DITTO FOR THE STRAIN RATIO ESTIMATE
C  DFI,DSIG,DXY = INTERVALS OF SEARCH FOR THE MEAN,ST. DEV.,STR. RATIO
      READ(5,910)FI0,FI1,DFI
      READ(5,910)SIG0,SIG1,DSIG
      READ(5,910)XY0,XY1,DXY
C
C  READ ORDINATES FREQ. HISTOGRAM
C
      READ(5,920) (HIS(I),I=1,18)
      FAC= PI / 180.
      RADEG= 180. / PI
      SQPI= N / SQRT( 2. * PI )
      DO 5 J=1,37
      I= J-1
      THETA(J)= I * 5 * FAC
      IF(THETA(J) .EQ. PI/2.) THETA(J)=THETA(J)-(1.E-5 )
      TTHETA(J)= TAN(THETA(J))
    5 CONTINUE
      NCTRL1= 0
      SUMH=0
      DO 10 I=1,18
 10   SUMH=SUMH+HIS(I)
      SUMMIN=1.E30
C
C  START CYCLE(S) OF ITERATION(S)
   11 CONTINUE
      NCTRL1= NCTRL1 + 1
      NFI=ABS((FI1-FI0)/DFI)+1
      NSIG=ABS((SIG1-SIG0)/DSIG)+1
      NXY=ABS((XY1-XY0)/DXY)+1
      DO 100 IPHI=1,NFI
      PHI=FI0+(IPHI-1)*DFI
      PHI= PHI * FAC
      DO 100 IS=1,NSIG
      S=SIG0+(IS-1)*DSIG
      TEMP= SQPI / S
```

```
      SD= S* FAC
      IF(S.EQ.0) GOTO 100
      DO 100 IE=1,NXY
      E=XY0+(IE-1)*DXY
      SUMY=0
      DO 20 J=1,37
      I=J-1
      TETLIN(J)= ATAN( E * TTHETA(J))
      IF(TETLIN(J) .LT. 0.) TETLIN(J) = TETLIN(J) + PI
      AUX= ( PI/2. -(TETLIN(J) + PHI))
      IF(AUX .EQ. 0. ) AUX= 1.E-6
      EXPN= EXP( -0.5 * (( AUX / SD )**2))
      AUX2= 1. + ((COS(TETLIN(J)))**2)*(E*E-1))
      FUNC= ( SQRT( AUX2**3))/ E
C
C  Y(J) = IS  THE ORDINATES OF FITTING  CURVE
      Y(J)=TEMP*EXPN*FUNC
      SUMY=SUMY+Y(J)
 20   CONTINUE
C
C  NORMILIZE CURVE BY SUMMING FREQUENCIES
      IF(SUMY - 0.) 21,21,22
  21  PNOR= 1.E30
      GOTO 30
  22  PNOR=SUMH*2/SUMY
      DO 30 J=1,37
      Y(J)=Y(J)*PNOR
  30  CONTINUE
      SUMSQR=0.
C
C  CALCULATE THE SUM OF SQUARED DIFFS. BETWEEN HISTOGRAM
C  AND NORMILIZED FREQUENCIES
C
      DO 50 K=2,36,2
 50   SUMSQR =SUMSQR +(Y(K)-HIS(K/2))**2
C
C  COMPARE WITH PREVIOUS RESULTS , STORE THE BEST ONES
C
      IF(SUMSQR.GE.SUMMIN) GOTO 100
      SUMMIN =SUMSQR
      PNORM= PNOR
      PHIM= PHI * RADEG
      SM=S
      EM=E
      DO 70 K=1,37
 70   YM(K)=Y(K)
 100  CONTINUE
C
C  OUTPUT RESULTS
C
      WRITE(6,1010)
      WRITE(6,1020)PHIM,FI0,FI1,DFI
      WRITE(6,1030)SM,SIG0,SIG1,DSIG
      WRITE(6,1040)EM,XY0,XY1,DXY
      WRITE(6,1050) N
      WRITE(6,1060)SUMMIN
C
C  STOP ITERATION CYCLE IF THE REQUIRED NUMBER IS COMPLETED
C  GO TO 31, OTHERWISE CALL SUBROUTINE OPTIM TO SET UP
C  NEW INTERVALS OF SEARCH
C
      WRITE(6,3001) NCTRL1
      IF( NCTRL1 .EQ. NCTRL2 ) GOTO 31
      CALL OPTIM(PHIM, SM, EM, FI0, FI1, DFI, SIG0, SIG1, DSIG, XY0,
     1 XY1, DXY )
      GOTO 11
C
C  AFTER COMPLETING THE REQUIRED NO. OF CYCLES
C  OUTPUT FINAL RESULTS
C
  31  WRITE(6,1070)
      DO 120 J=1,37
      I=(J-1)*5
      IF(J/2.EQ.J/2.) GOTO 110
C
C  OUTPUT : CLASS INTERVAL,CURVE ORDINATE AND CORRESPONDING
C  FREQUENCY HISTOGRAM
C
      WRITE(6,1080)I,YM(J)
      GOTO 120
  110 K=J/2
      WRITE(6,1080)I,YM(J), I, HIS(K)
  120 CONTINUE
      SUMH=SUMH*10
      WRITE(6,2000)SUMH,PNORM
      WRITE(6,3001) NCTRL1
  900 FORMAT(2I5 )
  910 FORMAT(3F10.5)
  920 FORMAT( 9F8.0)
 1010 FORMAT(1H ,47X,'OBLIQUE FOLD AXIS ANALYSIS',/, 1H ,'THETA IS ANGLE
```

```
     1 TO X-AXIS AFTER DEFORMATION .       RESULTS NORMALISED BY SUMMINGS
     2 FREQUENCIES')
 1020 FORMAT(   ' OBLIQUE STRETCHING (MU)  OF ',F10.3,
     1        ' CHECKED FROM PHI=',F8.3,5X,'TO PHI=',F8.3,5X,'BY STEPS
     2 OF',F8.3)
 1030 FORMAT(                 ' STD OF ORIGINAL FOLD AXIS DISTRIBUTION='
     1 ,F10.2,  ' CHECKED FROM S=',F8.3,5X,'TO S=',F8.3,5X,'BY STEPS
     2 OF',F8.3)
 1040 FORMAT(  ' STRETCHING (X/Y) =',F10.3,  ' CHECKED FROM X/Y=',F8.3,
     1 'TO X/Y=',F8.3,5X,'BY STEPS OF',F8.3)
 1050 FORMAT(1H ,'POPULATION SIZE = ',I5)
 1060 FORMAT(1H ,' SQUARE OF DEVIATIONS=',F20.10 )
 1070 FORMAT(1H ,5X,'THETA',5X,'Y(THETA)',10X,'THETA',5X,'HISTOGRAM')
 1080 FORMAT(1H ,5X,I5,5X,F8.3,10X,I5,5X,F8.3)
 2000 FORMAT(1H ,' SUMH=',F10.2,5X,'PNOP=',F20.10 )
 3001 FORMAT(1H ,' NO. OF CYCLES=',I5)
      STOP
      END
      SUBROUTINE OPTIM( PHIM, SM, EM, FI0, FI1, DFI, SIG0, SIG1, DSIG,
     1 XY0, XY1, DXY )
C
C
C  SUBROUTINE TO CHOOSE NEW BOUNDARIES OF SEARCH
C  CALLED AFTER COMPLETING EACH CYCLE OF ITERATION
C
C
      FI0= PHIM-( DFI * 2.1)
      FI1= PHIM + (DFI * 2. )
      DFI= (FI1 - FI0)/ 10.
      AUX3= ABS(DFI)
      IF( FI0 .LE. 0. .AND. FI1 .GE. 0.) DFI= AUX3
      IF( FI0 .GE. 0. .AND. FI1 .LE. 0. ) DFI = -AUX3
      IF( FI0 .LE. 0. .AND. FI1 .LE. 0. )  CALL AUXIL( FI0,FI1,DFI)
      SIG0= SM - ( DSIG * 2. )
      IF(SIG0 .LT. 1. ) SIG0= 1.
      SIG1= SM + ( DSIG * 2.1)
      IF(SIG1 .LT. 1. ) SIG1= 1.
      DSIG= (SIG1 - SIG0 )/ 10.
      XY0= EM - ( DXY * 2. )
      IF( XY0 .LT. 1. ) XY0= 1.
      XY1= EM + ( DXY * 2.1)
      IF(XY1 .LT. 1. )  XY1= 1.
      DXY=( XY1 - XY0 )/ 10.
      RETURN
      END
      SUBROUTINE AUXIL(FI0,FI1,DFI )
      IF(FI0 .LT. FI1 ) DFI= ABS(DFI)
      IF(FI0 .GT. FI1) DFI=-ABS(DFI)
      RETURN
      END
```

```
C
C   P R O G R A M M E     M O D E L 2
C
C*****************************************************************************
C
C  MODEL DERIVED BY  H. DAYAN
C  DIRECT SEARCH METHOD
C  STRAIN RATIO ESTIMATION PROGRAMME
C  VERSION : JAN 1979
C  DEVELOPED AT LEEDS' ICL 1906-A COMPUTER
C  BY  HENRIQUE DAYAN
C
C
C*****************************************************************************
C*****************************************************************************
C
C
C  THE FIRST CARD TO BE READ CONTAIN CONTROL PARAMETERS :
C  ---------------------------------------------------------------------------
C I  COLUMN   I  VARIABLE  I       U    S    A    G    E
C I___________I____________I__________________________________________________
C I  1 - 5    I     N      I  INTEGER VARIABLE . REFERS TO HISTOGRAM NO.
C I           I            I OF CLASS INTERVALS.
C I___________I____________I__________________________________________________
C I  6 - 10   I    NCY     I  INTEGER VARIABLE . ENTER  THE NUMBER OF
C I           I            I CYCLES OF ITERATIONS REQUIRED
C I___________I____________I__________________________________________________
C I 11 - 15   I   LIMIT    I  INTEGER VARIABLE . ENTER THE MINIMUN
C I           I            I NUMBER OF ITERATIONS REQUIRED.
C I___________I____________I__________________________________________________
C I  16- 26   I  ACURCY    I  REAL VARIABLE . ENTER THE REQUIRED ACCURACY
C I           I            I OF SEARCH.
C I___________I____________I__________________________________________________
C
C  THE NEXT THREE CARDS CONTROL THE BOUNDARIES AND INTERVALS OF SEARCH.
C  IN EACH CARD THE VARIABLES ARE READ WITH THE SAME FORMAT F10.0
C  ---------------------------------------------------------------------------
C I COLUMNS  I VARIABLES  I      U     S     A     G     E
C I__________I____________I___________________________________________________
C I          I    FI0     I
C I  1- 10   I    SIG0    I THE  LOWER BOUNDARY OF SEARCH
C I          I    XY0     I
C I__________I____________I___________________________________________________
C I          I    FI1     I
C I          I    SIG1    I THE UPPER BOUNDARY OF SEARCH
C I          I    XY1     I
C I__________I____________I___________________________________________________
C I          I    DFI     I
C I 21-30    I    DSIG    I THE  INITIAL INTERVAL OF SEARCH
C I          I    DXY     I
C I__________I____________I___________________________________________________
C
C  THE NEXT CARDS, INPUT THE ORDINATES OF THE FREQUENCY HISTOGRAM. EACH
C  CARD SHOULD CONTAIN REAL VARIABLES WITH FORMAT  F8.0
C
C*****************************************************************************
C*****************************************************************************
C
C
      DIMENSION HIS(100),Y(100),ABSC(100),ORD(100),THETA(100),TANLIN(100
     1),TETLIN(100)
      INTEGER CYCLES,CASE,CONTRL,LIMIT
C
C  I N P U T    D A T A
C  READ CONTROL  PARAMETERS
C  N = NO. OF CLASS INTERVALS
C  NCY= NO. OF CYCLES OF ITERATIONS
C  LIMIT= LOWER LIMIT OF ITERATIONS
C  ACURCY= ACCURACY  OF SEARCH
C
      READ(5,900) N,NCY,LIMIT,ACURCY
      PI=3.1415927
C
C  READ BOUNDARIES OF SEARCH
C  FI0,FI1 =INF. AND SUP. LIMITS  OF SEARCH  FOR THE MEAN
C  SIG0,SIG1 =DITTO FOR THE  ST. DEV. ESTIMATE
C  XY0,XY1= DITTO FOR THE STRAIN RATIO ESTIMATE
C  DFI,DSIG,DXY = INTERVALS OF SEARCH FOR THE MEAN,ST. DEV.,STR. RATIO
      READ(5,910)FI0,FI1,DFI
      READ(5,910) SIG0,SIG1,DSIG
      READ(5,910)  XY0,XY1,DXY
      SUMYM= 1.E40
      SUDTI=1.E40
      FAC= PI / 180.
C
C  READ ORDINATES FREQ.  HISTOGRAM
      READ(5,920)(HIS(I), I=1,N)
C
C  PRINT INPUT DATA
C
      WRITE(6,1300)  N,ACURCY
```

```
      WRITE(6,1400) FI0, FI1, DFI
      WRITE(6,1500) SIG0, SIG1,DSIG
      WRITE(6,1600) XY0, XY1, DXY
C          HISTOGRAM AREA CALCULATION ( FREQUENCY X DEGREES )
      SUMHIS= 0.
      AN= FLOAT(N)
      DO 10  I=1,N
   10 SUMHIS= SUMHIS + HIS(I)
      SUMH= SUMHIS * ( 180. / AN)
      SQPI=SUMH / SQRT(2. * PI)
      DO 5 J=1,N
      TETLIN(J)= (J - .5) * PI/AN
      IF( TETLIN(J)  .EQ. PI/2. )TETLIN(J)=TETLIN(J) - (1.E-6)
      TANLIN(J)= TAN(TETLIN(J))
C
C  START CYCLE(S) OF ITERATION(S)
    5 CONTINUE
      DO 104 L=1,NCY
      CYCLES= L
      NFI=ABS((FI1-FI0)/DFI)+1
      NSIG=ABS((SIG1-SIG0)/DSIG)+1
      NXY=ABS((XY1-XY0)/DXY)+1
      DO   100  IPHI=1,NFI
      PHI=FI0+(IPHI-1)*DFI
      PHI=PHI*PI/180.
      DO   100 IS=1,NSIG
      S=SIG0+(IS-1)*DSIG
      SD=S* FAC
      TEMP= SQPI / S
      DO   100 IE=1,NXY
      E=XY0+(IE-1)*DXY
      SUMY=0.
C          COMPUTING  THE SUM OF THE SQUARED        DIFFERENCES BETWEEN  T
C          CURVE  AND HISTOGRAM
      DO  20 I=1,N
      IF(HIS(I).EQ.0)GO TO 20
      THETA(I)= ATAN(E *  TANLIN(I))
      IF(THETA(I)  .LT. 0.) THETA(I)= THETA(I)  + PI
      AUX2= THETA(I) - PHI
      IF( AUX2 .EQ. 0.) AUX2= 2.E-6
      EXPN= EXP(-.5 * ((AUX2/ SD)**2))
      FUNC=(1.+((COS(THETA(I))**2) * (E*E-1.))) / E
C  Y(I) = IS  THE ORDINATES OF FITTING  CURVE
      Y(I)=TEMP*EXPN*FUNC
C  SUMY= OBJECTIVE FUNCTION
      SUMY=SUMY+(HIS(I)-Y(I))**2
   20 CONTINUE
C
C  COMPARE WITH PREVIOUS RESULTS , STORE THE BEST ONES
      IF(SUMY.LT.SUMYM) GO TO 30
      GOTO 100
   30 SUMYM=SUMY
      EM=E
      SM=S
      PHIM=PHI*57.29578
  100 CONTINUE
C     S U M Y M      TEMPORARY SUM OF SQUARED DIFFERENCES
C  OUTPUT RESULTS IN THE END OF EACH CYCLE OF ITERATIONS
C
      WRITE(6,1202)  CYCLES,SUMYM
      WRITE(6,1201)  PHIM,SM,EM
      WRITE(6,1203) DFI,DSIG,DXY
      DIF= ABS( SUOTI - SUMYM)
C
C  MAKE DECISION WHETHER OR NOT TO CONTINUE CYCLE(S) OF ITERS.
C
      IF(SUOTI-SUMYM)81,82,83
   81 CASE= 1
      GOTO 84
   82 CASE= 0
      GOTO 84
   83 CASE= 2
   84 IF(DIF - ACURCY) 91,91,92
   91 CONTRL= 1
      GOTO 93
   92 CONTRL= 2
   93 LX= L - LIMIT
   94 IF(LX - CYCLES) 95,95, 96
   95 DECISN= 1
   96 DECISN= 2
   97 IF( CASE .GT. 0) GOTO 98
      IF(DECISN .EQ. 1) GOTO 106
      GOTO 101
   98 IF(CASE .EQ. 2) GOTO 99
      IF(CONTRL .EQ. 2 .OR. DECISN .EQ. 2) GOTO 101
      GOTO 106
   99 IF(CONTRL .EQ. 2 .OR. DECISN .EQ. 2) GOTO 107
      GOTO 105
  107 CONTINUE
```

```
      SUOTI=SUMYM
      PHIOT=PHIM
      SOT=SM
      EOT=EM
  101 CONTINUE
C
C  SET UP NEW BOUNDARIES AND INTERVALS OF SEARCH:
C    A- FOR  ST. DEV.
      IF(DSIG .LT. 1.E-3) GOTO 120
      SIG0=SOT-(DSIG * 1.5)
      IF(SIG0.LT.1.) SIG0= 1.
      SIG1=SIG0 + (DSIG*2.85)
      DENSIG= NSIG - 1
      IF( DENSIG .LT. 1.) DENSIG= 1.
      DSIG= (SIG1 - SIG0) / DENSIG
C    B- FOR  STRAIN RATIO
  120 IF( DXY .LT. 1.E-3) GOTO 130
      XY0=EOT-(DXY * 1.7)
      IF( XY0.LT.1.) XY0= 1.
      XY1=XY0+(DXY * 3.3)
      DENOXY= NXY - 1
      IF( DENOXY .LT. 1.) DENOXY= 1.
      DXY=(XY1 - XY0) / DENOXY
  130 IF(DSIG .LE. 1.E-3 .AND.  DXY .LE. 1E-3) GOTO 104
C    C- FOR THE MEAN
      FI0=PHIOT-(DFI *5.1)
      IF(FI0.LT.0.) FI0= 0.
      FI1= FI0 +(DFI * 10.)
      IF(FI1 .GT. 180.)FI1= 180.
      DENOFI= NFI - 1
      IF( DENOFI .LT. 1.) DENOFI= 1.
      DFI=(FI1 - FI0)/ DENOFI
  104 CONTINUE
      IF(SUMYM .GT. SUOTI) GOTO 106
  105 SUOTI= SUMYM
      PHIOT=PHIM
      SOT=SM
      EOT=EM
C
C  OUTPUT  FINAL  RESULTS
C
  106 WRITE(6,1200)
      WRITE(6,1199) SUOTI
      WRITE(6,1201) PHIOT,SOT,EOT
      WRITE(6,1205)
C
C
C  CALL SUROUTINE PRINT TO OUTPUT :
C  CLASS INTERV.,HIST. FREQS., CURVE ABSCISSAE AND ORDINATES VALUES
C
      CALL PRINT(PHIOT,SOT,EOT,N,SUMH,HIS,ORD,ABSC)
 1200 FORMAT( 18H0     FINAL RESULTS)
 1205 FORMAT(1H0,2X,' CLASS INT. ',2X,'FREQ. HIST.',4X,' ABSC.',4X,' ORD
     1INATES')
 1206 FORMAT(1H0,' SUMYM=',F20.10)
 1199 FORMAT(9H0  SUOTI=,F20.10)
 1201 FORMAT( 1H ,' MEAN=',F20.10,2X,' ST.DEV.=',F20.10,2X,' STRAIN RATIO
     1=',F20.10 )
 1202 FORMAT(1H0,' CYCLES NO.=',I5,2X,' SUMYM=',F20.10)
 1203 FORMAT( 1H ,'DMEAN=',F20.10,2X,'DST.DEV.=',F20.10,2X,'DSTRAIN RATIO
     1=',F20.10 )
  900 FORMAT(3I5,F10.7)
  910 FORMAT(3F10.0)
  920 FORMAT( 9F8.0)
 1300 FORMAT(1H1,5X,'NUMBER OF CLASSES=', I5,5X,'PRECISAO=',F15.8)
 1400 FORMAT(1H0,'SEARCH FOR THE MEAN FROM=',F10.5,2X,'TO',F10.5,2X,'BY
     1 INITIAL INTERVALS OF=',F10.5)
 1500 FORMAT(1H0,'SEARCH FOR THE STD. DEVIATION FROM=',F10.5,2X,'TO',
     1F10.5,2X,'BY INITIAL INTERVALS OF=',F10.5)
 1600 FORMAT(1H0,'SEARCH FOR THE RATIO OF STRAIN FROM=',F10.5,2X,'TO',
     1F10.5,2X,'BY INITIAL INTERVALS OF=',F10.5)
      STOP
      END
      SUBROUTINE PRINT(AMEAN,SIGMA,RAT,N,SUMH,HIS,ORD ,ABSC )
C
C
C  SUBROUTINE TO OUTPUT RESULTS OF SEARCH
C
C
      DIMENSION HIS(100), ORD(100), ABSC(100)
      PI= 3.1415927
      FATOR= PI/ 180.
      AN= N
      SPAC= 180. / (2. * AN)
      NCL= N+N+ 1
      AM= AMEAN * FATOR
      STDV= SIGMA * FATOR
      T= SUMH / (SIGMA * SQRT(2. * PI))
      DO  500 I=1,NCL
      J= I-1
```

```
      TETLIN = (SPAC * J ) * FATOR
      TETA= ATAN( RAT * TAN( TETLIN ))
      IF ( TETA .LT. 0. ) TETA= TETA + PI
      EXPO= EXP( -.5 * (( TETA - AM ) / STDV ) **2 )
      FUNC= (( RAT * RAT ) * (( COS(TETA)) **2) + (SIN(TETA))**2)/RAT
      ORD(I)= T * EXPO * FUNC
      ABSC(I) = TETLIN/ FATOR
  500 CONTINUE
      DO 600 J =1,NCL
      I= (J-1) * 5
      IF (J/2 .EQ. J/2. ) GOTO 550
      WRITE(6,4000) ABSC(J),ORD(J)
      GOTO 600
  550 K= J/2
      WRITE(6,4001) I, HIS(K), ABSC(J), ORD(J)
  600 CONTINUE
 4000 FORMAT(1H ,30X,F5.0,5X,F10.5)
 4001 FORMAT( 1H ,5X,I5,5X,F10.5,5X,F5.0,5X,F10.5)
      RETURN
      END
```

```
C
C    P R O G R A M M E         I   S   T   R   A   E   S
C
C**************************************************************************
C**************************************************************************
C
C   IRROTATIONAL STRAIN RATIO ESTIMATION PROGRAMME
C
C**************************************************************************
C**************************************************************************
C
C   VERSION : JANUARY 1980
C   DEVELOPED AT  UNIV. OF LEEDS'  ICL 1906-A
C   BY  HENRIQUE  DAYAN
C
C.........................................................................
C
C   THIS PROGRAMME USES THE DISTRIBUTION OF HINGE DIRECTIONS OF SHEATH
C   OR CURVILINEAR FOLDS AS STRAIN MARKERS.
C.........................................................................
C   THE FIRST THREE CARDS CONTROL THE BOUNDARIES AND INTERVALS OF SEARCH
C   (USING THE DIRECT SEARCH METHOD) FOR EACH OF THE PARAMETERS : M E A N,
C   S T A N D A R D  D E V A T I O N  AND THE S T R A I N  R A T I O.
C   ENTER IN EACH CARD (I=1 TO 3) THE VALUES FOR THE FOLLOWING VARIABLES:
C_________________________________________________________________________
CI         I    REAL      I
CI COLUMNS I  VARIABLE    I           U    S    A    G    E
CI_________I______________I_______________________________________________
CI  1-15   I BOUNDS(I,1)  I THE LOWER BOUNDARY OF SEARCH
CI_________I______________I_______________________________________________
CI 16-30   I BOUNDS(I,2)  I THE UPPER BOUNDARY OF SEARCH
CI_________I______________I_______________________________________________
CI 31-45   I DELTAS(I)    I THE INITIAL INTERVAL OF SEARCH
CI_________I______________I_______________________________________________
C
C   THE FOURTH CARD REFERS TO PROGRAMME CONTROL OF SUBROUTINES , INPUT
C   TYPE AND OUTPUT MODE. THIS IS ACHIEVED THROUGH THE SUBSCRIPTED (REAL)
C   VARIABLES  C O N T R L  WHICH ARE SPECIFIED WITH THE SAME FORMAT F5.0
C_________________________________________________________________________
CI         I    REAL      I
CI COLUMNS I  VARIABLE    I           U    S    A    G    E
CI_________I______________I_______________________________________________
CI  1- 5   I CONTRL(1)    I NUMBER OF HISTOGRAM CLASS INTERVALS :
CI         I              I - IF 18 CLASSES IS THE REQUIRED NO. LEAVE
CI         I              I   THESE COLUMNS BLANK.
CI         I              I - OTHERWISE PUNCH THE REQUIRED NO. OF CLASSES.
CI_________I______________I_______________________________________________
CI  6-10   I CONTRL(2)    I NUMBER OF CYCLES REQUIRED BY THE DIRECT SEARCH
CI         I              I SUBROUTINE :
CI_________I______________I_______________________________________________
CI 11-15   I CONTRL(3)    I READING-DATA MODE :
CI         I              I - BLANK IF INPUT DATA ARE IN AZIMUTH AND DIP.
CI         I              I - ENTER ANY NUMBER IF DATA IS ALREADY IN
CI         I              I   DIRECTION COSINES .
CI_________I______________I_______________________________________________
CI 16-20   I CONTRL(4)    I RESULTS OUTPUT, FROM EACH CYCLE OF THE
CI         I              I DIRECT SEARCH SUBROUTINE :
CI         I              I - BLANK IF PRINTING IS REQUIRED .
C          I              I - ENTER NUMBER  1. OTHERWISE .
CI_________I______________I_______________________________________________
CI 20-21   I CONTRL(5)    I USE OR NOT OF THE GRADIENT ROUTINE  :
CI         I              I - BLANK IF THE GRADIENT METHOD IS REQUIRED .
CI         I              I - ENTER NUMBER  1.  OTHERWISE .
CI_________I______________I_______________________________________________
CI 26-30   I CONTRL(6)    I FREQUENCY - MODE :
CI         I              I - BLANK IF ABSOLUTE FREQUENCY IS REQUIRED .
CI         I              I - ENTER  NUMBER  1. FOR RELATIVE FREQUENCY .
CI_________I______________I_______________________________________________
CI 31-35   I CONTRL(7)    I USE OF THE DIRECT SEARCH ROUTINE :
CI         I              I - BLANK IF IT IS REQUIRED .
CI         I              I - ENTER NUMBER  1. OTHERWISE .
C__________I______________I_______________________________________________
CI 36-40   I CONTRL(8)    I INPUT - DATA MODE  :
CI         I              I - ENTER NUMBER  1. IF HISTOGRAM IS ALREADY
CI         I              I   AVAILABLE .
CI         I              I - BLANK OTHERWISE .
CI_________I______________I_______________________________________________
C
C   IN CASE  CONTRL(2) E Q U A L S   1.  THE HISTOGRAMS ARE READ FROM THE
C   NEXT TWO CARDS , 9 VALUES IN EACH CARD (WITH FORMAT F8.4). ENTER
C   HISTOGRAM ORDINATES IN COLUMNS : 1-8,9-16,17-24,25-32,33-40,41-48,
C   49-56,57-64,65-72 . THE ORDER IS  0 - 90 DEGREES IN THE FIRST CARD ,
C   AND 90 - 180 DEGREES IN THE SECOND CARD .
C.........................................................................
C   IN CASE CONTRL(3) IS GREATER THAN ZERO THE NEXT CARD IS USED FOR
C   IDENTIFICATION OF THE ESTIMATION . ENTER ANY PHRASE IN COLUMNS 1-80.
C
C
C**************************************************************************
C**************************************************************************
```

```
C
C
      DIMENSION XSP(1000),YSP(1000),ZSP(1000),SZ(3)
      DIMENSION XLM(1000),YLM(1000),ZLM(1000),SX(3)
      DIMENSION XFA(1000),YFA(1000),ZFA(1000),SF(3)
      DIMENSION HIS(72),SM(4),COL(80),AK(3)
      DIMENSION F(72),TL(72),Y(72),CONTRL(8)
      DIMENSION BOUNDS(3,2),DELTAS(3),PARS(3)
      COMMON/SCALA1/ PI,DUPI,DEGRAD,RADEG
      COMMON/SCALA2/ CTE,NCL
      COMMON/ARRAY1/ XSP,YSP,ZSP,XLM,YLM,ZLM,XFA,YFA,ZFA,SX,SZ
      COMMON/ARRAY2/ F,TL,Y,HIS
      DATA BLANK,CROSS,AST/1H ,1HX,1H*/
      PI= 3.141592654
      DEGRAD= PI / 180.
      RADEG= 1./DEGRAD
      DUPI= PI + PI
      HEIGHT= 0.
C
C          READ CONSTRAINTS OF SEARCH
      READ(1,200) ((BOUNDS(I,J),J=1,2),DELTAS(I),I=1,3)
C
C          READ CONTROL PARAMETERS
C
      READ(1,201) CONTRL
      NCL= IFIX(CONTRL(1))
      IF(NCL .EQ. 0) NCL= 18
      NCYCLE = IFIX(CONTRL(2))
      INDIC= IFIX(CONTRL(3))
      IPRINT= IFIX(CONTRL(4)) + 1
      NOP= IFIX(CONTRL(5)) + 1
      IN1= IFIX(CONTRL(6)) + 1
      IN2= IFIX(CONTRL(7)) + 1
      IN3= IFIX(CONTRL(8)) + 1
      GOTO( 7,6),IN3
    6 READ(1,205) (HIS(I),I=1,NCL)
      GOTO 16
    7 IF( INDIC) 8,8,9
    8 INDIC=1
      GOTO 10
    9 INDIC=3
      READ(5,203) (COL(I),I=1,80)
      WRITE(6,204)  COL
C
   10 SEH= 0.
      SUV= 0.
      NP= 0
      CALL READAT(INDIC,XSP,YSP,ZSP,NP,SEH,SUV,SZ,FK)
      AK(1)= FK
      NL= 0
      INDIC= INDIC + 1
      CALL READAT(INDIC,XLM,YLM,ZLM,NL,SEH,SUV,SX,FK)
      AK(2)= FK
      IF( SEH .EQ. 0. .OR. SUV .EQ. 0.) GOTO 11
      AUX= FLOAT(NP+NL)
      SEH= SEH/AUX
      SUV= SUV/AUX
      WRITE(6,202) SEH,SUV
   11 SEH= 0.
      SUV= 0.
      NF= 0
      CALL READAT(INDIC,XFA,YFA,ZFA,NF,SEH,SUV,SF,FK)
      AK(3)= FK
      IF( SEH .EQ. 0. .OR. SUV .EQ. 0.) GOTO 15
      SEH= SEH/FLOAT(NF)
      SUV= SUV/FLOAT(NF)
      WRITE(6,202) SEH,SUV
C
C             FORM FREQUENCY HISTOGRAM
C
   15 CALL HISTGM( NP,NL,NF,AK)
   16 ACL= FLOAT(NCL)
      TEMP= SQRT(DUPI)
      SUMHIS= 0.
      DO 20 I=1,NCL
      SUMHIS= SUMHIS + HIS(I)
      IF(HIS(I) .GT. HEIGHT) HEIGHT= HIS(I)
   20 CONTINUE
      CTE= (100./ACL)/TEMP
C
C             CHOOSE BETWEEN RELATIVE FREQUENCY(GOTO 30)   ,
C             OR ABSOLUTE FREQUENCY(GOTO 50)
C
   25 GOTO(50,30),IN1
   30 DO 40 I=1,NCL
      IF(HIS(I) .EQ. 0.) GOTO 40
      F(I)= HIS(I) / SUMHIS
   40 CONTINUE
      GOTO 50
   50 DO 55 I=1,NCL
```

```
   55 F(I)= HIS(I)
      CTE= SUMHIS*CTE
   60 DO 70 I=1,NCL
      TTL= (I-.5)*PI/ACL
      IF(TTL .EQ. PI/2.) TTL= TTL-1.E-6
      TI(I)= TAN(TTL)
   70 CONTINUE
      GOTO( 80,100),IN2
C
C            CALL SUBROUTINE MODEL2 TO PERFORM INTERVALS
C            ELIMINATION AND TO LOCATE THE FEASIBLE REGION
C
   80 CALL MODEL2(NCYCLE,IPRINT,BOUNDS,DELTAS,PARS)
C
C            IF REQUIRED :
C            FINALIZE OPTIMIZATION BY THE GRADIENT AND/OR
C            STEEPEST DESCENT METHOD(S)...( GOTO 90)
C            OTHERWISE PRINT HISTOGRAM AND FITTED CURVE..(GOTO 95)
C
      GOTO(90,95),NOP
   90 CALL GRADIT(PARS,SUOTI)
C
C            WRITE AND PRINT THE HISTOGRAM AND ITS FITTED CURVE
C
   95 NCL= NCL + NCI
      ACL= FLOAT(NCL)
      IN2= 2
      DO 96 I=1,NCL
   96 F(I)= 1.E-6
      GOTO 60
  100 CALL YPSLON( 1,PARS,SM)
        DO 105 I=1,NCI
      IF(Y(I) .GT. HEIGHT) HEIGHT= Y(I)
  105 CONTINUE
      SCALE= 64./HEIGHT
      PROP2= (HEIGHT*100.)/(SUMHIS*.8)
      PROP1= PROP2/2.
      WRITE(6,303)
      WRITE(6,304) PROP1,PROP2
      WRITE(6,305)
      BUX= 180./FLOAT(NCL)
      AUX= 0.
      M= 0
      DO 130 I=1,NCI
      AUX= AUX + BUX
      DO 110 J=1,80
  110 COL(J)= BLANK
      IF(I/2 .NE. I/2.) GOTO 115
      K= Y(I)*SCALE + 1
      COL(K)= AST
      WRITE(6,301) AUX,Y(I),COL
      GOTO 130
  115 M= M + 1
      K= HIS(M)*SCALE + 1
      IF(K) 122,122,120
  120 DO 121 J=1,K
  121 COL(J)= CROSS
  122 K= Y(I)*SCALE + 1
      IF(K-80) 125,125,127
  125 IF(K) 127,127,126
  126 COL(K)= AST
  127 WRITE(6,302) HIS(M),AUX,Y(I),COL
  130 CONTINUE
      WRITE(6,305)
  200 FORMAT(3F15.10)
  201 FORMAT(8F5.0)
  202 FORMAT(1H0,' CENTRE OF GRAVITY GIVEN BY GRID REFS. :',2F10.0)
  203 FORMAT(80A1)
  204 FORMAT( 1H0,80A1)
  205 FORMAT(9F8.4)
  301 FORMAT( 1H ,13X,F5.0,6X,F8.3,'  I',80A1,'I')
  302 FORMAT(1H ,1X,F9.5,3X,F5.0,6X,F9.3,'  +',80A1,'I')
  303 FORMAT(1H0,' FREQUENCY ABSCIS.  FITTED CURVE',28X,'S C A L E D   F
     1 R E Q U E N C Y')
  304 FORMAT(1H',' HISTOGRAM VALUES      ORDINATES     0.0',35X,F4.1,'%',35
     1X,F4.1,'%')
  305 FORMAT( 1H ,35X,1H+,38(1H-),1H+,39(1H-),1H+)
      STOP
      END
      SUBROUTINE READAT(IGO,XC,YC,ZC,KT,SUMEH,SUMUV,S,FK)
C
C
C  THIS SUBROUTINE READS DATA IN TWO MODES :
C
C     - AZIMUTH  AND  PLUNGE(REAL VARS. AZ,PL)
C                  OR
C     - DIRECTION  COSINES(REAL  VARS.  X,Y,Z)
C  IN BOTH MODES PROVISION WAS MADE FOR READING GRID CO-ORDINATES
C  AND USER'S STATION NUMBER . CONTROL OF THE READING MODE IS DONE
C  IN THE MAIN PROGRAM BY THE REAL VARIABLE  CONTRL(3)
```

```
C
C
      DIMENSION XC(1000),YC(1000),ZC(1000),STA(10),S(3)
      COMMON/SCALA1/ PI,DUPI,DEGRAD,RADEG
      A= 0.
      B= 0.
      C= 0.
    4 GOTO( 5,5,7,7),IGO
C
C          READ DATA IN TERMS OF AZIMUTH AND PLUNGE
    5 READ(5,50) AZ,DIP,EH,UV,STA,ISTOP
      IF(ISTOP .NE.0) GOTO 10
      KT= KT + 1
      GOTO ( 6,8,7,7),IGO
C
C          CONVERT TO POLE OF S-PLANE
    6 AZ= AZ + 180.
      IF(AZ .GT. 360.) AZ= AZ - 360.
      DIP= 90. - DIP
      GOTO 8
C
C          READ DATA ALREADY IN DIR. COSINES
    7 READ(5,51) X,Y,Z,EH,UV,STA,ISTOP
      IF( ISTOP .NE. 0) GOTO 10
      KT= KT + 1
      XC(KT)= X
      YC(KT)= Y
      ZC(KT)= Z
      GOTO 9
C
C          TRANSFORM AZIMUTH AND PLUNGE TO DIR. COSINES
    8 AX= AZ*DEGRAD
      DX= DIP*DEGRAD
      CA= COS(AX)
      CD= COS(DX)
      SA= SIN(AX)
      SD= SIN(DX)
      XC(KT)= CD*CA
      YC(KT)= CD*SA
      ZC(KT)= SD
    9 A= A + XC(KT)
      B= B + YC(KT)
      C= C + ZC(KT)
      SUMEH= SUMEH + EH
      SUMUV= SUMUV + UV
      GOTO 4
   10 AN= FLOAT(KT)
      A= A/AN
      B= B/AN
      C= C/AN
C
C          EVALUATE THE RESULTANT VECTOR
      R= A*A + B*B + C*C
      R= SQRT(R)
      S(1)= A/R
      S(2)= B/R
      S(3)= C/R
C
C          CALCULATE FISHERS' K-PARAMETER
      FK= AN - 1.
      FK= FK/(AN - R)
   50 FORMAT(4F10.3,10A1,I5)
   51 FORMAT(3F12.7,2F10.0,4X,10A1,I5)
      RETURN
      END
      SUBROUTINE HISTGM( NP,NL,NF,AK)
C
C
C   THIS SUBROUTINE GROUPS DATA INTO FREQUENCY HISTOGRAM . THE NUMBER
C   OF CLASS INTERVALS IS CONTROLLED ,IN THE MAIN PROGRAM, BY
C   THE REAL VARIABLE CONTRL(1).
C   THE LEAST SQUARES METHOD IS USED IN ORDER TO DETERMINE THE
C   PROJECTING PLANE( XY-PLANE OF THE FINITE STRAIN ELLIPSOID).
C
C
C
      DIMENSION XSP(1000),YSP(1000),ZSP(1000),SZ(3)
      DIMENSION XLM(1000),YLM(1000),ZLM(1000),SX(3)
      DIMENSION XFA(1000),YFA(1000),ZFA(1000),AK(3)
      DIMENSION D(3),E(2,3),X(3),P(3),TH(500),HIS(72)
      DIMENSION F(72),FL(72),Y(72)
      COMMON/SCALA1/ PI,DUPI,DEGRAD,RADEG
      COMMON/SCALA2/ CTF,NCL
      COMMON/ARRAY1/ XSP,YSP,ZSP,XLM,YLM,ZLM,XFA,YFA,ZFA,SX,SZ
      COMMON/ARRAY2/ F,FL,Y,HIS
C
C          THE ATTITUDE OF   X-AXIS
C
      CALL ATTITU( SX,AZX,DIPX)
      DO 10 I=1,3
   10 E(1,I)= SX(I)
```

```
C
C          MINIMIZE BY LEAST SQUARES . FIND THE BEST
C          FIT PLANE,CONTAINING THE X-AXIS.
C
      ANUM= 0.
      DENOM= 0.
      DO 20 I=1,NP
      D(1)= XSP(I)
      D(2)= YSP(I)
      D(3)= ZSP(I)
      AUX= 0.
      DO 15 J=1,3
   15 AUX= AUX + SZ(J)*D(J)
      AUX= ABS(AUX)
      IF( AUX .GT. 1.) AUX= 1.
      IF( AUX .LT. 1.E-20) AUX= 1.E-20
      TEMP= ACOS( AUX)
      IF( TEMP .EQ. PI/2.) TEMP= TEMP - 1.E-6
      TEMP= TAN( TEMP)
      AUX= AK(1)*TEMP
      W= 1./AUX
      AUX= E(1,1)*D(2)
      AUX= AUX - (E(1,2)*D(1))
      BUX= E(1,3)*D(2)
      BUX= BUX - (E(1,2)*D(3))
      ANUM= ANUM + (AUX*BUX*W)
      DENOM= DENOM + (AUX*AUX*W)
   20 CONTINUE
C
C          CALCULATE UNKNOWN PARAMETERS  A  AND  B
C
      A= -(ANUM/DENOM)
      AUX= -(A*E(1,1))-E(1,3)
      B= AUX/E(1,2)
C
C
C          THE ATTITUDE OF THE POLE OF THE BEST FIT PLANE  XZ .
C
      AUX= A*A + B*B + 1.
      AUX= 1./SQRT(AUX)
      X(1)= A*AUX
      X(2)= B*AUX
      X(3)= AUX
      DO 21 I=1,3
   21 E(2,I)= X(I)
      CALL ATITU( X,AZY,DIPY)
C
C           CALCULATE FOLD AXIS PROJECTIONS
C
      DO 25 I=1,NF
      P(1)= XFA(I)
      P(2)= YFA(I)
      P(3)= ZFA(I)
      CALFA= 0.
      CBETA= 0.
      DO 24 K=1,3
      CALFA= CALFA + E(1,K)*P(K)
      CBETA= CBETA + E(2,K)*P(K)
   24 CONTINUE
      AUX= CALFA*CALFA
      CBETA= CBETA*CBETA
C
C          CALCULATE THETA-2  ( XY-PLANE PROJECTION)
C
      TEMP= AUX + CBETA
      TEMP= 1./SQRT(TEMP)
      TEMP= CALFA*TEMP
      TH(I)= ACOS(TEMP)
   25 CONTINUE
      FATOR= 180./FLOAT(NCL)
C
C          FORM FREQUENCY HISTOGRAM
C
      DO 30 I=1,NCL
   30 HIS(I)= 0.
      DO 35 I=1,NF
      AUX= TH(I)*RADEG
      X(1)= XFA(I)
      X(2)= YFA(I)
      X(3)= ZFA(I)
      CALL ATITU( X,AZF,DIPF)
      IF( AZF .LE. AZX) AUX= 180. - AUX
      IF( AUX .GT. 180.) AUX= AUX - 180.
      AUX= AUX/FATOR
      J= IFIX(AUX) + 1
      HIS(J)= HIS(J) + 1.
   35 CONTINUE
      WRITE(6,100)
      WRITE(6,101) AZX,DIPX,AZY,DIPY
      WRITE(6,102)
```

```
      WRITE(6,103) (HIS(I),I=1,NCI)
  100 FORMAT(1H0,' ATTITUDE CF STRAIN ELLIPSOID PRINCIPAL AXES')
  101 FORMAT(1H ,' X-AXIS=',F7.3,'/',F6.3,10X,'Y-AXIS=',F7.3,'/',F6.3)
  102 FORMAT(1H0,' THETA-2= FOLD AXIS PROJECTION ON XY-PLANE')
  103 FORMAT(9(2X,F10.3))
  104 FORMAT(1H0,' BEST FIT PLANE PARAMETERS:',2X,' A=',F20.10,' B=',
     1F20.10)
      RETURN
      END
      SUBROUTINE MODEL2( NCY,IND,ED,DE,POT)
C
C
C  THIS SUBROUTINE USES A CONSTRAINED DIRECT SEARCH METHOD OF
C  MINIMIZATION ,TO INITIATE THE OPTIMIZATION PROCEDURE AND TO LOCATE
C  THE FEASIBLE REGION(IT INTENDS,AT EVERY CYCLE OF ITERATIONS,TO
C  RESTRICT THE INTERVALS OF SEARCH).
C  IF USED AS THE ONLY METHOD OF MINIMIZATION SEE IN THE MAIN PROGRAM:
C    - CONTRL(2) : MUST BE AT LEAST GREATER OR EQUAL TO  12
C    - CONTRL(5) : MUST BE EQUAL TO 1.
C    - CONTRL(7) : MUST BE EQUAL TO 0.  OR LEFT BLANK
C
C
      DIMENSION F(72),TL(72),Y(72)
      DIMENSION BD(3,2),RZ(3,2),CST(3,2)
      DIMENSION PA(3),NI(3),DB(3),POT(3),PAM(3),DEN(3)  ,YL(72)
      COMMON/SCALA1/ PI,DUPI,DEGRAD,RADEG
      COMMON/SCALA2/ CTE,NCL
      COMMON/ARRAY2/ F,TL,Y,HIS
      DATA RZ/1*5.1,1*1.5,1*1.7,1*10.,1*2.85,1*3.3/
      DATA CST/1*0.,1*1.,1*1.,1*180.,1*180.,1*100./
      DOUBLE PRECISION A3
      WRITE(6,100)
      WRITE(6,101)
      WRITE(6,102)
      WRITE(6,103) BD(1,1),BD(1,2),DB(1)
      WRITE(6,104) BD(2,1),BD(2,2),DB(2)
      WRITE(6,105) BD(3,1),BD(3,2),DB(3)
      IF( IND .EQ. 1) WRITE(6,106)
      SUMIN= 1.E40
      SUOTI= SUMIN
C
C           START CYCLE(S) OF COMBINATIONS
C
C
      DO 35 N=1,NCY
      DO 10 I=1,3
      AUX= BD(I,2) - BD(I,1)
      AUX= AUX/DB(I)
      AUX= ABS(AUX)
      NI(I)= IFIX(AUX) + 1
   10 CONTINUE
      NF= NI(1)
      NS= NI(2)
      NR= NI(3)
      DO 20 IR=1,NR
      PA(3)= BD(3,1) + (IR-1)*DB(3)
      DO 20 IS=1,NS
      PA(2)= BD(2,1) + (IS-1)*DB(2)
      DO 20 IFI=1,NF
      PA(1)= BD(1,1) + (IFI-1)*DB(1)
C
C           COMPUTE THE SUM OF THE SQUARED DEVIATIONS
C           BETWEEN FITTING CURVE AND HISTOGRAM
C
      SUM= 0.
      DO 15 I=1,NCL
      IF(F(I) .EQ. 0.) GOTO 15
      A1= TL(I)*PA(3)
      THR= ATAN(A1)
      IF(THR .LT. 0.) THR= THR+PI
      THD= THR*RADEG
      AUX= COS(THR)
      COS2= AUX*AUX
      A2= THD-PA(1)
      AUX= A2/PA(2)
      AUX= AUX*AUX
      A3= EXP(-.5*AUX)
      A4= PA(3)*PA(3) - 1.
      A4= 1. + COS2*A4
      ANUM= CTE* A4 * A3
      DENOM= PA(2)*PA(3)
      YL(I)= ANUM/DENOM
      AUX= YL(I) - F(I)
      AUX= AUX*AUX
      SUM= SUM + AUX
   15 CONTINUE
      IF( SUM .LT. SUMIN) GOTO 18
      GOTO 20
   18 SUMIN= SUM
      DO 19 I=1,3
```

```
   19 PAM(I)= PA(I)
   20 CONTINUE
      DIF= SUMIN - SUOTI
      IF( IND .NE. 1) GOTO 24
      WRITE(6,107) N,SUMIN
      WRITE(6,108) PAM(1),BD(1,1),BD(1,2),DB(1)
      WRITE(6,109) PAM(2),BD(2,1),BD(2,2),DB(2)
      WRITE(6,110) PAM(3),BD(3,1),BD(3,2),DB(3)
   24 IF( DIF) 25,30,30
   25 SUOTI= SUMIN
      DO 26 I=1,3
   26 POT(I)= PAM(I)
   30 CONTINUE
      IF( N .EQ. NCY) GOTO 35
      IAUX= 4
      DO 34 J=1,3
      ID= IAUX - J
      IF( DB(ID) .LE. 1.E-3) GOTO 35
      AUX= DB(ID)*RZ(ID,1)
      BD(ID,1)= POT(ID) - AUX
      IF( BD(ID,1) .LT. CST(ID,1)) BD(ID,1)= CST(ID,1)
      AUX= DB(ID)*RZ(ID,2)
      BD(ID,2)= BD(ID,1) + AUX
      NAUX= NI(ID) - 1
      AUX= FLOAT(NAUX)
      IF( AUX .LT. 1.) AUX= 1.
      DEN(ID)= AUX
      AUX= BD(ID,2) - BD(ID,1)
      AUX= AUX/DEN(ID)
      DB(ID)= AUX
   34 CONTINUE
   35 CONTINUE
      IF( SUMIN .GT. SUOTI) GOTO 40
      SUOTI= SUMIN
      DO 36 I=1,3
   36 POT(I)= PAM(I)
   40 CONTINUE
  100 FORMAT(1H0,' RESULTS FROM SUBROUTINE (MODEL2) WHICH MADE USE OF THI
     1E DIRECT SEARCH METHOD')
  101 FORMAT(1H0,' THE INITIALS CONSTRAINTS OF SEARCH WERE SET UP AS: ')
  102 FORMAT(1H0,6X,'PARAMETER',5X,'=',3X,'FROM',12X,'TO',11X,'BY INTERV
     1ALS OF')
  103 FORMAT(1H ,3X,'MEAN',8X,'=',F10.5,5X,F10.5,7X,F10.5)
  104 FORMAT(1H ,1X,'STANDARD DEVIATION =',F10.5,5X,F10.5,7X,F10.5)
  105 FORMAT(1H ,3X,'STRAIN RATIO',5X,'=',F10.5,5X,F10.5,7X,F10.5)
  106 FORMAT(1H0,' R E S U L T S    O F    S E A R C H')
  107 FORMAT(1H0,' IN THE END OF THE',I5,' CYCLE,THE MINIMUM SUM OF THE
     1 SQUARES IS= ',E14.7)
  108 FORMAT(1H ,'     MEAN =',F10.5,2X,'SEARCHED FROM:',F10.5,' TO:',F10.
     15,' BY INTERVALS OF:',F10.5)
  109 FORMAT(1H ,' ST.DEV.=',F10.5,2X,'SEARCHED FROM:',F10.5,' TO:',F10.
     15,' BY INTERVALS OF:',F10.5)
  110 FORMAT(1H ,' STRAIN =',F10.5,2X,'SEARCHED FROM:',F10.5,' TO:',F10.
     15,' BY INTERVALS OF:',F10.5)
      RETURN
      END
      SUBROUTINE GRADIT( PARMS,SUMOPT)
C
C
C     THIS SUBROUTINE WAS DERIVED FOR FINALIZING THE OPTIMIZATION
C     PROCEDURE BY MEANS OF THE GRADIENT TECNIQUE   (IF IT THE CASE)  ,
C     OTHERWISE IT SWITCHES TO THE STEEPEST DESCENT METHOD.
C     THE OBJECTIVE FUNTION EVALUATION IS GIVEN BY SUBROUTINE YPSILON
C     AND MATRIX INVERSION BY SUBROUTINE MATINV .
C
C
      DIMENSION PA(3),DPR(3),GRAD(3),P1(3),DX(3),PARMS(3)
      DIMENSION D1(3,3),D2(3,3),HV(3,3),SCH(4),DR(4)
      DIMENSION B(3),H(2),PF(3),IND(3),SUM(4)
      DIMENSION F(72),FL(72),Y(72)
      COMMON/SCALA1/ PI,DUPI,DEGRAD,RADEG
      COMMON/SCALA2/ CTF,NCL
      COMMON/ARRAY2/ F,FL,Y,HIS
      WRITE(6,200)
      WRITE(6,201) PARMS
      SUMIN= 1.E40
      KOUNT= 0
      DO 5 I=1,3
      IND(I)= 0
    5 PA(I)= PARMS(I)
C
C          START  ITERATIONS
C
   10 KOUNT= KOUNT + 1
      RETAIN= SUMIN
C
C          THE FIRST DERIVATIVES
C
      CALL YPSLON( 2,PA,SUM)
      DO 20 I=1,3
```

```
   20 DER(I)= SUM(I)
      SUMIN= SUM(4)
      NAUX= IND(1) + IND(2)
      IF(NAUX .NE. 0) GOTO 26
      DIF= ABS( RETAIN - SUMIN)
      IF( KOUNT .GE. 10) GOTO 25
      GOTO 26
   25 IF( ADIF .LE. 1.E-3) GOTO 170
   26 WRITE(6,202) KOUNT,SUMIN
      WRITE(6,203) PA
C
C            THE GRADIENT VECTORS
C
      DEN=0.
      DO 30 I=1,3
   30 DEN= DEN + (DER(I)*DER(I))
      DEN= SQRT(DEN)
      DO 40 I=1,3
   40 GRAD(I)= -DER(I)/DEN
C
C            IF REQUIRED SWITCH TO  THE STEEPEST DESCENT METHOD
C
      IF( IND(1) .NE. 0) GOTO 90
C
C            THE SECOND DERIVATIVES MATRIX(HESSIAN MATRIX)
C
      IND(2)= 0
      DELTA= .001
      DO 50 I=1,3
   50 P1(I)= PA(I)
      DO 60 I=1,3
      DX(I)= PA(I) * DELTA
      P1(I)= PA(I) + DX(I)
      CALL YPSLON( 2,P1,DR)
      DO 55 J=1,3
   55 D1(I,J)= DR(J)
      P1(I)= PA(I)
   60 CONTINUE
      DO 70 I=1,3
      DO 70 J=1,3
      IF( I .GT. J ) GOTO 65
      AUX= D1(I,J) - DER(J)
      D2(I,J)= AUX/DX(I)
      GOTO 70
   65 D2(I,J)= D2(J,I)
   70 CONTINUE
C
C            FIND THE INVERSE OF THE HESSIAN MATRIX
C
      CALL MATINV( D2,3,3,HV)
      DO 80 I=1,3
   80 B(I)= 0.
      DO 85 I=1,3
      DO 85 J=1,3
      B(I)= B(I) + HV(I,J) * GRAD(J)
   85 CONTINUE
      GOTO 100
   90 IND(1)= IND(1) - 1
      DO 95 I=1,3
   95 B(I)= GRAD(I)
      WRITE(6,204) KOUNT
C
C            INITIATE DIRECT SEARCH FOR STEP LENGTH H
C
  100 CONTINUE
      SUBEST= SUMIN
      ASUMIN= SUMIN
      SMIN= SUMIN
      ALEAST= SUMIN
      NRUN= 0
      LAP= 0
      H(1)= 0.
      H(2)= 0.
      HBEST= H(2)
      SPEED= 1.E8
      ALIMIT= 1.E-10
  105 DH= SPEED
  106 H(2)= H(1) + DH
      DO 110 I=1,3
      AUX= B(I) * H(2)
  110 PE(I)= PA(I) + AUX
      CALL YPSLON( 1,PE,SCH)
      SEARCH= SCH(4)
      IF( SEARCH .LT. SUBEST) SUBEST= SEARCH
      LAP= LAP + 1
      IF( ASUMIN - SEARCH) 115,115,120
  115 IF( NRUN .EQ. 0) ALIMIT= 1.E-40
      H(1)= H(1) - DH
      SPEED= SPEED / 10.
      IF(H(1) .LT. 0.) H(1)= 0.
```

```
      IF( ALIMIT .EQ. 1.E-40 .AND. SEED .LE. ALIMIT) GOTO 130
      IF( SEED .LE. ALIMIT) GOTO 131
      ASUMIN= SMIN
      GOTO 105
  120 NRUN= 1
      ALIMIT= 1.E-10
      SMIN= ASUMIN
      ASUMIN= SEARCH
      IF( SEARCH .GT. ALEAST) GOTO 125
      ALEAST= SEARCH
      HBEST= H(2)
  125 AB= H(2)-H(1)
      AB= ABS(AB)
      IF(AB .LT. ALIMIT) GOTO 131
      H(1)= H(2)
      GOTO 106
  130 HBEST= H(2)
  131 IF( H(2)   .LE. 1.E-37) GOTO 135
      GOTO 140
  135 IF(IND(1) .EQ. 0) GOTO 136
      GOTO 155
  136 IND(1)= 10
      IND(2)= 1
      GOTO 90
  140 WRITE(6,205) HBEST,SUBEST,IAP
C
C         OBTAIN  THE  NEW  CO-ORDINATES
C
      DO 150 I=1,3
      AUX= B(I)*HBEST
      PA(I)= PA(I)  + AUX
  150 CONTINUE
      GOTO 10
  155 WRITE(6,209)
  170 DO 171 I=1,3
  171 PARMS(I)= PA(I)
      WRITE(6,206) DIF
      SUMOPT= SUMIN
      WRITE(6,207)
      WRITE(6,208) SUMOPT
      WRITE(6,203) PARMS
  200 FORMAT(1H0,' ***********  MINIMISATION  BY  THE GRADIENT   METHOD
     1 ***********')
  201 FORMAT(1H0,' INPUT PARAMETERS : MEAN=',F11.7,5X,'ST. DEV.=',F11.7,
     15X,'STRAIN RATIO=',F11.7)
  202 FORMAT(1H0,' IN THE ',I5,'  ITERATION THE SUM OF SQUARED DEVIATION
     1S IS',E14.7,' WITH PARAMETERS :')
  203 FORMAT(1H ,' MEAN=',F11.7,5X,' STD. DEV.=',F11.7,5X,' STRAIN RATIO
     1=',F11.7)
  204 FORMAT(1H ,' *****  IN THE ITERATION NO.(',I5,') : THE PRESENT SUB
     1ROUTINE USED ONLY THE STEEPEST DESCENT METHOD')
  205 FORMAT(1H ,' SEARCH FOR STEP LENGTH(H)=',E14.7,'  YIELDS THE SUM
     1OF SQUARES=',E14.7,'.  NO. OF FUNC. EVALS.=',I5)
  206 FORMAT(1H0,' CONVERGENCE LIMIT (',E14.7,') ATTAINED.  END OF THE G
     1RADIENT MINIMISATION')
  207 FORMAT( 1H ,' F I N A L   R E S U L T S')
  208 FORMAT(1H ,' FINAL SUM OF SQUARED DEVIATIONS=',E14.7)
  209 FORMAT( 1H0,' *****REMARK : SEARCH IS OUT OF RANGE')
      RETURN
      END
      SUBROUTINE YPSION(NCTEL,PAM,SOMA)
C
C
C  THIS SUBROUTINE EVALUATES NOT ONLY THE OBJECTIVE FUNCTION,BUT ALSO
C  THE FIRST (ANALYTICAL) PARTIAL DERIVATIVES .
C
C
      DIMENSION F(72),TL(72),Y(72)
      DIMENSION P2(3),DIF(72),SOMA(4),DER(3)
      DIMENSION PAR(3),PAM(3)
      COMMON/SCALA1/ PI,DUPI,DEGRAD,RADEG
      COMMON/SCALA2/ CTE,NCL
      COMMON/ ARRAY2/ F,TL,Y,HIS
      DO 10 I=1,2
      PAR(I)= PAM(I)
   10 P2(I)= PAR(I) * PAR(I)
      PAR(3)= PAM(3)
      P2(3)= PAM(3) * PAM(3)
      DO 15 I=1,4
   15 SOMA(I)= 0.
      DO 21 I=1,NCL
      IF(F(I) .EQ. 0.) GOTO 21
      A1= PAR(3)*TL(I)
      A2= A1*A1
      THR= ATAN(A1)
      IF(THR .LT. 0.) THR= THR+PI
      THD= THR*RADEG
      COS2= COS(THR)
      COS2= COS2*COS2
      A3= THD-PAR(1)
```

```
      A4= A3*A3
      A5= EXP(-.5*(A4/P2(2)))
      A6= P2(3)-1.
      A7= 1.+COS2*A6
      Y(I) = (CTE*A5*A7)/(PAR(2)*PAR(3))
      DIF(I)= Y(I)-F(I)
      DIFF= DIF(I)
      IF( NCTRL .EQ. 1) GOTO 20
C
C           THE PARTIAL DERIVATIVES .
C             .MEAN
C
      DER(1) = (Y(I)*A3)/P2(2)
      SOMA(1)= SOMA(1) +(2.*DIFF*DER(1))
C
C             .STANDARD  DEVIATION
C
      AUX = A4-P2(2)
      AUX= AUX/(PAR(2)*P2(2))
      DER(2) = Y(I)*AUX
      SOMA(2)= SOMA(2) +(2.*DIFF*DER(2))
C
C             .STRAIN RATIO  ( R )
C
      A8= 2.*P2(3)*COS2
      A9= SIN(2.*THR)*A1*A6
      A9= A9/(1.+A2)
      A10= (A8-A9-A7)/P2(3)
      A11= A3*TL(I)*A7
      DN= P2(2)*PAR(3)*(1.+A2)
      A11= (A11/DN)*RADEG
      CUX= (CTE*A5)/PAR(2)
      DER(3)= CUX*(A10-A11)
      SOMA(3) = SOMA(3) +(2.*DIFF*DER(3))
C
   20 SOMA(4)= SOMA(4) +(DIFF*DIFF)
   21 CONTINUE
      RETURN
      END
      SUBROUTINE MATINV( A,N,N1,B)
      DIMENSION A(N1,N1), B(N1,N1)
      DO 100 I=1,N
      DO 101 J=1,N
      B(I,J)= 0.
  101 CONTINUE
      B(I,I)=1.
  100 CONTINUE
      DET= 1.
      DO 102 I=1,N
      DIV= A(I,I)
      DET= DET * DIV
      DO 103 J=1,N
      A(I,J)= A(I,J) / DIV
      B(I,J)= B(I,J) / DIV
  103 CONTINUE
      DO 104 J= 1,N
      IF(I-J) 1,104,1
    1 RATIO= A(J,I)
      DO 105 K=1,N
      A(J,K)= A(J,K) - RATIO * A(I,K)
      B(J,K)= B(J,K) - RATIO * B(I,K)
  105 CONTINUE
  104 CONTINUE
  102 CONTINUE
      RETURN
      END
      SUBROUTINE ATITU( X,AM,DM)
C
C
C   SUBROUTINE TO CONVERT DATA IN DIRECTION COSINES MODE
C   TO  AZIMUTH  AND  PLUNGE  (DEGREES) .
C
C
      DIMENSION X(3)
      COMMON/SCALA1/ PI,DUPI,DEGRAD,RADEG
      IF(X(3)) 1,3,3
    1 DO 2 I=1,3
    2 X(I) = -X(I)
    3 IF(X(1)) 4,9,5
    4 FAC= PI
      GOTO 8
    5 IF(X(2)) 6,10,7
    6 FAC= DUPI
      GOTO 8
    7 FAC= 0.
    8 AM= X(2)/X(1)
      AM= ATAN(AM) + FAC
      GOTO 11
    9 AM= PI/2.
      GOTO 11
```

```
10 AM= 0.
11 AUX= ASIN(X(3))
   DM= AUX*RADEG
   AM= AM* RADEG
   IF(DM - 90.) 13,13,12
12 DM= 180. - DM
   AM= AM + 180.
13 CONTINUE
   IF(AM .GT. 360.) AM= AM-360.
   RETURN
   END
```

```
C
C
C   P R O G R A M M E       F I T E I I
C
C* ** ** ** * ** ** ** ** * ** ** ** ** ** * ** ** ** ** ** ** **
C            PROGRAMME FOR TRIDIMENSIONAL STRAIN ESTIMATION
C* ** * ** * ** ** * ** ** ** ** ** ** ** ** ** ** ** ** ** ** **
C
C
C  VERSION : APRIL 1980
C  DEVELOPED AT  LEEDS'ICL-1906-A
C  BY  HENRIQUE DAYAN
C
C
C
C*********************************************************************
C
C  IF THE PROGRAMME IS TO BE USED O N L Y FOR FITTING PURPOSES  READ
C  THE INSTRUCTIONS IN PART A , OTHERWISE IF IT IS NEEDED 2D-STRAIN
C  ESTIMATION FOLLOW INSTRUCTIONS IN PART B.
C
C.....................................................................
C
C      P A R T   A
C   I N P U T   I N S T R U C T I O N S :
C  CARD    COLUMNS
C  1ST.       2          : INTEGER VARIABLE IOPT . DO NOT LEAVE IT BLANK(NOR
C                          ENTER ZERO) . IF YOU WANT THE PROGRAMME ONLY FOR
C                          FITTING PURPOSES ENTER ANY INTEGER .
C            3-72        : ENTER ANY PHRASE FOR SAMPLE IDENTIFICATION.
C  EVERY SAMPLE IS MADE OF TWO CARDS : THE FIRST IDENTIFIES  THE
C  SAMPLE (72 COLUMNS) . THE SECOND CONTAINS 6 REAL VARIABLES DEFINING
C  THE RATIOS OF 3 PERPENDICULAR ELLIPSES : XY(COLUMNS 1-7) ,YZ(CO-
C  LUMNS 15-25) AND THEIR ORIENTATION ANGLES : XY-PLANE(22-28) ,YZ
C  (29-35) AND ZX-PLANE(36-42).
C  THE LAST DATA 'CARD' SHOULD ALSO CONTAIN A SENTINEL(INTEGER VARIABLE
C  ISENT) . ENTER NUMBER 9 IN THE 44TH COLUMN IN ORDER TO END THE
C  CALCULATION.
C
C.....................................................................
C
C      P A R T   B
C   I N P U T   I N S T R U C T I O N S :
C  THE FIRST 'CARD' CONTAINS SPECIMEN REFERENCE . EVERY SAMPLE SHOULD
C  CONSIST OF THREE SETS OF PARTICLES MEASUREMENTS (I.E. IN THE XY,
C  YZ AND ZX-PLANE) . A CONTROL 'CARD' PRECEEDS EACH SET,WHILE THE LAST
C  'CARD' IN EVERY SET CONTAINS A SENTINEL.
C  CARD    COLUMNS
C  1ST.  72 COLUMNS   : ENTER ANY PHRASE FOR SAMPLE IDENTIFICATION
C  2ND.  COLUMN NO. 5: ENTER THE INTEGER VARIABLE DETERMINING THE
C                      CO-ORDINATE PLANE AND SENSE OF MEASUREMENT FOR
C                      EACH SET OF DATA (PUNCH AS FOLLOWS) ;
C         1            REFERING TO MEASUREMENTS FROM  X TOWARDS Y
C         2                      DITTO               Y  TWDS   Z
C         3                      DITTO               Z  TWDS   X.NOT
C                      NECESSARILY IN THAT ORDER.
C        6-15        : REAL VARIABLE C O R E C T .
C                      IT CORRECTS A SYSTEMATIC ERROR FOR THE WHOLE SET
C                      OF MEASUREMENTS IN THAT PLANE . BLANK IF THERE
C                      IS NOT ANY.
C  3RD.  COLUMNS 6-10: REAL VARIABLES:
C        1-10          A1= PARTICLE'S MAJOR SEMI-AXIS
C       11-20          A2= PARTICLE'S MINOR SEMI-AXIS
C       21-30          THETA= ANGLE(RANGE 0-180) BETWEEN  A1  AND
C                      THE APPROPRIATE REFERENCE AXIS :
C                      X  IN THE XY-PLANE , Y  IN THE YZ-PLANE  AND
C                      Z  IN THE ZX-PLANE .
C                      THE PROGRAMME ALSO CAN HANDLE ANGLES IN THE RANGE
C                      +90 TO -90 PROVIDED THAT THE  A P P R O P I A T E
C                      REFERENCE AND SENSE ARE EQUIVALENT TO THE ABOVE
C                      INDICATIONS.
C       31-35          INTEGER VARIABLE . INDICATES THE END OF EACH SET.
C                      LEAVE IT BLANK IF DATA INPUT IS NOT THE LAST ONE,
C                      OTHERWISE ENTER ANY INTEGERS WITHIN THE INTERVAL.
C
C  REMINDING ONCE MORE: THE   S E N S E   OF THETA (AS INDICATED ABOVE)
C  IS OF UTMOST IMPORTANCE . CORRECT THE WHOLE SET IN CASE OF  A N Y
C  SYSTEMATIC  ERROR  DURING MEASUREMENTS .
C
C*********************************************************************
C
C
      DIMENSION F(3),G(3),H(3),TITLE(72),AXA(3),AXB(3),FT(3)
      DIMENSION AX(3),RT1(3),AXIS(3),EB(3),AZ(3),D2(3),EX2(3)
      DIMENSION VAL(3,3),VEC(3,3),TH(3),KTT(3),CP(3,2),THET(3)
      DIMENSION R(3),SUMX(6),SCP(6,6),X(6),P(6),E(3,3),SPI(6,6)
      DIMENSION D2(2,2),HINV(2,2),V(2),D1(2),DIST(3),AMAX(3)
      PI= ATAN(1.)*4.
      HALFPI= PI/2.
      DEGRAD= PI/180.
```

```
      RADEG= 1./DEGRAD
      DUPI= PI + PI
      CB= 1./3.
      IND=0
C
C          READ AND WRITE SAMPLE RECORDS ( 70 COLUMNS)
C
      READ(5,1007) IOPT,(TITLE(I),I=1,70)
      WRITE(6,1008) TITLE
      IF( IOPT .EQ. 0) GOTO 10
    5 READ(5,2000) (TITLE(I),I= 1, 72)
      ISAFE= 0
      WRITE(6,2001) TITLE
      READ(5,2002) (R(I),I= 1, 3),(THTD(I), I=1, 3),ISENT
      DO 9 I=1,3
      AMAX(I)= R(I)
      AXA(I)= SQRT( R(I) )
      AXB(I)= 1./AXA(I)
      TH(I)= THTD(I)*DEGRAD
      TEMP= R(I) - AXB(I)*AXB(I)
      EX2(I)= TEMP/R(I)
    9 CONTINUE
      GOTO 59
C
C ROUTINE TO EVALUATE THE  2D-STRAIN AT EACH OF THE   THREE
C PERPENDICULAR PLANES . METHOD BY SHIMAMOTO AND IKEDA, 1976
C (TECTONOPHYSICS, 12 : 283 - 306) .
C
   10 READ(5,1000) I,CORECT
      IND= IND + 1
      KOUNT= 0
      RAMAX= 1.
      F(I)= 0
      G(I)= 0
      H(I)= 0
   20 READ(5,1001) A1,A2,THETA,ISTOP
      IF(ISTOP.NE. 0) GOTO 30
      KOUNT= KOUNT + 1
      IF(THETA .LT. 360..AND. A1 .GE. A2) GOTO 21
      WRITE(6,1003) IND
      WRITE(6, 1001) A1,A2,THETA,KOUNT
      GOTO 20
   21 IF( CORECT .NE. 90.) GOTO 25
      IF( CORECT - THETA) 22,23,23
   22 THETA= 270. - THETA
      GOTO 26
   23 THETA= CORECT - THETA
      GOTO 26
   25 THETA= THETA + CORECT
   26 RO= A1/A2
      IF(THETA .LT. 0.) THETA = 180. + THETA
      IF(RO .GT. RAMAX) RAMAX= RO
      THT= THETA*DEGRAD
      CT= COS(THT)
      CT2= CT*CT
      ST2= 1. - CT2
      ST= SQRT(ST2)
      F(I)= F(I)+(CT2/RO)+(RO*ST2)
      G(I)= G(I)+(ST2/RO)+(RO*CT2)
      H(I)= H(I)+(1./RO-RO)*ST*CT
      GOTO 20
   30 AN= KOUNT
      KTT(I)= KOUNT
      F(I)= F(I)/AN
      G(I)= G(I)/AN
      H(I)= H(I)/AN
      B= -(F(I)+G(I))
      AUX= (F(I)*G(I))-(H(I)*H(I))
      DS= (B*B)-(4.*AUX)
      IF(DS.LT.0.) GOTO 190
      DS= SQRT(DS)
      ROOT1= (-B+DS)/2.
      ROOT2= (-B-DS)/2.
      IF(ROOT1.LT.ROOT2) GOTO 40
      AUX= ROOT1
      ROOT1= ROOT2
      ROOT2= AUX
   40 AXA(I)= 1./SQRT(ROOT1)
      AXB(I)= 1./SQRT(ROOT2)
      TEMP= AXA(I)*AXA(I)
      EX2(I)= (TEMP - AXB(I)*AXB(I))/TEMP
      R(I)= AXA(I)/AXB(I)
      AMAX(I)= RAMAX
      AUX= H(I)+H(I)
      BUX= F(I)-G(I)
C
C          END OF SHIMAMOTO AND IKEDA ROUTINE
C
      IF(BUX) 43,48,44
   43 FC= PI
```

```fortran
      GOTO 47
   44 IF(AUX) 45,49,46
   45 FC= DUPI
      GOTO 47
   46 FC= 0.
   47 AT= ATAN(AUX/BUX)+FC
      THT= .5*AT
      GOTO 50
   48 THT= PI/4.
      GOTO 55
   49 THT= PI/2.
      GOTO 55
   50 IF( THT - PI/2.) 51,51,52
   51 THT= THT + (PI/2.)
      GOTO 55
   52 THT= THT - (PI/2.)
   55 TH(I)= THT
      THTD(I) = THT*RADEG
C
C
C            OBTAIN SOLUTION BY THE LEAST SQUARES METHOD
C
C
      IF(IND .LT. 3) GOTO 10
      WRITE(6,1005)
      WRITE(6,1006) KTT
C
C             USE NEWTON-RAPHSON ROUTINE FOR AXES SCALING
C
   59 CONTINUE
      DO 60 I=1,3
      FT(I)= 1.
      WRITE(6,1004) AXA(I),AXB(I),R(I),THTD(I),AMAX(I)
      CP(I,1) = AXB(I)/POL(EX2(I),TH(I))
      FI= TH(I) - HALFPI
      CP(I,2) = AXB(I)/POL(EX2(I),FI)
   60 CONTINUE
C
C             CALCULATE THE PARTIAL DERIVATIVES
C
      DO 62 I=1,2
   62 D2(I,I)= 2.*(CP(I+1,1)**2 + CP(I+1,2)**2)
      D2(1,2) = -2.*CP(3,1)*CP(2,2)
      D2(2,1) = D2(1,2)
      AUX= -2.*CP(1,2)*CP(2,1)
      BUX= -2.*CP(1,1)*CP(3,2)
      D1(1)= FT(2)*D2(1,1) + FT(3)*D2(1,2) + AUX
      D1(2)= FT(3)*D2(2,2) + FT(2)*D2(1,2) + BUX
C
C             INVERT THE  2ND. PARTIAL DERIVATIVES MATRIX
C
      CALL INVMAT(2,D2,HINV)
      DO 65 I=1,2
   65 V(I)= 0.
      DO 66 I=1,2
      DO 66 J=1,2
   66 V(I)= V(I) + HINV(I,J)*D1(J)
C
C           OBTAIN AND NORMALIZE THE SCALING FACTORS
C
      SMALL= FT(1)
      DO 68 I=1,2
      FT(I+1)= FT(I+1) - V(I)
      IF(FT(I+1) .GT. SMALL) GOTO 68
      SMALL= FT(I+1)
   68 CONTINUE
      DO 70 I=1,3
      FT(I)= FT(I)/SMALL
   70 AXB(I)= AXB(I)*FT(I)
      DO 71 I=1,3
      CP(I,1)= AXB(I) / POL(EX2(I),TH(I))
      FI= TH(I) - HALFPI
      CP(I,2)= AXB(I) / POL(EX2(I),FI)
   71 CONTINUE
      AUX= CP(1,1)*CP(2,1)*CP(3,1)
      BUX= CP(1,2)*CP(2,2)*CP(3,2)
      CHECK= AUX / BUX
      IF(CHECK .GT. 1.) CHECK= 1./CHECK
      AVELAC= 100.*(1. - CHECK**CB)
      FITLAC= 100.*(1. - CHECK)
      WRITE(6,1021) CHECK, FITLAC,AVELAC
C
C           COMPUTE CHORDS FROM EACH OF THE SCALED
C           ELLIPSES , USING POLAR EQUATION
C
      NCHORD= 6
      DIV= 2.*NCHORD
      DELTA= PI/DIV
      I= 1
      IA= 1
```

```
      JA= 2
      KT= 0
      DO 75 K=1,6
      DO 75 M=1,6
      SUMX(K) = 0.
   75 SCP(K,M)= 0.
   76 DO 77 K=1,6
   77 X(K)= 0.
      AUX= -(TH(I)+DELTA)
      DO 85 L=1,NCHORD
      AL= L - 1
      FI= AUX+DELTA
      FID= FI*RADEG
      AUX= FI
      RL= AXB(I)/POL(EX2(I),FI)
      AD= AL*DELTA
      UX= RL*COS(AD)
      VX= RL*SIN(AD)
      CX= UX*VX
C
C          COMPUTE THE SUM OF THE CROSS-PRODUCTS MATRIX
      X(IA)= UX*UX
      X(JA)= VX*VX
      MIX= IA+JA+1
      X(MIX) = CX
      KT= KT+1
      DO 84 KA=1,6
      SUMX(KA)= SUMX(KA) + X(KA)
      DO 84 MA=1,6
      SCP(KA,MA)= SCP(KA,MA) + X(KA)*X(MA)
   84 CONTINUE
   85 CONTINUE
      IA= JA
      GO TO(90,91,92),I
   90 JA= 3
      I= 2
      GOTO 76
   91 JA= 1
      I= 3
      GOTO 76
   92 AXX= NCHORD
      DO 95 K=1,6
      P(K)= 0.
      SUMX(K) = SUMX(K)/AXX
      DO 95 L=1,6
      SCP(K,L)= SCP(K,L)/AXX
   95 CONTINUE
C
C         INVERT CROSS PRODUCTS MATRIX
C
      CALL INVMAT(6,SCP,SPI)
      DO 100 I=1,6
      DO 100 J=1,6
      P(I)= P(I) + SPI(I,J)*SUMX(J)
  100 CONTINUE
      DO 110 I=1,3
      DO 109 J=1,3
      K= I + J + 1
      IF(I .EQ. J) GOTO 105
      E(I,J)= P(K)/2.
      VAL(I,J)= E(I,J)
      GOTO 109
  105 E(I,J) = P(I)
      VAL(I,J)= P(I)
  109 CONTINUE
  110 CONTINUE
C
C        OBTAIN EIGENVALUES AND EIGENVECTORS BY THE JACOBI METHOD,
C                    AND THEN COMPUTE ELLIPSOID RATIOS
C
      CALL EIGOBI(VAL,VEC)
      DO 115 I=1,3
      IF(VAL(I,I) .LE. 0.) GOTO 175
  115 AX(I)= 1./SQRT(VAL(I,I))
      WRITE(6,1002)
      WRITE(6,1010)
      DO 120 I=1,3
      WRITE(6,1011) (E(I,J),J=1,3),(VAL(I,J),J=1,3),(VEC(I,J),J=1,3)
  120 CONTINUE
      DO 125 I=1,3
  125 RT1(I) = AX(I)/AX(3)
      AUX= AX(1)*AX(2)*AX(3)
      VOL= 100.*(AUX - 1.)
      AUX= AUX**CB
      DO 130 I=1,3
      AXIS(I)= AX(I)/AUX
  130 DIST(I) = (AXIS(I) - 1.)*100.
      IF( IOPT .EQ. 0) WRITE(6,1012) VOL
      WRITE(6,1013) AX
      WRITE(6,1024) RT1
```

```
      WRITE(6,1014)
      WRITE(6,1013) AXIS
      WRITE(6,1022) DISP
C
C        COMPUTE ELLIPSOID CHARACTERIZATION PARAMETERS
C
      AUX= AXIS(1)/AXIS(2)
      BUX= AXIS(2)/AXIS(3)
      DO 135  I=1,3
  135 EB(I) = ALOG(AXIS(I))
C
C     FLINN'S PARAMETER (K)
      GAMA= (EB(1)-EB(2))**2 + (EB(2)-EB(3))**2 + (EB(3)-EB(1))**2
      GAMA= (2./3.)*SQRT(GAMA)
      ES= .5*SQRT(3.)*GAMA
      FK= (AUX-1.)/(BUX-1.)
C
C     RAMSAY'S PARAMETER (K)
      AUXLOG= ALOG(AUX)
      BUXLOG= ALOG(BUX)
      RK= AUXLOG/BUXLOG
C
C     LODE'S  PARAMETER (NU)
      XX= (2.*EB(2))-EB(1)-EB(3)
      ALODE= XX/(EB(1)-EB(3))
      WRITE(6,1015)
      WRITE(6,1016) FK,AUX,BUX,RK,AUXLOG,BUXLOG,ALODE
      WRITE(6,1023) GAMA,ES
C
C          COMPUTE ORIENTATION OF ELLIPSOID AXES
C          IN TERMS OF AZIMUTH OF PLUNGE
C
      WRITE(6,1017)
      DO 170  I=1,3
      IF( VEC(3,I)) 150,152,152
  150 DO 151  K=1,3
  151 VEC(K,I) = -VEC(K,I)
  152 C= VEC(1,I)
      S= VEC(2,I)
      D= VEC(3,I)
      IF( C ) 153,158,154
  153 FAC= PI
      GOTO 157
  154 IF( S ) 155,159,156
  155 FAC= DUPI
      GOTO 157
  156 FAC= 0.
  157 AZZ= ATAN( S/C ) + FAC
      GOTO 160
  158 AZZ= PI/2.
      GOTO 160
  159 AZZ= 0.
  160 DP(I)= ASIN( D ) * RADEG
      AZ(I)= AZZ*RADEG
      IF( DP(I) - 90.)  162,162,161
  161 DP(I)= 180.-DP(I)
      AZ(I)= AZ(I) + 180.
      IF( AZ(I) .GT. 360.) AZ(I)= AZ(I) - 360.
  162 WRITE (6,1018) I,AZ(I),DP(I)
  170 CONTINUE
      GOTO 180
  175 WRITE(6,1020)
  180 CONTINUE
      IF(IOPT .EQ. 0) GOTO 190
      IF( ISENT  .NE. 9) GOTO 5
  190 CONTINUE
 1000 FORMAT(I5,F10.5)
 1001 FORMAT( 3F10.5,I5)
 1002 FORMAT(1H0,43X,' RESULTS BY LEAST-SQUARES FITTING')
 1004 FORMAT(1H ,' MAJOR SEMI-AXIS=',F10.3,2X,' MINOR SEMI-AXIS=',F10.3,
     12X,' RATIO=',F10.3,2X,' THETA=',F10.3,'  MAX. RATIO=',F10.3)
 1005 FORMAT(1H0,' POPULATION IN EACH PLANE')
 1006 FORMAT( 1H ,' XY-PLANE=',I5,5X,' YZ-PLANE=',I5,5X,' ZX-PLANE=',I5)
 1007 FORMAT(I2,79A1)
 1008 FORMAT(1H0,70A1)
 1009 FORMAT( 1H0,' ***MESSAGE : ERROR IN INPUT DATA. CHECK DECK NO.',I3)
 1010 FORMAT(1H0,' ',12X,'INPUT MATRIX',24X,'MATRIX OF EIGENVALUES',19X,
     1'MATRIX OF EIGENVECTORS')
 1011 FORMAT( 1H ,3E13.4,1X,3E13.4,1X,3E13.4,/)
 1012 FORMAT(1H ,' ELLIPSOID WITH CHANGE IN VOLUME OF',F9.2,'  PERCENT')
 1013 FORMAT( 1H ,' AXES RATIO =',2(F10.3,' :'),F10.3)
 1014 FORMAT(1H0,' ELLIPSOID ASSUMING NO VOLUME CHANGE')
 1015 FORMAT(1H0,' CHARACTERIZATION PARAMETERS ACCORDING TO  :')
 1016 FORMAT(1H ,12H FLINN'S  K=,F5.3,'( A=',F5.3,2X,' B=',F5.3,')',15H
     1 RAMSAY'S  K=,F5.3,'( A=',F5.3,2X,' B=',F5.3,')',16H    LODE'S  (NU)
     2=,F6.3)
 1017 FORMAT( 1H0,' ATTITUDE OF THE ELLIPSOID AXES : X=1, Y=2 AND Z=3')
 1018 FORMAT(1H ,' AXIS=',I5, 2X, ' AZIMUTH=',F7.2,5X,' PLUNGE=',F7.2)
 1019 FORMAT( 1H0,' CHECK=',F20.10)
 1020 FORMAT(1H0,' ***REMARK : BAD RESULTS ! FITTING IS NOT OF AN ELLIPS
```

```
     1OID : CHECK THE ORIENTATION OF THE ANGLES IN THE XY,YZ,ZX-PLANES')
 1021 FORMAT(1H0,7H CHECK=,F10.7,37H    OVERALL ELLIPSES' INCOMPATIBILITY
     1=,F10.3,29H %    AVERAGE LACK OF FIT OF=,F7.3,14H % PER SECTION)
 1022 FORMAT(1H ,' PERCENTAGE  OF  DISTORTION IN EACH AXIS : X=',F8.3,'
     1%  Y=',F8.3,' %  Z=',F8.3,' %')
 1023 FORMAT(1H ,44H NADAI'S (NATURAL OCTAHEDRAL UNIT OF SHEAR)=,F6.3,5X
     1,' AND   EFFECTIVE STRAIN  (ES)=',F6.3)
 1024 FORMAT(1H ,' OR NORMILIZED TO THE SMALLER AXIS =',2(F10.3,' :'),F4
     1.1)
 2000 FORMAT(72A1)
 2001 FORMAT(1H1,72A1)
 2002 FORMAT(3F7.3,3F7.3,I2)
      STOP
      END
      FUNCTION POL(EX,PHI)
      POL= (1. - (EX*((COS(PHI))**2)))**.5
      RETURN
      END
      SUBROUTINE EIGGBI(VL,VC)
C
C
C  ROUTINE TO EVALUATE THE EIGENVALUES AND EIGENVECTORS OF
C  A SYMMETRIC  3 X 3 MATRIX.
C  INPUT MATRIX IS THROUGH ARRAY  VL WHICH IS LOST DURING
C  COMPUTATION. OUTPUT BY ARRAYS :
C           - VL =  MATRIX  OF EIGENVALUES
C           - VC =  MATRIX  OF EIGENVECTORS
C  METHOD BASED ON THE PAPER BY J.GREENSTADT,1960 -THE DETERMINATION
C  OF THE CHARACTERISTIC ROOTS OF A MATRIX BY THE JACOBI METHOD.
C  IN : MATHEMATICAL METHODS FOR DIGITAL COMPUTERS  , EDITED
C  BY  RALSTON AND WILF,WILEY,VOL I,1960.
C
C
      DIMENSION VL(3,3), VC(3,3)
      N= 3
      V= 0.
      DO 15 I=1,3
      DO  15 J=1,3
      IF( I .EQ. J) GOTO 5
      VC(I,J) = 0.
      V= V + VL(I,J)*VL(I,J)
      GOTO 15
    5 VC(I,J)= 1.
   15 CONTINUE
      AN= N
      V= SQRT(V)
      VF= (V*1.E-9)/AN
   16 V1= V/AN
      DO 50 I=1,2
      JA= I + 1
      DO 50 J=JA,N
      IF( ABS(VL(I,J)) .LT. V1) GOTO 50
      ANUM= -VL(I,J)
      DENOM= (VL(I,I)-VL(J,J))*.5
      W= ANUM/SQRT(ANUM*ANUM + DENOM*DENOM)
      IF(DENOM .LT. 0.) W= -W
      X= 1. + SQRT(1. - W*W)
      X= SQRT(2.*X)
      ST= W/X
      S2= ST*ST
      CT= SQRT(1. - S2)
      C2= CT*CT
      PROD= CT*ST
      DO 20 K=1,3
      IF( K .NE. I .AND. K .NE. J) KAXIS= K
      BUX= VC(K,I)*CT - VC(K,J)*ST
      VC(K,J) = VC(K,I)*ST + VC(K,J)*CT
      VC(K,I)= BUX
   20 CONTINUE
      K= KAXIS
      AUX= VL(K,I)*CT - VL(K,J)*ST
      VL(K,J) = VL(K,I)*ST + VL(K,J)*CT
      VL(K,I)= AUX
      DIF= VL(I,I) - VL(J,J)
      PD= VL(I,J)*PROD*2.
      AUX= VL(I,I)
      VL(I,I)= AUX*C2 + VL(J,J)*S2 - PD
      VL(J,J)= AUX*S2 + VL(J,J)*C2 + PD
      VL(I,J) = DIF*PROD + VL(I,J)*(C2 - S2)
      VL(J,I)= VL(I,J)
      DO 25 K=1,3
      VL(I,K)= VL(K,I)
   25 VL(J,K)= VL(K,J)
   50 CONTINUE
      V= V1
      IF(V .GE. VF) GOTO 16
      DO 70 I=1,2
      JA= I + 1
      DO 60 J=JA,3
      IF( ABS(VL(I,I)) .LT. ABS(VL(J,J))) GOTO 60
```

```
      AUX= VL(I,I)
      VL(I,I)= VL(J,J)
      VL(J,J)= AUX
      DO 55 K=1,3
      BUX= VC(K,I)
      VC(K,I)= VC(K,J)
      VC(K,J)= BUX
   55 CONTINUE
   60 CONTINUE
   70 CONTINUE
   10 CONTINUE
      RETURN
      END
      SUBROUTINE INVMAT(N1,A,B)
      DIMENSION A(N1,N1), B(N1,N1)
      N= N1
      DO 100 I=1,N
      DO 101 J=1,N
      B(I,J)= 0.
  101 CONTINUE
      B(I,I)=1.
  100 CONTINUE
      DET= 1.
      DO 102 I=1,N
      DIV= A(I,I)
      DET= DET * DIV
      DO 103 J=1,N
      A(I,J)= A(I,J) / DIV
      B(I,J)= B(I,J) / DIV
  103 CONTINUE
      DO 104 J=1,N
      IF(I-J) 1,104,1
    1 RATIO= A(J,I)
      DO 105 K=1,N
      A(J,K)= A(J,K) - RATIO * A(I,K)
      B(J,K)= B(J,K) - RATIO * B(I,K)
  105 CONTINUE
  104 CONTINUE
  102 CONTINUE
      RETURN
      END
```

```
C
C   P  R  O  G  R  A  M  M  E       F     T     E     L     A     M
C
C
C*  **  **  **  **  **  **  **  **  **  **  **  **  **  **  **  **  **  **  **
C              PROGRAMME FOR TRIDIMENSIONAL STRAIN ESTIMATION
C*  **  **  **  **  **  **  **  **  **  **  **  **  **  **  **  **  **  **  **
C   EXPERIMENTAL VERSION USING THE LAGRANGE MULTIPLIERS FOR CASES WHERE
C   THE MATRIX OF EIGENVALUES IS NON-POSITIVE DEFINITE.
C*  **  **  **  **  **  **  **  **  **  **  **  **  **  **  **  **  **  **  *
C   VERSION : DECEMBER 1980 , BASED ON AN EARLIER VERSION (APRIL 1980 ,
C             PROGRAMME FITELI ) .
C   DEVELOPED AT  LEEDS' AMDHAL 470
C   BY  HENRIQUE  DAYAN
C
C
C
C*************************************************************************
C   IF THE PROGRAMME IS TO BE USED  O N L Y FOR FITTING PURPOSES READ THE
C   THE INSTRUCTIONS IN PART A , OTHERWISE IF IT IS NEEDED 2D-STRAIN
C   ESTIMATION FOLLOW INSTRUCTIONS IN PART B.
C
C.........................................................................
C
C           P   A   R   T     A
C     I N P U T   I N S T R U C T I O N S :
C   CARD     COLUMNS
C   1ST.        2       : INTEGER VARIABLE IOPT . DO NOT LEAVE IT BLANK(NOR
C                         ENTER ZERO) . IF YOU WANT THE PROGRAMME ONLY FOR
C                         FITTING PURPOSES ENTER ANY INTEGER .
C            3-72       : ENTER ANY PHRASE FOR SAMPLE IDENTIFICATION.
C   EVERY SAMPLE IS MADE OF TWO CARDS : THE FIRST IDENTIFYIES THE
C   SAMPLE (72 COLUMNS) . THE SECOND CONTAINS 6 REAL VARIABLES DEFINING
C   THE RATIOS OF 3 PERPENDICULAR ELLIPSES : XY(COLUMNS 1-7) ,YZ(CO-
C   LUMNS 15-25) AND THEIR ORIENTATION ANGLES : XY-PLANE(22-28) ,YZ
C   (29-35) AND ZX-PLANE(36-42).
C   THE LAST DATA'CARD'SHOULD ALSO CONTAIN A SENTINEL(INTEGER VARIABLE
C   ISENT) . ENTER NUMBER 9 IN THE 44TH COLUMN IN ORDER TO END THE
C   CALCULATION.
C
C.........................................................................
C
C          P   A   R   T     B
C     I N P U T   I N S T R U C T I O N S :
C   THE FIRST 'CARD' CONTAINS SPECIMEN REFERENCE . EVERY SAMPLE SHOULD
C   CONSIST OF THREE SETS OF PARTICLES MEASUREMENTS (I.E. IN THE XY,
C   YZ AND ZX-PLANE) . A CONTROL 'CARD' PRECEEDS EACH SET,WHILE THE LAST
C   'CARD' IN EVERY SET CONTAINS A SENTINEL.
C   CARD    COLUMNS
C   1ST.   72 COLUMNS    : ANY PHRASE FOR SAMPLE IDENTIFICATION
C   2ND.   COLUMN NO. 5: INTEGER VARIABLE DETERMINING THE CO-ORDINATE
C                        PLANE AND SENSE OF MEASUREMENT OF EACH SET;
C            1           REFERING TO MEASUREMENTS FROM X  TOWARDS  Y
C            2                      DITTO                Y  TWDS    Z
C            3                      DITTO                Z  TWDS    X,NOT
C                        NECESSARILY IN THAT ORDER.
C           6-15       : REAL VARIABLE C O R E C T .
C                        IT CORRECTS A SYSTEMATIC ERROR FOR THE WHOLE SET
C                        OF MEASUREMENTS IN THAT PLANE . BLANK IF THERE IS
C                        NOT ANY.
C   3RD.   COLUMNS 6-10: REAL VARIABLES :
C            1-10        A1= PARTICLE MAJOR SEMI-AXIS
C           11-20        A2= PARTICLE MINOR SEMI-AXIS
C           21-30        THETA = ANGLE (RANGE 0-180) BETWEEN A1 AND THE
C                        APPROPRIATE REFERENCE AXIS   :
C                        X  IN THE  XY-PLANE ; Y  IN THE YZ-PLANE   AND
C                        Z  IN THE  ZX-PLANE .
C                        THE PROGRAMME ALSO CAN HANDLE ANGLES IN THE RANGE
C                        +90  TO  -90 , PROVIDED THAT THE APPROPTIATE
C                        REFERENCE AND SENSE ARE EQIVALENT TO THE  ABOVE
C                        INDICATIONS.
C           31-35        INTEGER VARIABLE . INDICATES THE END OF EACH SET.
C                        LEAVE IT BLANK IF DATA INPUT IS NOT THE LAST ONE,
C                        OTHERWISE ENTER ANY INTEGERS WITHIN THE INTERVAL.
C
C   REMINDING ONCE MORE: THE S E N S E OF THETA (AS INDICATED ABOVE)
C   IS OF UTMOST IMPORTANCE . CORRECT THE WHOLE SET IN CASE OF SYSTEMATIC
C   ERROR DURING MEASUREMENTS .
C
C*************************************************************************
C
C
      DIMENSION F(3),G(3),H(3),TITLE(72),AXA(3),AXB(3),FT(3)
      DIMENSION AX(3),RT1(3),AXIS(3),EB(3),AZ(3),D2(3),EX2(3)
      DIMENSION VAL(3,3),VEC(3,3),TH(3),KTT(3),CP(3,2),THT(3)
      DIMENSION R(3),SUMX(6),SCP(6,6),X(6),P(5),E(3,3),SPI(6,6)
      DIMENSION D2(2,2),HINV(2,2),V(2),D1(2),DIST(3),AMAX(3)
      DIMENSION DER2(12,12),HD2(12,12),DER1(12),SUH(12),SX(6)
      DIMENSION SP(6,6), B1(3)
      PI= ATAN(1.)*4.
```

```
      HALFPI= PI/2.
      DEGRAD= PI/180.
      RADEG= 1./DEGRAD
      DUPI= PI + PI
      ISAFE= 0
      CB= 1./3.
      IND=0
C
C          READ  AND  WRITE  SAMPLE  RECORDS ( 70 COLUMNS)
C
      READ(5,1007) IOPT,(TITLE(I),I=1,70)
      WRITE(6,1008) TITLE
      IF(IOPT .EQ. 0) GOTO 10
    5 READ(5,2000) (TITLE(I),I=1,72)
      ISAFE= 0
      WRITE(6,2001) TITLE
      READ(5,2002) (R(I),I=1,3),(THTD(I),I=1,3),ISEND
      DO 9 I=1,3
      AMAX(I)= R(I)
      AXA(I)= SQRT( R(I) )
      AXB(I)= 1./AXA(I)
      TH(I)= THTD(I)*DEGRAD
      TEMP= R(I) - AXB(I)*AXB(I)
      EX2(I)= TEMP/R(I)
    9 CONTINUE
      GOTO 59
C
C ROUTINE TO EVALUATE THE  2D-STRAIN  AT  EACH OF THE    THREE
C PERPENDICULAR PLANES . METHOD BY SHIMAMOTO AND IKEDA,1976
C (TECTONOPHYSICS,12 : 283 - 306) .
C
   10 READ(5,1000) I,CORECT
      IND= IND + 1
      KOUNT= 0
      RAMAX= 1.
      F(I)= 0
      G(I)= 0
      H(I)= 0
   20 READ(5,1001) A1,A2,THETA,ISTOP
      IF(ISTOP.NE. 0) GOTO 30
      KOUNT= KOUNT + 1
      IF(THETA .LT. 360..AND. A1 .GE. A2) GOTO 21
      WRITE(6,1002) IND
      WRITE(6,1001) A1,A2,THETA,KOUNT
      GOTO 20
   21 IF( CORECT .NE. 90.) GOTO 25
      IF( CORECT - THETA) 22,23,23
   22 THETA= 270. - THETA
      GOTO 26
   23 THETA= CORECT - THETA
      GOTO 26
   25 THETA= THETA + CORECT
   26 RO= A1/A2
      IF(THETA .LT. 0.) THETA= 180. + THETA
      IF(RO .GT. RAMAX) RAMAX= RO
      THT= THETA*DEGRAD
      CT= COS(THT)
      CT2= CT*CT
      ST2= 1. - CT2
      ST= SQRT(ST2)
      F(I)= F(I)+(CT2/RO)+(RO*ST2)
      G(I)= G(I)+(ST2/RO)+(RO*CT2)
      H(I)= H(I)+(1./RO-RO)*ST*CT
      GOTO 20
   30 AN= KOUNT
      KTT(I)= KOUNT
      F(I)= F(I)/AN
      G(I)= G(I)/AN
      H(I)= H(I)/AN
      B= -(F(I)+G(I))
      AUX= (F(I)*G(I))-(H(I)*H(I))
      DS= (B*B)-(4.*AUX)
      IF(DS.LT.0.) GOTO 450
      DS= SQRT(DS)
      ROOT1= (-B+DS)/2.
      ROOT2= (-B-DS)/2.
      IF(ROOT1.LT.ROOT2) GOTO 40
      AUX= ROOT1
      ROOT1= ROOT2
      ROOT2= AUX
   40 AXA(I)= 1./SQRT(ROOT1)
      AXB(I)= 1./SQRT(ROOT2)
      TEMP= AXA(I)*AXA(I)
      EX2(I)= (TEMP - AXB(I)*AXB(I))/TEMP
      R(I)= AXA(I)/AXB(I)
      AMAX(I)= RAMAX
      AUX= H(I)+H(I)
      BUX= F(I)-G(I)
C
C          END OF SHIMAMOTO AND IKEDA ROUTINE
```

```
C
      IF(BUX) 43,48,44
   43 FC= PI
      GOTO 47
   44 IF(AUX) 45,49,46
   45 FC= DUPI
      GOTO 47
   46 FC= 0.
   47 AT= ATAN(AUX/BUX)+FC
      THT= .5*AT
      GOTO 50
   48 THT= PI/4.
      GOTO 55
   49 THT= PI/2.
      GOTO 55
   50 IF( THT - PI/2.) 51,51,52
   51 THT= THT + (PI/2.)
      GOTO 55
   52 THT= THT - (PI/2.)
   55 TH(I)= THT
      THTD(I)= THT*RADEG
C
C
C           OBTAIN SOLUTION BY THE LEAST SQUARES METHOD
C
C
      IF(IND .LT. 3) GOTO 10
      WRITE(6,1005)
      WRITE(6,1006) KEP
C
C            USE NEWTON-RAPHSON ROUTINE FOR AXES SCALING
C
   59 CONTINUE
      DO 60 I=1,3
      FT(I)= 1.
      WRITE(6,1004) AXA(I),AXB(I),R(I),THTD(I),AMAX(I)
      CP(I,1)= AXB(I)/POL(EX2(I),TH(I))
      FI= TH(I) - HALFPI
      CP(I,2)= AXB(I)/POL(EX2(I),FI)
   60 CONTINUE
C
C            CALCULATE THE PARTIAL DERIVATIVES
C
      DO 62 I=1,2
   62 D2(I,I)= 2.*(CP(I+1,1)**2 + CP(I+1,2)**2)
      D2(1,2)= -2.*CP(3,1)*CP(2,2)
      D2(2,1)= D2(1,2)
      AUX= -2.*CP(1,2)*CP(2,1)
      BUX= -2.*CP(1,1)*CP(3,2)
      D1(1)= FT(2)*D2(1,1) + FT(3)*D2(1,2) + AUX
      D1(2)= FT(3)*D2(2,2) + FT(2)*D2(1,2) + BUX
C
C            INVERT THE  2ND. PARTIAL DERIVATIVES MATRIX
C
      CALL INVMAT(2,D2,HINV)
      DO 65 I=1,2
   65 V(I)= 0.
      DO 66 I=1,2
      DO 66 J=1,2
   66 V(I)= V(I) + HINV(I,J)*D1(J)
C
C         OBTAIN AND NORMALIZE THE SCALING FACTORS
C
      SMALL= FT(1)
      DO 68 I=1,2
      FT(I+1)= FT(I+1) - V(I)
      IF(FT(I+1) .GT. SMALL) GOTO 68
      SMALL= FT(I+1)
   68 CONTINUE
      DO 70 I=1,3
      FT(I)= FT(I)/SMALL
   70 AXB(I)= AXB(I)*FT(I)
      DO 71 I=1,3
      CP(I,1)= AXB(I) / POL(EX2(I),TH(I))
      FI= TH(I) - HALFPI
      CP(I,2)= AXB(I) / POL(EX2(I),FI)
   71 CONTINUE
      AUX= CP(1,1)*CP(2,1)*CP(3,1)
      BUX= CP(1,2)*CP(2,2)*CP(3,2)
      CHECK= AUX / BUX
      IF(CHECK .GT. 1.) CHECK= 1./CHECK
      AVELAC= 100.*(1. - CHECK**CB)
      FITLAC= 100.*(1. - CHECK)
      WRITE(6,1021) CHECK, FITLAC, AVELAC
C
C         COMPUTE CHORDS FROM EACH OF THE SCALED
C           ELLIPSES , USING POLAR EQUATION
C
      NCHORD= 6
      DIV= 2.*NCHORD
```

```
      DELTA= PI/DIV
      I= 1
      IA= 1
      JA= 2
      KT= 0
      DO 75 K=1,6
      DO 75 M=1,6
      SUMX(K)= 0.
   75 SCP(K,M)= 0.
   76 DO 77 K=1,6
   77 X(K) = 0.
      AUX= -(TH(I)+DELTA)
      DO 85 L=1,NCHORD
      AL= L - 1
      FI= AUX+DELTA
      FID= FI*RADEG
      AUX= FI
      RL= AXB(I)/POL(EX2(I),FI)
      AD= AL*DELTA
      UX= RL*COS(AD)
      VX= RL*SIN(AD)
      CX= UX*VX
C
C           COMPUTE THE SUM OF THE CROSS-PRODUCTS  MATRIX
      X(IA)= UX*UX
      X(JA)= VX*VX
      MIX= IA+JA+1
      X(MIX) = CX
      KT= KT+1
      DO 84 KA=1,6
      SUMX(KA)= SUMX(KA) + X(KA)
      DO 84 MA=1,6
      SCP(KA,MA)= SCP(KA,MA) + X(KA)*X(MA)
   84 CONTINUE
   85 CONTINUE
      IA= JA
      GO TO(90,91,92),I
   90 JA= 3
      I= 2
      GOTO 76
   91 JA= 1
      I= 3
      GOTO 76
   92 AXX= NCHORD
      DO 95 K=1,6
      P(K)= 0.
      SX(K) = -2.*SUMX(K)
      SUMX(K)= SUMX(K)/AXX
      DO 95 L=1,6
      SP(K,L)= 2.*SCP(K,L)
      SCP(K,L)= SCP(K,L)/AXX
   95 CONTINUE
C
C      INVERT CROSS PRODUCTS MATRIX
C
      CALL INVMAT(6,SCP,SPI)
      DO 100 I=1,6
      DO 100 J=1,6
      P(I) = P(I) + SPI(I,J)*SUMX(J)
  100 CONTINUE
  101 CONTINUE
      DO 110 I=1,3
      DO 109 J=1,3
      K = I + J + 1
      IF(I .EQ. J) GOTO 105
      E(I,J) = P(K)/2.
      VAL(I,J)= E(I,J)
      GOTO 109
  105 E(I,J) = P(I)
      VAL(I,J)= P(I)
  109 CONTINUE
  110 CONTINUE
C
C      OBTAIN EIGENVALUES AND EIGENVECTORS BY THE JACOBI METHOD,
C          AND THEN COMPUTE ELLIPSOID RATIOS
C
      CALL EIGCBI(VAL,VEC)
      DO 115 I=1,3
      IF(VAL(I,I) .LE. 0.) GOTO 175
  115 AX(I)= 1./SQRT(VAL(I,I))
      WRITE(6,1002)
      WRITE(6,1010)
      DO 120 I=1,3
      WRITE(6,1011) (E(I,J),J=1,3),(VAL(I,J),J=1,3),(VEC(I,J),J=1,3)
  120 CONTINUE
      DO 125 I=1,3
  125 RT1(I)= AX(I)/AX(3)
      AUX= AX(1)*AX(2)*AX(3)
      VOL= 100.*(AUX - 1.)
      AUX= AUX**CB
```

```
      DO 130 I=1,3
      AXIS(I)= AX(I)/AUX
  130 DIST(I)= (AXIS(I) - 1.)*100.
      IF( IOPT .EQ. 0) WRITE(6,1012) VOL
      WRITE(6,1013) AX
      WRITE(6,1024) RT1
      WRITE(6,1014)
      WRITE(6,1013) AXIS
      WRITE(6,1022) DIST
C
C        COMPUTE ELLIPSOID CHARACTERIZATION PARAMETERS
C
      AUX= AXIS(1)/AXIS(2)
      BUX= AXIS(2)/AXIS(3)
      DO 135 I=1,3
  135 EB(I)= ALOG(AXIS(I))
C
C     FLINN PARAMETER - K
      GAMA= (EB(1)-EB(2))**2 + (EB(2)-EB(3))**2 + (EB(3)-EB(1))**2
      GAMA= (2./3.)*SQRT(GAMA)
      ES= .5*SQRT(3.)*GAMA
      FK= (AUX-1.)/(BUX-1.)
C
C     RAMSAY  K- PARAMETER
      AUXLOG= ALOG(AUX)
      BUXLOG= ALOG(BUX)
      RK= AUXLOG/BUXLOG
C
C     LODE'S  PARAMETER (NU)
      XX= (2.*EB(2))-EB(1)-EB(3)
      ALODE= XX/(EB(1)-EB(3))
      WRITE(6,1015)
      WRITE(6,1016) FK,AUX,BUX,RK,AUXLOG,BUXLOG,ALODE
      WRITE(6,1023) GAMA, ES
C
C        COMPUTE ORIENTATION OF ELLIPSOID AXES
C        IN TERMS OF AZIMUTH OF PLUNGE
C
      WRITE(6,1017)
      DO 170 I=1,3
      IF( VEC(3,I)) 150,152,152
  150 DO 151 K=1,3
  151 VEC(K,I)= -VEC(K,I)
  152 C= VEC(1,I)
      S= VEC(2,I)
      D= VEC(3,I)
      IF( C ) 153,158,154
  153 FAC= PI
      GOTO 157
  154 IF( S ) 155,159,156
  155 FAC= DUPI
      GOTO 157
  156 FAC= 0.
  157 AZZ= ATAN( S/C ) + FAC
      GOTO 160
  158 AZZ= PI/2.
      GOTO 160
  159 AZZ= 0.
  160 DP(I)= ASIN( D ) * RADEG
      AZ(I)= AZZ*RADEG
      IF( DP(I) - 90.)  162,162,161
  161 DP(I) = 180.-DP(I)
      AZ(I)= AZ(I) + 180.
      IF( AZ(I) .GT. 360.) AZ(I)= AZ(I) - 360.
  162 WRITE (6,1018) I,AZ(I),DP(I)
  170 CONTINUE
      GOTO 400
C
C
C            SOLUTION USING LAGRANGE MULTIPLIERS
C
C
  175 ISAFE= ISAFE + 1
      IF(ISAFE .EQ. 1) WRITE(6,1020)
  180 CONTINUE
      KT= 0
      DO 200 I=1,3
      DO 200 J=4,6
      SP(I,J) = 2.* SP(I,J)
      SP(J,I)= SP(I,J)
  200 CONTINUE
      DO 211 I=4,6
      K= I - 3
      B1(K) = 1.
      SX(I)= 2.*SX(I)
      P(I) = P(I)/2.
      DO 210 J=4,6
      SP(I,J) = 4.* SP(I,J)
  210 CONTINUE
  211 CONTINUE
```

```
      SMIN= 1.E20
C
C         FIND THE UNKNOWNS BY THE NEWTON-RAPHSON TECHNIQUE
C         .FORM COLUMN VECTOR OF FIRST DERIVATIVES
C         .CALCULATE THE MATRIX OF 2ND. DERIVATIVES(HESSIAN)
C
  250 SUMIN= SMIN
      DO 260 I=1,12
      DO 260 J=1,12
      SUH(I) = 0.
      DER1(I)= 0.
      DER2(I,J)= 0.
  260 CONTINUE
      DO 270 I=1,6
      DO 270 J=1,6
      DER1(I)= DER1(I) + (SP(I,J)*P(J))
      DER2(I,J)= SP(I,J)
  270 CONTINUE
      KT= KT + 1
      DO 280 I=1,6
  280 DER1(I)= DER1(I) + SX(I)
      DER2(1,8)= P(2) + P(3)
      DER2(2,8)= P(1) + P(3)
      DER2(3,8)= P(1) + P(2)
      P12= P(1)*P(2)
      P13= P(1)*P(3)
      P23= P(2)*P(3)
      P16= P(1)*P(6)
      P25= P(2)*P(5)
      P56= P(5)*P(6)
      DER2(1,9)= P23 - P(6)**2
      DER2(2,9)= P13 - P(5)**2
      DER2(3,9)= P12 - P(4)**2
      DER2(4,9)= 2.*(P55 - P13)
      DER2(5,9)= 2.*(P(4)*P(6) - P25)
      DER2(6,9)= 2.*(P(4)*P(5) - P16)
      AUX= 0.
      BUX= 0.
      DO 290 I=1,3
      J= I + 3
      K= I + 6
      L= I + 9
      DER1(L)= B1(I)
      DER2(I,7)= 1.
      DER2(7,I)= 1.
      DER2(J,8) = -2.*P(J)
      AUX= AUX - P(J)**2
      BUX= BUX + P(I)
      DER2(K,L)= 2.*B1(I)
      DER2(L,K)= 2.*B1(I)
  290 CONTINUE
      DER2(8,11)= -DER2(8,11)
      DER2(11,8)= DER2(8,11)
      DO 300 I=8,9
      DO 300 J=1,6
      DER2(I,J) = DER2(J,I)
  300 CONTINUE
      DER1(7) = BUX + B1(1)**2
      DER1(8)= AUX + P23 + P13 + P12 - B1(2)**2
      AUX= P(1)*P23 - (2.*P(4)*P56) - (P(5)*P25)
      DER1(9) = AUX - (P(6)*P16) - (P(3)*P(4)**2) + B1(3)**2
      CALL INVMAT(12,DER2,HD2)
      DO 320 I=1,12
      DO 320 J=1,12
  320 SUH(I)= SUH(I) + HD2(I,J)*DER1(J)
      SMIN = 0.
      DO 330 I=1,6
      P(I)= P(I) - SUH(I)
      SMIN= SMIN + DER1(I)**2
  330 CONTINUE
      DO 340 I=1,3
  340 B1(I)= B1(I) - SUH(I+9)
      IF(SMIN .GE. SUMIN) WRITE(6,1026)
      DIF= ABS(SMIN - SUMIN)
      IF(ISAFE .GT. 10) GOTO 450
      IF(SMIN .LE. 1.E-3 .OR. DIF .LE. 1.E-3) GOTO 350
      IF( KT .LE. 10) GOTO 250
      WRITE(6,1025)
      GOTO 400
  350 CONTINUE
      DO 360 I=4,6
  360 P(I)= 2.*P(I)
      GOTO 101
  400 CONTINUE
      IF(ISAFE .NE. 0 .AND. SMIN .LE. SUMIN) WRITE(6,1027)
      IF(IDPT .EQ. 0) GOTO 450
      IF( ISENT  .NE. 9) GOTO 5
  450 CONTINUE
 1000 FORMAT(I5,F10.5)
 1001 FORMAT(3F10.5,I5)
```

```
1002 FORMAT( 1H0,43X,' RESULTS BY LEAST-SQUARES FITTING')
1004 FORMAT(1H ,' MAJOR SEMI-AXIS=',F10.3,2X,' MINOR SEMI-AXIS=',F10.3,
    12X,' RATIO=',F10.3,2X,' THETA=',F10.3,' MAX. RATIO=',F10.3)
1005 FORMAT( 1H0,' POPULATION IN EACH PLANE')
1006 FORMAT(1H ,' XY-PLANE=',I5,5X,' YZ-PLANE=',I5,5X,' ZX-PLANE=',I5)
1007 FORMAT(I2,70A1)
1008 FORMAT( 1H0,70A1)
1009 FORMAT(1H0,' ***MESSAGE : ERROR IN INPUT DATA. CHECK DECK NO.',I3)
1010 FORMAT( 1H0,' ',12X,'INPUT MATRIX',24X,'MATRIX OF EIGENVALUES', 19X,
    1'MATRIX OF EIGENVECTORS')
1011 FORMAT(1H ,3E13.4,1X,3E13.4,1X,3E13.4,/)
1012 FORMAT( 1H ,' ELLIPSOID WITH CHANGE IN VOLUME OF',F9.2,'  PERCENT')
1013 FORMAT(1H ,' AXES RATIO =', 2(F10.3,' :'),F10.3)
1014 FORMAT( 1H0,' ELLIPSOID ASSUMING NO VOLUME CHANGE')
1015 FORMAT(1H0,' CHARACTERIZATION PARAMETERS ACCORDING TO  :')
1016 FORMAT(1H ,12H FLINN'S  K=,F5.3,'( A=',F5.3,2X,'B=',F5.3,')',15H
    1 RAMSAY'S  K=,F5.3,'( A =',F5.3,2X,'B=',F5.3,')',16H   LODE'S  (NU)
    2=,F6.3)
1017 FORMAT( 1H0,' ATTITUDE OF THE ELLIPSOID AXES : X=1, Y=2 AND Z=3')
1018 FORMAT( 1H ,' AXIS=',I5,2X,' AZIMUTH=',F7.2,5X,' PLUNGE=', F7.2)
1019 FORMAT( 1H0,' CHECK=', F20.10)
1020 FORMAT( 1H0,' ***REMARK : BAD RESULTS ! FITTING IS NOT OF AN ELLIPS
    1OID : CHECK THE ORIENTATION OF THE ANGLES IN THE XY,YZ,ZX-PLANES')
1021 FORMAT (1H0,7H CHECK=,F10.7, 37H   OVERALL ELLIPSES' INCOMPATIBILITY
    1=,F10.3,29H %   AVERAGE LACK OF FIT CF=,F7.3,14H % PER SECTION)
1022 FORMAT(1H ,' PERCENTAGE  OF  DISTORTION IN EACH AXIS : X=',F8.3,'
    1%   Y=',F8.3,' %  Z=',F8.3,' %')
1023 FORMAT( 1H ,44H NADAI'S (NATURAL OCTAHEDRAL UNIT OF SHEAR)=, F6.3, 5X
    1,' AND   EFFECTIVE STRAIN  (ES) =', F6.3)
1024 FORMAT( 1H ,' OR NORMILIZED TO THE SMALLER AXIS =', 2(F10.3,' :'), F4
    1.1)
1025 FORMAT(1H0,' ***MESSAGE : NO SOLUTION WAS FOUND FOR THE NON LINEAR
    1 EQUATIONS( SOLUTION BY LAGRANGE MULTIPLIERS)')
1026 FORMAT(1H0,' ***MESSAGE : DIVERGENCE .')
1027 FORMAT(1H0,' ***REMARK : IT WAS NECESSARY TO USE THE LAGRANGE MULT
    1PLIERS')
2000 FORMAT(72A1)
2001 FORMAT( 1H1,72A1)
2002 FORMAT(3F7.3,3F7.3,I2)
     STOP
     END
     FUNCTION POL(EX,PHI)
     POL= (1. - (EX*((COS(PHI))**2)))**.5
     RETURN
     END
     SUBROUTINE EICOBI(VL,VC)
C
C
C    ROUTINE TO EVALUATE THE EIGENVALUES AND EIGENVECTORS OF
C    A SYMMETRIC  3 X 3 MATRIX.
C    INPUT MATRIX IS THROUGH ARRAY  VL WHICH IS LOST DURING
C    COMPUTATION. OUTPUT BY ARRAYS :
C          - VL = MATRIX OF EIGENVALUES
C          - VC = MATRIX OF EIGENVECTORS
C    METHOD BASED ON THE PAPER BY J.GREENSTADT, 1960 - THE DETERMINATION
C    OF THE CHARACTERISTIC ROOTS OF A MATRIX BY THE JACOBI METHOD.
C    IN : MATHEMATICAL METHODS FOR DIGITAL COMPUTERS  , EDITED
C    BY  RALSTON AND WILF,WILEY,VOL I,1960.
C
C
     DIMENSION VL(3,3), VC(3,3)
     N= 3
     V= 0.
     DO 15 I=1,3
     DO  15 J=1,3
     IF( I .EQ. J) GOTO 5
     VC(I,J) = 0.
     V= V + VL(I,J)*VL(I,J)
     GOTO 15
   5 VC(I,J)= 1.
  15 CONTINUE
     AN = N
     V= SQRT(V)
     VF= (V*1.E-9)/AN
  16 V1= V/AN
     DO 50 I=1,2
     JA= I + 1
     DO 50 J=JA,N
     IF( ABS(VL(I,J)) .LT. V1) GOTO 50
     ANUM= -VL(I,J)
     DENOM= (VL(I,I)-VL(J,J))*.5
     W= ANUM/SQRT(ANUM*ANUM + DENOM*DENOM)
     IF(DENOM .LT. 0.) W= -W
     X= 1. + SQRT(1. - W*W)
     X= SQRT(2.*X)
     ST= W/X
     S2= ST*ST
     CT= SQRT(1. - S2)
     C2= CT*CT
     PROD= CT*ST
```

```
      DO 20 K=1,3
      IF( K .NE. I .AND. K .NE. J) KAXIS= K
      BUX= VC(K,I)*CT - VC(K,J)*ST
      VC(K,J)= VC(K,I)*ST + VC(K,J)*CT
      VC(K,I)= BUX
   20 CONTINUE
      K= KAXIS
      AUX= VL(K,I)*CT - VL(K,J)*ST
      VL(K,J)= VL(K,I)*ST + VL(K,J)*CT
      VL(K,I)= AUX
      DIF= VL(I,I) - VL(J,J)
      PD= VL(I,J)*PROD*2.
      AUX= VL(I,I)
      VL(I,I)= AUX*C2 + VL(J,J)*S2 - PD
      VL(J,J)= AUX*S2 + VL(J,J)*C2 + PD
      VL(I,J)= DIF*PROD + VL(I,J)*(C2 - S2)
      VL(J,I)= VL(I,J)
      DO 25 K=1,3
      VL(I,K)= VL(K,I)
   25 VL(J,K)= VL(K,J)
   50 CONTINUE
      V= V1
      IF(V .GE. VF) GOTO 16
      DO 70 I=1,2
      JA= I + 1
      DO 60 J=JA,3
      IF( ABS(VL(I,I)) .LT. ABS(VL(J,J))) GOTO 60
      AUX= VL(I,I)
      VL(I,I)= VL(J,J)
      VL(J,J)= AUX
      DO 55 K=1,3
      BUX= VC(K,I)
      VC(K,I)= VC(K,J)
      VC(K,J)= BUX
   55 CONTINUE
   60 CONTINUE
   70 CONTINUE
   10 CONTINUE
      RETURN
      END
      SUBROUTINE INVMAT(N1,A,B)
      DIMENSION A(N1,N1), B(N1,N1)
      N= N1
      DO 100 I=1,N
      DO 101 J=1,N
      B(I,J)= 0.
  101 CONTINUE
      B(I,I)=1.
  100 CONTINUE
      DET= 1.
      DO 102 I=1,N
      DIV= A(I,I)
      DET= DET * DIV
      DO 103 J=1,N
      A(I,J)= A(I,J) / DIV
      B(I,J)= B(I,J) / DIV
  103 CONTINUE
      DO 104 J=1,N
      IF(I-J) 1,104,1
    1 RATIO= A(J,I)
      DO 105 K=1,N
      A(J,K)= A(J,K) - RATIO * A(I,K)
      B(J,K)= B(J,K) - RATIO * B(I,K)
  105 CONTINUE
  104 CONTINUE
  102 CONTINUE
      RETURN
      END
```

REFERENCES

Adby, P.R. and Dempster, M.A.H. (1974). Introduction to Optimization Methods. Chapman and Hall mathematics series. London 216pp.

Agterberg, F.P. and Briggs, G. (1973). Statistical analysis of the ripple marks in Atokan and Desmoinesian rocks in the Arkoma Basin and east-central Oklahoma; J. Sedim. Petrol., v.33, pp.393-410.

Agterberg, F.P. (1974). Geomathematics: Mathematical background and Geo-science Applications (Development in Geomathematics, 1). Elsevier. 596pp.

Allison, I (1979). Variations of strain and microstructure in folded pipe rock in the Moine Thrust Zone at Loch Eriboll and their bearing on the deformational history. Scott. J. Geol. 15 (4), pp.263-269.

Allison, J.W. (1974). A petrofabric investigation of shear zones from the Swiss Alps and North-West Scotland. PhD Thesis, Univ. London.

Anderson, E.M. (1948). On lineation and petrofabric structure and the shearing movement by which they have been produced. Geol. Soc. London, Quart. J. 104, pp.99-132.

Ardell, A.J., Christie, J.M. and Tullis, J.A. (1973). Dislocation structures in deformed quartz rocks. Cryst. Lattice Defects, v.4, pp.275-285.

Ashby, M.F. (1972). A first report on deformation-mechanism maps. Acta Metallurgica, v.20, pp.887-897.

Atkinson, B.K. (1976). Deformation mechanism maps for polycrystalline galena. Earth and Planetary Science Letters, v.29, pp.210-218.

Atkinson, B.K. (1977). The kinetics of ore deformation: Its illustration and analysis by means of deformation-mechanism maps. Geologiska Föuningens i Stockholm Förhandlingan. v.99, pp.186-197.

Bailey, E.B. (1955). Moine Tectonics and metamorphism in Skye. Trans. Edin. Geol. Sci., v.16, pp.93-166.

Barber, A.J. (1965). The history of the Moine Thrust Zone, Lochcarron and Lochalsh, Scotland. Proc. Geol. Assoc., v.76 (3), pp.215-242.

Barber, A.J. and Soper, N.J. (1973). Summer field meeting in the North-West Highlands of Scotland. Proc. Geol. Ass., v.84 (2), pp.207-235.

Barton, C.M. (1978). An Appalachian view of the Moine Thrust. Scott. J. Geol. 14 (3), pp.247-257.

Bartsch, H.J. (1974). Handbook of Mathematical Formulas. Academic Press Inc. N. York. and London. pp.527.

Bell, T.H. and Etheridge, M.A. (1973). Microstructure of mylonites and their descriptive terminology. Lithos 6, pp.337-48.

Bell, T.H. and Etheridge, M.A. (1976). The deformation and recrystallization of quartz in a mylonite zone, Central Australia. Tectonophysics, v.32, pp.235-267.

Bell, T.H. (1978). Progressive deformation and reorientation of fold axes in a ductile mylonite zone: The Woodroffe Thrust. Tectonophysics, 44, pp.285-320.

Berthé, D. and Brun, J.P. (1980). Evolution of folds during progressive shear in the south Armorican Shear Zone (France). J. Structr. Geol., v.2, no.1-2, pp.127-134.

Beveridge, G.S.G. and Schechter, R.S. (1970). Optimization: Theory and Practice. MacGraw Hill chemical engineering series. pp.773.

Bilby, B.A., Eshelby, J.D. and Kundu, A.M. (1975). The change in shape of a viscous ellipsoidal region embedded in a slowly deforming matrix having a different viscosity. Tectonophysics, v.28, pp.265-274.

Birch, F (1960). The velocity of compressional waves in rocks to 10 kilobars. J. Geophys. Res., v.66, pp.2199-2224.

Blay, P., Cosgrove, J.W. and Summers, J.M. (1977). An experimental investigation of the development of structures in multilayers under the influence of gravity. J. Geol. Soc. Lond., v.133, pp.329-342.

Borradaile, G.J. (1981). Particulate flow of rock and the formation of cleavage. Tectonophysics, 72, pp.305-321.

Bouchez, J.L. (1977). Plastic deformation of quartzites at low temperature in an area of natural strain gradient. Tectonophysics, 39, (1-3), pp.25-50.

Boullier, A.M. and Guegen, Y. (1975). SP-Mylonites: origin of some mylonites by superplastic flow. Contrib. Mineral. Petrol., v.50, pp.93-104.

Bowes, D.R. (1968). The absolute time scale and the subdivision of Precambrian rocks in Scotland. Geol. Für Stockholm Förh. v.90, pp.175-188.

Bowes, D.R. (1969). The Lewisian of Northwest Highlands of Scotland. In Kay, M. (ed), North Atlantic - Geology and continental drift, a symposium. Mem. Amer, Assoc, Petrol. Geol. v.12, pp.575-594.

Box, H.J., Davies, D. and Swann, W.H. (1969). Non-Linear Optimization Techniques. Monograph No.5. Oliver and Boyd. pp.60.

Brohnstein, I. and Semandaiev, K. (1971). Manual de Matemáticas para Ingenieros y Estudiantes. Editorial Mir, Moscú, pp.696.

Bryant, B. and Reed, J.C.,Jr. (1969). Significance of lineation and minor folds near major thrust faults in the southern Appalachians and the British and Norwegian Caledonides. Geol. Mag., v.106 (5), pp.412-429.

Burns, K.L. and Spry, A.H. (1969). Analysis of the shape of deformed pebbles. Tectonophysics, v.7, no.3, pp.177-196.

Cadell, H.M. (1888). Experimental Researches in Mountain Building. Trans. Roy. Soc. Edin., vol. xxxv, p.337.

Carreras, J., Estrada, A., and White, S. (1977). The effect of folding on the c-axis fabrics of a quartz mylonite. In G.S. Lister, P.F. Williams, H.J. Zwart and R.J. Lisle (eds). Fabrics, Microstructures and Microtectonics. Tectonophysics, v.39, pp.3-24.

Chapman, T.J., Milton, N.J. and Williams, G.D. (1979). Shape fabric variations and deformed conglomerates at the base of the Laksefjord Nappe, Norway. J. Geol. Soc. Lond., vol.136, pp.683-691.

Chapple, W.M. (1968). A mathematical theory of finite amplitude folding. Geol. Soc. Am. Bull., v.79, pp.47-68.

Chapple, W.M. (1978). Mechanics of thin;skinned fold- and thrust-belts. Geol. Soc. of America Bulletin, v.89, pp.1189-1198.

Chayes, F. (1956). Petrographic modal analysis. J. Wiley and Sons Inc. 113pp.

Christie, J.M., McIntyre, D.B. and Weiss, L.E. (1954). Appendix to McIntyre, D.B. The Moine Thrust. Proc. Geol. Assoc. v.65, pp.219-220.

Christie, J.M. (1955). Tectonic Phenomena Associated with the Post-Cambrian Movements in Assynt. Advancement of Science, v.12, pp.572-573.

Christie, J.M. (1963). The Moine Thrust zone in the Assynt region, Northwest Scotland. Univ. California pub. Geol. Sci. 40, pp.345-419.

Clark, S.P. (ed) (1966). Handbook of Physical Constants, rev. edn. Geol. Soc. Amer. Memoir 97.

Cloos, E. (1947). Lineation. Geol. Soc. Amer. Memoir, 18, 122pp.

Cobbold, P.R. and Quinquis, H. (1980). Development of sheath folds in shear regimes. J. Struct. Geol. v.2, no.1/2 pp.119-126.

Coble, R.L. (1963). A model for boundary diffusion controlled creep in polycrystalline materials. J. Appl. Phys. v.34, pp.1679-1682.

Coward, M.P. (1980). The Caledonian Thrust and Shear Zones of NW Scotland. J. Struct. Geol. v.2, no.1-2, pp.11-18.

Coward, M.P. and Kim. J.H. (1981). Strain within Thrust Sheets. Thrust and Nappe Tectonics. 1981 (Ed by McClay, K.R. and Price, N.J.) The Geological Society of London, pp.275-292.

Dahlstrom, C.D.A. (1970). Structural Geology in the eastern margin of the Canadian Rocky Mountains. Bulletin of Canadian Petroleum Geology, v.18 (3), pp.332-406.

DeHoff, R.T. (1962). The determination of the size distribution of ellipsoidal particles from measurements made on ramdom plane sections. Transactions of the Metallurgical Society of AIME, v.224, pp.474-477.

Delesse, A. (1848). Pour determiner la composition des roches. Ann. des Mines, v.13, fourth series, pp.379-388.

DePaor, D.G. (1980). Some limitations of the Rf/ϕ technique of strain analysis. Tectonophysics, v.64, T29-T31.

DePaor, D.G. (1981). Strain analysis using deformed line distributions. Tectonophysics 73, T9-T14.

Dewey, J.F. (1969). Structure and sequence in paratectonic British Caledonides. In M. Kay, (Editor), North Atlantic, Geology and Continental Drift. Am. Assoc. Pet. Geol. Memoir 12, pp.309-335.

Dixon, L.C.W. (1972). Non-Linear Optimization. The English Univ. Press Ltd. pp.213.

Douglas, R.J.W. (1950) Callum Creek, Langford Creek, and Gap map - areas Alberta. Geological Survey of Canada Memoir 255, pp.1-93. (no. 2493).

Dubey, A.K. (1977). An experimental and geological field study of flexural slip folds in multilayered materials. Unpublished PhD Thesis, University of Leeds.

Dunnet, D. (1969). A technique of finite strain analysis using elliptical particles. Tectonophysics 7, (2), pp.117-136.

Dunnet, D and Siddans, A.W.B. (1971). Non-random sedimentary fabrics and their modification by strain. Tectonophysics 12, pp.307-325.

Elliott, D. (1965). The Quantitative Mapping of Directional Minor Structures. J. Geol., v.73, pp.865-880.

Elliott, D. (1970). Determination of finite strain and initial shape from deformed elliptical objects. Geol. Soc. of America Bulletin, v.81, p.2221-2236.

Elliott, D. (1973). Diffusion Flow Laws in Metamorphic Rocks. Geol. Soc. of America Bulletin, v.84, pp.2645-2644.

Elliott, D. (1976-a) The Motion of Thrust Sheets. Journal of Geophysical Research, v.81 (5), pp.949-963.

Elliott, D. (1976-b) The energy balance and deformation mechanism of thrust sheets. Phil. Trans. R. Soc. Lond. A. v.283, pp.289-312.

Elliott, D. and Johnson, M.R.W. vs Price, N., Cosgrove. J.W. and Summers, J.M. (1978). Discussion on structures found in Thrust belts. J. Geol. Soc. Lond. v.135, pp.259-260.

Elliott, D. and Johnson, M.R.W. (1980). Structural Evolution in the Northern Part of the Moine Thrust Belt. Trans. Roy. Soc. Edin.

Escher, A. and Watterson, J. (1974). Stretching fabrics, fold and crustal shortening. Tectonophysics, 22, pp.223-231.

Escher, A., Escher, J.C. and Watterson, J. (1975). The Reorientation of the Kangâmint Dyke Swarm, West Greenland. Can. J. Earth. Sci., 12, pp.158-173.

Etheridge, M.A. and Wilkie, J.C. (1979-a). The Geometry and Microstructure of a range of QP-mylonite zones - a field test of the recrystallized grainsize palaeopiezometer. Proceedings of Conference VIII. Analysis of actual fault zones in Bedrock. US Geol. Survey, Menlo Park, California, pp.448-504.

Etheridge, M.A. and Wilkie, J.C. (1979-b). Grainsize reduction, grain boundary sliding and the flow strength of mylonites. In: T.H. Bell and R.H. Vernon (Eds), Microstructural Processes during deformation and metamorphism. Tectonophysics 58 pp.159-178.

Evans, A.G. and Langdon, T.G. (1976). Structural Ceramics Prog. Mater. Sci. v.21, pp.171-441.

Exner, H.E. (1972). Analysis of grain and particle size distributions in metallic materials. International Metallurgical Reviews, v.17, pp.25-42.

Fisher, R.A. (1953). Dispersion on a sphere. Proc. Roy. Soc. Lond. A217, pp.295-305.

Fleitout, L. and Froidevaux, C. (1980). Thermal and mechanical evolution of shear zones. J. Struct. Geol. v.2, no.1-2, pp.165-173.

Flinn, D. (1956). On the deformation of the Funzie Conglomerate, Fetlar, Shetland. J. Geol. v.64, pp.480-505.

Flinn, D. (1962). On folding during three-dimensional progressive deformation. Geol. Soc. London, Quart. J., v.118, pp.385-433.

Fry, N. (1979). Ramdom point distributions and strain measurement in rocks. Tectonophysics, 60, pp.89-105.

Fry, N. (1979). Density distribution techniques and strained length methods for determination of finite strains. J. of Struct. Geol, v.1 (3), pp.221-229.

Gay, N.C. (1968 a). The motion of rigid particles embedded in a viscous fluid during pure shear deformation of the fluid. Tectonophysics, 5 (2), pp.81-88.

Gay, N.C. (1968 b). Pure shear and simple shear deformation in inhomogeneous viscous fluids. 1. Theory. Tectonophysics, 5 (3), pp.211-234.

Gay, N.C. (1968 c). Pure shear and simple shear deformation in inhomogeneous viscous fluids. 2. The determination of the total finite strain in a rock from objects such as deformed pebbles. Tectonophysics. 5 (4), pp.295-302.

Gay, N.C. (1969). The analysis of strain in the Barberton Mountain Land, Eastern Transvaal, using deformed pebbles, J. Geol. v.77, pp.377-396.

Geikie, A. (1884). The Crystaline Rocks of the Scottish Highlands. Nature, pp.29-31. (Nov 13, 1884).

Gifkins, R.C. (1975). A theory for creep involving grain-boundary sliding. Acta metall.

Gifkins, R.C. (1976). Grain-Boundary Sliding and its accommodation furing creep and superplasticity. Metallurgical Transactions, A, v.7A, pp.1225-1232.

Gifkins, R.C. (1977). The effect of Grain size and Stress upon grain-boundary sliding. Metallurgical Transactions, A, v.8A, pp.1507-1516.

Goetze, C. (1975). Sheared Lherzolites: From the point of view of rock mechanics. Geology, v.3, p..172-173.

Gray, D.R. (1979). Geometry of crenulation-folds and their relationship to crenulation cleavage. J. Structural Geology, v.1, pp.187-206.

Griffiths, J.C. (1967). Scientific method in analysis of sediments: McGraw-Hill Inc., New York, 508p.

Griggs, D.T., (1967). Hydrolitic weakening of quartz and other silicates. Geophys. J. R. Astron. Soc. 14, pp.19-31.

Grocott J. (1977). The relationship between Precambrian shear belts and modern fault systems. J. Geol. Soc. Lond., vol.133, pp.257-262.

Grocott, J. (1979). Shape fabrics and superimposed simple shear strain in a precambrian shear belt, W Greenland.. J. Geol. Soc. Lond. v.136, pp.471-488.

Hallam, A. and Swett, K. (1966). Trace fossils from the Lower Cambrian Pipe Rock of the north-west Highlands. Scott. J. Geol. 2 (1), pp.101-106.

Hanna, S.S. and Fry, N. (1979). A comparison of methods of strain determination in rocks from southwest Dyfed (Pembrokeshire) and adjacent areas. J. of Struc. Geo. v.1 (2), pp.155-162.

Hansen, E. (1971). Strain Facies, Springer-Verlag, New York, 207pp.

Harbaugh, J.W. and Boham-Carter, G. (1970). Computer Simulation in Geology: J. Wiley and Sons Inc., New York, pp.575.

Herring, C. (1950). Diffusional viscosity of a polycrystalline solid. J. Appl. Phys. v.21, pp.437-445.

Hertzberg, R. (1976). Deformation and Fracture Mechanics, John Wiley and Sons, 604pp.

Hilliard, J.E. (1962). The counting and sizing of particles in transmission microscopy. Trans. AIME., v.224, p.906.

Hobbs, E., Means, W.D. and Williams, P.F. (1976). An Outline of Structural Geology. J. Wiley and Sons Inc., pp.571.

Hossack, J.R. (1968). Pebble deformation and thrusting in the Bygdin area (Southern Norway). Tectonophysics 5 (4), pp.315-339.

Hossack, J.R. (1978). The correction of stratigraphic sections for tectonic finite strain in the Bygdin area, Norway. J. Geol. Soc. Lond. v.135, pp.229-241.

Hubert, N.K. and Rubey, W.W. (1959). Role of fluid pressure in mechanics or overthrust faulting. Geol. Soc. Amer. Bull. v.70, pp.115-206.

Hudleston, P.T. (1969). The Morphology and Development of Folds. Unpublished PhD Thesis, University of London, 356pp.

Hudleston, P.J. (1973 a). The analysis and interpretations of minor folds developed in the Moine Rocks of Monar, Scotland. Tectonophysics 17, pp.89-132.

Hudleston, P.J. (1973 b). Fold morphology and some geometrical implications of theories of fold development. Tectonophysics 16, pp.1-46.

Huddleston, P.J. (1973 c). An analysis of 'single-layer' folds developed experimentally in viscous media. Tectonophysics 16, pp.189-214.

Hull, D. (1965). Introduction to dislocations. Oxford: Pergamon.

Hutchinson, C.S. (1974). Laboratory handbook of petropraphic techniques. Wiley, New York. 527pp.

Hutton, D.H.W. (1979). The strain history of a Dalradian slide: using pebbles with low fluctuations in axis orientation. Tectonophysics 55, pp.261-273.

Johnson, M.R.W. (1957). The structural geology of the Moine Thrust zone in Coulin forest, Western Ross. Quant. J. Geol. Soc. Lond. 113, pp.241-270.

Johnson, M.R.W. (1960). The structural history of the Moine Thrust Zone at Lochcarron, Western Ross. Trans. Roy. Soc. Edin. v.LXIV (7), 1960, pp.139-168.

Johnson, M.R.W. (1967). Mylonite Zones and Mylonite Banding. Nature pp.246-247.

Kerrich, R. and Allison, I. (1978). Flow mechanisms in rocks: Microscopic and mesoscopic structures, and their relation to physical conditions of deformation in the crust. Geoscience Canada, v.5 (3), pp.109-118.

Knipe, R. (1980). Distribution of impurities in deformed quartz and its implications for deformation studies. Tectonophysics v.64, T11-T18.

Kohlstedt, D.L. and Goetze, C. (1974). Low stress, high temperature creep in olivine single crystals. J. Geophys. Res., v.79, pp.2045-2051.

Kohlstedt, D.L., Goetze, C. and Durham. W.B. (1976). Experimental deformation of single crystal olivine with application to flow in the mantle, in The Physics and Chemistry of Minerals and Rocks, (ed. R.G.H. Sorens), J. Wiley and Sons Ltd, London, pp.35-49.

Kohlstedt, D.L., Cooper, R.F., Weathers, M.S. and Bird, J.M. (1979). Paleostress analysis of deformation - induced microstructures: Moine Thrust Zone and Ikertog Shear Zone. Proceedings of Conference VIII. Analysis of actual fault zones in Bedrock. US Geol. Survey, Menlo Park, California, pp.394-425.

Krumbein, W.C. (1935). Thin section Mechanical Analysis of Indurated Sediments. J. Geol. v.43, pp.482-496.

Kvale, A. (1948). Petrologic and structural studies in the Bergsdalen Quadrangle, Western Norway, Part II: Structural Geology. Bergens Mus. Arb., 1946-7. Naturn. Rekke 1, pp.1-255.

Kvale, A. (1963). Linear structures and their relation to the movement in the caledonides of Scandinavia and Scotland. Geol. Soc. Lond. Quart. J. 109, pp.51-73.

Lapworth, C. (1883 a). The Secret of the Highlands. Geol. Mag. 10, pp.120-128.

Lapworth, C. (1883 b). The Secret of the Highlands. Geol. Mag. v.5 (10), pp.191-199.

Lapworth, C. (1883 c). The Secret of the Highlands. Geol. Mag. v.10 (8). pp.337-343.

Lapworth, C. (1884). On the stratigraphy and metamorphism of the rocks of the Durness-Eriboll district. Proc. Geol. Ass. v.8, pp.438-442.

Lapworth, C. (1885 a). On the close of the Highland Controversy. Geological Magazine, v.2 (3), pp.97-106.

Lapworth, C. (1885 b). The Highland Controversy in British Geology: its causes, course and consequences. Nature, Oct.8, 1885. pp.558-559.

Lindstrom, M. (1961). Beziehungen zwischen Klein faltenurgenzen und andenn Gefugemertanalen in den Kaledoniden Skandinaviens. Geol. Rdssh., v.51, pp.144-180.

Lisle, R.J. (1977). Estimation of the tectonic strain ratio from the mean shape of deformed elliptical markers. Geol. Mijnbouw 56, pp.140-144.

Loudon, T.V.(1964). Computer Analysis of Orientation Data in Structural Geology: Tech. Report. Geog. Branch. Off. Naval Res., O.N.R.Task No.389-135, Contr. No. 1228 (26), No.13, pp.1-130.

McClay, K.R. (1977). Pressure solution and coble creep in rocks and minerals: a review. J. Geol. Soc. Lond. v.134, pp.57-70.

McClay, K.R. and Coward, M.P. (1981). The Moine Thrust Zone. An overview. Thrust and Nappe Tectonics 1981. The Geological Society of London. pp.241-260.

McIntyre, D.B. (1954). The Moine Thrust - its discovery, age and tectonic significance.. Proc. Geol. Assoc., v.65 (3), pp.203-223.

McLaren, A.C., Turner, R.G., Boland, J.N. and Hobbs, B.E. (1970). Dislocation structure of the deformation lamellae in synthetic quartz: a study by electron and optical microscopy. Contr. Min. and Petr. 29, pp.104-115.

McLeish, A. (1969). Strain analysis of deformed pipe rock in the Moine Thrust Zone, Northwest Scotland. Tectonophysics, v.12, pp.469-503.

McLeish, A.J. (1971). Strain analysis of deformed Pipe Rock in the Moine Thrust Zone, Northwest Scotland. Tectonophysics, 12, pp.469-503.

Mardia, K.V. (1972). Statistics of Directional Data. Academic Press Inc. (London) Ltd. pp.357.

Marjoribanks, R.W. (1976). The relation between microfabric and strain in a progressively deformed quartzite sequence from central Australia. Tectonophysics, 32, pp.269-293.

Matthews, P.E., Bond, R.A.B. and Van den Berg, J.J. (1974). An algebraic method of strain analysis using elliptical markers. Tectonophysics, 24, pp.31-67.

Mendum, J.R. (1976). A strain study of the Strathan Conglomerate, Northwest Sutherland, Scott. J. Geol. v.12, no.2, pp.135-146.

Mercier, J.C.C., Anderson, D.A. and Carter, N.L. (1977). Stress in the lithosphere: Inferences from steady state flow of rocks. Pageogh, v.115, pp.199-226.

Miller, D.M. and Oertel, G. (1979). Strain determination from the measurement of pebble shapes: a modification. Tectonophysics, 55, T11-T13.

Minnigh, L.D. (1979). Structural analysis of sheath-folds in a metachert from the Western Italian Alps. J. of Struct. Geol. v.1 (4), pp.275-282.

Milton, N.J. (1980-a). Determination of the strain ellipsoid from measurements on any three sections. Tectonophysics, 64, T19-T27.

Milton, N.J. (1980-b). Thrusts and related structures in the Scandanavian Caledonides. PhD Thesis, University of Wales, Cardiff.

Mitra, S. (1978). Microscopic deformation mechanisms and flow laws in quartzites within the South Mountain Anticline. Journal of Geology, v.86, pp.129-152.

Mitra, G. (1978). Ductile deformation zones and mylonites: the mechanical processes involved in deformation of crystalline basement rocks. American Journal of Science, v.278, pp.1057-1084.

Mittlefehldt, N.H. and Oertel, G. (1980). Strain determination from measurement of pebble shapes: the special case of a bent foliation. Tectonophysics, v.67, T1-T7.

Miyashiro, A. (1965). Metamorphism and metamorphic belts. George Allen and Unwin Ltd, 492p.

Mohamed, F.A. and Langdon, T.G. (1974). Deformation mechanism maps based on grain size. Metallurgical Transactions, v.5, pp.2339-2344.

Mukhopadhyay, D. (1965). Effects of compression on Concentric Folds and mechanism of similar folding. J. Geol. Soc. India, v.6, pp.27-41.

Mukhopadhyay, D. (1973). Strain measurements from deformed quartz grains in the slaty rocks from the Ardennes and the northern Eifel. Tectonophysics, 16, pp.279-296.

Mukhopadhyay, D. (1980). Determination of finite strain from grain centre measurements. Tectonophysics, 67-T9-T12.

Nabarro, F.R.N. (1948). Deformation of crystals by the motion of single ions. In Report of a conference on the strength of solids. Phys. Soc. Lond. pp.75-90.

Nadai, A. (1963). Theory of Flow and Fracture of Solids. McGraw-Hill book company, New York, 1950.

Nadir, P.Y. (1980). The Structure and Deformation History of the Cambro-Ordovician Sediments of the Moine Thrust Zone near Loch Eriboll, Northwest Scotland. PhD Thesis, University of Leeds (unpublished).

Nicol (1856). Quartzites, etc. of NW Scotland. Proceedings of the Geological Society, VXIII (part 1), pp.17-39.

Nicol (1860). NW Highlands. Proceedings of the Geological Society XVII (part 1) pp.85-113.

Nicolas, A. and Boudier, F. (1975). Kinematic interpretation of folds in alpine-type peridotites. Tectonophysics, 25, pp.233-260.

Nicolas, A. and Poirier, J.P. (1976). Crystalline placticity and solid state flow in metamorphic rocks. J. Wiley and Sons, Ltd 444p.

Nye, J.F. (1952). A comparison between the theoretical and the measured long profile of the Unteraar glacier. J. Glaciol. 2, pp.103-107.

Oertel, G. (1978). Strain determination from the measurement of pebble shapes. Tectonophysics, 50, T1-T7.

Oleson, N.O. (1971). The relative chronology of folds phases, metamorphism and Thrust movements in the Caledonian Troms, North Norway. Nor. Geol. Tidsskr., v.51, pp.355-377.

Park, R.G. (1970). Observations on Lewisian Chronology. Scott. J. Geol. 6 (4), pp.379-399.

Peach, B.N. and Horne, J. (1884). Report on the Geology of the North-West of Sutherland. Nature: Nov 13, 1994, pp.31-35.

Peach, B.N. and Horne, J.(1885). The geology of Durness and Eriboll with special reference to the Highland Controversy. Nature, Oct. 8, 1885, p.558.

Peach, B.N., Horne, J., Gunn, W., Clough, C.T., Hinxmann, L.W. and Teale, J.J.H. (1907). The geological structure of the Northwest Highlands of Scotland. Mem. Geol. Surv. UK.

Peach, B.N. and Horne, J. (1930). Chapters on the geology of Scotland. Oxford.

Peach, C.J. and Lisle, R.J. (1979). A FORTRAN IV program for the analysis of tectonic strain using deformed elliptical markers. Computers and Geosciences, v.5, pp.325-334.

Pettijohn, F.J. (1957). Sedimentary Rocks (2nd edit) Harper and Brothers, New York, 718pp.

Phemister, J.C. (1960). British Regional Geology: The Northern Highlands (3rd Edn.) H.M.S.O., London, p.104.

Phillips, F.C. (1937). A fabric study of some Moine Schists and associated rocks. Geol. Soc. Lond., Quart. J. v.93, pp.581-620.

Phillips, F.C. (1955). Structural Petrology and Problems of the Caledonides. Introduction Advancement of Science. pp.511-572.

Phillips, F.C. (1945). The micro-fabric of the Moine Schists. Geol. Mag., v.82, pp.205-220.

Pickering, F.B. (1976). The Basis of Quantitative Metallography. Institute of Metallurgical Technicians, Monograph no.1. pp.1-55.

Poirier, J.P. and Guillopé, M. (1979). Deformation induced recrystallization of minerals. Bull. Minerál, 102, pp.67-74.

Post, R.L. (1973). The Flow Laws of Mt Burnett Dunite. PhD Thesis University of California, Los Angeles, 272p.

Price, N.J. (1975). Rates of deformation. J. Geol. Soc. Lond. v.131. pp.553-575.

Price, N.J. (1977). Aspects of gravity tectonics and the development of listric faults. J. Geol. Soc. Lond., v.133, pp.311-327.

Price, R.A. and Mountjoy, E.W. (1970). Geologic structure of the Canadian Mountains between Bow and Athabasca Rivers: progress report, Geol. Ass. Can. Spec. Pap. 6, pp.7-25.

Quinquis, H., Andress, C.L., Brün, J.P. and Cobbold, P.R. (1978). Intensive progressive shear in Ile and Groix blueschists and compatibility with subduction or obduction. Nature, v.273, pp.43-45.

Raj, R and Ashby, M.F. (1971). On grain boundary sliding and diffusional creep. Metallurgical Transactions, v.2, pp.1113-1127.

Raleigh, C.B. and Kirby, S.H. (1970). Creep in the Upper Mantle. Min. Soc. Am. Spec. Pap. v.3, pp.113-121.

Ramberg, H. (1980). Diapirism and gravity collapse in the Scandinavian Caledonides. J. Geol. Soc. London. v.137, pp.261-270.

Ramberg, H. (1981). The role of gravity in orogenic belts. In McClay and Price (ed). Thrust and Nappe Tectonics. The geolocical Society of London. pp.125-140.

Ramsay, J.G. (1967). Folding and Fracturing of rocks. McGraw Hill, Inc. 568p.

Ramsay, J.G. and Graham, R.H. (1970). Strain variation in shear belts. Canadian Journal of Earth Sciences, 7, pp.786-813.

Ramsay, J.G. and Wood, D.S. (1973). The geometric effects of volume change during deformation processes. Tectonophysics 13, pp.263-277.

Ramsay, J.G. (1980). Shear zone geometry: a review. J. Struct. Geol. v.2, no.1-2, pp.83-100.

Rathbone, P.A., Coward, M.P. and Harris, A.L. (in press). Cover and basement: a contrast in style and fabrics.

Rhodes, S. and Gayer, R.A. (1977). Non-cylindrical folds, linear structures in the X direction adn mylonite developed during translation of the Caledonian Kalak Nappe Complex of Finmark. Geol. Mag. v.114 (5), pp.329-341.

Rich, J.L. (1934). Mechanics of low-angle overthrust faulting as illustrated by Cumberland Thrust block, Virginia, Kentucky and Tennessee. Bulletin of the American Assoc. of Petroleum Geologists, v.18 (12), pp.1684-1596.

Roberts, J.L. and Sanderson, D.J. (1974). Oblique fold axes in the Dalradian rocks of the Southwest Highlands. Scott. J. Geol. v.9 (4), pp.281-296.

Roberts, B. and Siddans, A.W.B. (1971). Fabric studies in the Lewyd Mawr Ignimbrite, Caernarvonshire, North Wales. Tectonophysics, 12, pp.283-306.

Robie, R.A., Betehke, P.M., Toulmin, M.S., Edwards, J.L. (1966). Handbook of Physical Constants. The Geol. Soc. of Am. 97pp.

Rodgers, D.F. and Adams, J.A. (1976). Mathematical Elements for Computer Graphics. McGraw Hill book company. 240p.

Rosiwal, A. (1898). Uber geometrische Gesteinrsanalysen, usw, Verhaudl. der K.K. gerlogischem Reischanstalt, 5/6, p.143.

Ross, J.V., Avelallement, H.G. and Carter, N.L. (1980). Stress dependence of recrystallized-grain and subgrain size in olivine. Tectonophysics, 70, pp.39-61.

Ross, J.V., Mercier, J.C.C., Avelallement, H.G., Carter, N.L. and Zimmerman, J. (1980). The Vourinos Ophiolite Complex, Greece: The Tectonite suite. Tectonophysics. 70, pp.63-83.

Rutter, E.H. (1976). The kinetics of suck deformation by pressure solution. Phil. Trans. R. Soc. Lond. A. 283, pp.203-219.

Sander, B. (1930). Gefugekünde der Gesteine: Springer, Vienna, 352pp.

Sanderson, D.J. (1973). The development of fold axes oblique to the regional trend. Tectonophysics, v.16, pp.55-70.

Sanderson, D.J. (1976). The superposition of compaction and plane strain. Tectonophysics. 30, pp.35-54.

Sanderson, D.J. (1977). The analysis of finite strain using lines with an initial random orientation. Tectonophysics 43, pp.199-211.

Seymour, D.B. and Boulter, C.A. (1979). Tests of computerised strain analysis methods by the analysis of simulated deformation of natural unstrained sedimentary fabrics. Tectonophysics 58, pp.221-235.

Shand, S.J. (1916). A recording micrometer for rock analysis. J. Geol. v.24, pp394-403.

Shimamoto, T. and Ikeda. Y. (1976). A simple algebraic method for strain estimation from deformed ellipsoidal objects 1. Basic Theory. Tectonophysics 36, pp.315-337.

Sibson, R.H. (1977). Fault rocks and fault mechanisms. J. Geol. Soc. Lond. Vol. 133, pp.191-213.

Siddans, A.W.B. (1971). The origin of Slaty Cleavage. PhD Thesis University of London, 555p.

Siddans, A.W.B. (1980 a). Analysis of three-dimensional homogeneous, finite strain using ellipsoidal objects. Tectonophysics 64, T1-16.

Siddans, A.W.B. (1980 b). Elliptical markers and non-coaxial strain increments. Tectonophysics 67, T21-T25.

Siddans, A.W.B. (1981). Some limitations of the Rf/ϕ technique of strain analysis - discussion. Tectonophysics 72, pp.155-158.

Soper, N.J. (1971). The earliest Caledonian structures in the Moine Thrust belt. Scott. J. Geol. v.7, pp.241-247.

Soper, N.J. and Barber, A.J. (1979). Proterozoic folds on the North-west Caledonian Foreland. Scott. J. Geol., v.15 (1) pp.1-11.

Soper, N.J. and Brown, P.E. (1971). Relationship between metamorphism and migmatization in the northern part of the Moine Nappe. Scott. J. Geol. v.7 (4), pp.305-325.

Soper, N.J. and Wilkinson, P. (1975). The Moine Thrust and Moine Nappe at Loch Eriboll, Sutherland. Scott. J. Geol. 11 (4), pp.339-359.

Spektor, A.G. (1950). Distribution Analysis of Spherical Particles in Non-Transparent Structures. Zavod. Lab. v.16, no.2, p.173.

Squires, R.L., Weiner, R.T. and Phillips, M (1963). Grain boundary denuded zones in a magnesium - ½ wt% zirconium alloy: Hour. Nuclear. Materials, v.8, pp.77-80.

Stabler, C.L. (1968). Simplified Fourier analysis of fold shapes. Tectonophysics 6, pp.343-350.

Stauffer, M.R. (1967). Tectonic strain in some volcanic sedimentary and intrusive rocks near Camberra, Australia: a comparative study in deformation fabrics. New Zealand. J. Geol. and Geophys. v.10, pp.1079-1108.

Stocker, R.L. and Ashby, M.F. (1973). On the Rheology of the Upper Mantle. Reviews of Geophysics and Space Physics, v.11 (2) pp.391-426.

Sutton, J. and Watson, J. (1951). The pre-torridonian metamorphic history of the Loch Torridon and Scourie areas in the North-West Highlands, and its bearing on the chronological classification of the Lewisian: Q. J. Geol. Soc. Lond. v.106 (for 1950), pp.241-307.

Sutton, J. and Watson, J. (1953). The supposed Lewisian inlier of Scardroy, Central Rosshire, and its relations with the Surrounding Moine rocks. Q. J. Geol. Soc. Lond. v.108, (for 1952), pp.99-126.

Sutton, J. and Watson, J. (1962). An Interpretation of Moine-Lewisian Relations in Central Rosshire. Geol. Mag. v.XCIX (6), pp.527-541.

Takeuchi, S. and Argon, A.S. (1976). Steady state creep of single phase crystalline matter at high temperature. J. Mater. Sci. II, pp.1542-1566.

Talbot, C.J. (1979). Fold trains in a glacier of salt in southern Iran. J. Struct. Geol. v.1, no.1, pp.5-18.

Tan, B.K. (1976). Oolite deformation in Windgällen, Canton, Uri, Switzerland. Tectonophysics, 31, pp.157-174.

Tullis, J., Christie, J.H. and Griggs, D.T. (1973). Microstructures and preferred orientations of experimentally deformed quartzites. Geol. Soc. of America Bulletin, v.84, pp.297-314.

Tullis, J.A. (1979). High Temperature Deformation of Rocks and Minerals. Reviews of Geophysics and Space Physics, v.17 (6), pp.1137-1154.

Turner, F.J. and Wiess, L.E. (1963). Structural Analysis of Metamorphic Tectonites. McGraw Hill book company. Inc. pp.545.

Twiss, R.J. (1977). Theory and Applicability of Recrystallized Grain Size Paleopiezometer.Pageoph., v.115, pp.227-244.

Underwood, E.E. (1970). Quantitative Stereology. Addison-Wesley Publishing Comp. 274-p.

van Breemen, O., Aftalion, M. and Johnson, M.R.W. (1979). Age of the Loch Borrolan complex, Assynt, and late movements along the Moine Thrust Zone. J. Geol. Soc. Lond. 136, pp.489-495.

Vauchez, A (1980). Ribbon texture and deformation mechanisms of quartz in a mylonitized granite of Great Kabylia (Algeria). Tectonophysics. 67, pp.1-12.

Vehoogen, J., Turner, J., Weiss, L.E., Wahrhaftig, C. and Fyfe, W.S. (1970). The Earth. An introduction to physical Geology. Holt, Rinehalt, and Winston, Inc. 750pp.

Weathers, M.S., Bird, J.M., Cooper, R.F. and Kohlstedt, D.L. (1979) Differential stress determined from deformation-induced microstructures of the Moine Thrust Zone. J. of Geophys. Research, v.84 (B13), pp.7495-7509.

Weathers, M.S., Bird, J.M., Cooper, R.F. and Kohlstedt, D.L. (1979-b). Microstructure and stress analysis of the Mullen Creek-Nash Fork shear zone, Wyoming. Proceedings of conference VIII. Analysis of actual fault zones in Bedrock. US Geol. Survey, Menlo Park, California. pp.426-447.

Weeterman, J. (1957). Steady state creep of crystals. J. Appl. Phys. v.28, p.1185.

Weiss, L.E. (1955). Fabric Analysis of a triclinic tectonite and its bearing on the geometry of flow in rocks. Am. J. Sci., v.253. pp.225-236.

Weiss, L.E. and McIntyre, D.B. (1957). Structural geometry of Dalradian rocks at Loch Leven, Scottish Highlands. J. Geol. 65, pp.575-602.

White, S. (1973 a). Syntectonic recrystallization and texture development in quartz. Nature, v.2-4, pp.276-278.

White, S. (1973 b). The dislocation structures responsible for the optical effects in some naturally-deformed quartzes. Journal of Materials Sciencs 8, pp.490-499.

White, S. (1973 c). Deformation lamellae in naturally deformed quartz. Nature Phys. Sci. 245, pp.26-28.

White, S. (1975). Estimation of strain rates from microstructures. J. Geol. Soc. Lond. v.131, pp.577-583.

White, S. (1976 a). The determination of deformation parameters from dislocation sub-structures in naturally deformed quartz. In: J.A. Venables (ed), Developments in electron microscopy and analysis. Academic Press, London, pp.505-509.

White, S. (1976 b). The effects of strain on the microstructures, fabrics and deformation mechanisms in quartzites. Phil. Trans. R. Soc. Lond. A. 283, pp.69-86.

White, S. (1976 c). The role of dislocation processes during tectonic deformations, with particular reference to quartz. "The Physics and Chemistry of Minerals and rocks" - London, Wiley, pp.75-91.

White, S. (1977). Geological significance of recovery and recrystallization processes in quartz. Tectonophysics 39, pp.143-170.

White, S. (1979-a). Difficulties associated with paleo-stress estimates. Bu-l. Mineral, 102, pp.210-215.

White, S (1979-b). Paleo-stress estimates in the Moine Thrust Zone, Eriboll, Scotland. Nature, 280, pp.222-223.

White, S. (1979-c). Grain and sub-grain size variations across a mylonite zone. Contrib. Mineral Petrol. 70, pp.193-202.

White, S. (1979-d). Large strain deformation; report on a Tectonic Studies Group Discussion meeting held at Imperial College, London on 14 November , 1979. J. of Struct-Geo., v.1 (4), pp.333-339.

White, S.H., Burrows, S.E., Carreras, J., Shaw, N.D. and Humphreys, J.F. (1980). On mylonites in Ductile Shear Zones. J. Struct. Geol. v.2, no.1-2, pp.175-188.

Whitten, E.H.T., (1966). Structural Geology of Folded Rocks. Rand McNally and Co, Chicago. 678pp.

Wilkinson, P. (1956). The structural history of the region east of Loch Eriboll, Sutherland. pp.573-575.

Wilkinson, P., Soper, N.J. and Bell, A.M. (1975). Skolithos pipe as strain markers in mylonites. Tectonophysics, 28, pp.143-157.

Williams, G.D. (1978). Rotation of contemporary folds into the X direction during overthrust processes in Laksefjord, Finnmark. Tectonophysics, 48, pp.29-40.

Winkler, H.G.F. (1974). Petrogenesis of metamorphic rocks. Springer-Verlag New York Inc., 334pp.

Wilson, C.J.L. (1973). The prograde microfabric in a deformed quartzite sequence, Mount Isa, Australia. Tectonophysics, 19, pp.39-81.

Wilson, C.J.L. (1975). Preferred orientations in quartz ribbon mylonites. Bull. Geol. Soc. Am. 86, pp.468-974.

Wismer, D.A. and Chattergy, R. (1978). Introduction to Nonlinear Optimization. North-Holland. New York. 395pp.

Wonnacott, T.H. and Wonnacott, R.J. (1977). Introductory Statistics, 3rd Ed. John Wiley and Sons. 650pp.

Zeuch, D.H. and Green, H.W.II, (1979). Experimental deformation of an 'anhydrous' synthetic dunite. Bull. Minéral. v.102, pp.185-187.

Fig. 2.1a Eriboll Area

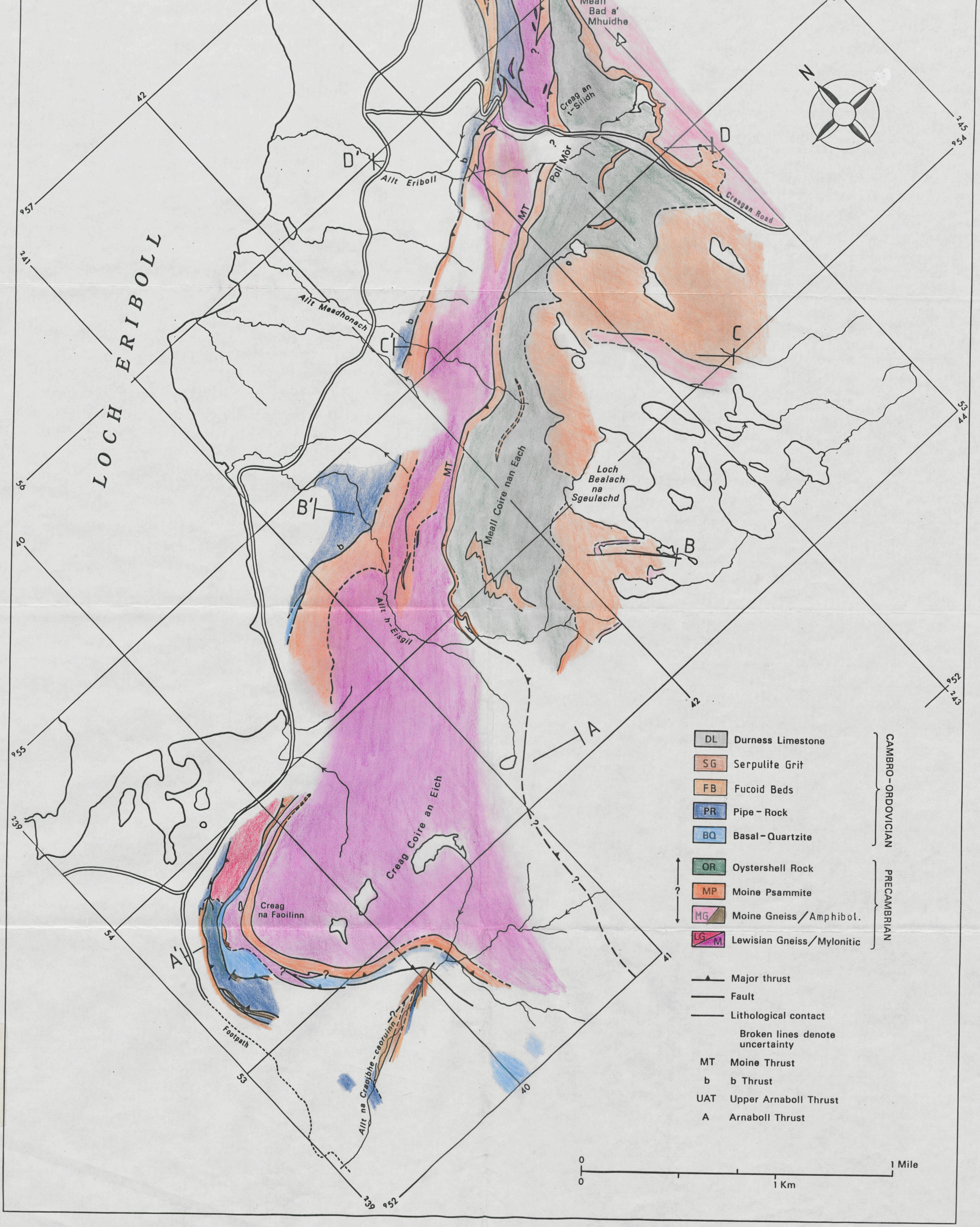

Fig. 2.1b Eriboll Area

Fig 2.2-a Eriboll Area

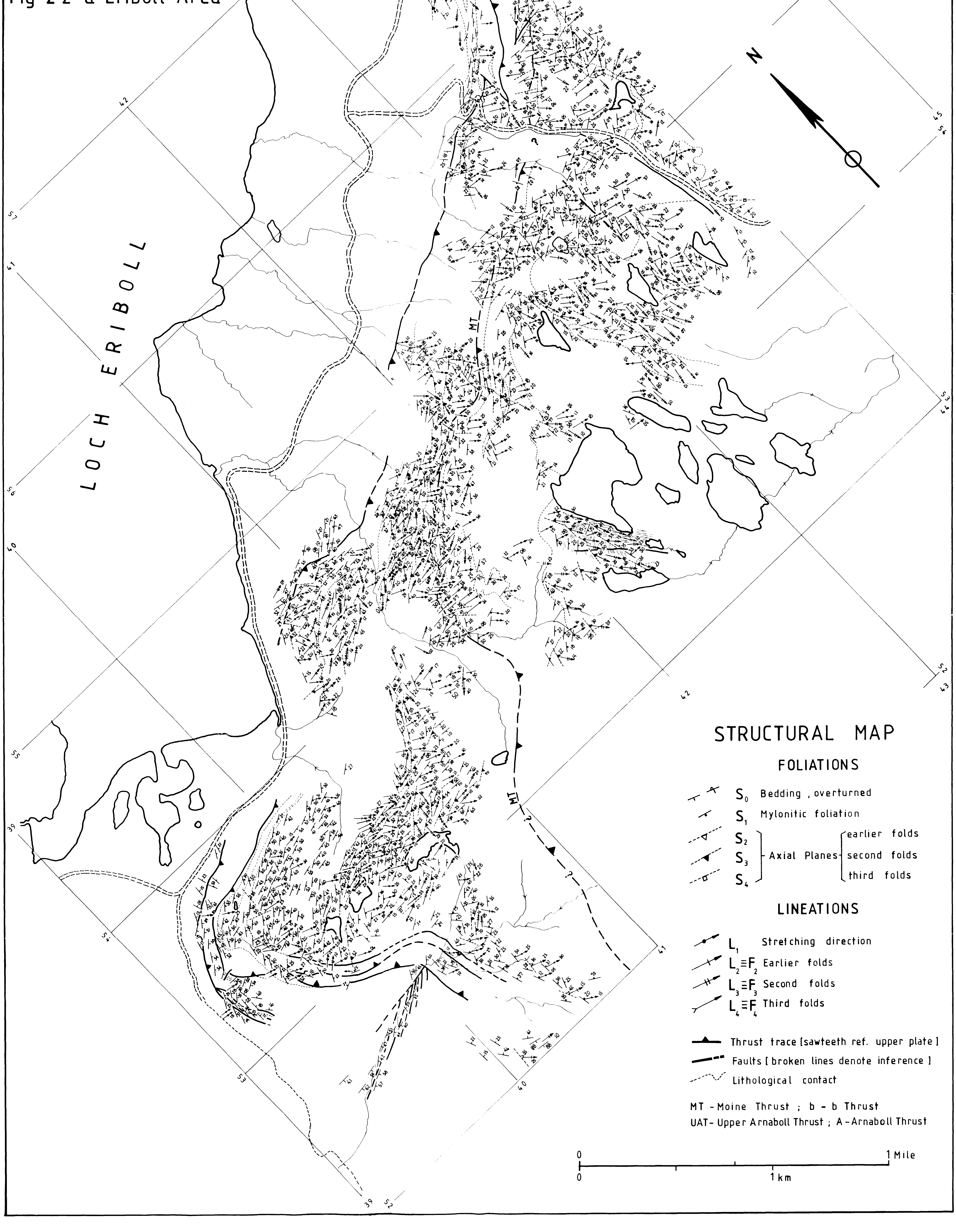

Fig. 2·2-b Eriboll Area